CRANFIELD UNIVERSITY

KING TIN LEUNG

ROAD VEHICLE STATE ESTIMATION USING LOW-COST GPS/INS

SCHOOL OF ENGINEERING

ENGD THESIS

This page intentionally left blank.

CRANFIELD UNIVERSITY

SCHOOL OF ENGINEERING

ENGD THESIS

Academic Year 2005-2009

KING TIN LEUNG

ROAD VEHICLE STATE ESTIMATION USING LOW-COST GPS/INS

Co-Supervisors:
Dr. J. Whidborne
Dr. D. Purdy
Dr. P. Baines
Dr. P. Barber

April 12, 2010

This thesis is submitted in partial fulfilment of the requirements for the degree of Engineering Doctorate

This page intentionally left blank.

Abstract

Due to noise and bias in the Inertial Navigation System (INS), vehicle dynamics measurements using the INS are inaccurate. Although alternative methods involving the integration of INS with accurate Global Positioning System (GPS) exist and are accurate, this kind of system is far too expensive to become value-adding to production vehicles. This thesis therefore considers two aspects: 1) the possibility of estimating vehicle dynamics using low-cost INS and GPS, and 2) the importance of vehicle dynamics in terms of handling in the eyes of customers upon vehicle purchase. The former aspect is considered from an engineering perspective and the latter is studied in a marketing context.

From an engineering point of view, knowledge of vehicle dynamics not only improves existing safety control systems, such the Anti-lock Braking System (ABS) and Electronic Stabilising Program (ESP), but also allows the development of new systems. Based on modelling and simulation in MATLAB/Simulink, low-cost GPS and in-car INS (such as accelerometers, gyroscopes and wheel speed sensors) measurements are fused using Kalman Filters (KFs) to estimate the vehicle dynamics. These estimations are then compared with the simulation results from IPG CarMaker. For most simulations, the speed of the vehicle is kept between 15 to 55kph. It is found that while triple KF designs are able to estimate the tyre radius, the longitudinal velocity and the heading angle accurately, an integrated KF design with known vehicle parameters is also able to estimate the lateral velocity precisely. Apart from studying and comparing different KF designs with restricted sensors quality, the effects and benefits of different sensor qualities in dynamic estimations are also studied via the variation of sensor sampling rates and accuracies. This investigation produces a design procedure and estimation error analyses (theoretical and graphical) which may help future engineers in designing their KFs.

From a marketing perspective, it is important to understand customers' purchase reasons in order to allocate resources more efficiently and effectively. As GPS/INS KF designs are able to enhance vehicle handling, it is vital to understand the relative importance of vehicle handling as a consumer purchase choice criterion. Based

on two surveys, namely the New Vehicle Experience Survey in the US (NVES_US) and the New Car Buyer Survey in the UK (NCBS_UK), analyses are performed in a computer program called the Predictive Analytics SoftWare (PASW), which is formerly known as the Statistical Package for the Social Sciences (SPSS). The number of purchase reasons are first reduced with factor analysis, the latent factors produced are then used in the SPSS Two Step Cluster analysis for customer segmentation. With the customer segments and the latent factors defined, a discriminant analysis is carried out to determine customer type in the automobile sector, in particular for Jaguar Cars. It is found that customers in general take vehicle handling for granted and often underrate its importance in their purchase. New vehicle handling-aided systems therefore need to be marketed in terms of the value they add to other benefits such as reliability and performance in order to increase sales and stakeholder value.

Acknowledgements

Throughout the four years of my EngD, I have experienced many ups and downs, successes and failures. To be able to write this section is really a miracle. I thank God for guiding me through these 4 years. It has been hard work, but the process has been filled with joy.

God has been so merciful to me. He has prepared me with a project that is sponsored by Jaguar Land Rover and EPSRC. He has granted me good supervisors, who are all charming, friendly, helpful and knowledgeable. He has not only given me one or two supervisors, but seven altogether. With no order of importance, thank you Dr. Martin Bayliss for his encouragement and teaching in vehicle dynamics at the start of the project. He pointed me in the right direction and helped my first conference publication. Thank you Prof. Robert Williams, Dr. Alain Dunoyer and Dr. Phil Barber for their continual support at Jaguar Land Rover. They provided me with chances of working in the company as well as survey data for my marketing research. Thank you Dr. Paul Baines for his guidance and expertise in the market research. Thank you Dr. David Purdy for his many ideas and support in vehicle dynamics and experimental work at the Shrivenham campus. Thank you Dr. James Whidborne for his support, guidance, patience and care throughout my EngD, he is always busy but always have time for me, teaching me and constantly correcting my materials with grammatical errors. And thank you Mrs. Kath Tipping from the Cranfield EngD centre for managing the EngD programme and organising industrial outings.

God has also given me additional support through Mr. Ian Crawford and Eric Collins, who proof read my thesis. The comments and changes they made were most appropriate and constructive. They are like the icing on the cake, allowing my thesis to flow and read better. My gratitude also goes towards my colleagues, Leo and Cip, for their company, which enlightened my stay at Cranfield with laughter. I would also like to thank my parents and my fiancee for their love and care. In my most despairing times, they have given me unlimited support and courage. Lastly, thank you for the numerous prayers from my brothers and sisters in church. Without the prayers, I do not think I could have endured the hardship.

The grace of God is countless, there are just too many people that I have to thank during these 4 years. So please then accept my apologies and my gratitude to anyone who I have missed out. Without any of you, this thesis would be incomplete.

Contents

This page intentionally left blank.

List of Figures

This page intentionally left blank.

List of Tables

Abbreviations

Axes & vehicle definition

4WS	Four Wheel Drive
b-frame	Body-frame (sensor)
v-frame	Vehicle-frame
DoF	Degree Of Freedom
ENU/e-frame	East, North, Up framework
NED	North, East, Down framework
RWD	Rear Wheel Drive
VM	Vehicle Model

In-car sensors

ABS	Anti-lock Braking System
CAN-bus	Controller Area Network
ECU	Electronic Control Unit
ESP	Electronic Stability Program
FOG	Fibre-Optic Gyroscope
GL	G sensors
INS	Inertial Navigation System
RLG	Ring Laser Gyroscope
WSS	Wheel Speed Sensor
YRS	Yaw Rate Sensor/Yaw Rate gyroscope

Satellite system

C/A code	Coarse/Acquisition code
DoP	Dilution of Precision
DDiff	Double Differencing
DGPS	Differential Global Positioning System
GLONASS	GLObal'naya NAvigatsionnaya Sputnikovaya Sistema (GLObal NAvigation Satellite System)

GNSS	Global Navigation Satellite System
GPS	Global Positioning System
SA	Selective Availability
SDiff	Single Differencing
WAAS	Wide Area Augmentation System

Intelligent estimators/observers

nKE	navigation Kinematic Estimator
sKE	sensor Kinematic Estimator
nKKF	navigation Kinematic Kalman filter
sKKF	sensor Kinematic Kalman Filter
ANN	Artificial Neutral Network
ASIR	Auxiliary Sampling Importance Resampling
CTPF	Continuous Time Particle Filter
EAKF	Extended Adaptive Kalman Filter
EKF	Extended Kalman Filter
EKKF	Extended Kinematic Kalman Filter
ELO	Extended Luenberger Observer
IE	Integrated Estimator
IEKF	Identification Extended Kalman filter
IF	Information Filter
IKF	Integrated Kalman Filter
KE	Kinematic-based Estimator/Kinematic Estimator
KF	Kalman Filter
KKF	Kinematic Kalman Filter
LKF	Linear Kalman Filter
LMO	Linear Modelled Observer
LO	Luenberger Observer
ME	Model-based Estimator
MEKF	Model-based Extended Kalman Filter
MKF	Model-based Kalman Filter
PF	Particle Filter
RK	Runge-Kutta method
RPF	Regularised Particle Filter
SIR	Sampling Importance Resampling
SMC	Sequential Monte Carlo
SMO	Sliding-Mode Observer

UKF	Unscented Kalman Filter

Business analysis notation

AGE	Age group
AO-tech	Add-On technology
BI-tech	Built-In technology
CF	Cluster Feature
CHD	Number of children in household
CPO	Certified Pre Owned
DMU	Decision Making Unit
EDU	Education
GM	General Motors
IBT	Total household income before tax
M/S	Marital status
NCBS_UK	New Car Buyer Survey UK
NVES_US	New Vehicle Experience Survey US
OCP	Occupation
PCA	Principal Component Analysis
SatNav	Satellite Navigation
SEX	Gender

Miscellaneous

NRMSD	Normalised Root Mean Square Deviation
RMSD	Root Mean Square Deviation

This page intentionally left blank.

Nomenclature

$\circledast^{*}$	plant model
$\circledast^{2gps}$, $\circledast_{2gps}$	dual GPS measurements
$\circledast^{gps}$, $\circledast_{gps}$	GPS measurements
$\circledast^{h}$	variable in the horizontal direction
$\circledast^{t}$	true value
$\circledast^{u}$	variable in the upward direction
$\circledast_{b}$	variable in the b-frame (vehicle body frame)
$\circledast_{e}$	variable in the e-frame (ENU frame)
$\circledast_{[ij]}$	variable at Front Right (FR), Front Left (FL), Rear Right (RR), Rear Left (RL) or variable at Front axle (F), Rear axle (R)
$\circledast_{ins}$	INS measurements
$\circledast_{k}$	variable at time k
$\circledast_{k+1}$	variable at time $k+1$
$\circledast_{k+1\|k}$	variable at time $k+1$, given information at time k
$\circledast_{max}$	maximum value in data set
$\circledast_{min}$	minimum value in data set
$\circledast_{v}$	variable in the v-frame (vehicle dynamics frame)
$\hat{\circledast}$	estimated variable
$\circledast_{k}$	discrete form at time k
a	distance from centre of gravity to front axle
$\vec{a}$	acceleration vector
b	distance from centre of gravity to rear axle
b_m	bias modelled by the Markov Process
b_x	bias in the longitudinal accelerometer
b_y	bias in the lateral accelerometer
b_ϕ	bias in the roll rate gyroscope

b_ψ	bias in the yaw rate gyroscope
b_θ	bias in the pitch rate gyroscope
b_P	longitudinal offset of INS
b_Q	lateral offset of INS
cg	centre of gravity
$\mathbf{f}$	non-linear function for process matrix
g	acceleration due to gravity, 9.81ms^{-2}
$\mathbf{g}$	non-linear function for measurement matrix
m	vehicle mass at centre of gravity
p_m	roll rate gyro measurement
q_m	pitch rate gyro measurement
r_m	yaw rate gyro measurement
u	input vector
v	measurement noise vector
w	input disturbance vector
w_{b_m}	disturbance in the Markov process
w_x	disturbance in the longitudinal accelerometer
w_y	disturbance in the lateral accelerometer
w_θ	disturbance in the pitch rate gyroscope
w_ϕ	disturbance in the roll rate gyroscope
w_ψ	disturbance in the yaw rate gyroscope
x	state vector
x	longitudinal displacement
$\dot{x}$	longitudinal velocity
$\ddot{x}$	longitudinal acceleration
y	lateral displacement
$\dot{y}$	lateral velocity
$\ddot{y}$	lateral acceleration
z	measurement vector
$\mathbf{A}$	process matrix
A_x	longitudinal accelerometer measurement
A_y	lateral accelerometer measurement
A_z	vertical accelerometer measurement
$\mathbf{B}$	input matrix
$\mathbf{C}$	measurement matrix
$C_{x,[ij]}$	longitudinal tyre stiffness

$C_{y,[ij]}$	lateral tyre cornering stiffness
$\mathbf{C_b^e}$	Direct Cosine Matrix (DCM), transformation matrix from body-frame to earth-frame
$F_{x,[ij]}$	Longitudinal force on tyre
$F_{y,[ij]}$	Lateral force on tyre
$F^v_{x,[ij]}$	longitudinal force in v-frame
$F^v_{y,[ij]}$	lateral force in v-frame
$\mathbf{F}$	Jacobian matrix for $\mathbf{f}$
$\mathbf{G}$	Jacobian matrix for $\mathbf{g}$
$\mathbf{H}$	discrete form of measurement matrix, $\mathbf{C}$
$\mathbf{I}$	identity matrix
$\mathbf{K}$	kalman filter gain matrix
$J_{[ij]}$	Second order moment of inertia about lateral axis of wheel
J_{zz}	Second order moment of inertia about vertical axis, Z_b
L	wheel base of the vehicle
M_z	moment of inertia
N	number of data points in set, X
$O(\cdot)$	truncated errors
$\mathbf{O}$	observability
$\mathbf{P}$	error covariance matrix
$\mathbf{Q}$	process covariance matrix
$R_{[ij]}$	wheel radius
$\mathbf{R}$	measurement covariance matrix
T_F	half of front track of vehicle
T_R	half of rear track of vehicle
T_s	sampling time
V	speed of vehicle at centre of gravity
$V_{[ij]}$	speed at the tyre
W	weight for the unscented Kalman filter
X	longitudinal axis
X	Data set
Y	lateral axis
$\mathcal{Z}$	measurement for the unscented Kalman filter
α	slip angle
β	sideslip angle at the centre of gravity
$\beta_{[ij]}$	sideslip angle at the tyre

$\mathcal{X}$	sigma point for the unscented Kalman filter
$\delta_{[ij]}$	steer angle on the tyres
ν	course angle about centre of gravity
$\omega_{[ij]}$	wheel rotational velocity at each wheel
ϕ, ϕ_{eb}	Euler roll angle
ϕ_{ev}	road bank angle, roll angle between the road (v-frame) and ENU axes (e-frame)
ϕ_{vb}	vehicle body roll angle, roll angle between the vehicle body (b-frame) and the road (v-frame)
ψ	Euler yaw angle
σ	standard deviation
$\tau_{[ij]}$	torque at each wheel
θ, θ_{eb}	Euler pitch angle
θ_{ev}	road grade, pitch angle between the road (v-frame) and ENU axes (e-frame)
θ_{vb}	vehicle body pitch angle, pitch angle between the vehicle body (b-frame) and the road (v-frame)
$\mathbf{\Gamma}_k$	discrete form of disturbance matrix
$\mathbf{\Delta}_k$	discrete form of input matrix, $\mathbf{B}$
$\mathbf{\Phi}_k$	discrete form of process matrix, $\mathbf{A}$

Chapter 1

Introduction

1.1 Motivations

In recent years, modern automobiles have included ever more sophisticated electronics and control systems, such as the Anti-lock Braking System (ABS) and the Electronic Stability Program (ESP). With the implementation of these intelligent systems, vehicles have become safer to drive [Van Zanten 2002] with less involvement in fatal accidents [Farmer et al. 1997, Farmer 2001]. Evidence of this can be seen in the increased demand for ABS since 1990 [Farmer et al. 1997]. In general, current and future development of more advanced and sophisticated control systems requires accurate and 'up-to-date' vehicle dynamic information. To achieve this direct measurements, namely the longitudinal and lateral velocities, are essential. Although these measurements are possible through speed-over-ground sensors, they are expensive, hard to maintain and subject to errors due to road terrain [Rock et al. 2005]. An alternative for vehicle dynamic measurements is through Inertial Navigation System (INS). However, measurements in INS are subjected to noise and bias, which cause numerical drifting when rotational rate and acceleration signals are integrated. To overcome this problem, a state estimator can be used instead of simple integration. This approach allows predictions of sensor bias as well as unmeasurable vehicle states.

To date, one of the most popular sensors used by drivers is the Global Positioning System (GPS). Unlike the INS, GPS provides absolute measurements without the need for numerical integrations. GPS receivers receive Coarse/Acquisition (C/A) codes from the satellite and compare them with its own signal to provide a distance from the receiver to the satellite, called pseudo-range. With four or more simultaneous pseudo-ranges, the location of the receiver can be determined. GPS velocities are then derived from the Doppler measurements [Grewal et al. 2007]. This drift-free

information from the GPS therefore provides an opportunity to be used as an external sensor in dynamic state estimation. Moreover, with the discontinued Selective Availability and the drive from other competitors, namely Galileo and COMPASS, GPS technology is very likely to increase in accuracy and decrease in cost in order to retain leadership against other Global Navigation Satellite System (GNSS) providers. With this motivation in mind, this project focuses on the opportunities that GPS offers in vehicle dynamic states estimation.

This project concentrates on the utilisation of GPS and INS. Although GPS remains at a relatively high cost, its rapid growth and pressure from other competitors gives it an indeterminable future. In fact, the technology is evolving so quickly that it is difficult to predict future cost and performance. To be more specific, this project focuses mainly on sideslip/lateral velocity estimation, one of the most difficult and challenging states to be obtained. The significance of sideslip estimation is highlighted by Manning and Crolla [2007], in which it is concluded that sideslip estimation is essential for a commercially viable sideslip stability control system. Despite its importance, one must not forget the fact that states are interdependent on one another, accuracy of sideslip estimation is only guaranteed if other state measurements/estimates are also sufficiently accurate. This project, therefore, also discusses the techniques that are used for estimating states that may have a close impact on sideslip estimation, for example the velocities, the roll angles and the pitch angles.

1.2 Project Aim and Objectives

This project is sponsored by Jaguar Land Rover under the Engineering Doctorate (EngD) programme at Cranfield University. In the EngD programme, it is a requirement to research both engineering and managerial aspects. This project therefore has two sets of aims and objectives: the engineering aspect and the managerial aspect. The managerial aim and objectives are re-stated in Chapter 6 for completeness.

1.2.1 Engineering Aspect

Aim

To design and investigate the feasibility of a state estimator utilising low cost GPS and INS, to continually provide dynamic state information for a ground vehicle with high accuracy and robustness.

Objectives

1. To design, analyse and compare different state estimators which utilise two or more in-car sensors, including GPS, so the benefits and drawbacks for each state estimator are identified;
2. To estimate vehicle dynamic states, e.g. the sideslip angle, with one or a combination of state estimator designs using measurements from noisy sensors with multi-sampling frequencies;
3. To study the effectiveness of using low cost sensors with a simple and easy-to-implement GPS/INS estimator;
4. To provide a design criteria and recommendation for future GPS/INS state estimator design.

1.2.2 Managerial Aspect

Aim

To investigate consumer reasons for purchase in the US and UK market in relation to their brand choice, along with a focus on the Jaguar brand and the importance of handling technologies.

Objectives

1. To identify customer purchase reasons;
2. To identify the relative importance of purchase reasons with a focus on vehicle handling characteristics;
3. To segment customers into groups with the same purchase reasons;
4. To segment brands of cars from the perspective of customers;
5. To identify the most important reason/s for purchasing Jaguar Cars.

1.3 Contribution to Knowledge

This section presents the contributions in the engineering aspect as well as the managerial aspect based on two surveys in the year 2007.

1.3.1 Engineering Aspect

Primary Outcomes

1. Designed and tested Kinematic Kalman Filter (KKF) in MATLAB/Simulink, which utilise GPS, accelerometer, gyroscope, steer wheel sensor and Wheel Speed Sensor (WSS) – the triple KF designs;

2. Designed and tested an Integrated Kalman Filter (IKF) in MATLAB/Simulink, which combines the Model-based Kalman Filter (MKF) and the KKF;

3. Provided a design criteria for the development of GPS aided state estimator;

4. Identified the gap for future study of the dynamic state estimator;

5. Presented a paper on 'A Study on the Effect of GPS Accuracy on a GPS/INS Kalman Filter' at the UKACC (International Conference on Control) in the year 2008 [Leung et al. 2008];

6. Presented and published a paper on 'Ideal Vehicle Sideslip Estimation using Consumer Grade GPS and INS' at the SAE World Congress and journal in the year 2009 [Leung et al. 2009*a*];

7. Published a paper on 'A Review of Ground Vehicle Dynamic State Estimations utilising GPS/INS' in the special issue of the Journal of Vehicle System Dynamics in the year 2009 [Leung et al. 2009*b*];

Secondary Outcomes

1. Presented a paper on 'Simulations for the use of GPS compensated sensors for vehicle dynamic systems control' at the ICSE (International Conference on Software Engineering) in the year 2006 [Leung et al. 2006];

2. Contributed in the paper on 'Four Wheel Steer Controller Development Utilising a GPS System Compensated Inertial Sensor Suite' in FISITA in the year 2006 [Bayliss et al. 2006] and presented in the student session of the same conference;

3. Developed bicycle and twin-track vehicle models in MATLAB/Simulink, which have two, three, five and seven Degrees of Freedoms (DoFs);

4. Developed a GPS and INS model with Controller Area Network (CAN-bus) and noise models in MATLAB/Simulink;

5. Theoretical and graphical parametric sensitivity analysis for 2DoF MKF state estimation;

1.3.2 Managerial Aspect

Primary Outcomes

1. Recommendations on how Jaguar Cars should focus in marketing their cars in the US and UK markets;
2. The importance of car handling technologies as a customer purchase criterion in the US and UK markets;

Secondary Outcomes

1. Determined top and bottom five vehicle attributes for the US customers;
2. Determined five customers segments in US market;
3. Determined the most mentioned vehicle purchase reason in the UK market;
4. Determined four customers segments in the UK market;
5. Provided recommendations for future study of the US and UK automobile market.

1.4 Methodology

The methodology in this section focuses mainly on the engineering aspect of the project. The managerial aspect is described in Chapter 6.

1.4.1 Simulation Tools

This project is based on simulations carried out in MATLAB/Simulink. GPS, INS and vehicle models are built in Simulink and the KF designs are written in MATLAB code. The inputs of the simulations are gathered from a professional simulation programme called IPG CarMaker. Noise and disturbances are added onto the inputs before processing through the sensor models and KF designs. The estimated results are then compared with the measurements from CarMaker, and errors are calculated as described in Section 1.4.2.

In this project in general six different track courses are used for simulations. These tracks are described below and are shown in Appendix C:

1. the *DoubleOval* – two oval shaped tracks, one turning left and the other one turning right;

2. the *LaneChangeISO* – a double lane change, which turns right and then left again;

3. the *Straight Road* (ST) – straight flat road without any obstacles or disturbance;

4. the *Right Turn course* (RT) – start with a straight road, then a 90° right hand turn and finish with a straight road;

5. the *figure Eight Course* (8C) – the shape of a figure eight;

6. the *Self-Defined* (SD) – contains numerous left and right turns with various radii and no straight roads between turnings apart from the starting position of the course.

1.4.2 Error measurement

To compare the estimations of the different KF designs and their effectiveness on various roads and manoeuvres, the error of the estimated states are determined with the reference measurement from CarMaker. This error is derived using the Root Mean Squared Deviation (RMSD) or the Normalised RMSD (NRMSD), which describes the amount of deviation of the estimated states (X_i^{est}) from the true value (X_i^t), given by the following relationship:

$$\%RMSD = \sqrt{\frac{\sum_{i=1}^{N}(X_i^{est} - X_i^t)^2}{N}} \times 100\% \tag{1.1}$$

$$\%NRMSD = \frac{\%RMSD}{(X_{max}^t - X_{min}^t)} \tag{1.2}$$

where N is the total number of data points, X_{max}^t is the maximum of the true data set, and X_{min}^t is the minimum of the true data set.

The NRMSD is a useful error measuring tool for any time-varying dynamic state, i.e. the yaw rate, the lateral velocity and the sideslip, while the RMSD is suitable for any states which are assumed as near constant, such as the vehicle speed and the bias of the sensors.

1.5 Thesis outline

This thesis is separated into eight chapters. This chapter introduces the motivation behind the project and the corresponding aims and objectives. A summary of the contribution to knowledge is also included for both the engineering and managerial aspects. Chapter 2 provides a literature review and background to the engineering aspect for this project. Up-to-date dynamic estimator designs are discussed with the focus on vehicle dynamic states, such as lateral velocity and sideslip. A detailed explanation and analysis of vehicle modelling is then given in Chapter 3. The vehicle models, namely the 2DoF, 3DoF, 5DoF and 7DoF, are compared with the professional IPG CarMaker simulation programme. With the knowledge in KF and INS modelling, Chapter 4 discusses and proposes new designs of the KKF, such as the Triple KF, utilising the Wheel Speed Sensor (WSS), the accelerometer and the gyroscopes. Moreover, the design criteria for a GPS/INS estimator is also discussed and analysed. In Chapter 5, the MKF is integrated with the KKF to produce an IKF. In Chapter 6, the business research for this project is discussed. Based on customer buying behaviour, a business literature review is presented. By using two surveys conducted in the year 2007 (one from the US, one from the UK), analysis is performed with recommendations and future studies. For the engineering aspect, a conclusion is drawn with recommendations and future opportunities in Chapter 7.

This page intentionally left blank.

Chapter 2

Literature Review and Background

2.1 Introduction

This chapter is based on the review paper of Leung et al. [2009*b*]. It provides a background and overview of the methods to determine vehicle dynamics. As will be discussed in Section 2.2, there are four ways to measure/estimate vehicle dynamics: the indirect, direct, model-based and blended approaches. While the first three simple methods are outlined in Section 2.3, the most common types of blended state estimator are described in Section 2.4. With a focus on GPS technology and the most commonly used blended estimator in the automotive industry – the KF, Sections 2.5 and 2.6 thoroughly discuss the current integration techniques. In Section 2.7, a few non GPS-aided estimators are introduced and described.

2.2 The Four Vehicle Dynamic Determination Approaches

With reference to Deng and Zhang [2006], there are in general four ways to measure/estimate the relevant states:

1. **Indirect sensor approach, also see Section 2.3.1:**
   This involves numerical integration from existing INS, such as accelerometers and rate gyroscopes. INS can be classified into two types: the gimballed and the strap-down [Grewal et al. 2007]. In the automotive sector strap-down INS are the most common as their costs are much lower than the gimballed. In addition, strap-down INS operate at 100 Hz, which allows a relatively fast

transient behaviour to detect dynamic changes in a vehicle. However, INS are also contaminated with noise and bias [Lawrence 1998]. Hence when integrated over a long period of time, errors accumulate and cause the predictions to drift. For a short time interval, however, the responsiveness of INS will allow accurate predictions, especially when estimating large dynamical changes such as large sideslip angles.

2. **Direct sensor approach, see also Section 2.3.2:**
   This approach uses a camera or GPS as a source of measurement that provides valuable information about vehicle dynamics without any numerical integrations (i.e. no integration error). However, both technologies have their drawbacks. GPS suffers from high price, low update rate and external environment influence. Although commercial GPS is getting cheaper, it typically works at a frequency of 1 Hz. Any dynamical changes in between samples are therefore undetectable. Faster sampling GPS is available but price rises exponentially with its frequency. Moreover, GPS signals are sensitive to surroundings (e.g. heavy foliage and urban canyon), which can cause temporary outages. Visual camera measurements also suffers from inaccuracy depending on road conditions (i.e. wet/dry and road layout). It is also relatively more expensive and susceptible to dirt and grime on the lens covers, hence requiring frequent maintenance.

3. **Model-based approach, also see Section 2.3.3 and Chapter 3:**
   Other than predicting dynamics using sensor measurements, one can also use a vehicle model for state estimations. This approach can give accurate results for both static and dynamic responses. However, models are normally highly nonlinear with a lot of demand for correct parameter specifications (e.g. spring stiffness, damping ratios and mass). In practise, the vehicle model is reduced to a linear bicycle model (i.e. 2 degrees of freedom) with a linear tyre model. This is able to generate some good results but is limited to the linear region.

4. **The blended approach – combination of (1) to (3):**
   By using different combinations of the above three independent approaches, the sensors and models can be utilised, compensating one another to produce better estimations. When fusing the different sensors and models together, one must make sure that the signals are properly synchronised in time.

One of the challenges that automotive industries now face is the cost-effectiveness ratio, in another words, using the cheapest components possible to achieve the best

result. Unsurprisingly, this phenomenon also applies to the design of vehicle control systems, in which cheap sensors are used to measure/estimate vehicle dynamics. As discussed above, there are three approaches in general and each has its own advantages and disadvantages. In order to achieve better estimations, it is therefore natural to combine them and utilise all of them in forming a fourth approach as described above.

From the four approaches discussed above, two main branches of state estimation can be defined: 1) simple state estimation approach (i.e. the direct, the indirect and model-based approaches), and 2) blended state estimation approach (i.e. the combination of the simple approaches). While a simple state estimator involves an accurate model of the sensors or vehicle, the blended state estimator requires techniques to fuse data from various sensors. As GPS navigation data is one of the main focuses of this project, the blended state estimation approach can be further classified into GPS-aided and non GPS-aided state estimator.

2.3 Simple State Estimation Approach

2.3.1 Inertial Navigation Sensor

As discussed earlier in the indirect sensor approach, the automotive industry in general prefers the strap-down INS over the gimballed type due to its low cost. For the strap-down INS, the linear and angular dynamics are measured with an accelerometer and a gyroscope respectively.

Accelerometers

Generally, accelerometers consists of a proof mass with some spring suspension. They operate by measuring the deflection of the spring or by applying a force required to keep the spring deflection at zero. Figure 2.1 shows a simple accelerometer, if the sensitivity axis is aligned with gravity, then there will be an extra component of force caused by the gravitational force. This additional force may induce an error to the true measurement if calibration is not done correctly. It must be noted that during vehicle manoeuvres, accelerometers do not only measure the translational acceleration of the vehicle, but also the acceleration caused by the angular motion of the vehicle.

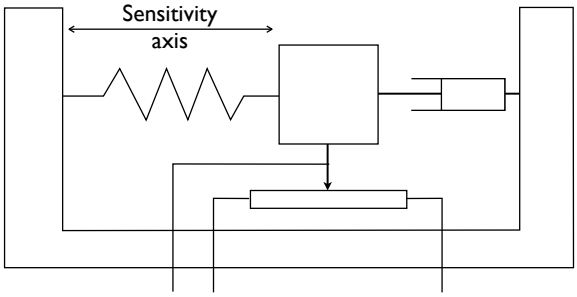

Figure 2.1: A simple accelerometer

Gyroscopes

Gyroscopes are important for navigation and vehicle dynamic determination purposes as they provide information for attitude and/or attitude rate measurements. In the majority of markets, two kinds of gyroscopes exist: optical and mechanical.

Optical gyroscopes rely on the phenomena of Sagnac effect, which is a measure of the phase difference between two phase-coherent counter rotating beams such as lasers. Two common designs for optical gyroscopes are the Ring Laser Gyroscopes (RLGs) and Fibre-Optic Gyroscopes (FOGs), see Figure 2.2. Although they are more precise and more stable when measuring than mechanical gyroscopes, they require an enclosed cavity and laser beams suffer from thermal and vibration sensitivity.

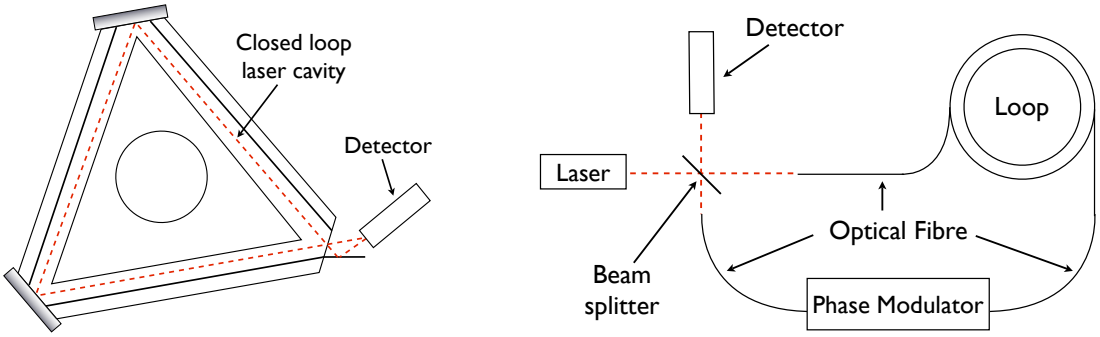

(a) Ring Laser Gyroscope

(b) Fibre-Optic Gyroscope

Figure 2.2: Optical gyroscope [Grewal et al. 2007]

Another kind of gyroscope is the mechanical gyroscope, or rate gyroscope. This has mechanical moving parts such as a conventional spinning rotor. Measurement of the rate gyroscope is in terms of the rate of change of orientation. This angular velocity is a measure of the reaction force used for maintaining a constant angular momentum in the rotor. Although the rate gyroscope is cheaper and easier to

maintain, its determined orientation/angle suffers from integration errors due to the existence of bias in the device.

INS Modelling and State Estimation

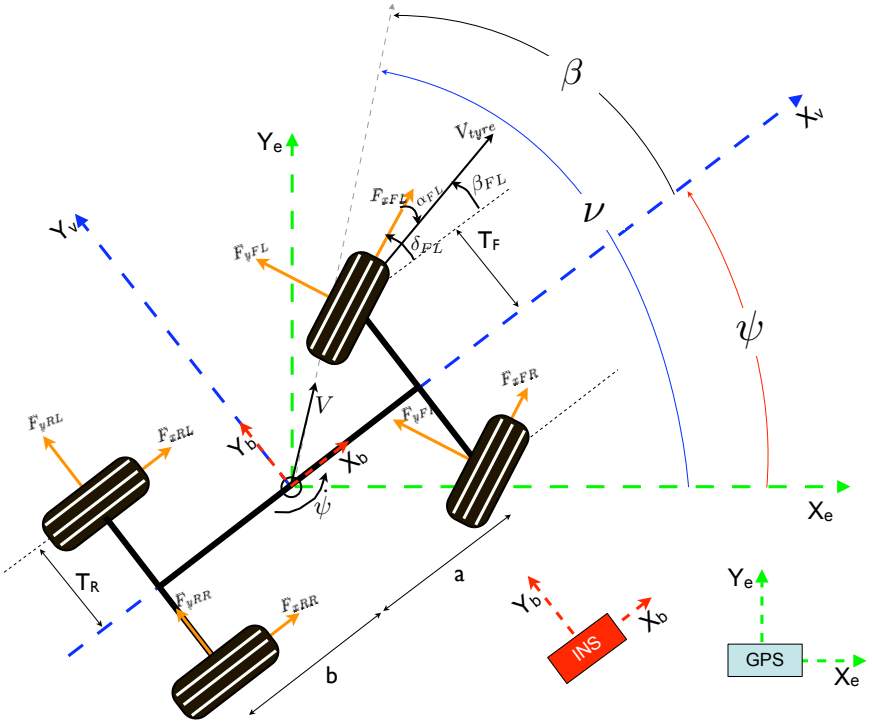

Figure 2.3: Plan view of a twin track vehicle model

In order to understand state estimation using the strap-down INS, we may consider the twin-track planar model as shown in Figure 2.3. On a typical vehicle there are in total three sets of coordinate frameworks: the East North Up frame (ENU/e-frame) for the GNSS, the body frame (b-frame) for the INS and the ISO vehicle frame (v-frame) for the vehicle. Note that although GNSS often uses the North East Down (NED) frame which is standard in aerospace applications, the ENU is the ISO standard (ISO 8855) for the automotive sector.

In Figure 2.3, the e-frame, b-frame and the v-frame are shown two-dimensionally with their corresponding subscripts. The majority of the INS used in ground vehicles nowadays are strap-down sensors, consisting of only two accelerometers (longitudinal and lateral) and a yaw rate gyroscope. This type of sensor moves and orientates with the vehicle, so the accelerometers and the gyro measure the accelerations (A_x, A_y) and yaw rate (r_m), respectively, in the b-frame.

The accelerometer measurements, A_x and A_y are sensitive to both translational and rotational movement of the vehicle. Assuming that the INS is located at the

centre of gravity (cg) and that it is aligned perfectly along and mounted rigidly on the vehicle. The accelerations in the b-frame are, hence, related to the accelerations at cg ($\ddot{x}_v$, $\ddot{y}_v$) in the v-frame by:

$$A_x = \ddot{x}_v - \dot{y}_v r_m \tag{2.1}$$

$$A_y = \ddot{y}_v + \dot{x}_v r_m \tag{2.2}$$

For a more precise sensor modelling, provided that roll and pitch angles are available, Ryu and Gerdes [2004*b*] have introduced the roll centre model with road grade and modified Equations 2.1 and 2.2 to:

$$A_x = \ddot{x}_v - \dot{y}_v\dot{\psi} + g\sin(\theta_{eb}) \tag{2.3}$$

$$A_y = \ddot{y}_v + \dot{x}_v\dot{\psi} + g\sin(\phi_{eb}) \tag{2.4}$$

where θ_{eb} is the vehicle body pitch angle due to the road grade; ϕ_{eb} is the vehicle body roll angle due to the road elevation.

Note that the above equations assume only vehicle body rolling motion. Moreover, the second term in Equations 2.3 and 2.4 have changed from r_m in previous equations to $\dot{\psi}$. This is because, precisely, the Euler angular rates ($\dot{\psi}$, $\dot{\theta}$, $\dot{\phi}$) are not simply equal to the integration of the measurements from the rate gyroscopes. As demonstrated in Ryu and Gerdes [2004*a*] and Dissanayake et al. [2001], the relation of the Euler angular rates with the measurements of the rate gyroscopes are given by

$$\begin{bmatrix}\dot{\phi}_{eb}\\ \dot{\theta}_{eb}\\ \dot{\psi}_{eb}\end{bmatrix} \text{ or } \begin{bmatrix}\dot{\phi}\\ \dot{\theta}\\ \dot{\psi}\end{bmatrix} = \begin{bmatrix}1 & \sin(\phi)\tan(\theta) & \cos(\phi)\tan(\theta)\\ 0 & \cos(\phi) & -\sin(\phi)\\ 0 & \sin(\phi)\sec(\theta) & \cos(\phi)\sec(\theta)\end{bmatrix}\begin{bmatrix}p_m\\ q_m\\ r_m\end{bmatrix} \tag{2.5}$$

where p_m is the gyroscopic roll rate; q_m is the gyroscopic pitch rate; $\dot{\phi}$ is the Euler roll rate; $\dot{\theta}$ is the Euler pitch rate; and $\dot{\psi}$ is the Euler yaw rate.

To obtain the Euler angles, the above equation is simply integrated. By assuming zero rolling and pitching in Euler angles (i.e. ϕ, $\theta = 0$) and in rate gyroscopes (p_m, $q_m = 0$), Equation 2.5 reduces to $\dot{\psi} = r_m$. These assumptions are used to form the simplified Equations 2.1 and 2.2 given earlier. With this, the vehicle sideslip at the cg can be estimated in terms of the ratio between the lateral to longitudinal velocity,

$$\beta = \frac{\dot{y}_v}{\dot{x}_v} = \frac{\int (A_y - \dot{x}_v r_m)\mathrm{dt}}{\int (A_x + \dot{y}_v r_m)\mathrm{dt}} \tag{2.6}$$

Referring back to Figure 2.3, an alternative way to obtain the sideslip and vehicle velocities in the v-frame is by transforming the accelerations measured from the sensor (b-frame) to the e-frame using the Euler angle, Equation 2.5:

$$\ddot{x}_e = A_x \cos(\psi) - A_y \sin(\psi) \tag{2.7}$$

$$\ddot{y}_e = A_x \sin(\psi) + A_y \cos(\psi) \tag{2.8}$$

To obtain the velocities and positions in e-frame, the above equation is integrated. Using the velocity in the e-frame, the track angle (or path angle) of the vehicle, ν, can be determined as

$$\nu = \tan^{-1}\left(\frac{\dot{y}_e}{\dot{x}_e}\right) \tag{2.9}$$

The sideslip angle, β, is simply the difference between the track angle and the yaw angle.

$$\beta = \nu - \psi \tag{2.10}$$

With the sideslip calculated from Equation 2.10, the vehicle velocity (v-frame) can also be derived as

$$\dot{x}_v = V \cos(\beta) \tag{2.11}$$

$$\dot{y}_v = V \sin(\beta) \tag{2.12}$$

where V is the resultant vehicle velocity with a relation of,

$$V = \sqrt{\dot{x}_e^2 + \dot{y}_e^2} = \sqrt{\dot{x}_v^2 + \dot{y}_v^2}. \tag{2.13}$$

When a vehicle is travelling on a straight road horizontally without any side force, the sideslip angle is zero. Thus, the track angle, ν, described by the GPS coincides with the yaw angle, ψ.

2.3.2 Global Navigation Satellite System

As discussed at the beginning of this chapter, a second approach to measuring / estimating vehicle dynamics is by the direct sensor method, in particular GNSS technology. To date, there exists four potential GNSS providers worldwide: the American GPS, the Russian GLObal'naya NAvigatsionnaya Sputnikovaya Sistema (GLONASS), the European Galileo, and the Chinese Compass. As GPS is the most

popular and most mature GNSS provider in the market, this project focuses on the opportunity provided by the GPS in dynamic estimation.

GPS

Currently, GPS is the only fully established satellite navigation system in the world. It is comprised of three elements: 1) orbiting satellites, 2) four Earth control stations, and 3) the user receiver unit.

GPS has between 24 to 32 satellites orbiting the earth. These satellites are distributed equally over 6 circular orbital planes and each plane is 60° apart and 55° tilted with respect to the earth's equator. This arrangement of the satellites in the earth orbit is done with care so at least six satellites are in sight at any time from anywhere on earth. Generally, GPS provides two types of services, namely civilian and military, and depending on the service, different satellite codes are utilised. For each GPS satellite, two frequencies, L1 (1.575GHz) and L2 (1.227GHz), are transmitted with a 20MHz maximum bandwidth through the Code Division Multiple Access (CDMA). Each satellite also has its own navigation codes, namely the C/A and the P code, which share the same frequency. The C/A code are modulated on L1. It is coarse and short for rapid acquisition purposes. P code, which is only available for the military service, is modulated in both L1 and L2. It contains a lengthy signal and requires secret short W code for encryption.

While the four Earth stations are responsible for the health and update of the timer in the satellite, user receivers decode the satellite signals and determine its location on earth by the trilateration method. When the code from one satellite is received, it is compared with that of the on-board receiver to determine the transmission time, see Figure 2.4. By multiplying the time taken for transmission with the speed of light, the distance (called the pseudorange) between the satellite and the receiver is known.

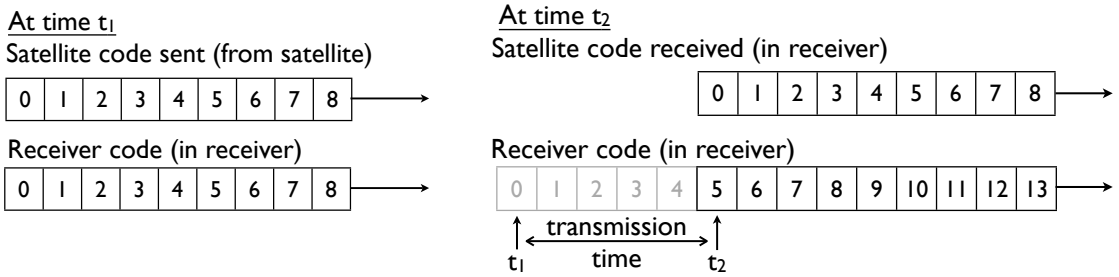

Figure 2.4: Transmission time determined from GPS receiver

By applying the method of trilateration with the pseudorange of three satel-

lites, two or less possible locations for the receiver can be determined in the three-dimensional space. For ground vehicles, the correct position is simply the one that is nearest to the earth's surface. Although the method of trilateration shows that only three satellites are needed for the determination of position, this method assumes perfect pseudorange measurements. In reality, GPS receiver suffers from clock error so a fourth satellite is required to correct this error. Hence, a good GPS position is achieved only with a minimum of four satellites. Errors in the GPS are caused by one or more of the following:

- **Dilution of Precision (DoP)** refers to the GPS satellite position accuracy related to the position of its neighbouring satellites. The further the satellites are apart, the greater the accuracy and the smaller the DoP;
- **Selective Available (SA)** is a degrading code induced in GPS codes for security purposes and only authorised users are supplied with the encrypting code. In the year 2000, however, it was announced that SA will be turned off completely by 2006;
- **Ephemerides** are signals that are part of an SA, used for 'worsening' the satellite position calculation;
- **Ionosphere** is the layer of the atmosphere above the earth that is electrically charged. This effect is caused by the atoms being ionised by UV light from the Sun, freeing electrons. The ionosphere has a large refractive index, causing a time delay owing to the structure of the code being too long or too short. A correction model can be induced to correct such error;
- **Troposphere and stratosphere** are the layers above the earth where signals from GPS can be attenuated or delayed. This delay can be addressed by an estimation of the troposphere delay. However, a wrong estimation will cause a clock bias error;
- **Antenna phase centre bias** refers to the error caused by the true position of the antenna, where the signal is being received or sent;
- **Foilage and precipitation** cause attenuation error;
- **Multipath** is an error caused by a multiple of reflected GPS signals from buildings. This causes a distortion in the GPS signal and thus an error in ranging. This error can be minimised by modifying the design of the antenna on the GPS receiver, making them sensitive to the right-hand polarised signals only;
- **City environments, aka city-canyons,** limit the GPS signal and caused outages when complete blockage occurs.

GPS Modelling and State Estimation

It is well understood that GPS is able to give us a position on earth, but it is also able to give us velocity measurements. This is done by carrying out either one or both of the following methods: GPS position differentiation and the use of Doppler measurements [Grewal et al. 2007].

Using the position and velocity measurements from GPS, vehicle dynamic information can be estimated. In order to understand this, first consider the planar vehicle model in Figure 2.3. Assuming that a GPS receiver is located at the cg of a vehicle, its measurements are referenced to the e-frame, with positions (x_e, y_e) and velocities ($\dot{x}_e$, $\dot{y}_e$). Using this information, the tracking angle and the resultant velocity of the vehicle can be determined by using Equations 2.9 and 2.13 respectively.

2.3.3 Vehicle Model-based approach

The third vehicle dynamic estimation method is by the use of a vehicle model. From Figure 2.3, a planar twin-track model is shown and the vehicle can be modelled by equating the force and inertia:

$$\begin{aligned} mA_x &= \Sigma F_{x,ij} \\ mA_y &= \Sigma F_{y,ij} \\ J_{zz}\ddot{\psi} &= \Sigma M_z \\ \tau_{ij} - RF_{x,ij} &= J_{ij}\ddot{\omega}_{ij} \end{aligned}$$

where m is the mass at cg; $F_{x,ij}$ is the longitudinal force; $F_{y,ij}$ is the lateral force; J_{zz} is the moment of inertia; ij denotes the wheel position: FR, FL, RR, RL; τ is the torque applied to a given wheel; R is the wheel radius; J_{ij} is the rotational inertia of the wheel; $\ddot{\omega}_{ij}$ is the angular acceleration of the wheel.

By solving these equations, the velocities and sideslip on the v-frame about the cg can be determined. In addition, a similar twin track model can also be found in Daily and Bevly [2004], but they have only considered the lateral and yaw dynamics. In a Model-based Estimator (ME), for the ease of computation, the employed model is normally a linearised two DoF bicycle model. This type of model assumes constant longitudinal velocity and small slip angles. The linearised bicycle model is very common and can be found in many text books [Ellis 1994, Genta 2003] and papers. For further details of the set-up and comparison of different vehicle models, a thorough discussion is included in Chapter 3.

2.4 Blended State Estimation Approach

As discussed earlier in this chapter, Deng and Zhang [2006] point out a fourth estimation method of combining the previous approaches using direct sensors, indirect sensors and vehicle model. This combined approach is termed blended state estimation approach and it requires data fusion techniques to integrate different measurements from the sensors and/or the vehicle model. In this section, a few of the most common data fusion techniques are described with a primary focus on the KF.

2.4.1 'Intelligent' methods

The 'Intelligent' method includes approaches such as the Fuzzy Logic and the Artificial Neural Network (ANN). The term 'intelligent' indicates the nature of its technique. Generally, a predefined set of values, containing both fit and unfit candidates, are simulated and trained. The unfit sets are then filtered out of the process and the remaining are carried downstream for the next training. This process continues until the specified training conditions are met. Unlike the predictive technique which has only '1' and '0' ('on' and 'off') in the logic, the intelligent method has an infinite number of predictive values (e.g. '0.222', '0.982' etc). A major advantage of such an approach is that it does not require any knowledge about the model. However, this also generates shortcomings such as long training time, limitation to the predefined training sets only, waste of resources in training unfit candidates, and the non-transferrable results between different models.

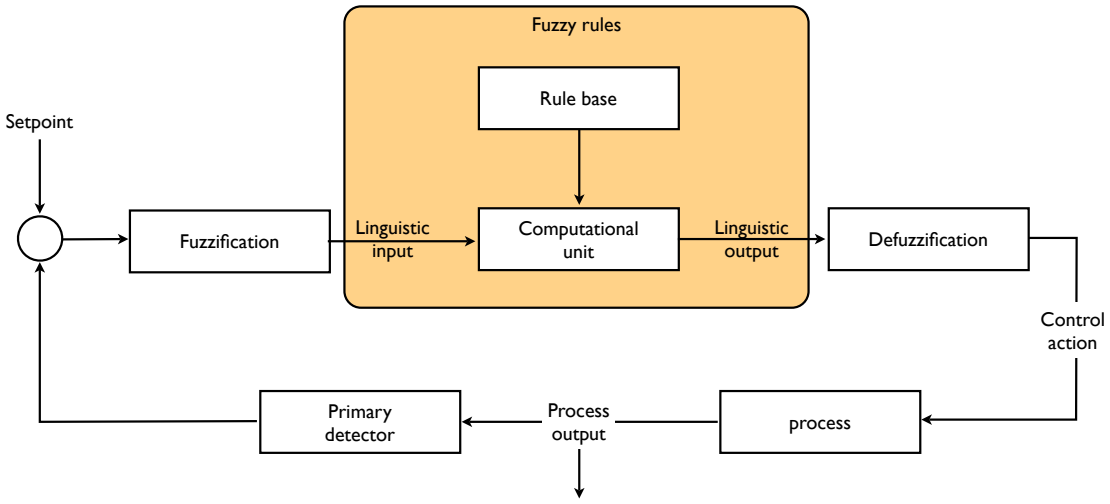

Figure 2.5: Generic fuzzy controller [Kickert and Mamdani 1978]

Figure 2.5 shows a generic structure for a fuzzy controller, which consists of three parts: the fuzzification, the fuzzy rules and the defuzzification. In the original design of Kickert and Mamdani [1978], they have also incorporated human 'experiences' inside this control. The fuzzy control starts with the transformation of inputs into a set of linguistic inputs through fuzzification with value between '1' and '0'. These linguistic inputs are then evaluated using a set of pre-defined fuzzy rules and the output for controller action is generated via the process of defuzzification. Nowadays, fuzzy logic is mostly used for identifying a suitable function for a system with predefined sets of data.

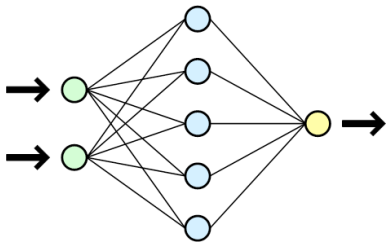

Figure 2.6: Typical neural network diagram

ANN, as the name suggests, is an information processing paradigm inspired by the human biological nervous system. Artificial neural networks contain a large number of interconnected networks of mathematical processes called neurones , Figure 2.6. Each neurone is connected from a collection of other neurones in the network and this creates the unique ability of ANN to process normally in situations when neurones are dis-functioning. Hence, ANN is robust to errors and any neurone failures. Moreover, as reported in Tan and Saif [2000] and Fisher and Rauch [1994], a well designed ANN is also adaptive to changes, enabling the system to 'learn' from experiences while acquiring additional 'knowledge' for the preparation of any future unforeseen problems. ANN also works well with modification features such as parallel processing, self organising and non-linear capabilities. However, it suffers from shortcomings such as long process time and the large amount of experimental data required for off-line training. Moreover, without a good set of data, ANN struggles to converge to a good solution and in such cases, Aykan et al. [2005] have used a KF to generates sufficient amount of data for the ANN training.

As described, the 'intelligent' method is mainly for model determination purposes, in which the model for the plant is treated as a black box. Having the estimated model trained, it is implemented into the system and states are predicted with the same type and number of inputs as the previous training sets.

2.4.2 Luenberger Observer (LO)

In previous 'intelligent' methods, although no model of the actual plant was needed, a large amount of data for training before implementation was required. Furthermore, these 'intelligent' methods did not filter out noise and bias from the inputs. Instead, they permitted the errors and included them in their model determination. Since 'intelligent' methods treat the plant as a black box, if any component or input source changes, the determined model will fail. For an automotive application, this is unfavourable as it is expensive to remodel using an 'intelligent' method whenever a new vehicle model is manufactured (or when the component changes). Furthermore, knowledge of sensor and vehicle modelling (see Section 2.3 and Chapter 3) are utilised in the LO and no pre-training is needed.

In brief, LO is a simple observer with a feedback mechanism, see Figure 2.7. The approximated model of the plant (i.e. **A**, **B** and **C**) forms the basis system of the simple observer with the same input as the plant. Outputs from the observer are compared with those from the plant and their error is fed back into the observer through a gain.With this feedback mechanism in LO, the design has surpassed the original purpose of an observer; and is able to correct errors and provide state estimations for the plant, i.e. called an estimator.

From the estimator design in Figure 2.7, the plant and observer have the following

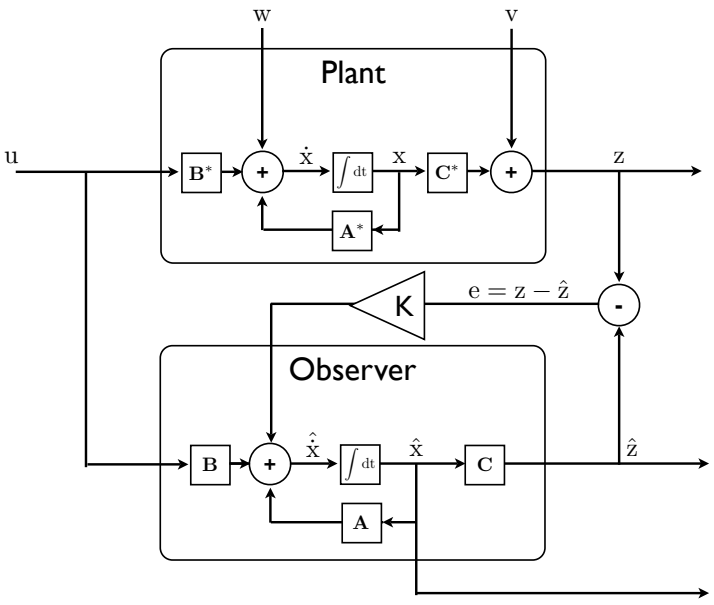

Figure 2.7: Typical structure for an estimator

dynamic equations:

$$\text{Plant}: \quad \begin{cases} \dot{\mathrm{x}} = \mathbf{A}^*\mathrm{x} + \mathbf{B}^*\mathrm{u} + \mathrm{w} \\ \mathrm{z} = \mathbf{C}^*\mathrm{x} + \mathrm{v} \end{cases} \tag{2.14}$$

$$\text{Observer}: \quad \begin{cases} \dot{\mathrm{x}} = \mathbf{A}\hat{\mathrm{x}} + \mathbf{B}\ \mathrm{u} \\ \hat{\mathrm{z}} = \mathbf{C}\hat{\mathrm{x}} \end{cases} \tag{2.15}$$

In discrete form, the two continuous dynamic equations above become:

$$\text{Plant}: \quad \begin{cases} \mathrm{x}_{k+1} = \mathbf{\Phi}^*{}_k\mathrm{x}_k + \mathbf{\Delta}^*{}_k\mathrm{u}_k + \mathbf{\Gamma}^*{}_k\mathrm{w}_k \\ \mathrm{z}_k = \mathbf{H}^*{}_k\mathrm{x}_k + \mathrm{v}_k \end{cases} \tag{2.16}$$

$$\text{Observer}: \quad \begin{cases} \hat{\mathrm{x}}_{k+1} = \mathbf{\Phi}_k\hat{\mathrm{x}}_k + \mathbf{\Delta}_k\mathrm{u}_k \\ \hat{\mathrm{z}}_k = \mathbf{H}_k\hat{\mathrm{x}}_k \end{cases} \tag{2.17}$$

Note that the observer assumes the process noise, w_k and measurement noise, v_k are zero, thus, excluding them from the equations. From the discretised observer equations, Equation 2.17, $\hat{\mathrm{x}}$ is the vector of estimated state variables. The estimated output, $\hat{\mathrm{z}}_k$, is compared with the actual output, z_k, of the plant, and the error, $e_k = \mathrm{z}_k - \hat{\mathrm{z}}_k$, is determined. This error is then fed through a matrix gain, $\mathbf{K}$, to the observer for correction,

$$\hat{\mathrm{x}}_{k+1} = \mathbf{\Phi}_k\hat{\mathrm{x}}_k + \mathbf{\Delta}_k\mathrm{u}_k + \mathbf{K}[\mathrm{z}_k - \hat{\mathrm{z}}_k] \tag{2.18}$$

$$\hat{\mathrm{z}}_k = \mathbf{H}_k\hat{\mathrm{x}}_k \tag{2.19}$$

With time, if the error converges to zero, the estimator is said to be asymptotically stable. Some examples for this type of estimator are presented in Stephant et al. [2004], Cherouat et al. [2005] and Deng and Zhang [2006].

Although the LO is simple to understand and implement, it only works well with accurate modelling and known inputs. In practice, the system plant is affected by stochastic process and measurement noise. These random errors make it impossible for LO to estimate states with certainty. Thus, another type of estimator namely the KF is employed.

2.4.3 Kalman Filter

KF is named after Rudolph E. Kalman. As described by Welch and Bishop [2001], KF is the best possible (optimal) estimator and is easy to understand and apply to our real world systems. KF is a special case of the Bayesian filtering under LQG

(Linear, Quadratic, Gaussian) circumstances [Ho and Lee 1964]. It operates under a sequential state estimation framework with the assumptions of linear system and gaussian distribution of noise and disturbances.

Given the discrete plant model in Equation 2.16, and assuming the noise to be Gaussian, a Linear Kalman Filter (LKF) can be applied. In general, KF is a two-stage process consisting of the correction and the prediction stages, in which the correction stage includes the following steps,

Correction stage:

$$\hat{\mathrm{z}}_k = \mathbf{H}_k \hat{\mathrm{x}}_{k|k-1} \tag{2.20}$$

$$\mathbf{K}_k = \mathbf{P}_{k|k-1}\mathbf{H}_k(\mathbf{H}_k\mathbf{P}_{k|k-1}\mathbf{H}_k^T + \mathbf{R}_k)^{-1} \tag{2.21}$$

$$\mathbf{P}_{k|k} = (\mathbf{I} - \mathbf{K}_k\mathbf{H}_k)\mathbf{P}_{k|k-1} \tag{2.22}$$

$$\hat{\mathrm{x}}_{k|k} = \hat{\mathrm{x}}_{k|k-1} + \mathbf{K}_k(\mathrm{z}_k - \hat{\mathrm{z}}_k) \tag{2.23}$$

Prediction stage:

$$\hat{\mathrm{x}}_{k+1|k} = \mathbf{\Phi}_k \hat{\mathrm{x}}_{k|k} + \mathbf{\Delta}_k \mathrm{u}_k \tag{2.24}$$

$$\mathbf{P}_{k+1|k} = \mathbf{\Phi}_k\mathbf{P}_{k|k}\mathbf{\Phi}_k^T + \mathbf{\Gamma}_k\mathbf{Q}_k\mathbf{\Gamma}_k^T \tag{2.25}$$

At time step k, the inputs to a LKF are the state variables estimated from the previous time step, $\hat{\mathrm{x}}_{k|k-1}$, and, the primary and referenced sensor measurements, $\mathrm{u_k}$ and $\mathrm{z_k}$. Firstly, the referenced measurements, $\hat{z}_k$, are predicted using the current estimated state variables, Equation 2.20. These predicted reference measurements are then compared with the actual measured reference value, $\mathrm{z}_k - \hat{\mathrm{z}}_k$. Their error is then multiplied by a weighing matrix called the Kalman gain, $\mathbf{K}_k$, and the old estimated states are updated using Equation 2.23. Using the updated state estimations, $\hat{\mathrm{x}}_{k|k}$, and the system equations in Equation 2.16, the states for the next time step, $k+1$, are predicted using Equation 2.24. At time step $k+1$, the estimated states from Equation 2.24 are inserted into Equation 2.20 and the process continues.

It is also worth mentioning that the update of matrices $\mathbf{K}$ and $\mathbf{P}$ at every time step are dependent upon the error covariance of matrices $\mathbf{Q}$ and $\mathbf{R}$, which correspond to the error covariance of the system process and measurement respectively. By comparing $\mathbf{Q}$ and $\mathbf{R}$ side-by-side, we can observe the relative 'trustworthiness' of the system as a whole. In addition, $\mathbf{Q}$ and $\mathbf{R}$ are normally pre-determined and stay as constant. During the iteration time steps, matrices $\mathbf{P}$ and $\mathbf{K}$ will eventually stabilise and become constant. Hence, it is also a common practice to obtain a steady state value for $\mathbf{P}$ and $\mathbf{K}$ before performing estimations using the LKF.

Extended Kalman Filter (EKF)

Although the LKF is simple to implement, in reality, most systems are non-linear and in such cases, an EKF can be applied. Consider a non-linear system (i.e. $\dot{\mathrm{x}} = \mathbf{f}(\mathrm{x}, \mathrm{u}, \mathrm{w})$) in discretised format:

$$\begin{aligned} \hat{\mathrm{x}}_{k+1} &= \hat{\mathrm{x}}_k + T_s \mathbf{f}(\hat{\mathrm{x}}_k, \mathrm{u}_k, \mathrm{w}_k) \\ &= \hat{\mathbf{f}}(\hat{\mathrm{x}}_k, \mathrm{u}_k, \mathrm{w}_k) \end{aligned} \tag{2.26}$$

$$\hat{\mathrm{z}}_k = \mathbf{g}(\hat{\mathrm{x}}_k, \mathrm{v}_k) \tag{2.27}$$

Similar to the LKF, the formulation for the estimation process in an EKF also involves a two-stage process. The difference lies within the equations for the covariance matrices, Equations 2.21, 2.22 and 2.25.

Correction stage:

$$\hat{\mathrm{z}}_k = \mathbf{g}(\hat{\mathrm{x}}_{k|k-1}, 0) \tag{2.28}$$

$$\mathbf{K}_k = \mathbf{P}_{k|k-1}\mathbf{G}_k(\mathbf{G}_k\mathbf{P}_{k|k-1}\mathbf{G}_k^T + \mathbf{R}_k)^{-1} \tag{2.29}$$

$$\mathbf{P}_{k|k} = (\mathbf{I} - \mathbf{K}_k\mathbf{G}_k)\mathbf{P}_{k|k-1} \tag{2.30}$$

$$\hat{\mathrm{x}}_{k|k} = \hat{\mathrm{x}}_{k|k-1} + \mathbf{K}_k(\mathrm{z}_k - \hat{\mathrm{z}}_k) \tag{2.31}$$

Prediction stage:

$$\hat{\mathrm{x}}_{k+1|k} = \hat{\mathbf{f}}(\hat{\mathrm{x}}_{k|k}, \mathrm{u}_k, 0) \tag{2.32}$$

$$\mathbf{P}_{k+1|k} = \mathbf{F}_k\mathbf{P}_{k|k}\mathbf{F}_k^T + \mathbf{\Gamma}_k\mathbf{Q}_k\mathbf{\Gamma}_k^T \tag{2.33}$$

From the EKF process, the inputs to the system are the same as the LKF. Since the system is non-linear, it cannot be written in a linear state space representation. The states and measurements, $\hat{x}$ and $\hat{z}$, are determined from Equations 2.26 and 2.27, without the noise and disturbance. The matrices, $\mathbf{F}$ and $\mathbf{G}$, are the partial derivatives, called Jacobian matrices, of the system.

$$\mathbf{F}_{[i][j]} = \frac{\delta \hat{\mathbf{f}}_{[i]}}{\delta \mathrm{x}_{[j]}}(\hat{\mathrm{x}}_k, \mathrm{u}_k, 0) \tag{2.34}$$

$$\mathbf{G}_{[i][j]} = \frac{\delta \mathbf{g}_{[i]}}{\delta \mathrm{x}_{[j]}}(\hat{\mathrm{x}}_k, 0) \tag{2.35}$$

Similar to the LKF, when matrices $\mathbf{P}$, $\mathbf{Q}$ and $\mathbf{R}$ are assumed constant, $\mathbf{K}$ in the EKF can be calculated offline to reduce the computational burden. However, in most cases, $\mathbf{P}$ will not remain constant as the partial derivatives of $\mathbf{f}$ and $\mathbf{g}$ are

changing according to the states and inputs.

In the process of EKF, the update of states in the prediction stage, Equation 2.32, is determined by the Euler approximation, which is derived using the first order Taylor series expansion of x_{k+1},

$$\begin{aligned}\mathrm{x}_{k+1} &= \mathrm{x}_k + \frac{\partial \mathrm{x}_k}{\partial t}T_s + \frac{1}{2!}\frac{\partial^2 \mathrm{x}_k}{\partial t^2}T_s^2 + \frac{1}{3!}\frac{\partial^3 \mathrm{x}_k}{\partial t^3}T_s^3 + ... \\ &= \mathrm{x}_k + T_s\mathbf{f}(\mathrm{x}_k) + O(T_s^2).\end{aligned} \tag{2.36}$$

By assuming the sampling time step is small, the truncated errors, $O(T_s^2)$, are negligible. This Euler approximation is not only used in the update of states, but also for the determination of the Jacobian matrices. Some examples for the application of EKF are demonstrated in Shieh [2005] and Wenzel et al. [2006].

Unscented Kalman Filter (UKF)

Although EKF is able to deal with the non-linear system by applying a Jacobian matrix, one major drawback is its assumption of small truncated error in higher order terms in the Taylor series expansion as shown in Equation 2.36. Based on this deficiency, Julier and Uhlmann [1997] have proposed a new extension for KF to non-linear system – UKF.

UKF utilises the Unscented Transformation (UT). The motivation behind this is inspired by Uhlmann [1994], who comments that it is easier to approximate a Gaussian distribution than it is to approximate an arbitrary non-linear function. When UT is applied to a KF, the mean and covariance of the original distribution (i.e. prior to the Jacobian matrix procedure), $\mathrm{x}_{k|k}$ and $\mathbf{P_{k|k}}$ respectively, are preserved, as no linearisation is needed.

In an UKF, the original state space equation is modified so that the state vector is augmented with both the original states (x), the process noise (w) and the measurement noise (v), such that,

$$\mathrm{x}^a = \begin{bmatrix}\mathrm{x} & \mathrm{w} & \mathrm{v}\end{bmatrix}^T. \tag{2.37}$$

Since the state vector is now in terms of states and noise, the process and measurement model is modified as a function of x^a such that in discrete format,

$$\mathrm{x}^a_{k+1} = \mathbf{f}^a(\mathrm{x}^a_k, \mathrm{u}_k); \tag{2.38}$$

$$\mathrm{z}_{k+1} = \mathbf{g}^a(\mathrm{x}^a_k). \tag{2.39}$$

As discussed, UKF does not linearise, but performs transformations. The procedure of the UT is similar to the Monte Carlo method but differs in its non-randomness in the sampling method of the sigma points. Using the specific algorithm in Equation 2.40, a set of discrete distribution of points (called the sigma points, $\mathcal{X}$) are selected with their corresponding weights, W_i. Note that this selection process preserves the sample mean and covariance, $\mathrm{x}_{k|k}$ and $\mathbf{P_{k|k}}$.

$$\begin{cases} \mathcal{X}_0^a = \hat{\mathrm{x}}_{k|k}^a & W_0 = \zeta/(n+\zeta) \\ \mathcal{X}_i^a = \hat{\mathrm{x}}_{k|k}^a + \left(\sqrt{(n+\zeta)\mathbf{P_{k|k}}}\right)_i & W_i = 1/2(n+\zeta) \\ \mathcal{X}_{i+n}^a = \hat{\mathrm{x}}_{k|k}^a - \left(\sqrt{(n-\zeta)\mathbf{P_{k|k}}}\right)_i & W_{i+n} = 1/2(n+\zeta) \end{cases} \tag{2.40}$$

$$\mathcal{X}_{k|k}^a = \begin{bmatrix} \mathcal{X}_0^a & \mathcal{X}_i^a & \mathcal{X}_{i+n}^a & ... \end{bmatrix}_{k|k} \tag{2.41}$$

where n is the total number of states in the augmented state vector, x^{a}; ζ is the fine tune parameter which is defined as $\zeta = 3 - n$ for a Gaussian distribution; $\left(\sqrt{(n-\zeta)\mathbf{P_{k|k}}}\right)_i$ is the i^{th} row or column of the matrix square root of $(n-\zeta)\mathbf{P_{k|k}}$; the number of sigma points is defined as $2n+1$.

Once the sigma points are defined, each point (i.e. $\mathcal{X}_{0,k|k}^a$, $\mathcal{X}_{i,k|k}^a$ etc.) is applied onto the non-linear system. The updated states, $\hat{\mathrm{x}}_{k+1|k}$ and the error covariance, $\mathbf{P}_{k+1|k}$, in the prediction stage are then computed using the weights as defined in Equation 2.40. With this, the correction stage is carried out easily with the UKF algorithm, which is summarised as follows:

Correction stage:

$$\hat{\mathcal{Z}}_{i,k} = \mathbf{g}^a(\mathcal{X}_{i,k|k-1}^a) \tag{2.42}$$

$$\hat{\mathrm{z}}_k = \sum_{i=0}^{2n} W_i \hat{\mathcal{Z}}_{i,k} \tag{2.43}$$

$$\mathbf{P}_{z_k,z_k} = \sum_{i=0}^{2n} W_i \left[\hat{\mathcal{Z}}_{i,k} - \hat{\mathrm{z}}_k\right] \left[\hat{\mathcal{Z}}_{i,k} - \hat{\mathrm{z}}_k\right]^T + \mathbf{R}_k \tag{2.44}$$

$$\mathbf{P}_{x_k,z_k} = \sum_{i=0}^{2n} W_i \left[\mathcal{X}_{i,k|k-1}^a - \hat{\mathrm{x}}_{i,k+1|k}^a\right] \left[\hat{\mathcal{Z}}_{i,k} - \hat{\mathrm{z}}_k\right]^T \tag{2.45}$$

$$\mathbf{K}_k = \mathbf{P}_{x_k,z_k} \mathbf{P}_{z_k,z_k}^{-1} \tag{2.46}$$

$$\mathbf{P}_{k|k} = \mathbf{P}_{k|k-1} - \mathbf{K}_k \mathbf{P}_{z_k,z_k} \mathbf{K}_k^T \tag{2.47}$$

$$\hat{\mathrm{x}}_{k|k}^a = \hat{\mathrm{x}}_{k|k-1}^a + \mathbf{K}_k(\mathrm{z}_k - \hat{\mathrm{z}}_k) \tag{2.48}$$

Prediction stage:

$$\mathcal{X}^a_{k|k} = \begin{bmatrix} \mathcal{X}^a_0 & \mathcal{X}^a_i & \mathcal{X}^a_{i+n} & ... \end{bmatrix}_{k|k} \text{ from Equations 2.40 and 2.41}$$

$$\mathcal{X}^a_{i,k+1|k} = \mathbf{f^a}(\mathcal{X}^a_{i,k|k}, \mathrm{u}_k) \tag{2.49}$$

$$\hat{\mathrm{x}}^a_{k+1|k} = \sum_{i=0}^{2n} W_i \mathcal{X}^a_{i,k+1|k} \tag{2.50}$$

$$\mathbf{P}_{k+1|k} = \sum_{i=0}^{2n} W_i \left[\mathcal{X}^a_{i,k+1|k} - \hat{\mathrm{x}}^a_{i,k+1|k}\right] \left[\mathcal{X}^a_{i,k+1|k} - \hat{\mathrm{x}}^a_{i,k+1|k}\right]^T + \mathbf{Q}_k \tag{2.51}$$

As shown in the UKF formulations above, there is no need for the calculation of Jacobian matrices. When the system is highly non-linear, UKF outperforms the EKF in accuracy and robustness. However, when higher order noises are negligible, the performance of the UKF is the same as that of the EKF. Some examples for the UKF application are given by Liu et al. [2006], Zhou et al. [2006] and Zhang et al. [2005].

2.4.4 Particle Filter (PF)

Other than the KF approach, an alternative approach to solve a non-linear and non-gaussian system is the PF. Djuric et al. [2003] considers that PF has become an important alternative to the EKF. Supporting his argument is the fact that PF enjoys a strong advantage over EKF - the ability to deal with any nonlinear system and non-Gaussian distributions. The two types of filter have been thoroughly compared in various areas of studies [Li et al. 2004, Yang et al. 2005, Gustafsson et al. 2002] and they all conclude that PF is able to estimate parameters more accurate than the well-known EKF.

Particle Filtering is a Sequential Monte Carlo (SMC) method based on 'particle point mass'. In other words, the system is approximated by some discrete random particles, which are samples of the unknown states from a state-space. These random particles have their own 'probability mass' or probability density that allows approximation of the posterior filtered distribution. Therefore, PF does not involve any linearisation process but the estimation of the sample distribution. This is important because the sampling and resampling techniques in the PF enables particles to propagate. Some sampling methods includes the Sequential Importance Sampling (SIS), the Sampling Importance Resampling (SIR), the Auxiliary Sampling Importance Resampling (ASIR) and the Regularised Particle Filter (RPF). And in some cases, PF sampling uses the KF to initiate a set of samples. With different sampling

algorithms, particles will be assigned to a different set of weightings and probability densities. With time, particles will converge to the probability distribution.

In a recent article, Ng et al. [2005] report the findings for the use of continuous time PF (CTPF) that is applied onto both discrete and continuous systems. They have concluded that the CTPF is more realistic and is more accurate than the discrete-time estimator.

Although the PF is proved to be more accurate and realistic than EKF, it suffers from a high demand for computation power and memory. Maskell and Gordon [2001] comment that the more particles there are for the PF, the more accurate the estimation will be.

2.5 GPS-aided Estimator

In Section 2.4, four common sensor fusion techniques, i.e. LKF, EKF, UKF and PF, were discussed. In the automotive industry, the KF is most commonly used due to its ease of implementation and simplicity to understand. This section therefore concentrates on the GPS-aided estimators. In the next subsection, an account on the difficulty in GPS/INS integration is given and followed by a discussion of the different architects of the GPS/INS design. This section then finishes with an overview of the GPS-aided estimator.

2.5.1 Sensor sampling and sideslip calculation

It must be noted that sensors may operate at different frequencies. Even though the majority of INS operate at 100Hz, measurements may not necessarily synchronise due to Controller-Area Network (CAN-bus) delays. In addition, due to hardware limitations, data received from GPS satellites is currently limited to a maximum rate of 50Hz; and cheap consumer grade GPS receivers, are normally available at 1Hz only. The difference between INS and GPS sampling rates causes error during their fusion process as INS measurements are forced to down-sample to synchronise with the GPS measurements.

As described earlier, the relationship between the INS (b-frame) and GPS (e-frame) is through the sideslip angle, Equation 2.10. With the sampling frequency of a consumer grade GPS (1Hz), the sideslip is calculated at a sample of 1Hz also. This delay is carried further downstream, affecting the accuracy of the velocities

measurements in the v-frame, i.e.

$$\begin{cases} \beta\Big|_{1Hz} = \nu\Big|_{1Hz} - \psi\Big|_{100Hz} \\ V\Big|_{1Hz} = \sqrt{\dot{x}_e^2 + \dot{y}_e^2}\Big|_{1Hz} \\ \dot{x}_v\Big|_{1Hz} = V\cos(\beta)\Big|_{1Hz} \\ \dot{y}_v\Big|_{1Hz} = V\sin(\beta)\Big|_{1Hz} \end{cases} \tag{2.52}$$

From Equation 2.10, the component that can resolve the problem of down-sampled sideslip estimation is obtaining a tracking measurement at a higher rate. In an expensive GPS receiver this can be obtained at a rate of up to 50Hz, but for lower grade receivers, the tracking angle has to be estimated through Equation 2.9. Taking one step backwards, velocities in the e-frame do not have to be taken from the low-sampled GPS. One can also transform the acceleration from the b-frame to the e-frame via the Euler heading angle using Equations 2.7 and 2.8,

$$\begin{cases} \ddot{x}_e\Big|_{100Hz} = A_x\cos(\psi)\Big|_{100Hz} - A_y\sin(\psi)\Big|_{100Hz} \\ \ddot{y}_e\Big|_{100Hz} = A_x\sin(\psi)\Big|_{100Hz} + A_y\cos(\psi)\Big|_{100Hz} \\ \nu\Big|_{100Hz} = \tan^{-1}\left(\frac{\dot{y}_e}{\dot{x}_e}\right)\Big|_{100Hz} \end{cases} \tag{2.53}$$

With the tracking calculated at a higher rate, the sideslip angle can also be calculated at a higher rate.

As presented here, there are two approaches to measure the sideslip angle: i) the low-sampling rate GPS/INS sideslip calculation, Equation 2.52, and ii) the high-sampling rate INS sideslip calculation, Equation 2.53. It may seem that the latter approach is more accurate as it provides a higher frequency for measurements. However, the high involvement of INS corrupts the estimations. As discussed earlier in Section 2.3, GPS and INS are contaminated with unwanted noise and bias, the two approaches, hence, cannot be operated on their own and must be accompanied by fusion with other sensors in the system. As will be discussed later in this thesis, the first approach is used as a reference measurement and sensor fusion takes place in the sensor frame, hence, the Sensor Kinematic Estimator (sKE). On the other hand, the second approach is used as the main process formulation with sensor fusion operating in the e-frame, hence, the Navigation Kinematic Estimator (nKE). In either approach, ensuring accuracy of the velocities in the v- or e-frames allows a good estimation of the sideslip.

2.5.2 Architecture for GPS-aided Kalman filter

Coupled and uncoupled Kalman filter

In order to fuse the GPS and INS, there are generally three different integration architectures to choose from: Uncoupled, loosely coupled and tightly coupled [Prasad and Ruggieri 2005, Grewal et al. 2007]. These architectures differ in terms of their input signals, type of filters, and number of filters.

Before going into details about the three different architectures, the structure of a basic sensor unit must be studied. This is because the type of architecture depends upon the nature of the signals. Figure 2.8 shows a typical sensor unit, which contains a receiver/measuring device, a filter, and a processor.

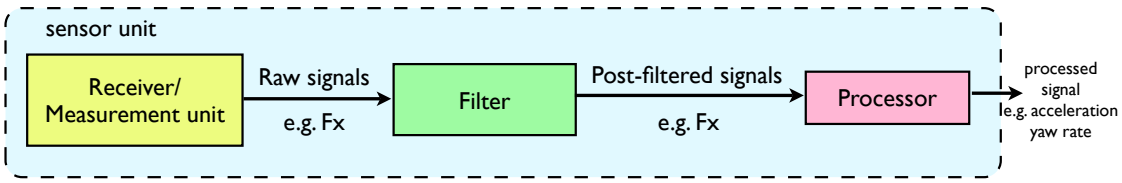

Figure 2.8: Sensor units

The receiver/measuring unit acquires raw information from an external source (for example, the GPS receiver acquires the raw C/A codes from the satellite, whilst the INS measuring unit acquires its raw data from an Inertia Measuring Unit, IMU, in terms of forces). As external equipment is contaminated with noise, the raw information gathered from the receiver/measuring unit is passed through a filter to remove any obvious uncertainties. In some sensors such as the GPS, a KF is used to improve the estimations. The pre-filtered signals are then calibrated and processed into the required measurements (for example, the GPS processor processes the velocity and positioning, whilst the INS processor calibrates the force into acceleration). These measurements, are hereby, referred to as processed signals for clarification. As a result, a sensor unit has three different signals that can be used: the raw signal, the post-filtered signal and the processed signal, see Figure 2.8.

Returning to the difference between the three architectures, the simplest of the three is the uncoupled structure. In this type of architecture each sensor unit is connected to its own navigation processor and has its own 'best' estimate. All these 'best' estimates are then fed into a filter (not necessarily a KF in this case) to obtain a final optimal prediction, see Figure 2.9. In some cases, such as a GPS/INS uncoupled filter, the filter is replaced by a simple switch and the solution is determined by selecting which signal is more appropriate at the time. Uncoupled architecture is

not only cheap, simple and easy to implement, it also has an advantage of continual data processing even when one or more sensors fail.

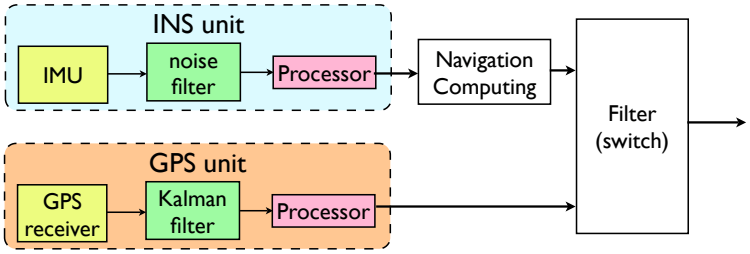

Figure 2.9: Uncoupled Kalman Filter

Loosely and tightly coupled architectures are different in terms of the input signals to the KF. Using GPS/INS integration as an example, a loosely coupled technique uses the processed signal from the GPS and INS unit as the inputs to the KF, Figure 2.10. The KF predicts the estimation errors of the INS. These are then used for correcting the INS state estimation as well as feeding back into the navigation processor unit to correct the processed signal. This type of architecture is relatively straight forward to implement, especially when dealing with commercial off-the-shelf sensor units, in which raw data may not be accessible. It also does not require the user to alter the system of the existing hardware. However, when GPS fails to receive information, INS becomes the only source that is available. For a short term GPS failure, this architecture should be able to cope, but for an extensive period, additional INS error control is required.

A GPS/INS tightly coupled integrated KF, Figure 2.11, uses the raw signal from the GPS unit, i.e. the raw C/A coding, and the processed signal from the INS. As GPS uses the range and Doppler to determine the position and velocity from the C/A coding, the INS processed signal is integrated with the raw signal to obtain a residual for the input of the KF. Similar to the loosely coupled architecture, the KF predicts the error estimates and uses them for corrections. This type of architecture is complex, difficult to implement and requires knowledge of GPS systems. However, it is robust and will not fail even when GPS becomes inaccurate (e.g. the number of satellites drop from four to three).

To summarise, the three architectures can be categorised into two different filtering approaches: centralised and decentralised, Figure 2.12. In a centralised filtering, all processed signals (or measurements) from different sensors are fed into the same KF for an optimal estimation. An example for such filtering is similar to a tightly coupled KF. In a decentralised filtering, each sensor unit has its 'best' private estimation. All these 'best' private estimations are then processed into one master filter

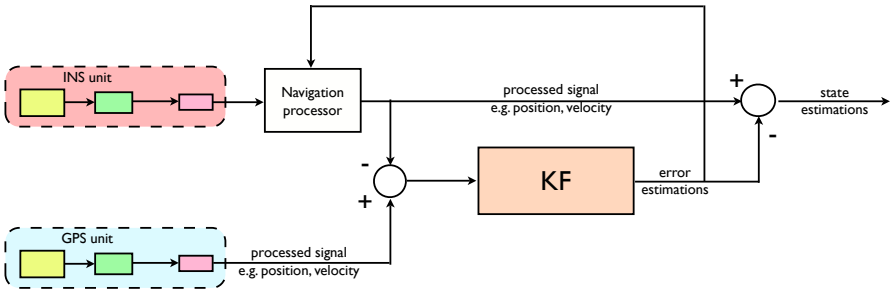

Figure 2.10: Loosely coupled Kalman Filter

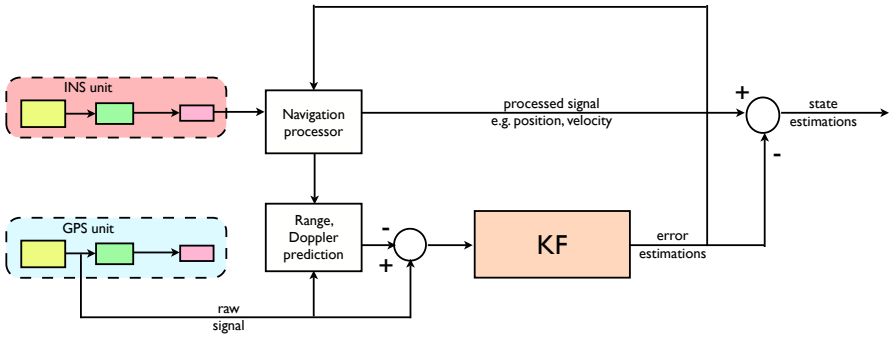

Figure 2.11: Tightly coupled Kalman Filter

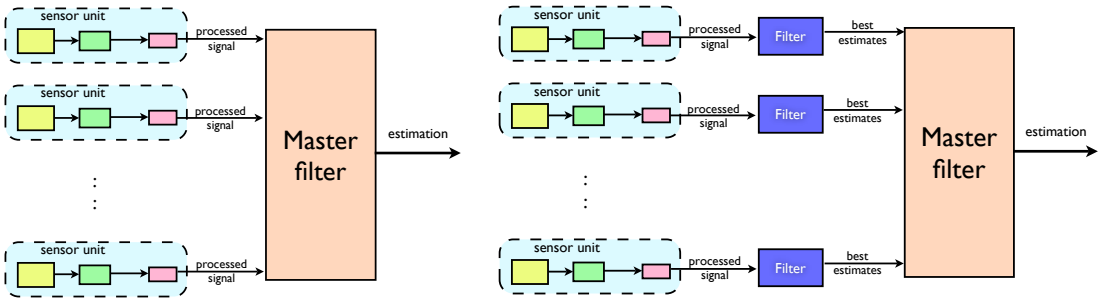

(a) Centralised filtering (b) De-centralised filtering

Figure 2.12: Two different filtering approaches [Brown and Hwang 1997]

for an optimal public estimation. This type of filtering approach is more flexible and easier to implement with multiple sensors. Examples are the uncoupled and loosely coupled KF. In all these cases, if error estimates are fed back into the sensor unit for correction, this is referred to as closed loop filtering.

2.5.3 GPS-aided Kinematic Estimator

Based on the observation of Deng and Zhang [2006], sideslip estimation can be generally categorised into either kinematic (combination of indirect and direct sensor)

or model-based approach. The Kinematic Estimator (KE) approach is concerned with the motion of objects without any reference to forces. A fair amount of work has been done by Bevly and colleagues on Mercedes M- and E-class vehicles [Bevly et al. 2000; 2001; 2002, Bevly 2004], in which they fuse GPS and INS with a KKF. As discussed previously, GPS suffers from a low update rate (typically 1Hz), so Bevly uses a KKF to predict the INS bias when GPS is available and integrating the 'corrected' INS signals when GPS becomes unavailable. This allows the INS biases to be estimated, hence attenuating the drifts in the sensor signal. In Bevly et al. [2000; 2001; 2002] and Bevly [2004], however, only a single GPS antenna is used and as a result, rate gyro bias can only be predicted while the vehicle is travelling on a straight road. Therefore, in Ryu et al. [2002] and Bevly et al. [2006], a dual GPS antenna setup has been introduced, so that the yaw angle of the vehicle can be measured at any instant.

As Bevly and Ryu comment in their papers, the dual GPS setup enables direct measurement of yaw and roll angles, thereby neatly de-coupling the estimation problems into two independent KKF (yaw KKF and velocity KKF), which improves the sideslip estimation. With the favourable outcome of the KKF, in Ryu and Gerdes [2004*b*], the KKF is extended to include a roll-centre model with road grade to estimate the roll and roll bias of a vehicle, resulting in an even more accurate prediction of the sideslip. Furthermore, Ryu and Gerdes [2004*b*] has also included a sensitivity factor to eliminate the cross coupling effect of the INS, making the bias settle onto a constant value.

The KKF (or generally KE) being discussed here works about the vehicle axes framework (v-frame), and their described motions are directly related to the motion of the sensors, i.e. the sKE approach as defined in Section 2.5.1. For the nKE approach, some examples can be found in Wang and Goh [1999], Dissanayake et al. [2001], Liu et al. [2005], Gao [2006], Lenain et al. [2006] and He [2006]. These papers perform estimation of the navigation frame (i.e. nKE) and transform the kinematic relationships of sensors from the sensor axes framework (b-frame) to e-frame.

One of the earliest papers, Wang and Goh [1999], constructed an nKE to include measurements from the odometer, the yaw gyro and the differential GPS (DGPS) to estimate the positions, velocities and the slip angles. Although their results look feasible, they are restricted to navigation prediction only. A more relevant approach in dynamic state estimation can be found in Dissanayake et al. [2001] and Liu et al. [2005], which includes vehicle non-holonomic constraints to restrict lateral and normal velocities in the v-frame (i.e. $\dot{y}_v$ and $\dot{z}_v$) to zero. This technique, however, only works on flat roads under ideal conditions. In more practical situations, as

noted by Gao [2006], sideslip will not be zero and non-holonomic constraints will no longer apply. To predict the sideslip, the use of GPS measurements and an observer-like estimator with path tracking control laws is suggested. With the path pre-specified, it has been shown that the sideslip of a low speed agricultural vehicle can be predicted with an average position tracking error of 0.08m [Lenain et al. 2006].

So far, estimators have been based upon different assumptions and constraints. For a more realistic vehicle behaviour, He [2006] and He et al. [2002] have constructed a system consisting of two nKE and a Runge-Kutta (RK) dead reckoning to estimate sideslip with a set of WSS. Apart from the WSS, Gao [2006] has also included four other sensors, namely the GPS, INS, G sensors (GL) and Yaw Rate Sensor (YRS). The GPS and INS are fused in a tightly coupled manner, which improves the accuracy of GPS positioning. During GPS outages, the system uses external aiding GL/YRS/WSS for estimations. Such a system structure is beneficial in reducing horizontal positioning error when compared to the non-holonomic constraint approach.

To summarise, KEs sub-divide into two classes: sKE and nKE. sKE operates in the sensor reference frame and nKE in the navigation frame. In general, KEs are easy and simple to implement, although their estimation effectiveness depends upon external aiding sensors. From the existing literature the majority of these KE use the KF technique. This is due to the ease of multi-sampling data fusion of a KF. Details of the KE are given in Section 2.6.

2.5.4 GPS-aided Model-based estimator

Apart from the kinematic approach, there is also the model-based approach (i.e. ME). As discussed by Stephant et al. [2004], there are in general two different kinds of estimators/observers depending on their model, namely linear and non-linear. In their paper, four different observers: Linear Modelled Observer (LMO), non-linear Extended LO (ELO), non-linear Model-based Extended Kalman Filter (MEKF) and non-linear Sliding-Mode Observer (SMO) are compared. Using a simple bicycle model with measurements from a YRS and WSS, Stephant et al. [2004] performed double lane change simulations at 20, 60 and 90 km/h as well as practical experiments. It was concluded that the observers (i.e. LMO, ELO and SMO) give better approximations of sideslip than EKF; and in the experiment LMO is the least accurate. The findings are interesting; however no external GPS measurements are included in the study.

With a dual GPS setup, vehicle attitude as well as vehicle yaw angle can be

obtained. Using this information, Ryu and Gerdes [2004*a*] have constructed a disturbance observer to allow the separation of the estimation of road bank angle from vehicle roll. This extra information from the GPS can also be applied to the bicycle model for cornering stiffness predictions. As reported in Rock et al. [2005] and Anderson and Bevly [2005], cornering stiffness can be accurately predicted and used during GPS absence. Although ME is able to produce accurate dynamic predictions, the model is very sensitive to parameter errors [Anderson and Bevly 2005, Li et al. 2005]. As Anderson and Bevly [2005] have shown, a simple incorrect weight split ratio can have a huge effect on the estimates precision. This disadvantage of a ME was later addressed by Best et al. [2007], who propose a two stage parameter estimation method: first to estimate the inertial parameters, and then the tyre parameters. They demonstrate that with an assumption of precise lateral velocity and yaw rate measurements, the parameters of a bicycle model and a magic tyre formula can be estimated by tuning only two parameters.

In GPS/INS ME, the majority of the literature uses a simple linear bicycle model with a linear tyre model. This is because linear models are relatively easier to implement with fewer parameters to specify. With correct parameters and tyres working in a linear region at constant forward velocity, ME generally works well.

2.6 Current Design for GPS-aided Vehicle Dynamic State Estimator

In the Sections 2.5.3 and 2.5.4, a general overview for the two types of GPS-aided vehicle dynamic estimator was discussed. This section aims to provide a more detailed explanation and design for recent developments. As a reminder, this project is based on KF estimators so other techniques such as the ANN and PF are not studied here.

2.6.1 GPS/INS Kinematic Estimator

Sensor Kinematic Kalman Filter (sKKF)

One of the earliest papers that involves vehicle state predictions and GPS was presented by Wang and Goh [1999]. In their paper, an Extended Kinematic Kalman Filter (EKKF) with fuzzy logic control is proposed. Using the steering encoders as an input, δ, and the rate gyros, odometer and Differential GPS (DGPS) as measurements, $\begin{bmatrix} r_m & V_b & x_e^{gps} & y_e^{gps} \end{bmatrix}^T$, the position, orientation and the sideslip of each wheel of a golf buggy are estimated. The fuzzy logic control in the system is used

to determine the magnitude of the process noise variance in the EKKF according to different driving manoeuvres. The EKKF constructed by Wang and Goh [1999] is based on a combination of sKE and nKE design, in which the system equations are based on the position in the e-frame, x_e and y_e, and the velocity in the v-frame, V_v,

$$\begin{bmatrix} x_e \\ y_e \\ V_v \\ \psi \\ \dot{\psi} \\ \alpha_f \\ \alpha_r \end{bmatrix}_{k+1} = \mathbf{\Phi}_k \begin{bmatrix} x_e \\ y_e \\ V_v \\ \psi \\ \dot{\psi} \\ \alpha_f \\ \alpha_r \end{bmatrix}_k + \mathbf{\Delta}_k \Big[\delta\Big]_k + \mathbf{\Gamma}_k \begin{bmatrix} \dot{V} \\ \ddot{\psi} \\ \dot{\alpha}_f \\ \dot{\alpha}_r \end{bmatrix}_k \tag{2.54}$$

As the golf buggy travels at very low speed (2m/s or less), the lateral and longitudinal slip is near zero. Hence, the use of velocity and yaw rate measurements from the odometer and gyro respectively as an accurate reference source is reasonable. However, if it is applied to a higher speed ground vehicle for estimations, the velocity and yaw angle will drift as INS is corrupted by biases.

Taking the bias of the INS into consideration, Bevly et al. [2000] designed a KKF, based on sKE, to estimate not only the yaw angle, but also the bias in the yaw rate gyro. In Bevly et al. [2000] a rate bias term, b_ψ, is included as well as a noise term, w_ψ, in the yaw rate gyro measurement, r_m, so that

$$r_m = \dot{\psi} + b_\psi + w_\psi \tag{2.55}$$

$$\begin{bmatrix} \psi \\ b_\psi \end{bmatrix}_{k+1} = \mathbf{\Phi}_k \begin{bmatrix} \psi \\ b_\psi \end{bmatrix}_k + \mathbf{\Delta}_k \Big[r_m\Big]_k + \mathbf{\Gamma}_k \Big[w_\psi\Big]_k \tag{2.56}$$

$$\Big[\nu\Big]_k = \mathbf{H}_k \begin{bmatrix} \psi \\ b_\psi \end{bmatrix}_{k+1} \tag{2.57}$$

To perform estimation correctly, Bevly et al. [2000] used the GPS measured tracking angle to compare with the predicted heading angle, ψ. However, as described in Section 2.3.3, the tracking angle is only equal to the heading angle when the vehicle is travelling on a straight road. Therefore, the measurement matrix, $\mathbf{H}_k$, changes to zero when the measured yaw rate exceeds a pre-defined threshold. Furthermore, as the INS and GPS each operate at a different sampling rate (i.e. 100Hz in INS and 10Hz in GPS in their paper), $\mathbf{H}_k$ also becomes zero in between GPS samples. Using the estimated heading angle, the sideslip at the cg of the vehicle, and the lateral and longitudinal slips at the tyres can be determined. Bevly et al. [2000]

have also commented on the effect that vehicle velocity has on the accuracy of the GPS measured tracking angle. Based on this KKF design, Bevly et al. [2000] have performed an experimental test on a ground vehicle travelling at 8m/s in an open-air car parking lot and have made some good sideslip estimations compared with the 2DoF bicycle model.

Using a similar set of equipment, Bevly et al. [2001] have continued their research and incorporated an additional KKF: lateral velocity KKF, which is described by,

$$A_y = \ddot{y}_v + \dot{x}_v r_m + b_y + \mathrm{w}_y, \tag{2.58}$$

$$\begin{bmatrix} \dot{y}_v \\ b_y \end{bmatrix}_{k+1} = \mathbf{\Phi}_k \begin{bmatrix} \dot{y}_v \\ b_y \end{bmatrix}_k + \mathbf{\Delta}_k \left[A_y - \dot{x}_v r_m \right]_k + \mathbf{\Gamma}_k \left[\mathrm{w}_y \right]_k, \tag{2.59}$$

$$\left[V_{gps} sin(\beta) \right] = \mathbf{H}_k \begin{bmatrix} \dot{y}_v \\ b_y \end{bmatrix}_{k+1}. \tag{2.60}$$

This KKF is used for lateral velocity and lateral accelerometer bias predictions. The state space description above assumed a constant vehicle speed of 7 to 10m/s and uses the corrected yaw rate from the yaw KKF as an input. The predicted velocities are then used with the bicycle model and sideslip to determine the slip angles and cornering coefficients at the tyres. In addition the predicted bias, b_y, can also be used as an approximation of the vehicle roll angle. Similar to the yaw KKF, the correction of this velocity KKF is also updated only when GPS signals are available. Due to the different sampling rates of GPS and INS, Bevly et al. [2001] have highlighted the significance of synchronising GPS with INS data. Up until this time, Bevly et al. [2000; 2001] had focused their KF design on a single GPS antenna, which created a limitation in the yaw KKF (namely the rate gyro bias prediction) during cornering. In Bevly et al. [2002], a thorough and detailed discussion on the feasibility of using single antenna GPS in state estimations is given.

Without the assumption of constant speed, the lateral velocity KKF can be

extended to include the longitudinal velocity:

$$\begin{bmatrix} \dot{x}_v \\ b_x \\ \dot{y}_v \\ b_y \end{bmatrix}_{k+1} = \mathbf{\Phi}_k \begin{bmatrix} \dot{x}_v \\ b_y \\ \dot{y}_v \\ b_y \end{bmatrix}_k + \mathbf{\Delta}_k \begin{bmatrix} A_x \\ A_y \end{bmatrix}_k + \mathbf{\Gamma}_k \begin{bmatrix} \mathrm{w}_x \\ \mathrm{w}_y \end{bmatrix}_k \tag{2.61}$$

$$\begin{bmatrix} V_{gps}cos(\beta) \\ V_{gps}sin(\beta) \end{bmatrix} = \mathbf{H}_k \begin{bmatrix} \dot{x}_v \\ b_x \\ \dot{y}_v \\ b_y \end{bmatrix}_{k+1} \tag{2.62}$$

This integrated velocity KKF is presented in Ryu et al. [2002] and is able to estimate the bias in the longitudinal accelerometer.

Furthermore, Ryu et al. [2002] have taken the dual KKF approach [Bevly et al. 2000; 2001] a step further and introduced a dual GPS antennae receiver. In fact, in an earlier paper of Bae et al. [2001], two GPS antennae receivers are placed in the pitch plane in order to estimate the pitch angle of a vehicle. This is then combined with engine torque information to estimate the mass, rolling resistance and aerodynamic drag from a simple longitudinal force balance. Such state estimations can also be obtained from sensor sets that exclude GPS [Lingman and Schmidtbauer 2002, Vahidi et al. 2005, McIntyre et al. 2009], but the GPS signal can improve the accuracy of both pitch and roll estimations [Baek et al. 2007]. In addition, GPS positional information can be used to fuse road grade estimations with road grade maps to provide predictions for look-ahead cruise control [Sahlholm, Jansson and Johansson 2007, Sahlholm, Jansson, Kozica and Johansson 2007, Sahlholm et al. 2008].

The setup of the GPS system proposed by Bae et al. [2001] is shown in Figure 2.13. The antennae are placed in the pitch plane to estimate the longitudinal dynamics state; for the lateral dynamics, e.g. [Ryu et al. 2002], the GPS antennae are placed in the roll plane, also shown in Figure 2.13, so that the system is able to measure the heading angle, the tracking angle and the velocities in the vertical and horizontal direction. This additional information allows the design of a new roll KKF which predicts the total roll angle, ϕ_{eb}, of the vehicle and the roll gyro bias,

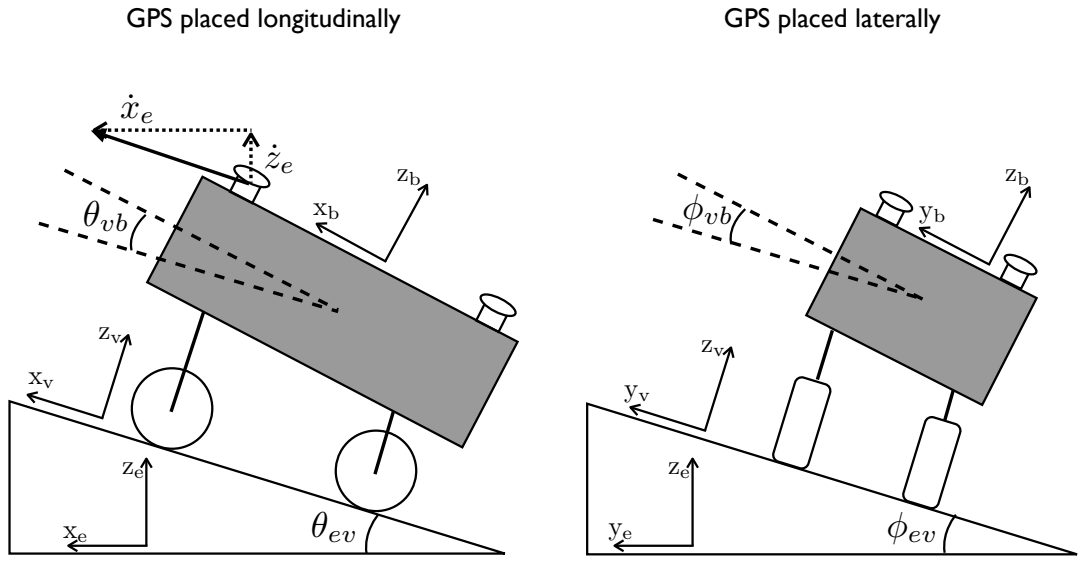

Figure 2.13: Dual GPS antennae setup [Bae et al. 2001, Ryu et al. 2002, Ryu and Gerdes 2004*b*, Ryu 2004]

b_ϕ, and the estimation of road grade, θ_{ev}, so that

$$p_m = \dot{\phi}_{eb} + b_\phi + \mathrm{w}_\phi$$
$$\phi_{gps} = \phi_{eb} + \mathrm{w}_{\phi_{gps}} \tag{2.63}$$
$$\hat{\theta}_{ev} = \tan^{-1}\left(\frac{V^u_{gps}}{V^h_{gps}}\right) \tag{2.64}$$

The dual GPS also allows a continual estimation of heading angle and yaw gyro bias as GPS heading measurements are now available during cornering. Recall Equations 2.3 and 2.4 with biases:

$$A_x = \ddot{x}_v - \dot{y}_v\hat{\dot{\psi}} + b_x + g\sin(\hat{\theta}_{eb})$$
$$A_y = \ddot{y}_v + \dot{x}_v\hat{\dot{\psi}} + b_y + g\sin(\hat{\phi}_{eb})$$

The longitudinal and lateral velocities in the v-frame are now more accurately predicted as vehicle pitching and rolling effects are taken into consideration. To further refine the model, Ryu and Gerdes [2004*b*] have modified the velocities KKF to include extra state variables to take account of the gyro sensitivity and accelerometer cross coupling effects.

Although experiments have shown the KF design to be effective, a de-coupling

problem exists with the roll estimations of the vehicle. As shown above, ϕ_{eb} can be predicted but this variable is equal to the sum of bank angle of road, ϕ_{ev}, and the actual vehicle body roll angle along its sensor axes, ϕ_{vb},

$$\phi_{eb} = \phi_{ev} + \phi_{vb} \tag{2.65}$$

To resolve this, Ryu and Gerdes [2004*a*] have combined a disturbance model with a bicycle model. This method allows the separation of vehicle roll from the bank angle, further improving the estimations. This added feature has given extra accuracy in state estimations, thereby enhancing velocity predictions. With the roll angle and roll gyro bias predicted, the roll stiffness and the damping ratio, and the mass can also be determined.

The designs of all aforementioned KKF assume a constant INS bias modelling (i.e. the derivative of the biases are zero). In reality, however, not all types of INS bias are constant. Some biases are driven by noise and some vary with external conditions such as temperature. This may cause the bias to drift over time. Bevly [2004] has, therefore, modified some of the biases, namely the longitudinal accelerometer, the roll rate and the yaw rate biases, to be modelled by a first order Markov Process driven by white noise,

$$\dot{b}_m = -\frac{1}{T_{b_m}} b_m + \frac{1}{T_{b_m}} \mathrm{w}_{b_m}, \tag{2.66}$$

in which the rate of change of bias, $\dot{b}_m$, is dependent on the time constant, T_{b_m}, and the normally distributed white noise, w_{b_m}.

Unlike the approach of Ryu and Gerdes [2004*a*], Bevly [2004] has assumed that rotational motion has no effect on the longitudinal acceleration. Hence, the rolling dynamics are entirely dependent on the road bank angle only. The longitudinal and lateral dynamics of a vehicle are modified from Equations 2.3 and 2.4 to

$$A_x = \ddot{x}_v + b_x + g(\theta_{ev} + \theta_{vb} + b_\theta) \tag{2.67}$$

$$A_y = \ddot{y}_v + \dot{x}_v \hat{\dot{\psi}} + b_y + g(\phi_{ev} + b_\phi) \tag{2.68}$$

which have a corresponding state space representation

$$V_{gps} = \dot{x}_v;\ V_{gps}\beta = \dot{y}_v;\ \theta_{gps} = \theta_b$$

$$\begin{aligned}
\begin{bmatrix} \dot{x}_v \\ \theta_{ev} \\ \theta_{vb} + b_x \\ b_\theta \end{bmatrix}_{k+1} &= \mathbf{\Phi}_k \begin{bmatrix} \dot{x}_v \\ \theta_{ev} \\ \theta_{vb} + b_x \\ b_\theta \end{bmatrix}_k + \mathbf{\Delta}_k \begin{bmatrix} A_x \\ q_m \end{bmatrix}_k + \mathbf{\Gamma}_k \begin{bmatrix} \mathrm{w}_x \end{bmatrix}_k \\
\begin{bmatrix} V_{gps} \\ \theta_{gps} \end{bmatrix}_k &= \mathbf{H}_k \begin{bmatrix} \dot{x}_v \\ \theta_{ev} \\ \theta_{vb} + b_x \\ b_\theta \end{bmatrix}_{k+1}
\end{aligned} \tag{2.69}$$

$$\begin{aligned}
\begin{bmatrix} \dot{y}_v \\ \phi_{ev} + b_y \\ b_\phi \end{bmatrix}_{k+1} &= \mathbf{\Phi}_k \begin{bmatrix} \dot{y}_v \\ \phi_{ev} + b_y \\ b_\phi \end{bmatrix}_k + \mathbf{\Delta}_k \begin{bmatrix} A_y - \dot{x}_v\hat{\dot{\psi}} \\ p_m \end{bmatrix}_k + \mathbf{\Gamma}_k \begin{bmatrix} \mathrm{w}_y \end{bmatrix}_k \\
\begin{bmatrix} V_{gps}\beta \end{bmatrix} &= \mathbf{H}_k \begin{bmatrix} \dot{y}_v \\ \phi_{ev} + b_y \\ b_\phi \end{bmatrix}_{k+1}
\end{aligned} \tag{2.70}$$

Similar to the KKF design of Ryu and Gerdes [2004*b*], two of the state variables in the above KKF require decoupling: $(\theta_{vb} + b_x)$ and $(\phi_{ev} + b_y)$. Bevly [2004] has considered the frequency nature of the variables and designed filters to separate them accordingly. As the rate of change of accelerometer biases is low relative to that of the angles, Bevly [2004] has used a low pass filter and a high pass filter with time constant, T_{sL} and T_{sH}, to separate the bias and angle from the state variable,

$$\begin{cases}
\hat{\theta}_{vb} = \dfrac{T_{sL}s}{T_{sL}s + 1}(\theta_{vb} + b_x) \\
\hat{b}_x = \dfrac{1}{T_{sL}s + 1}(\theta_{vb} + b_x) \\
\hat{\phi}_{ev} = \dfrac{T_{sH}s}{T_{sH}s + 1}(\phi_{ev} + b_y) \\
\hat{b}_y = \dfrac{1}{T_{sH}s + 1}(\phi_{ev} + b_y)
\end{cases} \tag{2.71}$$

The benefit of a dual GPS antenna setup over a single is apparent. As demonstrated in Bevly et al. [2006], without the use of KF, the sideslip prediction using GPS and integrated gyro, $\hat{\beta}_{GPS} = \nu_{GPS} - \int r_m \mathrm{dt}$, is more accurate than the integrated velocities from the accelerometers, $\hat{\beta}_{INS} = \tan^{-1}\left(\int \ddot{y}_v \mathrm{dt} / \int \ddot{x}_v \mathrm{dt}\right)$. Bevly et al. [2006] comment that this is because the gyro is less sensitive to errors induced by the roll

and that the cause of error is mainly due to the GPS measurements latency, which introduces an error of up to 30 – 50% error. This can be reduced by implementing GPS measurement in a KKF. Bevly et al. [2006] have used a single GPS antenna in a KKF, Equation 2.58, and improved the estimations of sideslip. Results show that the accelerometer bias is influenced by the rolling effect of the vehicle due to gravity. With a dual GPS antenna setup, the roll angle and yaw angle of the vehicle can be measured, thus enhancing the estimations of velocities and sideslips. With more accurate information, vehicle parameters such as cornering coefficients can be predicted and used to improve the MKF design as well as performance of modern control systems [Anderson and Bevly 2005, Daily and Bevly 2004].

With the sKKF, using an initial sideslip measurement from the GPS, the velocity in the v-frame and sensor biases are estimated. In between GPS samples, the 'corrected' INS is numerically integrated to give an estimation for the velocities in the v-frame as well as the sideslip angle.

Navigation Kinematic Kalman Filter (nKKF)

So far, the presented KFs are mainly sKKF, and GPS measurements are translated to the v-frame before being used in the filter. This approach is natural as the vehicle dynamic states operate and are most easily visualised in the v-frame. As described in Section 2.3, sideslip angles can also be estimated using the nKE approach,see Equation 2.53, by evaluating the velocities in the e-frame using sensor measurements from the b-frame. One benefit of this approach is that more GPS information can be utilised and used as reference measurements. With the estimator now based in the e-frame, not only the velocities, but also the position from the GPS can be fully utilised.

In Dissanayake et al. [2001], a filter called the Information Filter (IF) is applied instead of a KF. As discussed in their paper, the advantage and reason for using IF over KF is due to the ease of implementing multiple observations from various sensors, these being the positions and velocities from GPS, the speeds from the wheel encoders, and the velocity constraints. All three observations must operate in the same reference frame for comparison, and Dissanayake et al. [2001] have chosen the NED frame. In the paper, a complete transformation from its vehicle to NED frame is presented in a three-dimensional space, in which the pitch and roll angles are not zero. Similarly, measurements from the sensors in the b-frame are related to the e-frame with Euler angles by a transformation matrix, also known as the Direct

Cosine Matrix (DCM), $\mathbf{C_b^e}$:

$$\vec{a}_e = \mathbf{C_b^e}\vec{a}_b \tag{2.72}$$

where: $\vec{a}_e = \begin{bmatrix} \ddot{x}_e \\ \ddot{y}_e \\ \ddot{z}_e \end{bmatrix}, \vec{a}_b = \begin{bmatrix} A_x \\ A_y \\ A_z \end{bmatrix}$

$$\mathbf{C_b^e} = \begin{bmatrix} \theta^c\psi^c & -\phi^c\psi^s + \phi^s\theta^s\psi^c & \phi^s\psi^s + \phi^c\theta^s\psi^c \\ \theta^c\psi^s & \phi^c\psi^c + \phi^s\theta^s\psi^s & -\phi^s\psi^c + \phi^c\theta^s\psi^s \\ -\theta^s & \phi^s\theta^c & \phi^c\theta^c \end{bmatrix}$$

Subscripts s, c,represent sine and cosine respectively

It can be easily seen from the above that when the pitch and roll angles are neglected, the transformation matrix is the same as that shown by Equations 2.7 and 2.8. At this point, it is important to point out that the Euler angles (ϕ, θ and ψ) are not the same as the measurements from the rate gyros. They have a relationship as described by Equation 2.5.

In Dissanayake et al. [2001], the authors have applied the IF to a commercial vehicle travelling at 36km/h, with state variables in the e-frame: the position, velocities and the angles, $\mathrm{x} = \begin{bmatrix} x_e & y_e & z_e & \dot{x}_e & \dot{y}_e & \dot{z}_e & \phi & \theta & \psi \end{bmatrix}^T$, giving

$$\begin{bmatrix} \mathrm{x} \end{bmatrix}_{k+1} = \mathbf{\Phi}_k \begin{bmatrix} \mathrm{x} \end{bmatrix}_k + \mathbf{\Delta}_k \mathbf{C_b^e} \begin{bmatrix} A_x \\ A_y \\ A_z \end{bmatrix}_k + \mathbf{\Gamma}_k \begin{bmatrix} \mathrm{w}_x \\ \mathrm{w}_y \\ \mathrm{w}_z \end{bmatrix}_k \tag{2.73}$$

As discussed earlier, the observed measurements are taken from two sources, the GPS

$$\begin{bmatrix} x_e \\ y_e \\ z_e \\ \dot{x}_e \\ \dot{y}_e \\ \dot{z}_e \end{bmatrix}_k = \begin{bmatrix} x_{gps} \\ y_{gps} \\ z_{gps} \\ \dot{x}_{gps} \\ \dot{y}_{gps} \\ \dot{z}_{gps} \end{bmatrix}_k = \mathbf{H}_k \begin{bmatrix} \mathrm{x} \end{bmatrix}_k \tag{2.74}$$

and the speed encoder/holonomic constraints ($\dot{y}_b$ and $\dot{z}_b$ are equal to zero),

$$\begin{bmatrix} \dot{x}_e \\ \dot{y}_e \\ \dot{z}_e \end{bmatrix}_k = \mathbf{C_b^e} \begin{bmatrix} V_{encoder} \\ 0 \\ 0 \end{bmatrix}_k = \mathbf{H}_k \begin{bmatrix} \mathrm{x} \end{bmatrix}_k \tag{2.75}$$

The multiple observations above are weighted to obtain an improved state estimation. In Dissanayake et al. [2001], it is claimed that the IF design has an improvement of position estimations. However, for this approach, the vehicle requires more sensors than a commercial vehicle would normally have (e.g. pitch rate and roll rate sensors, and accelerometer in the vertical direction). Furthermore the system also suffers from the assumption of flat road operation with zero sideslip angles and zero lateral velocity.

He et al. [2002] have used two KFs in conjunction with a numerical integration method, namely RK analysis. They have designed this approach for a 4 Wheel Steered (4WS) mobile robot and have assumed that states remain constant between each sampling interval,

$$\begin{cases} V^i_{k+1} &= V^i_k + \mathrm{w}_V \\ \beta_{k+1} &= \beta_k + \mathrm{w}_\beta \\ \rho_{k+1} &= \rho_k + \mathrm{w}_\rho \end{cases} \tag{2.76}$$

where V^i is the velocity magnitude at each wheel, i; β is the sideslip angle at cg; ρ is the path curvature (1/turning radius).

With this process equation, the first KF has a state vector consisting of the four wheel velocities and the cg sideslip, $\begin{bmatrix} V^i & \beta \end{bmatrix}^T$, and a measurement vector comprising measurements from the wheel speed encoder and the steering sensor (see Equation 2.78 below). The predicted sideslip and wheel velocities are used in the process matrix of the second KF with state variables $\begin{bmatrix} x_e & y_e & \psi \end{bmatrix}^T$. The process equation is derived from a set of discrete kinematic equations,

$$\begin{cases} x_e\big|_{k+1} = x_e\big|_k + T_s V \cos(\psi\big|_k + \beta) \\ y_e\big|_{k+1} = y_e\big|_k + T_s V \sin(\psi\big|_k + \beta) \\ \psi\big|_{k+1} = \psi\big|_k + T_s \dfrac{V}{\mathrm{b}} \sin(\beta) \end{cases} \tag{2.77}$$

The measurement vector for this second KF uses the GPS positions, x_e and y_e. During the loss of GPS information, the quality of the second KF estimations reduces, and the system switches from the second KF estimation to the RK analysis. The kinematic relationship is

$$V^i = V\cos(\beta)\sqrt{\left(1 \mp \frac{T\rho}{\cos(\beta)} + \tan^2(b_j)\right)} \tag{2.78}$$

where V is the velocity at the cg; β is the sideslip angle at cg; T is the half wheel

base; ρ is the path curvature, 1/turning radius; b_j is the steer angle at the front or rear, j.

This relationship is nonlinear so an EKF is employed. Recalling Equation 2.26:

$$\hat{\mathrm{x}}_{k+1} = \hat{\mathrm{x}}_k + T_s \mathbf{f}(\hat{\mathrm{x}}_k, \mathrm{u}_k, \mathrm{w}_k) = \hat{\mathbf{f}}(\hat{\mathrm{x}}_k, \mathrm{u}_k, \mathrm{w}_k)$$

The discretised expression only makes use of the first two terms of a Taylor series expansion. Information from higher derivatives are therefore lost during each interval. If higher order terms are included, the process covariance matrix will be more complex and the level of nonlinearity will also increase. However, the higher the level of complexity, the closer the representation is to reality. Discrepancies between estimations and measurements (i.e. innovation) will also be minimised. As a result, during GPS outages and in between GPS samples (i.e. GPS downtime), estimations will be more accurately predicted by the EKF.

Apart from increasing the complexity of the process matrix during GPS downtime, some papers [Bevly et al. 2001; 2002] have simply switched the measurement off, i.e. $\mathbf{H}_k = 0$ in Equation 2.16, and interpret estimations through numerical interpolation, such as the trapezoidal interpolation, or other analytical formulation [Chen and Hsieh 2008]. Other papers such as Gao [2006] have taken the obvious step of increasing the number of sensors and available measurements during GPS downtime. In Gao [2006], GPS, INS, G sensors (GL), YRS and WSS are used for the study of estimation accuracy. Four different combinations of sensors and strategies are investigated during GPS downtimes. They are:

1. GPS/INS: with no external sensors aiding;

2. GPS/INS/GL/YRS/WSS: with two non-holonomic constraints on the lateral and upward velocities while the longitudinal velocity is measured by the WSS(i.e. $\dot{x}_v = V_{WSS}$, $\dot{y}_v = 0$, $\dot{z}_v = 0$);

3. GPS/INS/GL/YRS/WSS: with only one non-holonomic constraint on the upward direction. The lateral velocity is measured with the GL/YRS sensor and the longitudinal velocity from WSS;

4. GPS/INS/GL/YRS/WSS: with only one non-holonomic constraint on the upward direction. The longitudinal and lateral are both derived from the velocity from the WSS and the sideslip determined from the GL/YRS.

Gao [2006] has compared the above four strategies for the horizontal position estimation. Results show that strategies with external aiding sensors (strategies 2,

3 and 4) provide an estimation improvement of at least 80%. He also concludes that with a large sideslip of over 7 degrees, non-holonomic constraints in the lateral velocity are inappropriate as actual lateral velocity can no longer be assumed to be zero.

sKKF and nKKF

In a more recent paper, Travis and Bevly [2008] have revisited their previous model [Bevly et al. 2000; 2001] and successfully combined the sKKF and nKKF to form an expanded navigation model. This model takes the advantage of measurements in both the sensor and navigation frame, in which the EKF is described as:

$$\dot{\mathrm{x}} = \begin{bmatrix} \ddot{x}_v = A_x - b_x + \dot{y}_v(r_m - b_r) \\ \dot{b}_x = 0 \\ \ddot{y}_v = A_y - b_y - \dot{x}_v(r_m - b_r) \\ \dot{b}_y = 0 \\ \dot{\psi} = r_m - b_r \\ \dot{b}_r = 0 \\ \dot{\phi} = p_m - b_p \\ \dot{b}_\phi = 0 \\ \dot{x}_e = \sqrt{\dot{x}_v^2 + \dot{y}_v^2}\cos(\psi + \tan^{-1}(\frac{\dot{y}_v}{\dot{x}_v})) \\ \dot{y}_e = \sqrt{\dot{x}_v^2 + \dot{y}_v^2}\sin(\psi + \tan^{-1}(\frac{\dot{y}_v}{\dot{x}_v})) \end{bmatrix}, \mathrm{u} = \begin{bmatrix} A_x \\ A_y \\ r_m \\ p_m \end{bmatrix}, \mathrm{z} = \begin{bmatrix} \dot{x}_v^{gps} = V^{gps}\cos(\beta) \\ \dot{y}_v^{gps} = V^{gps}\sin(\beta) \\ \psi^{gps} \\ \phi^{gps} \\ x_e^{gps} \\ y_e^{gps} \end{bmatrix}, \tag{2.79}$$

where β can be estimated from either a single or dual GPS setup, and the roll, ϕ^{gps}, is captured by a dual GPS setup as described previously.

In general, KKF is more favourable towards industrial applications. This is mainly due to the fact that it does not require any physical vehicle parameters, such as the mass and cornering coefficients. Hence, KKF systems will be more economical and robust as they can be implemented for different vehicles without any readjustments. However, KKF suffers from inaccuracy when there is a GPS downtime. As pointed out by Travis and Bevly [2005; 2008], sideslip measurement/estimation is crucial for dynamic estimations in KKF, especially during GPS downtime. Since sideslip is derived from the heading and the course angle, and the heading is integrated from the yaw gyro, the course angle measurement becomes an essential measurement. Although magnetometers are capable of measuring the heading angle of the vehicle, Travis and Bevly [2005] have criticised it on the grounds of its

ineffectiveness for sideslip estimation. On the other hand WSS is able to aid the sideslip estimation but is restricted to constant slip during cornering.

2.6.2 GPS/INS Model-based Estimator

Another approach for state estimation is the MKF, which contains a vehicle dynamic model as described in Section 2.3. For simplicity and ease of implementation, MKF normally employs the 2DoF bicycle model. In addition, v-frame is normally assumed to be on the same plane as the b-frame, in which tilt angles, ϕ_{vb} and θ_{vb} are ignored resulting in $\phi_{eb} = \phi_{ev}$ and $\theta_{eb} = \theta_{ev}$. Unlike the KKF, MKF is very sensitive to the physical vehicle parameters. In Anderson and Bevly [2005], the yaw KKF and a 2DoF bicycle MKF is augmented to predict the sideslip, yaw rate, vehicle heading and gyro bias,

$$\dot{\mathrm{x}} = \mathbf{A}\mathrm{x} + \mathbf{B}\mathrm{u}$$

$$\begin{bmatrix} \dot{\beta} \\ \ddot{\psi} \\ \dot{\psi} \\ \dot{b}_r \end{bmatrix} = \begin{bmatrix} \frac{C_{yF}+C_{yR}}{mV} & \frac{aC_{yF}-bC_{yR}}{mV^2} - 1 & 0 & 0 \\ \frac{aC_{yF}-bC_{yR}}{J_{zz}} & \frac{a^2C_{yF}+b^2C_{yR}}{J_{zz}V} & 0 & 0 \\ 0 & 1 & 0 & 0 \\ 0 & 0 & 0 & 0 \end{bmatrix} \begin{bmatrix} \beta \\ \dot{\psi} \\ \psi \\ b_r \end{bmatrix} + \begin{bmatrix} \frac{-C_{yF}}{mV} \\ \frac{-aC_{yF}}{J_{zz}} \\ 0 \\ 0 \end{bmatrix} \delta \quad (2.80)$$

$$\mathrm{z} = \mathbf{C}\mathrm{x}$$

$$\begin{bmatrix} r_{gyro} \\ \nu_{gps} \end{bmatrix} = \begin{bmatrix} 0 & 1 & 0 & 1 \\ 1 & 0 & 1 & 0 \end{bmatrix} \begin{bmatrix} \beta \\ \dot{\psi} \\ \psi \\ b_r \end{bmatrix} \quad (2.81)$$

Anderson and Bevly [2005] have shown that with a single GPS antenna (measuring only course angle, $\nu = \psi + \beta$) and incorrect value of cornering coefficient, C_{yF} and C_{yR}, the MKF is unable to predict the sideslip with an acceptable accuracy. However, when a dual GPS antennae setup is used, the sideslip and yaw rate of the vehicle can be measured and C_{yF} and C_{yR} can be determined more accurately using

$$C_{yR} = \frac{mVr}{\left(\frac{b}{a}+1\right)\left(\beta - \frac{br}{V}\right)}; \qquad C_{yF} = \frac{bC_{yR}\left(\beta - \frac{br}{V}\right)}{a\left(\beta + \frac{ar}{V} - \delta\right)}. \quad (2.82)$$

With more accurate tyre cornering coefficients, the initial sideslip and yaw rate measurements from the dual GPS are improved through the MKF estimations. From

their work, it is clear that MKF is very sensitive to parameter accuracy.

Similar to the work by Anderson and Bevly [2005], Rock et al. [2005] have used a model-based approach for estimations. But instead of the MKF method, a model-based observer to combine the GPS and INS was used. Rock et al. [2005] extended the number of GPS to a triple antennae setup, allowing the system to measure the velocity with one antenna as well as sideslip and vehicle heading with two antennae. Estimations of sideslip and velocity agreed favourably with the measurements from a two axes optical sensor. Moreover, the GPS/INS setup is used to estimate the cornering coefficient, C_{yF} and C_{yR}, which are used in the observer design. The model of the observer in Rock et al. [2005] is based on the 2DoF bicycle model with states, $\mathrm{x} = \begin{bmatrix}\beta & \dot{\psi}\end{bmatrix}^T$. The state space representation for such an observer is,

$$\dot{\mathrm{x}} = \mathbf{A}\mathrm{x} + \mathbf{B}\mathrm{u}$$

$$\begin{bmatrix}\dot{\beta}\\ \ddot{\psi}\end{bmatrix} = \begin{bmatrix}\frac{C_{yF}+C_{yR}}{mV} & \frac{aC_{yF}-bC_{yR}}{mV^2} - 1\\ \frac{aC_{yF}-bC_{yR}}{J_{zz}} & \frac{a^2C_{yF}+b^2C_{yR}}{J_{zz}V}\end{bmatrix}\begin{bmatrix}\beta\\ \dot{\psi}\end{bmatrix} + \begin{bmatrix}\frac{-C_{yF}}{mV}\\ \frac{-aC_{yF}}{J_{zz}}\end{bmatrix}\delta \tag{2.83}$$

$$\mathrm{z} = \mathbf{C}\mathrm{x} + \mathbf{D}\mathrm{u}$$

$$\begin{bmatrix}A_y\\ r_m\end{bmatrix} = \begin{bmatrix}\frac{C_{yF}+C_{yR}}{m} & \frac{aC_{yF}-bC_{yR}}{m\dot{x}_v}\\ 0 & 1\end{bmatrix}\begin{bmatrix}\beta\\ \dot{\psi}\end{bmatrix} + \begin{bmatrix}\frac{-C_{yF}}{m}\\ 0\end{bmatrix}\delta. \tag{2.84}$$

This differs from the MKF in Anderson and Bevly [2005], Equations 2.80 to 2.81, by the measurement matrix, Equation 2.84. Note that the measurement matrix, $\mathbf{C}$, in Equation 2.84 is derived from the lateral acceleration Equation 2.2 with the assumption of small sideslip angle and constant longitudinal velocity, resulting in $A_y = \dot{x}_v(\dot{\beta} + \dot{\psi})$. The expression of $\dot{\beta}$ in Equation 2.83 is then inserted into this approximated lateral acceleration to obtain A_y in Equation 2.84. The measurement that is used for comparison in this case is not the GPS course angle, ν_{gps}, but rather the measurements from the lateral accelerometer, $\ddot{y}_{b,ins}$.

Although the 2DoF MKF is able to estimate sideslip and yaw rate as shown in Rock et al. [2005] and Anderson and Bevly [2005], it is restricted to manoeuvres on level ground. As briefly mentioned in Section 2.6.1, Ryu and Gerdes [2004*b*] incorporated a disturbance filter with the 2DoF MKF to estimate the vehicle roll and the bank angle. In general, the bank angle and the derivative of the roll gyro

are treated as disturbances with a relationship of,

$$\dot{\phi}_{ev} = \cos(\theta)p_m + \sin(\phi)\sin(\theta)q_m + \cos(\phi)\sin(\theta)r_m. \tag{2.85}$$

A further assumption on small pitch angle results in,

$$\begin{aligned}\dot{\phi}_{ev} &\approx p_m + \sin(\phi)\theta q_m + \cos(\phi)\theta r_m \\ &\approx p_m + \epsilon.\end{aligned} \tag{2.86}$$

Implementing this relationship into the MKF/disturbance filter, the state vector is defined as, $\begin{bmatrix}\beta & r_m & \phi_v & \dot{\phi}_v & \phi_{ev} & p_m & \dot{p}_m & \epsilon\end{bmatrix}^T$. Using the dual GPS antennae set-up as presented in Ryu et al. [2002], accurate yaw rate and sideslip angle can be estimated and used as reference measurements. With this, the sideslip estimation can be refined with estimations for the vehicle roll and road bank angle.

From Anderson and Bevly [2005] and Rock et al. [2005], one can see the importance of parameter accuracy in dynamic modelling. Having this in mind, Best et al. [2007] have taken one step further and designed an Identifying EKF (IEKF) to estimate vehicle parameters (i.e. mass, inertia, geometry). The IEKF is based upon his earlier work on real time state estimation without GPS [Best et al. 2000]. In Best et al. [2000], an Extended Adaptive KF (EAKF) is proposed, which has the ability not only to estimate the important dynamic states, but also important tyre parameters, namely the cornering coefficient (C_{yF} and C_{yR}). Best et al. [2000] have used a 4DoF (ψ, $\dot{y}_v$, $\dot{x}_v$ and ϕ_{eb}) bicycle model in their EAKF, the state vector does not only include the 5 states to be estimated, but also C_{yF} and C_{yR}:

$$\begin{bmatrix} \dot{\psi} \\ \ddot{y}_v \\ \ddot{x}_v \\ \ddot{\phi}_{eb} \\ \dot{\phi}_{eb} \\ - - - \\ \dot{C}_{yF} \\ \dot{C}_{yR} \end{bmatrix} = \begin{bmatrix} \\ \\ \mathbf{f}(\mathrm{x}(t)) \\ \\ \\ - - - - \\ 0_{(7\times7)} \\ 0_{(7\times7)} \end{bmatrix} \begin{bmatrix} \psi \\ \dot{y}_v \\ \dot{x}_v \\ \dot{\phi}_{eb} \\ \phi_{eb} \\ - - - \\ C_{yF} \\ C_{yR} \end{bmatrix} + \begin{bmatrix} \\ \mathrm{w}(t) \\ \\ \\ \\ - - - \\ \mathrm{w}_\alpha(t) \end{bmatrix} \tag{2.87}$$

The EAKF takes sensor measurements solely from five accelerometers on the vehicle and results show that EAKF is able to track the changing tyre characteristics, hence giving an improved performance over traditional KF. Note that the EAKF differs from the EKF in the covariance matrices. Any disturbance from the vehicle,

$\mathrm{w}(t)$, may cause noise in the sensor measurement, $\mathrm{v}(t)$. Thus, expectation of the correlation of noise and disturbance, $E(\mathrm{w}, \mathrm{v})$, can no longer be assumed to be zero.

With the assumption of accurate vehicle dynamic measurements in the v-frame, obtained from an expensive GPS/INS system, namely the RT3002 [OXTS 2008], Best et al. [2007] have taken the EAKF a step further and converted it into a parameter-based IEKF. In the IEKF, Best et al. [2007] have placed the parameters of the vehicle, namely the mass, m, the inertia, J_{zz}, and the distance from the cg to the front axle, a, in the state vector,

$$\begin{bmatrix} \dot{m} \\ \dot{J}_{zz} \\ \dot{a} \end{bmatrix} = \begin{bmatrix} \\ 0_{(3\times 3)} \\ \\ \end{bmatrix} \begin{bmatrix} m \\ J_{zz} \\ a \end{bmatrix} + \mathrm{w}(t) \tag{2.88}$$

Since vehicle parameters do not change abruptly during driving manoeuvres, it is assumed that their derivatives are zero and changes are only due to disturbances. With the IEKF predicting the vehicle parameters, the accurate vehicle dynamic measurements form the measurement vector and matrix, which is described by a bicycle model with a Pacejka non-linear tyre model,

$$\begin{bmatrix} \dot{y}_v \\ \\ \dot{\psi} \end{bmatrix} = \begin{bmatrix} \\ \mathbf{H(t)} \\ \\ \end{bmatrix} \begin{bmatrix} m \\ J_{zz} \\ a \end{bmatrix} + \mathrm{v}(t). \tag{2.89}$$

where: $\mathbf{H(t)}$is the Jacobian of the bicycle model, $\mathbf{h(t)}$, and,

$$\mathbf{h(t)} = \begin{cases} \dot{y}_v\Big|_k = \dot{y}_v\Big|_{k-1} + T_s \dfrac{F_{yF} + F_{yR}}{mM_0 - \dot{x}_v\dot{\psi}}\Big|_k \\ \dot{\psi}\Big|_k = \dot{\psi}\Big|_{k-1} + T_s \dfrac{aF_{yF} - (L-a)F_{yR}}{J_{zz}J_0}\Big|_k \end{cases}, \tag{2.90}$$

M_0 is the normalised mass,

J_0 is the normalised yaw moment of inertia.

Similar to the EAKF, measurement noise, $\mathrm{v}(t)$, is correlated with the disturbance in the state vector, $\mathrm{w}(t)$. Thus, the expectation, $E(\mathrm{w}, \mathrm{v})$, will not be zero. As shown in Best et al. [2007], the IEKF is able to converge to the vehicle parameters and a further three conclusions are reported in Best et al. [2007]:

1. Parameters to be estimated must be contained in a strictly smooth non-linear model, and the parameters must be independent of each other.

2. The filter depends on only two tuning parameters and self-regulates.

3. Varying the filter time constant allows the the filter to change its nature in off-line identification from a data set, or on-line parameter adaptation to compensate changes in the vehicle.

2.7 Non GPS-aided Estimator

In Section 2.7, the design and architecture of GPS/INS integrated estimators are described. Without GPS, estimators can utilise other measuring devices such as the WSS and/or vehicle model.

As commented in Liu et al. [2005], the purpose of GPS in an estimator is to limit the drifting errors caused by the INS integration. In the vast literature, there also exist other state estimation approaches that do not require the use of GPS measurements. These methods include the modelling of the INS drifting dynamics, the application of vehicle constraints, and the integration of odometer and gyros data.

2.7.1 Non GPS-aided Kinematic Estimator

In Liu et al. [2005], vehicle constraint is employed onto the vertical velocity, which is modelled as a Gaussian white noise with zero mean and variance,

$$\dot{z}_v = \mathrm{w}_z(0, \sigma_z^2). \tag{2.91}$$

Liu et al. [2005] have also derived the longitudinal and lateral velocities from the rear WSS alone, in which the rotational velocities of the left, ω_{RL}, and right, ω_{RR}, are measured and averaged:

$$\omega_R = \frac{1}{2}(\omega_{RL} + \omega_{RR}).$$

The velocities of the vehicle are then derived in terms of the average wheel rotation:

$$\dot{x}_v = \frac{\omega_R R}{R_{RR} + \frac{L}{2}} \times (R_{RR} + \frac{L}{2} - b_Q) \tag{2.92}$$

$$\dot{y}_v = \frac{\omega_R b_P R}{R_{RR} + \frac{L}{2}} \tag{2.93}$$

where R is the radius of wheel; L is the length of vehicle wheelbase; b_P is the longitudinal offset of INS; b_Q is the lateral offset of INS,; R_{RR} is defined as $\left(\frac{\omega_{RR} L}{\omega_{RL} - \omega_{RR}}\right)$.

Liu et al. [2005] have translated Equations 2.91 to 2.93 into the e-frame and implemented them into a KF. The state vector and measurement matrix of the KF are

$$\mathrm{x} = \begin{bmatrix} x_e \\ y_e \\ z_e \\ \dot{x}_e \\ \dot{y}_e \\ \dot{z}_e \\ \psi \end{bmatrix}, \quad \mathrm{z} = \mathbf{C}_{\mathbf{b}}^{\mathbf{e}} \begin{bmatrix} \dot{x}_b \\ \dot{y}_b \\ \dot{z}_b \\ \psi \end{bmatrix} = \begin{bmatrix} 0 & 0 & 0 & 1 & 0 & 0 & 0 \\ 0 & 0 & 0 & 0 & 1 & 0 & 0 \\ 0 & 0 & 0 & 0 & 0 & 1 & 0 \\ 0 & 0 & 0 & 0 & 0 & 0 & 1 \end{bmatrix} \begin{bmatrix} x_e \\ y_e \\ z_e \\ \dot{x}_e \\ \dot{y}_e \\ \dot{z}_e \\ \psi \end{bmatrix}, \tag{2.94}$$

where $\dot{x}_b$ and $\dot{y}_b$ are obtained from the odometers, $\dot{z}_b$ is the vehicle constraint in Equation 2.91 and ψ is measured with an accurate single-axis gyro. Experimental results from Liu et al. [2005] have shown that the proposed method is able to provide positions, velocities and heading information with reasonable accuracy without the aid of GPS. However, their model is tested only at a very low speed (6 m/s), and so there is a negligible longitudinal slip on the tyres for accurate velocities determination. Moreover, this model assumes a constant tyre radius, which will become invalid when the vehicle enters a corner at a higher speed.

An alternative approach for a non GPS-aided KE is presented in Chen and Hsieh [2008], in which the estimator design is based upon the INS model given by Equations 2.1 and 2.2 and that of the yaw rate gyro with disturbances ($\mathrm{w}_x, \mathrm{w}_y, \mathrm{w}_r$) added. These are recalled here:

$$\begin{aligned} A_x &= \ddot{x}_v - \dot{y}_v\dot{\psi} + \mathrm{w}_x \\ A_y &= \ddot{y}_v + \dot{x}_v\dot{\psi} + \mathrm{w}_y \\ r_m &= \dot{\psi} + \mathrm{w}_r \end{aligned}$$

Chen and Hsieh [2008] have used the above formulae to construct a discrete EKF with states $\dot{x}_v$ and $\dot{y}_v$:

$$\begin{aligned} \begin{bmatrix} \dot{x}_v \\ \dot{y}_v \end{bmatrix}_{k+1} = \begin{bmatrix} 1 & r_m T_s \\ -r_m T_s & 1 \end{bmatrix} \begin{bmatrix} \dot{x}_v \\ \dot{y}_v \end{bmatrix}_k + \begin{bmatrix} T_s & 0 \\ 0 & T_s \end{bmatrix} \begin{bmatrix} A_x \\ A_y \end{bmatrix}_k \\ + \begin{bmatrix} -\dot{y}_v T_s & -T_s & 0 \\ \dot{x}_v T_s & 0 & -T_s \end{bmatrix} \begin{bmatrix} \mathrm{w}_r \\ \mathrm{w}_x \\ \mathrm{w}_y \end{bmatrix}_k \end{aligned} \tag{2.95}$$

As noted from the above equation, the disturbance matrix contains states to be estimated and an EKF is used. The measurement of their estimator is taken from the longitudinal velocity derived from wheel rotational speed, ω_w, the gear ratio of the final drive, n_f and R:

$$\dot{x}_v^w = \omega_w n_f R = \begin{bmatrix} 1 & 0 \end{bmatrix} \begin{bmatrix} \dot{x}_v \\ \dot{y}_v \end{bmatrix}_k . \tag{2.96}$$

In the event of yaw rates lower than the specified threshold, $|r_k| < r_{th}$, the Kalman gain, $\mathbf{K}$, becomes zero, and the lateral velocity, $\dot{y}_v$, is determined using the vehicle model:

$$\begin{aligned} & \dot{y}_v = A_y - \dot{x}_v \dot{\psi}, \\ \text{where:} \quad & A_y = \frac{1}{m} \left\{ C_{yF} \left[\tan^{-1} \left(\frac{\dot{y}_v + a r_m}{\dot{x}_v} - \delta \right) \right] + C_{yR} \tan^{-1} \left(\frac{\dot{y}_v - b r_m}{\dot{x}_v} \right) \right\} \end{aligned}$$

Chen and Hsieh [2008] have evaluated their proposed estimator in a professional simulation software, CarSim®, under a Double Lane Change (DLC) and slalom manoeuvres. Simulation results have shown that the approach is able to provide an improvement on state estimations over Farrelly and Wellstead [1996] and Aoki et al. [2004]. Furthermore, Chen and Hsieh [2008] claim that their Kinematic-MEKF is able to overcome the error induced by inaccurate parameters, namely the cornering coefficients, C_{yF} and C_{yR}.

2.7.2 Non GPS-aided Model-based Estimator

Previously Chen and Hsieh [2008] have shown the implementation of MKF. In Cherouat et al. [2005], a LO has been designed to estimate vehicle sideslip and yaw rate. Their observer is very similar to that presented in Rock et al. [2005], and differs only by the inclusion of an extra yaw moment term generated by longitudinal force, M, and the steering control input, $\mathbf{\Delta}_k \delta$,

$$\begin{cases} \begin{bmatrix} \dot{\beta} \\ \ddot{\psi} \end{bmatrix} = \begin{bmatrix} \frac{C_{yF}+C_{yR}}{mV} & \frac{aC_{yF}-bC_{yR}}{mV^2} - 1 \\ \frac{aC_{yF}-bC_{yR}}{J_{zz}} & \frac{a^2C_{yF}+b^2C_{yR}}{J_{zz}V} \end{bmatrix} \begin{bmatrix} \beta \\ \dot{\psi} \end{bmatrix} + \begin{bmatrix} \frac{-C_{yF}}{mV} \\ \frac{-aC_{yF}}{J_{zz}} \end{bmatrix} \delta + \begin{bmatrix} \frac{-C_{yF}}{mV} & 0 \\ \frac{-aC_{yF}}{J_{zz}} & 1 \end{bmatrix} \begin{bmatrix} \mathbf{\Delta}_k \delta \\ M \end{bmatrix}; \\ \begin{bmatrix} A_y \end{bmatrix} = \begin{bmatrix} \frac{C_{yF}+C_{yR}}{m} & \frac{aC_{yF}-bC_{yR}}{mV} \end{bmatrix} \begin{bmatrix} \beta \\ \dot{\psi} \end{bmatrix} + \begin{bmatrix} \frac{-C_{yF}}{m} \end{bmatrix} \delta + \begin{bmatrix} \frac{-C_{yF}}{m} \end{bmatrix} \begin{bmatrix} \mathbf{\Delta}_k \mathbf{H}_k \delta \\ M \end{bmatrix}. \end{cases} \tag{2.97}$$

Moreover, the velocity, V, is defined with R, ω_w, and the two states, ψ and β,

$$V = R\omega_w - \psi\left(\frac{L}{2} - b\beta\right). \tag{2.98}$$

Cherouat et al. [2005] have incorporated the above into their observer model, Equation 2.97, to form a non-linear model. The model is linearised with the Jacobian and is stabilised with the use of a Lyapunov function. Estimation results from simulation have shown that the observer is able to reduce the noise from the accelerometer, A_y, and provides reasonable estimations for sideslip and yaw rate only when the steering angle is under 2 degrees. This is because the tyre dynamics are no longer in the linear region. For a better estimation, a more sophisticated tyre model must be used, such as the Fiala or the Pacejka (Magic) tyre models. It is well understood that the more closely the tyre model represents the true tyre dynamics, the more realistic the vehicle state estimations are. In Grip et al. [2007], a non-linear observer is designed based upon their previous work [Grip et al. 2006]. Their new observer does not use one fixed tyre model (i.e. Fiala or magic tyre), but a range of tyre models that allow the observer to adapt to the changing road surface conditions. Estimations results have shown that the observer is robust with respect to the changing errors in the model.

From the previous literature it is noticeable that the majority of MKF uses a 2DoF bicycle model. This model heavily simplifies the complete vehicle model and reduces a four wheeled vehicle to two wheeled. In critical driving condition (i.e. snow and rain, low μ), assumptions such as constant longitudinal velocity and evenly distributed weight on the left and right are no longer applicable. Slips and velocities on each wheel will be different and these will affect the overall state estimations of the vehicle. As a result, a higher order of vehicle model is required for improved estimations. In Wenzel et al. [2007] an extended four-wheel vehicle model (5DoF) is used for the MEKF design. The 5DoF model includes the longitudinal and lateral motions, and the three angular motions (namely ϕ, θ and ψ). The TMeasy tyre model is used which is not simply linear [Hirschberg et al. 2003]. Distinct from other state estimators, Wenzel et al. [2007] have additionally included parameter estimations in the state vector:

$$\mathrm{x} = \begin{bmatrix} \dot{x}_v & \dot{y}_v & a_y & \dot{\psi} & \dot{\phi} & \phi & \dot{\theta} & \theta & \alpha_{fl} & \alpha_{fr} & \alpha_{rl} & \alpha_{rr} & \ldots \\ & F_{zfl} & F_{zfr} & F_{zrl} & F_{zrr} & s_{fl} & s_{fr} & s_{rl} & s_{rr} & m & b & & \end{bmatrix}^T. \tag{2.99}$$

The inputs of the vehicle model are taken from the steering angle and WSS, and measurements are taken from the yaw rate gyro, lateral accelerometer and vehicle

velocity,

$$\mathrm{u} = \begin{bmatrix} \delta & \omega_{FL} & \omega_{FR} & \omega_{RL} & \omega_{RR} \end{bmatrix}^T \tag{2.100}$$

$$\mathbf{y} = \begin{bmatrix} r_m & A_y & v_x \end{bmatrix}^T \tag{2.101}$$

The estimations from the MEKF are then used to determine other unmeasureable variables in a vehicle, such as the true lateral acceleration and sideslip angle.

2.8 Conclusion

Of the four state estimation approaches described by Deng and Zhang [2006], the blended approach is the least expensive and is also the most reliable. Using GPS and in-car sensors, they are integrated in the estimator to determine vehicle dynamic states. Examples of such estimators includes fuzzy logic, ANN, KF and PF. As one of the purposes of the GPS/INS integrated system is to provide a real-time continual estimation in any vehicle model with minimal adjustments (via plug & play), techniques that requires a large amount of data and training, such as fuzzy logic and ANN, are unsuitable. Moreover, estimations currently used in vehicles are also considerably constrained by the amount of computational power. This makes the PF unsuitable. However, it is believed that in the future, when computational power has further reduced in cost, PF may become a good candidate for similar studies. At the moment, in the automotive industry, KF designs are the most popular and widely accepted estimation technique.

In general, there are two types of KF: the kinematic based (i.e. KKF) and the model-based (i.e. MKF). The KKF can be further categorised into the navigation frame-based (i.e. nKKF) and the sensor frame-based (i.e. sKKF). For simple KKF designs [Bevly et al. 2000; 2001], only yaw rate gyroscope, accelerometers and a GPS receiver are used to predict the sensor bias. In more complicated KKF estimators [Bae et al. 2001, Ryu et al. 2002, Ryu and Gerdes 2004*b*], pitch and roll gyroscopes are used with a set-up of dual GPS antennae. For the MKF designs, most literature [Anderson and Bevly 2005, Rock et al. 2005] use the 2DoF linear bicycle model. Although MKF is accurate in estimation, it is highly sensitive to the precision of the parameters and requires continual parameter estimations [Best et al. 2000; 2007].

To conclude, in the automotive industry where cost is one of the major concerns, it is unlikely that car manufacturers will increase the number and quality of sensors without a good justification of the benefit outcomes. Based on the constraint in cost, the most suitable KF designs from the vast literature are the KKF designed

by Bevly et al. [2000; 2001], in which they have based their simple KF design on a limited number of INS that are available in most existing vehicles and a 5Hz GPS receiver. Although other KKF designs [Bae et al. 2001, Ryu et al. 2002, Ryu and Gerdes 2004*b*] are better and more accurate, they require more sensors and GPS receivers, and hence, more costly. Other than KKF design, another cost effective KF design is the MKF. Although some good results are presented in [Anderson and Bevly 2005, Rock et al. 2005], they generally are parameter sensitive and would cause difficulties when transferring between different vehicles. As a result, this project is focused mainly on the design and use of the KKF and simple MKF (2DoF mainly with small number of parameters). Using the KF designs of Bevly et al. [2000] and Anderson and Bevly [2005] as a starting point, while utilising additional existed in-car sensors (e.g. the WSS and the Steer Wheel Sensor (SWS)) with low-cost GPS (1Hz) receiver, an innovative KF is designed and studied; not only its feasibility of estimating vehicle dynamic states is discussed, but also the benefit of having additional and better sensors through simulations.

Chapter 3

Vehicle Modelling

3.1 Introduction

The aim of this study is to show the suitability and quality of various vehicle models in representing a real vehicle. This is done in order to 1) provide a model for MKF, and 2) test against other KF designs, which closely represents the real vehicle in a controlled environment with added noise, disturbance and uncertainties. In general, the best vehicle model for the MKF design is the simplest model that captures the important dynamics of the vehicle with a sufficient accuracy. With the vertical, pitching and rolling motion ignored, these are the longitudinal, lateral and yaw dynamics of a vehicle.

In this chapter, there are seven sections. In the next section, the planar vehicle dynamic formulations for the bicycle and twin-track models are derived. Three most commonly used tyre model are also given in Section 3.3. By combining the tyre model and the vehicle dynamic formulations, five vehicle models are derived in Section 3.4. In order to compare the suitability of the vehicle models with a professional simulated programme, the main features of the IPG CarMaker are described in Section 3.5. The five vehicle models are compared with CarMaker in Section 3.6 and conclusions are drawn in the last section.

3.2 The Vehicle Dynamic Formulation

To reduce the complexity of the vehicle modelling, only the horizontal planar dynamics of the vehicle are considered. In other words, only the longitudinal and lateral direction (i.e. surge, sway and yaw motion) is of concern while the vertical, the pitching and the rolling motions of the vehicle are ignored. This reduction approach is suitable as vertical motion is negligible in the v-frame, and while the

vehicle is travelling at low velocity, pitching and rolling motion contributes little to the horizontal planar dynamics of a vehicle.

3.2.1 The Bicycle Model

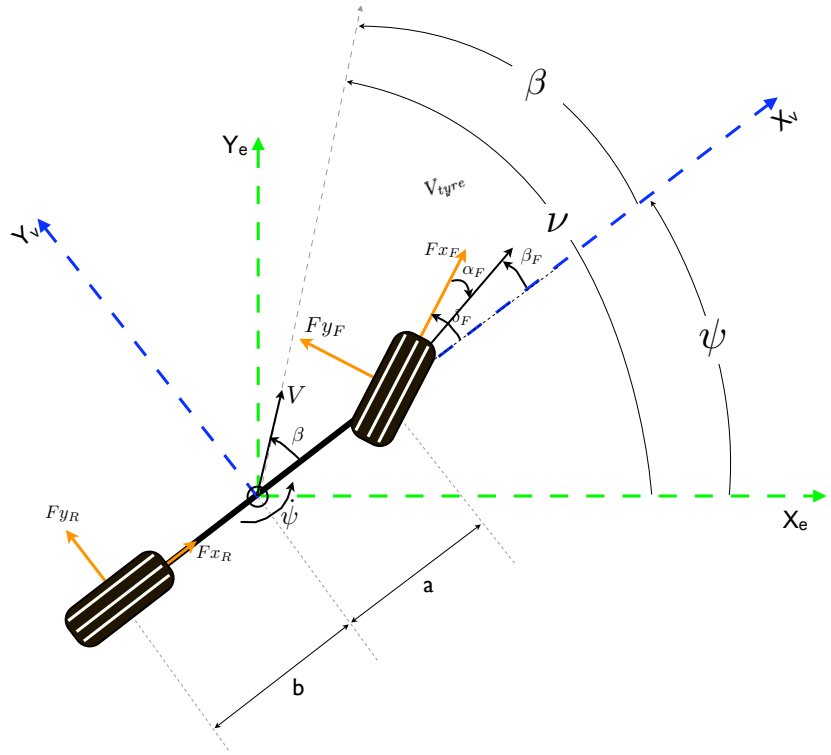

Figure 3.1: A typical bicycle model

Figure 3.1 shows a typical schematic diagram for the bicycle model. It reduces from four wheel to two wheels on the centre line, with assumptions such as constant longitudinal velocity and average tyre steering angle. These assumptions are further discussed in detail in Section 3.2.3. From Figure 3.1, the three equations of motion are:

longitudinal motion

$$
\begin{aligned}
mA_x = m\left(\ddot{x}_v - \dot{y}_v\dot{\psi}\right) &= \sum\left(F_{xF}^v + F_{xR}^v\right) \\
\ddot{x}_v = \frac{1}{m}&\left(m\dot{y}_v\dot{\psi} + F_{xF}\cos\delta_F + F_{xR}\cos\delta_R - F_{yF}\sin\delta_F - F_{yR}\sin\delta_R - F_{xA}\right)
\end{aligned}
\tag{3.1}
$$

$$
where \quad F_{xA} = \frac{1}{2}\rho C_d A_{aero} V^2
$$

lateral motion

$$mA_y = m\left(\ddot{y}_v + \dot{x}_v\dot{\psi}\right) = \sum\left(F_{yF}^v + F_{yR}^v\right)$$
$$\ddot{y}_v = \frac{1}{m}\left(-m\dot{x}_v\dot{\psi} + F_{xF}\sin\delta_F + F_{xR}\sin\delta_R + F_{yF}\cos\delta_F + F_{yR}\cos\delta_R\right) \quad (3.2)$$

rotation about the vertical axis - yaw motion

$$J_{zz}\ddot{\psi} = a\sum F_{yF}^v - b\sum F_{yR}^v$$
$$\ddot{\psi} = \frac{1}{J_{zz}}\left[a\left(F_{xF}\sin\delta_F + F_{yF}\cos\delta_F\right) - b\left(F_{xR}\sin\delta_R + F_{yR}\cos\delta_R\right)\right] \quad (3.3)$$

wheel angular motion - rear wheel drive

$$J_F\dot{\omega}_F = -R_F\sum F_{xF}$$
$$\dot{\omega}_F = -\frac{1}{J_F}\left(R_F F_{xF}\right) \quad (3.4)$$
$$J_R\dot{\omega}_R = \sum\tau - R_R\sum F_{xR}$$
$$\dot{\omega}_R = \frac{1}{J_R}\left(\tau_R - R_R F_{xR}\right) \quad (3.5)$$

3.2.2 The Twin-track Model

The twin-track model shown in Figure 3.2 considers all four tyres of the vehicle. Similar to the bicycle model, the twin track model has the three equations of motion in the longitudinal, lateral and yaw directions. However, the forces on the left and right are no longer assumed equal.

longitudinal motion

$$mA_x = m\left(\ddot{x}_v - \dot{y}_v\dot{\psi}\right) = \sum\left(F_{xF}^v + F_{xR}^v - F_{xA}\right)$$
$$\ddot{x}_v = \frac{1}{m}\Big(m\dot{y}_v\dot{\psi} + F_{xFL}\cos\delta_{FL} + F_{xFR}\cos\delta_{FR} + F_{xRL}\cos\delta_{RL} + F_{xRR}\cos\delta_{RR}$$
$$-F_{yFL}\sin\delta_{FL} - F_{yFR}\sin\delta_{FR} - F_{yRL}\sin\delta_{RL} - F_{yRR}\sin\delta_{RR} - F_{xA}\Big) \quad (3.6)$$

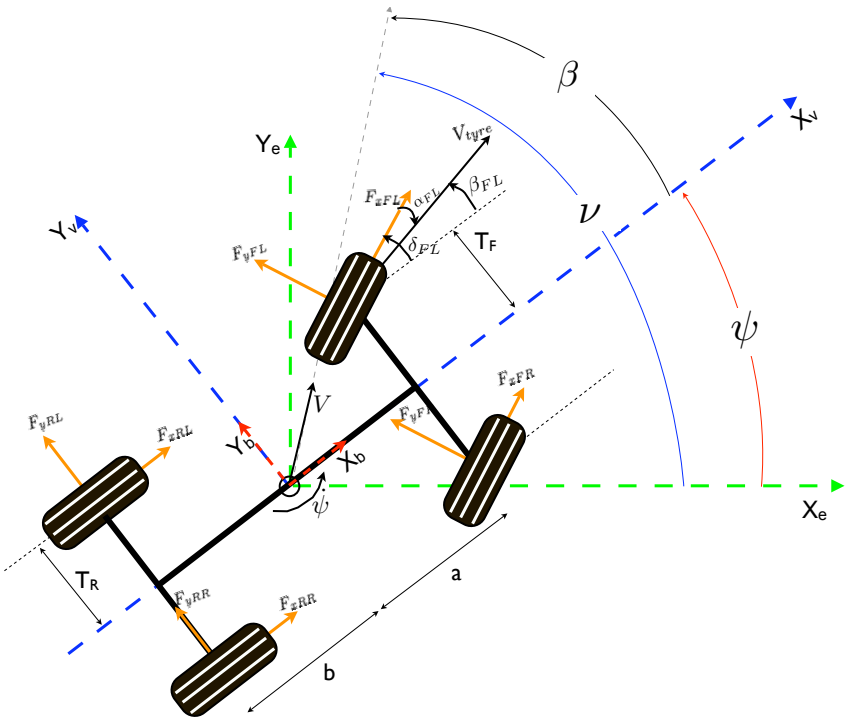

Figure 3.2: A typical twintrack model

lateral motion

$$
\begin{aligned}
mA_y = m\left(\ddot{y}_v + \dot{x}_v\dot{\psi}\right) &= \sum\left(F_{yF}^v + F_{yR}^v\right) \\
\ddot{y}_v = \frac{1}{m}\Big(&-m\dot{x}_v\dot{\psi} + F_{xFL}\sin\delta_{FL} + F_{xFR}\sin\delta_{FR} + F_{xRL}\sin\delta_{RL} + F_{xRR}\sin\delta_{RR} \\
&+F_{yFL}\cos\delta_{FL} + F_{yFR}\cos\delta_{FR} + F_{yRL}\cos\delta_{RL} + F_{yRR}\cos\delta_{RR}\Big)
\end{aligned}
\tag{3.7}
$$

rotation about the vertical axis - yaw motion

$$
\begin{aligned}
J_{zz}\ddot{\psi} &= a\sum F_{yF}^v - b\sum F_{yR}^v + T_F\sum F_{xF}^v + T_R\sum F_{xR}^v \\
\ddot{\psi} = \frac{1}{J_{zz}}\Big[&a\left(F_{xFL}\sin\delta_{FL} + F_{xFR}\sin\delta_{FR} + F_{yFL}\cos\delta_{FL} + F_{yFR}\cos\delta_{FR}\right) \\
&-b\left(F_{xRL}\sin\delta_{RL} + F_{xRR}\sin\delta_{RR} + F_{yRL}\cos\delta_{RL} + F_{yRR}\cos\delta_{RR}\right) \\
&+T_F\left(-F_{xFL}\cos\delta_{FL} + F_{xFR}\cos\delta_{FR} + F_{yFL}\sin\delta_{FL} - F_{yFR}\sin\delta_{FR}\right) \\
&+T_R\left(-F_{xRL}\cos\delta_{RL} + F_{xRR}\cos\delta_{RR} + F_{yRL}\sin\delta_{RL} - F_{yRR}\sin\delta_{RR}\right)\Big]
\end{aligned}
\tag{3.8}
$$

wheel angular motion - rear wheel drive

$$\dot{\omega}_{FL} = -\frac{1}{J_{FL}}\left(R_{FL}F_{xFL}\right) \tag{3.9}$$

$$\dot{\omega}_{FR} = -\frac{1}{J_{FL}}\left(R_{FR}F_{xFR}\right) \tag{3.10}$$

$$\dot{\omega}_{RL} = \frac{1}{J_{FL}}\left(\tau_{RL} - R_{RL}F_{xRL}\right) \tag{3.11}$$

$$\dot{\omega}_{RR} = \frac{1}{J_{FL}}\left(\tau_{RR} - R_{RR}F_{xRR}\right) \tag{3.12}$$

3.2.3 Model Complexity Reduction

For the bicycle and twin-track models, a large number of parameters and measurements are required to implement the model. Table 3.1 shows a summary of the parameters and measurements required for each type of model.

Table 3.1: Parameters and variables required for the bicycle and twin-track model

		Bicycle model	**Twin-track model**
parameters	a	√	√
	b	√	√
	m	√	√
	ρ	√	√
	C_d	√	√
	A_{aero}	√	√
	J_{zz}	√	√
	J_F	√	
	J_{FR}		√
	J_{FL}		√
	J_R	√	
	J_{RR}		√
	J_{RL}		√
	T_F		√
	T_R		√
	R_F	√	
	R_{FR}		√
	R_{FL}		√
	R_R	√	
	R_{RR}		√
	R_{RL}		√
	Total	**11**	**17**

		Bicycle model	**Twin-track model**
measurements	$\dot{x}_b$	√	√
	$\dot{y}_b$	√	√
	$\dot{\psi}$	√	√
	δ_F	√	
	δ_{FR}		√
	δ_{FL}		√
	δ_R	√	
	δ_{RR}		√
	δ_{RL}		√
	τ_F	√	
	τ_{RL}		√
	τ_{RLR}		√
	F_{xF}	√	
	F_{xFR}		√
	F_{xFL}		√
	F_{xR}	√	
	F_{xRR}		√
	F_{xRL}		√
	F_{yF}	√	
	F_{yFR}		√
	F_{yFL}		√
	F_{yR}	√	
	F_{yRR}		√
	F_{yRL}		√
	Total	**10**	**17**

Table 3.1 shows that the twin-track model requires nearly twice as many parameters and measurements as the bicycle model. Although some of the parameters

stay almost constant throughout the vehicle life, i.e. T_F and T_R, other parameters, such as the mass and tyre radii, vary with external vehicle weight distributions and affecting the dynamics of the vehicle. The large number of required variables shown in Table 3.1 can be reduced and the complexity of the equations of motions can be simplified with the following assumptions:

1. **constant longitudinal velocity** means zero longitudinal acceleration, $\ddot{x}_v = 0$. Together with small yaw rate and lateral velocity, $\dot{y}_v\dot{\psi} \approx 0$, this allows the removal of Equation 3.1 from the bicycle model and Equation 3.6 from the twin-track model. The zero longitudinal force assumption also simplifies the remaining equations of motion, reducing the number of required measurements to 8 and 13 for the bicycle and twin-track models respectively. The absence of longitudinal force also implies that the wheels are turning at a constant rotational velocity, thus, $\dot{\omega} \approx 0$. Furthermore, with zero longitudinal force, the aerodynamic (or drag) force, F_{xA}, is also reduced to zero.

2. **zero rear tyre angle**, δ_R, δ_{RL} and δ_{RR}, is a valid assumption as most production vehicles are front wheel steer only. Although there will be steer effects due to compliance in suspension and steer linkages, these errors are normally ignored in calculations. This assumption therefore allows further reduction in equation complexity, i.e. $\cos\delta_R = 1$ and $\sin\delta_R = 0$, and in the number of terms of the equations. With Assumptions 1 and 2, the equations are simplified, which required 8 and 13 measurements in the bicycle and twin-track model respectively.

3. **average tyre steering angle** assumes the steering on the front is equal to the average steering angle on the left and right, i.e. $\delta_F = \frac{1}{2}(\delta_{FR} + \delta_{FL})$. In a normal city vehicle, wheels are normally set with a toe-in approach. During straight road driving, lateral forces on the left and right tyres are equal but opposite, cancelling each other out and resulting in a zero lateral force. During a turn, the front lateral force can be approximated as the net difference between the lateral forces on the left and the right. This, in theory, is similar to taking the average between the left and right tyre steering angles, i.e. δ_F. Furthermore, with a small tyre steering angle assumption, its trigonometric function can measurable simplified to: $\cos\delta_F \approx 1$ and $\sin\delta_F \approx \delta_F$.

4. **infinitesimal tyre radius change** allows the reduction of parameters to 7 and 11 in a bicycle and twin-track model respectively. Although it is not true that the tyre radius stays constant while driving, typically varying with the

load distribution and the temperature, the change in the radius is small. On the other hand, as will be presented later in Section 4.3, tyre radius can be predicted using a KKF approach utilising GPS and INS.

5. **average torque output** means that the torque from the engine is assumed to be distributed evenly between the left and right wheels. With more sophisticated engines and power management, the assumption of even distribution may not be entirely valid. However, this assumption is aimed at simplifying the model for an average vehicle.

6. **small sideslip angle** at the centre of gravity and at the tyres allows sideslip to be approximated as the ratio of lateral to longitudinal velocity in the v-frame, i.e. $\beta \approx \frac{\dot{y}_v}{\dot{x}_v}$ and $\beta_w \approx \frac{\dot{y}_w}{\dot{x}_w}$.

7. **the time derivative of sideslip angle** can be approximated by using Assumptions 1 and 6, in which,

$$\beta \approx \frac{\dot{y}}{\dot{x}} \qquad \text{(Assumption 6)}$$

$$\dot{\beta} = \frac{\ddot{y}}{\dot{x}} - \frac{\ddot{x}\dot{y}}{\dot{x}^2} \approx \frac{\ddot{y}}{\dot{x}} \qquad \text{(Assumption 1)}$$

With these assumptions, the equation of motions can be simplified. However, one must bear in mind that the more assumptions made, the more details of the model are lost. Some of these simplifications may affect the dynamics of the vehicle significantly and designers must make judgements carefully and wisely. On the other hand, some of these variables are either not measurable or too expensive to measure. In such cases, estimation is required if knowledge of the variables/parameters is needed.

3.3 Tyre Modelling

Table 3.1 shows that nearly half of the measurements relate to the longitudinal and lateral forces on the tyres. These forces are dependent on the tyre characteristics and the friction between the tyre and the road. As a result selection of a suitable tyre model is very important as it provides an estimation of the forces in the vehicle model, which is vital to accurately estimate all states from a vehicle model.

It must be noted that different tyre models are derived from different parameters and under different assumptions. A good tyre model that fits one type of driving condition well does not necessarily mean that it is the best fit for other conditions.

Each model has its own advantages and limitations. Furthermore, it must be borne in mind that accuracy is not dependent on the number of parameters, but on continuous testing, modifying and research. Since there is no 'best' tyre model, each in-car Electronic Control Unit (ECU) may have a specific model to which it is best suited. The idea of having only one centralised global control unit that is adaptable to changing parameters is then apparent to the modelling of tyres.

This section is not concerned with how well a tyre model fits into a particular model, but rather gives a general overview of the three most popular tyre models used in the current literature: the linear model, the Fiala model and the 'Magic Formula' tyre. In order to give a more thorough background in tyre modelling, some experimental data of the tyre characteristics is first presented.

3.3.1 Tyre Characteristics Experiment

This experiment involves a tyre fixed at its centre and a moving platform, Figure 3.3. The tyre is restricted to rotate only about its lateral axis (i.e. rotating forward) and the platform can be rotated between ± 10 deg about the vertical axis. The rotated platform forms an angle, α, with the tyre, which is known as the slip angle, see Figure 3.3. It is well understood that the lateral force on a tyre has a close relationship with the slip angle.

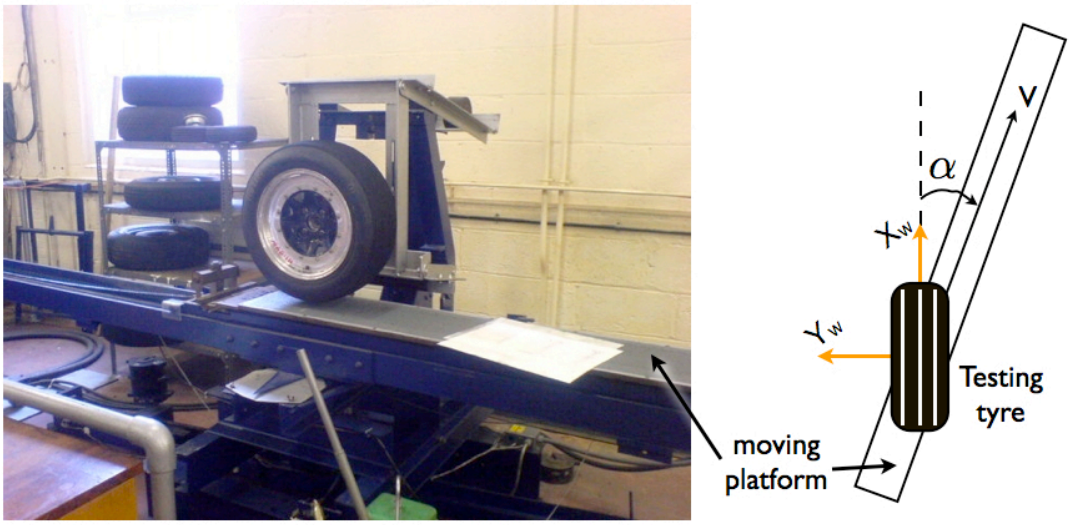

Figure 3.3: Moving platform for tyre characteristic testing, taken in Shrivenham, Cranfield.

During the experiment the platform runs from left to right to mimic the forward motion of a vehicle. Measurements for the displacement travelled and lateral force

are recorded.

Results

Three sets of experiments with different tyre pressures (18psi, 20psi and 22psi) are performed. For each set of experiments, the platform angle (i.e. slip angle) is varied from 0 to -8 degrees. Figures 3.4 and 3.5 show the results obtained from the experiment with the tyre pressure at 18psi.

As the displacement increases, the tyre accelerates to a constant velocity. As can be seen from Figure 3.4, the lateral force increases from the start and reaches a steady value after some distance of travel. Note that the more negative the slip angle is, the higher the lateral force. This is not hard to imagine because when the slip angle reaches 90 degrees, all forces on the moving platform are transferred to the negative lateral direction. Taking the steady state value of the lateral force for each slip angle, Figure 3.5 is constructed, which shows a typical curve when lateral force is plotted against the slip angle. The cornering coefficient for the tyre is the function that transforms the slip angle to the lateral force, $C = \mathbf{f}(F_y, \alpha)$. As clearly shown in Figure 3.5, the lateral force increases linearly with the slip angle initially between 0 to -2 degrees and then saturates to a steady constant after -6 degrees.

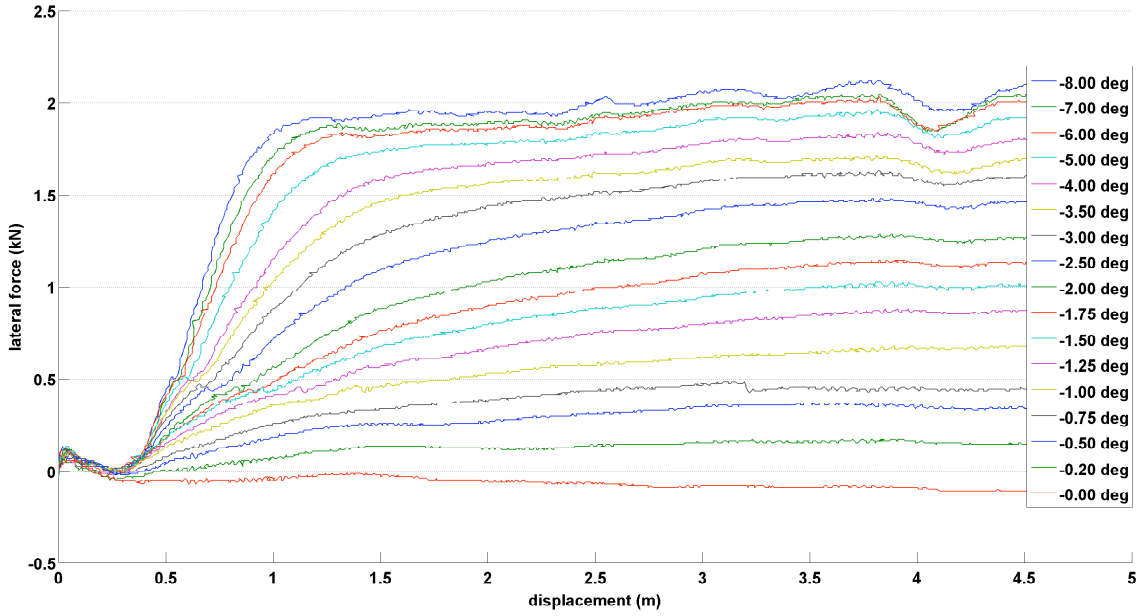

Figure 3.4: Lateral force variation with the change in slip angle at 18 psi tyre pressure

From Figure 3.5, one may notice that the curves do not intercept at the origin even when the slip angle is zero. This extra lateral force at zero slip angle is due to one or more of the following reasons: 1) the camber angle of the tyre, 2) the

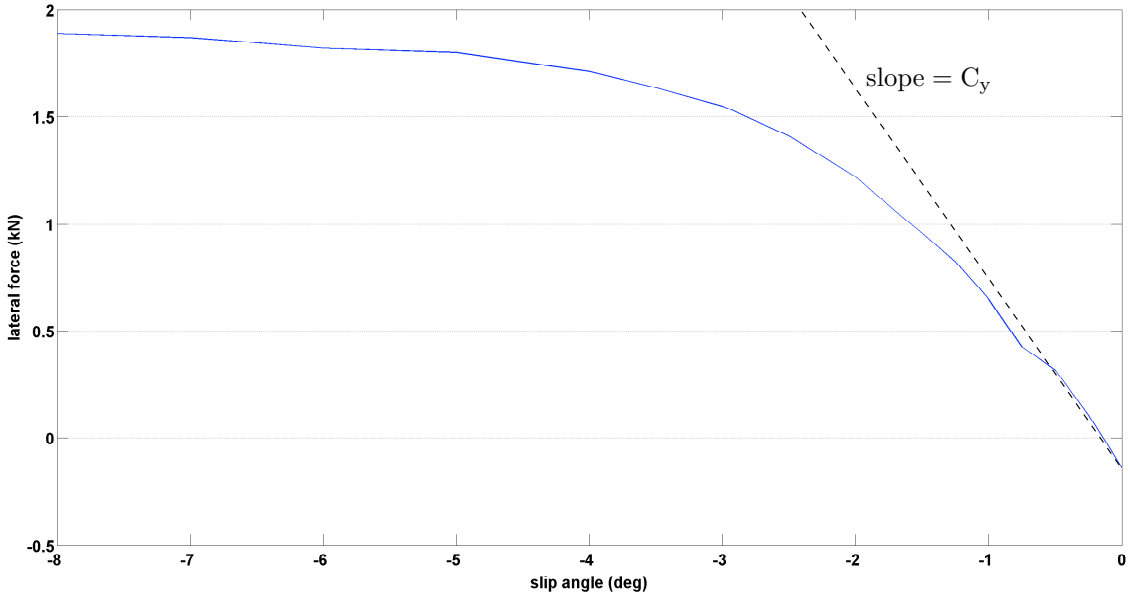

Figure 3.5: Saturated lateral force of tyre with 18 psi pressure

imperfection of the tyre, such as the surface and thread, 3) the conicity and ply steer, and 4) experimental errors.

3.3.2 The Linear Tyre Model

As shown in Figure 3.5, when the slip angle is small, the relationship of the lateral force and slip angle can be approximated by a linear relationship. The cornering stiffness is therefore the slope of the line. This tyre model is called the linear tyre model and is the simplest of its kind. By definition, the cornering stiffness, C_x and C_y, is related to the longitudinal and lateral cornering forces by the longitudinal slip angle, κ, and lateral slip angle, α:

$$F_x = C_x \kappa \tag{3.13}$$

$$F_y = C_y \alpha \tag{3.14}$$

Longitudinal slip, κ, depends on the motion of the vehicle, i.e. braking or driving. The definition of κ is given in Kiencke and Nielsen [2005] as,

$$\begin{cases} \textbf{Braking:} & \kappa_b = \dfrac{R\omega_w \cos\alpha - V_w}{V_w} \\ \textbf{Driving:} & \kappa_d = \dfrac{R\omega_w \cos\alpha - V_w}{R\omega_{tyre} \cos\alpha}. \end{cases} \tag{3.15}$$

From the two equations of κ, the required variables are all included in the list of

parameters and measurements in Table 3.1, no extra variables are required. The wheel angular speed, ω_w, can be derived from the equation of wheel rotation and/or measured from the WSS of the ABS module. The velocity at the wheel, V_w, is determined by transforming the velocities at the centre of gravity, $\dot{x}_v$ and $\dot{y}_v$, to individual wheels.

In the existing literature, the relationship of the lateral force with the cornering coefficient and slip angle, i.e. Equation 3.14, often includes a negative sign but without a clear explanation. The reason for this negative sign is due to the initial definition of the axis system. As discussed in Section 2.3.1, the ISO co-ordinate system is used and therefore anticlockwise rotation about an axis is defined as positive. Since the definition of slip angle, α, is the angle from the longitudinal body axis to the direction of travel of the body, the experimental set-up in Figure 3.3 then gives a slip in the clockwise direction – negative slip angle. Referring to Equation 3.14, a positive lateral force is achieved only with a negative cornering coefficient when the slip angle is negative, see also Figure 3.5. In many references, these cornering coefficients are set as a positive instead, so an additional negative sign is required in Equation 3.14.

From Figure 3.5, the linear tyre model works well only when the slip angle magnitude is less than 2 degrees. When the slip angle increases, the linear tyre model is no longer valid as the lateral force saturates. In such cases, alternative tyre models exist, such as the Fiala and the 'Magic Formula' models.

3.3.3 The Fiala Tyre Model

Figure 3.5 shows that in order to model the tyre cornering force more accurately, a non-linear model must be applied. One of the most common methods is the Fiala tyre model. As described in Blundell and Harty [2004], one major advantage of this model is that it only requires ten input variables (when compared to more than 30 inputs for the 'Magic Formula' tyre formula) and they are directly related to the physical properties of the tyres.

The standard formulations are not given here as they can be found in Blundell and Harty [2004]. In general, the determination of forces depends on two tyre states: the elastic deformation state and the sliding state. By comparing the longitudinal slip, κ, and the lateral slip, α, with the calculated critical slips, κ^* and α^*, respectively, the tyre state can be determined. With the state identified, different formulations are applied and the longitudinal force, the lateral force, the resistance moment and the aligning moment are obtained. Although the Fiala tyre model is able to produce a good prediction, as described by Blundell and Harty [2004], this

model suffers from limitations such as:

1. the inability to model complex dynamics that involve both cornering and braking, or cornering with driving;

2. forces and moments caused by the camber angle not being modelled;

3. the change in cornering stiffness at zero slip angle where tyre force is not considered;

4. the offsets in forces or moments caused by coincity and ply steer at zero slip angle not being represented.

3.3.4 The 'Magic Formula' Tyre Model

The 'Magic Formula' tyre model was developed in 1986 and 1989 by Bakker et al. [1989] and later modified by Pacejka and Bakker [1993]. Researchers continue to build around this model, adding more useful and meaningful interpretations. To date, the 'Magic Formula' tyre model has been enhanced by Pacejka and Besselink [1997] to allow it to operate with small slip angles as well as backward manoeuvres.

As the name of the tyre model suggests, it involves a series of formulas which calculate the tyre dynamics 'magically'. These 'magic' components of the model are the coefficients used in the formulas which have neither relationship with tyre engineering nor any physical meaning. They are merely coefficients used for polynomial curve fittings. In fact, the original idea of the 'Magic Formula' [Bakker et al. 1986] was not to predict, but to fit a curve onto tyre models based upon polynomials and Fourier series techniques. Although the coefficient inputs of the 'Magic Formula' tyre model do not explain much about tyres, with structured measure test data, these coefficients can be interpreted, giving a good correlation with the tyre dynamics [Bakker et al. 1989, Makita and Torii 1992].

The 'Magic Formula' tyre model has different versions. In the later version of Pacejka and Bakker [1993], four sets of formulas exist: a set of general formula and three other sets for the longitudinal force, the lateral force and the aligning moment. Altogether, there are over 30 input coefficients to be interpreted before implementing the tyre model. For detail of the 'Magic Formula' tyre model, one can refer to Blundell and Harty [2004] and Genta [2003] for data on 'Magic Formula' coefficients.

3.4 The Simplified Vehicle Model

Sections 3.2 and 3.3 have given the basis for constructing a vehicle model. The number of degrees of freedom of the vehicle model depends on how many equations of motion are used. In this section, four different vehicle models with different degrees of freedom are presented. Their general formulation are based on those described in Section 3.2.

As stated at the beginning of this chapter, the main focus for this study is the suitability of different vehicle models for state estimations. Ultimately, the vehicle model must also be universal to any type of vehicle and tyre, so it can be used as a kind of 'plug-and-play' state estimator. For this reason, the linear tyre model is best suited for this purpose as it requires the fewest parameters. Therefore the vehicle models presented in this section uses the linear tyre model.

3.4.1 The Two Degrees of Freedom Model

The two degrees of freedom model is the simplest vehicle model used for evaluating vehicle dynamics. It is based on the bicycle model and assumes constant longitudinal velocity, $\dot{x}_v = V$, (i.e. zero longitudinal force and zero wheel angular acceleration). Hence, the five equations of motion reduce to two. Therefore, the 2DoF are the lateral motion and the rotation motion, Equations 3.2 and 3.3 respectively. In additional, applying the small rear steer angle, resulting in,

lateral motion

$$\ddot{y}_v = \frac{1}{m}\left(-m\dot{x}_v\dot{\psi} + F_{yF} + F_{yR}\right)$$

rotation about the vertical axis - yaw motion

$$\ddot{\psi} = \frac{1}{J_{zz}}\left(aF_{yF} - bF_{yR}\right)$$

The lateral force on the tyres are calculated with the linear tyre model, thus,

$$F_{yF} = C_{yF}\alpha_F; \tag{3.16}$$

$$F_{yR} = C_{yR}\alpha_R. \tag{3.17}$$

The cornering coefficient for a single tyre is normally pre-determined from a tyre test similar to the one shown in Section 3.3. The determined value must then be doubled to give the axle cornering stiffness as required in Equations 3.16 and 3.17. This is because the tyre test only accounts for a single tyre.

Referring back to Figure 3.1 and as described in Section 3.3, the slip angle is defined as the difference between the sideslip angle and the steering angle at the tyres. Note that the sideslip at the tyres is not the same as that at the centre of gravity, β, due to the difference in velocities at the tyres. Therefore, applying the small sideslip assumption, slip at the tyres can be approximated as,

$$\begin{aligned} \alpha_F &= \beta_F - \delta_F \\ &\approx \frac{\dot{y}_v + a\dot{\psi}}{\dot{x}_v} - \delta_F = \beta + \frac{a\dot{\psi}}{\dot{x}_v} - \delta_F \end{aligned} \tag{3.18}$$

$$\begin{aligned} \alpha_R &= \beta_R \\ &\approx \frac{\dot{y}_v - b\dot{\psi}}{\dot{x}_v} = \beta - \frac{b\dot{\psi}}{\dot{x}_v} \end{aligned} \tag{3.19}$$

Combining Equations 3.16 to 3.19, putting them into the two equations of motion and finally approximating $\ddot{y}_v \approx \dot{\beta}\dot{x}_v$, the state space representation is:

$$\begin{bmatrix} \dot{\beta} \\ \ddot{\psi} \end{bmatrix} = \begin{bmatrix} \frac{C_{yF}+C_{yR}}{mV} & \frac{aC_{yF}-bC_{yR}}{mV^2} - 1 \\ \frac{aC_{yF}-bC_{yR}}{J_{zz}} & \frac{a^2C_{yF}-b^2C_{yR}}{J_{zz}V} \end{bmatrix} \begin{bmatrix} \beta \\ \dot{\psi} \end{bmatrix} + \begin{bmatrix} \frac{-C_{yF}}{mV} \\ \frac{-aC_{yF}}{J_{zz}} \end{bmatrix} \delta_F \tag{3.20}$$

From the state-space model in Equation 3.20, the input is the tyre steering angle, δ_F and the states are the sideslip and the yaw rate, $\begin{bmatrix} \beta & \dot{\psi} \end{bmatrix}^T$. This model is very popular with automotive manufacturers as it is simple, easy to implement and requires relatively few parameters.

3.4.2 The Three Degrees of Freedom Model

The 3DoF model also uses the bicycle model as a basis and makes the same assumptions as the 2DoF except constant longitudinal velocity. Therefore, the 3DoF model takes the longitudinal motion into consideration as well. With this configuration, the longitudinal acceleration is no longer restricted to zero, allowing both longitudinal force, F_x, and wheel angular acceleration, $\dot{\omega}$, to be non-zero.

The 3DoF model focuses on the dynamic behaviour of the vehicle body, so the wheel angular dynamics are de-coupled and ignored. The three degrees of freedom are therefore:

longitudinal motion

$$\ddot{x}_v = \frac{1}{m}\left(m\dot{y}_v\dot{\psi} + F_{xF} + F_{xR} - F_{yF}\delta_F - F_{xA}\right)$$

lateral motion

$$\ddot{y}_v = \frac{1}{m}\left(-m\dot{x}_v\dot{\psi} + F_{xF}\delta_F + F_{yF} + F_{yR}\right)$$

rotation about the vertical axis - yaw motion

$$\ddot{\psi} = \frac{1}{J_{zz}}\left[a\left(F_{xF}\delta_F + F_{yF}\right) - bF_{yR}\right]$$

As for the 2DoF bicycle model, the lateral force in the 3DoF model uses the same formula. The cornering coefficients and slip angles are also determined using the same method and formulas as previously described for the 2DoF model, see Equations 3.16 to 3.19. The longitudinal force, as discussed in Section 3.3, has a formula of $F_x = C_x\kappa$. The longitudinal slip, κ, as Equation 3.15 stated, is calculated depending on whether the vehicle is braking or driving. Applying the small angle approximation on the slip angle, $\cos\alpha = 1$, the two equations can be simplified,

$$\begin{aligned} \textbf{Braking:} \qquad \kappa_b &= \frac{R\omega_w - V_w}{V_w} \\ \textbf{Driving:} \qquad \kappa_d &= \frac{R\omega_w - V_w}{R\omega_{tyre}}. \end{aligned}$$

The velocities at the wheels are calculated from the velocities at the cg,

$$\begin{cases} V_{wF} = \sqrt{\dot{x}_v^2 + \left(\dot{y}_v + a\dot{\psi}\right)^2} \\ V_{wR} = \dot{x}_v \end{cases} \tag{3.21}$$

Since the wheel angular dynamics are not considered in the 3DoF model, the wheel angular velocity is measured from the WSS. Similar to the lateral force, the front or rear longitudinal force in a bicycle model accounts for two tyres and normally the determination of the coefficient is for a single tyre. Thus, C_{xF} and C_{xR} is roughly double that measured from experiment. From the equations of longitudinal slip, another parameter required is the radius of the tyre. As commented in Section 3.2, the radius is assumed to be constant. Any variations in the tyre can be captured by a KKF, which is discussed in Section 4.3.

Combining all the formulas into the three equations of motion, one can see that

the 3DoF bicycle model is a set of non-linear equations. Moreover, the 3DoF model also requires four extra parameters (R_F, R_R, C_{xF} and C_{xR}) and two additional measurements (ω_F and ω_R) for determining the longitudinal force.

3.4.3 The Five Degrees of Freedom Model

The 5DoF model is also based upon the bicycle model, which considers all five equations of motion. With the same assumptions made in the 3DoF model, the equations for the five degrees of freedom simplify to:

longitudinal motion

$$\ddot{x}_v = \frac{1}{m}\left(m\dot{y}_v\dot{\psi} + F_{xF} + F_{xR} - F_{yF}\delta_F - F_{xA}\right)$$

lateral motion

$$\ddot{y}_v = \frac{1}{m}\left(-m\dot{x}_v\dot{\psi} + F_{xF}\delta_F + F_{yF} + F_{yR}\right)$$

rotation about the vertical axis - yaw motion

$$\ddot{\psi} = \frac{1}{J_{zz}}\left[a\left(F_{xF}\delta_F + F_{yF}\right) - bF_{yR}\right]$$

wheel angular motion - rear wheel drive

$$\dot{\omega}_F = -\frac{1}{J_F}\left(R_F F_{xF}\right)$$
$$\dot{\omega}_R = \frac{1}{J_R}\left(\tau_R - R_R F_{xR}\right)$$

The main difference between a 5DoF and 3DoF model is the inclusion of the wheel angular motion. Previously in the 3DoF model, the longitudinal forces require measurements from the WSS to determine the wheel angular speed. With the 5DoF model, ω_F and ω_R can be determined from the two equations of wheel angular motion. Therefore, the number of input measurements reduces to two, δ_F and τ_F. We should remember here that τ_F is the total torque applied on two wheels as this is a bicycle model. Similar to the 3DoF bicycle mode, the 5DoF model is non-linear and cannot be written in the form of a linear state-space representation.

3.4.4 The Seven Degree of Freedom Model

With the bicycle model described in Section 3.2, the maximum degrees of freedom is five. The 7DoF model is based on the twin-track model, in which the dynamics

of the four wheels are considered. With the small angle assumption and zero rear wheel steer, the equations of motion for the twin-track are simplified to,

longitudinal motion

$$\ddot{x}_v = \frac{1}{m}\left(m\dot{y}_v\dot{\psi} + F_{xFL} + F_{xFR} + F_{xRL} + F_{xRR} - F_{yFL}\delta_{FL} - F_{yFR}\delta_{FR} - F_{xA}\right)$$

lateral motion

$$\ddot{y}_v = \frac{1}{m}\left(-m\dot{x}_v\dot{\psi} + F_{xFL}\delta_{FL} + F_{xFR}\delta_{FR} + F_{yFL} + F_{yFR} + F_{yRL} + F_{yRR}\right)$$

rotation about the vertical axis - yaw motion

$$\begin{aligned}\ddot{\psi} = \frac{1}{J_{zz}}\,[&a\left(F_{xFL}\delta_{FL} + F_{xFR}\delta_{FR} + F_{yFL} + F_{yFR}\right) - b\left(F_{yRL} + F_{yRR}\right)\\ &+T_F\left(-F_{xFL} + F_{xFR} + F_{yFL}\delta_{FL} - F_{yFR}\delta_{FR}\right) + T_R\left(-F_{xRL} + F_{xRR}\right)]\end{aligned}$$

wheel angular motion - rear wheel drive

$$\begin{aligned}\dot{\omega}_{FL} &= -\frac{1}{J_{FL}}\left(R_{FL}F_{xFL}\right)\\ \dot{\omega}_{FR} &= -\frac{1}{J_{FL}}\left(R_{FR}F_{xFR}\right)\\ \dot{\omega}_{RL} &= \frac{1}{J_{FL}}\left(\tau_{RL} - R_{RL}F_{xRL}\right)\\ \dot{\omega}_{RR} &= \frac{1}{J_{FL}}\left(\tau_{RR} - R_{RR}F_{xRR}\right)\end{aligned}$$

In fact, if the wheel angular motion is ignored, the vehicle model is reduced from a 7DoF to a 3DoF twin-track model. For the twin-track model, the formulas for the sideslip angle and both longitudinal and lateral slip angles are different to those used for the bicycle model, as velocity at the left and right tyres is no longer assumed to be equal. Referring back to Figure 3.2, the longitudinal and lateral velocities at the tyres in the v-frame are,

$$\begin{cases}\dot{x}_{FL} = \dot{x}_v - T_F\dot{\psi} & \dot{y}_{FL} = \dot{y}_v + a\dot{\psi}\\ \dot{x}_{FR} = \dot{x}_v + T_F\dot{\psi} & \dot{y}_{FR} = \dot{y}_v + a\dot{\psi}\\ \dot{x}_{RL} = \dot{x}_v - T_R\dot{\psi} & \dot{y}_{RL} = \dot{y}_v - b\dot{\psi}\\ \dot{x}_{RR} = \dot{x}_v + T_R\dot{\psi} & \dot{y}_{RR} = \dot{y}_v - b\dot{\psi}\\ V_w = \dot{x}_w & \text{where: } \circledast_w \text{ is the index for the tyres}\end{cases} \tag{3.22}$$

The sideslip for individual wheels is, therefore, defined as the ratio of the lateral

velocity to the longitudinal velocity when sideslip is small.

$$\beta_{FL} \approx \frac{\dot{y}_v + a\dot{\psi}}{\dot{x}_v - T_F\dot{\psi}} \tag{3.23}$$

$$\beta_{FR} \approx \frac{\dot{y}_v + a\dot{\psi}}{\dot{x}_v + T_F\dot{\psi}} \tag{3.24}$$

$$\beta_{RL} \approx \frac{\dot{y}_v - b\dot{\psi}}{\dot{x}_v - T_R\dot{\psi}} \tag{3.25}$$

$$\beta_{RR} \approx \frac{\dot{y}_v - b\dot{\psi}}{\dot{x}_v + T_R\dot{\psi}} \tag{3.26}$$

With the velocities and sideslip determined at the tyres, the longitudinal and lateral slip angles can be calculated. As the forces in the twin-track model act on a single wheel, the cornering and slip coefficients obtained from experiments or estimations can be implemented directly into the formulation. Similarly, the torque applied on the wheel is measured individually and not as the total.

3.5 Professional Car Simulator, IPG CarMaker

In this project, sensor signals and reference measurements are taken from a virtual vehicle under a simulation environment, IPG CarMaker. This is done so that the external environment is controlled and stay consistent throughout each simulation/experiment. In addition, this also allows a more extensive access to vehicle dynamic information at any location of the virtual vehicle, thus encouraging a more thorough understanding of the vehicle behaviour in different manoeuvres and driving conditions.

The main purpose of CarMaker is to offer a simulated environment for the test and development of control systems, components and complete vehicles [*IPG CarMaker* 2009]. At the highest level, CarMaker is divided into two versions: the standalone version and the MATLAB/Simulink version. While the standalone version allows quick analysis of a pre-design vehicle model, the MATLAB/Simulink version provides more freedom in measuring dynamic data, and designing new and existing control algorithms.

For both versions of the CarMaker, there are generally four main areas that require special attention in this project before running the simulations:

1. the vehicle model,

2. the tyre model,

3. the driving manoeuvre, and

4. the data collection.

Over the next subsections, a brief introduction for each subsystem is given. Moreover, comments related to the use of CarMaker for this project are also given.

3.5.1 The Vehicle Model

CarMaker utilises a 14 DoF vehicle model (i.e. 6 DoF in the 3 body axes and 2 DoF on each wheels). It is made up of the vehicle chassis (geometry, masses and inertia), the steering system, the suspension system, the braking system, the aerodynamics, and the power-train system. Users are required to defined all the vehicle parameters before any simulations. Fortunately, default values for different types of cars (e.g. Saloon and Luxury) are also provided in order to reduce the mundane work on data input.

CarMaker has 3 coordinate systems; one is fixed on the earth of the 'virtual world' (Fr0, e-frame equivalent), one is fixed at the rear of the moving vehicle body (Fr1, v-frame equivalent), and a further four are fixed at the centre of each wheel (Fr2), see Figure 3.6. When collecting and analysing the data, the definition of the coordinate system becomes crucial.

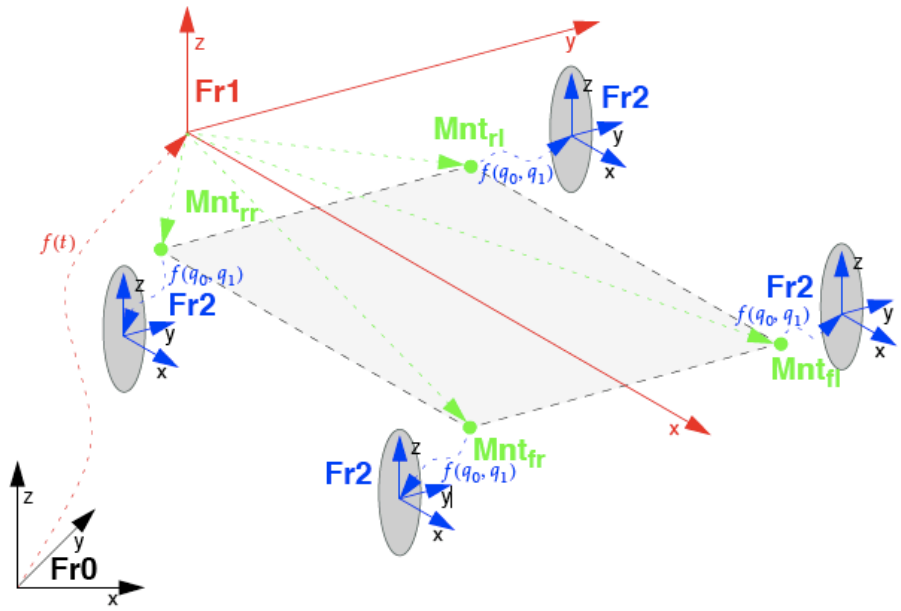

Figure 3.6: CarMaker coordinate systems [*IPG CarMaker* 2009]

3.5.2 The Tyre Model

In any vehicle model, the tyre model is the most critical as it provides the relation between the road and the chassis.

By default, CarMaker uses its own tyre model called the Real Time Tire (RT-Tire) model. This in-house model is more sophisticated than a series of look-up tables, it reads tyre measurement data and converts the data for use in the tyre model calculations, which makes a two-dimensional grid interpolation using spline coefficients for drive forces and a plausible generation of lateral forces, brake forces and the self aligning torque.

Apart from the RT-Tire model, users are also given the option of using the magic tyre model or their own designed tyre model. The magic tyre model is pre-programmed in CarMaker but the self-designed tyre model requires use of the MATLAB/Simulink for implementation. In this project, the RT-Tire model is used, so the CarMaker model is as representative of a real vehicle as possible with the dynamic behaviour in reality under a controlled environment.

3.5.3 The Driving Manoeuvre

After defining the vehicle chassis and its tyres the next step is to construct a manoeuvre for the virtual vehicle to perform. In general, the driving manoeuvre contains two elements that need to be defined: 1) the course, and 2) the longitudinal and lateral dynamics manoeuvres.

For the course, the track can either be imported digitally or built in CarMaker by specifying different segments of the road. In the latter case, users are given three types of road segments to choose from: a straight line, a curve (i.e. circular arc) or a clothoid (i.e. transition from straight to curve). By choosing the road segments and specifying their geometry (i.e. length of the segment, angle of the segment, radius of turn, gradient of road climb, slope of road tilt and camber for the curvature of the road), the simulation track is constructed. Moreover, additional features are also provided by CarMaker to add extra complexity to the defined track. These features include: 1) friction strip, 2) side winds, 3) velocity signs, and 4) obstacles (e.g. cylinders, beams, waves and cones).

After the simulation track is defined, the longitudinal and lateral dynamics of the manoeuvre must also be specified. By default, the dynamics of the virtual vehicle are controlled by the driver model provided in CarMaker. This model consists of two types of drivers – standard driver and racer driver; depending on the type of driver and the driver parameters (e.g. maximum cruising speed, the corner cutting

coefficient) the virtual vehicle is driven in different ways. Additionally, manoeuvre dynamics can also be specified without the use of a driver model. In such case, the longitudinal and lateral dynamics must be defined. For the longitudinal dynamics, users can manually control the speed, the acceleration or the gas and brake pedals. For the lateral dynamics, users can choose from having a sinus steering, a step steering or a steer control.

3.5.4 The Data Collection

There are two ways of collecting simulation data from CarMaker. One way is to output the required data from CarMaker into a data file during the simulation. Another way is to run CarMaker from MATLAB/Simulink and read and output the data into the workspace in MATLAB.

When collecting the vehicle data directly from CarMaker, data is recorded in a special format. This then requires a specific MATLAB programme (i.e. an m-file) to interpret and extract the data. On the other hand, when data is extracted directly from MATLAB/Simulink, the process of interpretation is omitted. Another benefit of using the MATLAB/Simulink version is that it allows sensor measurements to be collected from any position on the virtual vehicle by specifying the location of the sensor.

In this project simulations are based primarily on the MATLAB/Simulink version. Sensors are defined at various locations on the virtual vehicle and their measurements are returned to CarMaker and collected in a specific data file together with other dynamic data.

3.5.5 CarMaker in relation to the project

Due to inaccessible experimental instruments, this project is mainly concentrated on the performance of estimators in a simulated environment. This method is limited by the fact that simulation environment is controlled, and it differs from the real world by additional assumptions and reduced uncertainties. A developed system that operates well in a simulation may not necessarily work as it should be when transferred to the real world environment. In this project, therefore, noise and disturbance are introduced to the simulation measurements in order to represent the real world data as closely as possible.

For the vehicle and tyre parameters used in this project, Appendix A, they are collected from a previous study of Tardy [2007], in which he has validated his 3DoF (lateral, yaw and roll) bicycle model with the IPG CarMaker model. Using the

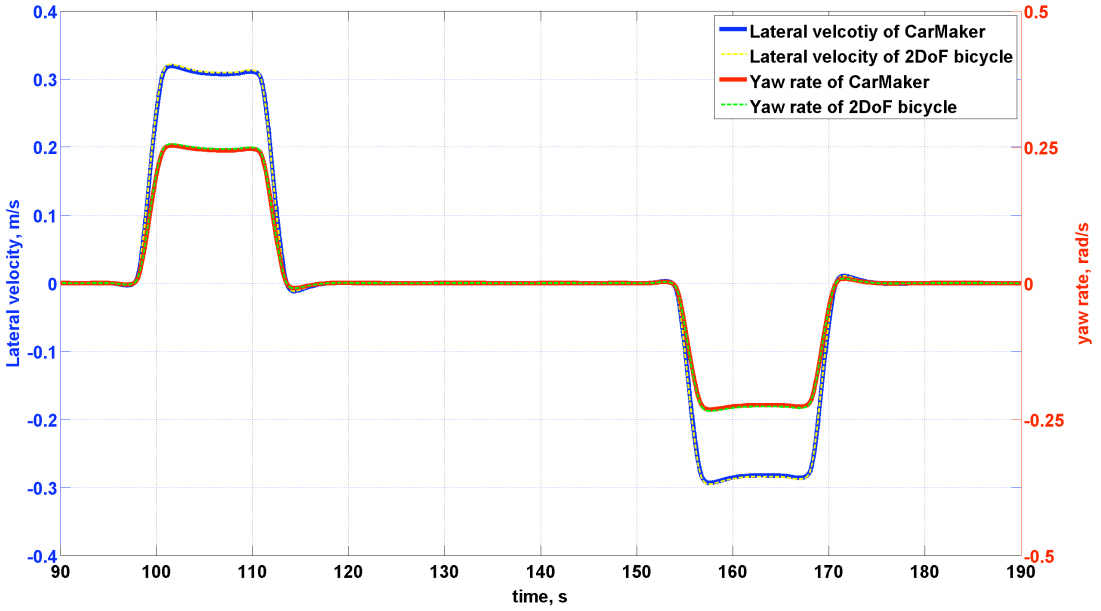

Figure 3.7: Lateral velocity and yaw rate of 2DoF bicycle model and CarMaker, section of *DoubleOval_25kph*

same set of vehicle and tyre parameters, the 2DoF bicycle model described earlier is validated with the CarMaker model on the *DoubleOval* track at 25kph, Figure 3.7. The results show that at 25kph, the lateral velocity and yaw rate of the 2DoF model are similar to that of the CarMaker model.

In this project, the longitudinal dynamics of the virtual vehicle in CarMaker is executed by a constant speed; and the lateral dynamics is carried out by the standard driver model in CarMaker with minimum corner cutting steering behaviour. As already described, virtual sensors are placed at the cg of the vehicle with gravitational effect turned 'on'/'off' depending on the simulation and their type (i.e. GPS or INS). The measurements from the virtual sensors are imported into Matlab/Simulink, where noise are added before passing through the virtual CAN-bus model.

3.6 Performance of Vehicle Models

With the vehicle models described in the last section, this section looks at the performance and accuracy of each model when compared to the IPG CarMaker. This section also serves as a background for Chapter 5, presenting a justification for the selection of the 2DoF bicycle model as the model for the MKF.

Using IPG CarMaker with its real-time tyre model as the basis of the simulation, the vehicle models under investigation are tuned with simple driving manoeuvres

to estimate parameters such as the longitudinal and lateral tyre coefficients. More complicated manoeuvres are then simulated with the tuned vehicle models and their performances are compared. The vehicle models that are studied in this section are:

- 2DoF bicycle model;
- 3DoF bicycle model;
- 3DoF twin-track model;
- 5DoF bicycle model;
- 7DoF twin-track model.

In these vehicle models the linear tyre model is applied to reduce model complexity as well as computation time. Their formulations were previously described in Section 3.4.

3.6.1 Parameters determination

Table 3.2 below summaries the parameters require for each vehicle model. Table 3.2 differs from Table 3.1 by the assumption of linear tyre model, hence the four extra cornering coefficients.

From Table 3.2 fewer parameters are required for the bicycle models than the twin-track models. The separation of both the front and rear tyres into left and right tyres adds extra parameters, such as the tyre radius and the tyre track distance, that are needed for the modelling. Furthermore, Table 3.2 also shows that the twin-track model is more computationally expensive. In the bicycle model, only a maximum of two sets of slip angles are needed to be solved for the longitudinal and lateral forces. However in the twin-track model four sets of slip angles are required. These extra sets of slip angles are the result of different velocities at each tyre as shown in Equation 3.22.

Looking at the number of DoF of the two model approaches in Table 3.2, it is not hard to see that the higher the degree of freedom of the model, the more parameters are needed. The extra consideration of the longitudinal motion has introduced an additional four parameters into the model as a whole; and inclusion of the wheel rotational dynamics further doubled the number of parameters. In general, the parameters of the vehicle model can be further categorised into three groups: the static, the conditional and the dynamic parameters.

Table 3.2: Parameters required for vehicle model with linear tyre model

		Bicycle mode			**Twin-track mode**	
	Parameters	**2DoF**	**3DoF**	**5DoF**	**3DoF**	**7DoF**
static	T_F				√	√
	T_R				√	√
	ρ		√	√	√	√
	C_d		√	√	√	√
	A_{aero}		√	√	√	√
conditional	a	√	√	√	√	√
	b	√	√	√	√	√
	m	√	√	√	√	√
	J_{zz}	√	√	√	√	√
	J_F			√		
	J_{FR}					√
	J_{FL}					√
	J_R			√		
	J_{RR}					√
	J_{RL}					√
dynamic	R_F		√	√		
	R_{FR}				√	√
	R_{FL}				√	√
	R_R		√	√		
	R_{RR}				√	√
	R_{RL}				√	√
	C_{xF}		√	√		
	C_{xFR}				√	√
	C_{xFL}				√	√
	C_{xR}		√	√		
	C_{xRR}				√	√
	C_{xRL}				√	√
	C_{yF}	√	√	√		
	C_{yFR}				√	√
	C_{yFL}				√	√
	C_{yR}	√	√	√		
	C_{yRR}				√	√
	C_{yRL}				√	√
	Total	**6**	**13**	**15**	**21**	**25**

The static and conditional parameters

As the name suggests, the static parameters are those that define the dimension and the geometry of the vehicle. These are the total length and height of the vehicle, which do not change much during vehicle motion. Notice that the dimension for lengths a and b do not fall into this category as the cg may change due to the change in mass and/or the rolling/pitching motion of the vehicle. Overall, there are only two static parameters in the vehicle models presented in this study, T_F and T_R, and they are normally specified before manufacturing during the design stage of a

vehicle. These parameters are normally precise and have minimal errors. However, their values can change if there are modifications in the type of tyres used.

Conditional parameters are those that change mainly due to the vehicle loading conditions. They can be pre-measured after the vehicle is manufactured when it is in the 'unload' condition. The conditional parameters depend not only on the total amount of the load, but also the distribution of load. With the resultant weight of the vehicle distributed unevenly, the cg changes, affecting the distance from the axles, a and b, as well as the moments of inertia about the cg. The moments of inertia of the wheels are affected by the position of the rotating axis, as the tyre radius changes. Although the conditional parameters are more likely to change while driving, they do not tend to cause too many problems as they do not fluctuate or change significantly.

In this study the tracks at the front and rear, T_F and T_R, are assumed to be equal. The mass of the vehicle, m, the distances from the axles to the cg and all the moments of inertia are assumed to be constant and measured with the 'unload' condition. These parameters are pre-specified in CarMaker before simulations, see Appendix A for details.

The Dynamic Parameters

Dynamic parameters are those which are sensitive to vehicle motion and have a significant effect on the dynamic states determination. Although these parameters can be obtained experimentally or through direct measurement, they are heavily affected by the vehicle conditions, the external environment and driving manoeuvres. Moreover, unlike the conditional parameters with a clear definition, derivation and understanding, the dynamic parameters are more complex in their definition. There is a close relationship between the dynamic parameters and tyre dynamics. They provide the only connection between forces on the road and forces on the vehicle via the longitudinal and lateral slip angles (refer to Equations 3.13 to 3.15). This characteristic of the dynamic parameters has made them vital to the dynamics of the vehicle as a whole.

Although tyre radius change is relatively small, accurate tyre radius is critical as it determines the longitudinal speed of the vehicle. In this study, the effective rolling radius, R_{eff}, is used as the radius for the tyres. In CarMaker, this value is not directly available, but can be determined from the wheel rotational velocity, ω_w, and wheel velocity, V_w, as defined in CarMaker,

$$V_w = R_{eff}\omega_w \tag{3.27}$$

As mentioned at the beginning of this section, the parameters for each model are estimated with a simple manoeuvre before testing on more complicated ones. Thus, straight road driving with constant speed is simulated.

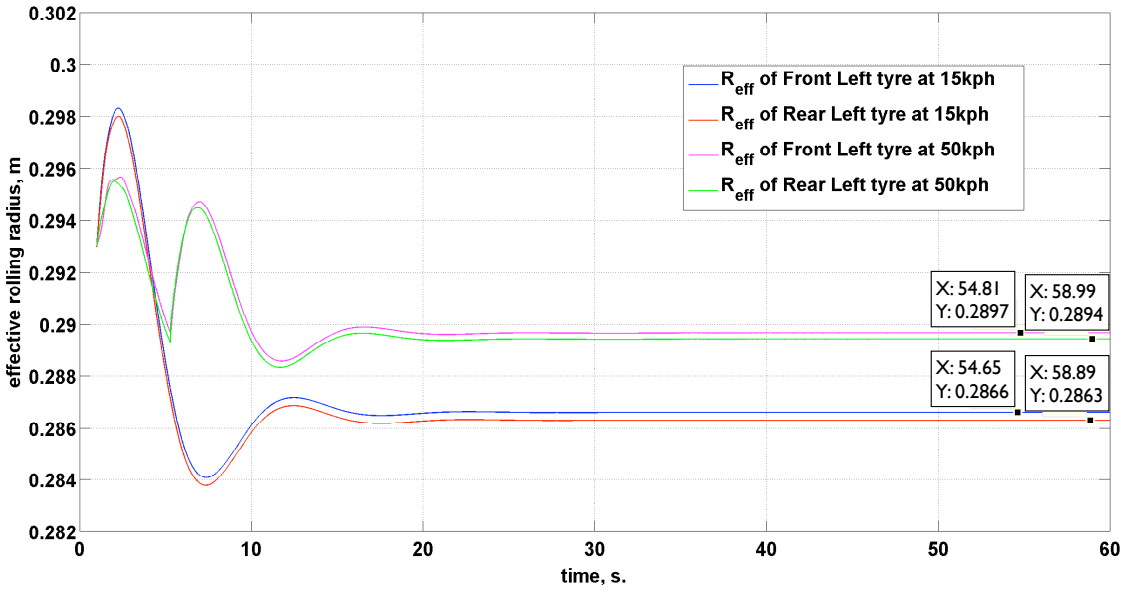

Figure 3.8: Effective rolling radius of front left and rear left tyres, determined from a straight road manoeuvre at 15kph and 50kph.

Figure 3.8 shows the variation of rolling radius with time for the front left and rear left tyres at 15 and 50kph. Initially, the effective rolling radius is the same as the pre-specified kinematic radius of the tyres at 0.293m, but after 20s., the vehicle enters a stable condition and the rolling radius reduces and settles at around 0.2865m and 0.2895m when the vehicle is travelling at 15kph and 50kph respectively. For this study, the effective rolling radius is taken as the average of the stabilised value at 15kph and 50 kph, $R_{eff} = 0.288$.

To approximate the cornering coefficients of the tyres, a *DoubleOval* manoeuvre (see Appendix C.1) is simulated at a constant speed of 15kph. This manoeuvre allows the tyre to remain in the linear region while generating a a good lateral velocity, Figure 3.9. By plotting the forces against the slip angles, the cornering coefficient can be determined from the slope of the plot. Figure 3.10 shows the longitudinal and lateral tyre forces varying with their corresponding slip angles at a speed of 15kph. It can be seen from the figures that the tyres behave linearly across the slip angles. Hence it is appropriate to use the linear tyre model to model the tyre dynamics in this case.

Figure 3.10a shows that the longitudinal forces experienced by the vehicle come mainly from the rear wheels and that the front wheels contribute mostly to the

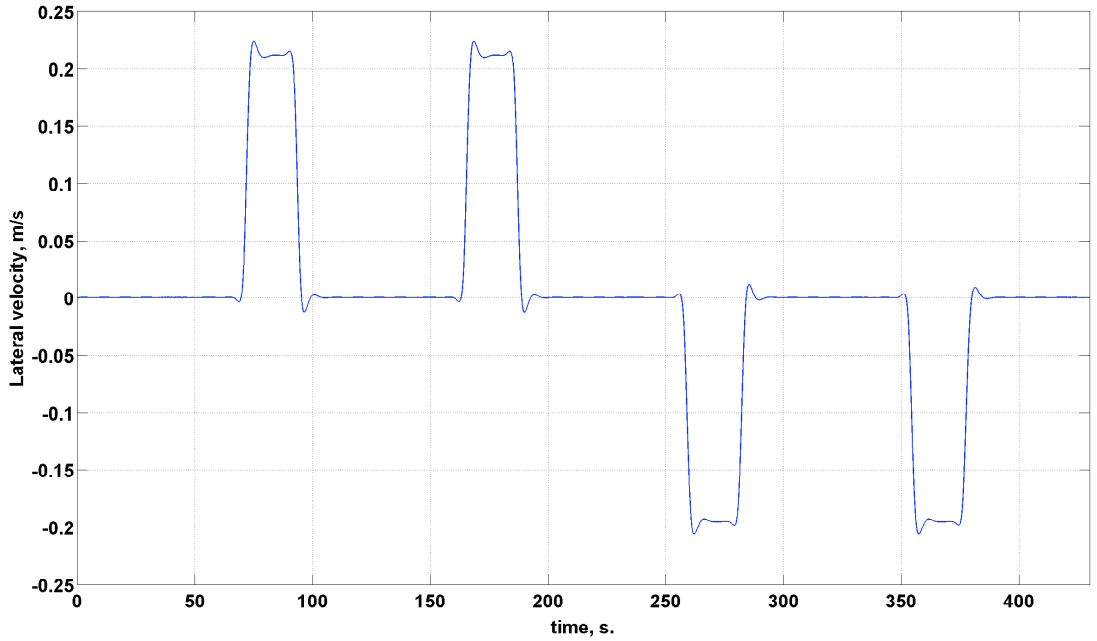

Figure 3.9: Lateral velocity produced by CarMaker on the *DoubleOval* manoeuvre at a constant speed of 15kph

small negative forces. This is because the vehicle in the simulation is Rear Wheel Drive (RWD) and torque from the engine is supplied to the rear only. Further down the longitudinal slip at around 10 thousandths of slip-ratio, the linear line begins to split into two. This effect is due to the variation of weight distribution as the vehicle corners. For a twin-track model, the four longitudinal coefficients are approximated as the slope of each line in Figure 3.10a. However, for a bicycle model, the left and right wheels are assumed to be equal, thus, the longitudinal coefficient is estimated as the average gradient of the left and right.

$$\begin{cases} C_{xFL} = 1.688 \times 10^5 (\mathrm{N}); & C_{xFR} = 1.689 \times 10^5 (\mathrm{N}); \\ C_{xRL} = 1.437 \times 10^5 (\mathrm{N}); & C_{xRR} = 1.439 \times 10^5 (\mathrm{N}); \\ - - - - - - - - - - - - - - - & - - - - - - - - - - - - - - - \\ \text{Ave: } C_{xF} = 1.688 \times 10^5 (\mathrm{N}); & C_{xR} = 1.438 \times 10^5 (\mathrm{N}). \end{cases} \tag{3.28}$$

Similarly, the cornering coefficients are obtained by approximating the slope for the lines in Figure 3.10b. But unlike the longitudinal force, the lateral force distributes evenly amongst the four wheels, with the left and right wheel each occupying a positive and negative force region. From the same figure, two other observations can be made. i) The fact that the lines go through the origin means that there are no camber angles or other physical features such as the ply steer or conicity; and

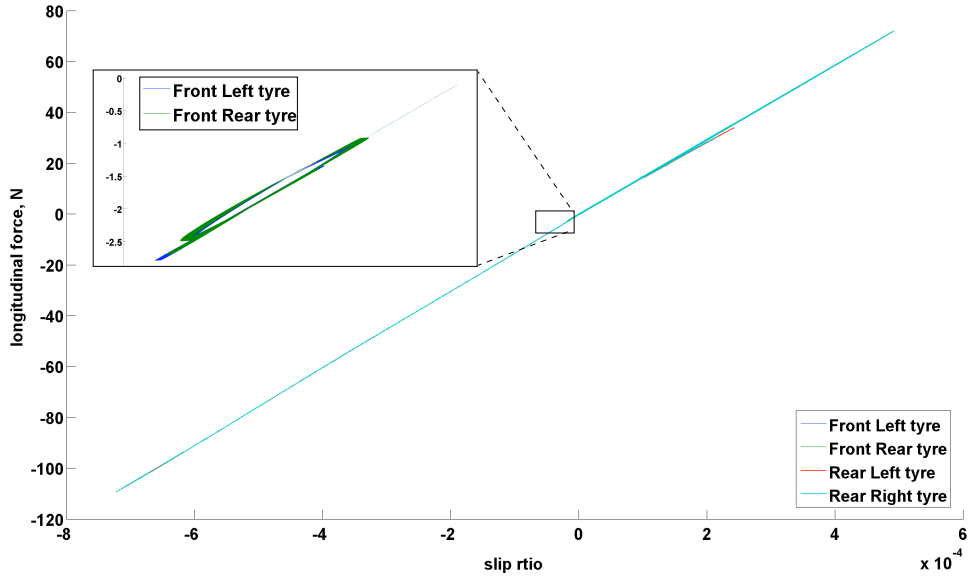

(a) Longitudinal force at the four wheels

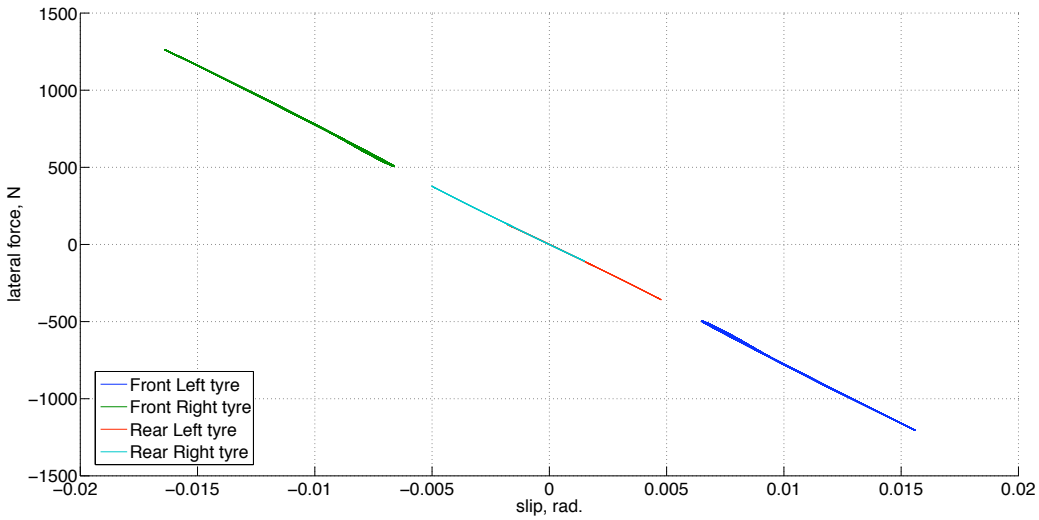

(b) Lateral force at the four wheels

Figure 3.10: Forces at the four tyres when simulated on a DoubleOval travel travelling at 15kph

ii) the symmetric positioning of the four lines suggests a toe in wheel set-up. The cornering coefficients are estimated as:

$$\begin{cases} C_{yFL} = -7.740 \times 10^4 (\text{N/rad.}); & C_{yFR} = -7.739 \times 10^4 (\text{N/rad.}); \\ C_{yRL} = -7.373 \times 10^4 (\text{N/rad.}); & C_{yRR} = -7.380 \times 10^4; (\text{N/rad.}) \\ - - - - - - - - - - - - - - - - & - - - - - - - - - - - - - - - - \\ \text{Ave: } C_{yF} = -7.739 \times 10^4 (\text{N/rad.}); & C_{yR} = -7.377 \times 10^4 (\text{N/rad.}). \end{cases} \tag{3.29}$$

3.6.2 Frequency Response for the Vehicle Model

With the parameters defined for the vehicle model, a frequency response of the states can be evaluated with oscillatory inputs. While Table 3.2 summaries the parameters required for each vehicle model, Table 3.3 summaries the inputs and the initial conditions required for each model.

Table 3.3: The input and initial conditions specified for the vehicle models

		Bicycle model			**Twin-track model**	
	Parameter	**2DoF**	**3DoF**	**5DoF**	**3DoF**	**7DoF**
input	δ	√	√	√		
	δ_{FL}				√	√
	δ_{FR}				√	√
	ω_F		√			
	ω_{FL}				√	
	ω_{FR}				√	
	ω_R		√			
	ω_{RL}				√	
	ω_{RR}				√	
	τ_R			√		
	τ_{RL}					√
	τ_{RR}					√
initial condition	$\dot{x}_v(0)$		√	√	√	√
	$\dot{y}_v(0)$	√	√	√	√	√
	$\dot{\psi}(0)$	√	√	√	√	√
	$\omega_F(0)$			√		
	$\omega_{FL}(0)$					√
	$\omega_{FR}(0)$					√
	$\omega_R(0)$			√		
	$\omega_{RL}(0)$					√
	$\omega_{RR}(0)$					√

Table 3.3 shows that the common input for all five vehicle models is the steer wheel angle, δ, δ_{FL} and δ_{FR}. For the 3DoF models, extra wheel rotational speeds, ω_i, are required to calculate the longitudinal slip; and for the 5DoF and 7DoF, the wheel torque, τ_i, is needed for the determination of wheel dynamics and forces. To start each simulation, initial conditions are used for defining the starting point for the states in each model. In reality, these are normally assumed to be constants or zeros at start. For this study: $\dot{x}_v(0)$ = speed of vehicle, $\dot{y}_v(0) = 0$, $\dot{\psi} = 0$, and $\omega_i(0) = \dot{x}_v/R_w$ Note that the longitudinal velocity, $\dot{x}_v(0)$, is assumed to be constant and not a state in the 2DoF bicycle model, see Section 3.2.

Figures 3.11 and 3.12 show the frequency responses of the lateral velocity when steer wheel angles vary in frequency. The two figures show four Bode plots of absolute magnitude and phase at speeds of 10, 50, 60 and 100kph. Each Bode plot

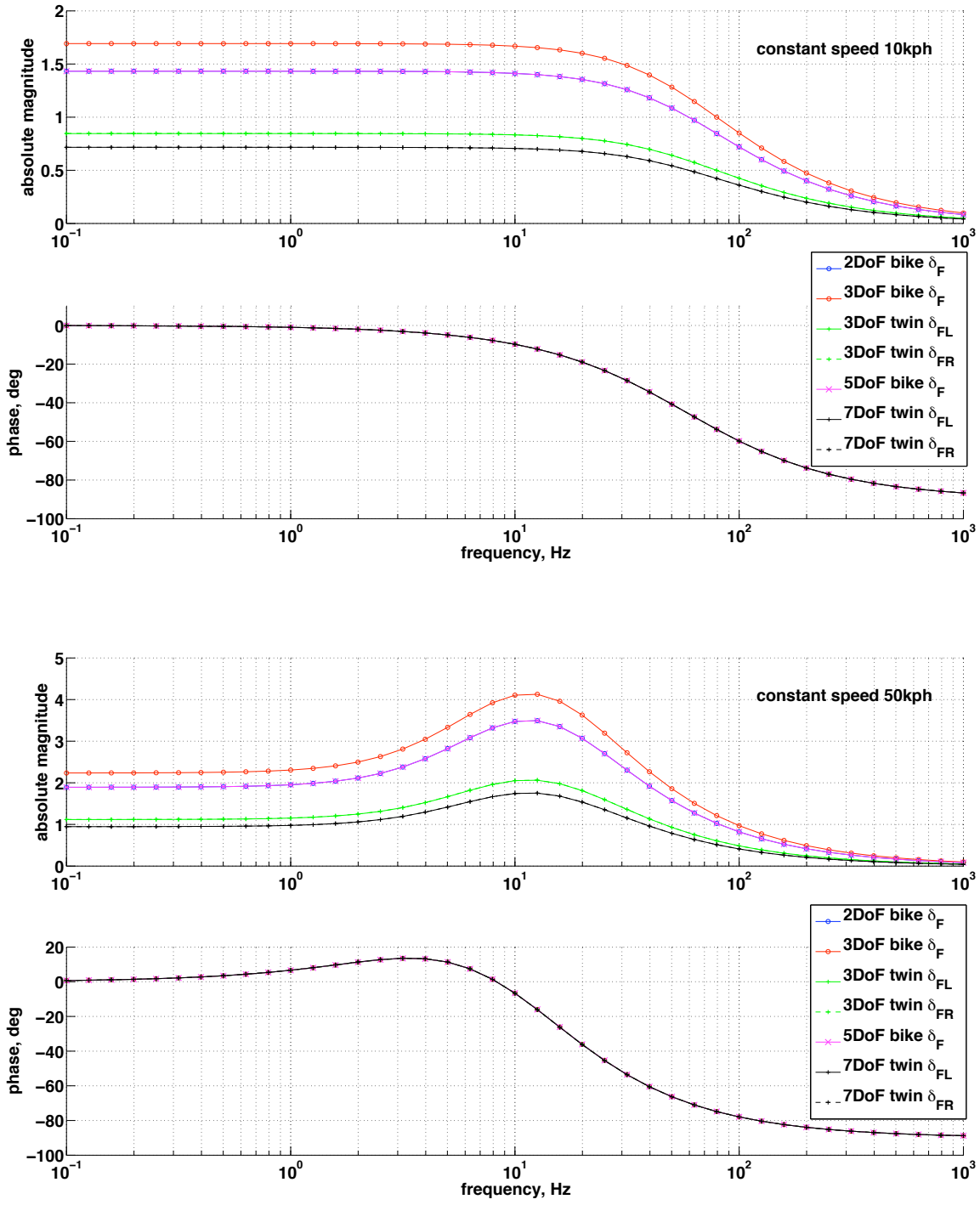

Figure 3.11: Frequency response of lateral velocity with steering inputs for different models, 10 and 50kph

shows the responses of the five vehicle models (i.e. 2DoF bicycle, 3DoF bicycle, 3DoF twin-track, 5DoF bicycle, and 7DoF twin-track).

From the magnitude plots of Figures 3.11 and 3.12, the bicycle models and the

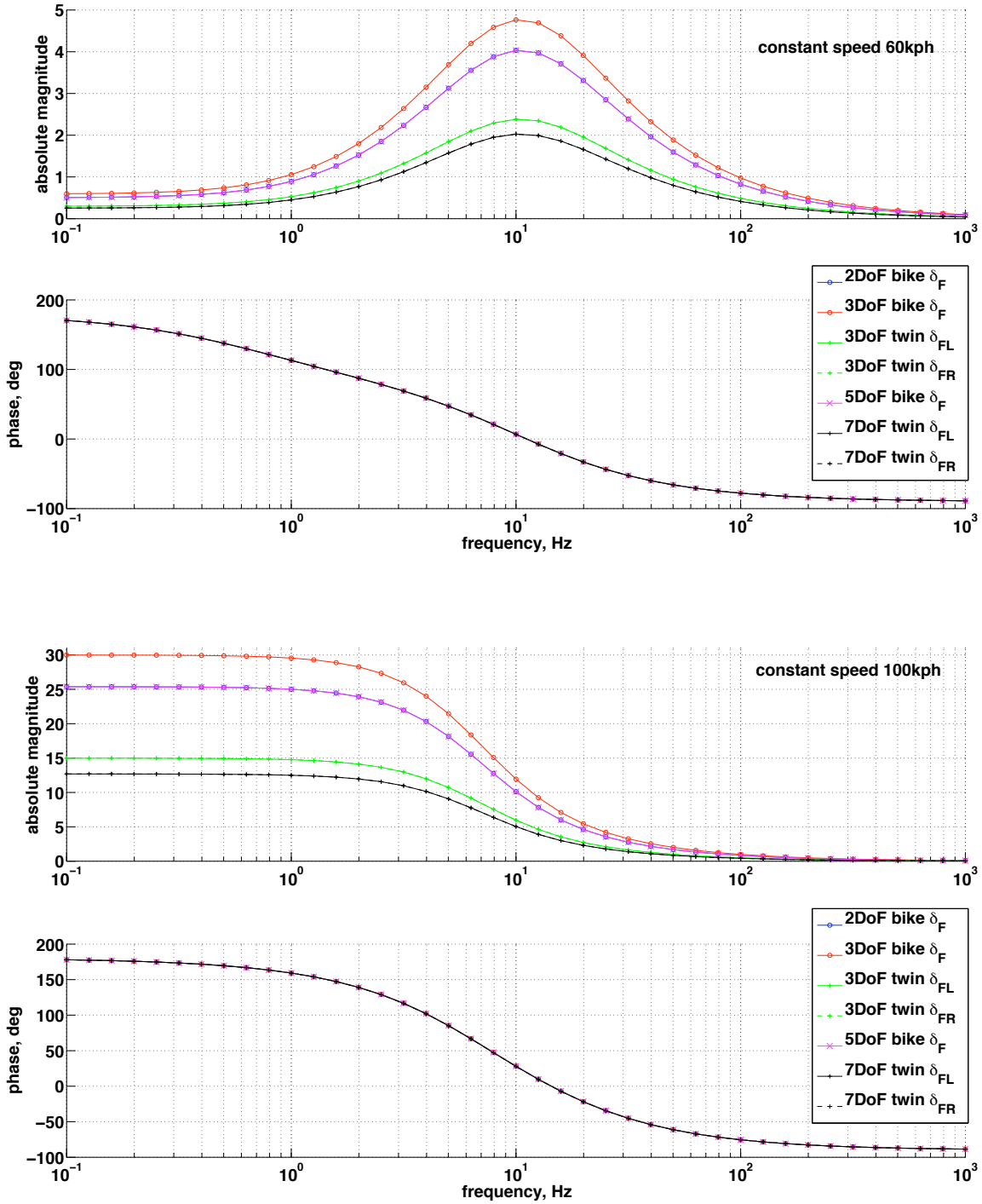

Figure 3.12: Frequency response of lateral velocity with steering inputs for different models, 60 and 100kph

twin-track models are clearly separated by a gap. This obvious difference is due to the principle formulation assumption of the two vehicle modelling approaches (see Section 3.2). For the bicycle model, the left and right wheels are merged into one.

The steer wheel angle of the bicycle model is, therefore, a measure of the average steer angle of the left and right wheel, δ_{FL} and δ_{FR}, of the vehicle. As cornering stiffness remains unchanged (determined from a single wheeled station as discussed in Section 3.3), force due to the axle slip on the combined single tyre (i.e. α_F or α_R) of the bicycle model must be doubled to equal the total force on the twin-track, so:

$$F_{yF} = C_{yFR}\alpha_{FR} + C_{yFL}\alpha_{FL} = 2C_{yF}\alpha_F$$

where C_{yF} is the average of C_{yFR} and C_{yFL}.

Hence, for the same lateral velocity, the single combined tyre steer input on the bicycle model (i.e. δ_F) must produce roughly twice the force of the single tyre steer of the twin-track (i.e. δ_{FR} or δ_{FL}). In other words, the single steering of the bicycle model has double the effect of the steering of a single tyre of the twin-track, i.e. the double magnitude in both Figures 3.11 and 3.12. For example, the magnitude of the two 7DoF responses are summed up (i.e. 7DoF twin δ_{FR} + 7DoF twin δ_{FL}) to equal the magnitude of either the 2DoF bicycle δ_F or the 5DoF bicycle δ_F responses.

Looking at the class of bicycle models, one would expect the models to have similar frequency responses. This is indeed the case for the 2DoF and 5DoF models, but not for the 3DoF. The reason for this is due to the fact that the 3DoF model has inputs of the wheel speed, adding in extra uncertainties to the output of the system.

Analysing the magnitude plot with constant speed 10kph in Figure 3.11, at a frequency below 10Hz, the lateral velocity output has a stable absolute magnitude with an in-phase relationship with the steer wheel angle. As frequency rises above 100Hz, the lateral velocity output becomes out-of-phase and non-responsive. This phenomenon is also observed in the other Bode plots of different speeds, see Figures D.1 to D.5 in the Appendices.

At 50kph, the vehicle manages to maintain a steady lateral velocity output at a steering frequency below 1Hz. However, continual increase of steering rate to 10Hz causes the vehicle to go unstable, hence, the increase in absolute magnitude. With further increase in vehicle speed, i.e. 60kph, the steering has become less responsive at the low frequency range (below 1Hz). Above 1Hz, the magnitude rises quickly and reaches the maximum at around 10Hz. In fact, with careful inspection of the Bode plots, Figures D.1 to D.5, it can be seen that the magnitude increases and decreases with the formation of peaks as vehicle speed increases:

1. from 10kph to 40kph, the magnitude in general increases with a resonant peak formation;

2. at 50kph and 60kph, the magnitude at the low frequencies decreases and forms a peak at roughly 10Hz. Moreover, the phase changes from in-phase at 50kph to out-of-phase at 60kph;

3. from 70kph to 100kph, the magnitude at low frequencies increases again, flattening the peak.

In case 1, when the vehicle increases its speed from 10kph to 40kph, the yaw rate and the slip angles increase, causing the overall lateral velocity magnitude to increase. At frequencies below 10Hz of the 40kph simulation, the lateral velocity magnitude remains constant and further increase of frequency above 10Hz causes the front slip to rise and become 90° out-of-phase to the rear slip. This increases the lateral velocity further and starts to form a peak, Figure D.2.

In case 2, when the speed of the vehicle is increased further from 40kph to 60kph, the vehicle becomes unstable, in which case the the yaw rate dominates the vehicle motion (i.e. oversteering). The lateral motion of the vehicle at this time decreases as the lateral velocity is 180° out-of-phase to the steering input. As frequency continues to increase up to 10Hz, the lateral velocity becomes in-phase with the steering input, causing the lateral magnitude to reach the maximum. With the further increase of speed from 60kph to 100kph in case 3, the lateral velocity dominates.

It can be concluded from Figures 3.11 and 3.12 that the five models show some similarity and compatibility with each other: each of them gives similar lateral velocity response with the changes in the steer wheel angle. From the plots it can be deduced that the 2DoF model produces responses that are similar to those in the 5DoF, suggesting that the reduction of 5 to 2DoF does not cause significant difference in the relationship between the lateral velocity accuracy and the steer wheel angle. On the other hand, as discussed previously, the inclusion of the longitudinal motion and wheel speed in the 3DoF model has affected the relationship between the lateral velocity and the steer wheel angle. As a result, the 2DoF model seems to be the best of the three bicycle models in terms of its simplicity, and low number of parameters and inputs.

Although the frequency response diagrams help us to understand the input-output relationship and the model behaviour, the output (lateral velocity in this case) is based upon the model itself and does not relate to the value of an actual vehicle. Thus, in the next part of this section, more manoeuvres are simulated and states estimated from the vehicle models, which are then compared against each other.

3.6.3 Transient Response for the Vehicle Model

This section compares the feasibility of five vehicle models in comparison with the higher order IPG CarMaker model. For each simulation, the vehicle static and conditional parameters for each model are taken from Appendix A. The dynamic parameters, such as the tyre stiffness, are pre-measured with a single tyre using the *DoubleOval_15kph* manoeuvre. The inputs and initial conditions, Table 3.3, are taken directly from the IPG CarMaker without any additional noise or bias. In this study, due to the linear cornering coefficients assumption in the tyre model, only two low slip manoeuvres are simulated:

1. constant low slip manoeuvre, *DoubleOval_25kph*
2. fast dynamic low slip manoeuvre, *LaneChangeISO_25kph*

Table 3.4: State estimation error of five vehicle models, %NRMSD

Yaw rate estimation

	Bicycle model			**Twin-track model**	
Manoeuvres	**2DoF**	**3DoF**	**5DoF**	**3DoF**	**7DoF**
DoubleOval_25kph	0.2017	0.2126	2.9606	0.3800	0.7096
LaneChangeISO_25kph	0.1263	0.1543	1.0734	0.2245	0.1846

Lateral velocity estimation

	Bicycle model			**Twin-track model**	
Manoeuvres	**2DoF**	**3DoF**	**5DoF**	**3DoF**	**7DoF**
DoubleOval_25kph	0.2043	0.2319	1.2737	0.2051	0.5000
LaneChangeISO_25kph	0.3010	0.3395	0.5272	0.3416	0.3040

While Table 3.4 summarises the %NRMSD of yaw rate and lateral velocity estimations, Figures 3.14 and 3.16 show the differences between the estimated states of the vehicle model and the actual states from IPG CarMaker. Before further analysis it is important to point out the main difference between each model again. With the parameters and inputs as shown in Tables 3.2 and 3.3, the 3DoF models (i.e. both bicycle and twin-track) differ from the 2DoF bicycle models with the inclusion of tyre radius, R_w, longitudinal stiffness, C_{xw}, and angular velocity of wheels, $\dot{\theta}_w$. Similarly, the 5DoF and 7DoF vehicle models differ from the 2DoF bicycle model with the inclusion of not only R_w and C_{xw}, but also the moments of inertia of wheels, J_w, and the wheel torque, τ_w.

With pre-defined parameters, the two 3DoF models do not have a large difference in terms of their %NRMSD of the state estimation in each manoeuvre. Their small

difference in error is the result of single-track and twin-track modelling, of which the latter involves additional parameters for the left and right. Moreover, errors in the 3DoF models are also similar to those obtained using the 2DoF model. This suggests that the inclusion of tyre radius, R_w, longitudinal stiffness, C_{xw}, and wheel rotational speed, ω_w, do not contribute a large amount of error. In another perspective, the small errors also indicate that the parameters and inputs are correct when they are implemented in the 2DoF and 3DoF models.

Continuing with the sequence, apart from adding the tyre radius and longitudinal coefficients, the 5DoF/7DoF model also includes the moment of inertia as well as the torque of each wheel. Unlike the 3DoF models, these additional parameters and inputs have caused an increase in errors in the 5DoF and 7DoF models, in particular the 5DoF bicycle model and the *DoubleOval_25kph* manoeuvre. Since the parameters are defined or measured before each simulation, the errors in the 5DoF and 7DoF models are mainly due to the torque input. As this is directly affecting the longitudinal velocity through the longitudinal slip ratio, the effect of the inclusion of torque is therefore better explained by comparing the longitudinal velocities of the models, see Figure 3.13a. As clearly shown in the figure, the 5DoF and 7DoF vehicle models have an accumulating error on the longitudinal velocity determination. Moreover, it also shows that the 7DoF twin-track model has less error than the 5DoF by having a separate wheel torque. When a vehicle corners, the rotational speed on the left and right tyres differ. By separating the determination of left and right wheel speed, states can be estimated more precisely.

Comparing the %NRMSD of the 5DoF and 7DoF models, in general the error from the *LaneChangeISO_25kph* manoeuvre is lower. This is because the steer angle in the *LaneChangeISO_25kph* manoeuvre is much less than that in the *DoubleOval_25kph* manoeuvre, hence less variation in the longitudinal velocity during a corner. As a result, the states %NRMSD is also lower for the *LaneChangeISO_25kph*.

Of the five vehicle models, Table 3.4 reveals that the state estimation errors are the lowest for the 2DoF model. Figure 3.13a also shows that the WSS is sufficient to provide a good measurement of the longitudinal velocity, but only when the wheel radius is correctly identified. When the longitudinal velocity is correctly determined, the 2DoF model with constant speed assumption gives the best solution with the least %NRMSD in the states.

Figures 3.14 and 3.16 show the state estimation error of each model in time series. When the vehicle is travelling on a straight road all five vehicle models estimate well. It is during vehicle cornering that the state estimations between models become interesting. For both manoeuvres, the 5DoF model gives the greatest errors in both

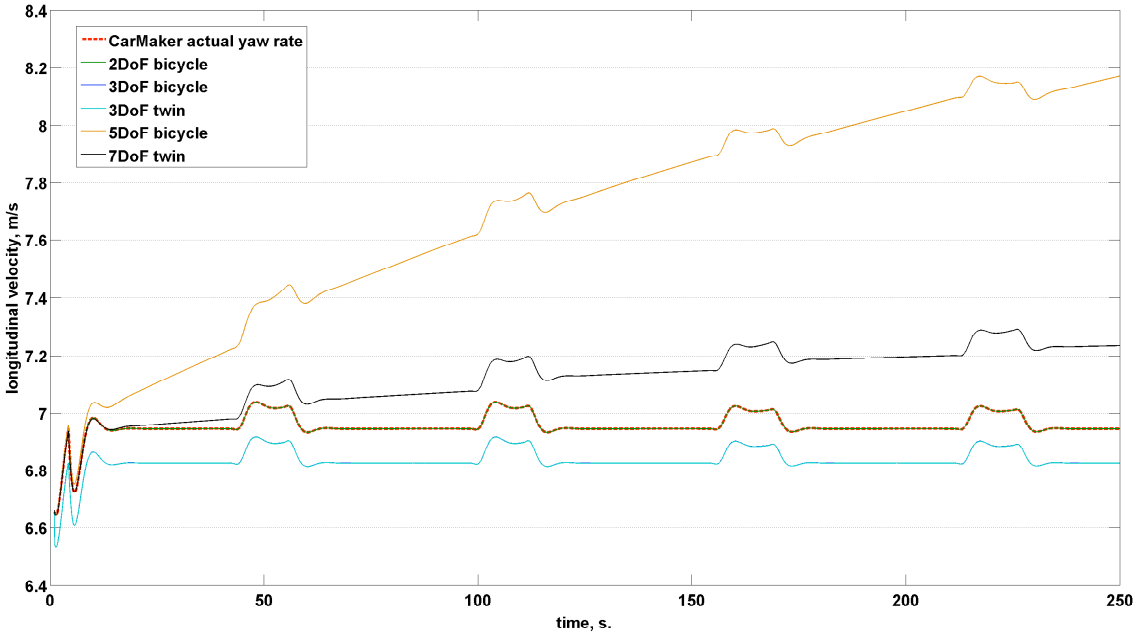

(a) Longitudinal velocity from vehicle model and CarMaker

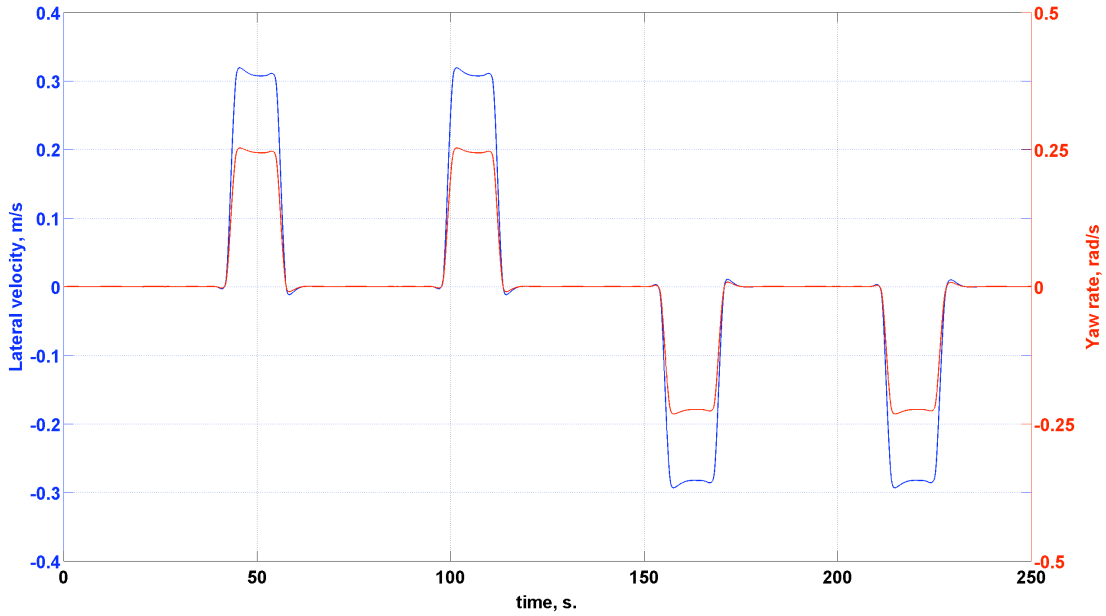

(b) Lateral velocity and yaw rate from CarMaker

Figure 3.13: Vehicle dynamics from CarMaker and vehicle models, *DoubleOval_25kph*

state estimation. This finding confirms the previous %NRMSD in Table 3.4. For the *DoubleOval_25kph* manoeuvre, see Figure 3.14, while the 3DoF models have the fewest errors in the lateral velocity estimation, the 2DoF model is better in predicting the yaw rate. For the *LaneChangeISO_25kph* manoeuvre however, see Figure 3.16, the 2DoF and 7DoF models both achieve similar accuracy for the yaw

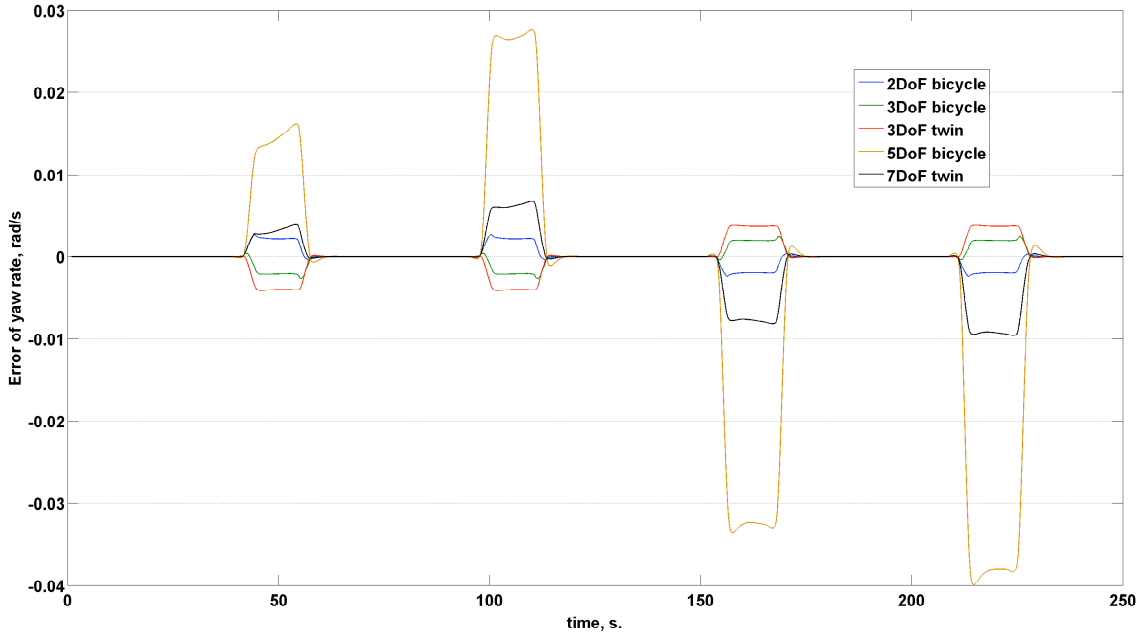

(a) Yaw rate estimation error

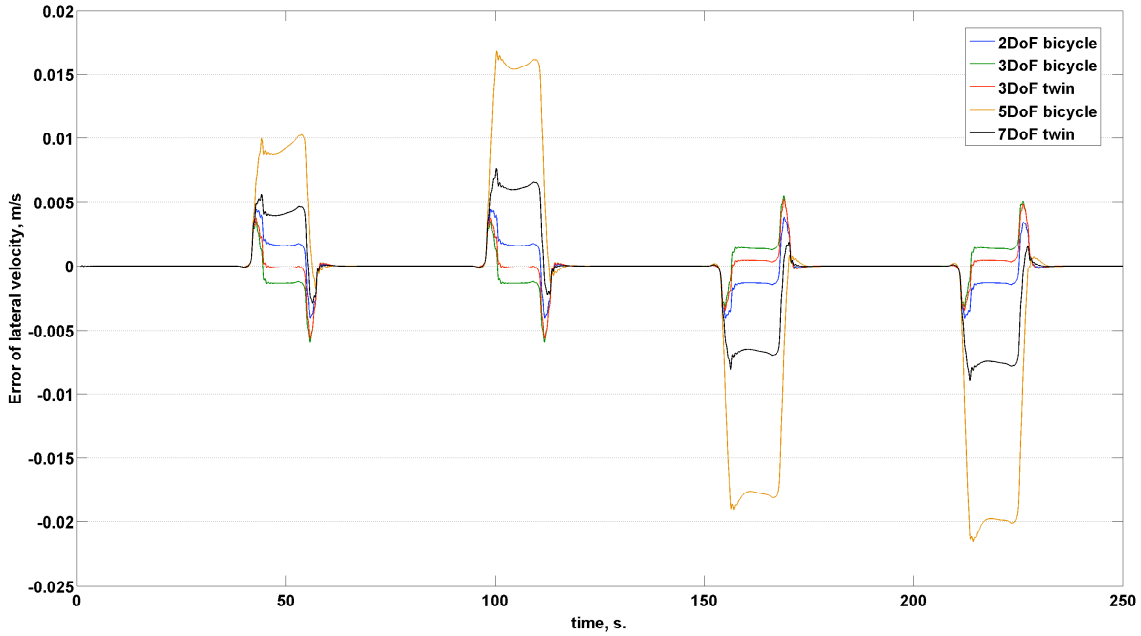

(b) Lateral velocity estimation error

Figure 3.14: Estimation error of five vehicle models (*DoubleOval_25kph*)

rate and lateral velocity estimation.

3.7 Conclusion

In Section 3.2, the basic vehicle formulation for the bicycle and twin-track model is given along with the assumptions and simplifications for the models. The exper-

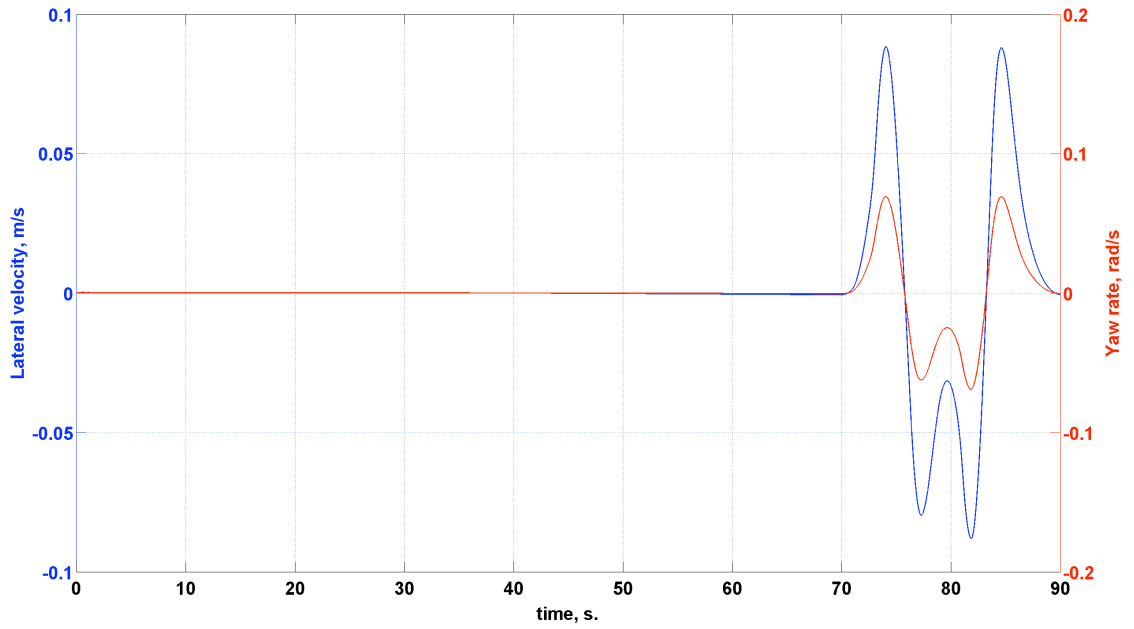

Figure 3.15: Lateral velocity and yaw rate from CarMaker, *LaneChangeISO_25kph*

imentation result for a tyre and three types of tyre model, namely the linear, the Fiala and the 'Magic Formula' tyre model, are presented in Section 3.3. Using the linear tyre model, five simplified vehicle models are derived in Section 3.4: the 2DoF bicycle, 3DoF bicycle, 3DoF twin-track, 5DoF bicycle and 7DoF twin-track model. In Section 3.6, the performance of the five vehicle models is compared in terms of their frequency and transient response.

The frequency response plots, Figures 3.11 and 3.12, provide a comparison between the five vehicle models and their suitability in representing the complex vehicle model. A good vehicle model in MKF must be sufficiently accurate to the true vehicle with relevant dynamics and low complexity (i.e. simple equations and few parameters). Although a higher DoF model represents the true vehicle more precisely, the number of parameters and the effects on uncertainties also increases. From the frequency response analysis, we can see that a higher DoF model does not provide a benefit that outweighs the effect of the increased number of uncertainties. As a result, the 2DoF bicycle model remains the most suitable model.

The transient response analysis (Table 3.4) compares the yaw rate and lateral velocity estimations of the five vehicle models when simulations are carried out in manoeuvres with linear tyre models, e.g. *DoubleOval_25kph* and *LaneChangeISO_25kph*. Results show that the 3DoF and 2DoF models are superior to the rest, but considering the number of parameters in the model the 2DoF bicycle model is more suitable

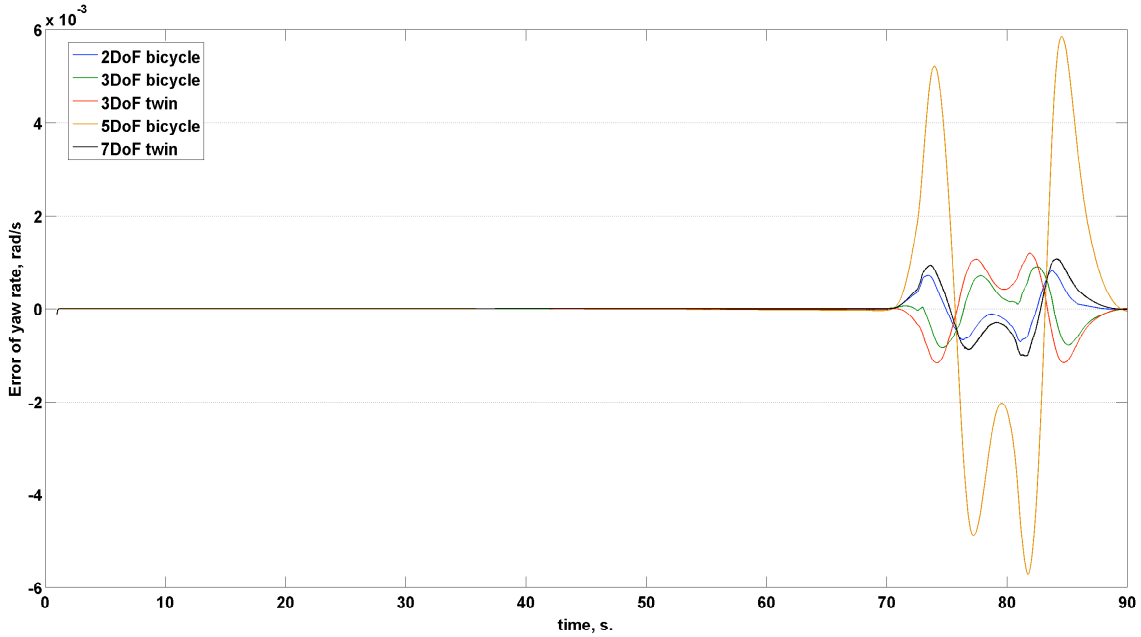

(a) Yaw rate estimation error

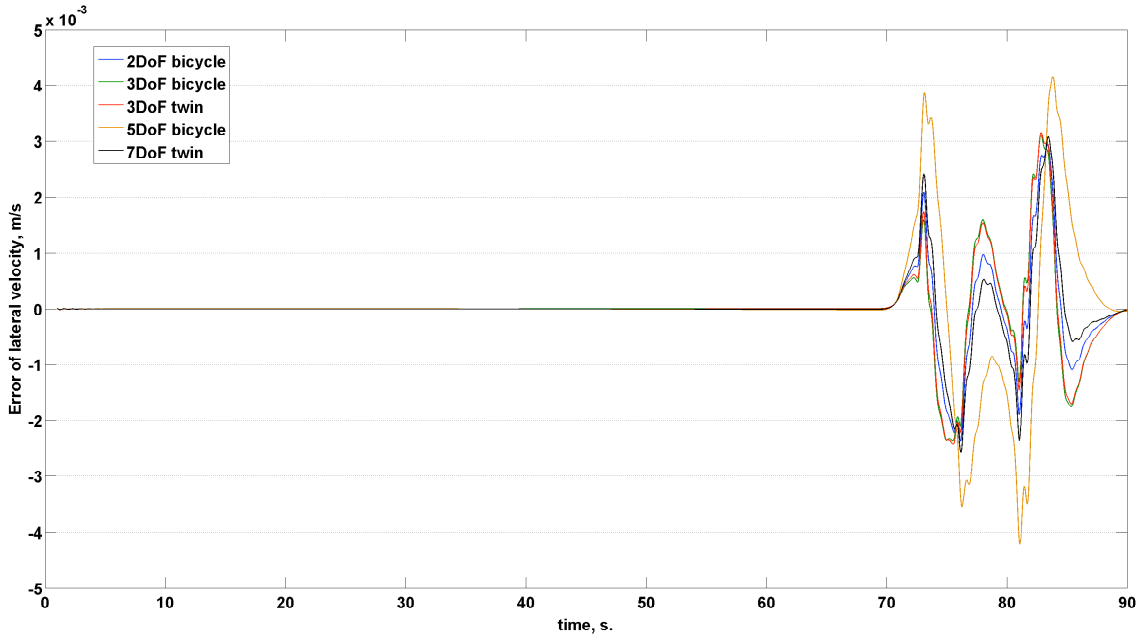

(b) Lateral velocity estimation error

Figure 3.16: Estimation error of five vehicle models (*LaneChangeISO_25kph*)

for MKF implementation.

In conclusion, the 2DoF bicycle model is the most suitable vehicle for the MKF. This is due to its accurate state estimations as well as its low requirement in the number of parameters. However, designers must note that the performance analysis carried out here is restricted to manoeuvres with linear tyre characteristics. For non-linear tyre behaviour, either a more sophisticated tyre model such as the 'Magic

Formula' tyre model is used or a continual update of the axle cornering stiffness is performed. The effect of using the linear 2DoF bicycle model in non-linear driving manoeuvres is presented later in Chapter 5. As the focus of this project is on state estimations, research on parametric estimation is not investigated further in this thesis.

Chapter 4

Design and Performance of GPS-aided Kinematic Estimators

4.1 Introduction

As discussed in Chapter 2, there are in general two types of a KF applicable to this problem, namely the KKF and the MKF. Much work has been done in the last decade while sensors have been getting smaller and cheaper. In particular, GPS has become more mature and reliable, together with a wide acceptance by the public in terms of its price and usage. It is, therefore, natural to consider using such technology in vehicle dynamics determination.

Previous work, such as Bevly et al. [2000; 2001], Anderson and Bevly [2005], Ryu et al. [2002], and Best et al. [2007], has shown that the KF is able to provide good solutions for vehicle dynamics estimation. However, the systems used in these works are either expensive top-of-the-range GPS units or tested under linear tyre conditions. A system that can be integrated into an everyday commercial vehicle has to be accurate, robust, cheap and reliable. This chapter, therefore, provides a thorough investigation into the feasibility of implementing consumer grade GPS with INS to provide vehicle dynamic state estimations, in particular, sideslip estimation.

The chapter is split into six sections. The existing design based on Bevly et al. [2000; 2001] is presented in Section 4.2 and is tested with simulations produced from IPG CarMaker using consumer grade GPS parameters. Section 4.3 provides an account of some possible approaches to improve state estimations focusing on a single GPS antenna design. Section 4.4 describes two summaries of studies analysing the nature of GPS, see also Leung et al. [2008; 2009*a*]. Moving on from a single antenna to multi-antennae GPS system, Section 4.5 focuses on a dual GPS setup and opens the discussion on its architecture and benefits. The effect of the dual

GPS setup on state estimations, in particular sideslip and velocity, are investigated. This chapter finishes with a discussion on the design methodology using graphical charts.

4.2 Single GPS antenna dual KKF design

According to the literature, the most simple and straight forward GPS/INS KF design is presented in Bevly et al. [2000; 2001], and Ryu et al. [2002]. These have used a sKKF approach, which is suitable for car manufacturers as it is not dependent on vehicle parameters, such as mass, inertia and tyre coefficients. As briefly described in Section 2.6.1, this kind of KF system consists of two sKKF, namely the *yawKKF* and the *velKKF*, see Figure 4.1. Note that due to the neglected roll and pitch angle in this KF, b-frame of the sensors is actually aligned with the v-frame of the vehicle motion.

The *yawKKF* consists of a state vector of two states: heading angle, ψ, and yaw rate gyro bias, b_r. The measurement for the *yawKKF* is taken from the GPS tracking angle only, ν, and is related to the heading only when the vehicle is travelling on a straight road: $\nu = \psi$. This is because vehicles generate a sideslip angle only during cornering, making the tracking angle equal to the sum of the heading and sideslip angles: $\nu = \psi + \beta$. Therefore, the measurement for this sKKF switches on and off depending on two circumstances:

1. the presence of GPS signals, and

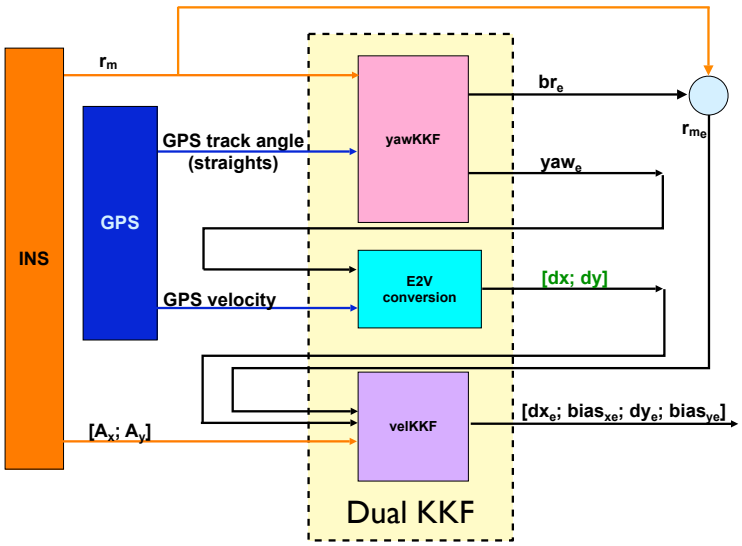

Figure 4.1: Dual KKF architecture [Bevly et al. 2000; 2001, Ryu et al. 2002]

2. whether the vehicle is traveling straight or not.

The presence of GPS signals is often detected by a GPS tag sent from the receiver and the determination of vehicle cornering can be determined from the yaw rate gyro or the steering wheel sensor. We propose using the former as rate gyro bias can be estimated using a simple *yawKKF*.

After the states are estimated from the *yawKKF*, the yaw rate measurements are corrected $(r_m - \hat{b_r})$ and the estimated heading angle is combined with the GPS tracking angle and velocity to produce the longitudinal and lateral velocities in the v-frame as reference measurements for the *velKKF* :

$$\begin{aligned} \dot{x}_v^{ref} &= V_{gps}\cos(\nu_{gps} - \hat{\psi}) \\ \dot{y}_v^{ref} &= V_{gps}\sin(\nu_{gps} - \hat{\psi}). \end{aligned} \tag{4.1}$$

Using these reference measurements, the *velKKF* predicts the longitudinal and lateral velocities in v-frame as well as the biases in the corresponding accelerometers. A summary for the dual KKF setup is presented below:

yawKKF:

$$\begin{bmatrix} \psi \\ b_\psi \end{bmatrix}_{k+1} = \begin{bmatrix} 1 & -T_s \\ 0 & 1 \end{bmatrix} \begin{bmatrix} \hat{\psi} \\ \hat{b}_r \end{bmatrix}_k + \begin{bmatrix} T_s \\ 0 \end{bmatrix} \begin{bmatrix} r_m \end{bmatrix}_k \tag{4.2}$$

$$\begin{bmatrix} \nu \end{bmatrix}_k = \mathbf{H_{yaw}} \begin{bmatrix} \hat{\psi} \\ \hat{b}_r \end{bmatrix}_k \tag{4.3}$$

where: $\mathbf{H_{yaw}} = \begin{bmatrix} 1 & 0 \end{bmatrix}$ when the GPS is available travelling on a straight road, or
$= \begin{bmatrix} 0 & 0 \end{bmatrix}$ when either GPS is off or the vehicle is turning

velKKF:

$$\begin{bmatrix} \dot{x}_v \\ b_x \\ \dot{y}_v \\ b_y \end{bmatrix}_{k+1} = \begin{bmatrix} 1 & -T_s & T_s(r_m - \hat{b_r}) & 0 \\ 0 & 1 & 0 & 0 \\ -T_s(r_m - \hat{b_r}) & 0 & 1 & -T_s \\ 0 & 0 & 0 & 1 \end{bmatrix} \begin{bmatrix} \dot{x}_v \\ b_x \\ \dot{y}_v \\ b_y \end{bmatrix}_k + \begin{bmatrix} T_s & 0 \\ 0 & 0 \\ 0 & T_s \\ 0 & 0 \end{bmatrix} \begin{bmatrix} A_x \\ A_y \end{bmatrix}_k \tag{4.4}$$

$$\begin{bmatrix} \dot{x}_v^{ref} \\ \dot{y}_v^{ref} \end{bmatrix} = \begin{bmatrix} 1 & 0 & 0 & 0 \\ 0 & 0 & 1 & 0 \end{bmatrix} \begin{bmatrix} \dot{x}_v \\ b_x \\ \dot{y}_v \\ b_y \end{bmatrix}_k \tag{4.5}$$

As commented in Bevly et al. [2001], GPS tracking angle must be aligned properly with the heading estimate from the *yawKKF* in time, in order to 'correctly' determine the sideslip angle. Another important point to bear in mind is the definition and magnitude of the two angles. As GPS measures the tracking angle in terms of velocity, $\nu_{gps} = \text{ATAN2}\,(\dot{y}_e, \dot{x}_e)$, the angle will always be measured in the range $-\pi$ to π region. On the other hand, heading angle is a numerical integration from the yaw rate gyro and is therefore unbounded.

As discussed, the *yawKKF* compares the heading angle with the tracking angle when travelling on a straight road. As the tracking and heading angles may be operating in a different numerical range, they have to be converted to the same working numerical range before making comparison. A common working region for angles is the trigonometric region, in which angles are converted to their cosine and sine. As a result, the measurement expression in Equation 4.3 is no longer a direct comparison with the GPS tracking angle, i.e. $\nu_k = \hat{\psi}_k$, but a non-linear trigonometric relationship,

$$\begin{bmatrix} \cos\nu \\ \sin\nu \end{bmatrix}_k = \begin{bmatrix} \cos\hat{\psi} \\ \sin\hat{\psi} \end{bmatrix}_k .$$

This change causes the simple measurement matrix, $\mathbf{H_{yaw}}$, to be replaced by a non-linear Jacobian matrix, $\mathbf{J_H}$, in the KF formulation:

$$\mathbf{J_H}^{i,j} = \left[\frac{\partial z_i}{\partial x_j}\right]^{i,j=1,2} = \begin{bmatrix} -\sin\hat{\psi}_k & 0 \\ \cos\hat{\psi}_k & 0 \end{bmatrix}. \tag{4.6}$$

In the absence of GPS signals, the measurement matrix, $\mathbf{H_{yaw}}$, becomes zero. However, for the *velKKF*, it is recommended later in Section 4.4 and in Leung et al. [2009*a*] that the measurement matrix must remain 'ON' even when the GPS is unavailable. Instead of turning the matrix into zeros, the measurement covariance of the *velKKF*, $\mathbf{R_{vel}}$, is set to a large value, reducing the effect of the measurements on the estimated states.

4.2.1 Analysis of dual KKF design approach

Using virtual sensor measurements from IPG CarMaker simulations, errors (see Appendix B) are added to the sensors before passing through a virtual CAN-bus, which quantises, limits and delays the signals. Vehicle dynamic states are then estimated with the dual KKF setup as described previously.

Although the simulation from CarMaker provides a 3-axis accerometer/gyroscope

Table 4.1: Sensors that are commonly found on a Jaguar

Sensors
Yaw rate gyroscope
Longitudinal accelerometer
Lateral accelerometer
Wheel speed sensor
Steering wheel sensor

combination, it is not common to find such setups in every commercial vehicle. For instance, in most Jaguar production cars, only the sensors listed in Table 4.1 can be commonly found. Due to this constraint on the availability of sensors in vehicles, the dual KKF setup has become a more suitable and attractive solution for the state estimation problem.

With the error standard deviation described in Appendix B.1, the covariance matrices for the *yawKKF* and *velKKF* are defined as follows:

$$\mathbf{P_{0|yaw}} = \begin{bmatrix} 0 & 0 \\ 0 & 0 \end{bmatrix}; \qquad \mathbf{P_{0|vel}} = \begin{bmatrix} V_{wss} & 0 & 0 & 0 \\ 0 & 0 & 0 & 0 \\ 0 & 0 & 0 & 0 \\ 0 & 0 & 0 & 0 \end{bmatrix};$$

$$\mathbf{Q_{yaw}} = \begin{bmatrix} {\sigma_{r_m}}^2 & 0 \\ 0 & {\sigma_{br}}^2 \end{bmatrix}; \qquad \mathbf{Q_{vel}} = \begin{bmatrix} {\sigma_{A_x}}^2 & 0 & 0 & 0 \\ 0 & {\sigma_{b\ddot{x}}}^2 & 0 & 0 \\ 0 & 0 & {\sigma_{A_y}}^2 & 0 \\ 0 & 0 & 0 & {\sigma_{b\ddot{y}}}^2 \end{bmatrix};$$

$$\mathbf{R_{yaw}} = \begin{bmatrix} {\sigma_{\cos\nu}}^2 & 0 \\ 0 & {\sigma_{\sin\nu}}^2 \end{bmatrix}; \qquad \mathbf{R_{vel}} = \begin{bmatrix} {\sigma_{\dot{x}_v^{ref}}}^2 & 0 \\ 0 & {\sigma_{\dot{y}_v^{ref}}}^2 \end{bmatrix}.$$

where:
$$\begin{aligned} \sigma_{br}, \sigma_{b\ddot{x}}, \sigma_{b\ddot{y}} &= 1 \times 10^{-6}; \\ \sigma_{\cos\nu} &= (\sin\nu)\sigma_\nu; \\ \sigma_{\sin\nu} &= (\cos\nu)\sigma_\nu; \\ {\sigma_{\ddot{x}_v^{ref}}}^2 &= \cos^2(\nu-\psi){\sigma_V}^2 + V^2\sin^2(\nu-\psi){\sigma_\nu}^2 + V^2\sin^2(\nu-\psi){\sigma_\psi}^2 \\ {\sigma_{\ddot{y}_v^{ref}}}^2 &= \sin^2(\nu-\psi){\sigma_V}^2 + V^2\cos^2(\nu-\psi){\sigma_\nu}^2 + V^2\cos^2(\nu-\psi){\sigma_\psi}^2 \end{aligned}$$

The above matrices are implemented into the dual KKF design and two tracks (*DoubleOval* and *LaneChangeISO*, see Section 1.4 for detailed description) are simulated using the IPG CarMaker with a speed ranging from 15kph to 55 kph. The

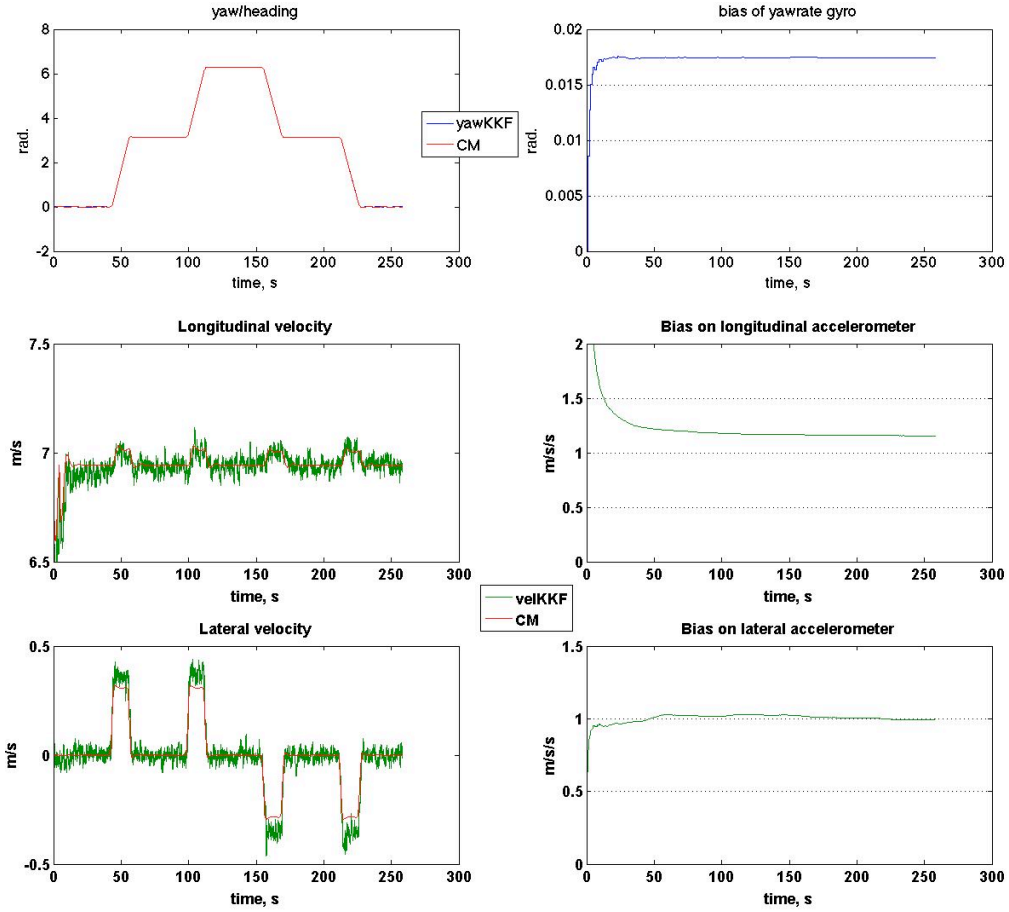

Figure 4.2: State estimations of *yawKKF* and *velKKF* in *DoubleOval_25kph* manoeuvre

estimated error for the state estimations in each simulation are given in terms of the RMSD or the NRMSD as described in Section 1.4.2.

For the *DoubleOval_25kph*, both *yawKKF* and *velKKF* perform reasonably well, especially in the bias estimation, giving an average error of 0.03% (b_r), 15.18% (b_x) and 0.16% (b_y), see Table 4.2. The bias estimates converge in a very short period of time, allowing the heading and velocity to be estimated more precisely with minimum drifting.

In the *yawKKF*, the heading estimation has an error of 0.04%. From Figure 4.2, the heading estimations are so close to the actual simulation values that the plots are indistinguishable. Although the heading errors are small and insignificant for the heading estimations, they are not trivial when determining the sideslip angles. This is because sideslip angles developed in this study are less than 0.05 rad ($\approx 3^\circ$) with a low update rate (1Hz). Hence, a small error in heading will cause a significant error in the sideslip estimation.

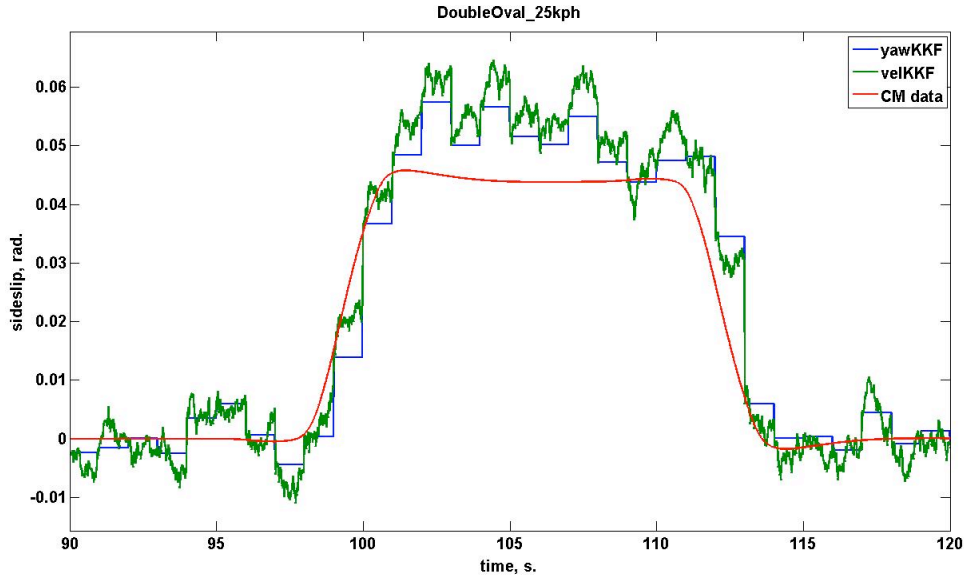

Figure 4.3: Comparison of sideslip estimation from *yawKKF* and *velKKF* in a *DoubleOval_25kph*

In addition, as sideslip is measured from the GPS tracking angle and the estimated heading angle, the slow sampling rate of the consumer GPS unit (1Hz) causes the estimated heading angle to be down-sampled from 100Hz to 1Hz. This results in a stair-case plot similar to the one shown in Figure 4.3. The sideslip error is then carried downstream to the *velKKF* via the measurement, i.e. $\dot{x}_v^{ref} = V_{gps}\cos(\hat{\beta})$ and $\dot{y}_v^{ref} = V_{gps}\sin(\hat{\beta})$.

With this *velKKF* setup, velocity estimation places a greater weight on the measurement when GPS is available and lower during its absence. As a result, the sideslip estimation from the *velKKF*, $\hat{\beta}_{velKKF} \approx \dot{y}_v/\dot{x}_v$, develops a strong relationship with that predicted from the *yawKKF*, see Figure 4.3 and Table 4.2. Throughout the simulation, the largest estimated bias error in the dual KKF design comes from the bias prediction of the longitudinal accelerometer.

As shown in Figure 4.2, the estimated bias does not converge to the pre-set value, 1 m/s^2, and this error is due to the weak and short excitation of the longitudinal dynamics in the driving manoeuvre (constant speed). As longitudinal acceleration is a function of the longitudinal and lateral dynamics, i.e. $\ddot{x}_v = A_x + \dot{y}_v\dot{\psi}$, the lateral dynamics response will dominate when the longitudinal dynamics response is weak and short, therefore making it hard for the *velKKF* to identify the longitudinal bias from all the errors in the longitudinal acceleration.

In the *LaneChangeISO_25kph* manoeuvre, results are very similar to the previous simulation in terms of estimation performance. Both *yawKKF* and *velKKF* manage

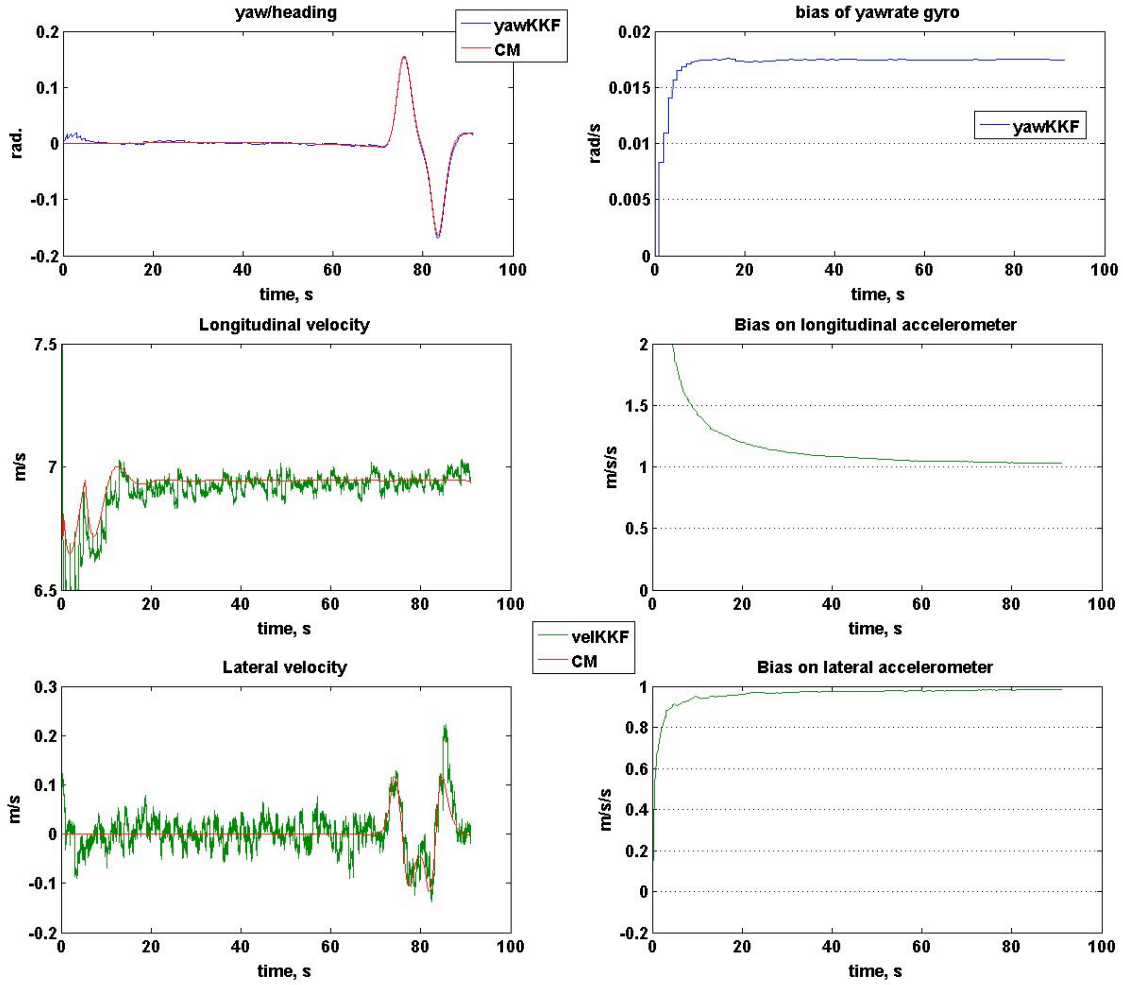

Figure 4.4: State estimations of *yawKKF* and *velKKF* in *LaneChangeISO_25kph* manoeuvre

to predict their corresponding bias with an average error: 0.10% (b_r), 3.24% (b_x) and 0.46% (b_y), see Table 4.2. The bias prediction ability for the two tracks are similar apart from the longitudinal bias, which improved by a factor of 5. Comparing Figure 4.4 with Figure 4.2, the main differences are twofold: i) the longitudinal dynamics, and ii) the time on the straight. Because typically more time is spent on straight road driving, longitudinal dynamics play a stronger part in the *velKKF*, thus encouraging the longitudinal bias to be estimated more precisely.

With the same driving speed, the *LaneChangeISO* manoeuvre has a smaller lateral velocity, noise then becomes a more significant problem as it contaminates the sideslip angle estimation. Changes in lateral velocity are also sharper, more vigourous and shorter in time for the *LaneChangeISO* manoeuvre (2 sharp turns under 30 seconds as compared to 1 turn in 20 seconds for the *DoubleOval* manoeuvre). This short and sharp manoeuvre causes problems in estimation at high vehicle

Table 4.2: Average errors of estimated states over 10 simulation runs

		yawKKF			**velKKF**				
		NRMSD		RMSD	RMSD	NRMSD		RMSD	
	Estimated states:	$\hat{\psi}$	$\hat{\beta}$	$\hat{b}_r$	$\hat{\dot{x}}_v$	$\hat{\dot{y}}_v$	$\hat{\beta}$	$\hat{b}_x$	$\hat{b}_y$
Simulated manoeuvre	*DoubleOval_15kph*	0.04	5.72	0.03	3.01	6.86	6.90	13.96	0.22
	DoubleOval_25kph	0.04	5.15	0.06	3.38	6.37	6.40	15.18	0.16
	DoubleOval_35kph	0.05	7.04	0.08	3.88	9.76	9.75	17.35	0.41
	DoubleOval_45kph	0.06	15.13	0.09	4.96	24.52	24.44	20.03	0.57
	DoubleOval_55kph	0.08	14.15	0.09	8.27	21.43	21.25	23.22	1.08
	LaneChangeISO_15kph	0.81	12.64	0.09	3.19	14.92	14.96	0.49	0.44
	LaneChangeISO_25kph	0.59	10.93	0.10	4.12	11.72	11.76	3.24	0.46
	LaneChangeISO_35kph	0.58	14.73	0.23	5.37	15.85	15.89	23.55	1.07
	LaneChangeISO_45kph	0.55	18.86	0.16	7.48	21.39	21.46	30.46	1.48
	LaneChangeISO_55kph	0.52	47.10	0.21	10.01	62.16	62.46	39.09	2.06

speed, because the update rate of the dual KKF (1Hz) is not fast enough to track the changes.

Table 4.2 provides a summary of the average estimated error for the two tracks over 10 simulations each. In general, it shows that the higher the speed the vehicle is travelling, the higher the state estimation errors are. This is partly due to the sampling rate of the devices used in the dual KKF and partly due to the unmodelled dynamics. As discussed earlier, when the vehicle increases in speed, its transient dynamics change more rapidly and they become harder to capture. Owing to the slow sampling nature of the consumer GPS, the system is being corrected less frequently, resulting in a higher estimation error.

This can also be clearly observed from Figure 4.5. When the speed increases from 25kph to 45 kph for both simulated tracks. The time taken for the cornering manoeuvres in both cases reduces as speed increases, thereby shortening the time allowed for the KKF to update. Comparing the *LaneChangeISO_45kph* with *LaneChangeISO_25kph* in Figure 4.5, it can be seen that the number of successive *yawKKF* updates reduces greatly by a factor of 2. This relative lack of updates causes the increase in estimation error in the *yawKKF* and *velKKF* in the downstream.

Moreover, as pointed out earlier, error in the *velKKF* (especially in the lateral direction) is also a cause of the unmodelled dynamics, such as the vehicle roll, θ. At low speed cornering, vehicle roll is negligible and roll can be assumed as zero in the lateral dynamics. However, during a high speed manoeuvre, roll angle is no longer small enough to be ignored as it affects the lateral acceleration via gravity, i.e. $g\sin(\theta)$. Therefore, it is important to measure or estimate this state.

Comparing the two simulation cases, *DoubleOval* represents a more benign driving track with a larger cornering radius while the *LaneChangeISO* is more vigorous with two sharp turns. Considering the nature of the two tracks, the unmodelled dynamics plays a more important role in the latter track, and thus, higher estimation error results.

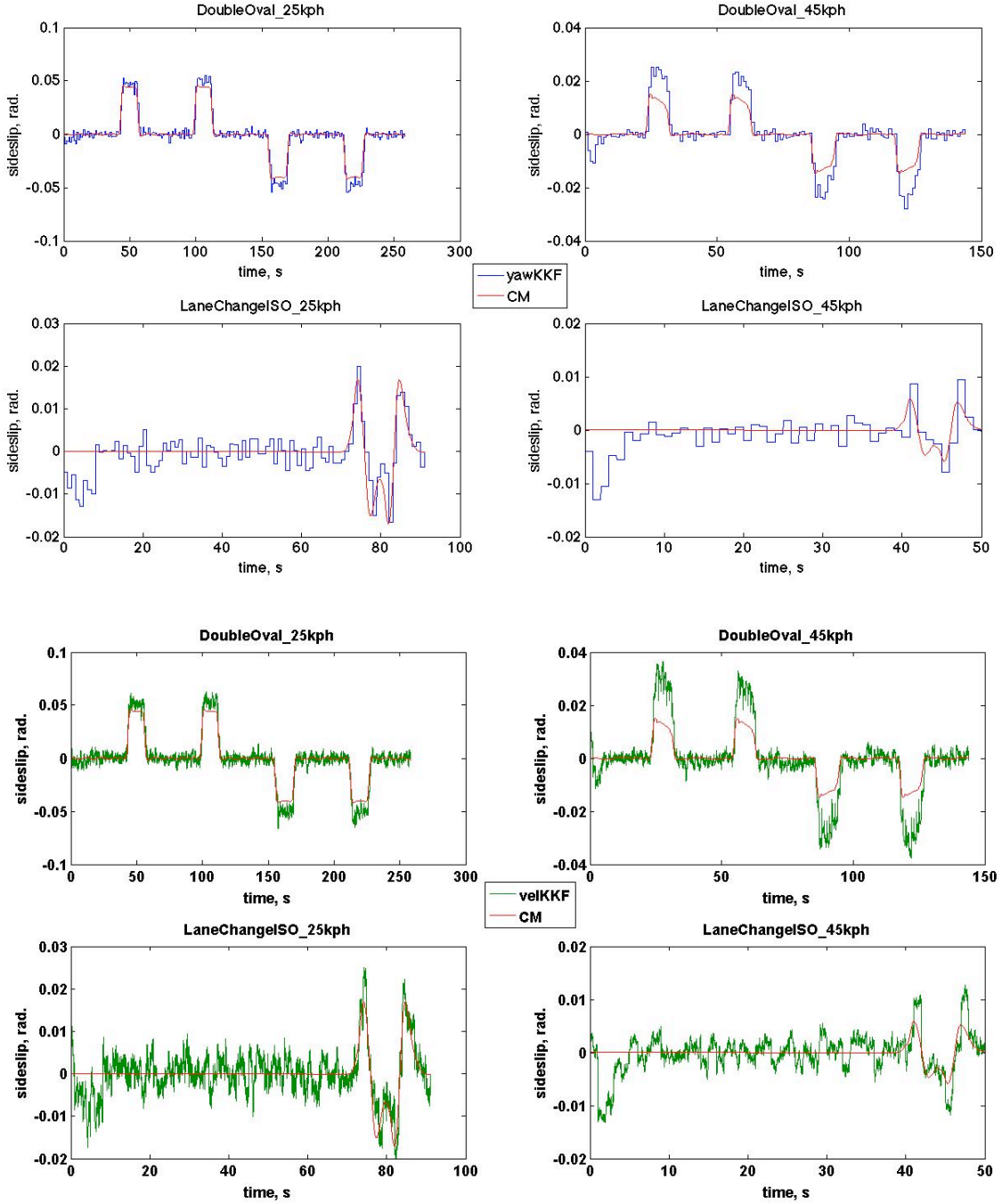

Figure 4.5: Sideslip estimation from *yawKKF* in *DoubleOval* and *LaneChangeISO* simulated tracks

4.2.2 Critique for the dual KKF

Through the analysis of the dual KKF, a few state estimation accuracy dependent factors are identified. They are listed below with no order of significance.

1. The approximation of the discrete time model:
   The dual KKF described previously uses a discrete process matrix $\mathbf{\Phi_k} \approx (\mathbf{I} - \mathbf{A}T_s)$, which is a first order approximation of the definition of $\mathbf{\Phi_k} = e^{\mathbf{A}T_s} = \sum_{k=0}^{\infty} \frac{1}{k!} (\mathbf{A}T_s)^k$. This approximation performs well when its frequency, $1/T_s$, is higher than the dynamic frequency of the actual plant. In many practical situations, the sensor update frequency is not high enough to capture all the dynamics of the vehicle. As a result, a higher order of the $\mathbf{\Phi_k}$ or a different approximation, such as the bilinear transform, $e^{\mathbf{A}T_s} \approx \left(\mathbf{I} + \frac{1}{2}\mathbf{A}T_s\right)\left(\mathbf{I} - \frac{1}{2}\mathbf{A}T_s\right)^{-1}$, is required.

2. The sensor model:
   The sensor model used in *velKKF* does not take the vehicle roll angle into consideration. At low speed cornering with low lateral velocity, the absence of roll angle does not have a large impact on the state estimations. However, as pointed out earlier, the error increased dramatically once the vehicle enters a high speed cornering manoeuvre. An improved sensor model to compensate for this error is given as, $A_y = \ddot{y}_v + \dot{x}_v\dot{\psi} + g\sin(\theta) + b_y$. This formulation contains the vehicle roll angle, θ, which is not a direct numerical integration of the roll rate gyro, but a measurement from the euler angle relation as given in Section 4.5.

3. The effect of the CAN-bus:
   The CAN-bus prioritised and quantised the measurements of the INS before they enter the dual KKF system, thus creating a delay and round-off error at the input of the system. Figure 4.6 shows a perfect yaw rate signal (i.e. without noise), with and without going through the CAN-bus before the *yawKKF*. It is clear that the CAN-bus has added errors to the original signal. Since the measurements of the yaw rate are relatively small, the quantisation has down-sampled the original 100Hz yaw rate gyro measurement to about 5Hz. The loss of information results in an inaccurate heading and sideslip estimation by the *yawKKF*, see Figure 4.6.

Theoretically, this error can be treated as a dynamic time-variant bias and can be tracked by the bias estimation in the *yawKKF*. However, with this *yawKKF* setup, bias estimation only updates when the vehicle is travelling straight and remains

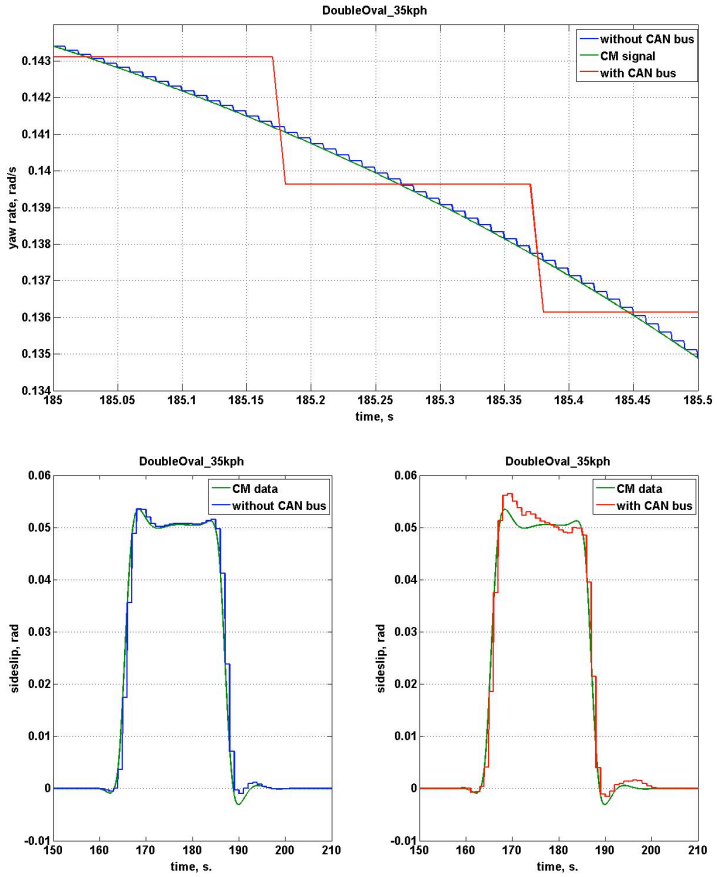

Figure 4.6: Perfect yaw rate signal and sideslip estimation comparison with/without CAN-bus

constant during cornering. Any over- or under-estimation of the bias creates an error in heading and sideslip estimation. Thus, it is better to obtain measurements directly rather than via passing through the CAN-bus and estimations can be more accurate if the *yawKKF* can be continuously updating even during cornering. However, as the project is aimed at designing an estimator using 'in-the-practical' on-vehicle measurements, the CAN-bus system must remain in the simulation to represents 'real world' signals.

4.3 Introduction to the wheel speed sensor aided triple KF

As discussed in the previous section, a continuous update of the heading angle in the *yawKKF* may benefit the overall dual KKF state estimations. It is assumed that a bias-free heading angle measuring device is available (e.g. magnetometer or

a dual GPS receiver setup) continuously at a rate of 100Hz, with a white noise of standard deviation $\sigma = 0.10$ rad ≈ 5.7 ° .

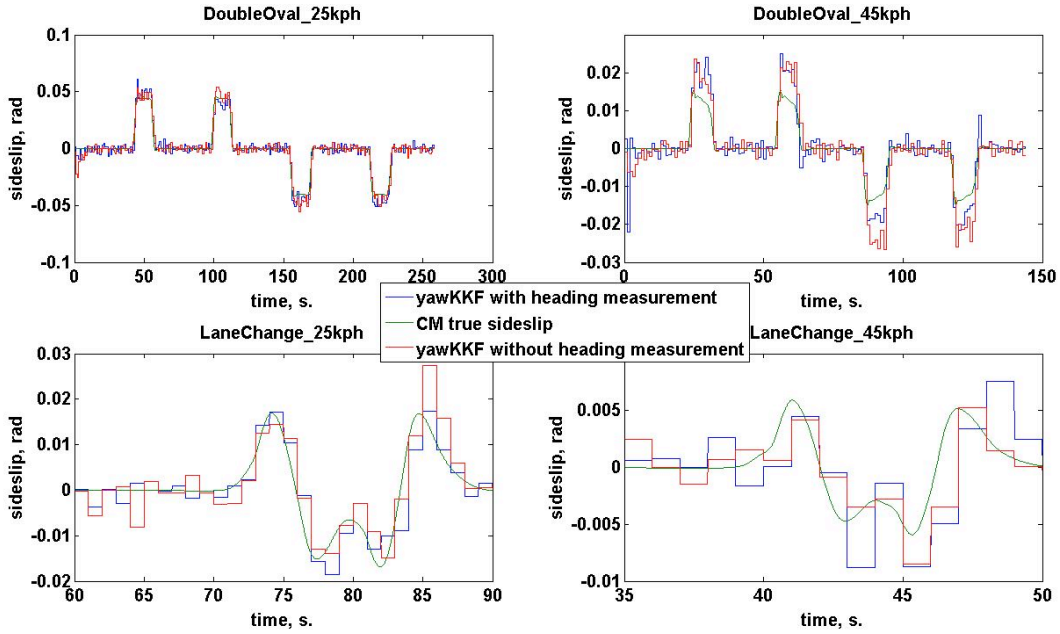

Figure 4.7: Sideslip estimation from *yawKKF* with and without heading measurement

Figure 4.7 shows the sideslip estimation comparison of a dual KKF design with and without heading measurement in the *yawKKF*. At 25kph, the sideslip estimates are similar, the extra heading measurement for the *yawKKF* does not seem to be giving an advantage over estimation. However, for the *DoubleOval_45kph*, it is clear that the modified *yawKKF* is benefiting the sideslip estimation, giving more accurate estimations than the previous KKF. The estimation errors for this study are summarised in Table 4.3.

The upper rows in Table 4.3 represent the dual KKF design with heading measurement in the *yawKKF*. Comparing the errors for the two designs, the inclusion of heading measurement only marginally improves the sideslip and lateral velocity estimations for the *DoubleOval* manoeuvre. The only significant improvement is during the *DoubleOval_45kph* simulation, where the sideslip estimation error is approximately 3% to 4% lower than the original dual KKF setup. Although the inclusion of heading measurement has been shown to give a better estimation in the simulated environment, the amount of improvement is so little that investment in a new sensor is unlikely to be economically value-adding.

Table 4.3: Comparison of the estimated errors of dual KKF with and without heading measuring devices

		yawKKF			**velKKF**				
		NRMSD		RMSD	RMSD	NRMSD		RMSD	
	Estimated states:	$\hat{\psi}$	$\hat{\beta}$	$\hat{b}_r$	$\hat{\dot{x}}_v$	$\hat{\dot{y}}_v$	$\hat{\beta}$	$\hat{b}_x$	$\hat{b}_y$
manoeuvre	with heading measurement:								
	DoubleOval_25kph	0.04	4.80	0.04	3.11	5.94	5.97	15.12	0.29
	DoubleOval_45kph	0.05	12.77	0.04	4.33	22.33	22.30	19.74	0.61
	DoubleOval_55kph	0.07	13.81	0.07	7.59	20.71	20.52	22.98	0.81
	LaneChangeISO_25kph	0.59	11.17	0.16	3.50	11.92	11.95	2.84	0.56
	LaneChangeISO_45kph	0.51	20.99	0.26	5.63	22.59	22.66	30.77	1.16
	LaneChangeISO_55kph	0.66	60.05	0.20	7.17	74.65	74.88	39.22	1.34
	without heading measurement:								
	DoubleOval_25kph	0.04	5.35	0.08	3.14	6.49	6.52	15.24	0.43
	DoubleOval_45kph	0.07	16.26	0.08	4.24	26.02	25.94	20.11	0.64
	DoubleOval_55kph	0.08	14.99	0.08	7.53	22.55	22.36	23.08	1.07
	LaneChangeISO_25kph	0.61	11.47	0.15	3.59	12.29	12.31	3.00	0.72
	LaneChangeISO_45kph	0.60	19.94	0.20	5.42	21.81	21.89	30.88	1.60
	LaneChangeISO_55kph	0.54	51.69	0.19	7.33	67.94	68.21	39.39	2.08

4.3.1 The wheel speed sensor

Another possible solution is to utilise the WSS on a vehicle. With a given wheel radius, R_i, and rotational speed, ω_i, the velocity of the wheel about its centre axis can be derived,

$$V_{[ij]} = \omega_i R_i \tag{4.7}$$

where: $[ij]$ = position of the wheel, i.e FR, FL, RR, RL

From the diagram of a twin track model, Figure 3.2, four kinematic equations can be determined:

$$V_{FR}\cos(\delta_{FR}) = \dot{x}_v + T_F\dot{\psi} \tag{4.8}$$

$$V_{FL}\cos(\delta_{FL}) = \dot{x}_v - T_F\dot{\psi} \tag{4.9}$$

$$V_{RR} = \dot{x}_v + T_R\dot{\psi} \tag{4.10}$$

$$V_{RL} = \dot{x}_v - T_R\dot{\psi} \tag{4.11}$$

Using the above equations, the longitudinal velocity and the yaw rate at the cg can be determined. However, in order to reduce the number of dependent variables and

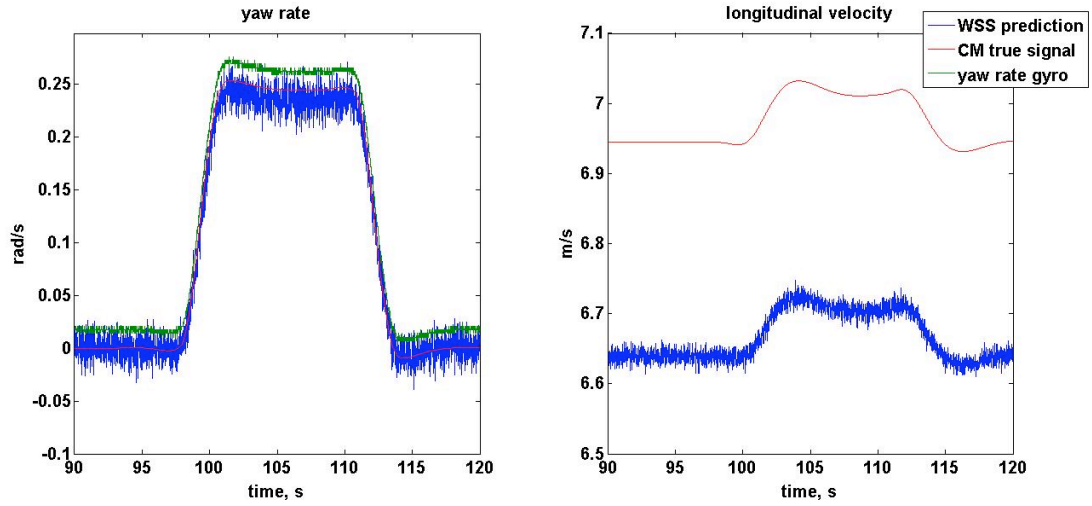

Figure 4.8: Yaw rate and longitudinal velocity calculated using the WSS measurements

uncertainties, only Equations 4.10 and 4.11 are used for calculation:

$$\dot{x}_v = \frac{V_{RR} + V_{RL}}{2} = \frac{(\omega_{RR} + \omega_{RL})R_w}{2} \tag{4.12}$$

$$\dot{\psi} = \frac{V_{RR} - V_{RL}}{2T_R} = \frac{(\omega_{RR} - \omega_{RL})R_w}{2T_R} \tag{4.13}$$

Both the wheel velocity and rotational speed are available from the CAN-bus. For a better representation of the error in the WSS, the wheel rotational speed is used for the calculation. With this approach, not only the noise in the WSS is taken into account, but also the approximation error of the tyre radius. Although noise in the sensor varies with the vehicle speed, it is taken here as having a constant standard deviation of $4 \times 10^{-2} rad/s$, as speed is maintained at a constant throughout the simulation.

Figure 4.8 shows the comparison of the two simulated noise signals of equations 4.12 and 4.13 with the signal of the noisy yaw rate gyro and the "true" values from IPG CarMaker. Despite the noisy predictions from the WSS, it does not have a bias as large as that in the yaw rate gyro. The bias in the WSS mainly comes from the uncertainty of the tyre radius, as it is affected by the load and driving manoeuvre.

In order to utilise the WSS predictions, the bias (tyre radius) must be estimated to a certain degree of accuracy before implementing into the dual KKF. Therefore, a KF is implemented with the GPS to estimate the bias in the WSS. Adding the

bias term into previous equations and after discretisation, the new equations are:

$$\begin{aligned} \dot{x}_v &= \frac{1}{2}(\omega_{RR} + \omega_{RL})(R_w + b_w) \\ x_v^{k+1} &= x_v^k + T_s \left(\frac{1}{2}(\omega_{RR} + \omega_{RL})(R_w + b_w) \right) \end{aligned} \tag{4.14}$$

$$\begin{aligned} \dot{\psi} &= \frac{1}{2T_R}(\omega_{RR} - \omega_{RL})(R_w + b_w) \\ \psi^{k+1} &= \psi^k + T_s \left(\frac{1}{2T_R}(\omega_{RR} - \omega_{RL})(R_w + b_w) \right) \end{aligned} \tag{4.15}$$

4.3.2 The simple wheel speed sensor EKF, *wssEKF*$_a$

The WSS EKF, *wssEKF*$_a$, uses Equation 4.15 and not Equation 4.14 because it does not require any other estimated values, such as the sideslip angle, to determine the reference measurement. The states for this KF are $\begin{bmatrix} \psi & b_w \end{bmatrix}^T$ and the input is $\frac{R_w}{2T_R}(\omega_{RR} - \omega_{RL})$. The equation is non-linear and an EKF is implemented. This gives a state space representation of,

$$\begin{aligned} \begin{bmatrix} \psi \\ b_w \end{bmatrix}_{k+1} &= \mathbf{\Phi_{wss}}\left(\psi, b_w\right)_k + \frac{R_w}{2T_R}(\omega_{RR} - \omega_{RL}) \\ \begin{bmatrix} \cos(\nu_{gps}) \\ \sin(\nu_{gps}) \end{bmatrix}_k &= \mathbf{H_{wss}}\left(\psi, b_w\right)_k \end{aligned} \tag{4.16}$$

where $\mathbf{\Phi_{wss}}$ and $\mathbf{H_{wss}}$ are the non-linear functions of the estimated states at time step k. During the EKF operation, the function is partially differentiated to obtained the Jacobian matrix, refer also to Section 2.4.3:

$$\begin{aligned} Jf_{wss} &= \frac{\partial \mathbf{\Phi_{wss}}}{\partial \mathbf{x}_k} = \begin{bmatrix} 1 & \frac{1}{2T_R}(\omega_{RR} - \omega_{RL})T_s \\ 0 & 1 \end{bmatrix}_k ; \\ Jh_{wss} &= \frac{\partial \mathbf{H_{wss}}}{\partial \mathbf{x}_k} = \begin{bmatrix} -\sin(\psi) & 0 \\ \cos(\psi) & 0 \end{bmatrix}_k . \end{aligned}$$

Similar to the *yawKKF*, during cornering (when $\dot{\psi} > 1°/s$) and GPS outages, the terms in the measurement matrix becomes zero to avoid updating the EKF with incorrect measurements. Figure 4.9 shows that the *wssKKF*$_a$ is able to produce a corrected heading angle estimation with a NRMSD error of 0.52% in the *DoubleO-val_25kph* simulation. From the zoom-in plot, at the end of the first turn, just before the GPS measurement activates, the heading estimation of the *wssEKF*$_a$ does not closely predict the true data, having an error of approximately 6°. It is after the

GPS signal returns that the $wssEKF_a$ begins to perform correction.

This type of error is typical in a KF when the sensors have multi-frequency sampling with unknown dynamic behaviour in the bias errors, i.e. assumed constant, $\dot{b}_w = 0$. As shown in the bottom plot of Figure 4.9, the bias estimation, b_w, is in the shape of a stair-case. Since there are no predefined dynamics for the bias estimation, it only updates whenever the GPS measurement is available. Between each GPS samples and cornering manoeuvre, the latest bias prediction update is carried forward and used during the absence of GPS reference measurements. When the measurement matrix is once again activated, the bias starts to make corrections again.

There are four corners in the simulation, the four steps representing the differ-

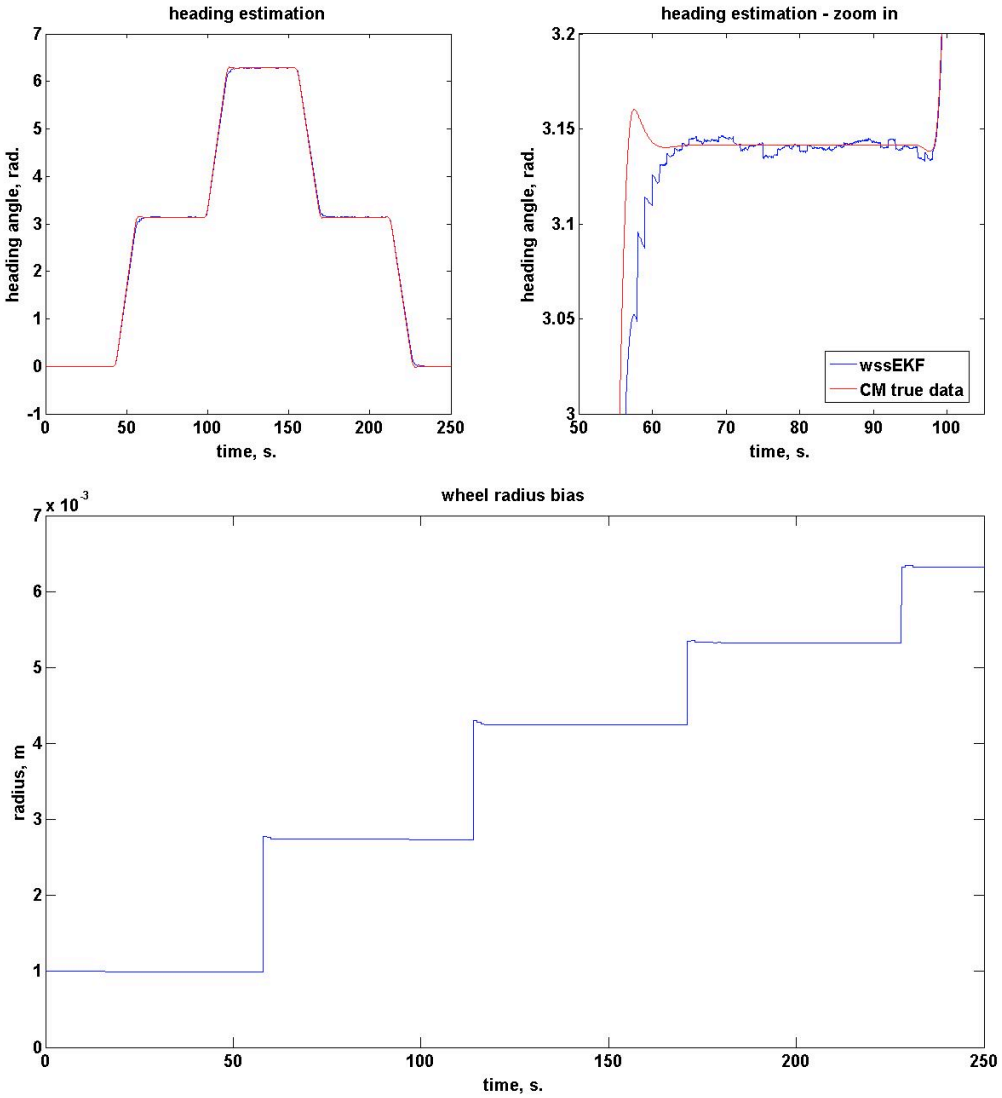

Figure 4.9: State estimation of $wssEKF_a$ from *DoubleOval_25kph* simulation

ence in angles between the estimation from the 'corrected WSS' and the GPS after individual cornering. The large steps suggest that the prediction of the radial bias of the tyres before the cornering is incorrect, further confirming the offset error in the heading estimation plots. Although the initial error is large, it reduces gradually as time proceeds. Determining from the trend here, the bias should slowly converge to a single value, i.e. $\approx 13 \times 10^{-3}$ in this simulation when $R_w = 0.28m$.

From a more careful inspection of Figure 4.9 and a comparison with Figure 4.2, the bias prediction in the *yawKKF* seems to have outperformed that in the $wssEKF_a$, especially in the initial stage ($0s.$ to $40s.$) when the vehicle is on the straight road. The fact is that the $wssEKF_a$ has not under-performed, but is unobservable on the straight road. Reconsidering Equation 4.15 and applying a discrete linear state space representation to it,

$$\begin{bmatrix} \psi \\ b_w \end{bmatrix}_{k+1} = \begin{bmatrix} 1 & \frac{T_s}{2T_R}(\omega_{RR} - \omega_{RL}) \\ 0 & 1 \end{bmatrix} \begin{bmatrix} \psi \\ b_w \end{bmatrix}_k + \begin{bmatrix} \frac{1}{2T_R}(\omega_{RR} - \omega_{RL}) \\ 0 \end{bmatrix} R_w.$$

When travelling on a straight road, without a split-μ condition, the left and right tyres should be rotating at the same rate or very close range, i.e. $\omega_{RR} \approx \omega_{RL}$. As a result, the above expression is modified to,

$$\mathbf{X_{k+1}} = \mathbf{\Phi_k X_k} + \mathbf{\Delta_k u}$$
$$\begin{bmatrix} \psi \\ b_w \end{bmatrix}_{k+1} = \begin{bmatrix} 1 & 0 \\ 0 & 1 \end{bmatrix} \begin{bmatrix} \psi \\ b_w \end{bmatrix}_k + \begin{bmatrix} 0 \\ 0 \end{bmatrix} R_w.$$

With the measurement output from the GPS, the simplified matrix is,

$$\mathbf{Z_k} = \mathbf{H_k X_k}$$
$$\begin{bmatrix} \nu \end{bmatrix} = \begin{bmatrix} 1 & 0 \end{bmatrix} \begin{bmatrix} \psi \\ b_w \end{bmatrix}_k.$$

The observability for this system on a straight road is then determined by calculating the number of unobservable states in the system by subtracting the rank of observability matrix, $\mathbf{O}$, from the rank of process matrix in $wssEKF_a$, $\mathbf{\Phi_k}$,

$$\mathbf{O} = \begin{bmatrix} \mathbf{H_k} & \mathbf{H_k \Phi_k} & \mathbf{H_k \Phi_k^2} & \cdots & \mathbf{H_k \Phi_k^{n-1}} \end{bmatrix}^T; \tag{4.17}$$

where n is the number of state variables

From the above formulation, it can be concluded that the bias state is unobservable in the system under straight road conditions. At cornering, although

$\omega_{RR} \neq \omega_{RL}$, due to the lack of heading measurement, $\mathbf{H_k}$ changes to zeros and the bias state estimation stays unobservable. The only time for the bias to update is the short period just before the end of the corner when the sideslip is negligibly small. This simple and quick analysis gives an explanation of the shape and behaviour of the estimation.

One way to resolve this unobservability problem is by providing a heading angle measurement during cornering. This can be done by fusing in the heading estimation from the *yawKKF*, but doing so will destroy the initial idea of using the WSS to provide an external heading angle source for the *yawKKF*. Another approach is to provide other sources of measurement to the $wssEKF_a$ while it is on the straight road.

4.3.3 The inclusion of external constraints, $wssEKF_b$

Referring back to Equation 4.12, on a straight road the yaw rate is zero and the vehicle motion is mainly in the forward direction. This allows an assumption of longitudinal velocity being the same as the velocity measured from the GPS. Hence, Equation 4.12 can be modified to:

$$\begin{aligned} \dot{x}_v|_{straight} \approx V_{gps} &= \frac{(\omega_{RR} + \omega_{RL})(R_w + b_w)}{2} \\ b_w &= \frac{2V_{gps}}{\omega_{RR} + \omega_{RL}} - R_w = b_{w|gps}. \end{aligned} \tag{4.18}$$

With this extra measurement, the system becomes observable and the measurement of state space representation is modified to include the new measurement, $b_{w|gps}$,

$$\begin{bmatrix} \nu \\ b_{w|gps} \end{bmatrix} = \begin{bmatrix} 1 & 0 \\ 0 & 1 \end{bmatrix} \begin{bmatrix} \psi \\ b_w \end{bmatrix}_k .$$

Similar to the previous dual KKF setup, during GPS outage and vehicle cornering, the measurement matrix switches from the identity matrix to zeros. The variance for the new measurement, $\sigma^2_{bw|gps}$, is given as,

$$\sigma^2_{bw|gps} = \left[\left(\frac{1}{\omega_{RL} + \omega_{RR}} \right) \sigma_{Vgps} \right]^2 + \left[\left(\frac{2V_{gps}}{(\omega_{RL} + \omega_{RR})^2} \right) \sigma_{\omega_{RR,RL}} \right]^2 \times 2$$

Figure 4.10 shows the heading and bias estimation for the modified *wssEKF*. It is not obvious from the plots that the heading estimations have improved, but from the %NRMSD error, the new $wssEKF_{b1}$ has actually improved from a previous error

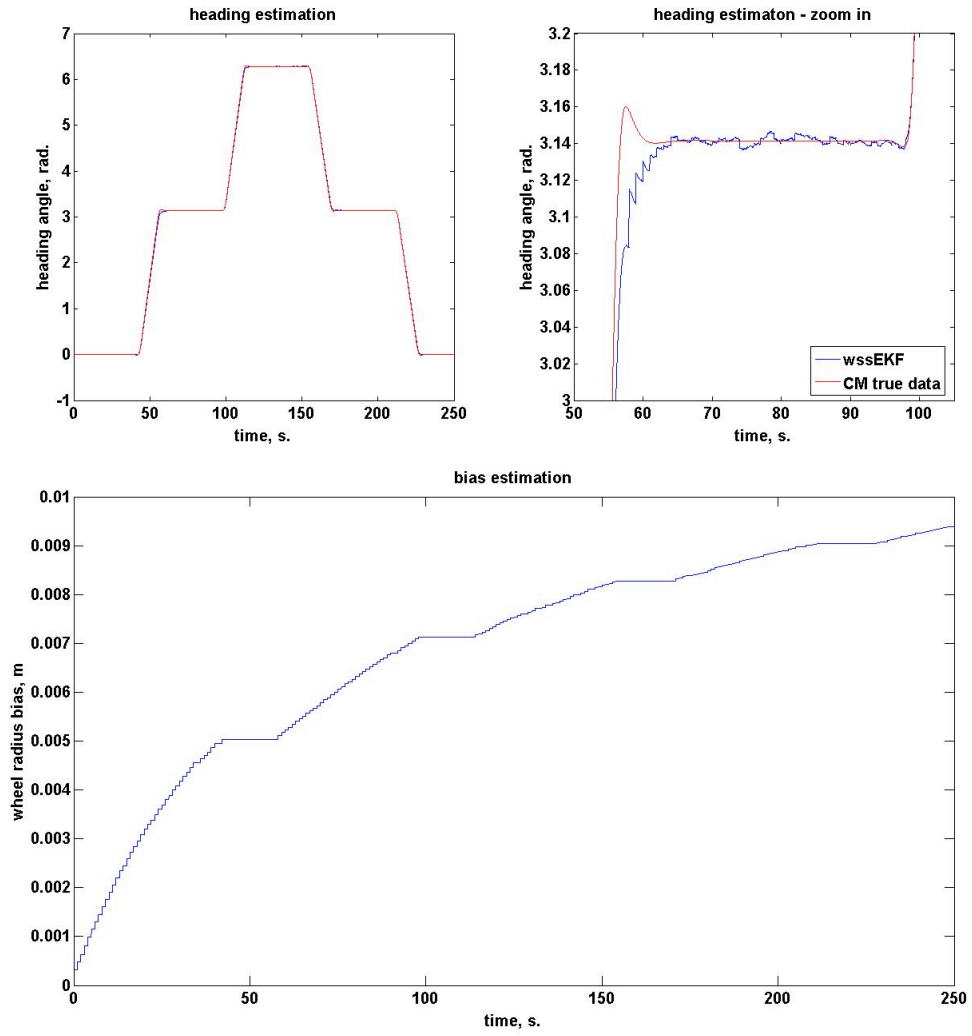

Figure 4.10: State estimation of $wssEKF_{b1}$ with new measurement from *DoubleOval_25kph* simulation

of 0.52% to 0.33%. In the bias estimation plot, the staircase has disappeared and it is clear that the bias is estimating when the vehicle is on the straight road. However, the rate of the estimation is not fast enough to converge to a constant.

From the $wssEKF_{b1}$ setup, states are updated when GPS is available, therefore, the update is operated at the same sample frequency as the GPS, 1Hz. For a state with known time derivative function, the state is numerically integrated between updates. However, if the time derivative is unknown, the state has to stay constant between updates, hence, the staircase pattern at every second. In straight road driving, Equation 4.18 stands and assumes that the speed does not change much during GPS samples. The equation will therefore still be valid even between GPS samples. The $wssEKF_{b1}$ measurement update is modified with the following rules:

1. Corners:

$$\begin{bmatrix} \nu \\ b_{w|gps} \end{bmatrix} = \begin{bmatrix} 0 & 0 \\ 0 & 0 \end{bmatrix} \begin{bmatrix} \psi \\ b_w \end{bmatrix}_k ;$$

2. Straight road and GPS is 'ON':

$$\begin{bmatrix} \nu \\ b_{w|gps} \end{bmatrix} = \begin{bmatrix} 1 & 0 \\ 0 & 1 \end{bmatrix} \begin{bmatrix} \psi \\ b_w \end{bmatrix}_k ;$$

3. Straight road and GPS is 'OFF':

$$\begin{bmatrix} \nu \\ b_{w|gps} \end{bmatrix} = \begin{bmatrix} 0 & 0 \\ 0 & 1 \end{bmatrix} \begin{bmatrix} \psi \\ b_w \end{bmatrix}_k .$$

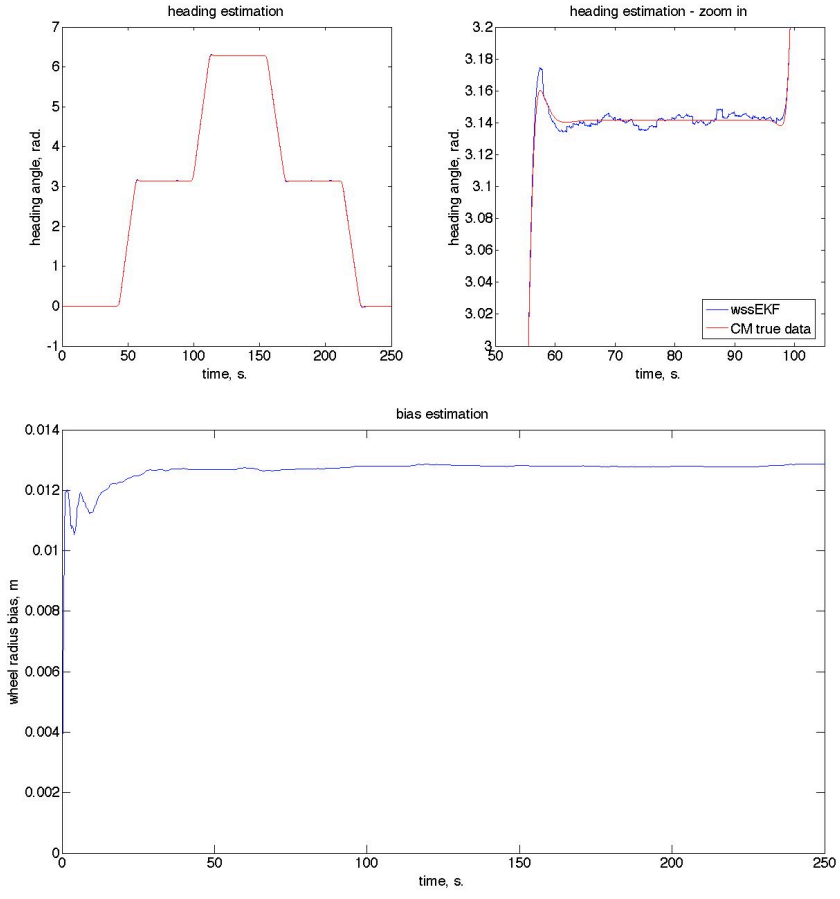

Figure 4.11: State estimation of $wssEKF_{b2}$ with new measurement and rules from *DoubleOval_25kph* simulation

Using the rules above, the bias is estimated at any time as long as the vehicle

is travelling on a straight road. From the bias estimation plot in Figure 4.11, the modified rules have shown to be useful and effective in bias estimations. Within 30 seconds, the $wssEKF_{b2}$ is able to converge to the correct bias and maintain at the same value throughout the rest of the simulation. The correct bias has enabled a more accurate heading angle estimation, in which the % NRMSD error has reduced dramatically to as little as 0.06%. Table 4.4 shows average error for 10 manoeuvres over 10 simulations. Note that due to different load is applied onto the vehicle model, R_w is now started with 0.329m.

Table 4.4: Comparison of the estimated errors of $wssEKF_{b2}$ and *yawKKF*

		$\boldsymbol{wssEKF_{b2}}$		***yawKKF***	
		NRMSD	RMSD	NRMSD	RMSD
	Estimated states:	$\hat{\psi}$	$\hat{b}_w$	$\hat{\psi}$	$\hat{b}_r$
manoeuvre	*DoubleOval_15kph*	0.11	0.18	0.04	0.03
	DoubleOval_25kph	0.07	0.30	0.04	0.06
	DoubleOval_35kph	0.20	0.35	0.05	0.08
	DoubleOval_45kph	0.93	0.12	0.06	0.09
	DoubleOval_55kph	4.38	0.14	0.08	0.09
	LaneChangeISO_15kph	1.23	0.33	0.81	0.09
	LaneChangeISO_25kph	0.98	0.36	0.59	0.10
	LaneChangeISO_35kph	1.02	0.22	0.58	0.23
	LaneChangeISO_45kph	1.12	0.34	0.55	0.16
	LaneChangeISO_55kph	1.39	0.39	0.52	0.21

* $R_w = 0.329m$
* true tyre bias for *DoubleOval* $= -0.036m$
* true tyre bias for *LaneChangeISO* $= -0.049m$

In the *DoubleOval* manoeuvre, as the speed of the vehicle increases, the accuracy of the heading estimation decreases, especially when the speed is above 35kph. The increase of the heading error in the $wssEKF_{b2}$ is not a cause of the tyre bias estimations, see Figure 4.12, but of the rolling angle of the vehicle. The inclusion of this angle affects the load distribution at each wheel and causes them to deflect accordingly. The tyre bias estimated here represents the static deflection of the tyres and not the dynamic deflection. As shown in the table, the static bias of the tyre is estimated accurately at different speeds. Similarly in the *LaneChangeISO* cases, the bias estimation is estimated with a low error; however, unlike the *DoubleOval* simulations, the heading estimation error remains more or less the same as speed varies. The main reason for this is the relatively shorter cornering period (1 second compared to 7 seconds at 55kph in the *LaneChangeISO* and *DoubleOval* manoeuvre respectively) in the *LaneChangeISO* manoeuvres. Hence, a longer cornering manoeuvre causes a longer delay in KF correction. Since dynamic deflection bias exists

in the tyres during a high speed cornering, without KF correction, errors accumulate, see Figure 4.12. In general, of the two types of manoeuvres, the *LaneChangeISO* gives a greater heading estimation error. This is because of the induced rolling angle as mentioned previously.

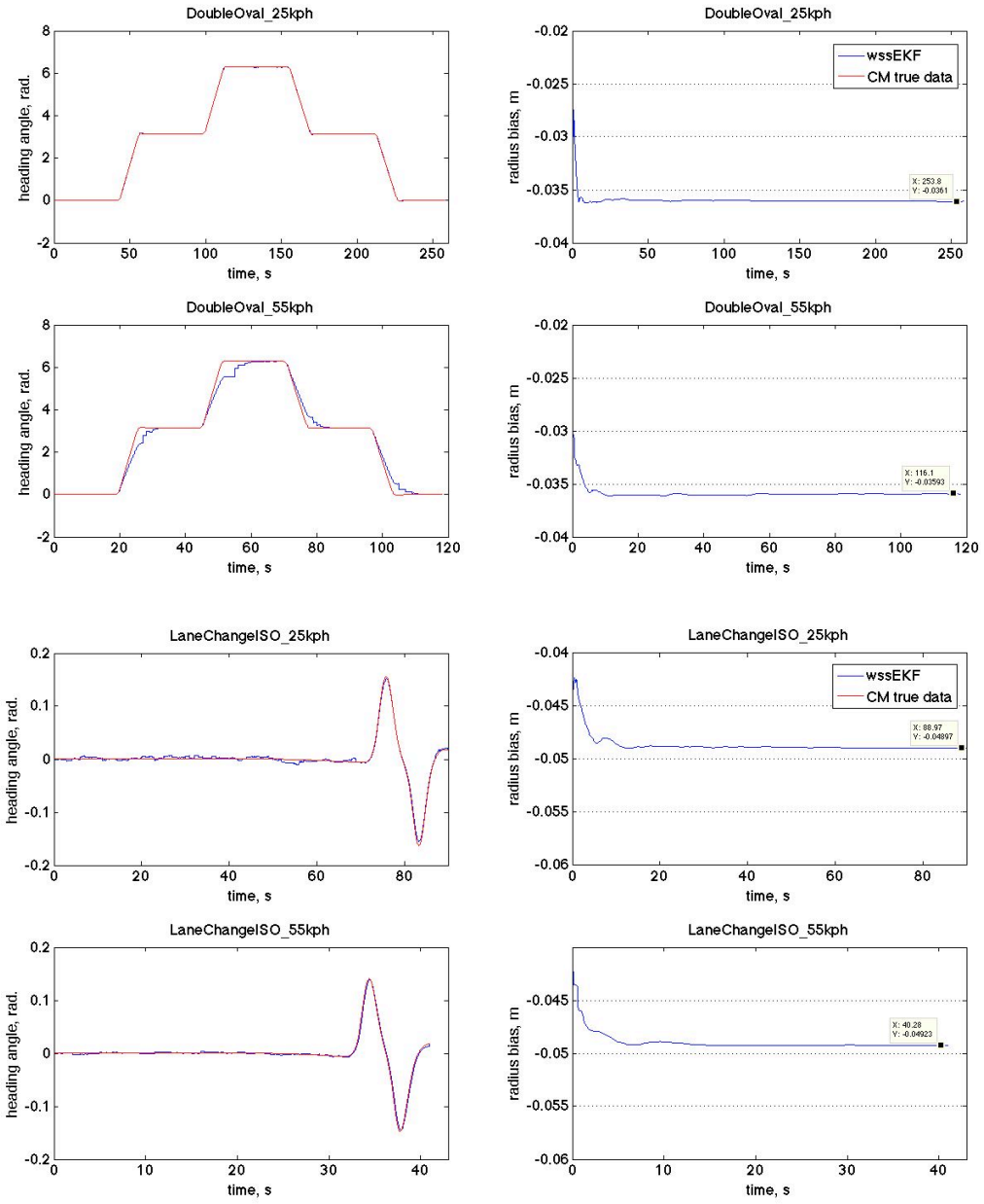

Figure 4.12: State estimated by the *wssEKF*

When comparing the results of the *yawKKF* with those of the $wssEKF_{b2}$, it is clear that the performance of the *yawKKF* is superior. This suggests that the *wssEKF*s in general does not contribute much benefit to the estimations of the *yawKKF* during cornering. If the heading estimation $\hat{\psi}_{wss}$ is used as a measurement

in the *yawKKF*, depending on the measurement covariance matrix, estimations from the *yawKKF* will either be contaminated with unwanted disturbances (i.e. using small measurement covariance) or have no influence at all (i.e. using large measurement covariance).

It seems that from this investigation the $wssEKF_{b2}$ has nothing to offer to the system, but the determination of the static tyre bias enables us also to estimate the longitudinal velocity as discussed at the beginning of this subsection, recalling Equation 4.14. Figure 4.13 shows the longitudinal velocity estimation comparison of *velKKF* and $wssEKF_{b2}$ in the *DoubleOval_25kph* simulation.

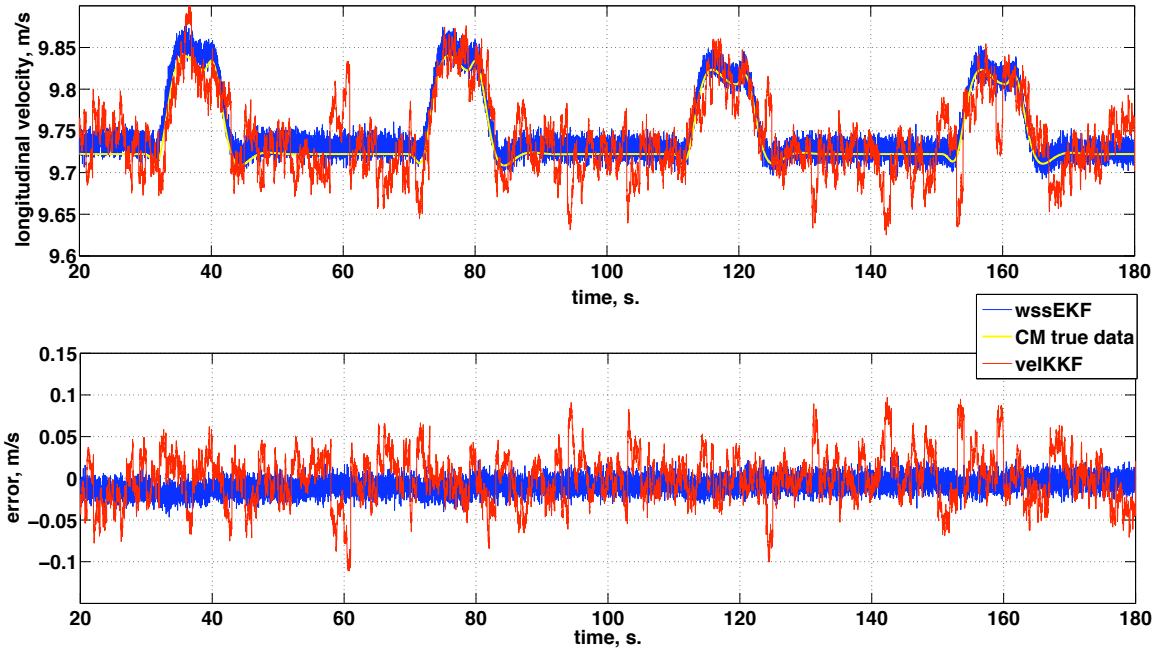

Figure 4.13: Comparison of longitudinal state estimated of $wssEKF_{b2}$ and *velKKF* in *DoubleOval_25kph*

It can be seen that the $wssEKF_{b2}$ gives a more structured and stable longitudinal velocity estimation than the *velKKF*. The error of the $wssEKF_{b2}$ also reduces with time because the static bias in the tyres gets predicted better. Over the 10 manoeuvres and simulations, see Table 4.5, apart from the *DoubleOval_55kph*, all the longitudinal velocity estimations in $wssEKF_{b2}$ have been predicted more accurately than those in the *velKKF*.

The exceptional error at 55kph is due to the pitching and rolling of the vehicle during a high speed cornering, which causes a change in dynamic tyre deflection and tyre slip angle. These changes are significant when determining the velocities

Table 4.5: Average longitudinal velocity estimation error from *wssEKF* and *velKKF* over 10 simulations each

		wssEKF	***velKKF***
		RMSD	RMSD
	Estimated states:	$\hat{\dot{x}}_v$	$\hat{\dot{x}}_v$
manoeuvre	*DoubleOval_15kph*	0.85	2.96
	DoubleOval_25kph	0.89	3.05
	DoubleOval_35kph	1.10	2.91
	DoubleOval_45kph	2.19	3.42
	DoubleOval_55kph	10.04	6.71
	LaneChangeISO_15kph	0.88	2.82
	LaneChangeISO_25kph	0.93	3.03
	LaneChangeISO_35kph	0.90	2.92
	LaneChangeISO_45kph	0.99	3.04
	LaneChangeISO_55kph	1.06	2.98

as they affect the load and the forces applied on the tyres. The pitching and rolling angles can be obtained from pitch rate and roll rate gyroscopes. As these sensors are not yet common instruments onboard vehicles, they are not considered here.

From Table 4.5, the error in the *DoubleOval_55kph* simulation is also greater than the *LaneChangeISO_55kph*. As explained earlier, this is mainly due to the accumulation of errors during the time of cornering.

4.3.4 The Triple KF Design, $wssEKF_c$

From previous results, each KF is good at estimating one particular state. When the vehicle starts off on a straight road with available GPS, the *yawKKF* is good at heading estimation while $wssEKF_{b2}$ and *velKKF* are good at longitudinal and lateral velocity estimation respectively. Therefore, it is natural to combine the three KF to form a triple KF setup, see Figure 4.14.

The triple KF design differs from the original dual KKF by the inclusion of the $wssEKF_c$, an upgraded version of previous $wssEKF_{b2}$. In $wssEKF_c$, the heading estimations from the *yawKKF* are added to the measurement vector. During cornering, the *yawKKF* estimations provide an update for the heading estimation in $wssEKF_c$. This allows $wssEKF_c$ to estimate its states more accurately, hence, improving also the longitudinal velocity estimation. This velocity estimation is then implemented into the *velKKF* to provide a continual source of longitudinal velocity measurement when the GPS is unavailable.

Table 4.6 shows the state estimation errors for the triple KF. The results obtained from these simulations agree with the previous analysis on a single *wssEKF*. With the

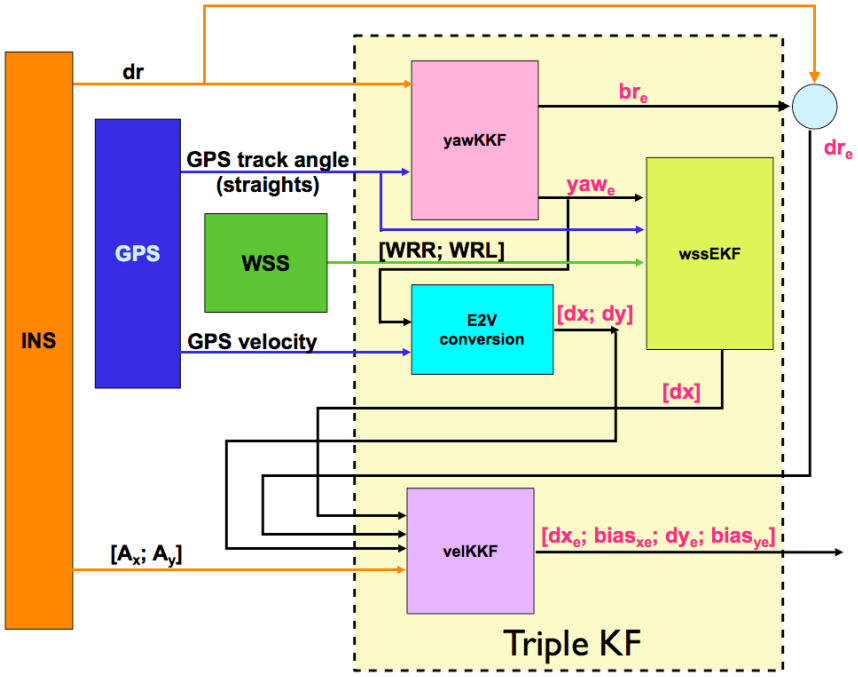

Figure 4.14: The triple KF design

Table 4.6: State estimation errors for a triple KF

		yawKKF		***velKKF***				***wssEKF$_c$***	
		NRMSD	RMSD	RMSD	NRMSD	RMSD		NRMSD	RMSD
	Estimated states:	$\hat{\psi}$	$\hat{b}_r$	$\hat{\dot{x}}_v$	$\hat{\dot{y}}_v$	$\hat{b}_x$	$\hat{b}_y$	$\hat{\psi}$	$\hat{b}_w$
manoeuvre	*DoubleOval_15kph*	0.04	0.04	0.87	6.75	13.14	0.21	0.04	0.34
	DoubleOval_25kph	0.04	0.06	0.90	6.09	13.15	0.38	0.04	0.37
	DoubleOval_35kph	0.05	0.09	0.99	9.37	13.21	0.40	0.05	0.31
	DoubleOval_45kph	0.06	0.05	2.28	24.78	13.85	0.79	0.10	0.08
	DoubleOval_55kph	0.08	0.08	10.22	20.45	13.68	1.29	0.29	0.24
	LaneChangeISO_15kph	1.24	0.09	0.84	16.67	2.31	0.14	1.25	0.25
	LaneChangeISO_25kph	1.08	0.08	0.94	14.77	2.69	0.58	1.13	0.31
	LaneChangeISO_35kph	0.65	0.16	0.98	16.95	12.81	0.91	0.68	0.20
	LaneChangeISO_45kph	0.64	0.18	0.95	24.54	12.65	1.27	0.71	0.32
	LaneChangeISO_55kph	0.60	0.25	1.04	74.65	12.74	2.19	0.78	0.38

heading estimates from *yawKKF*, *wssEKF$_c$* is able to predict the heading angle more accurately, refer to Table 4.4. Comparing these results with those obtained from the dual KKF results, Table 4.2, the longitudinal velocity from the *velKKF* clearly shows a smaller estimated error. This reduction is due to the accurate determination of velocity using the estimated states from the *wssEKF$_c$*. However, when the speed is increased to 55kph or over, the error caused by pitching and rolling of the vehicle still remains an issue, see manoeuvres at 55kph and Figures 4.15 and 4.16. Unless these angles are accurately measured/predicted, the triple KF is limited to manoeuvres that have negligible pitching and rolling angles. As mentioned earlier, studies on pitching and rolling angles are beyond the scope of this thesis, and therefore they

will not be investigated further here.

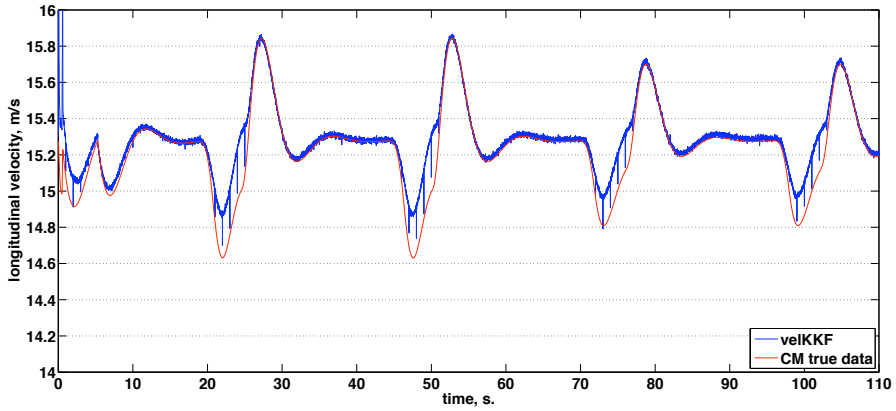

Figure 4.15: The longitudinal velocity from the *velKKF* in the triple KF design, *DoubleOval_55kph*

However, the error in Figure 4.15 can be reduced by including an extra dynamic bias, b_d, in the original longitudinal equation, $\ddot{x}_v = A_x + \dot{y}_v\dot{\psi} - b_x - b_d$, to compensate for the pitching motion. So b_d can be estimated by assuming it to be zero on the straight road and equal to the difference between the GPS velocity and the WSS velocity on the curve:

$$\begin{aligned} &\text{Striaght:} && b_d = 0; \\ &\text{Curve:} && b_d = (V_{gps}\cos\left(\nu_{gps} - \hat{\psi}\right) - \hat{V}_{wss})\frac{1}{T_s^{gps}}. \end{aligned} \tag{4.19}$$

Although this is able to address the error for the 55kph cases, care must be taken during the implementation. This is because Equation 4.19 assumes that the GPS estimation is always accurate and uses the measurements as a reference. From Figure 4.16 one can notice that the WSS is more accurate than the GPS at low speed and the effect of pitching becomes apparent at higher speed.

4.3.5 Summary for the WSS aided triple KF

Table 4.7 shows a summary for the different versions of *wssEKF* used in this study. The inclusion of the WSS has demonstrated some useful features. It is able to estimate the heading angle accurately with the aid of heading estimation from the *yawKKF*. The triple KF is able to improve the longitudinal velocity estimations but only when the speed of the vehicle is below a critical speed (45kph in this case). When the speed increases above the critical speed, pitching and rolling effect can no longer be neglected. Although the KF is capable of reducing the error of the

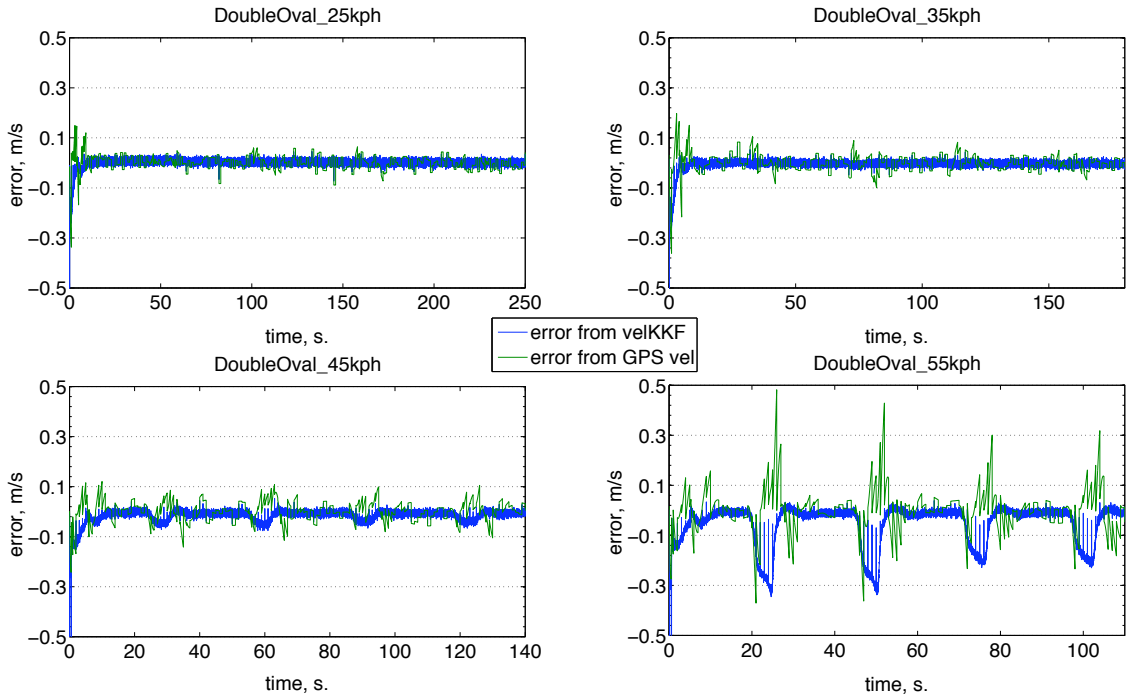

Figure 4.16: Estimation error of longitudinal velocity from the *velKKF* and raw GPS signals

estimation by including a virtual bias, such as the dynamic bias mentioned in the last section, this requires an accurate reference measurement.

Table 4.7: Summary for WSS aided triple KF

Types of *wssEKF*	**Features**
$wssEKF_a$	original EKF
$wssEKF_{b1}$	measurement constrained on the straight road
$wssEKF_{b2}$	rules applied
$wssEKF_c$	heading estimation from *yawKKF* is implemented as measurement

4.4 Effects of GPS precision

In the dual KKF and triple KF design, GPS measurements are used as a primary source for referencing: the *yawKKF* and *wssEKF* uses the GPS tracking angle while the *velKKF* uses the predicted sideslip angle and GPS velocity. In the *yawKKF*, when yaw rate is higher than the magnitude of noise, the estimated heading angles will be accurate with only minimal error. As discussed previously, the sideslip angle is determined at a low sampling rate to compromise with the slow GPS frequency. This, as a result, causes delay and error in the sideslip calculation, and it becomes

highly sensitive to the GPS precision, namely its accuracy (error variance) and its sampling rate.

Sideslip angle is an important state because it is the only connection between the actual dynamics and the dynamics in the v-frame. In Equation 4.1, the longitudinal and lateral velocity can be referenced to the GPS velocity and sideslip prediction. As discussed in Section 4.3, GPS is not always capable of providing accurate measurements. In such cases, the implementation of *wssKKF* is able to compensate for this deficiency but is strictly limited to longitudinal velocity estimations. Theoretically, the sideslip can be re-engineered into, $\cos\beta = \hat{\dot{x}}_v / V_{gps}$, but due to the small sideslip and contamination of noise, the results are almost useless.

Without any other means of determining the sideslip, the lateral velocity can only be determined via Equation 4.1. Lateral velocity estimation is, therefore, highly dependent on the predicted sideslip angle of the vehicle. This section looks at the limitations and the level of influence that GPS has on KF predictions. In addition, a guided chart of different types of GPS is proposed in order to aid designers to choose suitable devices against their error criterion.

4.4.1 Precision of GPS in the market

Table 4.8: GPS receivers accuracy

Types of GPS grade	**Price range (in US$)**	**Accuracy****
*Survey	> 12000	0.01 (0.01)
*Mapping	500 – 12000	2 – 5 (0.10)
*Consumer	< 500	15 – 20 (0.50)
GlobalSat® DG-100	≈ 75	3–4 (0.04)
GlobalSat® DG-100 with external antenna	≈ 95	1–2 (0.017)

* data taken from Wing et al. [2005]
** standard deviation of position(m) and velocity (ms^{-1}), in parentheses

Table 4.8 shows the prices and varying accuracies of the 3 types of GPS receiver described in Wing et al. [2005] and the GlobalSat® DataLogger DG-100 purchased in year 2007. For detailed evaluation of the accuracy of the DG-100, please refer to Appendix B.2.

From the table it is clear that whereas price has decreased, the accuracy of GPS receivers in general has increased enormously throughout a two-year period. With a price of much less than US$500, users are now able to obtain accuracy similar to a mapping grade GPS in 2005. This improvement is due to the introduction of the latest SiRF Star III GPS Chipset, which has a faster satellite fix time, a higher

sensitivity to satellite position, and advanced Wide Area Augmentation System (WAAS). With an extra external antenna attached, the DG-100 GPSlogger shows some improvement in both position and velocity determination. For details on the DG-100 test, please refer to Appendix B.2.

With current competition in the GNSS sector, there is little doubt that the price-to-accuracy ratio of GPS receivers will be further reduced in the coming years. Furthermore, as other GNSS technologies become mature and available, they can be considered to replace or cooperate with the GPS measurements in the proposed dual KKF or triple KF.

4.4.2 Simulation setup

In this study, 5 different manoeuvres are simulated:

i) Straight road (ST),

ii) Right Turn (RT),

iii) Figure of Eight Course (8C),

iv) Lane Change (LC), and

v) Self-Defined course (SD).

Each course has its own characteristics, ranging from simple straight to windy, from low to high demand on driver response. Details on the 5 courses can be found in Appendix C. This, enables the investigation into the influence of the different courses in state estimation. Moreover, in order to concentrate on the effects of GPS precision on state estimations while minimising other errors due to unmodelled dynamics, each manoeuvre above is simulated 10 times with the vehicle travelling at a low constant speed of 5m/s. The state estimation utilises the dual KKF setup discussed previously with noise and bias defined as Table B.2 in Appendix B.1.

In order to reduce the error effect from the yaw rate gyro and concentrate on the GPS precision effect on the KF state estimation performance, the dual KKF assumes perfect measurements from the gyroscope. This assumption is reasonable since the *yawKKF* is able to estimate heading angle accurately below an error of 1%, refer to Table 4.2 in Section 4.3. Moreover, the accelerometers in this study are assumed to be not sensitive to gravity, in other words, the pitching and rolling of the vehicles does not have any effect on the accelerometer measurements. This assumption is not entirely true in reality, but given this assumption, the results are easier to analyse.

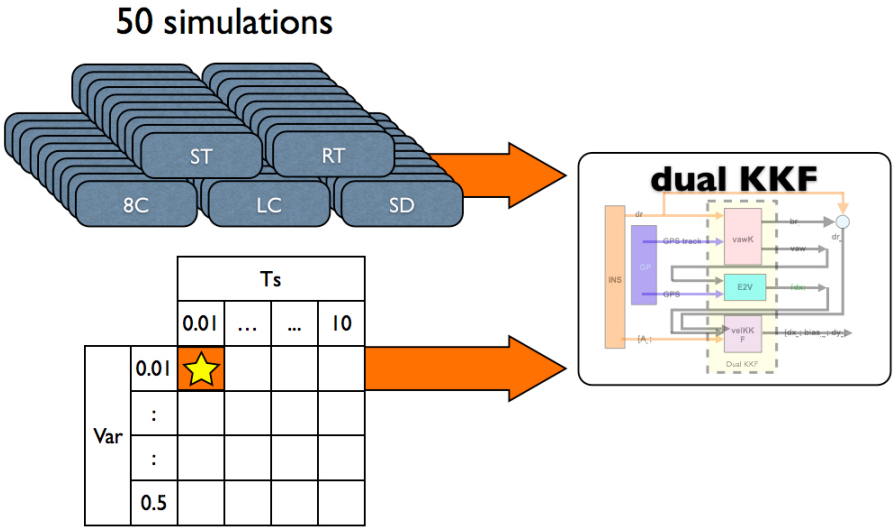

Figure 4.17: The simulation structure for the GPS precision study

The primary objective of this section is to look at the influence of the GPS sampling time and GPS error variance on the dual KKF state estimation. With a perfect heading reading, the estimated error is concentrated at the state estimations of *velKKF* as its measurement vector is dependent upon the speed and tracking angle of the GPS. By varying the sampling rate and velocities variance of the GPS between 0.1Hz to 100Hz and 0.01 to 0.5m/s (standard deviation of GPS velocity) respectively, the estimation error for the longitudinal and lateral velocities can be obtained. At this point, it is important to bear in mind that the maximum rate of GPS message received is 50Hz. Any frequency higher than 50Hz in the simulation is regarded as future technology.

To understand the simulation structure for this study in more detail, refer to Figure 4.17. At first, the sampling rate and variance are divided into sets. For each set, 50 simulations (10 simulations on each manoeuvre) are performed in the dual KKF and the average error of the velocity estimations are obtained. The errors are plotted against sampling time and GPS velocity variance, with colour bands representing the different sensors as described in Table 4.8.

4.4.3 The effect of GPS sampling rate

In Section 4.2.1, it was shown that the dual KKF is able to predict biases efficiently. To see the effect of different sampling rates on the velocity estimations, a typical consumer GPS receiver is assumed, which has a velocity variance of 5e-4 m^2/s^2. The estimated errors for the longitudinal and lateral velocity estimations are plotted in Figures 4.18 and 4.19.

From the longitudinal velocity error, Figure 4.18, the error plots of the five manoeuvres are very close to one another, suggesting that the longitudinal velocity is not sensitive to different manoeuvres. As the vehicle is travelling on straight road, the bias of the longitudinal accelerometer is estimated. As the speed of the vehicle is constant, the change in longitudinal velocity is minimal even during the heavy cornering manoeuvres, namely the LC and SD.

As the sampling frequency increases, GPS measurements are received more regularly and accelerometer biases in the *velKKF* are estimated more frequently. This, as a result, reduces the errors in the longitudinal velocity estimations. Note that the estimations are improved more significantly between 0.1 and 5Hz when compared with the change between 5 to 100Hz. This suggests that a GPS receiver with a higher frequency may not necessarily benefit the overall design, as cost tends to rise exponentially after the typical consumer grade GPS (1Hz).

Figure 4.19 shows the the lateral velocity estimation error for the five manoeuvres. Different to Figure 4.18, the error curves do not coincide with one another. The lateral velocity estimation itself is sensitive to the manoeuvres, with simulations ST and SD having the least and the most average error respectively. Although there are no lateral dynamics in the ST manoeuvre, the GPS measurements are accurate enough to correct the bias in the lateral accelerometer.

When the manoeuvre involves more lateral motion, the error increases. This

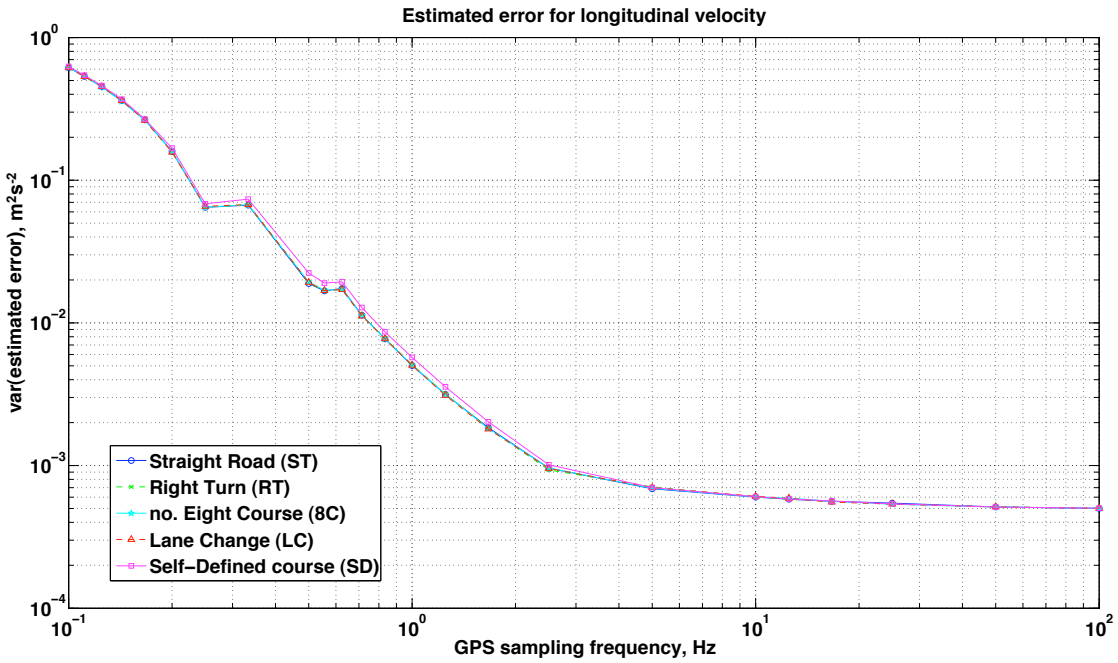

Figure 4.18: Estimation error of longitudinal velocity over GPS velocity variance. σ_{vel} = 5e-4

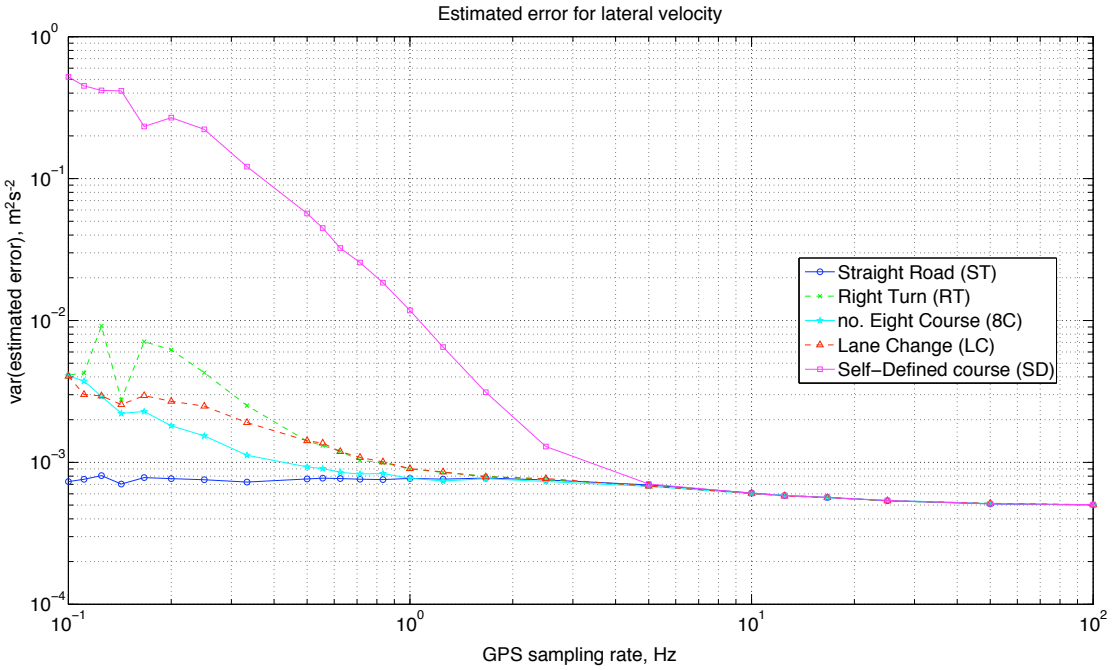

Figure 4.19: Estimation error of lateral velocity over GPS sampling rate. σ_{vel} = 5e-4

is because the GPS sideslip prediction ($\beta_{gps} = \nu_{gps} - \psi_{ins}$) fails to keep up with the change in lateral motion in between GPS samples. To explain the cause for this error, one must refer back to the original KF Equations 2.20 to 2.25. During the GPS outage time, without any sideslip dynamic equation, the sideslip angle is retained at the last reading. Since the measurement matrix $\mathbf{H_{vel}}$ of *velKKF* is configured as $\begin{bmatrix} 1 & 0 & 0 & 0 \\ 0 & 0 & 1 & 0 \end{bmatrix}$ during GPS outage, the correction phase of the KF remains valid:

$$\hat{x}_k = \hat{x}_k^{ins} + \mathbf{K_{vel}}(z_k^{gps} - z_k^{ins}).$$

As GPS measurements are placed on hold, their 'trustworthiness' is not the same as when GPS is available. Therefore, the measurement covariance, $\mathbf{R_{vel}}$, is set to $1.0^2 m^2/s^2$. This allow the GPS measurements to have some effect on the final estimations. If the covariance is changed to, say $100^2 m^2/s^2$, $\mathbf{K_{vel}}$ will become near zero and this is equivalent to setting the $\mathbf{H_{vel}}$ components to zeros, see Figure 4.20.

From Figure 4.20, one can see that during GPS outages, e.g. 55 to 56s., the Kalman gain is a lot higher when the measurement covariance is set to $1.0^2 m^2/s^2$. Although this gain is still relatively small compared to the gain when GPS is available (about 1), it is enough to cause error in the estimation during the GPS outages,

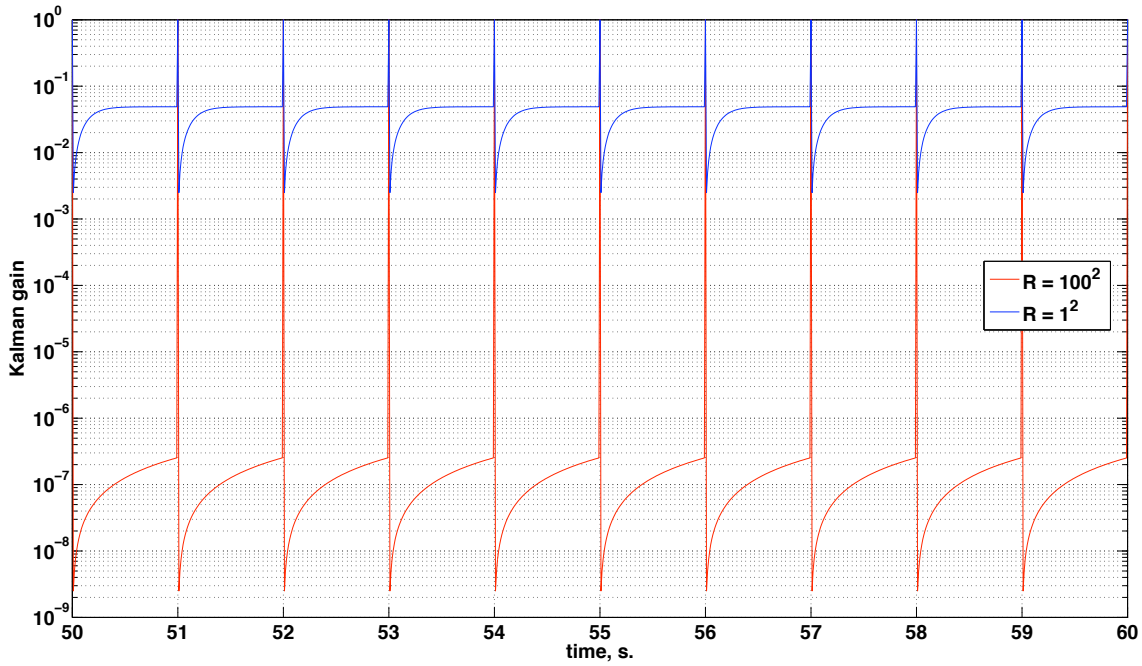

Figure 4.20: The lateral dynamics component of Kalman gain, $\mathbf{K}_{\mathbf{vel}}^{\mathbf{32}}$, of *velKKF* with GPS sampling rate of 1Hz, in the SD course

see Figure 4.21. With a decreasing sampling frequency, the GPS measurements and estimation ($\mathbf{R}_{\mathbf{vel}} = 1.0^2$) extend, producing more errors. On the other hand, when the vehicle is travelling on a straight road (the sideslip is zero), the configuration with $\mathbf{R}_{\mathbf{vel}} = 1.0^2$ becomes more accurate, see Figure 4.21.

Referring back to Figure 4.19, an interesting region is between 5 to 100Hz, in which the plots of the five manoeuvres join up closely. Within this sampling range, varying the types of manoeuvre longer has a significant effect on the estimation error. This suggests that a 5Hz GPS receiver is able to capture the main lateral dynamics and produce a reasonably accurate sideslip for the lateral velocity. Furthermore, the 5Hz sampling frequency also explains the good results obtained in Bevly et al. [2000; 2001; 2002], Bevly [2004] and Anderson and Bevly [2005], as the authors have performed their simulations and experiments based on a 5Hz GPS receiver.

4.4.4 The effect of GPS variance

This section looks at the effect of the GPS variance on state estimations. The simulations are carried out with different velocity variances ranging from 1e-4 to $1.0m^2/s^2$. As described in Table 4.8, GPS receivers are classified into three grades and they are represented with different colour regions in Figures 4.22 and 4.23. In

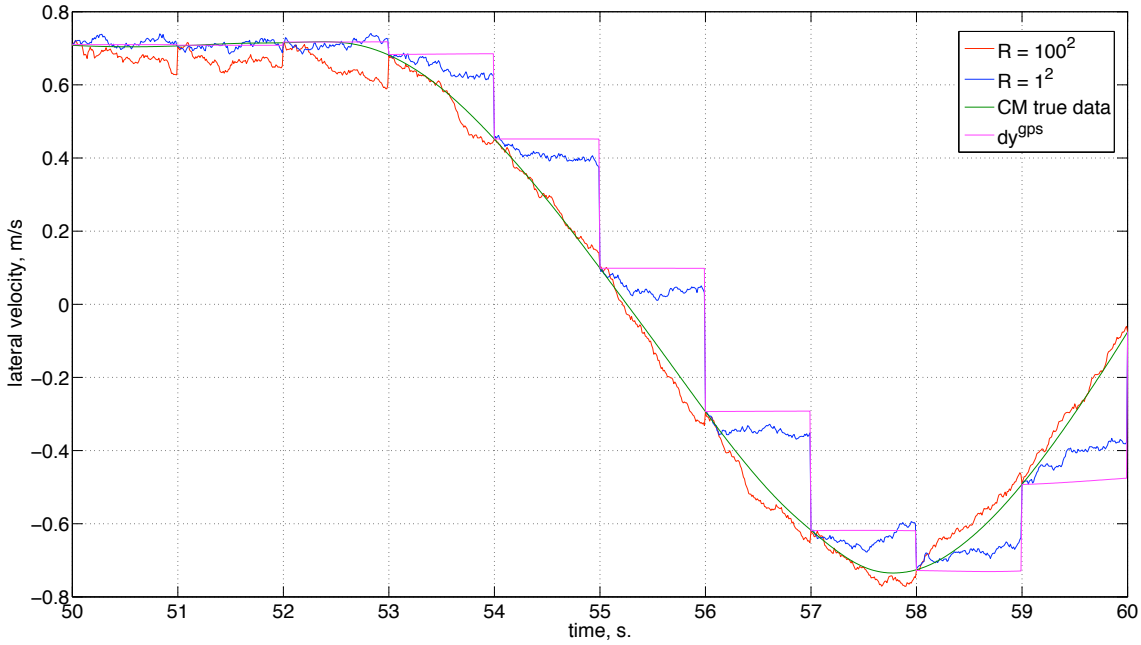

Figure 4.21: Lateral velocity estimated from the *velKKF* with GPS sampling rate of 1Hz, in the self-defined course

this study, the typical commercial GPS sampling rate is assumed, 1Hz.

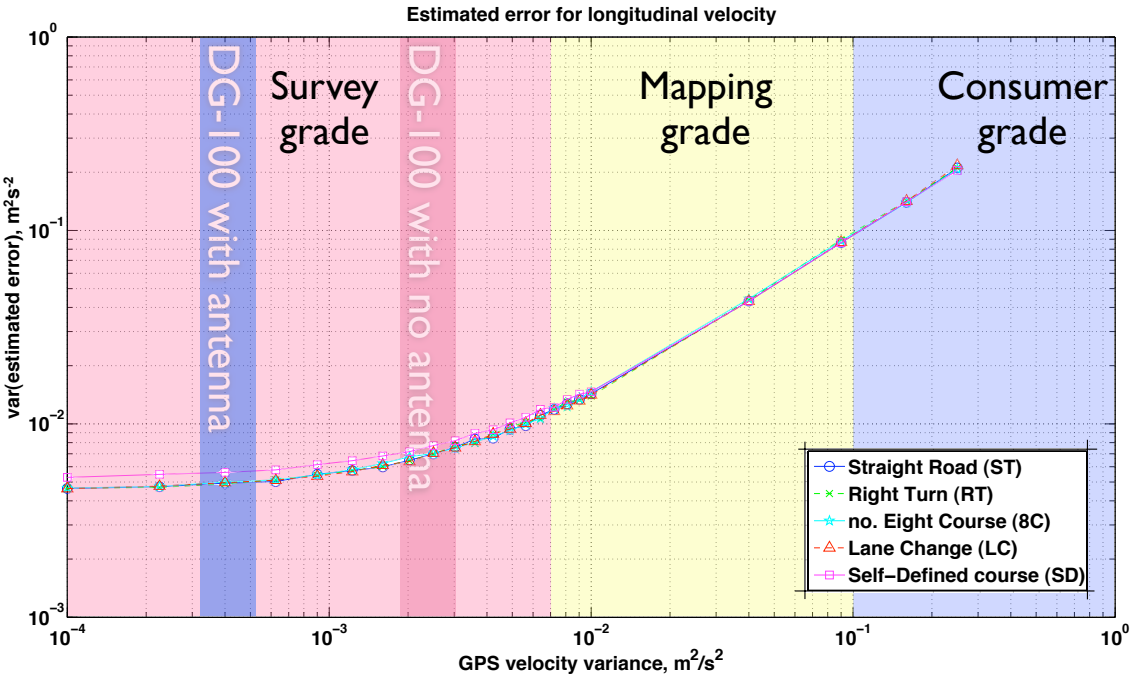

Figure 4.22: Estimation error of longitudinal velocity over GPS velocity variance. $T_s = 1$s.

The increase of the GPS velocity variance corresponds to the reduction in measurement accuracy in the *velKKF*. As the measurement covariance matrix, $\mathbf{R_{vel}}$, increases in value, the Kalman gain reduces. The *velKKF*, therefore, puts less weight on the innovation and begins to rely on the INS model more. The loss in 'trust' of the GPS measurements causes the bias to be estimated less accurately. As a result, from Figure 4.22, the longitudinal velocity estimation error increases as the GPS variance rises from 1e-4 to $1.0 m^2/s^2$.

At variance of 1e-2 m^2/s^2 in Figure 4.22, one can notice the separation of the error plot of SD manoeuvre from the rest. With a less accurate GPS receiver, manoeuvres do not affect the estimations much. However, when the GPS gets more accurate, the error due to the manoeuvre becomes apparent.

Similar to Figure 4.22, Figure 4.23 shows that the lateral velocity estimation error increases while the GPS variance increases. However, the error caused by different manoeuvres is now so significant that it cannot be ignored. The reason for this difference is due to the incorrect sideslip angle prediction as discussed earlier in this section. For this set of simulations, the sampling time is assumed to be 1s. The sideslip angle stays on hold between each sample, and errors occur due to the values of the measurement covariance between GPS samples, see Figure 4.21. As the variance of the GPS reduces, lateral velocity estimation is more accurately corrected whenever GPS becomes available, thus, a smaller estimation error. This error, however, saturates due to the fact that measurement covariance matrix tends to zero as GPS velocity variance decreases.

Figures 4.22 and 4.23 are also subdivided into 3 regions that correspond to the 3 GPS grades. Unsurprisingly, the survey grade GPS region has the lowest error while the consumer grade has the highest. These regions aim to provide designers with a sense of cost. With time, the size of these regions will change. The consumer grade region will occupy more space to the left as the other two shrink.

4.4.5 The effect of GPS measurements during outages

As discussed, the lateral velocity estimation error is caused by the continuous update from the GPS measurements in the correction stage during GPS outages. This section looks at the consequences of switching the corrective phase of the KF 'OFF' during GPS outages. Note that GPS outage means the time when GPS information is not available, e.g. GPS dropouts and between GPS samples, and in the section, the latter is being studied.

In the original dual KKF, GPS measurements in *velKKF* are available at all instances, even during GPS outages. When the same simulations are run with the

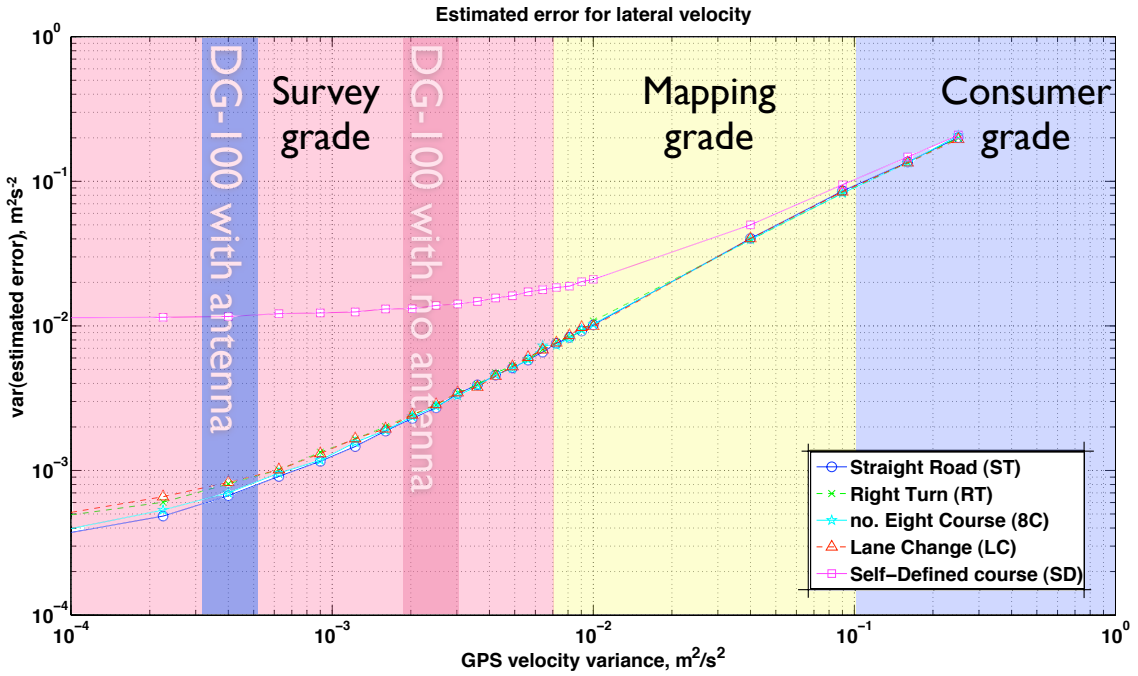

Figure 4.23: Estimation error of lateral velocity over GPS velocity variance. $T_s = 1$ s.

GPS measurements turned off during outages, i.e. $\mathbf{H_{vel}} = \mathbf{0_{2\times 4}}$, the estimations seem to follow the actual value more closely but with occasional overshoots. Figure 4.24 shows the lateral velocity estimations obtained from the two configurations as well as the absolute estimation error.

From Figure 4.24, it is clear from the error plot that the configuration with $\mathbf{H} = 1.0$ is more accurate when the lateral velocity is 0 and becomes inaccurate during a turn. This, agrees with the previous analysis and results in Figure 4.19, in which the straight road manoeuvre has a small error over the whole range of the sampling rate.

Figures 4.25 and 4.26 compare the lateral estimation errors of the 5 different manoeuvres with the 2 configurations. It is clear from the two graphs that the $\mathbf{H_{vel}} = \mathbf{0}$ configurations have 'unified' the estimations, so they are no longer dependent on driving manoeuvres. With this configuration in the dual KKF, designers do not need to worry about the performance of the estimations in different situations.

However, in terms of the performance for individual manoeuvres the only benefit of the $\mathbf{H_{vel}} = \mathbf{0}$ configuration is the improvement made on the SD manoeuvre. On the SD course, straight road is very limited and therefore one can conclude that bias estimations on straight roads are sufficiently accurate for the accelerometer to make essential corrections. During a corner when GPS is 'out', lateral velocity estimations

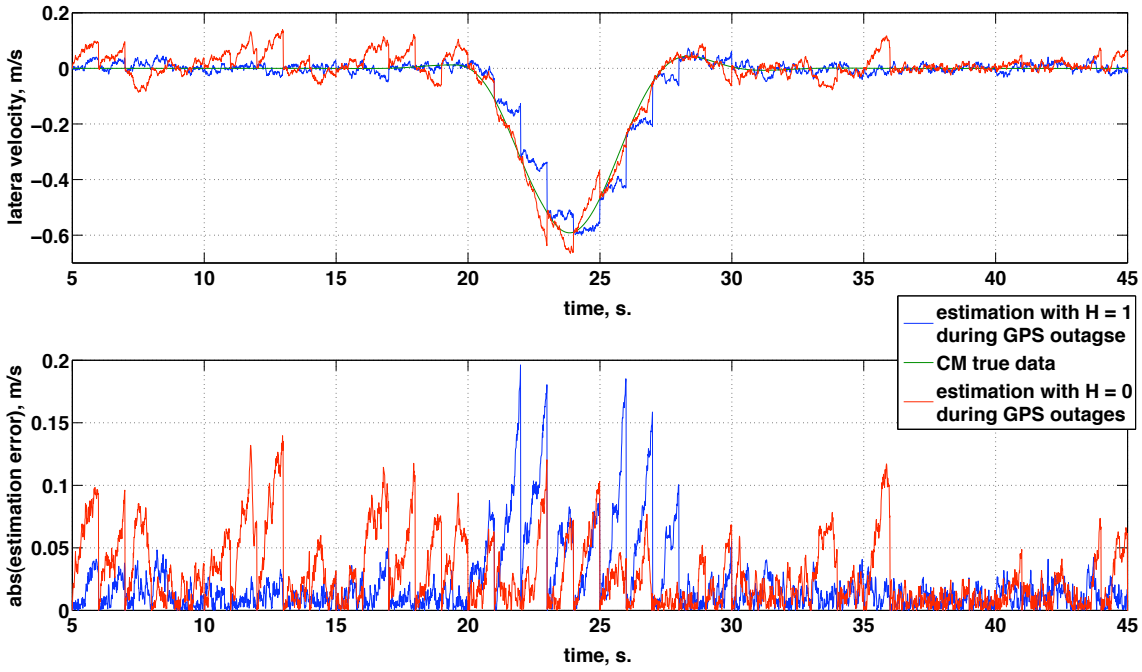

Figure 4.24: The lateral velocity estimation of the two configurations and their corresponding errors, $T_s = 1s$.

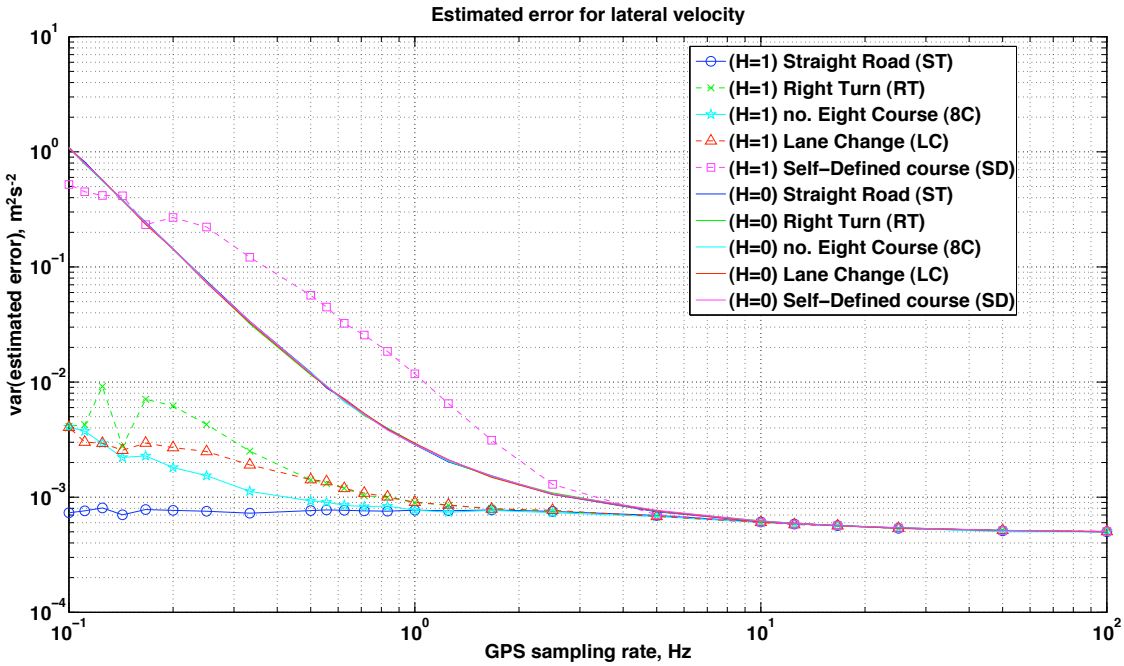

Figure 4.25: Estimation error of lateral velocity over GPS sampling rate, $\sigma_v^2 = 5\text{e-}4$.

from the corrected INS model are more accurate than relying on the 'out-dated' GPS measurements.

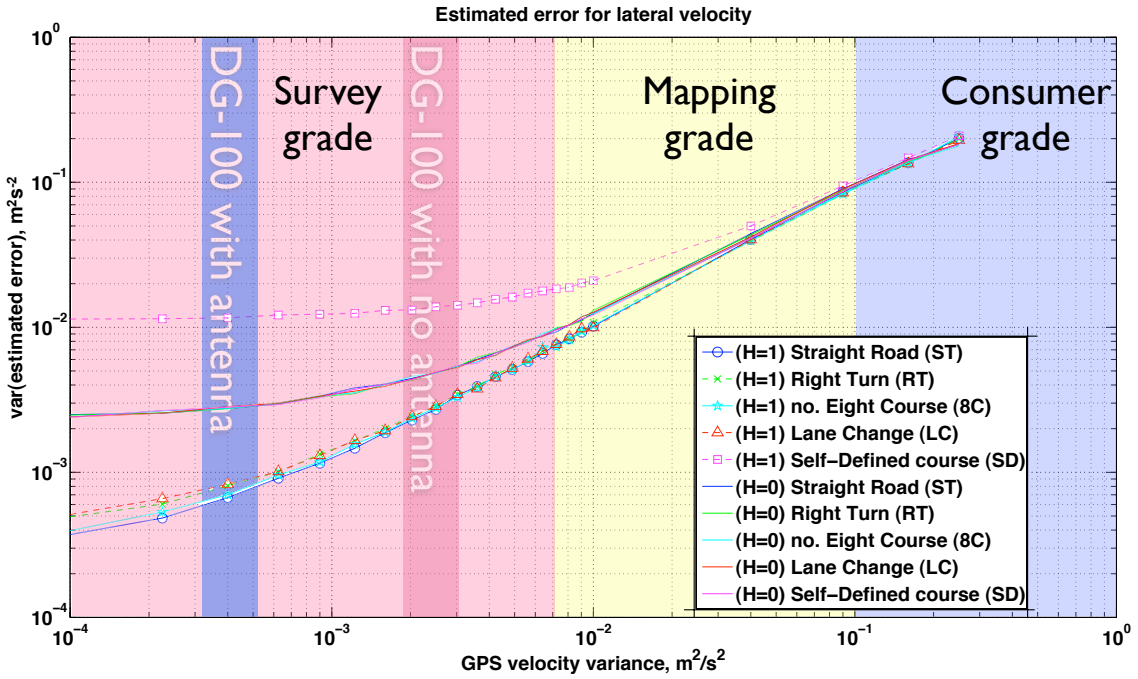

Figure 4.26: Estimation error of lateral velocity over GPS velocity variance, T_s = 1s.

On the other hand this is not true when the vehicle is on a straight road. As discussed previously and also shown in Figures 4.25 and 4.26, the continuous dependency of 'out-dated' GPS measurements during GPS outage on a straight road allows more accurate velocity estimations. This is because the longitudinal dynamics on a straight road do not change as vigourously as the lateral dynamics during a cornering. Therefore, the assumption of constant longitudinal velocity is valid.

4.4.6 The extension of GPS measurements

It has been shown from previous results that state estimations deteriorate when predictions place too much emphasis on the GPS measurements during GPS outages. One solution to this issue is to simply turn the GPS update off during the GPS outage, but this relies heavily on the accuracy of the bias estimates as well as how representative the kinematic model is to the true dynamics.

Another possible solution to improve estimations is to extend the GPS measurements during outages. Without knowledge of GPS measurements in the next sample, measurements can be predicted using an interpolation method applied to previous GPS values. In this study, the first and second order interpolations are considered and a schematic diagram for the first order is shown in Figure 4.27.

From Figure 4.27, GPS measurements are sampled at a constant rate represented

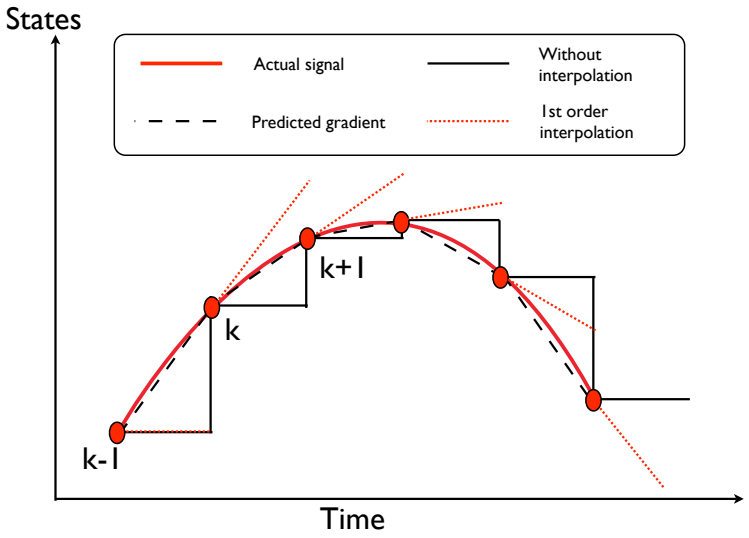

Figure 4.27: First order interpolation applied on the measurement

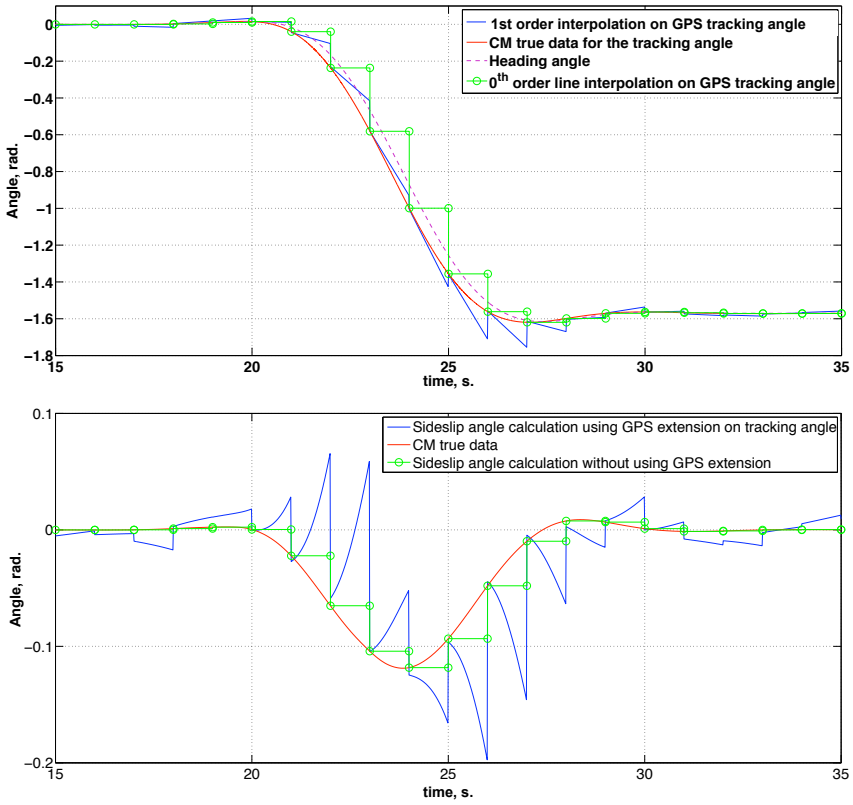

Figure 4.28: (Top): First order interpolation applied on GPS tracking angle measurement; (Bottom): Sideslip angle calculation

by the red dots. In the original dual KKF set-up, the GPS measurements are placed on hold during GPS outages, i.e. the solid black line. Using a first order interpolation technique, the gradient for the current GPS measurement is determined by, $\dot{z}_k = (z_k - z_{k-1})/T_s^{gps}$, see dashed black line. The gradient is extended from the current

GPS measurements and used as a reference for the KF until the next available GPS sample, see dashed red line. The GPS measurements, therefore, predict at the same rate as the KF with $z_{t+1} = z_k + \dot{z}_k(T_s^{KF})$.

However, this extension technique cannot be applied directly to the GPS measurement, especially when calculating the sideslip angle. Figure 4.28 shows the extended tracking angle from the GPS and the perfect heading angle from the yaw rate gyro.

As defined, the extended tracking angle of the GPS extends the gradient from the last measurements. Due to the low sampling rate of GPS, the interpolation technique is not able to follow the fast dynamic changes of the tracking angle in the vehicle. When calculating the sideslip angle, this generates more error than that without the extension method, see bottom plot of Figure 4.28. As a result, the interpolation method must not apply to the GPS measurements directly, but to the resultant quantities such as the sideslip angle.

The dual KKF modification - dual KKF$_\beta$

Figure 4.29 shows the calculated sideslip angle and lateral velocity when a first order interpolation is applied on the low-sampled sideslip calculation. As shown clearly in the figure, one of the major errors comes from the overshoots. Sideslip is calculated using a delayed sideslip gradient and errors occur whenever the true measurements saturate. Moreover, the figure also shows errors when the vehicle is travelling on a straight road. This error is due to the noise in the GPS and INS. When this extended sideslip is applied to the *velKKF*, the lateral velocity produces results as shown in Figure 4.29. In regions when the sideslip is changing constantly, the lateral velocity estimated well. However during sideslip changes, the lateral velocity overshoots. From this one can see the close relationship between the sideslip and the estimated lateral velocity.

The error that occurs on the straight road is unfavourable but can be improved by incorporating the sideslip calculation into the *yawKKF*, see Figure 4.30. The original two-component *yawKKF* can be modified to include a sideslip estimation,

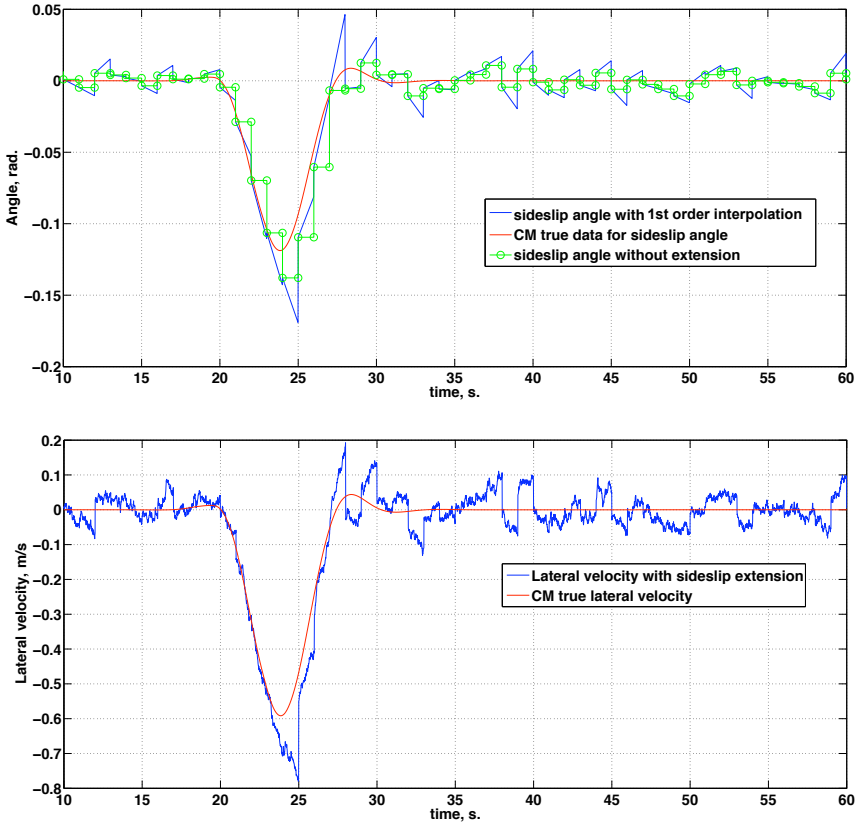

Figure 4.29: (Top): First order interpolation applied on sideslip angle; (Bottom): Lateral velocity as a result of the sideslip

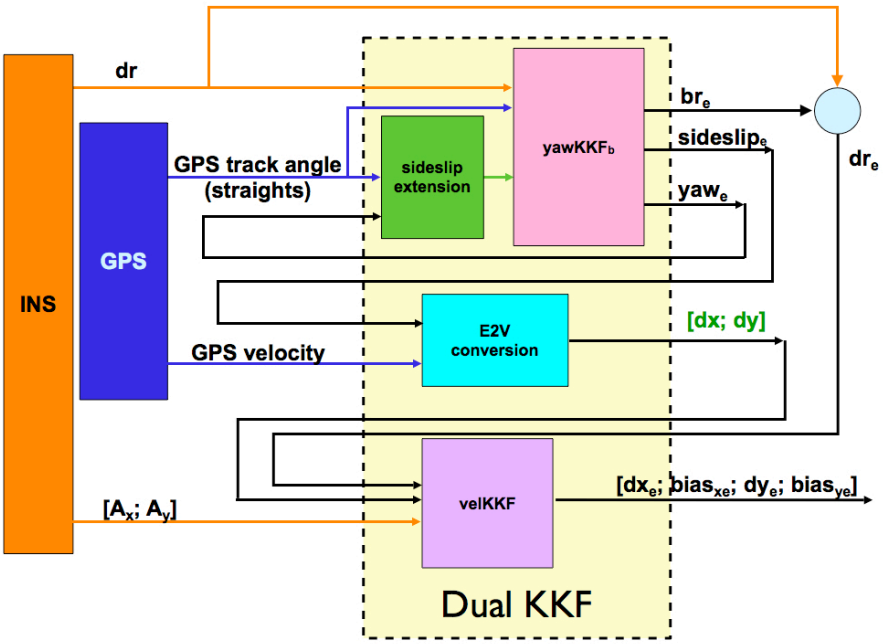

Figure 4.30: The modified dual KKF with sideslip extension and $yawKKF_b$

forming a new three-component $yawKKF_b$, which is described by:

$$\begin{bmatrix} \hat{\psi} \\ \hat{b}_r \\ \hat{\beta} \end{bmatrix}_{k+1} = \begin{bmatrix} 1 & -T_s & 0 \\ 0 & 1 & 0 \\ 0 & 0 & 1 \end{bmatrix} \begin{bmatrix} \hat{\psi} \\ \hat{b}_r \\ \hat{\beta} \end{bmatrix}_k + \begin{bmatrix} T_s \\ 0 \\ 0 \end{bmatrix} [r_m]_k \tag{4.20}$$

$$\mathbf{z_k} = \mathbf{H_{yaw_b}} \begin{bmatrix} \hat{\psi} \\ \hat{\delta}_\psi \\ \hat{\beta} \end{bmatrix}_k . \tag{4.21}$$

In addition to the extra state, the measurement vector, $\mathbf{z_k}$, and matrix, $\mathbf{H_{yaw_b}}$, also change according to different driving circumstances with the following rules:

Rule 1: During cornering when GPS is available

$$\begin{bmatrix} \nu_{gps} \\ \beta_{ext} \end{bmatrix} = \begin{bmatrix} 1 & 0 & 1 \\ 0 & 0 & 1 \end{bmatrix} \begin{bmatrix} \hat{\psi} \\ \hat{b}_r \\ \hat{\beta} \end{bmatrix} \tag{4.22}$$

Rule 2: During cornering when GPS is not available

$$\begin{bmatrix} \beta_{ext} \end{bmatrix} = \begin{bmatrix} 0 & 0 & 1 \end{bmatrix} \begin{bmatrix} \hat{\psi} \\ \hat{b}_r \\ \hat{\beta} \end{bmatrix} \tag{4.23}$$

Rule 3: Travelling on straight road regardless of the presence of GPS

$$\begin{bmatrix} \nu_{gps} \\ 0 \end{bmatrix} = \begin{bmatrix} 1 & 0 & 0 \\ 0 & 0 & 1 \end{bmatrix} \begin{bmatrix} \hat{\psi} \\ \hat{b}_r \\ \hat{\beta} \end{bmatrix} \tag{4.24}$$

Similar to the original *yawKKF*, the measurement vector is also evaluated as a trigonometric function before comparing with the state predictions. Therefore, the measurement matrix will become non-linear and the Jacobean matrix must be determined.

The implementation of the $yawKKF_b$ allows more control over the sideslip determination, especially in the reduction of error during straight road driving, see Figure 4.31. From the figure, it is clear that Rule 3 is working well and substantially attenuates the fluctuation of sideslip estimation due to GPS and INS noise.

Furthermore, the comparison of the velocity estimation plots in Figures 4.29 and 4.31 in detail allows one to see the reduction in discontinuities when $yawKKF_b$

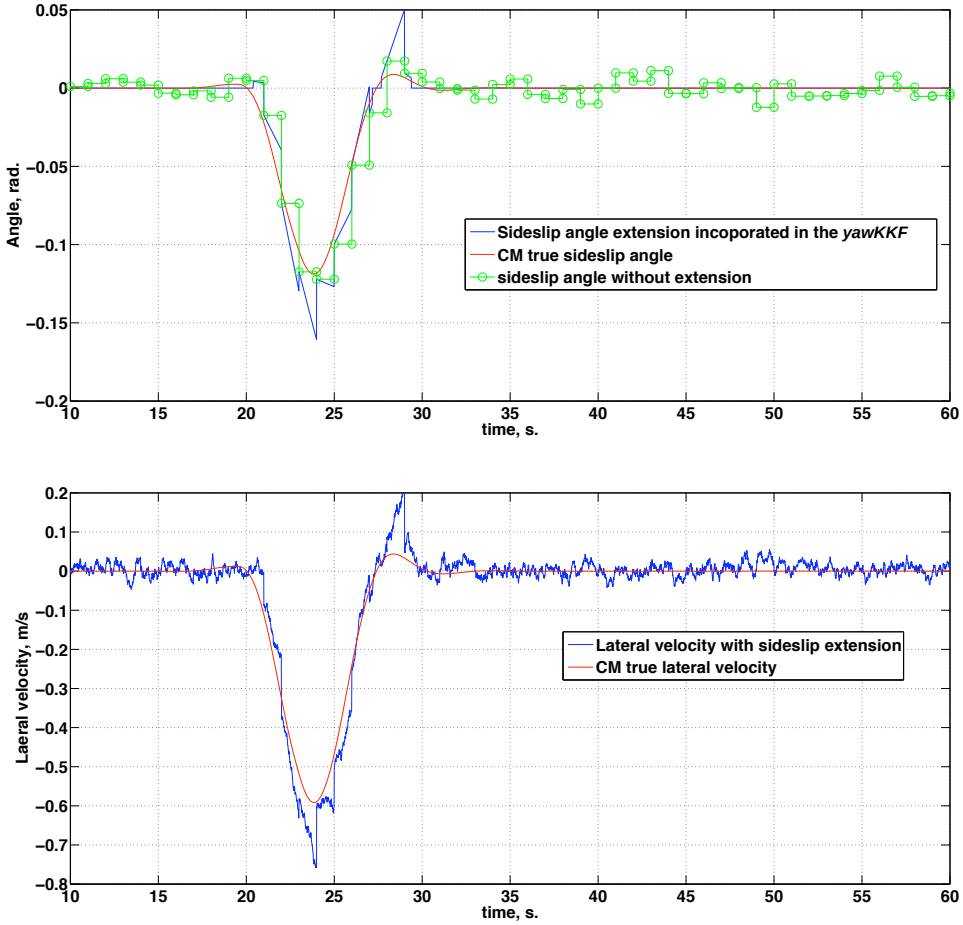

Figure 4.31: (Top): Sideslip estimation of the $yawKKF_b$; (Bottom): Lateral velocity as a result of the sideslip estimation

is applied. The continual update and correction of the *velKKF* is enhanced by the sideslip prediction to produce estimations that are more suitable for control systems, as discontinuous inputs may cause instability during control operations.

Interpolation applied in simulation

Table 4.9 shows the comparison of the lateral velocity estimation error of the five manoeuvres with and without the interpolation algorithm in the sideslip. As clearly indicated from the table, the introduction of the interpolation into the dual KKF does not guarantee an improved estimation.

Moving from top to bottom, the manoeuvres in Table 4.9 are arranged in order of increased cornering frequency. This shows that the more corners the vehicle is involved in during a manoeuvre, the higher the estimation error is. The reason for this error can be explained by Figure 4.32.

Table 4.9: Percentage variance of the state estimation on the simulated manoeuvre utilising *yawKKF* and $yawKKF_b$

	lateral velocity estimation error (%)		
Manoeuvres	dual KKF	dual $KKF_\beta + 1^{st}$ order*	dual $KKF_\beta + 2^{nd}$ order**
Striaght Road (ST)	0.09	0.03	0.03
Right Turn course (RT)	0.11	0.05	0.05
Lane Change (LC)	0.10	0.07	0.11
figure of Eight Course (8C)	0.43	0.44	0.58
Self-Defined (SD)	1.52	2.34	2.81

* use of $yawKKF_b$ with 1^{st} order extension on sideslip prediction
** use of $yawKKF_b$ with 2^{nd} order extension on sideslip prediction

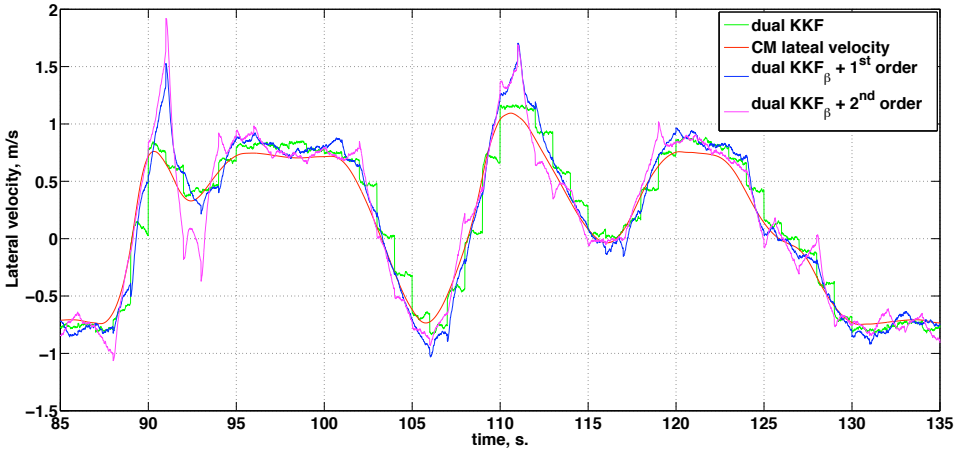

Figure 4.32: Lateral velocity estimation using the dual KKF and dual KKF_β

With the original dual KKF, the error is due to the 'stair-case' effect of the estimation as a result of the configuration of the *velKKF* as described previously in Section 4.4.5. As described at the beginning of this study and as shown in Figure 4.32, the 'stair-case' error has been effectively dealt with by incorporating the interpolation method. Errors of the dual KKF_β as shown in Table 4.9 are mainly caused by the rapid rate of change in the dynamic states (i.e. at the turning points in Figure 4.32). The results also show that the accumulated error from the overshoots are much greater than those from the 'stair-case' effect, hence, a higher estimation error in the dual KKF_β.

The overshoots of the two dual KKF_β setup as shown in Figure 4.32 depend upon the rate of change of the gradient of the state, in this case, the lateral jerk, $\dddot{y}_v$. As the gradient/jerk changes slowly, the interpolation estimates well without overshooting. However, when the gradient/jerk changes rapidly, overshoots occur. This overshooting behaviour can be observed in the figure when the vehicle enters

a turn with varying radius (90-93s., high jerk) and a constant radius turn (95-100s., low jerk).

From Table 4.9, one can also see the benefits of the application of the proposed rules in the $yawKKF_b$. On the ST manoeuvre, the two dual KKF$_\beta$ have a clear improvement over the original dual KKF. This benefit, however, reduces as the amount of straight road driving decreases. As mentioned earlier, one of the major benefits of the interpolation is the reduction of estimation discontinuity. This, is shown clearly with the use of the first order interpolation in Figure 4.32.

Comparing the lateral velocity estimation of the two different interpolation approaches in Figure 4.32, the second order interpolation gives a sharper and greater overshoot than the first order, therefore, giving a higher estimation error as shown in Table 4.9. Of the two interpolations, the first order gives smoother and less fluctuated estimations.

The real track testing

After successfully implementing the dual KKF$_\beta$ with the simulated data, two sets of track test are analysed here. The data is supplied by the sponsor company, Jaguar Land Rover, and it is collected using an Oxford Technical Solutions RT3100 device [OXTS 2008], which logs raw measurements from the GPS as well as the INS via the CAN-bus. This recorded data accurately represents the dynamics of the vehicle as the device is mounted rigidly on the vehicle with no faults or bias in the sensors (which are checked and corrected when the vehicle is stationary). The RT3100 runs at 100Hz, with the GPS and INS updating at 10Hz and 100Hz respectively. The GPS data is down-sampled to 1Hz to represent a consumer grade GPS unit. No additional noise is required to add to the data collected, as measurements are recorded in raw form without post-processing or filtering. The noise for the GPS and INS is defined in Table 4.10.

Table 4.10: Initial covariance matrices for GPS and INS in RT3100, all states are in SI units.

GPS & heading (R_0), 1Hz		**INS (Q_0), 100Hz**	
state variables	Standard deviation	state variables	Standard deviation
V_{gps}	3×10^{-2}	A_x	5×10^{-1}
$\dot{x}_e$	3×10^{-1}	A_y	5×10^{-1}
$\dot{y}_e$	3×10^{-1}	r_m	5×10^{-3}
ν	$1^\circ \times 10^{-1}$	β	1.0×10^{-1}
ψ_{sns}	$1^\circ \times 10^{-1}$	δ_x	1.0×10^{-8}
		δ_y	1.0×10^{-8}
		δ_{r_m}	1.0×10^{-8}

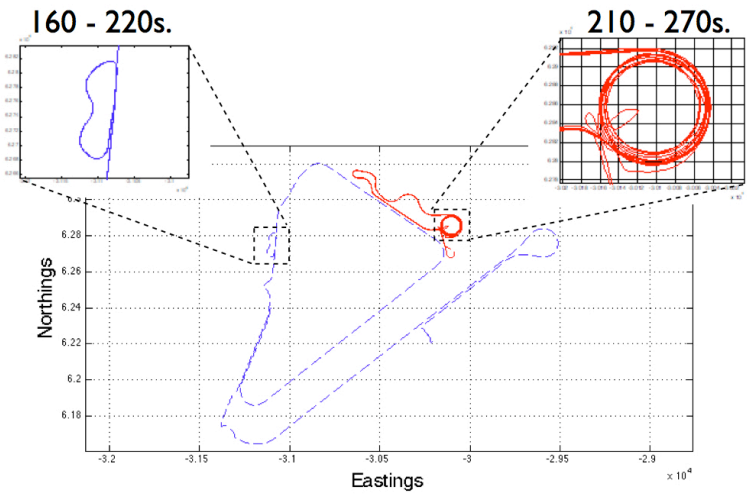

Figure 4.33: Mira test track: dashed blue line = dry track; solid red line = wet track

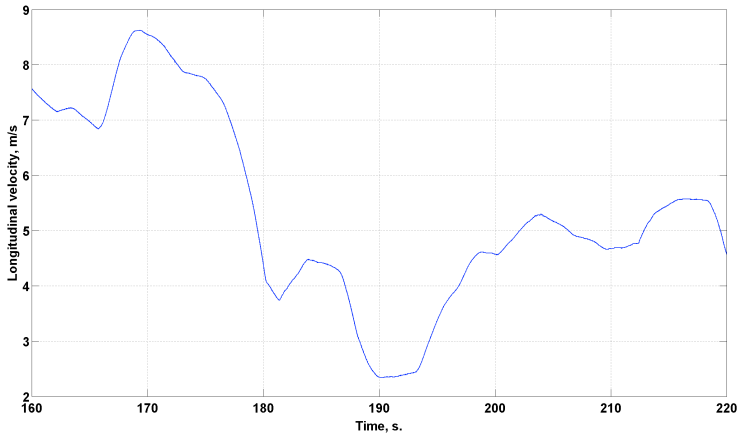

(a) Longitudinal velocity

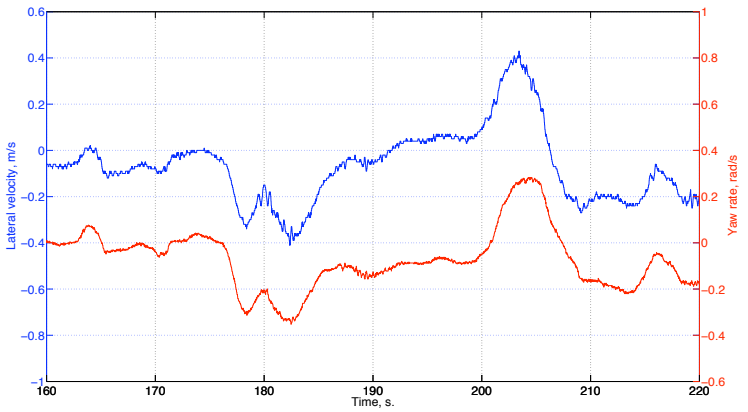

(b) Lateral velocity and yaw rate

Figure 4.34: Vehicle dynamics on Mira dry track

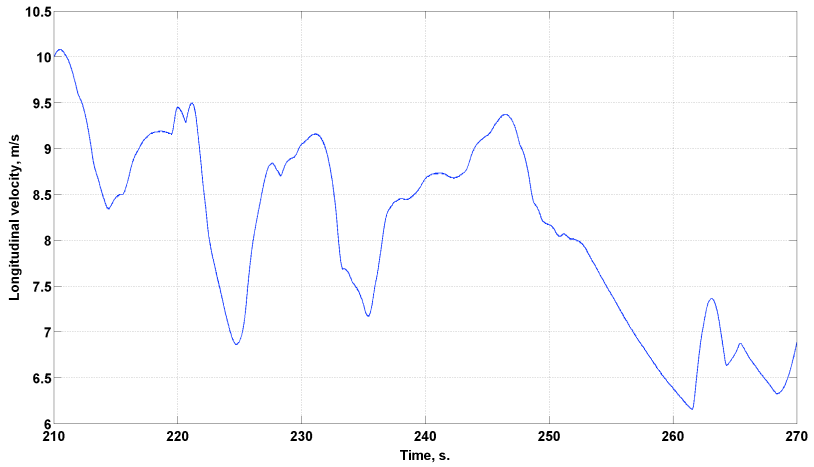

(a) Longitudinal velocity

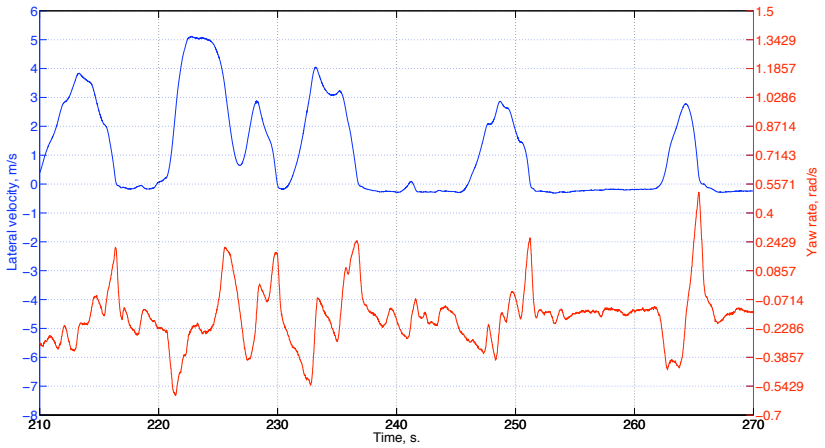

(b) Lateral velocity and yaw rate

Figure 4.35: Vehicle dynamics on Mira wet track

The map for the two track tests is shown in Figure 4.33, which consists of a dry (dashed blue line) and a wet track (solid red line). The state estimations evaluation for the two tracks focus on the section which has the most lateral dynamics, so the effect of the interpolation can be observed more clearly. The vehicle dynamics, namely the longitudinal velocity, lateral velocity and yaw rate, for the sections of the dry and wet track are shown in Figures 4.34 and 4.35 respectively.

Interpolation applied in real track test

It is shown that the interpolation method is able to reduce estimation discontinuities in state estimations under simulated environments. In this subsection, two sets of real test track data, wet and dry, are analysed with the original dual KKF and the modified dual KKF$_\beta$.

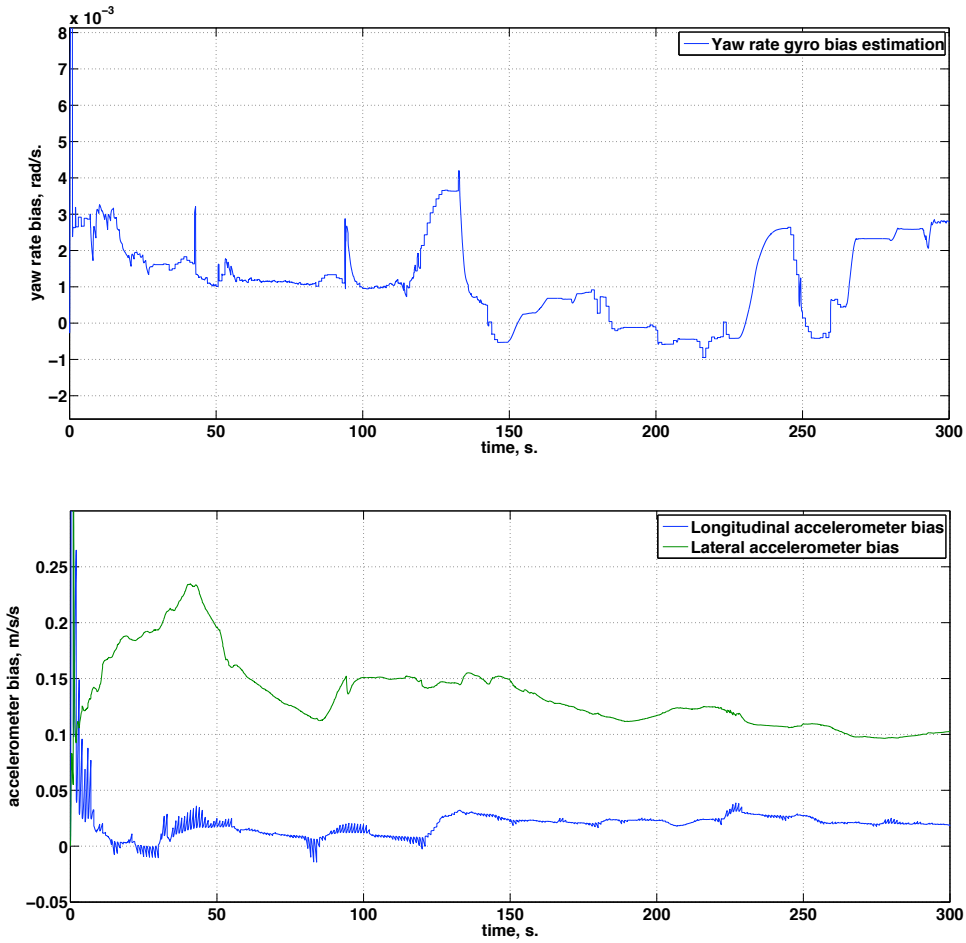

Figure 4.36: Yaw rate gyro bias and accelerometer biases estimations when running on the dry track

As described, the test data is obtained directly from the sensor via the CAN-bus, noise and disturbances are already included in the data. Without any knowledge of the biases, the proposed dual KKF$_\beta$ manages to obtain an estimation for each of the rate sensors, see Figure 4.36.

However, the bias estimations do not converge to a constant, suggesting the existence of unmodelled dynamics in the INS modelling equations. The incorrect modelling of the yaw rate causes errors in both heading and sideslip estimation, thereby, carrying their errors downstream and affecting the velocity estimations, see Figure 4.37.

From Figure 4.37, the effect of the first order interpolation and the sideslip rules are clearly shown. The sideslip estimations are suppressed to zero when the yaw rate measurement from the gyro is lower than a threshold (in this case, 1 degree per second). In-between GPS samples, the first order interpolation produces an extension, causing small overshoots during sharp changes in dynamics.

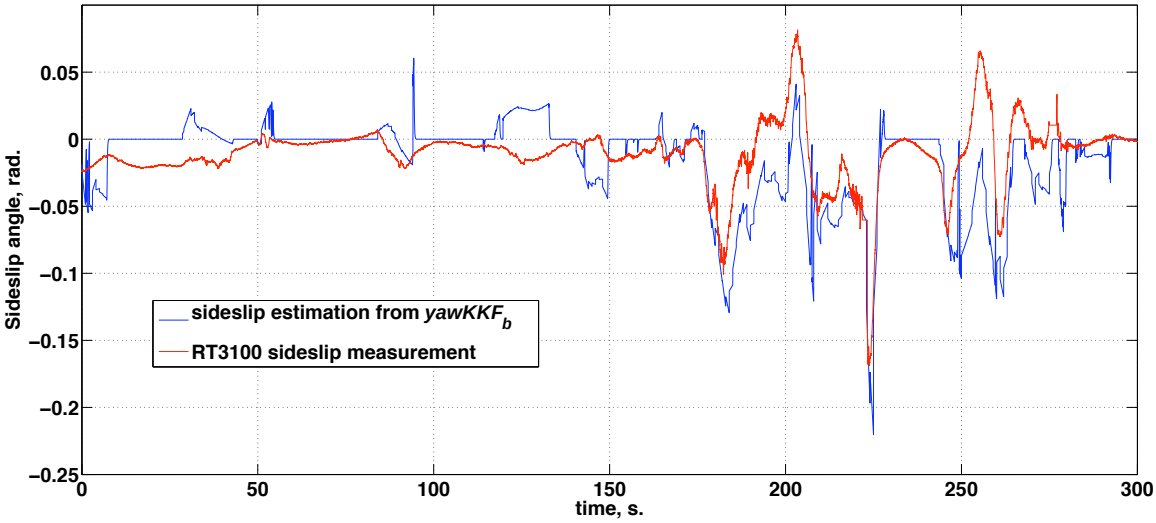

(a) Sideslip estimation

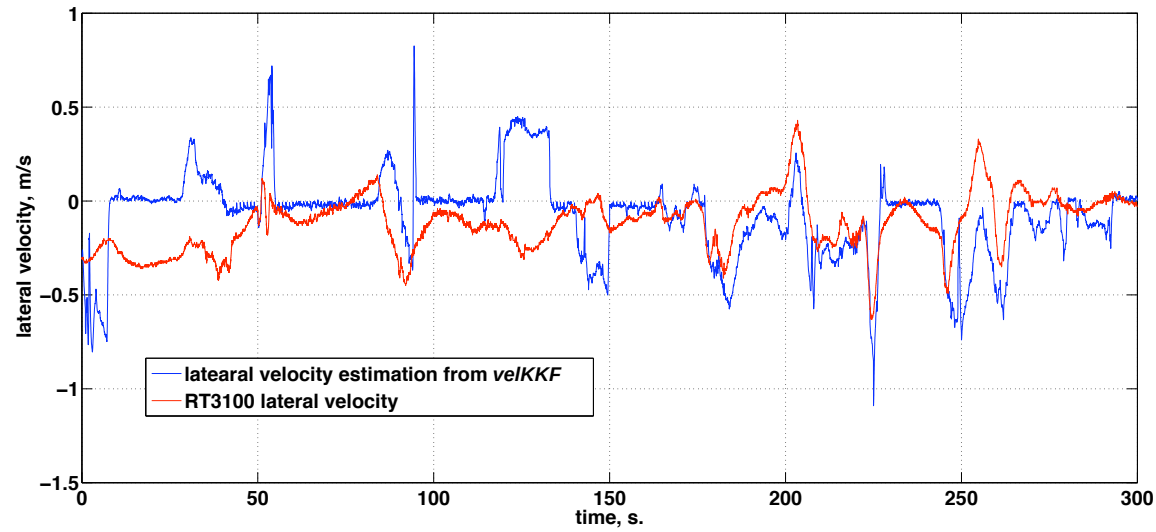

(b) Lateral velocity estimations estimation

Figure 4.37: Estimations on dry track

Although the $yawKKF_b$ is performing as it is configured, the estimations are not as good as those estimated with the simulated manoeuvres data. The assumption of zero sideslip at low yaw rate does not seem to be applicable for this track test. This implies that a low yaw rate measurement does not necessarily give a vehicle heading angle that is the same as the tracking angle. This is due to the pitching and rolling of the vehicle as a result of hard acceleration and braking. Providing that the RT3100 device is functioning properly and measuring accurately, these errors are simply a cause of incorrect modelling of the KF and/or any hidden dynamics in

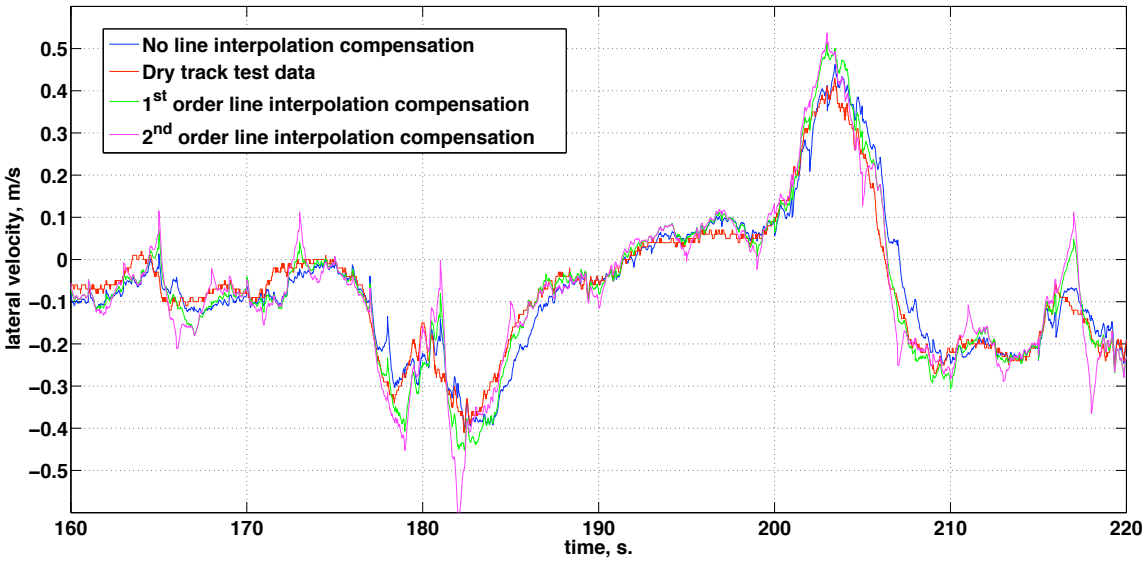

(a) Dry track

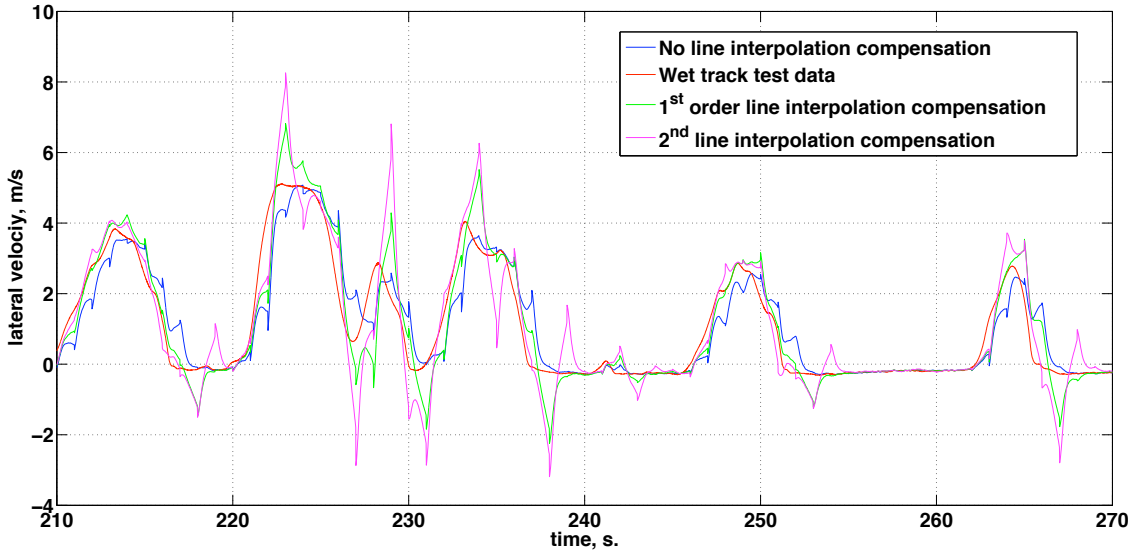

(b) Wet track

Figure 4.38: Lateral velocity estimations with external heading measurement

the INS.

To continue with the investigation on the real track data, the heading angle is assumed to be available externally and correcting the yaw rate gyros. Table 4.11 shows the estimation error for the two tracks with and without the deployment of the interpolation technique.

The table shows that the system with a first order interpolation gives a better lateral velocity estimation in both sets of track data. This is because the extended

Table 4.11: %NRMSD of state estimation on the Mira test track using *yawKKF* and $yawKKF_b$

	lateral velocity estimation error (%)		
Manoeuvre	*yawKKF*	$yawKKF_b$ 1^{st} order	$yawKKF_b$ 2^{nd} order
Dry (160 - 220s.)	5.25	5.01	6.44
Wet (210 - 270s.)	11.79.	11.69	15.03

* $yawKKF_b$ with 1^{st} order extension on sideslip prediction
** $yawKKF_b$ with 2^{nd} order extension on sideslip prediction

sideslip gradient is allowing a more precise estimation of lateral velocity in-between GPS samples. On the other hand, a second order interpolation gives an inferior estimation due to its overshoot, see Figure 4.38.

From Figure 4.38, the lateral velocity developed when driving on the wet track is higher than that in the dry track. This difference is due to a smaller radius of turn as well as a lower tyre-contact friction with the road on the wet track. In this case, the greater lateral velocity also means greater lateral acceleration, which causes greater overshoot as acceleration equals zero (turning point).

Comparing the lateral velocity estimation obtained from the dual KKF_β in Figures 4.37 and 4.38, one can see the improvement of the estimation when an external heading measurement is added to the dual KKF system. It is, therefore, critical to maintain a good measurement for the tracking angle as well as an accurate estimation for the heading angle during sideslip predictions. The effect these two angles have on the determination of sideslip is discussed later in Section 4.5.

4.4.7 Summary for the GPS precision

In this section, five CarMaker simulated manoeuvres have been used for investigating the accuracy of state estimations as a result of the variation of GPS precision. In addition, two sets of real track test data have been used for testing and evaluation of the interpolation technique as a solution to provide GPS measurements in-between GPS samples.

GPS receivers are classified into three grades, see Table 4.8, and their precision depends on their sampling rates and measurement variances. With a dual KKF and simulated noisy measurements via a virtual CAN-bus, a few interesting findings are summarised as follows:

1. The configuration of $\mathbf{H_{vel}} = \begin{bmatrix} 1 & 0 & 0 & 0 \\ 0 & 0 & 1 & 0 \end{bmatrix}$ with $\mathbf{R_{vel}} = 1.0^2$, should be applied when the vehicle is:

(a) on straight road with GPS present,

(b) on straight road with no GPS present, and

(c) cornering with GPS present;

2. The configuration of $\mathbf{H_{vel}} = \begin{bmatrix} 0 & 0 & 0 & 0 \\ 0 & 0 & 0 & 0 \end{bmatrix}$ or $\mathbf{R_{vel}} = 100^2$, if and only if the dynamic model is clearly defined in the KF with available measurements, such as pitch and roll angles. Then this configuration can be applied when the vehicle is:

   (a) cornering with no GPS presence;

   Furthermore, this configuration can also apply when when the effects of pitching and rolling are minimal.

3. With the typical off-the-shelf consumer GPS receiver (T_s =1Hz, $\sigma^2_{vel} \approx$ 3e-4, refer to Table 4.8), items 1 and 2 should apply. If GPS receiver of same variance at 5Hz is available, the configuration of the dual KKF will not have a significant effect on the estimations.

Depending on the design criterion and the purpose of the designed system, designers must make a sensible judgement and compromise between cost and performance. With a known accuracy and sampling rate of a GPS device, the plots in this section also provide designers with a tool for the error expectancy of the estimations before the real testing and/or simulations.

In reality, the configuration in item 2 above can never be utilised with existing in-car sensors. This is due to the shortage of correct measurements and other hidden dynamics. It is, therefore, important to maintain $\mathbf{H_{vel}} = \begin{bmatrix} 1 & 0 & 0 & 0 \\ 0 & 0 & 1 & 0 \end{bmatrix}$ at all times in order to keep the estimations bounded. However, the $\mathbf{H_{vel}}$ matrix also creates another issue: discontinuity effects, see Figure 4.32. This, however, can be improved by applying an interpolation technique to the sideslip to extend measurements between GPS samples.

Both the simulated and test track results (with external heading) favour the first order interpolation, showing a reduction in discontinuity, a closer match to the real lateral velocity between GPS samples, and a similar overall error compared to the estimations not using the technique.

From the real test data the importance of heading and tracking measurements to the dual KKF estimation has also been clarified. With a single GPS antenna, heading measurement is not available during cornering and gyro bias can only be

estimated when the vehicle is travelling on a straight road, i.e. tracking angle equals the heading angle. If, however, there is a lack of straights and/or an inaccurate tracking angle measurement, the heading estimation will be corrupted, giving wrong sideslip and lateral velocity estimations.

Lastly, the interpolation can also be applied before or after the KF correction. The evaluation shown in this section is applied after the correction. When applied before the correction, the estimated states show a delay but no overshoots occur. This allows the INS to be corrected and states to be estimated accurately if realtime estimation is not an issue.

4.5 Dual GPS antennae and six-axes INS EKF design

In Sections 4.2 and 4.3, the use of a single antenna GPS was studied and several designs and configuration schemes for the KF were proposed. The results showed the importance of external heading measurement in the KF. In Section 4.3, the triple KF design was presented to utilise the WSS to provide estimations for the longitudinal velocity and heading angle. However, it was shown via simulation that estimations from the *wssEKF* were not necessarily more accurate than those predicted from the *yawKKF*. The significance of the requirement of accurate heading and tracking angle measurements were further highlighted and confirmed in Section 4.4, where the dual KKF was applied onto the real track test data.

The fact that a single GPS antenna is not able to provide any angle measurements apart from the tracking angle has made KF estimations less robust with limitations. Therefore, this section explores the possibility of the use of multi-GPS antennae in KF designs. Since sideslip angle is an important yet hard-to-measure state in vehicle dynamics, an account is also given of the accuracy of the sideslip estimations as a result of the error in the tracking and heading angle.

4.5.1 The six-axes INS and dual GPS antennae set-up

Before discussion, it is important to point out that the following study repeats some of the formulation as show in Chapter 2. It must be remembered that the Euler angles defined in Equation 2.5 represent the angles between the e-frame and the sensor (i.e. b-frame), so $\begin{bmatrix}\dot{\phi}_{eb} & \dot{\theta}_{eb} & \dot{\psi}_{eb}\end{bmatrix}^T = \begin{bmatrix}\dot{\phi} & \dot{\theta} & \dot{\psi}\end{bmatrix}^T$.

In Ryu et al. [2002], Ryu and Gerdes [2004*b*], and Ryu [2004], the authors have shown two possible ways of positioning the multi GPS antenna on a vehicle: longi-

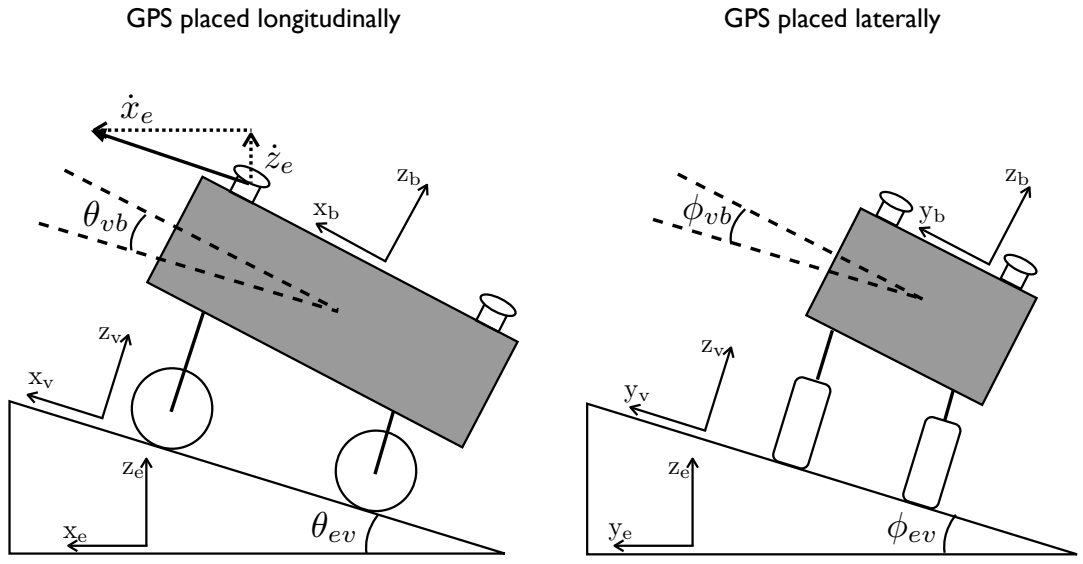

$$\theta_{2gps} = \theta_{ev} + \theta_{vb} \qquad \phi_{2gps} = \phi_{ev} + \phi_{vb}$$
$$\theta_{eb} = \theta_{2gps} \qquad \phi_{eb} = \phi_{2gps}$$

Figure 4.39: Multi GPS antenna location on a vehicle [Bae et al. 2001, Ryu et al. 2002, Ryu and Gerdes 2004*b*, Ryu 2004]

tudinally and laterally, see Figure 4.39.

With the multi GPS antennae longitudinal set-up, the heading angle as well as the total pitching angle, θ_{2gps}, can be measured. The total pitching angle is the sum of the vehicle pitch at the cg, θ_{vb}, and the road gradient, θ_{ev}. Using velocity measurements from a single GPS antenna, the road grade can be approximated by:

$$\theta_{ev} = -\tan^{-1}\left(\frac{\dot{z}_e}{\dot{x}_e}\right) \text{ or } -\tan^{-1}\left(\frac{\dot{z}_e}{\sqrt{\dot{x}_e^2 + \dot{y}_e^2}}\right). \tag{4.25}$$

With this set-up, the pitching of the vehicle, θ_{vb}, can be determined. By utilising a pitch rate gyro, q_m, the bias in the gyro can be estimated and corrected using a similar KF design as the *yawKKF*:

pitchKKF

$$\begin{bmatrix} \dot{\theta}_{vb} + \dot{\theta}_{ev} \\ \dot{b}_q \end{bmatrix} = \begin{bmatrix} 0 & 1 \\ 0 & 0 \end{bmatrix} \begin{bmatrix} \theta_{vb} + \theta_{ev} \\ b_q \end{bmatrix} + \begin{bmatrix} 1 \\ 0 \end{bmatrix} q_m \tag{4.26}$$

$$\begin{bmatrix} \theta_{2gps} \end{bmatrix} = \begin{bmatrix} 1 & 0 \end{bmatrix} \begin{bmatrix} \theta_{vb} + \theta_{ev} \\ b_q \end{bmatrix} \tag{4.27}$$

With the total pitching state, $\theta_{vb} + \theta_{ev}$, estimated, the vehicle pitch, θ_{vb}, can be

determined by subtracting the road gradient measured by the single GPS antenna as Equation 4.25.

In Figure 4.39, the lateral set-up measures the heading angle and the total sum of rolling of the vehicle, ϕ_{2gps}, which comprises road grade, ϕ_{ev}, and vehicle roll angle at the cg, ϕ_{vb}. Similar to the longitudinal set-up, with the installation of a roll rate gyro, the total roll angle can be measured and bias can be corrected using a KKF:

rollKKF

$$\begin{bmatrix} \dot{\phi}_{vb} + \dot{\phi}_{ev} \\ \dot{b}_p \end{bmatrix} = \begin{bmatrix} 0 & 1 \\ 0 & 0 \end{bmatrix} \begin{bmatrix} \phi_{vb} + \phi_{ev} \\ b_p \end{bmatrix} + \begin{bmatrix} 1 \\ 0 \end{bmatrix} p_m \tag{4.28}$$

$$\begin{bmatrix} \phi_{2gps} \end{bmatrix} = \begin{bmatrix} 1 & 0 \end{bmatrix} \begin{bmatrix} \phi_{vb} + \phi_{ev} \\ b_p \end{bmatrix} \tag{4.29}$$

Unlike the *pitchKKF* (which can de-couple the total pitch, θ_{eb}, with GPS velocity measurements in Equation 4.25), the total roll angle state, $\phi_{eb} = \phi_{vb} + \phi_{ev}$, in *rollKKF* cannot be de-coupled easily due to the lack of ϕ_{ev} measurements.

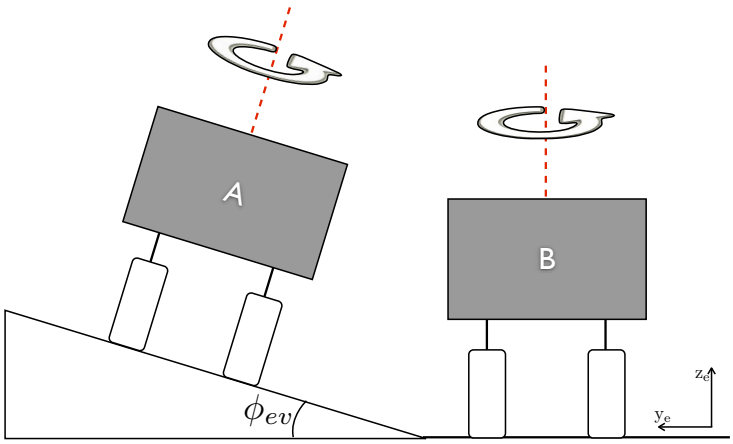

Figure 4.40: Simple schematic diagram showing the operation axis for the yaw rate gyro in red dashed line

Theoretically, the *pitchKKF*, *rollKKF* and *yawKKF* described previously is correct but restricted to gyros rotating about their own axis that are fixed and parallel to the e-frame. For example, without pitching and rolling on the road surface or the body, the yaw rate gyro operates about its axis parallel to the z_e axis and with its b-frame coinciding with the v-frame. The turning rate of the vehicle is simply the turn rate of the yaw rate gyro about its axis, $\dot{\psi} = r_m$, see vehicle B in Figure 4.40. However, if the vehicle is not operating on a flat plane (and still without any body roll or pitch with respect to the road), i.e. vehicle A in Figure 4.40, the axis of the yaw rate gyro is no longer parallel to the z_e axis, but rotated by a roll angle,

ϕ_{ev}. In this situation, the vehicle body yaw rate with respect to the e-frame, $\dot{\psi}_{eb}$, is evaluated as the turn rate about the rotated yaw rate axis, i.e. $\dot{\psi}_{eb} = r_m \cos\phi_{ev}$. The vehicle, therefore, turns an angle of $\psi_{eb} = \int r_m \cos\phi_{ev}\ \mathrm{dt}$ radians with respect to the e-frame. If the roll angle is not taken into consideration here, the heading angle measurement will be corrupted. For three-axes gyros attached to a vehicle in the b-frame, the rate of rotation in e-frame (i.e. Euler rates) are derived by,

$$\begin{bmatrix} \dot{\phi}_{eb} \\ \dot{\theta}_{eb} \\ \dot{\psi}_{eb} \end{bmatrix} = \begin{bmatrix} 1 & \sin\phi_{eb}\tan\theta_{eb} & \cos\phi_{eb}\tan\theta_{eb} \\ 0 & \cos\phi_{eb} & -\sin\phi_{eb} \\ 0 & \sin\phi_{eb}\sec\theta_{eb} & \cos\phi_{eb}\sec\theta_{eb} \end{bmatrix} \begin{bmatrix} p_m \\ q_m \\ r_m \end{bmatrix} \tag{4.30}$$

Equation 4.30 shows the conversion of gyro measurements, $\begin{bmatrix} p_m & q_m & r_m \end{bmatrix}^T$, to the Euler rates, $\begin{bmatrix} \dot{\phi}_{eb} & \dot{\theta}_{eb} & \dot{\psi}_{eb} \end{bmatrix}^T$. From the equation, Euler yaw rate, $\dot{\psi}_{eb}$, is equal to the yaw rate gyro, r_m, only when the pitch and roll angles are zero. Similarly, $\dot{\phi}_{eb} = p_m$ when θ_{eb} is zero and $\dot{\theta}_{eb} = q_m$ when ϕ_{eb} is zero. With these conditions, the original angular KFs perform accurately. However, the Euler angles can never be guaranteed to be zeros and the angular KFs must be modified to replace the gyro measurements with the Euler rates.

As the rate gyros each contain a bias and are coupled together to form the Euler rates, the three angular KFs can no longer be a standalone KF. They are combined in an EKF, *angEKF*, with kinematic relationship,

$$\begin{bmatrix} \dot{\phi}_{vb} + \dot{\phi}_{ev} \\ \dot{\theta}_{vb} + \dot{\theta}_{ev} \\ \dot{\psi}_v \\ \dot{b}_p \\ \dot{b}_q \\ \dot{b}_r \end{bmatrix} = \begin{bmatrix} \mathbf{A_{ang}} & -\mathbf{A_{ang}} \\ \mathbf{0_{3\times 3}} & \mathbf{0_{3\times 3}} \end{bmatrix} \begin{bmatrix} p_m \\ q_m \\ r_m \\ b_p \\ b_q \\ b_r \end{bmatrix} \tag{4.31}$$

where:
$$\mathbf{A_{ang}} = \begin{bmatrix} 1 & \sin\phi_{eb}\tan\theta_{eb} & \cos\phi_{eb}\tan\theta_{eb} \\ 0 & \cos\phi_{eb} & -\sin\phi_{eb} \\ 0 & \sin\phi_{eb}\sec\theta_{eb} & \cos\phi_{eb}\sec\theta_{eb} \end{bmatrix}$$

The estimated state vector for *angEKF* is $\begin{bmatrix} \phi_{vb} + \phi_{ev} & \theta_{vb} + \theta_{ev} & \psi_v & b_p & b_q & b_r \end{bmatrix}^T$ with measurements from a dual GPS antennae set-up, $\begin{bmatrix} \phi_{2gps} & \theta_{2gps} & \psi_{2gps} \end{bmatrix}^T$.

With the three Euler angles estimated using the three angular KFs, the accelerometer measurement in the b-frame can be rewritten more precisely with the inclusion of all the gyro measurements and the gravitational terms as given in Klier

et al. [2008]. Note that the gravitational acceleration is in the e-frame, $\vec{g}_e$, but the subject to be evaluated is in b-frame. In this case, the DCM is applied to convert from e-frame to b-frame,

$$\begin{aligned}\vec{g}_b &= \mathbf{C_e^b}\vec{g}_e \\ &= \begin{bmatrix} \theta_{eb}^c\psi_{eb}^c & \theta_{eb}^c\psi_{eb}^s & -\theta_{eb}^s \\ -\phi_{eb}^c\psi_{eb}^s + \phi_{eb}^s\theta_{eb}^s\psi_{eb}^c & \phi_{eb}^c\psi_{eb}^c + \phi_{eb}^s\theta_{eb}^s\psi_{eb}^s & \phi_{eb}^s\theta_{eb}^c \\ \phi_{eb}^s\psi_{eb}^s + \phi_{eb}^c\theta_{eb}^s\psi_{eb}^c & -\phi_{eb}^s\psi_{eb}^c + \phi_{eb}^c\theta_{eb}^s\psi_{eb}^s & \phi_{eb}^c\theta_{eb}^c \end{bmatrix} \begin{bmatrix} 0 \\ 0 \\ -g \end{bmatrix}\end{aligned} \tag{4.32}$$

$$\vec{g}_b = -g \begin{bmatrix} -\sin\theta_{eb} \\ \sin\phi_{eb}\cos\theta_{eb} \\ \cos\phi_{eb}\cos\theta_{eb} \end{bmatrix} \tag{4.33}$$

The acceleration kinematic relationship for the INS hence becomes,

$$\begin{bmatrix} A_x \\ A_y \\ A_z \end{bmatrix} = \begin{bmatrix} \ddot{x}_b \\ \ddot{y}_b \\ \ddot{z}_b \end{bmatrix} + \begin{bmatrix} 0 & -\hat{r}_m & \hat{q}_m \\ \hat{r}_m & 0 & -\hat{p}_m \\ -\hat{q}_m & \hat{p}_m & 0 \end{bmatrix} \begin{bmatrix} \dot{x}_b \\ \dot{y}_b \\ \dot{z}_b \end{bmatrix} + g \begin{bmatrix} \sin\theta_{eb} \\ \sin\phi_{eb}\cos\theta_{eb} \\ \cos\phi_{eb}\cos\theta_{eb} \end{bmatrix} \tag{4.34}$$

Note that the above equation has replaced the v-frame vectors in Equations 2.3 and 2.4 by the b-frame variables. This is because the INS attached to the vehicle body on the b-frame no longer aligns with the vehicle road dynamic plane on the v-frame, see Figure 4.39. This misalignment results in a small angle of difference, called the tilt angle. In a commercial vehicle, tilt angles refer to the rolling and pitching tilt angles, ϕ_{vb} and θ_{vb} respectively. Using Equations 4.30 and 4.34, with the measurements from the INS, the velocities in the b-frame can be determined. To obtain the dynamic measurements in the v-frame, a DCM is applied with the tilt angles,

$$\begin{bmatrix} \dot{x}_v \\ \dot{y}_v \\ \dot{z}_v \end{bmatrix} = \begin{bmatrix} \cos\theta_{vb} & \sin\phi_{vb}\sin\theta_{vb} & \cos\phi_{vb}\sin\theta_{vb} \\ 0 & \cos\phi_{vb} & -\sin\phi_{vb} \\ -\sin\theta_{vb} & \sin\phi_{vb}\cos\theta_{vb} & \cos\phi_{vb}\cos\theta_{vb} \end{bmatrix} \begin{bmatrix} \dot{x}_b \\ \dot{y}_b \\ \dot{z}_b \end{bmatrix} \tag{4.35}$$

The simulation: difference in working frame

In order to show the difference and importance of working in the correct framework, a simulation is performed in IPG CarMaker with the track as shown in Figure 4.41.

The simulated track starts from $(0, 0)$ and combines pitching, rolling and yawing motion to form a track with an uphill slope, road banking and turning. Table 4.12 summaries the road profile of the simulation.

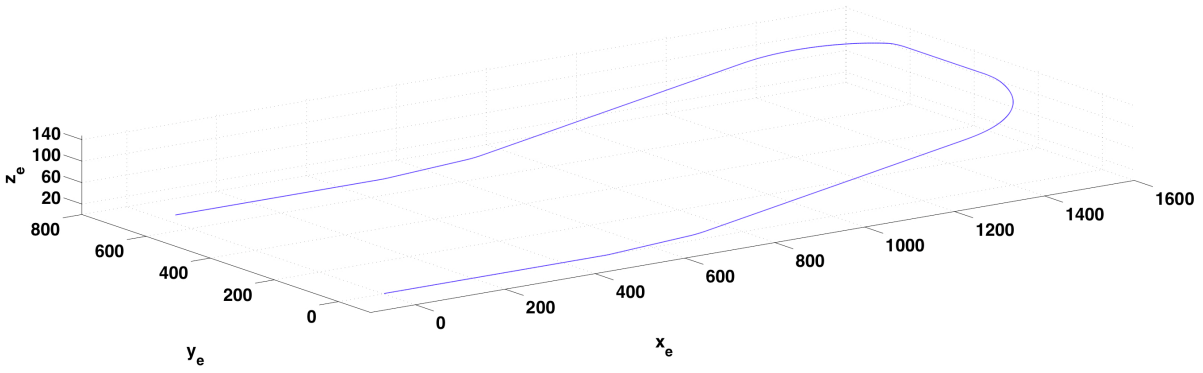

Figure 4.41: CarMaker Simulated track in three-dimensional view

Table 4.12: Simulated track detail

	Road definition			
Road section	road type	length	uphill slope gradient (%)	banking gradient (%)
1	straight	500	0	0
2	straight	200	5	0
3	straight	200	15	0
4	straight	200	15	5
5	straight	200	15	15
6	left turn	–	15	15
7	straight	200	0	0
8-13	repeats from section 6 down to 1 with a downhill slope			

In the simulation, the virtual vehicle is travelling at a constant speed of 80 kph with a three-axes accelerometers and rate gyroscopes installed at the cg. Moreover, two GPS receivers are fixed on the vehicle, one placed at the cg and one placed longitudinally away from the cg. Figure 4.42 shows the vehicle body pitching angle, θ_e, measured by the GPS receivers using Equation 4.36 and the uphill gradient, θ_{ev}, measured by Equation 4.25. Both angles are calculated in the e-frame as GPS operates with reference to the ECEF coordinates.

$$\theta_{ev} = -\tan^{-1}\left(\frac{z_e^{gps2} - z_e^{gps}}{\sqrt{\left(x_e^{gps2} - x_e^{gps}\right)^2 + \left(y_e^{gps2} - y_e^{gps}\right)^2}}\right). \tag{4.36}$$

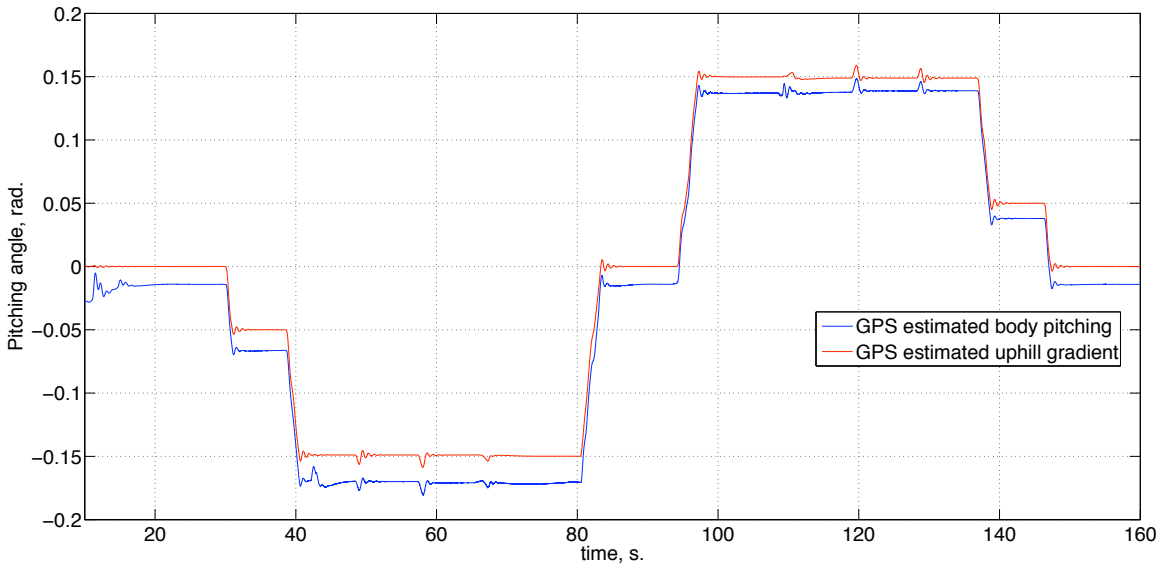

Figure 4.42: GPS measured body pitching and uphill gradient

Figure 4.42 shows the distinct difference between the two pitching angles. This suggests that the vehicle body is no longer parallel to the surface of the road. As velocities determined using Equation 4.34 are no longer the same as those acting on the road surface, a transformation from the vehicle body to the surface axes is essential, see Equation 4.35.

As shown in Equation 4.35 and Figure 4.39 previously, the two tilt angles (ϕ_{vb} and θ_{vb}) are required for the calculation of surface velocities. The pitching tilt angle can be estimated in two ways. The first one is via GPS measurements, simply taking the difference between the two pitching angles as given in Figure 4.42, i.e. $\theta_{vb} = \theta_{eb} - \theta_{ev}$. This method is straight-forward but GPS receivers tend to suffer from low sampling rate and outages. The second method is utilising the velocities estimation in the b-frame, i.e. $\begin{bmatrix} \dot{x}_b & \dot{y}_b & \dot{z}_b \end{bmatrix}^T$. This is more accurate but sensitive to sensor noise and disturbances:

$$\theta_{vb} = -\tan^{-1}\left(\frac{\dot{z}_b}{\sqrt{\dot{x}_b^2 + \dot{y}_b^2}}\right). \tag{4.37}$$

The rolling tilt angle of the vehicle body, however, is not as easy to de-couple from the Euler angles as the pitching tile angle. As suggested in Ryu and Gerdes [2004*a*], with the use of a MKF and a GPS/INS based KKF, the road banking angle, ϕ_{ev}, can be estimated when a roll rate gyro is utilised. However, Leung et al. [2009*b*] has commented that the weakness of this approach lies in the assumption

of constant bias as well as the dependence of accurate GPS measurements with the dual antennae set-up.

Nevertheless, assuming that the rolling and pitching tilt angles are accurately available with all other INS and GPS measurements, Figure 4.43 shows the vertical velocity of the vehicle when taken from the vehicle body axes, b-frame, and the vehicle motion/surface axes, v-frame. The figure shows the significant difference

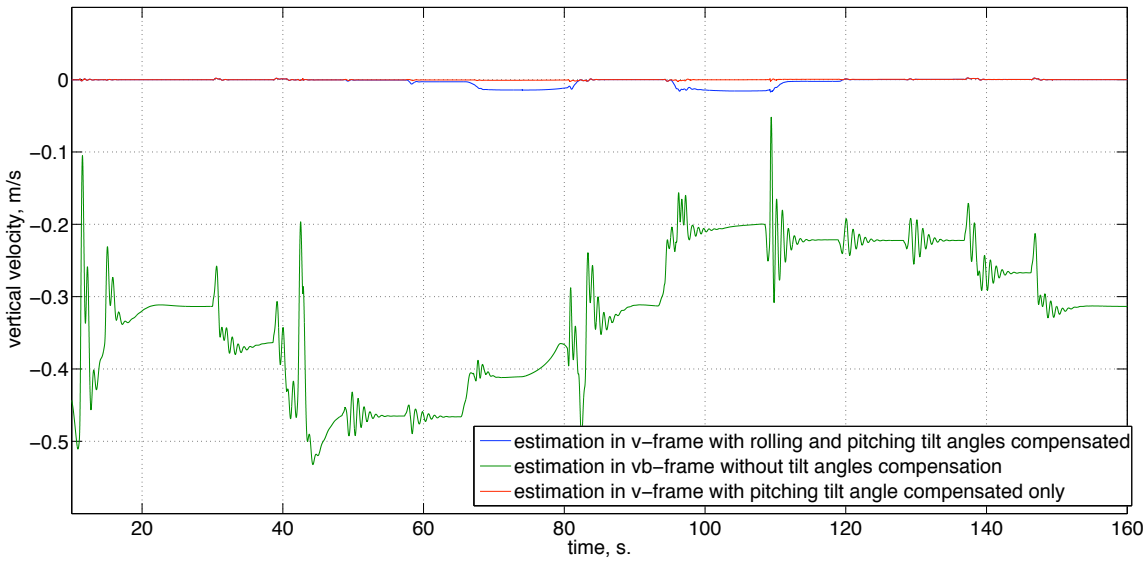

Figure 4.43: Vertical velocity estimated in the v-frame and b-frame

between the vertical velocity of the vehicle in different frames of reference. When using Equation 4.34, the vertical velocity estimation is very noisy and unstructured. The fact that its estimation is non-zero during the entire simulation (even on straight road travelling) suggests the existence of initial pitching.

A closer look at the estimation in the v-frame, see Figure 4.44, allows one to see the difference between 'with' and 'without' the rolling tilt angle. As identified from the figure, the main contribution of rolling tilt angle is during heavy road banking and turning (60 to 80s. and 95 to 120s.). Otherwise, the rolling tilt angle is not as critical as the pitching tilt angle.

As shown in previous figures, tilt angles have a significant effect on vertical velocity estimations. Similarly, tilt angles also have an effect on the longitudinal and lateral velocity, and thus the sideslip angle. However, as shown in Figure 4.45, the effect of the tilt angles are not as great when applied to the vertical velocity. Although results from the figure show only a small effect at the cg, when transferred to the estimations of tyre dynamics, this small difference may lead to a significant error in determining slip angles and tyre forces.

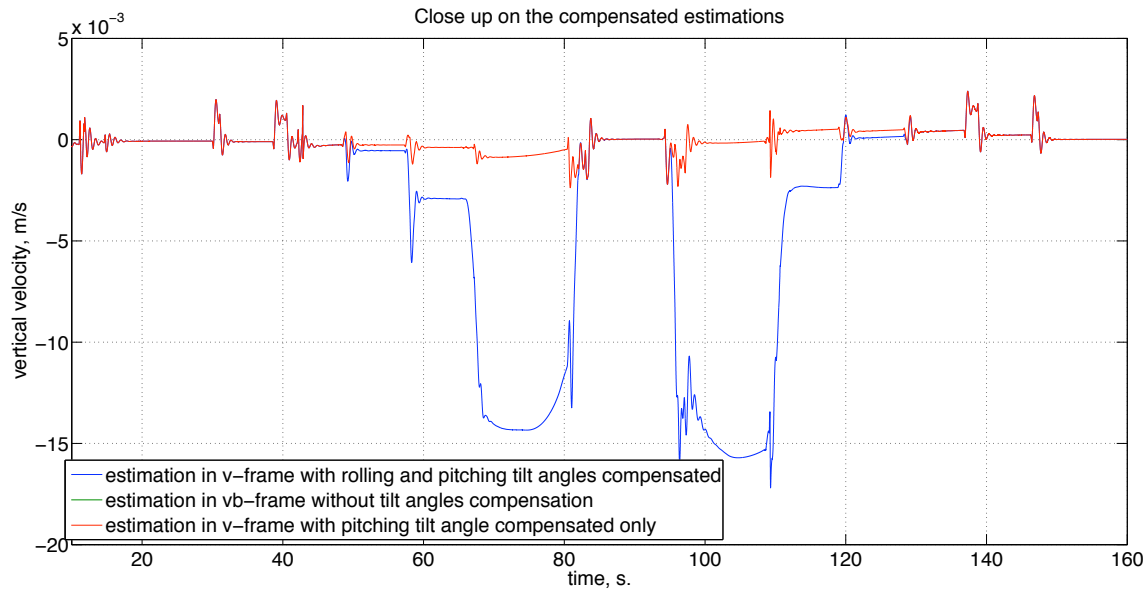

Figure 4.44: Vertical velocity estimated in the v-frame and b-frame - close up

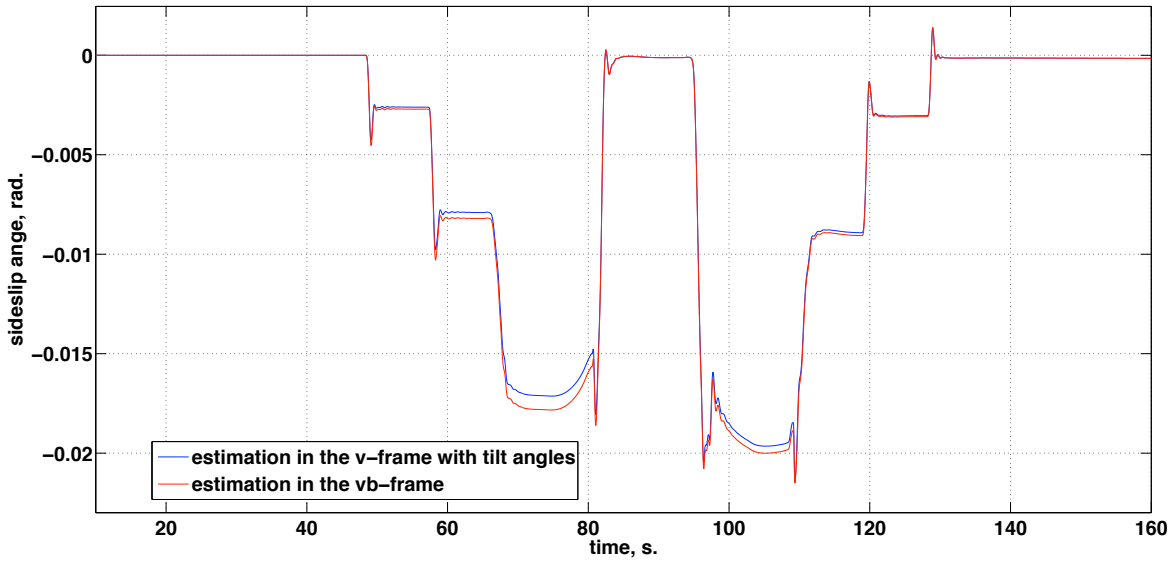

Figure 4.45: Sideslip angle estimated in the v-frame and b-frame

To conclude, with the Euler rates and Euler angles determined, a better sensor model for the INS is available. Together with a dual GPS antennae set-up, the bias in the three gyros can be estimated. Simulation has also shown the importance of working in the correct framework. As GPS operates at e-frame, INS in b-frame and vehicle motion in v-frame, vehicle dynamics must be correctly transformed before comparison and usage in the KFs.

Transforming from a b-frame to v-frame is straight forward and easy, but requires extra measurements not commonly found in the standard sensor package (i.e. yaw rate gyro, accelerometer and single GPS antenna receiver). Depending on the requirements of estimation precision, designers must juggle between cost and benefit to decide whether to invest in extra sensors and GPS antennae/receivers. Without

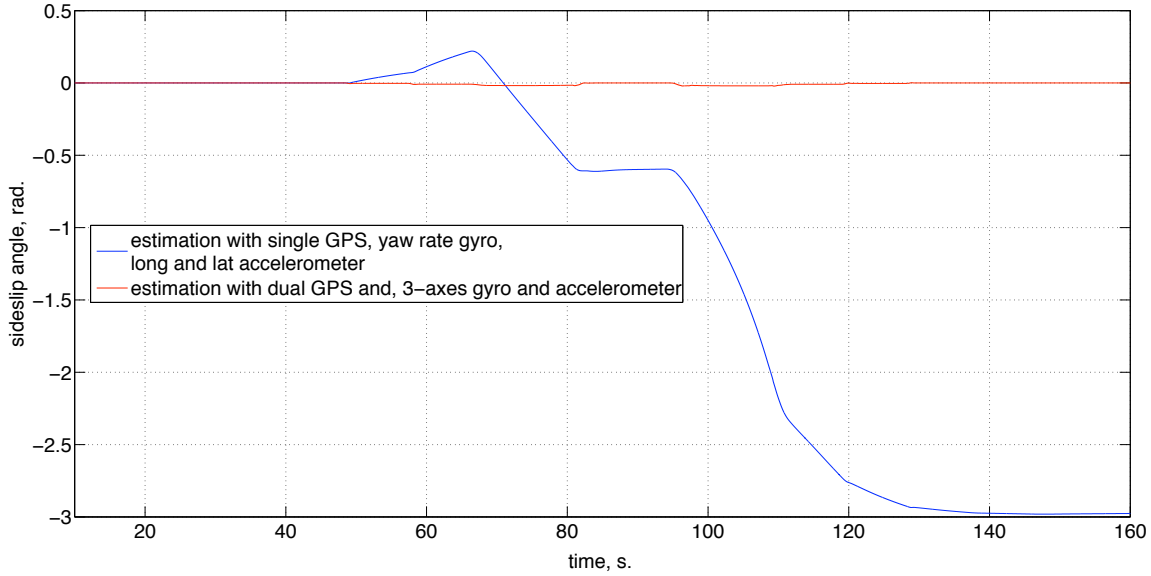

Figure 4.46: Sideslip angle estimated in the b-frame without gravitational components

any extra sensors, there will be no knowledge for the Euler angles to supply to the gravitation components in Equation 4.34. Ignoring this term, and using only the standard package results in a sideslip estimation as presented in Figure 4.46, this shows the importance of the gravitational terms in the INS model of the KF when the vehicle is travelling up and downhill.

4.5.2 Dual-GPS antennae heading estimation

As discussed earlier, the advantage of having a multiple GPS antennae is the availability of heading angle measurements. With multiple antennae and GPS units on the vehicle, multiple GPS positions will be available. It is, therefore, natural to try to use these position measurements with simple geometry to obtain a heading measurement for the vehicle. However, due to the inaccuracy of the GPS (1-4m for a typical consumer GPS receiver, Table 4.8), it is important to know the consequences and errors of using this technique in estimating the sideslip angle before implementation.

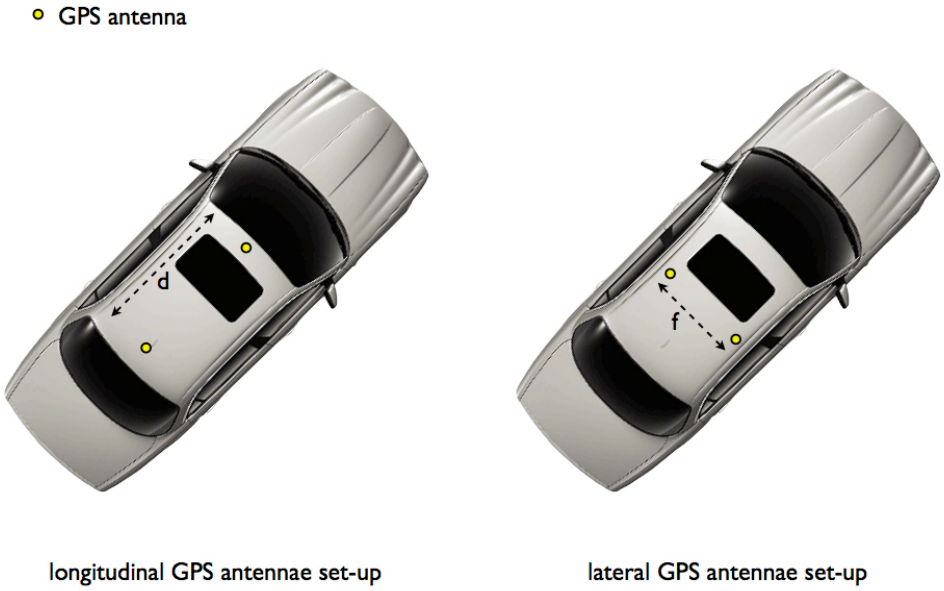

Figure 4.47: Diagram showing the possible dual GPS antennae set-up on a Jaguar XJ

With two antennae, there are basically two ways to arrange the sensors: longitudinally and laterally, see Figure 4.47. The longitudinal set-up has a heading-position relationship of $\hat{\psi}_{2gps} = \tan^{-1}\left(\frac{y_e^{(1)} - y_e^{(2)}}{x_e^{(1)} - x_e^{(2)}}\right)$. With known distance, d, between the two antennae, the variance of the heading estimation, $\sigma^2_{\psi_{2gps}}$, in terms of the variance of the GPS position, σ_P^2, is expressed as

$$\sigma^2_{\psi_{2gps}} = \frac{2\sigma_P^2}{d^2}. \tag{4.38}$$

Similarly, for the lateral GPS set-up, with the distance between the two antennae as, f, the heading variance yields:

$$\sigma^2_{\psi_{2gps}} = \frac{2\sigma_P^2}{f^2}. \tag{4.39}$$

Using Equation 4.38 or 4.39 , for a typical GPS with 3m standard deviation, Table 4.8, the antennae must be at least 243m apart in order to achieve a heading variance of (1° ^{2}) ($\approx 3 \times 10^{-4}$ rad.). Or, if a heading variance of (1° ^{2}) is to be achieved with a distance of 1m, the standard deviation for the GPS position must be better than 0.01m.

The analysis above has shown that an acceptable accuracy for the heading estimation is not achievable via simple geometric relationship using position estimations from consumer grade GPS. An alternative method exists which utilises the concept

of interferometry. In short, interferometry is a technique that is used for studying the interference of waves. Figure 4.48 shows two GPS antennae with distance, d, apart. Satellite code is transmitted and received by the two antennae at an angle. This results in a phase difference between the two codes received by the two antennae.

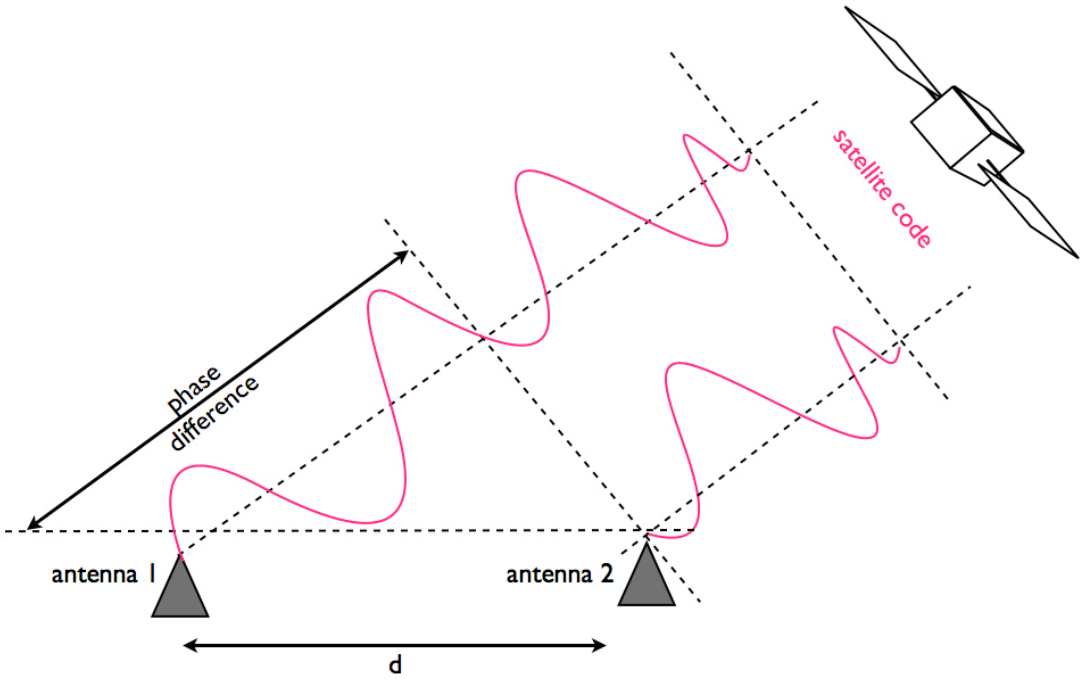

Figure 4.48: Diagram showing phase differencing when GPS antennae receive satellite code

This phase difference is combined with the pseudo-range and geometry data from the satellite to produce a measurement for the rate rotation in the b-frame. This information can be implemented into the *angEKF* for bias prediction and noise filtering.

As described in Parikh [2006], there are two types of GPS interferometry: i) Single Differencing (SDiff) and, ii) Double Differencing (DDiff). The two schemes differ in terms of complexity and as commented in Van Graas and Braasch [1991], the use of DDiff requires not only a set-up of dual GPS antennae, but also two GPS receivers. The extra component on GPS is going to increase the cost for the overall system and judgement must be made carefully to compensate between cost and accuracy. In order to help designers to choose the components for their GPS/INS integrated system, Section 4.6 provides a detail analysis of the accuracy of the cross-relationship between tracking, heading and sideslip angle.

4.6 Graphical-aided GPS/INS design

Section 4.5 discussed the set-up of a dual GPS antennae and 6-axes INS system. A brief introduction was also given on the use of GPS interferometry for accurate heading angle measurements. By using the *angEKF* proposed in Equation 4.31 with measurements from the dual GPS set-up, biases in the gyros can be estimated.

Although state estimations are improved by including more sensors, this also increases the cost per vehicle. As a result, it is important to be able to justify the extra cost spent on the system and to understand how the extra cost benefits the overall system. This section, therefore, focuses on the effect of the sideslip angle precision when its two major components, tracking and heading angle, vary in their accuracy. It is true that tracking angle and heading angle (with corresponding accuracy) are available in a dual GPS antennae set-up as discussed in Section 4.5. However, designers may not necessarily require/want to use such a sophisticated system due to restricted budget or other criteria. Thus, this section goes one step further to look into the typical method of deriving the tracking and heading angle from the perspective of a single GPS antenna and three-axes INS set-up. With this knowledge, designers can choose the most suitable components to fit the design criterion.

4.6.1 Tracking, heading and sideslip angle

As mentioned at the beginning of Section 4.5, sideslip angle is an important state for local velocity determination in the b-frame for a GPS. A simple approach to obtain the sideslip is to subtract the heading angle from the tracking angle, recall $\beta = \nu - \psi$. The accuracy of the sideslip estimated is, therefore, dependent on the precision of the tracking and heading angle measurements. As the effect of GPS sampling rate has already been addressed in Section 4.4, this section focuses on the general effect of tracking and heading angle on sideslip estimations, as a result of noise and disturbances. Therefore the simulations use a sampling rate at the consumer grade level: 100Hz for the INS (and heading angle measurement) and 1Hz for GPS (and tracking angle measurement).

Figure 4.49 shows the result of a series of simulations when sideslip angle and yaw rate is set as constant (0.5 rad. and 1 rad/s respectively). In the series of simulations, a different level of white noise (σ = 0 to 1°) is added to the heading and tracking angle. The sideslip is estimated with the corrupted angle measurements and the variance of the sideslip error is calculated and represented in colour code in Figure 4.49.

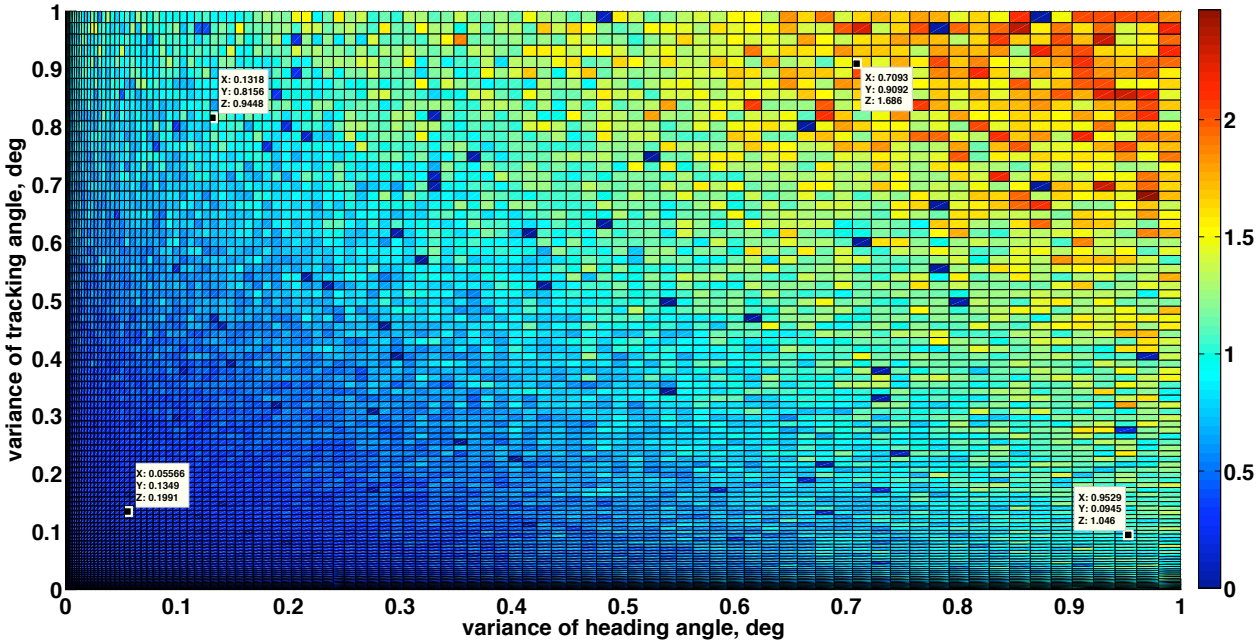

Figure 4.49: Variance for sideslip estimation error in degrees. Sideslip estimated with $\beta = \nu - \psi$

In general, the smaller the error in both tracking and heading angle, the better the sideslip estimation, i.e. a proportional relationship. Due to random seeding of noise in Matlab/Simulink, a few variance combinations manage to achieve a relatively small sideslip error, producing uneven colouring regions in Figure 4.49. With repeated simulations, these uneven coloured regions will be reduced.

Figure 4.49 also shows similar colour bands (blue, green and orange) in the inversely proportional direction (top left to bottom right). When the tracking angle has a high variance, the sideslip estimation remains low only if the variance of the heading angle is low. This, also happens in the reverse order when heading angle variance is high. This phenomena is better explained with the mathematical relationship of the three variances, $\sigma_\beta^2 = \sigma_\nu^2 + \sigma_\psi^2$, which agree with the graphical representation in the figure. Using this formula, it can easily be seen that when both tracking and heading variances are small (or large), the sideslip variance becomes correspondingly small (or large). But the sideslip variance can also remain at a similar value with different combinations of tracking and heading variances, thus, the diagonal colour bands are in the inversely proportional direction.

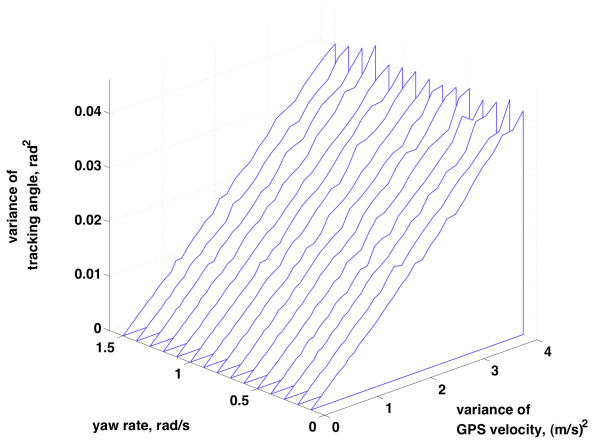

(a) GPS velocity is kept at 10m/s

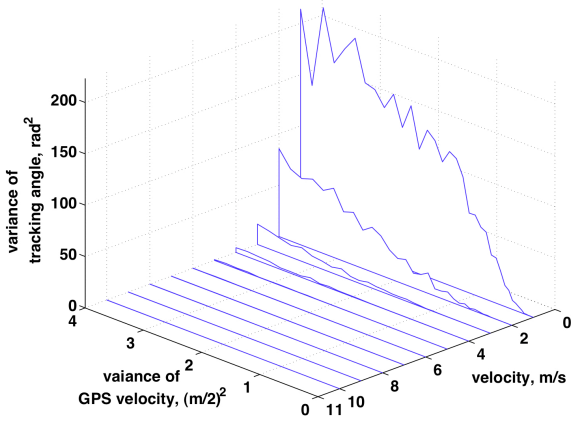

(b) yaw rate is kept at 0.5 rad/s

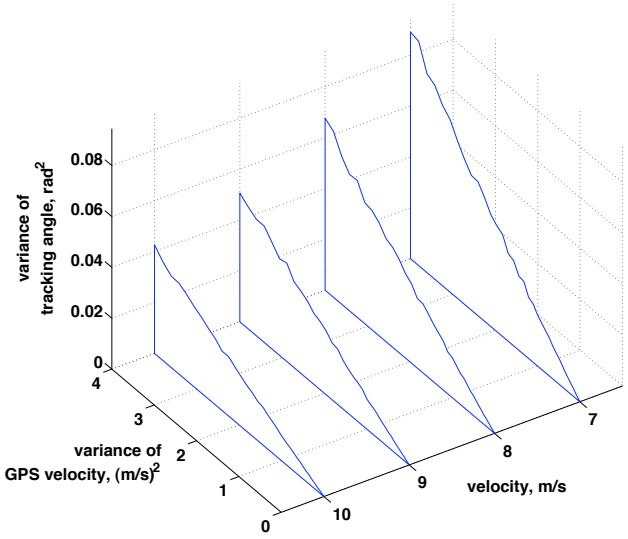

(c) close-up view with yaw rate kept at 0.5 rad/s

Figure 4.50: Variance for tracking angle in radians

4.6.2 GPS Tracking Angle Estimation

In a single GPS receiver, tracking angle is typically measured by taking the inverse tangent of the lateral to longitudinal velocity ratio in the e-frame, $\nu = \tan^{-1}\left(\frac{\dot{y}_e}{\dot{x}_e}\right)$. With this formula, the variance for the tracking angle is

$$\sigma_\nu^2 \approx \frac{\sigma_V^2}{V^2}. \tag{4.40}$$

A detailed derivation for this variance approximation is given in Appendix B.2 with the assumption of the same GPS velocity variance in the lateral and longitudinal direction, i.e. $\sigma_{\dot{x}_e}^2 = \sigma_{\dot{y}_e}^2 = \sigma_V^2$. It is not hard to see from Equation 4.40 that the

faster the vehicle is travelling, the lower the tracking angle variance. This is because velocity variance is a measure of the average squared deviation from its mean value, $\bar{V}$, thus,

$$\sigma_\nu^2 \approx \frac{\sigma_V^2}{V^2} = \frac{\frac{1}{n}\sum_{i=1}^{n}\left(V_i - \bar{V}\right)^2}{V^2}.$$

As GPS velocity variance, σ_V^2, is referenced to a fixed speed (in many cases this speed is zero), the variance does not change with speed. Therefore, when the speed, V, of the vehicle increases, the velocity variance will have less effect on the GPS measured speed. Hence, a more accurate velocity measurement and tracking angle estimation is obtained.

Figure 4.50 shows the tracking angle variance (in rad^2) obtained from various simulations, in which the speed of the vehicle and yaw rate vary. The bottom plot in Figure 4.50 shows agreement with Equation 4.40. However, for lower speeds (1 to 6m/s), see top-right plot of Figure 4.50, the approximated tracking variances do not seem to agree with the approximation made in Equation 4.40. This is because the GPS velocity variance is close to or larger than the actual speed of the vehicle, which makes the velocity error too great. From the simulation, it can be seen that with a velocity variance lower than $\frac{V}{2}$, the use of Equation 4.40 for tracking angle estimation is acceptable, refer to bottom plot Figure 4.50. As a result, for $V = 2m/s$, the tracking angle variance is correctly predicted only when the velocity variance is smaller than $1.0(m/s)^2$.

In addition, as shown in the simulation, Equation 4.40 does not vary with the change in vehicle yaw rate. With yaw rate increases from 0 to 1.5 rad/s at a constant speed of 10m/s, the tracking angle variance stay close to one another. The upward slope is entirely due to the variation of the GPS velocity variance as presented in Equation 4.40.

4.6.3 Numerically integrated heading estimation

Using consumer grade INS, heading estimations are normally numerically integrated from gyro measurements. Integrated heading accuracy and variances are dependent on the sampling time, T_s, the run time, t, the accuracy of the gyro, σ_{r_m}, and the

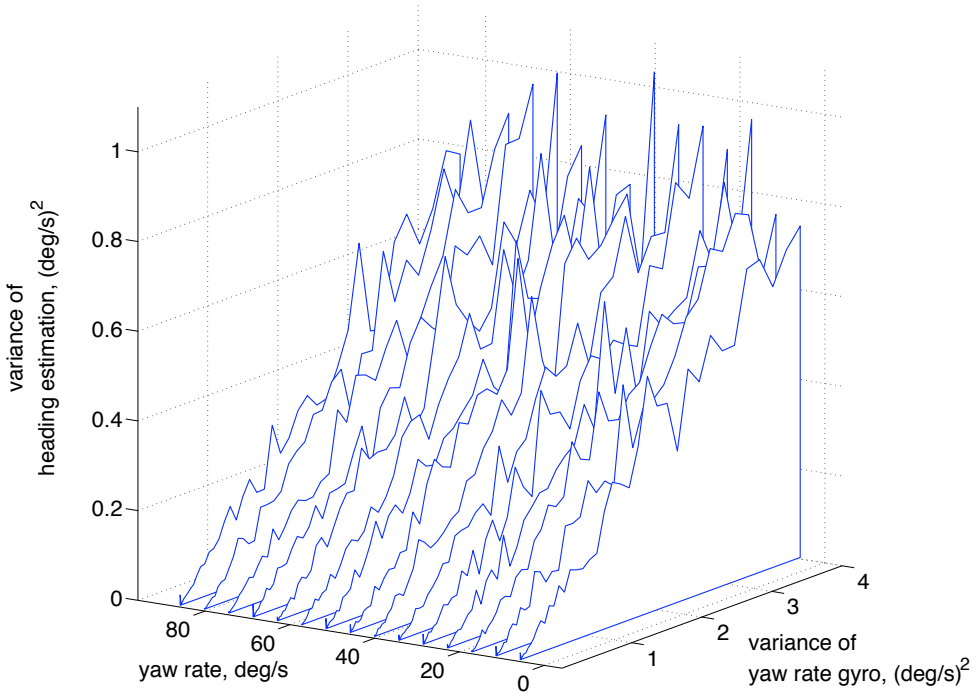

Figure 4.51: Variance for heading estimation in degrees, numerically integrated from the yaw rate gyro

variance of previous estimation, σ_{ψ_n},

$$\begin{aligned}
\psi_k &= \psi_{k-1} + T_s r_m \\
\sigma^2_{\psi_k} &= \sigma^2_{\psi_{k-1}} + T_s^2 \sigma^2_{r_m} \\
\therefore \sigma^2_{\psi_1} &= \sigma^2_{\psi_0} + T_s^2 \sigma^2_{r_m} \\
\sigma^2_{\psi_2} &= \sigma^2_{\psi_0} + 2T_s^2 \sigma^2_{r_m} \\
&\vdots \qquad\qquad \vdots \\
\sigma^2_{\psi_n} &= \sigma^2_{\psi_0} + nT_s^2 \sigma^2_{r_m} \\
&= \sigma^2_{\psi_0} + \frac{t}{T_s} T_s^2 \sigma^2_{r_m} \\
&= \sigma^2_{\psi_0} + tT_s \sigma^2_{r_m}
\end{aligned} \tag{4.41}$$

From Equation 4.41 it is clear that with the absence of bias, variance of heading estimation derived from numerical integration is unbounded. With time, the variance of the heading angle increases to equal the variance of the rate gyro and a longer duration causes the variance to continue to increase. As shown in Equation 4.41 and Figure 4.51, when the variance of rate gyro increases, the heading variance also increases.

Moreover, Figure 4.51 shows that the heading variance has a minimum influence from the variation of the yaw rate when compared with the rate gyro variance. The spikes shown in Figure 4.51 are random and dependent upon all the heading estimations throughout each simulation. The heading estimation results show that with the absence of bias, error continues to grow and it is essential to have an external heading measurement to correct the errors.

4.6.4 Summary and application

In this section, various figures showing the variance of tracking angle, heading angle and sideslip angle are presented while varying the vehicle speed, yaw rate, GPS velocity variance and yaw rate gyro variance. With known GPS velocity and yaw rate gyro variance, Figures 4.49 to 4.51 and Equation 4.40 to 4.41, can be implemented together to approximate the variance of sideslip estimation.

On the other hand, without a dedicated type of sensor to be used, the charts can also aid designers in choosing appropriate GPS and/or INS devises to suit their design purpose of a GPS/INS integrated system. Here, below, shows a recommended procedure in which there exists a design criterion for sideslip estimation:

1. What is the range of accuracy (variance) of the estimated sideslip angle? (use Figure 4.49)

2. What is the range of variance of tracking angle and heading angle that will produce the sideslip criterion as specified in step 1?

3. Are you considering a dual GPS antennae set-up? If yes, stop here as a dual GPS system should provide a variance for heading and tracking estimation; if not, continue.

4. What is the variance for the yaw rate gyro required to produce the heading accuracy the same as or higher than that found in step 2? (use Equation 4.41 and Figure 4.51)

5. What is the variance for the GPS velocity required to produce the tracking angle accuracy the same as or higher than that found in step 2? (use Equation 4.40 and Figure 4.50)

6. What is the speed range for the vehicle when the designed system is operating? i.e. GPS velocity variance must be lower than half of the vehicle speed.

This page intentionally left blank.

Chapter 5

Model-based Estimator and Integrated Kalman Filter

5.1 Introduction

In Sections 4.2 to Section 4.5, the focus was the use of a KKF. It was shown that the KKF is a viable solution for state estimation, but requires a six-axis INS for accurate estimations to be obtained for most driving manoeuvres. With the standard three-axis INS set-up (longitudinal accelerometer, lateral accelerometer and yaw rate gyroscope), the KKF struggles to estimate states correctly during high speed manoeuvres that involve hill climbing/descending. Additional sensors can improve the estimations but at the same time, also increase the cost per vehicle.

As discussed in Chapter 2, an alternative method for estimating states is the use of a MKF. Although this approach benefits from a close representation of the actual vehicle, MKF is highly dependent on the model accuracy and that of the parameters and coefficients used. In Chapter 3, it has been shown that the 2DoF model is the simplest and least costly to implement. This chapter therefore focuses on the MKF based on the 2DoF bicycle model.

The chapter is divided into four sections. In the next section, a thorough study is carried out using both simulations and theoretical analysis. Limitations and robustness of the 2DoF bicycle model-based on the accuracy of parameters and sensor inputs are investigated. Section 5.3 combines the KKF and MKF to form an IKF; the structure and simulated results for this filter are also presented. In the last section, a summary of findings for this chapter is given.

5.2 Limitations and Robustness of 2DoF Bicycle Model Estimator

The higher the number of degrees of freedom in the model the more accurately it represents the real vehicle. However at the same time it becomes more complicated to implement, and includes more sources of uncertainty. As shown in Bayliss et al. [2006], a 5DoF bicycle MKF is able to give good estimations for unmeasurable dynamic states but accuracy is only guaranteed when the parameters in the MKF are known accurately. It becomes obvious that the understanding of the sensitivity of the estimated state due to parameter variations is vital during the design process. Moreover, in order to reduce the complexity of the vehicle model, the 2DoF bicycle model is to be studied. It should also be noted that this study involves no KF and only the vehicle model itself. So the sensitivity of the states can be observed on their own without any correction from external sources such as GPS. As a reminder, the 2DoF bicycle model is given by,

2DoF bicycle model

$$\begin{bmatrix} \dot{\beta} \\ \ddot{\psi} \end{bmatrix} = \begin{bmatrix} \frac{C_{yF}+C_{yR}}{mV} & \frac{aC_{yF}-bC_{yR}}{mV^2} - 1 \\ \frac{aC_{yF}-bC_{yR}}{J_z} & \frac{a^2C_{yF}+b^2C_{yR}}{J_zV} \end{bmatrix} \begin{bmatrix} \beta \\ \dot{\psi} \end{bmatrix} + \begin{bmatrix} \frac{-C_{yF}}{mV} \\ \frac{-aC_{yF}}{J_z} \end{bmatrix} \delta_F$$

$$\text{inputs} = \begin{bmatrix} \delta_F & V \end{bmatrix}^T$$

$$\text{states to be estimated} = \begin{bmatrix} \beta & \dot{\psi} \end{bmatrix}^T$$

$$\text{parameters} = m, C_{yF}, C_{yR}, a, b, J_z$$

In general, there are two types of error in the vehicle model: 1) errors from parameters, and 2) errors from inputs and initial conditions.

5.2.1 Parameter Related Errors

As defined in Section 3.6.1, vehicle parameters are classified into three groups (i.e. static parameters, conditional parameters and dynamic parameters) and each of these contributes to some errors in the vehicle model. In the 2DoF model, only the conditional and dynamic parameters are present. In order to simplify the investigation, this section only looks at the effect of mass, moment of inertia and the two

axle cornering coefficients. The effect of the geometric ratio is discussed later in the sensitivity analysis in Section 5.2.2.

For each case, a low speed manoeuvre at 20kph is performed in IPG CarMaker with sensors bias and noise set to zero. These perfect input signals and initial conditions allow a better understanding of the effects of parameter variation on the accuracy of state estimation. Each study is first started with the original value of the parameters given in Appendix A.1 and a percentage variation is then added to the corresponding parameter to investigate their effect. The states from the 2DoF model, namely sideslip and yaw rate (also heading angle), are recorded and compared with the actual states.

Variation of Mass

The mass of the model is varied between ±50% with increments of 1% of the unloaded mass (only the finished vehicle without fuel, nor passenger, nor luggage). While the unloaded mass stays almost constant during the lifetime of a vehicle, the variation of mass is mainly due to the changes in the number of passengers, and amount of luggage and fuel. This variation range is adequate as 50% of the total mass of the vehicle ($\approx 900kg$) in this study is much heavier than the likely maximum mass ($550kg$), which is the total mass of five adults ($400kg = 5 \times 80kg$), 50L fuel ($50kg$) and luggage ($100kg$).

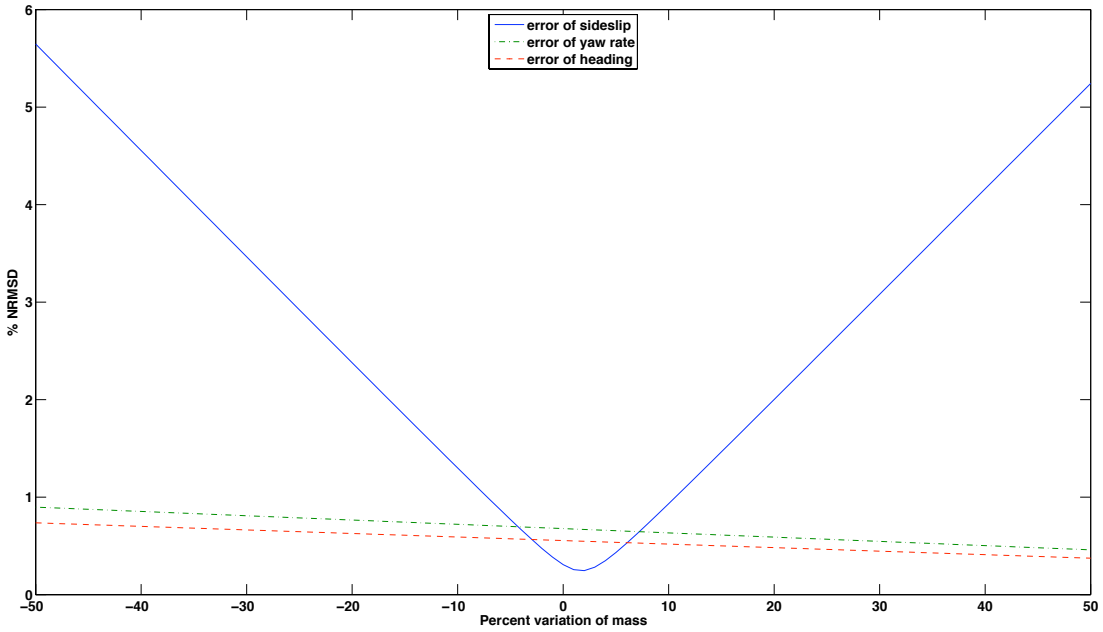

Figure 5.1: Effect on estimated states with variation in mass at 20kph, %NRMSD

Figure 5.1 shows the %NRMSD of the three estimated states during mass vari-

ation. It is interesting to see that at 0% mass variation, the state estimation errors are not 0%. This means that the 2DoF vehicle model is not a perfect representation of the original vehicle in IPG CarMaker and some of the dynamics are left unmodelled. Inspecting the %NRMSD of yaw rate and heading angle, the figure reveals that their errors are always under 1% throughout the entire range of variation, with a maximum at -50% mass variation.

For the sideslip estimation, however, the %NRMSD is over 5% at both ends of the mass variation spectrum. While the error of yaw rate and heading estimations decreases linearly and slowly from variation of -50% to $+50\%$, the %NRMSD of the sideslip estimate reduces quickly from its maximum error at variation of -50% to near 0% and then increases to over 5% at $+50\%$. From Figure 5.1, it can be concluded that sideslip estimations are more sensitive to the mass variation.

Although Figure 5.1 has shown the high sensitivity of the sideslip estimations at both ends of the mass variation, in reality, the unloaded mass of a vehicle does not change much as wear and tear contribute little to the variation of mass. As the unloaded mass stays almost constant, the fully loaded vehicle mass varies due to the variation in the number of passengers, luggage and amount of fuel. With the maximum mass allowance, $550kg$, this is equivalent to 32% of the total variation of the vehicle unloaded mass. From Figure 5.1, therefore, the maximum expected %NRMSD for sideslip estimation is about 3.2%.

Variation of Moment of Inertia

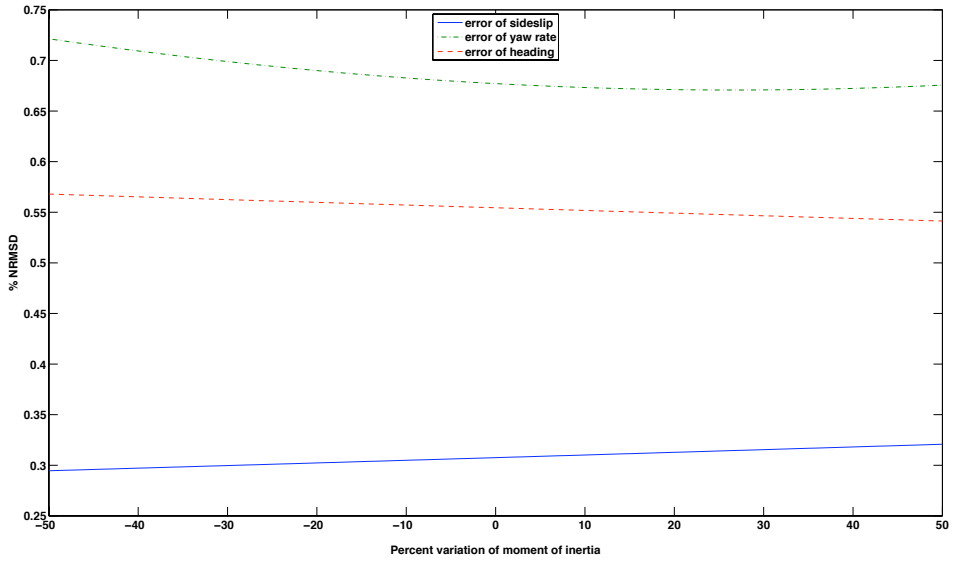

Figure 5.2: Effect on estimated states with variation in moment of inertia at 20kph, %NRMSD

With regard to the moment of inertia, it is varied from -50% to +50% again with an interval of 1% of its unloaded value given in IPG CarMaker. Similar to the mass variation, due to unmodelled dynamics, Figure 5.2 shows that the state estimation errors are not zero at 0% variation. Comparing this with Figure 5.1 demonstrates that the state estimates are less sensitive to the change in the moment of inertia. All three error curves in Figure 5.2 have a %NRMSD less than 1%. A major difference is the error of the sideslip estimation, which is lower than both errors of the yaw rate and heading angle throughout the entire range. In general, all states are not very sensitive to variation in the moment of inertia.

Variation of Cornering Coefficients

In the 2DoF bicycle model, apart from the mass and moment of inertia, another two extremely important parameters are the front and rear axle cornering coefficients, C_{yF} and C_{yR}. As described in Chapter 3, they hold the key linkage between the surface of the road and the motion of the body via the force generated by the tyres.

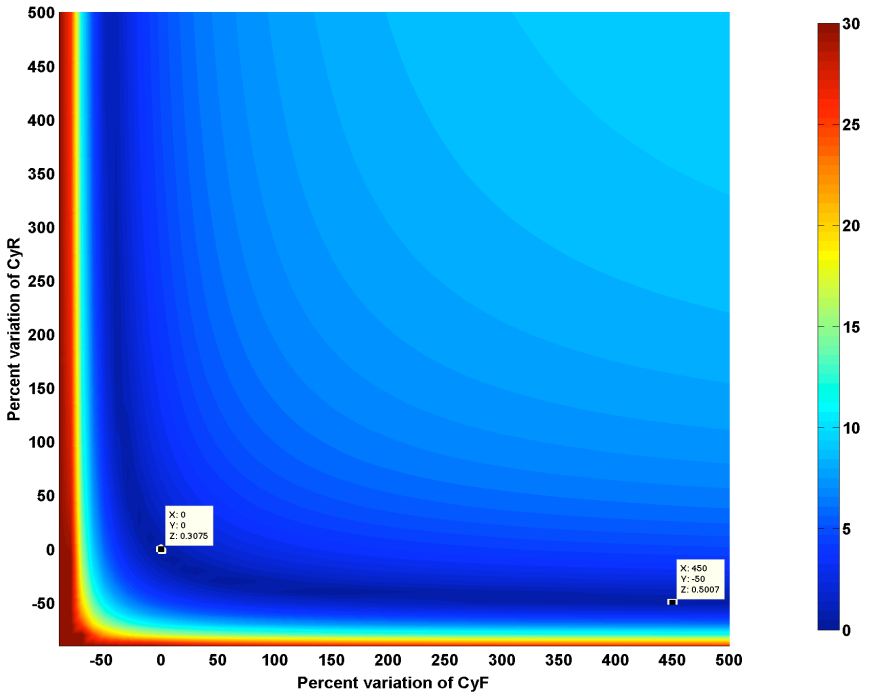

Figure 5.3: Effect on sideslip estimation with variation in axle cornering coefficients at 20kph, %NRMSD

For this particular study, the starting cornering coefficients are determined from the *DoubleOval_20kph* manoeuvre in IPG CarMaker (for details please refer to Sec-

tion 3.6.1) and they are varied from -90% to +500% of their starting values. Figures 5.3 to 5.5 show the %NRMSD of the state estimates in a colour map. It must be pointed out that the maximum %NRMSD is over 100%. For the purpose of better visualisation, the figures display only the range from 0% to above 30%.

Similar to the previous cases, the figures show a small error at 0% cornering coefficient variations. For the sideslip state estimation, Figure 5.3, the maximum %NRMSD occurs at -90% variation for both C_{yF} and C_{yR}. It is interesting to see the error variation in the figure, in which similar errors are achieved with a combination of either a large C_{yF} and small C_{yR} or a small C_{yF} and large C_{yR} variation. This pattern is due to the determination of lateral acceleration from the sum of front and rear tyre forces,

$$\ddot{y} \quad = \tfrac{1}{m} \left(F_{yF} + F_{yR} \right).$$

When the force at the front changes, the force at the rear has to vary inversely with respect to the front axle forces in order to maintain the same lateral acceleration and sideslip angle. This relationship of the front and rear axle forces generates the pattern in Figure 5.3. Furthermore, the error also seems to grow faster in the westward direction, which suggests that the reduction of C_{yF} results in more sideslip errors when compared to the reduction of C_{yR}. In the other dimension, variation of +500% of C_{yF} and C_{yR}, the error is still in the range of 10-13%.

For the yaw rate and heading estimations, shown in Figures 5.4 and 5.5, the maximum errors occur on the west and south-most of the two figures when the cornering coefficients have a negative variation. Compared with the error pattern in the sideslip estimation, those in the yaw rate and heading estimation have a more symmetrical pattern. This is because yaw acceleration is estimated with the difference in forces at the front and rear axles,

$$\ddot{\psi} \quad = \tfrac{1}{J_z} \left(a F_{yF} - b F_{yR} \right).$$

Hence, in order to maintain the same output, when force at the front changes, the force at the rear also has to change proportionally. The two figures show that a large cornering coefficients variation of 500% generates an error in the range of 3 to 5%NRMSD.

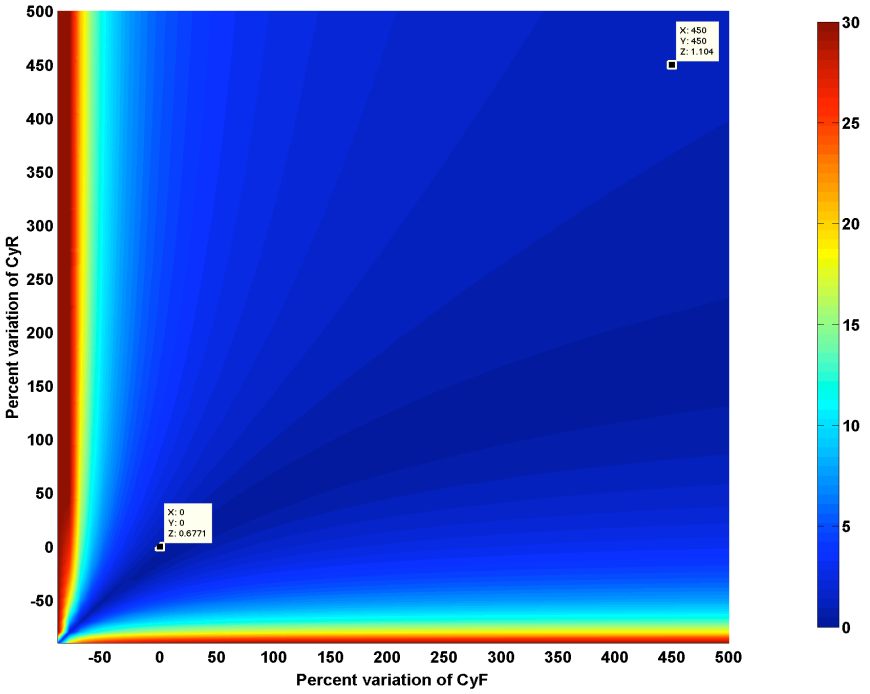

Figure 5.4: Effect on yaw rate estimation with variation in axle cornering coefficients at 20kph

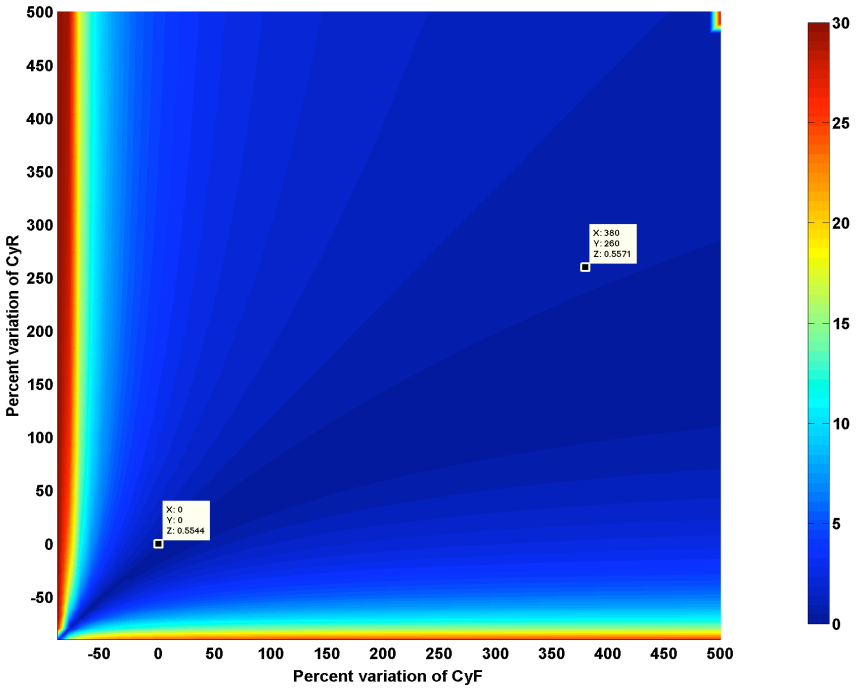

Figure 5.5: Effect on heading estimation with variation in axle cornering coefficients at 20kph

5.2.2 Parametric Sensitivity Analysis

As shown graphically in the previous section, sideslip estimations are relatively sensitive to changes in cornering coefficients when compared to mass and inertia. However, one interesting observation from the graphs is that changes in cornering coefficients do not cause the sideslip estimation errors to increase indefinitely. It is therefore concluded that it is better to set cornering stiffness larger than smaller.

In this section, a sensitivity analysis is carried out on the 2DoF model in order to give a theoretical explanation for the previous graphical observations on the variation of cornering coefficients, mass, moment of inertia and geometric ratio, $\frac{a}{b}$. Consider the 2DoF bicycle model in discrete state space representation:

$$
\begin{aligned}
\Theta_{k+1} &= \mathbf{A}\Theta_k + \mathbf{B}\mathrm{u}_k \\
\text{where: } \Theta &= \begin{bmatrix} \beta & \dot{\psi} \end{bmatrix}^T \\
\mathrm{u} &= \delta \\
\mathbf{A} &= \begin{bmatrix} 1 + T_s\left(\frac{C_{yF}+C_{yR}}{mV}\right) & T_s\left(\frac{aC_{yF}-bC_{yR}}{mV^2} - 1\right) \\ T_s\left(\frac{aC_{yF}-bC_{yR}}{J_z}\right) & 1 + T_s\left(\frac{a^2C_{yF}+b^2C_{yR}}{J_zV}\right) \end{bmatrix} \\
\mathbf{B} &= \begin{bmatrix} T_s\left(\frac{-C_{yF}}{mV}\right) \\ T_s\left(\frac{-aC_{yF}}{J_z}\right) \end{bmatrix}
\end{aligned}
$$

The sensitivity for the parameter, P_m, is defined as the derivatives of the final state vector, Θ_n, over the paramter in consideration, therefore:

$$
S_{P_m} := \frac{\partial \Theta_n}{\partial P_m} = \frac{\partial \Theta_n}{\partial \mathbf{A}} \frac{\partial \mathbf{A}}{\partial P_m} + \frac{\partial \Theta_n}{\partial \mathbf{B}} \frac{\partial \mathbf{B}}{\partial P_m} \tag{5.1}
$$

The final state vector is derived through the following steps:

$$
\begin{aligned}
\Theta_1 &= \mathbf{A}\Theta_0 + \mathbf{B}\mathrm{u}_0 \\
\Theta_2 &= \mathbf{A}\Theta_1 + \mathbf{B}\mathrm{u}_1 \\
&= \mathbf{A}(\mathbf{A}\Theta_0 + \mathbf{B}\mathrm{u}_0) + \mathbf{B}\mathrm{u}_1 \\
&= \mathbf{A}^2\Theta_0 + \mathbf{A}\mathbf{B}\mathrm{u}_0 + \mathbf{B}\mathrm{u}_1 \\
\Theta_3 &= \mathbf{A}^3\Theta_0 + \mathbf{A}^\mathbf{2}\mathbf{B}\mathrm{u}_0 + \mathbf{A}\mathbf{B}\mathrm{u}_1 + \mathbf{B}\mathrm{u}_2 \\
\vdots & \qquad\qquad \vdots
\end{aligned}
$$

$$\Theta_n = \mathbf{A}^n\Theta_0 + \mathbf{A^{n-1}B}\mathrm{u}_0 + \mathbf{A^{n-2}B}\mathrm{u}_1 + \ldots \mathbf{IB}\mathrm{u}_{n-1}$$

$$\Theta_n = \mathbf{A}^n\Theta_0 + \begin{bmatrix}\mathbf{A}^{n-1} & \mathbf{A}^{n-2} & \ldots & \mathbf{I}\end{bmatrix}\mathbf{B}\begin{bmatrix}\mathrm{u}_0\\ \mathrm{u}_1\\ \vdots\\ \mathrm{u}_{n-1}\end{bmatrix}$$

With the final state vector derived with respect to the initial system, the sensitivity can be written as:

$$\begin{aligned} S_{P_m} = {} & n\mathbf{A}^{n-1}\frac{\partial \mathbf{A}}{\partial P_m}\Theta_0 \\ & + \begin{bmatrix}(n-1)\mathbf{A}^{n-2} & (n-2)\mathbf{A}^{n-3} & \ldots & \mathbf{0}\end{bmatrix}\frac{\partial \mathbf{A}}{\partial P_m}\mathbf{B}\begin{bmatrix}\mathrm{u}_0\\ \mathrm{u}_1\\ \vdots\\ \mathrm{u}_{n-1}\end{bmatrix} \\ & + \begin{bmatrix}\mathbf{A}^{n-1} & \mathbf{A}^{n-2} & \ldots & \mathbf{I}\end{bmatrix}\begin{bmatrix}\mathrm{u}_0\\ \mathrm{u}_1\\ \vdots\\ \mathrm{u}_{n-1}\end{bmatrix}\frac{\partial \mathbf{B}}{\partial P_m} \end{aligned} \tag{5.2}$$

Applying the following properties of the Frobenius norms,

1. $\|ab\| \leq \|a\|\|b\|$, and
2. $\|a+b\| \leq \|a\| + \|b\|$,

to the sensitivity anaylsis, Equation 5.2.

$$\begin{aligned} \|S_{P_m}\| \leq {} & n\|\mathbf{A}^{n-1}\|\|\frac{\partial \mathbf{A}}{\partial P_m}\|\|\Theta_0\| \\ & + \begin{bmatrix}(n-1)\|\mathbf{A}^{n-2}\| & (n-2)\|\mathbf{A}^{n-3}\| & \ldots & \mathbf{0}\end{bmatrix}\|\frac{\partial \mathbf{A}}{\partial P_m}\|\|\mathbf{B}\|\begin{bmatrix}\mathrm{u}_0\\ \mathrm{u}_1\\ \vdots\\ \mathrm{u}_{n-1}\end{bmatrix} \\ & + \begin{bmatrix}\|\mathbf{A}^{n-1}\| & \|\mathbf{A}^{n-2}\| & \ldots & \mathbf{I}\end{bmatrix}\begin{bmatrix}\mathrm{u}_0\\ \mathrm{u}_1\\ \vdots\\ \mathrm{u}_{n-1}\end{bmatrix}\|\frac{\partial \mathbf{B}}{\partial P_m}\| \end{aligned} \tag{5.3}$$

Property (1) also gives rise to the inequality of $\|\mathbf{A}^n\| \leq \|\mathbf{A}\|^n$. If the system is

stable, the eigenvalues of $\mathbf{A}$ are smaller than one, $|\lambda(\mathbf{A})| < 1$, therefore, when n tends to ∞, $\|\mathbf{A}\|^n$ tends to 0 and so is $\|\mathbf{A}^n\|$. Suppose $y = nX^{n-1}$, where X is the Frobenius norm of $\mathbf{A}$. As $|\lambda(\mathbf{A})| < 1$, $X < 1$ and this can also be expressed in a fraction as $\frac{1}{C}$, where $C > 1$. This function of y can therefore be rearranged to,

$$\begin{aligned} y &= nX^{n-1} \\ &= n\left(\frac{1}{C}\right)^{n-1} \\ &= \frac{nC}{C^n} \end{aligned}$$

As $n \to \infty$, $C^n > nC$, therefore, $y \to 0$. As a result, with the eigenvalues of $\mathbf{A}$ and its derivatives smaller than one, Equation 5.3 will become small and the sensitivity is stable.

Vehicle Parameters

The values for the vehicle parameters used for this analysis are taken from a simulation performing at 5ms^{-1}. Applying the Saloon parameters in Table 5.1 to matrices $\mathbf{A}$ amd $\mathbf{B}$ of the bicycle model, and taking the Frobenius norm of the matrices:

Table 5.1: Vehicle Parameters (Jaguar Saloon)

Parameter	**Value**
Mass, m	1858 kg
Inertia, J_z	3515 kgm^2
Front wheelbase, a	1.36 m
Rear wheelbase, b	1.55 m
Front cornering stiffness, C_{yF}	-140,000
Rear cornering stiffness, C_{yR}	-120,000
Sampling time, T_s	0.01 s.
longitudinal velocity, V	5 ms^{-1}

$$\mathbf{A} = \begin{bmatrix} 0.7201 & -0.0109 \\ -0.0125 & 0.6886 \end{bmatrix}; \qquad \|\mathbf{A}\| = 0.9965 < 1;$$

$$\mathbf{B} = \begin{bmatrix} 0.1507 \\ 0.5417 \end{bmatrix} \qquad \|\mathbf{B}\| = 0.5623 < 1;$$

The Frobenius norms of matrix $\mathbf{A}$ amd $\mathbf{B}$, both are smaller than one, hence, $n||\mathbf{A}^{n-1}|| < 0$ and $n||\mathbf{B}^{n-1}|| < 0$. Therefore, the parameter sensitivity, Equation 5.3, tends to zero if the Frobenius norms of the parameter derivative, $||\frac{\partial A}{\partial P_m}||$ and

$||\frac{\partial B}{\partial P_m}||$, also tend to zero.

Sensitivity to the Front Cornering Coefficient

With the front cornering coefficient, i.e. $P_m = C_f$, the parameter derivatives are:

$$\frac{\partial \mathbf{A}}{\partial C_{yF}} = \begin{bmatrix} \frac{T_s}{mV} & \frac{aT_s}{mV^2} \\ \\ \frac{aT_s}{J_z} & \frac{a^2T_s}{J_zV} \end{bmatrix}; \qquad \frac{\partial \mathbf{B}}{\partial C_{yF}} = \begin{bmatrix} \frac{-T_s}{mV} \\ \\ \frac{-aT_s}{J_z} \end{bmatrix}.$$

Applying the vehicle parameters in Table 5.1, the Frobenius norms for the derivatives are,

$$\frac{\partial \mathbf{A}}{\partial C_{yF}} = \begin{bmatrix} 0.1076 & 0.0293 \\ 0.3869 & 0.1052 \end{bmatrix} \times 10^{-5}; \qquad \|\frac{\partial \mathbf{A}}{\partial C_{yF}}\| = 4.1617 \times 10^{-6};$$
$$\frac{\partial \mathbf{B}}{\partial C_{yF}} = \begin{bmatrix} -0.1076 \\ -0.3869 \end{bmatrix} \times 10^{-5}; \qquad \|\frac{\partial \mathbf{B}}{\partial C_{yF}}\| = 4.0161 \times 10^{-6}.$$

With this set of vehicle parameters, the norms on the system matrices and derivatives are all below one. State estimations therefore do not grow indefinitely when the front axle cornering stiffness changes.

The sensitivity of states to the rear cornering coefficients, the mass and the moment of inertia share the same analytical method as shown here: taking derivatives with respect to the parameter and then substituting the values to solve for the Frobenius norms. To avoid unnecessary repetitive work, a summary of their Frobenius norms is presented in Table 5.2. For the sensitivity to the geometric ratio, an extra step is required.

Sensitivity to the Geometric ratio

With a fixed vehicle wheelbase, the variation of the location of the cg depends on the ratio between the front and rear wheelbase. This ratio is called the geometric ratio which is defined as $\bar{\bar{a}} = \frac{a}{b}$. With this newly defined parameter, matrices $\mathbf{A}$ and $\mathbf{B}$ can be rewritten as,

$$\mathbf{A} = \begin{bmatrix} 1 + T_s\left(\frac{C_{yF}+C_{yR}}{mV}\right) & T_s\left(\frac{\bar{\bar{a}}bC_{yF}-bC_{yR}}{mV^2} - 1\right) \\ \\ T_s\left(\frac{\bar{\bar{a}}bC_{yF}-bC_{yR}}{J_z}\right) & 1 + T_s\left(\frac{\bar{\bar{a}}^2b^2C_{yF}+b^2C_{yR}}{J_zV}\right) \end{bmatrix} \quad \mathbf{B} = \begin{bmatrix} T_s\left(\frac{-C_{yF}}{mV}\right) \\ \\ T_s\left(\frac{-\bar{\bar{a}}bC_{yF}}{J_z}\right) \end{bmatrix}$$

Since there are no extra components in the two matrices, the Frobenius norms of matrix **A** and **B** are the same as previously determined. The derivatives of these two matrices in terms of the geometric ratio are,

$$\frac{\partial \mathbf{A}}{\partial \bar{\bar{a}}} = \begin{bmatrix} 0 & T_s\left(\frac{bC_{yF}}{mV^2}\right) \\ T_s\left(\frac{bC_{yF}}{J_z}\right) & T_s\left(\frac{2\bar{\bar{a}}b^2C_{yF}}{J_zV}\right) \end{bmatrix}; \qquad \frac{\partial \mathbf{B}}{\partial \bar{\bar{a}}} = \begin{bmatrix} 0 \\ T_s\left(\frac{-bC_{yF}}{J_z}\right) \end{bmatrix}.$$

Taking the Frobenius norm for the two derivative matrices with the pre-defined values in Table 5.1:

$$\frac{\partial \mathbf{A}}{\partial \bar{\bar{a}}} = \begin{bmatrix} 0 & -0.0467 \\ -0.6174 & -0.3358 \end{bmatrix}; \qquad \|\frac{\partial \mathbf{A}}{\partial \bar{\bar{a}}}\| = 0.7043;$$

$$\frac{\partial \mathbf{B}}{\partial \bar{\bar{a}}} = \begin{bmatrix} 0 \\ 0.6174 \end{bmatrix}; \qquad \|\frac{\partial \mathbf{B}}{\partial \bar{\bar{a}}}\| = 0.6174.$$

Summary for Sensitivity

Table 5.2 summarises the parametric sensitivities of the linear 2DoF bicycle model. The values are obtained by applying the parametric constants and velocity in Table 5.1 to the Frobenius norm. It must be noted that this sensitivity analysis is only applicable for vehicles which are travelling on a road with linear force to slip relationship. When this relationship becomes non-linear, the linear 2DoF model no longer holds due to its assumption of the linear relationship between the lateral force and slip.

Table 5.2: Summary for the parametric sensitivity

$\mathbf{V = 5ms^{-1}}$		**Parameter,** $P_m, (\times 10^{-3})$				
	Frobenius norm	C_{yF}	C_{yR}	m	J_z	$\bar{\bar{a}}$
$\|\mathbf{A}\| = 0.9965$	$\|\frac{\partial \mathbf{A}}{\partial P_m}\|$	0.00416	0.00475	0.151	0.0887	703
$\|\mathbf{B}\| = 0.5623$	$\|\frac{\partial \mathbf{B}}{\partial P_m}\|$	0.00402	0	0.0811	0.154	617
$\mathbf{V = 10ms^{-1}}$		**Parameter,** $P_m, (\times 10^{-3})$				
	Frobenius norm	C_{yF}	C_{yR}	m	J_z	$\bar{\bar{a}}$
$\|\mathbf{A}\| = 1.205$	$\|\frac{\partial \mathbf{A}}{\partial P_m}\|$	0.00394	0.00450	0.0753	0.0444	640
$\|\mathbf{B}\| = 0.547$	$\|\frac{\partial \mathbf{B}}{\partial P_m}\|$	0.00391	0	0.0406	0.154	617

From Table 5.2, for the $5ms^{-1}$, all twelve parametric Frobenius norms are smaller

than 1. This implies that state estimations are stable to the parameter variation and will not grow indefinitely. Amongst the parameters, the geometric ratio has Frobenius norms that are closest to 1, which means state estimations are most sensitive to the change in geometric ratio of the vehicle model. With the same loaded mass, different mass distribution on the vehicle causes the location of the cg, and therefore the geometric ratio, to vary. This change has an effect on the characteristic behaviour of a vehicle (i.e. under-steer, neutral steer or over-steer) and will cause different vehicle dynamic behaviour.

Suppose the position of the cg stays unchanged at the 5ms^{-1}, state estimations are sensitive to the loaded mass and moment of inertia. From Table 5.2 we can see that the process matrix $\mathbf{A}$ is more sensitive to the change in loaded mass and the input matrix $\mathbf{B}$ is more sensitive to the change in the moment of inertia. In other words, previous estimated states and steering inputs are greatly influenced by the vehicle mass and the moment of inertia respectively.

The two cornering coefficients in the 5ms^{-1} case are relatively low in their Frobenius norms, which suggests that the state estimations are relatively less sensitive to the variation of C_{yF} and C_{yR} than the other parameters. Of the two measurements of cornering stiffness, the previous states are more influenced by the rear while the input is more influenced by the front. Table 5.2 also shows that the input is not sensitive to C_{yR} at all with a value of zero for $\frac{\partial \mathbf{B}}{\partial C_{yR}}$. Comparatively, C_{yF} has shown its effects on both process and input matrices, suggesting that it is more sensitive to the overall state estimations when compared to C_{yR}. The relatively greater sensitivity of the variation of C_{yF} can also be observed in Figures 5.3 to 5.5, in which a larger proportion of error is situated in the western region.

Referring back to Table 5.2, for a higher velocity, 10ms^{-1}, the ten parametric Frobenius norms decrease. However, the Frobenius norm of the process matrix has increased above 1. This suggests that state estimations are no longer bounded and more likely to become unstable.

5.2.3 Variation on Different Manoeuvre

Previous simulations and theoretical studies have shown that the state estimations are relatively insensitive to the parameters in the 2DoF bicycle model, i.e. bounded and will not grow indefinitely. However this is only the case when the vehicle is operating in low speed manoeuvres such as the *DoubleOval_20kph*. It is understood from Chapter 3 that lateral tyre forces behave linearly with the slip angle at low velocity, but at higher speeds their relationship becomes non-linear. Based on the parameter variation in Section 5.2.1, this section looks at the accuracy of state estimations in

a high speed manoeuvre at 50kph. The starting value for the parameters are as in Table 5.1 and the cornering coefficients are predicted from the average gradient of the lateral force-slip curve.

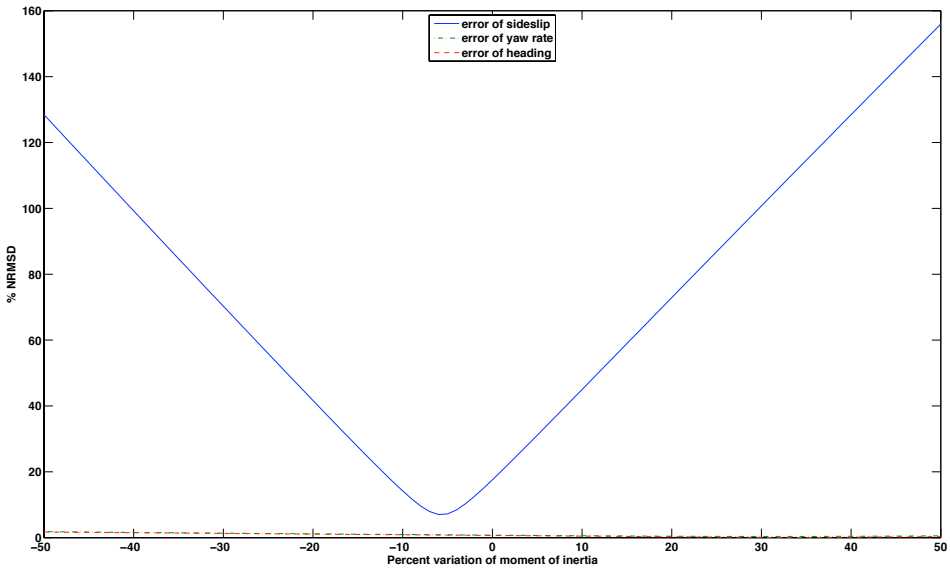

Figure 5.6: %NRMSD of state estimations with variation of mass at 50kph

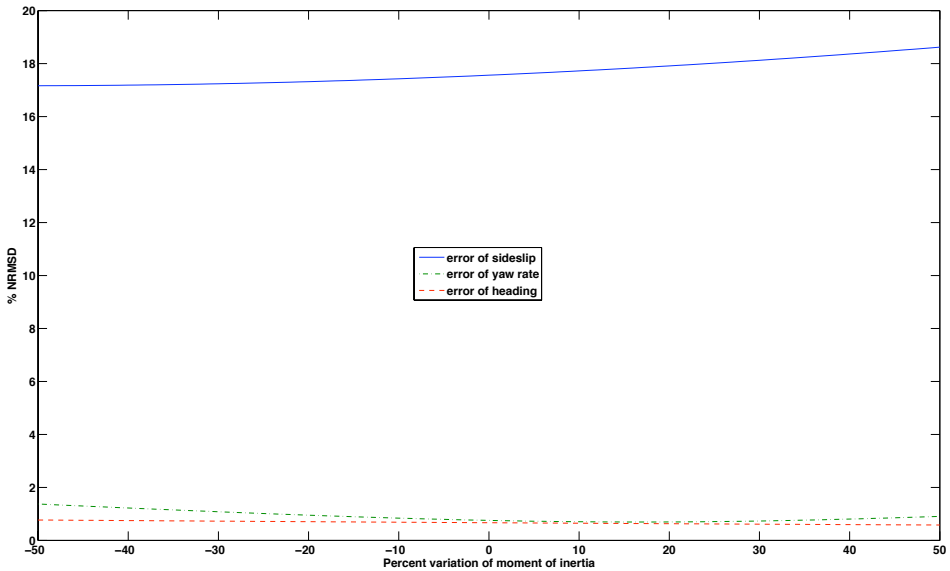

Figure 5.7: %NRMSD of state estimations with variation of moment of inertia at 50kph

Figures 5.6 to 5.9 show the %NRMSD of the state estimations with parameter variations under a 50kph manoeuvre. Comparing the %NRMSD measured from the variation of mass at 50kph (Figure 5.6) with that obtained from the 20kph simulation

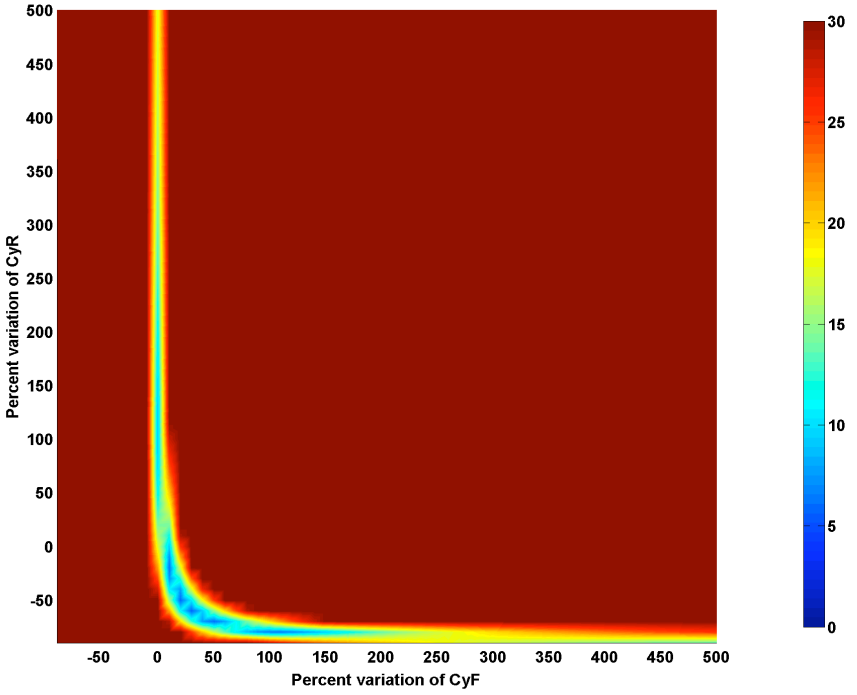

Figure 5.8: %NRMSD of sideslip angle estimation with variation of cornering coefficients at 50kph

(Figure 5.1) the general shape of the plot has not changed – the sideslip %NRMSD remains V-shaped; but the %NRMSD from the 50kph has increased by at least 20 times. At this speed, the tyre force-slip relationship has entered the non-linear region. Cornering coefficients determined previously from the 20kph simulation are no longer applicable. Therefore, %NRMSD in Figure 5.6 is never as small as that in Figure 5.1, especially for the sideslip %NRMSD which has a minimum of about 10%. In addition, Figure 5.6 also demonstrates the sensitivity of sideslip estimation to the mass. This strong influence of the vehicle mass can also be explained by using the first component of the partial derivatives $\frac{\partial \mathbf{A}}{\partial m}$ in previous theoretical analysis, Section 5.2.2. Although the theoretical analysis in Section 5.2.2 is based on low velocity, 20kph, the partial derivative formulations are still applicable for the 50kph case as the same 2DoF model is used in the system with the same parametric values.

Similarly, in Figure 5.7, the %NRMSD due to the variation of moment of inertia is a lot higher than that from previous 20kph case. Moreover, the position of the three error curves have also swapped places between the 20kph and 50kph manoeuvre. While the sideslip estimation in the low speed case has the least error, it has the most in the high speed case. This is because the cornering coefficients are wrong and fail to predict the tyre force in the non-linear region.

For the variation of cornering coefficients, the %NRMSD plots, Figures 5.8 to

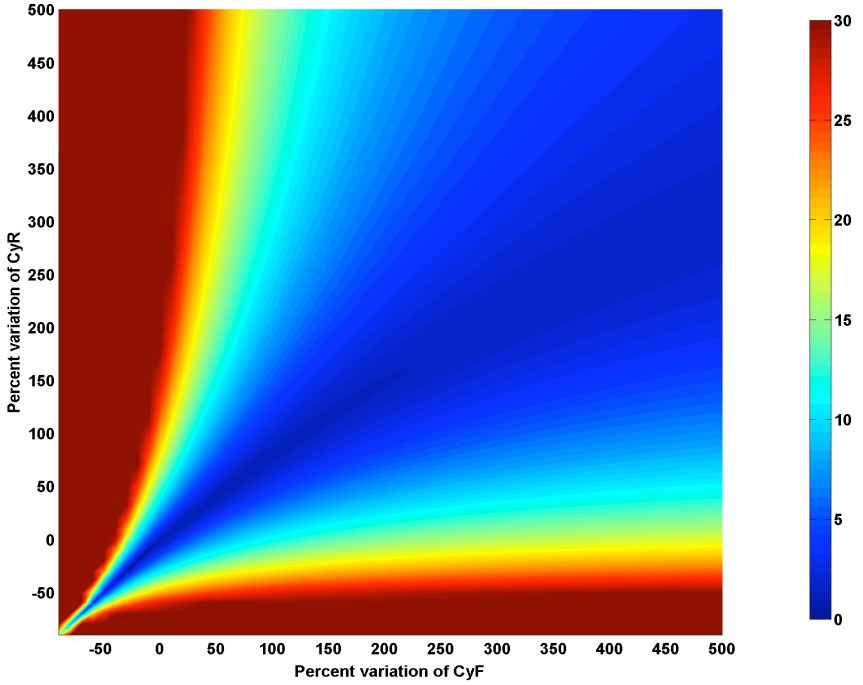

Figure 5.9: %NRMSD of yaw rate estimation with variation of cornering coefficients at 50kph

5.9, are very different to the previous low speed case. This is especially true for the sideslip estimation, which has a very small region with error less than 20%. The rest of the region is above 30% error. For the yaw rate and heading estimations, the accuracy has also decreased with a higher velocity. The above 30% error zone has been extended both west and south of the figure, but the least error remains in a region where the two cornering coefficients vary by the same amount. This pattern is due to the derivation of yaw rate in the original 2DoF model, in which it is a measure of the difference between the two lateral forces at the front and rear (i.e. $J_z\ddot{\psi} = aC_{yF}\alpha_F - bC_{yR}\alpha_R$). When the front and rear axle cornering coefficients vary, the yaw rate estimation will have error from both coefficients; however, since the coefficients are subtracting one another, the error will be smaller and growing at a slower rate. For a particular proportion of variation, the error maintains at a certain level, see the colour band in Figure 5.9. Notice that the colour band is not linear as C_{yF} and C_{yR} do not have the same value, nor the same slip, nor a 1:1 geometric ratio.

It has been concluded in the earlier section that cornering coefficients are best set larger than smaller as state estimates are relatively insensitive to them. However, for a higher speed manoeuvre, tyre forces no longer depend linearly with the lateral slip. State estimations therefore becomes sensitive to parameter variations. In

terms of the sensitivity analysis, the Frobenius norm of matrix **A** for the high speed manoeuvre is larger than one. State estimations then can grow indefinitely with time.

5.2.4 Input Related Errors

Referring back to the 2DoF vehicle model with the assumption of accurate initial conditions, the only input errors of the 2DoF bicycle model come from the longitudinal velocity, V, and the steering angle, δ_F. These two inputs are crucial as they are used for determining the slip and vehicle motion. Unlike the parameters, which are pre-set as constants, the inputs are measured continually from sensors. It is a common practice that longitudinal velocity is measured from the WSS of the ABS while the steering angle is measured from a position sensor.

Using the virtual sensors (including virtual CAN-bus) described in Appendix B.1, ten manoeuvres are simulated using two different tracks (i.e. *DoubleOval* and *LaneChangeISO*) and five different speeds (i.e. 15kph, 25kph, 35kph, 45kph and 55kph). The parameters for the 2DoF model are taken from Appendix A and the cornering coefficients are pre-determined from each manoeuvre before the analysis.

Table 5.3: %NRMSD of state estimations of 2DoF bicycle model

	sideslip, β		**yaw rate,** $\dot{\psi}$	
Manoeuvre	without noise	with noise	without noise	with noise
DoubleOval_15kph	0.0725	2.4016	0.1601	2.4212
DoubleOval_25kph	0.1585	2.5198	0.2151	2.3939
DoubleOval_35kph	0.7168	2.7793	0.2438	2.3401
DoubleOval_45kph	5.0745	4.2327	0.2335	2.3016
DoubleOval_55kph	6.8651	4.8325	2.0390	2.8444
LaneChangeISO_15kph	0.1103	7.1125	0.0997	6.8090
LaneChangeISO_25kph	0.3190	8.5723	0.1290	8.0845
LaneChangeISO_35kph	0.7219	8.8540	0.2200	8.9877
LaneChangeISO_45kph	1.6872	8.8018	0.3901	9.2137
LaneChangeISO_55kph	6.9634	9.4187	0.4318	9.5051

In the analysis 10 simulations are run per manoeuvre. The average %NRMSD of the two state estimations for each manoeuvre is presented in Table 5.3. For the *DoubleOval* manoeuvres, in general state estimations become less accurate when the velocity of the vehicle increases, especially when the velocity exceeds 35kph. Although the 2DoF bicycle model predetermines the cornering coefficients linearly before the simulations, due to the non-linear tyre characteristics at high speed, the linear cornering coefficients are no longer applicable. This results in an increase in error at speeds above 35kph. Table 5.3 also shows that velocity is not as sensitive to

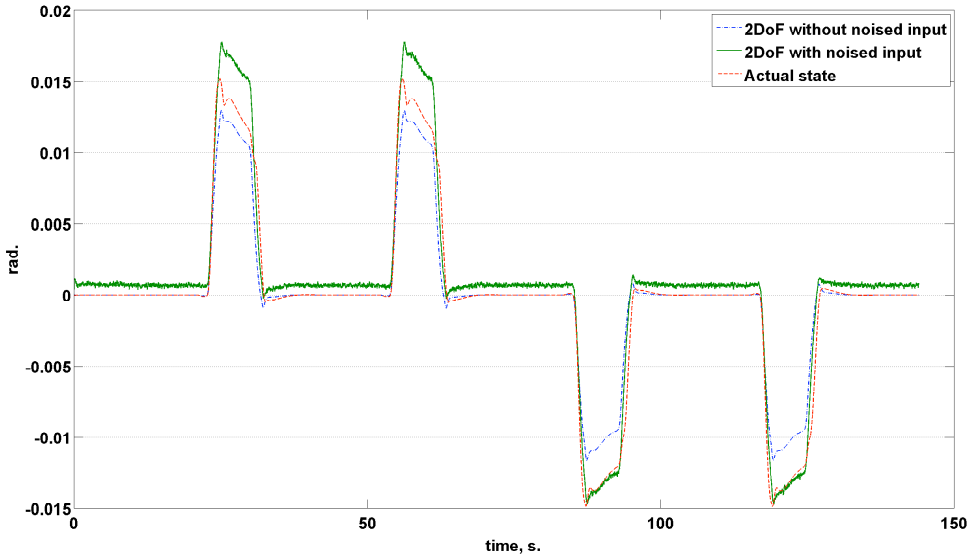

Figure 5.10: Sideslip angle estimation with *DoubleOval_45kph* manoeuvre

the yaw rate as to the sideslip estimations, which stays between 2 and 3%NRMSD and is independent of the change in velocity. Furthermore, it is interesting to see that the %NRMSD of sideslip estimation is lower for 45kph and 55kph on the *DoubleOval* manouvre. Referring to the sideslip estimations for *DoubleOval_45kph*, Figure 5.10, it is shown that there are more errors in the estimation with noisy inputs. However, the overall error is reduced when the vehicle enters the third and fourth corners, in which the bias of the steering unexpectedly compensates for the shortcomings of the noise.

As described in Section 4.2.1, the lateral velocities of the *LaneChangeISO* manoeuvres are smaller than those in the *DoubleOval* manoeuvres. The tyre characteristics therefore remain in the linear region and cornering coefficients determined from the linear relationship remain applicable to the model. However, *LaneChangeISO* manoeuvres have more vigourous dynamics with sharper turns. This causes the vehicle to roll and errors are introduced into the estimations via lateral acceleration. In other words, F_y is no longer equal to $(\ddot{y}_v + \dot{x}_v\dot{\psi})$, but with an additional gravitational term, $g\sin\phi$. The roll motion of the vehicle also causes the loads on the left and right tyres to redistribute (i.e. affecting the values for the cornering coefficients). But since the 2DoF model is based on the single-track bicycle approach, left and right load reallocation will have less/no effect on the modelling.

Figure 5.11 shows the actual roll angles of the *LaneChangeISO* manoeuvres. As discussed, due to the vigourous manoeuvre, the vehicle rolls during a corner. When the velocity of a vehicle increases, more lateral force is required to hold the vehicle

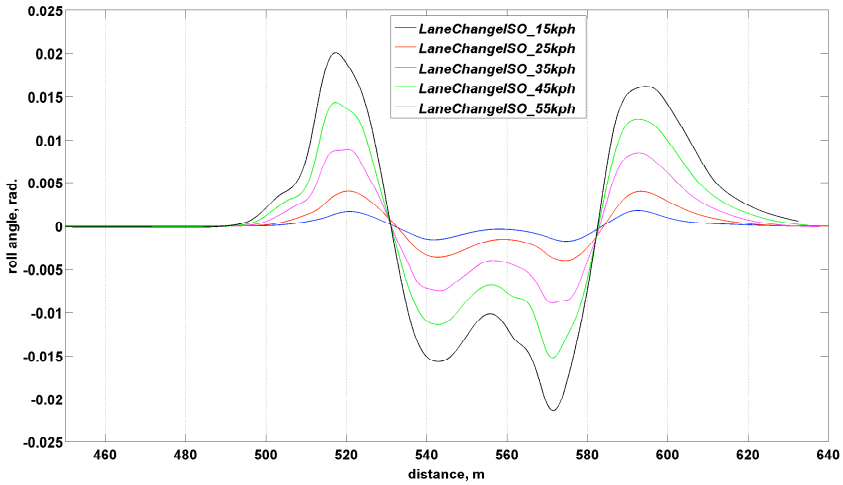

Figure 5.11: sideslip angle estimation with *DoubleOval_45kph* manoeuvre

on track, resulting in an increase of roll angle. Since the 2DoF model is without roll compensation, the presence of roll angle induces an error to the estimations. As a result, state estimations are expected to be less accurate at a higher velocity.

5.2.5 Summary for 2DoF Model Limitations and Robustness

As clarified at the beginning of this section, two types of errors are involved in a vehicle model which will affect the accuracy of the state estimates: 1) parameter related errors, and 2) input related errors. It is shown from the simulation and theoretical results that state estimations are sensitive to the cornering coefficients and also the unmodelled dynamics, such as the rolling and pitching angles. For the noisy inputs, it is important to reduce the bias in the steering as it is directly related to the determination of slip angle (i.e. $\alpha = \delta - \beta$).

It must be noted that the main concern for this project is to estimate the vehicle dynamic states. Parameter estimations, therefore, are not investigated further. It is assumed that parameters are pre-determined for the vehicle before it is launched onto the market.

5.3 Integrated Kalman Filter Design

As concluded in the last section, state estimations are dependent upon the parameters and inputs accuracies. Focusing on the inputs for the linear 2DoF bicycle model,

this section looks at the benefit for state estimations when the MKF is combined with the KKF.

5.3.1 Model-based Kalman Filter

As discussed in Chapter 2, a typical MKF is based on the 2DoF bicycle model with reference measurements from the GPS tracking angle, ν_{gps}, and the INS yaw rate gyro, $\dot{\psi}_{ins}$. Since the yaw rate gyro is contaminated with noise and bias, the MKF is modified to include the yaw rate bias, b_r, in the state vector [Anderson and Bevly 2005].

Based on the MKF of Anderson and Bevly [2005], it can be further modified to include the trigonometric function of angles in the correction matrix. As discussed in Chapter 4, the use of trigonometric function is essential as angles (i.e. GPS tracking angle, INS heading angle, and estimated sideslip angle) being compared must be bounded between positive and negative π. This adds non-linearity into the correction stage of the KF and an EKF must be used for the estimation. This modified filter, $MEKF_{2a}$, therefore has the following state space equations,

***MEKF*$_{2a}$:**

Prediction stage:

$$\begin{bmatrix} \dot{\beta} \\ \ddot{\psi} \\ \dot{\psi} \\ \dot{b}_r \end{bmatrix} = \begin{bmatrix} \frac{C_{yF}+C_{yR}}{mV} & \frac{aC_{yF}-bC_{yR}}{mV^2}-1 & 0 & 0 \\ \frac{aC_{yF}-bC_{yR}}{J_z} & \frac{a^2C_{yF}+b^2C_{yR}}{J_zV} & 0 & 0 \\ 0 & 1 & 0 & 0 \\ 0 & 0 & 0 & 0 \end{bmatrix} \begin{bmatrix} \hat{\beta} \\ \hat{\dot{\psi}} \\ \hat{\psi} \\ \hat{b}_r \end{bmatrix} + \begin{bmatrix} \frac{-C_{yF}}{mV} \\ \frac{-aC_{yF}}{J_z} \\ 0 \\ 0 \end{bmatrix} \delta_F \tag{5.4}$$

Correction stage:

$$\begin{cases} r_m = \hat{\dot{\psi}} + \hat{b_r} \\ \cos\nu = \cos(\hat{\psi}+\hat{\beta}) \\ \sin\nu = \sin(\hat{\psi}+\hat{\beta}) \end{cases} \tag{5.5}$$

With the $MEKF_{2a}$, not only the sideslip and the yaw rate of the vehicle can be estimated, but also the heading angle, ψ, and gyro bias, b_r.

However, as discussed in Section 5.2.4, state estimations are sensitive to the steering input. As shown in Figure 5.10, sideslip estimation is estimated incorrectly with an offset when a bias is present in the steering of the 2DoF model. Hence, it is essential to remove the steer bias, b_δ, in order to give an accurate state estimation. To acheive this, b_δ is added into the state vector of $MEKF_{2a}$. This new KF, $MEKF_{2b}$,

has a prediction stage with state space representation of,

***MEKF*$_{2b}$:**

Prediction stage:

$$\begin{bmatrix} \dot{\beta} \\ \ddot{\psi} \\ \dot{\psi} \\ \dot{b}_r \\ \dot{b}_\delta \end{bmatrix} = \begin{bmatrix} \frac{C_{yF}+C_{yR}}{mV} & \frac{aC_{yF}-bC_{yR}}{mV^2}-1 & 0 & 0 & \frac{-C_{yF}}{mV} \\ \frac{aC_{yF}-bC_{yR}}{J_z} & \frac{a^2C_{yF}+b^2C_{yR}}{J_zV} & 0 & 0 & \frac{-aC_{yF}}{J_z} \\ 0 & 1 & 0 & 0 & 0 \\ 0 & 0 & 0 & 0 & 0 \\ 0 & 0 & 0 & 0 & 0 \end{bmatrix} \begin{bmatrix} \hat{\beta} \\ \hat{\ddot{\psi}} \\ \hat{\dot{\psi}} \\ \hat{b}_r \\ \hat{b}_\delta \end{bmatrix} + \begin{bmatrix} \frac{-C_{yF}}{mV} \\ \frac{-aC_{yF}}{J_z} \\ 0 \\ 0 \\ 0 \end{bmatrix} \delta_F \tag{5.6}$$

With the INS and GPS sensor noise defined in Appendix B, the steering input for the vehicle is taken from the driver's steering wheel and the speed, V, is taken from the wheel rotational speed. Simulating five speeds using the *DoubleOval* track, the steer bias and its %NRMSD to the actual bias is presented in Figure 5.12.

	DoubleOval				
	15kph	25kph	35kph	45kph	55kph
%NRMSD of b_δ	0.1950	0.1478	0.0990	0.0868	0.5363

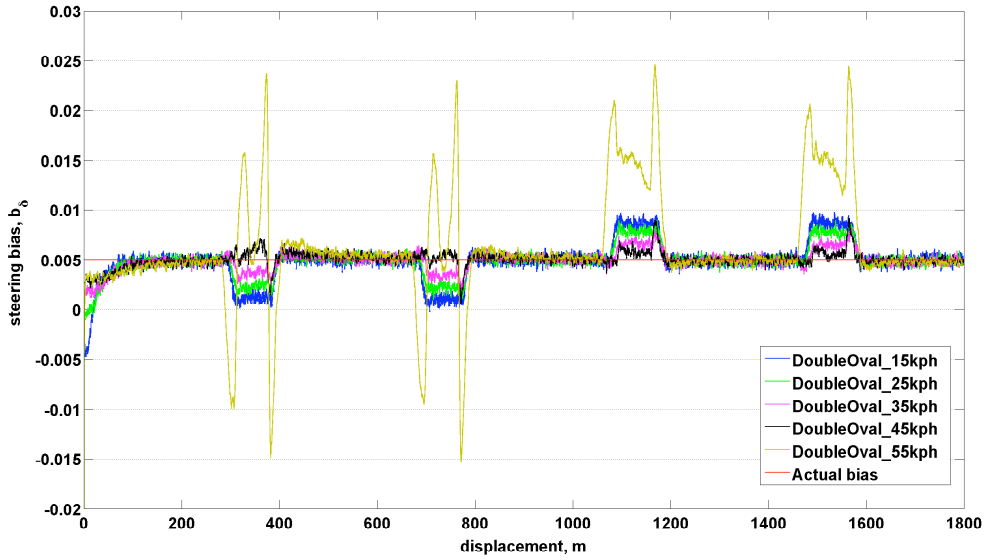

Figure 5.12: Steering bias estimation of the *MEKF*$_{2b}$ in *DoubleOval* manoeuvres

For the steer bias estimation, Figure 5.12 shows the %NRMSD determined from the *MEKF*$_{2b}$ on the *DoubleOval* manoeuvres. As shown, the steer bias is estimated accurately regardless of the vehicle velocities when it is travelling on a straight road.

However, when cornering, the accuracy of bias estimations vary with the velocity of the vehicle. For the *DoubleOval* manoeuvre, linear axle cornering coefficients are valid under a speed of 45kph; for speeds that are 45kph or above, non-linear characteristics of tyres occur and predetermined linear stiffness are no longer applicable to the linear 2DoF model.

Assuming precise reference measurements, accuracy of steer bias is dependent on the accuracy of the vehicle model. Therefore, inaccurate axle cornering stiffness causes error in the steer bias estimations, hence, the large %NRMSD of steer bias at 55kph. However, at 45kph, an unexpectedly accurate estimation has occurred despite the inappropriate representation of the linear cornering coefficients at this speed. This result is due to coincidence, in which the errors of the parameters have been compensated by those from the inputs, e.g. the offset of the longitudinal velocity measured from the WSS (refer to Figure 5.16 in Section 5.3.2).

For speeds between 15kph to 35kph in the *DoubleOval* simulation, the errors are related to the longitudinal speed and the cornering stiffness. As discussed, when the reference measurements are accurate, the error of the steer bias, $\delta(b_\delta)$, depends on the accuracy of the the 2DoF bicycle model. This can be expressed as a function proportional to the cornering stiffness and geometry, and inversely proportional to the velocity, mass and moment of inertia, as follows,

$$\delta(b_\delta) \propto \frac{\delta(C_y)\delta(a)\delta(b)}{\delta(m)\delta(J_z)\delta(V)} \approx \frac{\delta(C_y)}{\delta(V)}. \tag{5.7}$$

For speeds of 35kph or under, geometric ratio, mass and moment of inertia of a vehicle do not change much during the manoeuvre. Therefore, the error of the steer bias can be simplified as an accuracy ratio of cornering stiffness to velocity, Equation 5.7.

As described earlier in this section, longitudinal velocity for the vehicle model is determined from the WSS by applying Equation 4.12. With this equation, the errors are contributed from the changing of rotational speed in the wheels, $\delta(\omega_R)$, and the wheel radius, $\delta(b_w)$. So the steer bias in Equation 5.7 can be further modified to,

$$\delta(b_\delta) \approx \frac{\delta(C_y)}{\delta(V)} = \frac{\delta(C_y)}{\delta(\omega_R)\delta(b_w)}. \tag{5.8}$$

From Equation 5.8 we can see that the error of the steer bias is dependent on the accuracy ratio of the cornering stiffness to the rotational speed and wheel radius. Between 15kph to 35kph on the *DoubleOval* manoeuvre, lateral force behaves linearly with the slip. The predetermined linear cornering coefficients are therefore

applicable to the 2DoF vehicle model. When vehicle speed increases from 15kph to 35kph, the errors in the rotational speed and wheel radius increases more than those of the cornering coefficients, resulting a reduction in steer bias estimation error.

MEKF with steer bias averging, $MEKF_{2c}$

It has been seen that steer bias can be estimated accurately on a straight but fails to be tracked once the vehicle enters a corner. As steer bias does not change much during a corner, its estimated value on the straight road can be averaged and applied onto the vehicle model when it enters a corner. Therefore, in the $MEKF_{2c}$, a 10 seconds equal weighted moving average window is applied on the steer bias.

Simulating ten manoeuvres with ten runs each with the $MEKF_{2c}$, Table 5.4 shows the average %NRMSD of steer bias, as well as the sideslip and yaw rate estimations from the 2DoF bicycle model and the $MEKF_{2c}$.

Table 5.4: State estimation errors of 2DoF bicycle model and $MEKF_{2c}$

	%NRMSD				%RMSD
	sideslip, $\hat{\beta}$		**yaw rate,** $\hat{\dot{\psi}}$		**steer bias,** b_δ
Manoeuvre	2DoF	$MEKF_{2c}$	2DoF	$MEKF_{2c}$	$MEKF_{2c}$
DoubleOval_15kph	2.4019	0.6062	2.4209	0.8362	0.1011
DoubleOval_25kph	2.5188	0.8253	2.3923	0.5631	0.0872
DoubleOval_35kph	2.7803	1.2146	2.3419	0.3609	0.0636
DoubleOval_45kph	4.2303	3.5376	2.3035	0.2580	0.0649
DoubleOval_55kph	4.8329	10.1776	2.8420	0.7895	0.0843
LaneChangeISO_15kph	7.1101	2.3481	6.8070	2.1964	0.1787
LaneChangeISO_25kph	8.5864	2.3685	8.0985	2.0595	0.1346
LaneChangeISO_35kph	8.8404	1.9844	8.9756	1.6298	0.0966
LaneChangeISO_45kph	8.7876	2.7409	9.1996	1.4280	0.0934
LaneChangeISO_55kph	9.4020	9.8130	9.4889	1.2488	0.0817

Table 5.4 shows that the $MEKF_{2c}$ has achieved a lower %NRMSD of the steer bias than that obtained previously with the $MEKF_{2b}$. This is because steer bias in the $MEKF_{2c}$ is more accurately predicted during corners, see Figure 5.13. When the average window technique is applied during the corners, Figure 5.13 shows a great enhancement for the steer bias prediction. Not only the low speed manoeuvres benefit from this approach, but also the high speed ones. With the steer bias more accurately estimated, the relationship between the speed and the %NRMSD becomes more apparent, Equation 5.8. For linear lateral force to slip relationship, i.e. *DoubleOval_15kph* to *DoubleOval_35kph* and *LaneChangeISO_15kph* to *LaneChangeISO_55kph*, error caused by the cornering coefficients are less than those in the WSS. Hence, a reduction in %NRMSD in the steer bias.

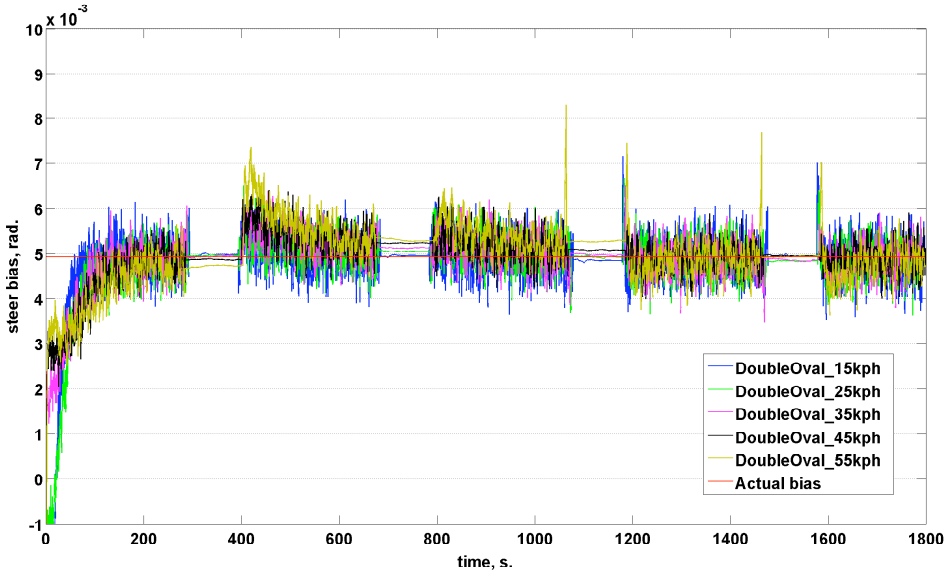

Figure 5.13: Steer bias estimation of the $MEKF_{2c}$ with the *DoubleOval* manoeuvres

Comparing the errors of the estimated states in Table 5.4, it is clear that the $MEKF_{2c}$ provides a more accurate estimation compared to the 2DoF vehicle model. This is because the 2DoF vehicle model is an open loop estimation while the $MEKF_{2c}$ is a closed loop estimation with error feedback. The correction stage in the $MEKF_{2c}$ provides a continuous update of reference measurement to modify and correct the errors accumulated, thereby allowing better state predictions.

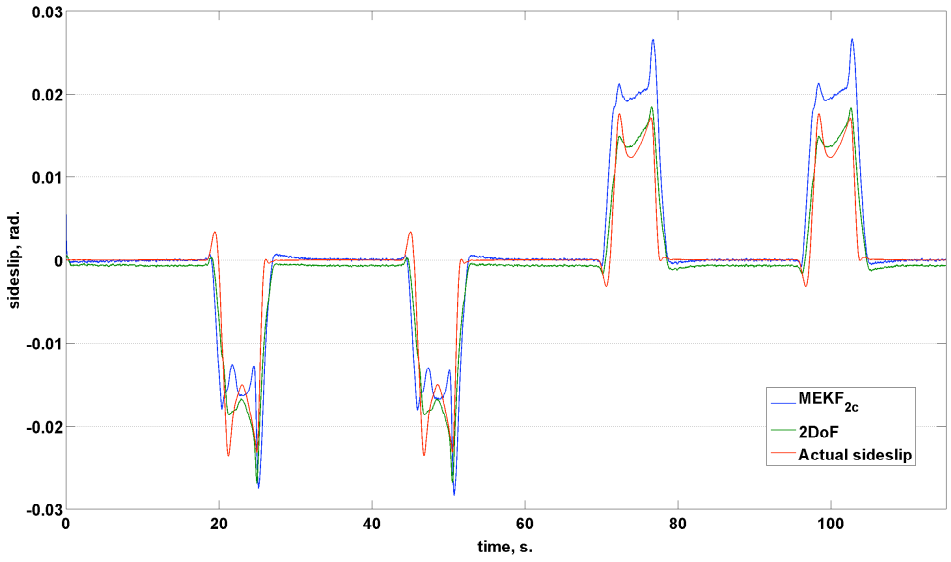

Figure 5.14: Sideslip estimation of the 2DoF bicycle model and $MEKF_{2b}$ (in *DoubleOval_45kph*)

It must also be pointed out that model-based simulations, with parameter and input uncertainties, may result in unexpectedly accurate estimations in certain manoeuvres. Such a result occured previously in the comparison of the linear 2DoF model with and without noise in the *DoubleOval_45kph* (Figure 5.10), and also during the %NRMSD steer bias estimation of the $MEKF_{2b}$ in the *DoubleOval_45kph* (Figure 5.12). Another example of this is the sideslip estimation in the *DoubleOval_55kph* manoeuvre (Figure 5.14), in which the linear 2DoF bicycle model predicts the sideslip state more accurately than the $MEKF_{2b}$. Similarly, this result is due to the coincidence of the error in the parameters compensated by the sideslip offset caused by the steer bias.

Table 5.4 shows that more errors are constituted in the state estimations of the *LaneChangeISO*. As the linear cornering coefficients are applicable in all five manoeuvres of the *LaneChangeISO*, their errors are due to the fast changing dynamics of the vehicle, which introduce extra rolling angles into the vehicle model.

5.3.2 The Design of Integrated Kalman Filter, IKF

It is clear from the last section that accuracy of steer bias prediction is sensitive to the accuracy of the speed measurement, see Equation 5.8. By the use of the proposed IKF, MKFs are combined with KKFs to produce state estimations with fewer errors.

For this study, the IKF design is based on the $MEKF_{2c}$ and the triple KF described in Section 4.3. The reason for this choice is the ability of the triple KF to give good estimations for the longitudinal velocity. Amongst the many versions of the *wssEKF*, the $wssEKF_c$ is used with the inclusion of an additional pitch bias, b_d and measurement Equation 4.18. This triple KF is named $TripleKF_b$ and is able to provide a better longitudinal velocity estimation than the other versions. By combining the $TripleKF_b$ with the $MEKF_{2c}$, the IKF_a is constructed and its structure is shown in Figure 5.15.

Unlike the solo $MEKF_{2c}$, $MEKF_{2c}$ of the IKF_a has an additional reference measurement from the heading estimation of the *yawKKF*. In Figure 5.15 the *yawKKF* provides a good continual heading angle estimation, and the $wssEKF_c$ provides a good update of longitudinal velocity estimations. Together, the two KFs allow a continuous estimation of vehicle velocities in the *velKKF* regardless of the GPS outages. This longitudinal velocity estimation from the *velKKF* and the corrected yaw rate from the *yawKKF* are then fed into the $MEKF_{2c}$ to estimate the vehicle dynamic states, $\begin{bmatrix}\beta & \dot{\psi} & \psi & b_r & b_\delta\end{bmatrix}^T$. Similar to previous $MEKF_{2b}$, the 2DoF model parameters are predetermined and can be found in Appendix A.

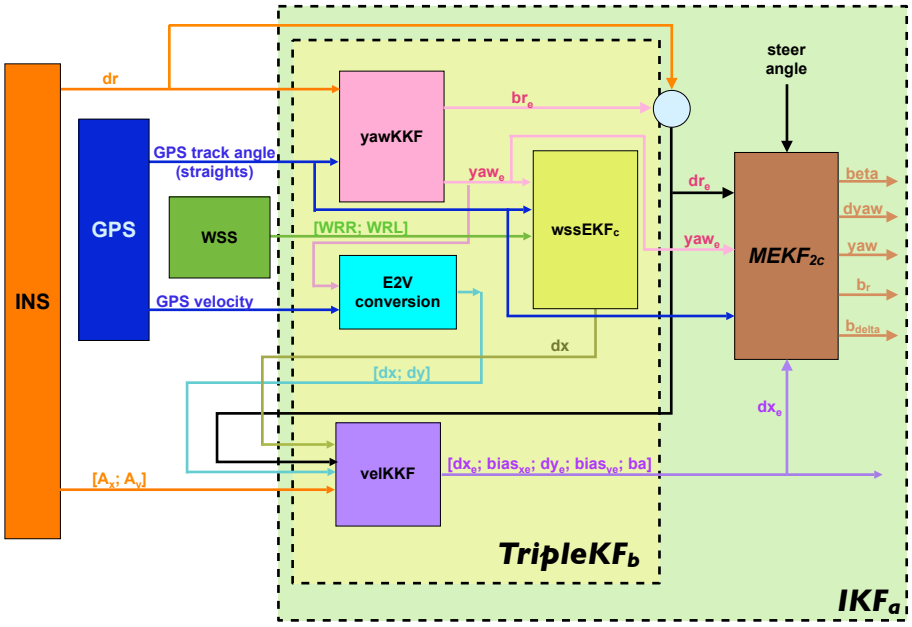

Figure 5.15: The design of IKF_a ($TripleKF_b$+$MEKF_{2c}$)

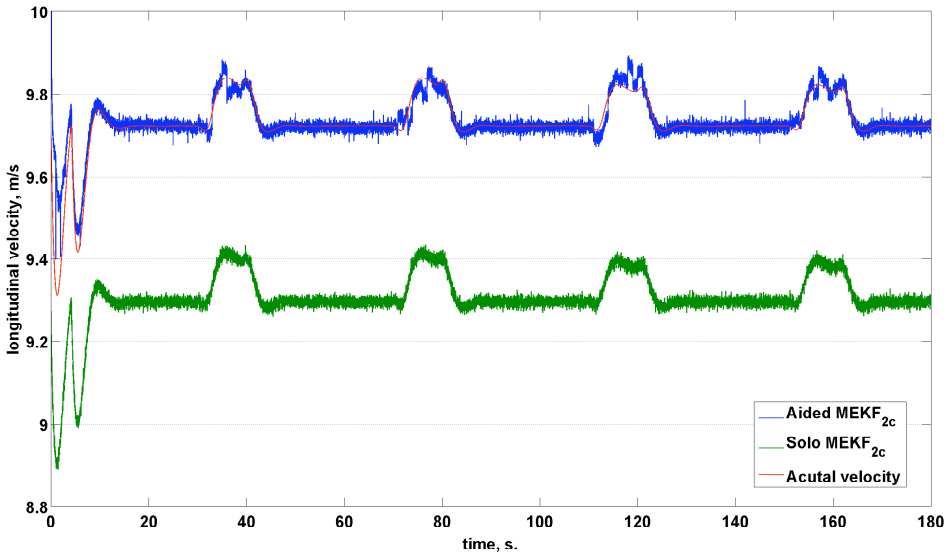

Figure 5.16: Longitudinal velocity inputs to the *Solo* $MEKF_{2c}$ and the *Aided* $MEKF_{2c}$ in the *DoubleOval_35kph* manoeuvre

Figure 5.16 shows the longitudinal velocity inputs of the *Solo* $MEKF_{2c}$ and the $MEKF_{2c}$ in the IKF_a (hereafter calls the *Aided* $MEKF_{2c}$). As a reminder, the *Solo* $MEKF_{2c}$ uses the longitudinal velocity determined from the WSS as inputs, while the *Aided* $MEKF_{2c}$ uses longitudinal velocity estimations from the *velKKF*. Comparing the two velocities, it is clear that the *Aided* $MEKF_{2c}$ has a better longitudinal

velocity input. The benefit of the accurate longitudinal velocity determination has been demonstrated in Table 5.5, in which both sideslip and yaw rate estimations are more accurate when the linear cornering coefficients are applicable to the 2DoF bicycle model (i.e. *DoubleOval_15kph* to *DoubleOval_35kph* and *LaneChangeISO_15kph* to *LaneChangeISO_55kph*), see also Appendix E.1 for detail vehicle dynamics (i.e. lateral velocity, sideslip velocity, yaw rate and heading angle estimations and errors) results.

Table 5.5: State estimation error of $TripleKF_b$, IKF_a and $MEKF_{2c}$, %NRMSD

	sideslip, $\hat{\beta}$			**yaw rate,** $\hat{\dot{\psi}}$		
Manoeuvre	$TripleKF_b$	IKF_a	$MEKF_{2c}$	$TripleKF_b$	IKF_a	$MEKF_{2c}$
DoubleOval_15kph	6.8045	0.4174	0.6062	0.7560	0.4377	0.8362
DoubleOval_25kph	5.2610	0.3232	0.8253	0.4946	0.3555	0.5631
DoubleOval_35kph	6.9596	0.5600	1.2146	0.3849	0.3683	0.3609
DoubleOval_45kph	15.1912	4.0282	3.5376	0.3259	0.3511	0.2580
DoubleOval_55kph	12.7709	12.8077	10.1776	0.2911	0.7194	0.7895
LaneChangeISO_15kph	21.0481	1.8495	2.3481	2.6157	1.8660	2.1964
LaneChangeISO_25kph	17.8751	1.4995	2.3685	2.109	1.4815	2.0595
LaneChangeISO_35kph	17.2353	1.4223	1.9844	1.7858	1.2260	1.6298
LaneChangeISO_45kph	24.3931	2.2926	2.7409	1.5617	1.0856	1.4280
LaneChangeISO_55kph	69.7912	9.2321	9.8130	1.4422	0.99748	1.2488

For manoeuvres which do not have a linear lateral tyre force to slip behaviour, Table 5.5 shows that the state estimations are more accurate with the $MEKF_{2c}$ alone. Similar to previous cases, this result is purely coincidence, due to the compensation between parametric errors and state estimation errors.

For the steer bias prediction, Figure 5.17 shows that the IKF_a is able to converge onto the steer bias quickly for both tracks. Comparing the estimated steer bias in the *DoubleOval* track with that of the $MEKF_{2c}$, Figure 5.13, one can see that the IKF_a converges faster and more accurately to the steer bias at the start and after a corner. This improvement of estimation is because of the more accurate prediction in longitudinal velocity and heading angle. Examining the %NRMSD of the steer bias estimation, (Table 5.4 and Figure 5.17), reveals that IKF_a is able to produce better steer bias estimations for both tracks.

Referring to the yaw rate estimation in the $TripleKF_b$ and the $MEKF_{2c}$, Table 5.5, we can see that the $TripleKF_b$ is able to provide an accurate heading and longitudinal velocity while the $MEKF_{2c}$ is good at estimating fast dynamic change of the vehicle (i.e. relatively low %NRMSD for the *LaneChangeISO* manoeuvres). By utilising these advantages from the two approaches, the IKF_a gives the most accurate state estimations when the linear 2DoF bicycle model is valid.

	DoubleOval				
	15kph	25kph	35kph	45kph	55kph
%NRMSD of b_δ	0.0761	0.0607	0.0495	0.0509	0.0685

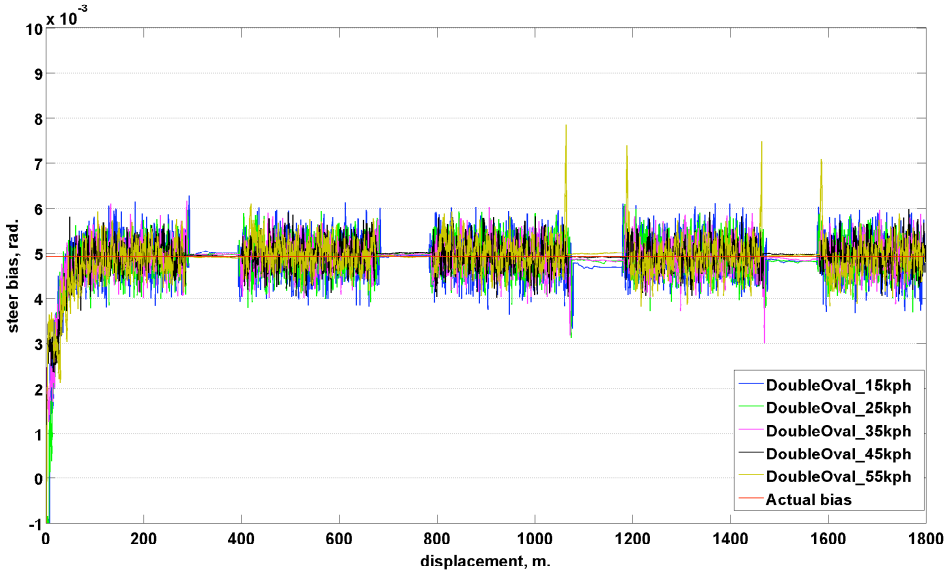

(a) *DoubleOval* manoeuvres

	LaneChangeISO				
	15kph	25kph	35kph	45kph	55kph
%NRMSD of b_δ	0.1312	0.0833	0.0763	0.0731	0.0726

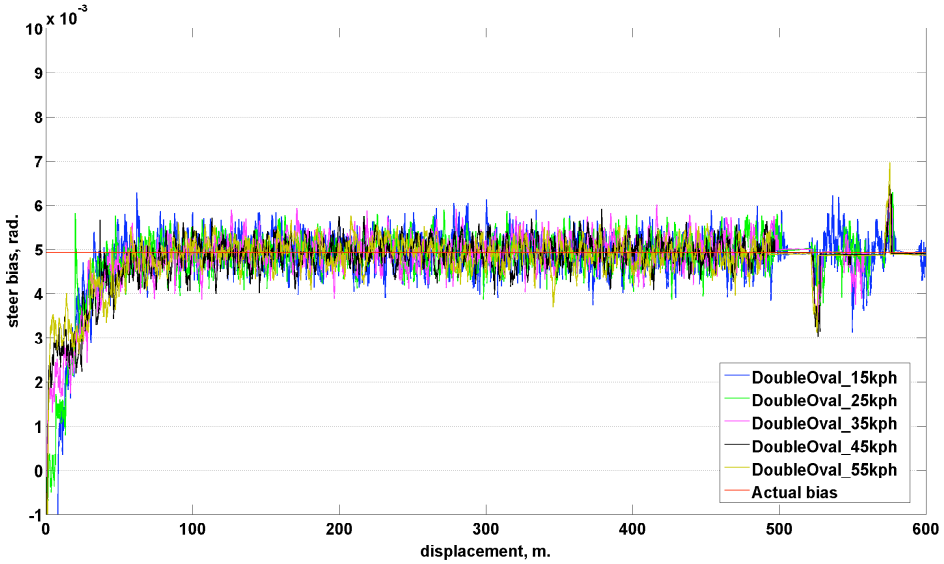

(b) *LaneChangeISO* manoeuvres

Figure 5.17: Steering bias estimation of the IKF_a

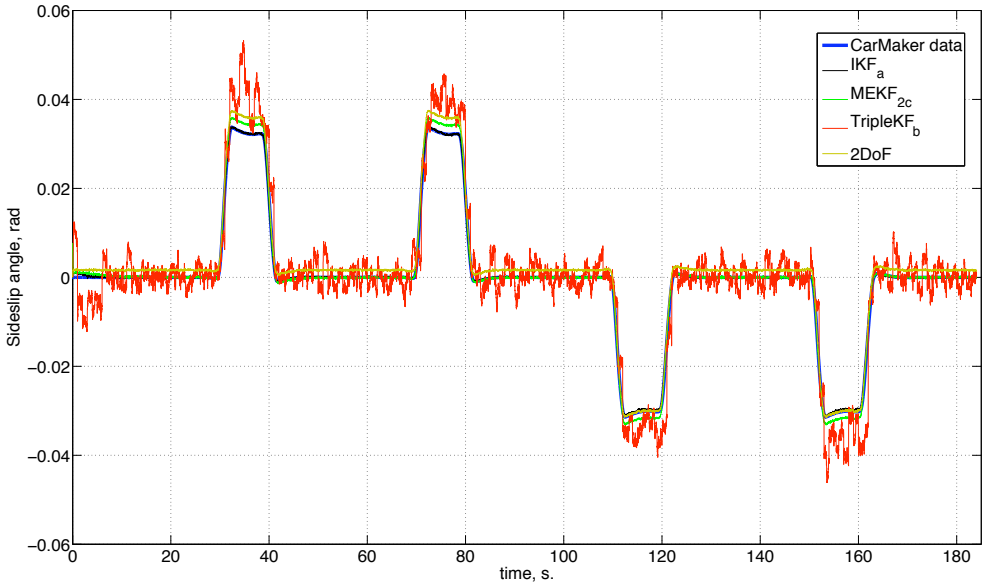

(a) Sideslip angle estimations

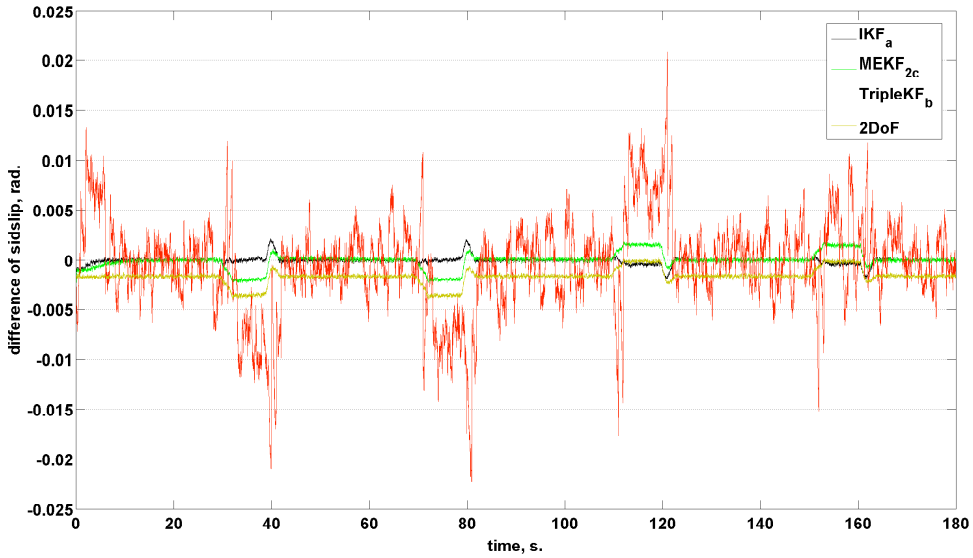

(b) Error in sideslip angle estimations

Figure 5.18: State estimations and errors of sideslip angle of *DoubleOval_35kph* manoeuvre

Figures 5.18 to 5.21 show the errors of the sideslip and heading estimations of different estimation approaches, namely the IKF_a, the $MEKF_{2c}$, the $TripleKF_b$ and the original linear 2DoF bicycle model. Results for two manoeuvres with valid linear 2DoF vehicle model, i.e. *DoubleOval_35kph* and *LaneChangeISO_35kph*, are presented in this section and the rest are attached in Appendix E.1.

Figures 5.18 and 5.19 show the state estimation errors from when the vehicle is travelling on the *DoubleOval_35kph* manoeuvre. For the sideslip estimation, Figure

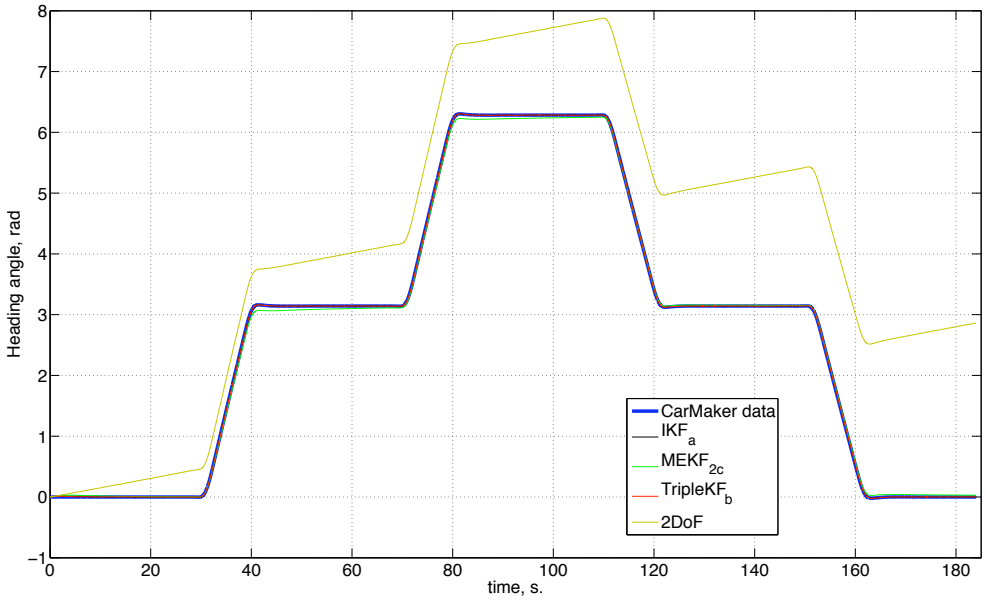

(a) Heading angle estimations

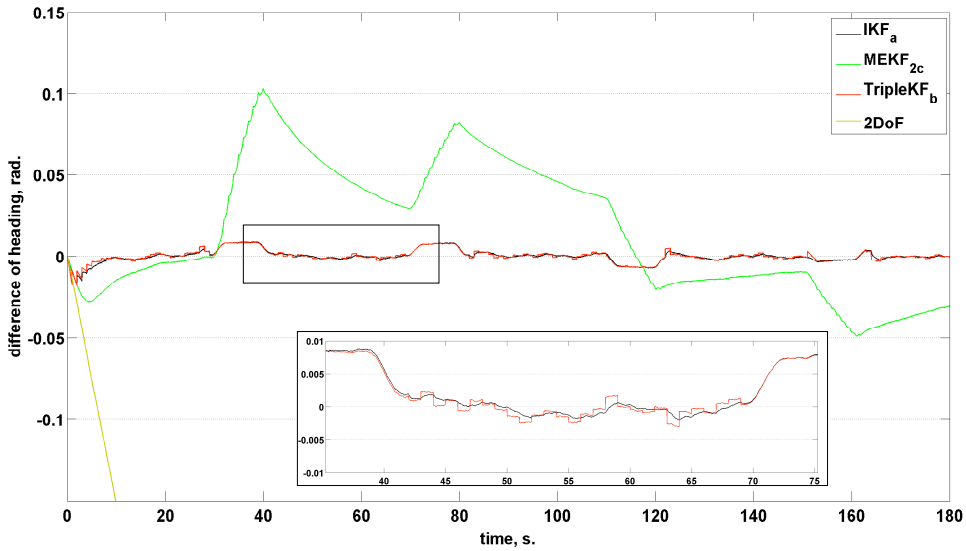

(b) Error in heading angle estimations

Figure 5.19: State estimations and errors of heading angle of *DoubleOval_35kph* manoeuvre

5.18 reveals that the $TripleKF_b$ provides a very noisy and possibly unstable estimation, which is due to the inaccuracy of lateral velocity estimation in the *velKKF*. On the other hand, approaches based on the vehicle model are able to give more stable estimations. However, without any error feedback and bias estimation algorithm, the 2DoF vehicle model estimates the sideslip with an offset. When MKF is introduced into the 2DoF model, $MEKF_{2c}$, the offset is compensated but during corners, sideslip errors increase. Notice that the sideslip estimation of the $MEKF_{2c}$

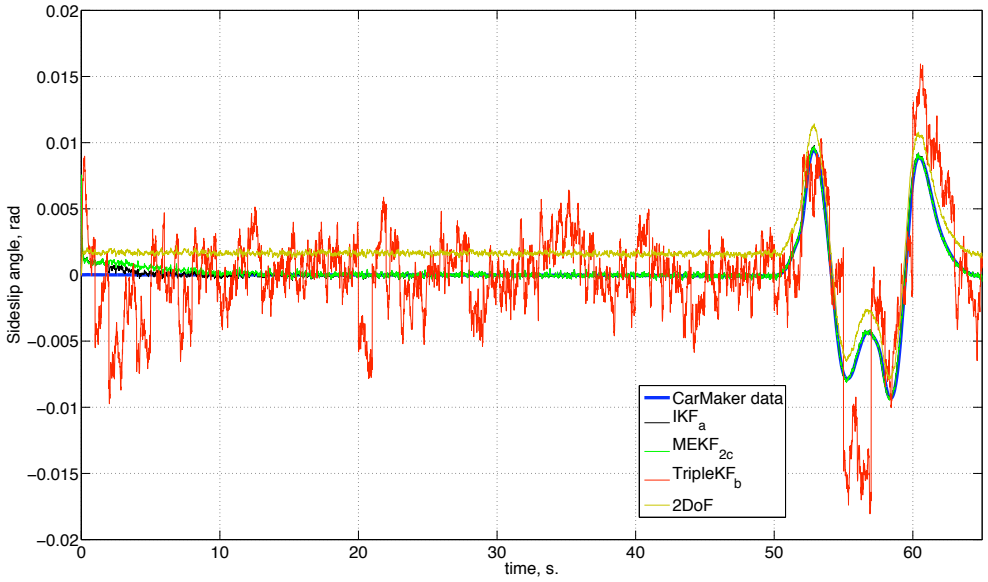

(a) Sideslip angle estimations

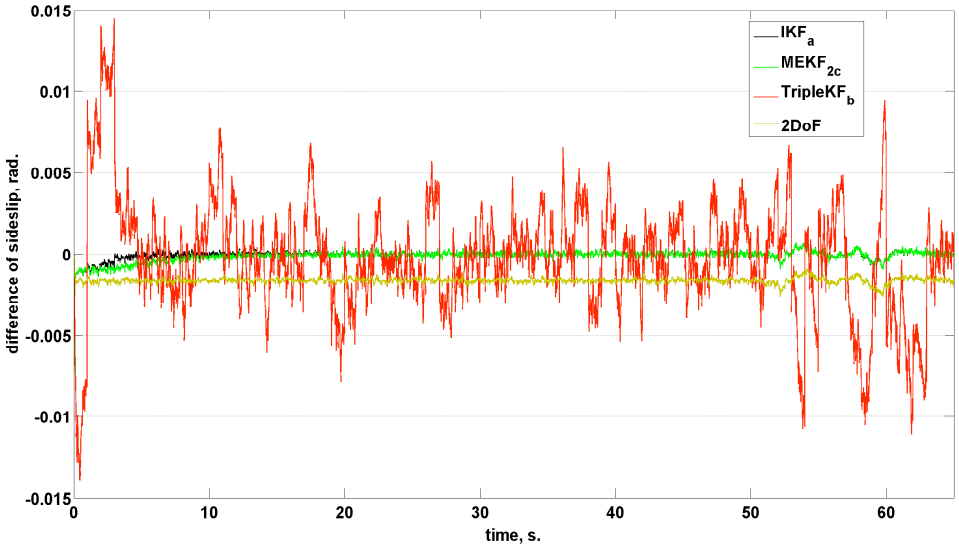

(b) Error in sideslip angle estimations

Figure 5.20: State estimations and errors of sideslip angle of *LaneChange_35kph* manoeuvre

and the 2DoF model are almost the same but with an offset. For the third and fourth corners, where the vehicle is turning right, the offset error of the 2DoF model has become beneficial to the sideslip estimation. This 2DoF result is only good for this particular simulation and cannot be used as a general explanation for all vehicle systems. The most accurate sideslip estimation produced by combining the $TripleKF_b$ with the $MEKF_{2c}$, i.e. IKF_a. Whether the vehicle is travelling straight or cornering, the sideslip is predicted accurately with small overshoots just before

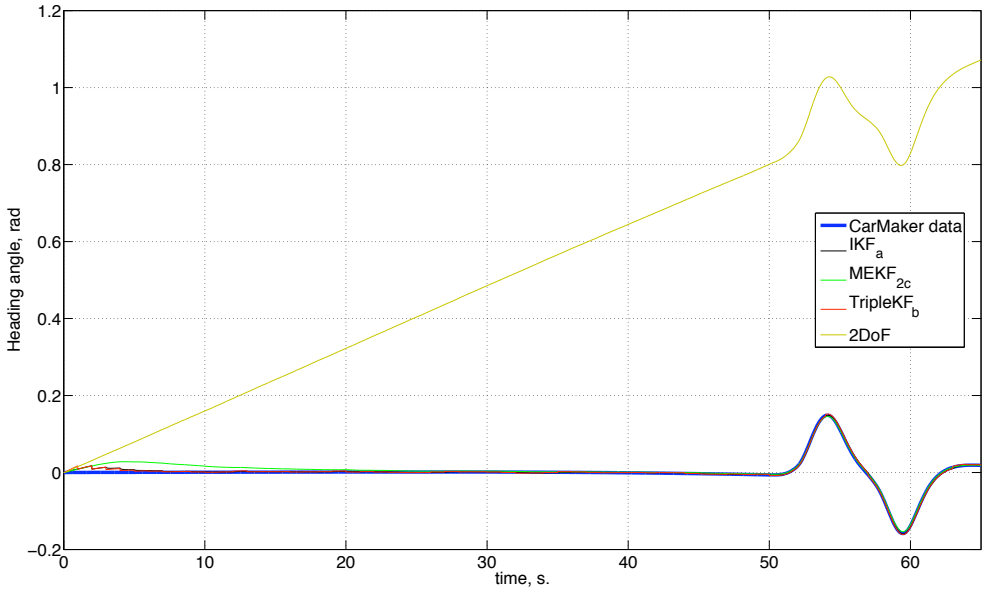

(a) Heading angle estimations

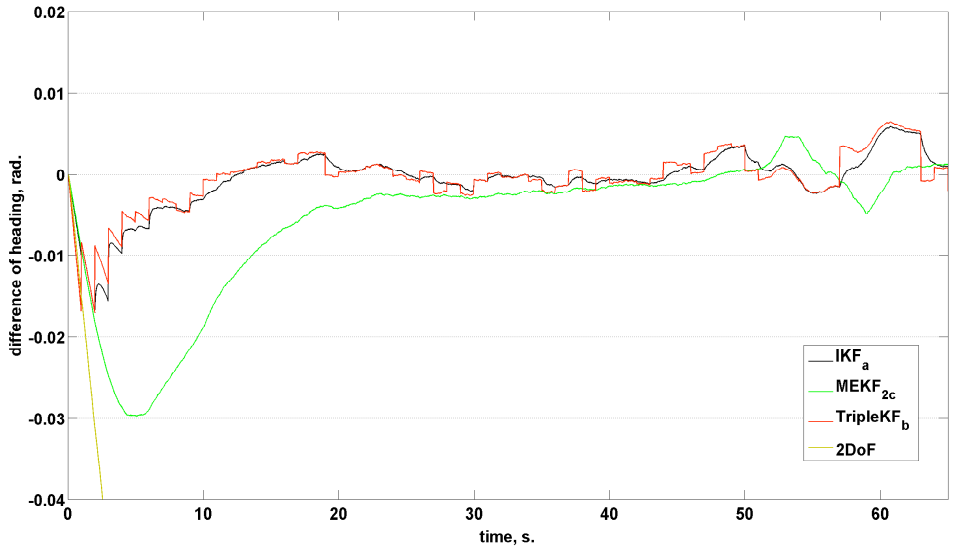

(b) Error in heading angle estimations

Figure 5.21: State estimations and errors of heading angle of *LaneChange_35kph* manoeuvre

the vehicle exits the corner.

For the heading estimations, Figure 5.19 shows that the 2DoF vehicle model has increasing errors due to the biases from the yaw rate gyroscope and steering wheel. Even with the bias predicted, Figure 5.19 shows that the $MEKF_{2c}$ is not able to track the heading of the vehicle accurately, but bounds the errors. As commented in Section 4.3, the $TripleKF_b$ manages to predict the yaw rate and heading accurately. Utilising these estimations in the IKF_a, the heading estimations are as accurate

as those predicted from the $TripleKF_b$. In fact, from the zoom-in region of the graph, it can be seen that the IKF_a provides smoother heading estimations than the $TripleKF_b$.

For fast dynamic manoeuvres such as the *LaneChangeISO_35kph*, Figure 5.20 shows that the sideslip estimation is not accurately predicted when solely using the $TripleKF_b$. Similar to the *DoubleOval_35kph*, the model-based approaches are more accurate, especially for the $MEKF_{2c}$ and IKF_a, in which the biases are estimated. Unlike the *DoubleOval_35kph*, the fast cornering dynamic of the vehicle in the *LaneChangeISO* manoeuvres does not generate a large sideslip angle. Hence, the difference between the sideslip estimations in the $MEKF_{2c}$ and the IKF_a are small, see Figure 5.20.

Examining the heading estimations of the four estimation approaches, Figure 5.21 presents similar findings to those in the *DoubleOval_35kph*. While the 2DoF vehicle model fails to track the heading of the vehicle, the $MEKF_{2c}$ corrects slowly. Moreover, the results show that approaches utilising the $TripleKF_b$ give better heading estimations. This is because of the corrected yaw rate from the *yawKKF* and the more accurate longitudinal velocity determination from $wssEKF_c$.

5.4 Conclusions

To summarise, this chapter uses a linear 2DoF bicycle model as the basis for the proposed MKF. The sensitivity of the model parameters to the state estimations are studied in Section 5.2. It is found that when the linear cornering coefficients are applicable to the vehicle model, the location of the cg is the most influential factor in the state estimations. In a non-linear tyre force to slip region, however, the cornering coefficients become critical to the accuracy of state estimations, see Figure 5.8. Furthermore, in Section 5.2, the importance of steering and longitudinal velocity are also discussed. Without a good measurement of inputs, states will be incorrectly estimated. As the aim of this project is to design an estimator for vehicle dynamic states, parameter estimations are not the main focus here.

In Section 5.3, the MKF of Anderson and Bevly [2005] is modified with a trigonometric GPS measurement and steer bias state, i.e. $MEKF_{2b}$. It is found that the steer bias can be accurately predicted on a straight road and a window averaging technique must be applied to the steer bias for improved estimations during corners, i.e. $MEKF_{2c}$. The $MEKF_{2c}$ is further enhanced by combining with the $TripleKF_b$ to produce the proposed IKF, IKF_a. IKF_a differs from $MEKF_{2b}$ by its inputs, which are taken from the $TripleKF_b$. Comparisons are made between the linear 2DoF

bicycle model, the $TripleKF_b$, the $MEKF_{2c}$ and the IKF_a.

From the findings, it is found that, in general, MKF is better for sideslip estimations and KKF is better for heading estimations. For fast dynamics, however, KKF suffers from continuous update and correction. Unless the update rate of reference sensors are increased, KKF is not superior to the MKF in state estimations. By combining the MKF and KKF, the benefits of the two approaches are utilised. Results show that as long as the linear cornering coefficients are applicable to the vehicle model, the IKF_a is good at both sideslip and heading estimations.

Although the IKF_a is able to estimate the dynamic states of the vehicle in both types of manoeuvres, it is restricted to linear tyre region only. For future work, it is recommended to combine the MKF design of Wenzel [2005] with the proposed $TripleKF_b$. New or existing techniques for cornering stiffness estimation should also be investigated to enhance the new design of the IKF.

Chapter 6

The Business Research: The Relative Importance of Handling as a Consumer Choice Criterion

This chapter forms part of the research of the Engineering Doctorate (EngD) programme. It focuses on the marketing aspect of the technology designed and discussed earlier. This chapter can be viewed as an extension to the researched technology in the business fields, or as an individual study concerning the relative importance of vehicle attributes to customer's purchasing habits.

6.1 Introduction

In 1802, the era of steam coaches was heralded in when William Trevethick built and successfully tested a three-wheeled steam vehicle for transportation. The steam engine design, however, did not open the private automobile market, this occurred with the invention of the internal combustion engine nearly one hundred years later.

6.1.1 A Brief History of the Rise of the Automotive Market

The beginning of the production of private automobiles can be traced back to the late 19th century, when auto-manufacturers such as Benz, Daimler and Peugeot started to establish factories around Europe [Eckermann 2001]. Automobiles at that time were seen as a luxury item, and not yet as an alternative to bicycles and railways. With the expansion of railways and the reduction of bicycle price, the automotive

market at the beginning of the 20th century was an up-market niche and hardly affordable to the ordinary worker.

In America, however, the door to the mass market was opened when Henry Ford, the founder of Ford Motor Company (hereafter called Ford), introduced the Model T (also known as 'Tin Lizzie') to the American market in 1908. The success of 'Tin Lizzie' was due to its affordability to the working class [Zlotin et al. 2002], which enabled Ford to grab 9.4% of the market share in America. Ford's share was further increased after introducing the concept of a moving assembly line, which reduced the number of employees as well as the production time (shortened from 12.5 hours to 2.6 hours for making one car in 1913) [Eckermann 2001]. This allowed 'Tin Lizzie' to be mass produced and further widened the market share to an amazing 39.6% in 1913 and 48% in 1914 [Zlotin et al. 2002].

The success of Ford, however, was only sustained until 1924, when its rival companies, General Motors (GM) and Chrysler caught up by introducing new technological innovations with better business and marketing strategies. By 1926, the market share had been turned around, with GM taking 43%, Chrysler 25% and Ford just 22%. This great reduction in Ford's market share was the result of failing to foresee and adapt during the structural crisis of the time [Zlotin et al. 2002]. The U.S. 'Big 3' further consolidated their grip on the US market after the second world war ended in 1945.

While the automotive market in America was expanding, the European market grew more slowly and to a smaller scale. In 1929, British automotive production (private and commercial) accounted for just 239,000 units compared to over 5,000,000 produced in America in the same year. The big difference was due to lower living standards, a smaller national market and more restrictive tax policies [Britannica 2009]. During this period 70% of the British market was occupied by three companies - Austin, Morris and Singer, and in France there was a similar consolidation with Citroen controlling 40% of the French market. Although the market grew slowly, the direction of the automotive industry towards mass production did not change. In 1934 for example Morris installed the first moving assembly line into in its manufacturing process.

Thirty-five years after the second world war in 1980, world automobile production had increased by a factor of 10. This significant increase is attributable mainly to European and Japanese carmakers, who now account for 80% of the worldwide market, with American global automobile share reduced to the remaining 20% [Britannica 2009].

As described by Zlotin et al. [2002], structural crisis and changes occur in any

business. Failing to see the crisis and/or adapt to changes may cause one to lag behind or lose in the race. Zlotin et al. [2002] have identified four such structural changes in the automobile industry in the 20th century and also suggest a paradigm shift in the current industry to an 'E-paradigm', which stands for: Environment, Electronic communication, and Energy. Recently, like all other businesses, the automotive industry has suffered from the consequences of another unexpected crisis – the 2007/08 credit crunch.

6.1.2 A Quick Glance at the Current Automotive Industry in UK

The beginning of the credit crunch dates back to August 2007, but the actual financial crisis did not begin until the collapse of Lehman Brothers in September 2008. During this grey period (Aug07 to Sept08), forecasts based upon current market were misleading as the effect of the crunch had been camouflaged by the rapid rise of commodity prices due to increasing demands in both China and India [Oxlade 2009]. In the May KeyNote [2008] report, an annual growth of 4.4% (worth £61.58bn) was reported (motor vehicles and components) between 2006 and 2007. In the same report it was also forecast that new car registrations would be reduced by 2.7% to 2.34m in 2008, due to the credit crunch, but the overall market value for new cars would not be affected due to the strong British export trading history. At this point in time, the effect of the credit crunch has not yet been fully revealed. In fact, KeyNote [2008] forecast that the total value of new cars would rise by 1.5% in 2008, and that new car registrations would rise again between 2009 and 2012 due to consumers' confidence in the economy.

This optimistic forecast did not last long. In the October report of Mintel [2008*b*], forecasts began to show the impact of the credit crunch. Although forecasts in new car registration from Mintel [2008*b*] showed a similar trend to that of KeyNote [2008], the trend for the total value of new car sales was forecast to decrease from 2008 to 2013. With the reduction in credit availability for financing new car purchases, it was also predicted that consumers would turn to used cars instead. Thus, a steady increase of used car sales was expected between 2009 to 2013.

In March 2009, another report [Mintel 2009*b*] was published in order to amend changes and re-forecast the trend of the automotive market. It showed that the 2007/08 credit crunch has damaged the automotive industry more severely than previously predicted. The trend for the total value sales of cars (used and new) initially forecast for 2008 to 2013 [Mintel 2008*b*; 2009*a*] had changed to a V-shape with a sharp decrease from 2007 to 2009, see Figure 6.1. According to Mintel [2009*b*], the

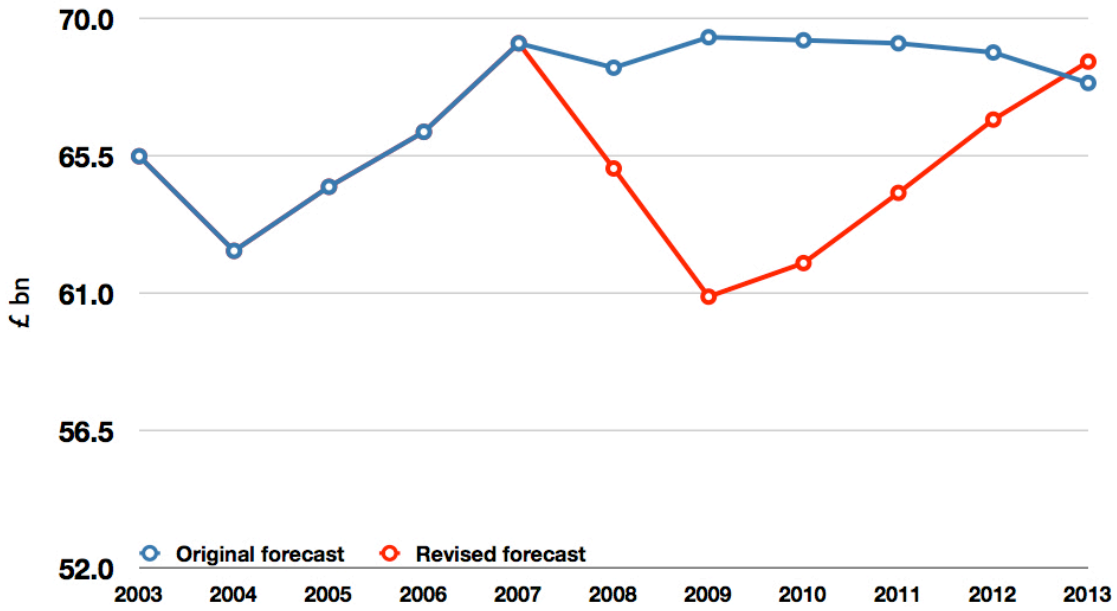

Figure 6.1: Total values sales of cars at current price from 2003 to 2013 [Mintel 2009*b*]

value of new car sales was forecast to decline steeply in 2009 and continue to fall in 2010 and 2011.

In another web report in May 2009, Zino [2009] commented that the current worldwide volumes will not return to pre-crisis level until 2012 due to worsening economic conditions. It is evident that economic decline is far worse than initially forecast and debate is still ongoing as to whether there will be a second dip in the economy before the crisis ends. Polk [2009] has predicted that emerging markets, such as India and China, will come out of the crisis earlier than other saturated regions due to their relatively loose regulations on emission and safety in cars.

In these difficult times, both carmakers and governments have implemented strategies and policies to reduce losses. Carmakers have focused more on cost reduction strategies such as factory/product line closure, worker redundancy and salary reduction. Governments, such as those in Western Europe, have implemented scrappage schemes to boost new car sales. These schemes have been effective, easing the falling market from an initial forecast of 20% to a mere 8%, as reported in Polk [2009].

6.1.3 Motivation for Research

Although cost cutting has an immediate effect in reducing losses, in the long run, such a strategy will cause stagnation and make it difficult to innovate. Carmakers therefore should not solely focus on cost cutting strategies, but also look to the future for opportunities. A KPMG [2009] report reveals that the fundamental drivers of automotive success from the perspective of auto-executives have remained unchanged during the current crisis (i.e. technology, fuel efficiency, environment). Hence, it is essential for carmakers to continue to design new products and technologies in order to gain a competitive advantage once the crisis ends..

In addition, carmakers should be more customer-focused and try to understand their needs more thoroughly. In today's sophisticated auto-market, customers are usually swamped by too many choices (e.g. makes, price, features, options etc...) so they tend to try and rationalise their needs into just a few purchase reasons. By understanding these reasons and aligning them with new product design strategies, carmakers can produce more effective marketing strategies.

In today's customer-demand-driven-world, technological innovation alone no longer gives a leading edge to carmakers in the market.Competitive advantage is created by fulfilling customer demands via a combination of technology design and marketing strategies. Carmakers need to listen more carefully to customers in delivering what they want.

6.1.4 Aim and Objectives

From previous discussion it is clear that understanding customer needs in the overall market as well as customer perception of the brand is vital for successful sales. Motivated by this, the aim and objectives of this chapter are based on the Jaguar brand as given below.

> **Aim:** To investigate consumer purchase reasons in the US and UK markets in relation to brand choice, along with a particular focus on the Jaguar brand and the importance of handling technologies.
>
> **Objectives:** Using survey data in the US and UK from 2007 to,
>
> 1. identify customer purchase reasons,
> 2. identify the relative importance of purchase reasons with a focus on vehicle handling characteristics,
> 3. segment customers into groups with the same purchase reasons,

4. segment brands of cars from the perspective of customers,
5. identify the most important purchase reasons for choosing Jaguar Cars.

In today's economy, it is important to invest wisely and 'correctly' in order to stay competitive. Results from this chapter will enable Jaguar to identify the attribute/s that it should concentrate on, and to prepare competitive strategies to strengthen its current market as well as future opportunities.

6.1.5 Outline of Chapter

This chapter is composed of six sections. This section has given a brief introduction to the past and current automobile market, as well as the aim and objectives for this study. A literature review of the automotive technology, consumer behaviour and automotive segmentation are presented in Section 6.2. The statistical method used in this study is presented and explained in Section 6.3, along with a brief introduction to the two surveys used. The analytical results and discussions are given in Section 6.4. Managerial implications and recommendations are then given in Section 6.5. Section 6.6 offers a conclusion and gives some indications as to possible future work in this field.

6.2 Literature Review

6.2.1 Automobile Technology

To date published data on technology and consumer purchase decisions are limited. Consultancies provide private services such as technology change research to companies but findings typically remain confidential. In general automotive technology can be divided into two areas: 1) Built-In technology (BI-tech), and 2) the alternative Add-On technology (AO-tech). Traditionally, BI-tech only involves technologies that are related to vehicle performance, such as power-steering and ABS (Anti-slip Braking System), and other technology such as entertainment systems are regarded as options or AO-tech.

With growing interest in multi-media technology over the past few years (growing from £591m in 2001 to £1,621m in 2007 [Mintel 2007]), the variety of AO-techs has however increased. Drivers no longer simply own solely the radios and CD players, but also gadgets such as MP3 players, DVD players and satellite navigation systems (SatNav). Nowadays, consumers are overloaded with this fast changing technology. Young adults in particular are beginning to judge the quality of a car based upon both its in-car technology as well as performance. Carmakers have started to include a greater range of gadgets as part of the BI-techs. One obvious example is SatNav, which was initially available only as a portable device (e.g. TomTom). Nowadays, SatNav comes with most luxury cars or as an option to many other models. Although many of these former AO-techs do not add value to the vehicle performance or drivability, they do add value to the driving experience.

In a recent survey by KPMG [2009], 200 automotive executives were interviewed. Results showed that the primary issue of concern is the need to strive for a rebalance in the industry. Although most executives expect a fall in profit margins as well as increase in the numbers of bankrupt companies, their long-term focus over a five year period has not changed (i.e. technology, fuel efficiency and environment). Moreover, within the technology area the issues of most concern are related to cost savings (i.e. manufacturing process and product materials). In fact, the findings from KPMG [2009] support those reported by Davies and Schreck [2008] a year before the economic crisis had fully hit, namely that cost reduction has been the top challenge in the automotive industry for the past three years from 2006. Furthermore, Davies and Schreck [2008] have also reported that the two most important vehicle attributes for consumers are fuel efficiency and environmental friendliness.

Research on consumer purchase priorities in KPMG [2009] shows an increased emphasis on fuel efficiency and affordability compared to previous years. This im-

plies that automotive manufacturers are becoming more aware of the cost of running a vehicle. Compared with the data in 2007, a clear change in priorities has occurred. In 2007, the top three areas of importance were: 1) quality, 2) fuel efficiency, and 3) safety of the vehicle. In 2008, however, the top three areas were: 1) fuel efficiency, 2) quality, and 3) affordability (only 2% lower than quality). This change is a result of the global economic downturn, which has altered consumers' behaviour in terms of expenditure.

In order to succeed in the near future, KPMG [2009] has identified three top management factors: 1) leveraging technology, 2) meeting customer expectations, and 3) producing affordable/cost-efficient cars. Of these three factors, leveraging technology scores the highest, implying it is important for carmakers to develop new technologies based on existing product/s and processes, rather than designing new products from ground up.

By comparing the reports before and during the economic crisis, one can see that the technological direction of vehicles has remained unchanged (i.e. fuel efficiency and environmental friendliness). As commented by Zlotin et al. [2002], the automotive industry has entered the 'E' paradigm (i.e. Environment, Electronic communication, and Energy). Although there is a clear focus for future technological development, perceptions of technology differ: What constitutes 'E' for a carmaker may not be same for a consumer. Therefore, educating consumers about a new technology is as important as carrying out a deep analysis of their needs.

6.2.2 Consumer Behaviour

Consumer behaviour is a complex and multi-disciplinary subject, which crosses and integrates several schools of thought such as psychology, economics and sociology. By understanding how consumers behave, companies can design, manufacture and launch products that better suit the needs of consumers and their buying patterns. Consumer behaviour is a large topic, which considers four areas: 1) who the customers are, 2) what their needs are, 3) where they are, and 4) how to target them for a particular product [Evans et al. 2006]. In addition to these four areas, another area that needs to be considered is when to target the customer. This area is essential as it defines the execution phase that links up the rest of the four areas to form an on-going process of consumer behaviour, see Figure 6.2. Nowadays, businesses talk about brand value, customer relationships and loyalty, which are built upon customers' experience with a product/service before, during and after the purchase. It is inevitable that businesses have to become more customer-focused in order to sustain their market share. Companies have to continually innovate in their technology

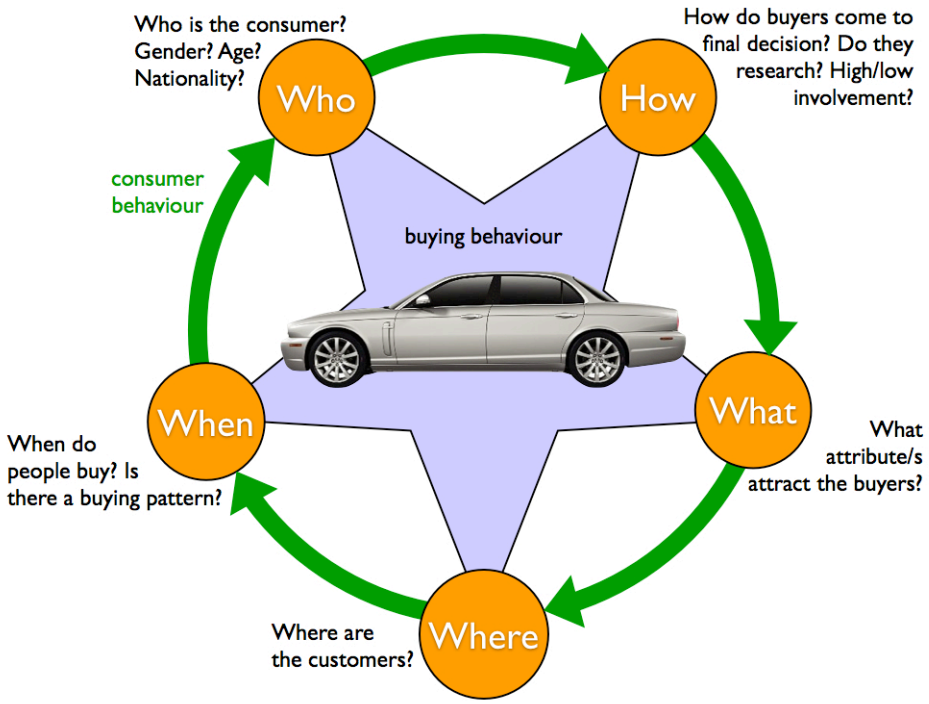

Figure 6.2: Five areas in consumer behaviour

and management to meet customers' expectations.

Buying is frequently described as a problem solving exercise [Paul et al. 1999, Solomon et al. 2002]. Consumers detect a problem, evaluate possible solutions and then carry out the action. This rationale is well-known and is presented as a generic model in Figure 6.3. Using this model, the buying logic and key decision factor/s of a customer can be identified. With this information, the five areas of consumer behaviour in Figure 6.2 can be employed to target the consumer. As living standards increase, consumers' expectations and ideals rises with them. Therefore, it is important for marketers to analyse and evaluate the five areas continuously from the consumers' perspective. The rest of this section gives a brief introduction and explanation for each of the five categories, with a focus on the automobile industry.

Who are the Customers?

Whether in a large organisation or in a small family, the buying process is carried out by a Decision Making Unit (DMU) or 'buying centre'. The DMU is in turn made up of smaller units which includes the initiators, influencers, decision-makers, buyers, end-users and gatekeepers. Each discrete unit has its own function which is carried out by one or more members in an organisation/family. Depending on the purchase

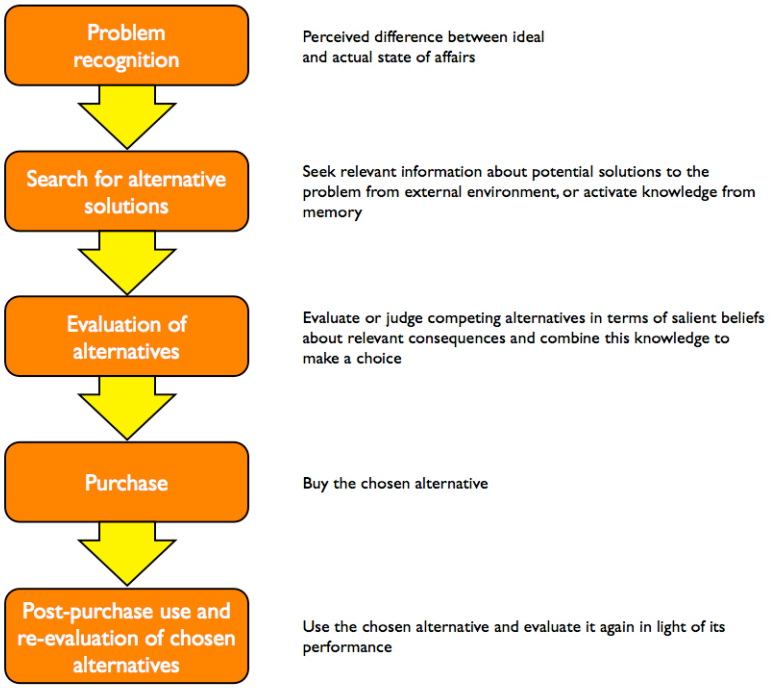

Figure 6.3: Generic model of consumer problem solving/buying behaviour [Paul et al. 1999]

Table 6.1: The five categories of Kenkel [1961]

Wife personal	e.g. clothes, jewellery
Wife household	e.g. washing machine, cooking utemsils
Husband	e.g. books, clothes, watch
Joint family	e.g. furniture, car
Children	e.g. toys, clothes

product/service, the member/s in each small unit may change. Moreover, it is also normal to see some member/s involved in more than one small unit. In a small organisation, such as a family, Kenkel [1961] distinguished five categories, each related to several types of product purchase, see Table 6.1. Davis and Rigaux [1974] have further investigated the buying behaviour of 73 Belgian families and characterised the family decision-making process into three main classes: 1) husband-dominant, 2) wife-dominant, and 3) joint, in which the joint class is sub-divided into autonomic (less than half the family made decisions) and syncratic (more than half the family made decisions).

When making a decision on which vehicle to buy, Davis and Rigaux [1974] have categorised this process in the syncratic joint decision region. This allocation is supported by previous studies of Kenkel [1961], who placed car in the 'Joint family' category, see Table 6.1. In a recent study, Belch and Willis [2001] have shown

that since 1985 women have gained significant influence inside the family in the initiation, evaluation as well as final decision stage for vehicle purchase. In fact, Belch and Willis [2001] have detected an increase in female influence upon many other purchase decisions such as household applicants, household furniture and vacations. Through an understanding of the gender of the decision-maker, a more suitable product design and marketing strategy can be applied. It must be noted that in order to be successful, other demographic details of the decision-maker, e.g. age, residential location and nationality, are also important. In a report, Prasitphol [2002] presents results concerning the cultural influence in vehicle buying decisions from 200 respondents in three countries (i.e. Japan, Thailand and United States). Prasitphol [2002] concludes that Japanese and American consumers emphasise feeling (i.e. attitudes towards the purchased vehicle in general) and reliability, while Thai consumers are more price-sensitive.

How to Target the Customers?

After knowing and understanding the decision-maker for a particular product, organisations will be able to make a more accurate prediction about how to upgrade their current product. However, consumers themselves do not simply 'know' about a product, they go through different channels for research, analysis and comparison. During a buying decision process, there are generally two areas where customers make contact with a product/service: 1) through marketing and advertising, and 2) through the buying experience. It is therefore important for organisations to learn about these channels of contact in order to understand the 'best' way to approach customers. Traditionally, products were advertised through television, radio, billboards and magazines. Customers then browsed the actual product in a shop/dealer before buying it. Nowadays, products are advertised through the internet on interactive web-based banners. Customers are also encouraged to buy the product online with incentives, such as a discount prices or free gifts. With the global popularisation of the web, consumers now have access to a larger pool of information with more choices. Organisations, hence, should identify the types of channels that customers are using, in order to perform strategic marketing campaign.

In the 21st century, everything is going 'on-line'. An article in the Birmingham Post [2009] shows that internet advertising is now in third place in advertising spending, not far behind the top two areas of expenditure (i.e. television and press advertising). The standing of internet advertising is further strengthened by its 19% growth and 12% decline of the press and television in their own markets. This amazing growth is a result of the increased use of the internet as a channel for

information. As reported in KeyNote [2009], 84% of respondents in the survey use internet for finding information about goods and/or services. This high percentage is only 3% lower than the top internet usage - emailing. In another study, Wolin and Korgaonkar [2003] has provided some insights into the different internet usage reasons. He concludes from his survey of 420 consumers that males tend to use the internet more for entertainment and functional purposes, while females use it for shopping.

Although the future of online advertising is clearly very positive compared to traditional advertising, organisations should not solely invest in the internet. This is because each advertising medium has its own audience, and different benefits and drawbacks. To successfully market to a variety of people, it is important to communicate through different sources. While businesses are fighting for space in the cyber-world, a recent article [McMains and Morrissey 2009] reports a move-back to traditional advertising (especially TV adverts) for three online brands: Kayak.com, Zappos.com and Amazon.com. As chief marketing officer at Kayak commented,

> **In these bad times, we can actually accelerate our growth. If I spend this money [on traditional ads], I'm actually going to get a positive return. [McMains and Morrissey 2009]**

This clearly illustrates that TV advertising still retains some benefits over online advertising. As explained by McMains and Morrissey [2009], one of the limitations of online advertising is the type of audience. TV, however, does not have this constraint and has the advantage of a broad audience which can bring new customers into the company. In practice, human beings do not spend their entire day in front of computers and internet; they will watch TV, read newspapers and magazines, and go outdoors. The enduring value of TV advertising is backed up by Sharp et al. [2009], who have compared the TV watching pattern of 2008 with that in the 1970s. They have discovered continuities in television-viewing behaviour as well as the obvious increase of channels over 40 years. In addition, genre-specific channels do not necessarily attract specific pre-defined audiences. For example, the majority of subscribers to the UK channel, 'Men & Motors', are mainly women (30% women compared to 5% men). By carefully identifying the audience and viewing frequencies for different channels, organisations can advertise more effectively. In general, traditional and digital advertising complement one another. In a recent interview, Clay and James [2009] commented that brands cannot stay alive on TV adverts alone. Best results can be achieved by integrating TV with online adverts.

While one of the main reasons for advertising is to attract customers to purchase, the internet has evolved from a research tool to a shopping tool. Businesses nowadays

do not only use the internet merely to advertise their goods and services, but also incorporate the function of convenient buying with simple 'clicks'. A report from Mintel [2009*c*] details a rise of 1% in online purchasing in a 4-month period during the economic downturn (July to October 2008). This is further supported by the findings obtained in the Lightspeed survey, which reports that about 4 in 10 people intend to shop more online and less on the high street in the year 2009. Without doubt, the rise of the internet is a phenomenon. It has promoted customers to a higher level of product involvement as well as pulling businesses closer to them. However, despite all the benefits from online shopping, high street shopping remains an important source of purchasing. This is especially true for expensive goods shoppers, who prefer to 'feel' the actual product with their own senses through experience before buying. Other customers also enjoy high street shopping due to its lack of waiting time and better customer service. As both online and high street shopping have their advantages and disadvantages, Mintel [2009*c*] concludes that a multi-channel retailing approach must be adopted by businesses in order to survive in this competitive climate.

In the automobile industry, Mintel [2008*a*] reveals that traditional dealerships remain the top preferred method for purchasing a vehicle. Even the younger generations who demonstrate a clear growth in internet usage tend to use it mainly for research and comparison purposes. This behaviour shows that information given on web sites is typically inadequate/inappropriate to trigger a buying decision. Customers tend to behave differently in the real world and the internet has merely transformed their method of shopping but not buying. Again, a two-year real-life study in marketing Certified Pre Owned (CPO) Lexus, Pettit [2008] has found that information broadcast through TV adverts may not necessarily reached or be listened by customers. Pettit [2008] also points out the significance of understanding customers from their own perspectives, so that a proactive and well-considered research can be applied.

What are Customers' Needs?

After identifying the types of consumer and their channels of knowledge, the next step is to understand their needs in order to develop a product that matches expectations. However, as pointed out by Jean Philippe [1989], proceeding to this step may cause four complications: 1) customers do not know what they want or what they may want in the future, 2) customers do not always buy what they think they want, 3) customers want different things, and 4) customers continue to upgrade their expectations. It is therefore important to distinguish carefully between

the 'needs' and the 'wants' of customers. A customer may want a particular feature/service/function based on his/her own short-term desires. Customers' 'needs', on the other hand, are the reasons for their 'wants'. 'Needs' explain why a customer wants a particular feature/service/function and normally relate to long-term desires. For example, an iPod may be someone's 'want', but the 'need' may be fashion rather than an mp3 player. Distinguishing between 'needs' and 'wants' will allow an organisation to understand the short and long-term desires of its customers, thereby, planning ahead to the future.

In many situations, however, customers unconsciously replace their 'needs' with their 'wants' based on their current lifestyle and problems. In a technological-based industry, 'needs' and 'wants' sometimes become even more vague as they may be based on previous experience. It is commonplace that customers do not always understand the technologies behind a product and simply take them for granted [Luckhurst and Smith 2006]. From another perspective, customers fail to understand their 'needs' because they simply do not have the physical knowledge and 'dictionary' of a technical expert in order to 'truly' appreciate the technology. Moreover, a new technology normally requires a three to five year time span from concept to fully developed product. By the time customers experience the technology within a product, a technology time lag exists. Unless the technology is followed closely, it is unlikely to answer to the supposed 'needs'. In addition, a customer may also transfer what 'feels good' from perception of one product to 'needs' in another product. On some occasions, technologies are indeed transferable between products, such as the ABS used in cars and aircraft. In others, technologies are not transferable due to cost, safety and/or technical issues (e.g. autopilot in aircraft). Correctly identifying the 'needs' and 'wants' of customers is critical to product success. This requires careful design, planning and execution for the market research.

As human beings are not constrained by logical rules, customers' 'wants' may not remain the same over time. Instead, the 'wants' are dynamic, and may be subject to psychological factors at the time of decision. Customers' 'wants' may change quickly once they realise their actual 'needs' during a buying process. For example, the popularity of a GPS navigation device may trigger a customer's 'want' and then the 'need' for a GPS device. The 'need' is created simply because GPS is the only navigation system that is known about. However, when the new generation GNSS technology is explained (i.e. comprising the American 'GPS', the Russian 'GLONASS', the European 'Galileo' and the Chinese 'COMPASS'), customers are likely to wish to upgrade their 'needs' from GPS to the most current satellite based navigation system. This example demonstrates the difficulty of defining customers'

'needs' when knowledge and future vision to the technology is lacking. It is therefore important to make a distinction between 'experts' with technical knowledge, and the rest of the consumer buying public. Furthermore, it is equally important to educate and communicate with customers in their language, making sure that their 'wants' are aligned with their actual 'needs'. As reported by Taylor-West et al. [2008], customers' expertise, product involvement and familiarity with product will allow companies to more accurately segment customers and deploy more suitable marketing tools.

While customer demand is the driver of businesses, it is also important to satisfy their needs. But as discussed, customers do not always understand their 'needs' and sometimes 'wants' and 'needs' get mixed up. Organisations blindly accepting customers' every 'want' and 'need' are almost certain to achieve disappointing sales. Therefore, the question that needs to be addressed here is how to accurately predict the true future 'needs' of customers from their own perspective. One obvious answer is to design surveys more appropriately to detect the satisfaction level of customers. According to Jamison [1999], a survey can be made more effective and meaningful if it is designed to determine the most important features, to capture the customers' perceptions and expectations, to identify their zones of tolerance, and to prioritise critical areas of delivery. In other words, businesses should try to understand the difference between customer and business perceptions. As commented by Jamison [1999], "It is neither necessary, nor profitable, to try and implement the best service." Companies should develop products based on the consideration of customers' tolerance level and their priority in order to be more cost-effective. Maurer [2007] also emphasises the importance of customer relationship, in which leaders should keep an open mind to meet and actively listen to customers. Hence, real customers' 'needs' can be identified through a good structured survey. By identifying the 'expert' in the surveys and determining the most important attributes as well as their relative importance, a more realistic forecast can be made for future products.

In the automobile industry the general future direction is clear. As discussed previously, KPMG [2009] has identified the three most important attributes for customers from the perspective of automotive executives: 1) fuel efficiency, 2) quality, and 3) affordability. These three attributes are supported by customers' positive response to environmental friendly vehicles and their primary concern towards costs (i.e. running costs, vehicle costs, fuel price and fuel efficiency) [Mintel 2008*a*]. The alignment of the results from the two surveys suggests that carmakers should aim for a cheaper and 'greener' vehicle with better fuel efficiency. In fact, fuel efficiency has always been one of the top concerns of consumers when they buy a new vehicle.

Going back to 1981, Towriss [1981] reported the five most important concerns of consumers: 1) good fuel economy, 2) reliability, 3) comfort, 4) styling, and 5) value of money. When comparing the rankings with that in the KPMG [2009], cost is always one of the primary concerns. With time, comfort, styling and reliability have lost their position and been replaced by environmental concerns. Interestingly in both reports safety and vehicle handling are never the top attributes for car purchase. This suggests that customers already have high expectations of these two attributes in most vehicles and that they therefore do not affect their choice significantly.

Where and When to Target the Customers?

For a product or service to achieve success, a designed marketing plan simply including three elements previously mentioned (who, how and what) is not sufficient. It also needs to include an execution schedule which coordinates these elements. The schedule has two purposes; firstly, it must be able to locate the area where targeted customers have most activities, and secondly, it must be able to provide a time frame for when to execute the marketing plans. If the execution schedule is not well designed, resources will be wasted and, more importantly, market share will be lost.

Once the target customers are identified along with knowledge of their needs and buying channels, it is important to execute the marketing plan by interacting with customers directly. To do this, it is essential to understand customers' personal lives as thoroughly as possible. With the introduction of loyalty cards and club cards, demographic details and buying behaviour have become easier to acquire. This information allow more accurate predictions of the customers' lifestyle, personal preferences, and personality. Marketing plans can then be deployed to the 'correct' audience more suitably, for example through optimal advertising slots on TV, internet etc. In a case study a 7-11 store in Japan had detected a growth in women's stocking sales. The store then increased its stocks of women's cosmetics but found that no concomitant profit had been made. It was later discovered that the customers who shop for the stockings were actually the husbands. By repositioning the stockings next to the beer, the beer sales rose. This example is given by Verespej [2003] and it underlines the significance of correctly identifying the customers and their lifestyle. It is not hard to see from this example the close relationship between the two elements of 'who' and 'where'.

Having studied the personal details of the target customers, it is also vital to get the timing correct, because any miscalculation or wrong prediction can be costly in terms of money and market position. The timing of the launch of a new product

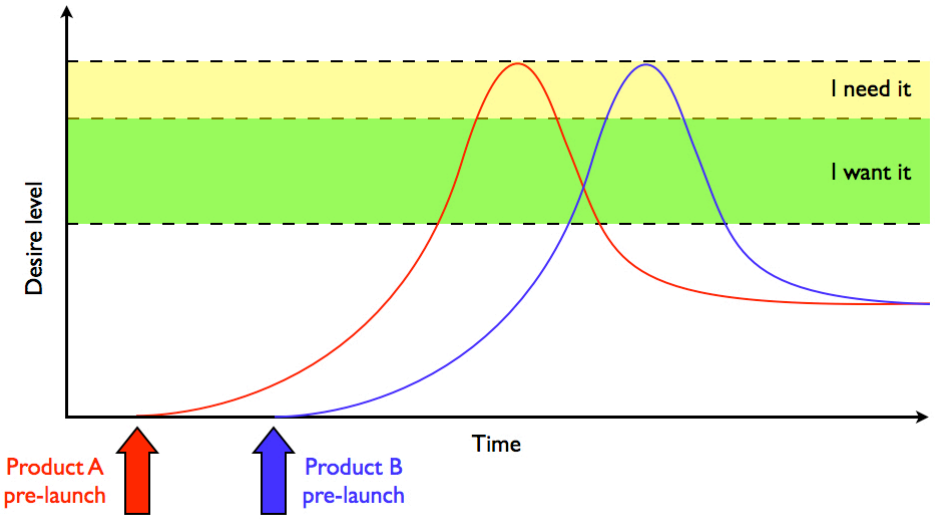

Figure 6.4: Desire level of a customer after the pre-launch phase

is as important as its design. To predict the optimal launch time, companies must understand the market and the buyers' behaviour thoroughly. In an expanding market, companies may want to launch products early to secure a position in the market. On the other hand, if the market is weak and shrinking, a new product launch may be better delayed or modified for another market. It must be noted that the release of a new product intensifies competition in the market, which may include and earlier version of the new product. Hence, before any new product launch, a series of marketing and advertising activities are executed to strengthen its image and future sales. These activities may include advertising, promotions, demonstrations and test days, which are used to bring the new product to the attention of customers. Here, two timings are detailed: 1) the pre-launch time; and 2) the launch time.

The pre-launch time is the time taken between the announcement and the actual launch of the product. Within this time, customers' desire level for a product builds up until it reaches its maximum, then drops over time, see Figure 6.4. If the pre-launch time is too short (i.e. early launch time or delayed announcement), marketing activities will become ineffective as information cannot be delivered/spread to 'all' potential consumers of the new product. If the pre-launch time is too long (i.e. delayed launch or early announcement), consumers may become frustrated and their initial desire for the new product may start to diminish, see Figure 6.4. A long delay on product launch also creates a threat to the new product, and potential customers may redirect their desire towards a similar alternative product. The pre-launch time is like a psychological waiting game, it is crucial to get the timing correct in order

to hit customers' maximum desire levels.

Furthermore, the pre-launch programme must also maintain a buyer focus, which defines activities such as which time slot and which channel to advertise. Pre-launch is a powerful strategy which can cause as much harm as benefit if not managed wisely. Companies, therefore, must master the art of defining the pre-launch time and programme in order to boost sales.

6.2.3 Segmentation in the Automotive Industry

As discussed in Section 6.2.2, the target customers are identified through market segmentation. By focusing on particular segments, a marketing plan can be carried out more cost-effectively. Three formal definitions for market segment and segmentation are given below:

> **Market segmentation is the process of dividing the market into smaller divisions by attempting to define the physical differences between sectors and/or by price discrimination.** – Skillern [1967]
>
> **Market segments consist of groups of people or organisations that are similar in terms of how they respond to a particular marketing mix or in other ways that are meaningful for marketing planning purposes.** – Myers [1997]
>
> **Market segmentation is the division of customer markets into group of customers with distinctly similar needs.** – Baines et al. [2008]

Although the three definitions above originate from texts over a 50 year time span, the main purpose of segmentation remains – to reduce the market to smaller and more meaningful groups. As described in Baines et al. [2008], there are two segmentation methods: the breakdown and the build-up method. The breakdown method separates customers who have the same differences, while the build-up method groups customers with similarities. This chapter focuses on the breakdown method which is better established.

When segmenting a market it is important to first define the segments themselves. This can be done either before collecting customer data (called A priori) or after data are collected (called Post hoc). The post hoc method is more complex and involves multidimensional analysis, but it tends to represent customers' views more accurately [Myers 1997]. In Baines et al. [2008], the post hoc method is given with six general steps:

1. Sample design,
2. Decision on data analysis methodology (e.g. Clustering methods, CHAID),
3. Data collection,
4. Data analysis – apply methodology to form segments,
5. Establishment of profile for all segments and selection of segment descriptors (basis variables), and
6. Translation of the findings into marketing strategies.

The above market segmentation procedure can be applied to both customer and product/service segmentation. In the customer-based segmentation, the basis variables are mostly derived from customers' details, which are classified into their profile, their lifestyles/ psychographics and their behaviour. In a product/service-based segmentation, the basis variables are the quantity, patterns, features desired, attribute deficiencies and other variables such as brand, price sensitivity and media usage.

With the basis variables, the market can be segmented in many different ways. In the most extreme case, each basis variable forms a segment of its own. This approach does not describe much about the market and is inefficient when applying marketing strategies. As there is no formula for the correct number of segments, it is subject to the analysis of researchers/marketers. But in general, the number of segments must be small enough to describe the variety of items in the market.

In the automobile industry, the market is normally segmented according to the physical specification of a vehicle. In 1967 for example Chrysler cars were defined into eight car segments according to engine size and the Overall bumper-to-bumper Length (OAL) of the car [Skillern 1967], Table 6.3a. Skillern [1967] criticised on this segmentation approach in that it considered only the physical attributes of the cars and ignored the actual marketing factors in the industry. Furthermore, he argued that it was inappropriate to apply the defined car segments from the US market to the European market; because the 'image' of cars perceived by European customers is different to that of American customers. Extending this argument, Truscott [1967] divided the automobile market into 'home release' and 'imported release'. In each market, the cars were in turn grouped into six basic segments based on their size and performance, Figure 6.3b. In each market, the 6 basic segments were further divided into 32 segment characteristics according to the price and the physical specification of the car, such as engine size, length and top speed, see Table

Table 6.2: Different car segmentation approach

Car segments	**Examples**
mini cars	Fiat 500, Bianchina
economy cars	Austin Mini, Citroen 2CV
small family cars	Mini Cooper, Morris Minor 1000
light family cars	Mini Cooper 1275's', MG 1100
medium family cars	Toyota Corona, Austin A60
deluxe family cars	Peugeot 404, Audi
luxury cars	Rover 3 Litre, Jaguar - A11
sports & high performance cars	Aston Martin, Jaguar 'E'

(a) Car segmentation of Chrysler in 1967, [Skillern 1967]

Car segments	**Examples in home-release (UK)**
small cars	Austin Mini, Mini Cooper
light cars	MG 1100, Cortina GT
medium cars	Austin A60, Jaguar 240
large cars	Rover 3 Litre, Jaguar MkX
sports cars	Mini Cooper 1275's', Jaguar 'E' Open
grand touring cars	Aston Martin

(b) Six basic car segmentation suggested by Truscott [1967]

Car segments		**Examples**
(A)	mini cars	Renault Twingo, Toyota Aygo
(B)	small cars	Ford Fiesta, Opel Corsa
(C)	medium cars	Ford Focus, VW Golf
(D)	large cars	Audi A4, BMW 3 Series
(E)	executive cars	Jaguar XF, Mercedes E-Class
(F)	luxury cars	BMW 7 Series, Jaguar XJ
(S)	sport cars	Jaguar XK, Ferrari Enzo
(M)	multi purpose cars	Ford Fusion, Toyota Previa
(J)	sport utility cars	Land Rover, BMW X5

(c) Official car segmentation used in UK and Europe, [Van Miert 1999]

F.1 in the appendix. Truscott's segmentation allowed him to see, to forecast and to provide recommendations for the market at that time. Nowadays, the automobile market is generally divided into nine segments, Table 6.3c. They are segmented based on the price and the size of the car. This segmentation is still very subjective but, is widely accepted throughout the UK and other European countries.

Although segmenting the brands by physical features allows cars to be categorised into different classes(i.e. small, luxury and sporty), it does not provide any insight into the reasons for customers' purchase. This is because customers of a particular brand do not necessarily have purchase reasons that are related solely to the physical features of the vehicle. Customers may be buying a vehicle simply because it looks good or easy to drive. Their decision making process may be less related to

their demographic details (e.g. age, gender and income) than, their psychographics. Evans et al. [2006] describes consumer psychographics as the lifestyle, the personality and the self-image of consumers. By analysing this kind of information one can explain customers' motives and behaviour in greater depth. In the US, using VALS^{TM} , the English speaking population aged 18 or older is segmented into eight groups[1] according to their psychographic characteristics: 1) Innovators, 2) Thinkers, 3) Believers, 4) Achievers, 5) Strivers, 6) Experiencers, 7) Makers, and 8) Survivors. In the automotive industry, there are four psychographics segments [Mitchell 1994]: 1) participants, 2) Ego show-offs, 3) functionalists, and 4) do-it-yourselfers. And for Porsche, consumers are separated into five psychographics segments [Taylor 1995]: 1) Top Guns, 2) Elitists, 3) Proud, 4) Bon Vivants, and 5) Fantasists.

As discussed, there are numerous ways to segment the automobile market. Although there is no best solution for segmentation, they all share one common purpose – to group and identify similar customers so marketing strategies can be tailored for the targeted segment. As commented by Myers [1997], the 'best' approach for market segmentation is to distinguish and focus on the heaviest users in the particular segment. But since this approach is being used by almost all major competitors in the market, it no longer provides sustainable competitive advantages. In addition, some products/services do not even have a sizeable group of heavy users. In today's highly competitive market, Myers [1997] have suggested a use of the needs-based segments approach, which bases on customers' wanted benefits and unmet needs. He commented that these segments are usually the best way to segment both consumer and business-to-business markets as they identify the fundamental buying objectives.

[1] http://www.sric-bi.com

6.3 Methodology

This project is sponsored by Jaguar Land Rover (JLR) and the following study focuses mainly on the Jaguar Cars brand. The study is based on two surveys conducted in 2007, they are:

1. the New Vehicle Experienced survey from the United States (NVES_US), and

2. the New Car Buyer survey from the United Kingdom (NCBS_UK).

Details of the two surveys are described in sections 6.3.1 and 6.3.2. The analytical methods for this study are described in Section 6.3.3. At this point, it is also worth noting that the two surveys are conducted before the credit crunch and the results analysed in this study may have changed since.

6.3.1 Survey: NVES_US

The New Vehicle Experienced Survey in US (NVES_US) is an annual survey completed by Strategic Vision with a sample size of approximately 115,000 vehicles. This sample size is acceptable as it is larger than the minimum sample size of 16,604 [Creative Research Systems 2007]. This recommended size is calculated from the total number of passenger cars sold in the US in 2007 (i.e 7.5 million) at 99% confidence level with an interval of 1. For each make/model of vehicles, a typical sample size is about 350. Candidates for each sample set are selected randomly without any criteria.

The sampling plan is divided into three waves: Wave One consisting of September to November buyers; Wave Two consisting of December to March buyers; and Wave Three consisting of April to August buyers.

For data collection, an 8-page questionnaire is sent out by mail after three months of car ownership. All respondents who do not return the questionnaire will receive an additional 2-page questionnaire which contains key demographic and loyalty questions. Those who fill out the questionnaire then receive a second mailing consisting of a 4-page questionnaire (if email address is given, then the questionnaire is sent out through the internet instead of mail). In addition, those who also indicate that they would like to offer more opinions and have internet access, are asked to answer extra questions which are not in the survey. Alternatively, respondents are also given the option to fill out the questionnaire in Spanish over the internet.

6.3.2 Survey: NCBS_UK

The New Car Buyer Survey in UK (NCBS_UK) is conducted every year by GfK NOP with a sample size of approximately 42,000 vehicles. This sample size is adequate as it is larger than the recommended sample size of 16,526 (with 99% level of confidence and an interval of 1) determined from the total number of passenger cars sold in the UK in 2007 (i.e. 2.4 million). In addition, this large sample size is made up of smaller samples of different vehicle models, which are supplied by individual car manufacturers based on its market share. Jaguar Land Rover, for example, sets the sample size according to their sales and selects candidates randomly from manufacturer-owner lists.

For the sampling plan, NCBS_UK includes car models registered between September in the previous year to June in the following year. Therefore, the NCBS_UK 2007 includes car models from September 2006 to June 2007. The exclusion of July and August is because they are the low sales months. The 10 months of surveying is then divided into five waves, each wave consisting of two months.

After approximately three months of car ownership, an 8-page self-completion questionnaire is sent out by post to the new car buyer. The questionnaire is to be completed by the principal driver of the car and it is estimated to take 45 minutes on average to complete. There is, however, no incentive provided to the respondents. If, after three weeks, there is no reply from the buyer then a reminder questionnaire is mailed out. Overall, the gross response rate is about 30%. However, due to incomplete or blank returned questionnaire, the useable response rate is reduced to 25%.

The data collected is then published twice in a year: in June 2007 (data for September to December 2006) and in December 2007 (data for September 2006 to June 2007).

6.3.3 Analytical Strategy

As discussed in Section 6.2, the understanding of customers' 'needs' is important for a company to sustain and stay competitive in today's economic climate. Moreover, it is also crucial for a brand to understand itself through the eyes of consumers. As a reminder, the aim of this study is to investigate the relative importance of the handling characteristics of a car as a consumer purchase criterion. In order to better achieve this goal, a more systematic approach is taken, in which the aim is broken down into problem statements.

As the two surveys, NVES_US and NCBS_UK, are conducted by different com-

panies, their structure and the types of question also vary. This study is interested in the customers' purchase reasons and the most relevant part/s in the two surveys are as described below:

NVES_US Question on "Your purchase decision...". This question consists of 47 variables, each uses an ordinal rating from 1 to 5, with 1 being "Extremely important" and 5 being "Not important at all";

NBC_UK Question on "Part D3 – For what reasons did you buy this particular new car rather than some other one?". This question is a qualitative open question.

Due to the different nature of the questions in the two surveys, the analytical methods being used also differ. Hence, for each problem statement, a suggested method is given for each survey.

The Problem Statements and the Corresponding Methods

1. What are the major attributes that determine the customers' vehicle choice upon purchase?

   NVES_US There are a total of 47 attributes for the customers' purchase decision. Analysing all 47 attributes is computationally expensive and many of these attributes share similarities, e.g. vehicle's image and exterior styling. To reduce the number of attributes, Factor Analysis technique is applied.

   NCBS_UK The question used in this survey for purchase reasons uses an open question format. The first answer written down is assumed to be the most important reason for the respondent. From initial observation, there are in total over 90 different reasons given by the respondents. Based on the latent factors deduced from NVES_US, the purchase reasons from the NCBS_UK are grouped in a similar manner. This method is used for two reasons: 1) to reduce the total number of different reasons, and 2) to facilitate easy comparisons with the US market.

2. Which type of customers consider handling as a car purchase criterion?

   NVES_US Using the SPSS TwoStep Cluster Analysis with the customers' purchase decision attribute scorings (or the latent Factor loading from previous) and their demographic details, the car market is segmented into

groups of customer types. This exploratory study provides an insight into customer segmentation in terms of their purchase decision.

NCBS_UK Using discriminant analysis, a model for the purchase reasons is determined with the demographic details of customers.

3. How important is handling relative to other attributes from the customers' point of view when making a buying decision?

   NVES_US To obtain the relative importance between attributes, a discriminant analysis is performed to identify and separate out the major difference (i.e. attributes) amongst customers' brand choices. These discriminated attributes are regarded as the most influential attributes made by customers during their purchase decision making progress.

   NCBS_UK The importance of the attributes can be observed from the total number of respondents citing each attribute.

4. How do customers perceive brands in terms of vehicle attributes? How do they perceive Jaguar Cars?

   NVES_US With the discriminant function identified previously, the two most influential functions are selected and plotted as a perceptual map (X and Y axes). The determined brand centroid are also plotted in the same map together with the rest of the attributes. This allows an easy visualisation of how the brand relates to the customers' perception in terms of attributes.

   NCBS_UK The purchase reason (or the classified group of reasons) are plotted using perceptions superimposed onto the brand positions, from the customer's perceptions, to show the relationships between brands and purchase reasons.

The Filtered Analytical Data

Both surveys contain a huge amount of information and it is important to pre-filter the data before using it for analysis. The vehicles used for analysis in this study had to satisfy the following conditions:

- purchased and not leased,
- owned by an individual and not a company,
- the purchase decision is made by the owner or his/her family.

In addition, this study focuses on car brands and not individual models; it concentrates on customers' purchase decisions (and reasons) that are related to the car manufacturer and not the dealers. Therefore, reasons such as good dealer network and good salesperson are less relevant to this study.

6.3.4 Limitations

It is assumed in NVES_US analysis that the importance ratings of vehicle attributes given by customers are directly related to the vehicle which they bought. In other words, what they state is important about a vehicle is represented in the car that they buy. In NCBS_UK, it is assumed that the first mentioned purchase reason is the most critical decision made by customers when deciding the vehicle to buy.

6.4 Results and Discussion

The US Automotive Market

Using the NVES_US conducted in the year 2007, customer purchase decisions are studied to determine the relative importance of vehicle handling in the American auto-market.

6.4.1 The American Perspective on Purchase Criteria

The question on "Your purchase decision..." in the NVES_US is composed of 47 attributes. Each respondent was asked to give a score from 1 (Extremely important) to 5 (Not at all important). Table 6.3 gives a descriptive summary of the attributes.

The table is arranged in an ascending order according to the mean of the total attribute scores. For each attribute, the standard deviation (Std. deviation), the skewness and the kurtosis are also given. While std. deviation measures the width of the spread, skewness and kurtosis measure the shape of the spread. To be more precise, a normal distribution has a skewness and a kurtosis of 0. The more positive the skewness, the more the spread tends to the left and visa versa; and the more positive the kurtosis, the more pointed the shape. For an attribute with extreme importance, therefore, the mean score should be near to 1 with a small std. deviation; the skewness and kurtosis also have to be as largely positive as possible. With these criteria in mind, the top five most important candidates from Table 6.3 are "Reliability", "A Well Made Vehicle", "Durability", "Good Running Engine" and "Ease of Handling"; and the least important attribute from Table 6.3 is "Leasing Terms", which has a large mean (4.6) with the most negative skewness (-2.5) and most positive kurtosis (5.28). This indicates a high proportion of answers in the 5s ("not at all important"). It is also interesting to see that "Price or Deal Offered" and media reviews do not score high in the table. This suggests that buyers tend to be more careful with what they buy while having more concerns in vehicle safety and comfort. Furthermore, by inspecting the total number of respondents for each attribute, most of them have a number near or above 40,000, except for " An Alternative To A Family Car" (22,689). This relatively low response rate is due to the nature of the attribute, which is designed especially for new truck owners. Since this study focuses on family cars, " An Alternative To A Family Car" will be neglected from here onwards.

Although the statistics given in Table 6.3 provide a general picture of the importance of each attribute, a number of them are actually very similar and even

Table 6.3: Description analysis for the purchase decision attributes in NVES_US (1 = "Extremely important", 5 = "Not important at all")

	N	Mean	Std. deviation	Skewness	Kurtosis
Reliability	45407	1.45	0.66	1.59	3.33
A Well Made Vehicle	45656	1.46	0.66	1.53	2.96
Durability	45340	1.58	0.73	1.29	2.11
Good Running Engine	45280	1.60	0.76	1.37	2.44
Ease Of Handling	45510	1.64	0.74	1.09	1.44
Safety Features	45510	1.66	0.80	1.19	1.38
Riding Comfort	45487	1.70	0.78	1.09	1.44
Fun To Drive	45186	1.76	0.92	1.32	1.69
Manufacturer's Reputation	45081	1.76	0.91	1.32	1.78
Seating Comfort	45252	1.76	0.82	1.09	1.51
Interior Roominess	45299	1.80	0.84	1.02	1.16
Warranty Coverage	45372	1.83	0.93	1.10	1.07
Value For The Money	45209	1.85	0.92	1.13	1.26
Exterior Styling	45283	1.87	0.93	1.09	1.16
Price Or Deal Offered	45314	1.89	0.99	1.12	0.98
Interior Styling	45253	1.93	0.86	0.76	0.49
Interior Package	45218	1.97	0.90	0.79	0.50
Quietness	45448	1.97	0.90	0.77	0.40
Handling in Inclement Weather	44361	1.99	1.12	1.15	0.71
Dealer's Service	45324	1.99	1.03	0.97	0.48
Fuel Economy	45407	2.00	0.98	0.82	0.26
Exterior Colour	45257	2.03	1.07	0.99	0.48
Power & Pickup	44964	2.05	1.00	0.90	0.55
Technical Innovations	44741	2.07	0.96	0.77	0.41
Costs Of Service & Repairs	44532	2.15	1.04	0.74	0.13
Future Trade-In Or Resale Value	44967	2.21	1.09	0.77	0.08
Vehicle's Image	45023	2.23	1.18	0.83	-0.08
Large Trunk Or Cargo Space	44196	2.40	1.20	0.64	-0.39
Previous Experience With Make	43941	2.50	1.52	0.59	-1.12
Size/Weight	44450	2.55	1.28	0.58	-0.61
Convenient Dealer Location	44915	2.59	1.31	0.46	-0.83
Passenger Seating Capacity	44741	2.60	1.28	0.50	-0.71
Interior Versatility/Convertibility	43709	2.72	1.32	0.37	-0.92
An Alternative To A Family Car	22689	2.84	1.46	0.28	-1.27
Environmental Impact	43898	2.90	1.30	0.19	-0.96
Prestige	44109	3.05	1.41	0.05	-1.25
American Made	43988	3.16	1.60	-0.12	-1.54
Availability of AWD	38508	3.24	1.63	-0.18	-1.58
Interest Rate, Credit Terms	44046	3.28	1.57	-0.18	-1.50
Availability of Rear Wheel Drive	39817	3.28	1.53	-0.18	-1.44
Availability of 4WD	38700	3.31	1.65	-0.26	-1.59
Media Reviews	43386	3.37	1.41	-0.22	-1.27
Ease Of Customizing	43090	3.56	1.45	-0.48	-1.17
Advice Of Friends/Relatives	43569	3.57	1.41	-0.49	-1.09
Towing Capability	41134	3.67	1.48	-0.61	-1.12
Off-road Capability	42047	3.83	1.45	-0.82	-0.82
Leasing Terms	38806	4.60	0.98	-2.50	5.28

Table 6.4: Kaiser-Meyer-Olkin (KMO) and Bartlett's Test for NVES_US

KMO Measure of Sampling Adequacy		0.95
Bartlett's Test of Sphericity	Approx. Chi-Square	642103.09
	df	703.00
	Sig.	0.0000

Table 6.5: Total variance explained with Principle Component Analysis (PCA) for the first 7 components, for detail refer to Table F.2

	Initial Eigenvalues		
Component	**Total**	**%Var**	**%Cum**
1	12.70	31.74	31.74
2	3.59	8.98	40.72
3	2.33	5.82	46.54
4	1.59	3.98	50.51
5	1.41	3.51	54.03
6	1.12	2.81	56.84
7	1.02	2.55	59.38

inter-changeable. To make these attributes more useful and less time consuming to analyse, they are grouped into several areas of interest by the use of a reduction process called Factor Analysis. This is suitable as it is reasonable to assume similar customer scores for attributes belonging to the same group.

However, before applying Factor Analysis, it is important to filter out any attributes that are not directly related to the physical features of a vehicle. This is because this study focuses on vehicle features and not the influence from dealerships (e.g. service) or cultural background (e.g. nationality). Inclusion of these unrelated attributes will affect the analysis. Therefore, the omitted attributes are:

"Warranty Coverage"	"Price Or Deal Offered"
"Dealer's Service"	"Convenient Dealer Location"
"An Alternative To A Family Car"	"Interest Rate, Credit Terms"
"Leasing Terms"	"Advice Of Friends/Relatives"
"American Made"	

With the remaining 38 attributes, Factor Analysis is applied. When inspecting the correlation matrix of the attributes, we can see that there are many coefficients of 0.3 and above. Table 6.4 shows that the Kaiser-Meyer- Olkin value is 0.95, exceeding the recommended value of 0.6 [Kaiser 1970; 1974]. The value of the Barlett's Test of Sphericity [Barlett 1954] also reaches statistical significance, with Chi-Square of 642103.09 and significance value of 0.0000. These values support the factorability of the correlation matrix and the Principal Component Analysis (PCA) is carried out.

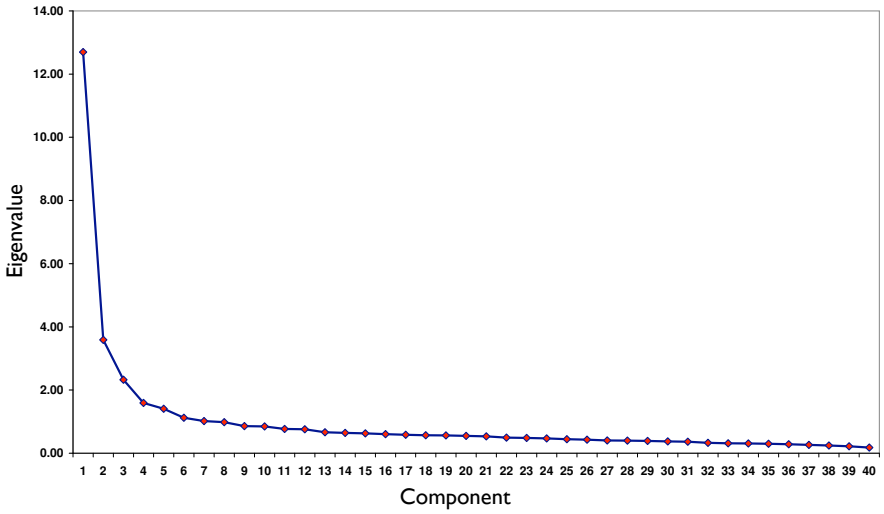

Figure 6.5: Screeplot for NVES_US

Table 6.6: Component Correlation Matrix for the rotated solution

Component	1	2	3	4	5	6	7	8	9	10
1	1.00									
2	0.10	1.00								
3	-0.33	-0.13	1.00							
4	0.27	0.17	-0.35	1.00						
5	0.30	0.22	-0.16	0.24	1.00					
6	-0.20	-0.16	0.10	-0.21	-0.26	1.00				
7	-0.12	-0.36	0.23	-0.18	-0.22	0.19	1.00			
8	0.16	0.24	-0.25	0.31	0.17	-0.22	-0.22	1.00		
9	-0.13	-0.12	0.23	-0.17	-0.08	0.14	0.18	-0.18	1.00	
10	0.41	-0.01	-0.20	0.30	0.23	-0.22	-0.02	0.15	-0.10	1.00

Examining the PCA, Table 6.5, reveals seven components with eigenvalues above 1, with 31.74%, 8.98%, 5.82%, 3.98%, 3.51%, 2.81% and 2,55% of the variance respectively, which sums up to a total of 59.38%. An inspection of the screeplot, Figure 6.5, however does not provide a clear break after the seventh component. It is therefore decided to take 7-, 8-, 9-, and 10-components set forward for further investigation.

For each component set, an Oblimin rotation is applied and correlation tables are constructed. After careful inspection and comparison amongst the 7-, 8-, 9-, and 10-components set, it is decided to retain the 10-components set. The reason for this is twofold: 1) the attributes grouped in each of the ten components are reasonably similar, and 2) the correlations among the ten components are relatively low, see Table 6.6.

From the rotated pattern matrix, Table 6.7, loadings are classified as strong when they are 0.3 or above (shown red in the same figure). Inspecting the table shows

Table 6.7: Rotated Pattern Matrix from Factor Analysis

	Component									
	1	**2**	**3**	**4**	**5**	**6**	**7**	**8**	**9**	**10**
Safety Features	0.73	0.05	0.04	-0.01	0.08	-0.14	-0.02	0.06	-0.04	0.07
Ease Of Handling	0.67	0.01	-0.11	0.22	-0.05	-0.03	-0.07	0.03	0.01	0.09
Quietness	0.59	0.06	-0.17	0.08	0.18	-0.16	0.05	0.16	0.11	-0.11
Availability of 4WD	-0.04	0.92	0.02	-0.04	0.01	0.07	0.00	-0.02	-0.03	0.07
Availability of AWD	0.13	0.89	0.01	-0.08	0.01	0.03	0.08	-0.08	-0.13	0.05
Off-road Capability	-0.19	0.58	0.00	0.04	0.04	-0.02	-0.38	0.09	0.05	-0.01
Handling in Inclement Weather	0.35	0.52	0.15	-0.01	0.10	-0.05	-0.04	-0.03	-0.04	0.20
Availability of RWD	-0.02	0.50	-0.15	0.24	-0.08	-0.13	-0.06	0.14	0.10	-0.25
Towing Capability	-0.22	0.49	0.02	0.13	0.17	-0.03	-0.28	0.18	0.16	-0.10
Exterior Styling	-0.03	-0.02	-0.73	0.11	0.10	0.09	0.00	-0.06	-0.11	0.12
Exterior Colour	0.05	-0.02	-0.72	-0.04	-0.04	-0.08	-0.16	0.06	0.07	0.00
Interior Styling	0.12	0.02	-0.65	0.09	0.18	-0.03	0.04	-0.02	-0.04	0.11
Vehicle's Image	-0.01	0.02	-0.62	-0.05	-0.14	-0.05	-0.16	0.21	-0.15	0.01
Interior Package	0.41	0.01	-0.42	0.11	0.14	0.10	-0.06	0.01	-0.05	-0.05
Fun To Drive	0.19	-0.03	-0.39	0.30	-0.16	0.16	-0.11	0.03	-0.16	0.12
Seating Comfort	0.32	-0.02	-0.38	0.07	0.26	-0.01	-0.12	0.02	0.15	0.12
Technical Innovations	0.15	0.05	-0.35	0.20	0.12	-0.10	0.02	-0.02	-0.18	0.08
Power & Pickup	0.09	0.04	-0.09	0.77	0.04	0.13	-0.07	-0.01	-0.11	-0.03
Good Running Engine	0.12	-0.02	0.03	0.62	-0.01	0.00	-0.09	0.03	-0.02	0.34
Value For The Money	-0.02	-0.08	0.07	0.41	0.09	-0.36	-0.02	-0.02	-0.17	0.23
Passenger Seating Capacity	-0.03	0.04	-0.02	-0.10	0.79	0.00	-0.07	-0.01	-0.15	-0.03
Large Trunk Or Cargo Space	0.02	0.01	0.19	0.16	0.68	0.00	-0.15	0.17	-0.02	-0.05
Interior Roominess	0.12	0.04	-0.25	0.01	0.63	-0.06	0.04	0.01	0.10	0.20
Riding Comfort	0.24	0.05	-0.35	0.10	0.37	-0.08	0.11	-0.02	0.10	0.23
Fuel Economy	0.02	-0.07	-0.03	-0.06	0.06	-0.78	-0.04	-0.08	0.02	0.22
Environmental Impact	0.29	0.05	0.06	-0.17	-0.05	-0.59	-0.26	0.03	-0.20	-0.07
Costs Of Service & Repairs	0.06	-0.02	0.09	0.42	0.12	-0.50	0.00	0.12	0.01	0.00
Future Trade-In Or Resale Value	-0.05	0.13	-0.25	0.19	0.02	-0.41	0.22	0.24	-0.08	0.03
Size/Weight	0.03	-0.01	0.01	0.07	0.03	0.00	-0.75	0.01	0.01	0.10
Interior Versatility/Convertibility	0.09	0.00	-0.10	-0.03	0.25	-0.02	-0.61	-0.02	-0.08	-0.01
Ease Of Customizing	-0.07	0.19	-0.23	0.04	-0.05	-0.13	-0.57	-0.01	-0.09	-0.09
Previous Experience With Make	0.01	-0.03	0.04	-0.07	0.07	0.04	0.04	0.91	0.01	-0.01
Manufacturer's Reputation	0.11	-0.05	-0.02	0.01	-0.03	0.04	-0.03	0.58	-0.16	0.37
Media Reviews	-0.04	0.05	0.06	0.05	0.12	-0.07	-0.04	0.02	-0.82	-0.04
Prestige	-0.06	0.09	-0.40	0.08	-0.01	0.02	0.00	0.15	-0.56	-0.08
Reliability	-0.02	0.07	-0.08	0.07	0.05	-0.14	-0.01	0.07	0.05	0.79
Durability	-0.05	0.09	-0.11	0.07	0.08	-0.19	-0.03	0.08	0.05	0.74
A Well Made Vehicle	0.36	0.02	-0.03	0.12	-0.08	0.10	-0.07	0.16	-0.03	0.51

a number of strong loadings in the variables of each component and the variables load significantly on only one component (see the stair-case pattern in the pattern matrix, Table 6.7). Together, the ten components explain 67.52% of the variance, with 32.45%, 9.04%, 6.11%, 4.02%, 3.59%, 2.85%, 2.61%, 2.47%, 2.25% and 2.14% for component 1 to 10 respectively.

Looking at the component correlation matrix, Table 6.6, most coefficients are below 0.3, suggesting that the ten components are unique and do not correlate to one another significantly. By interpreting the pattern matrix in Table 6.7, a name to represent each component is determined and summarised in Table 6.8.

Using Factor Analysis, the 38 attributes in the NVES_US are reduced to 10. These 10 areas represent the 10 latent factors of customers, which consist of both physical features of a vehicle and customer's feeling towards a brand. In Table 6.8, "Intended positioning" refers to the features, atttributes and perceptions that

Table 6.8: Interpretation for the ten components derived from the Factor Analysis

Component	**Interpretation of component**	**Significant contributed attributes**
1	Vehicle driving comfort/safety	Safety Features Ease Of Handling Quietness
2	Vehicle toughness	Availability of 4WD Availability of AWD Off-road Capability Handling in Inclement Weather Availability of Rear Wheel Drive Towing Capability
3	Vehicle appearance	Exterior Styling Exterior Colour Interior Styling Vehicle's Image Interior Package Fun To Drive Seating Comfort Technical Innovations
4	Vehicle performance	Power & Pickup Good Running Engine Value For The Money
5	Vehicle interior comfort	Passenger Seating Capacity Large Trunk Or Cargo Space Interior Roominess Riding Comfort
6	Vehicle long-term value	Fuel Economy Environmental Impact Costs Of Service & Repairs Future Trade-In Or Resale Value
7	Vehicle customisation	Size/Weight Interior Versatility/Convertibility Ease Of Customising
8	Customer experience	Previous Experience With Make Manufacturer's Reputation
9	Intended positioning	Magazine/Newspaper/T.V.. Reviews Prestige
10	Vehicle reliability	Reliability Durability A Well Made Vehicle

communicators project in the messages contained within their advertising and other promotional commnications to persuade customers to identify with, accept and pur-

chase their products and services [Baines 2010]. Looking at the four attributes in components 8 and 9 in Table 6.8, with the aid of Table 6.3, we can see that the most important purchase decision of the four is the "Manufacturer's Reputation". The remaining three attributes all have a mean near to 3 ("somewhat important") and a negative kurtosis (i.e. evenly distributed scoring), which implies that customers tend to buy a vehicle with a good brand image, based on an individual's experience and his/her interpretation of a particular model.

6.4.2 Customer Segmentation

Having derived the 10 latent factors, they are segmented with regard to customers' details, so those with similar purchase decisions can be identified and grouped. In this analysis the salient customers' details are:

- Age
- Gender
- Marital status
- Education
- Occupation
- Total household income before tax
- Number of children in household

To perform segmentation, the SPSS TwoStep Clustering method[2] is applied to the whole population. As the name suggests, the clustering technique involves two steps: 1) sub-clustering the data with a modified Cluster Feature (CF) tree, and then 2) clustering the sub-clusters with the traditional hierarchical clustering method. The TwoStep Clustering method is accurate for large data sets and this suits the present study well.

The TwoStep Clustering method provides an option for auto-clustering, but using this feature produces only two clusters. Inspection of the two cluster distribution in Table 6.9 reveals that this setup is unfavourable due to the uneven distribution of cases amongst the two clusters.

Table 6.9: Auto-cluster by TwoStep Clustering Analysis in SPSS

	Cluster				
	1	**2**	**Combined**	**Excluded Cases**	**Total**
N	10692	16915	27607	19111	46718
% of Combined	38.73	61.27	100.00		
% of Total	22.89	36.21	59.09	40.91	100.00

Further study of the Schwarz's Bayesian Criterion (BIC) in the TwoStep Clustering Analysis, Table 6.10, shows that not only the two clusters setup give a large

[2]This algorithm applies to SPSS 11.5 and later releases

Table 6.10: BIC results from Auto-clustering in TwoStep Clustering

Number of Cluster	Schwarz's Bayesian Criterion (BIC)	BIC Change[1]	Ratio of BIC Changes[2]	Ratio of Distance Measures[3]
1	225863.81			
2	194596.14	-31267.67	1.00	2.99
3	184286.69	-10309.45	0.33	1.54
4	177645.69	-6641.00	0.21	1.04
5	171294.31	-6351.37	0.20	1.26
6	166279.29	-5015.02	0.16	1.19

Table 6.11: Cluster distribution for three and five clusters

	Three clusters			Five clusters				
	1	**2**	**3**	**1**	**2**	**3**	**4**	**5**
N	10365	10606	6636	5518	5027	5642	5664	5756
% of Combined	37.54	38.42	24.04	19.99	18.21	20.44	20.52	20.85
% of Total	22.19	22.70	14.20	11.81	10.76	12.08	12.12	12.32

"Ratio of BIC Change" and "Ratio of Distance Measures"; so does the three and five clusters setup. Table 6.11 shows the distribution of cases for the three and five clusters. It shows that the five clusters setup has a better and more even spread of cases (i.e. respondents) in each cluster. Therefore, the population is segmented with five clusters.

Reduced Purchase Reasons in the Five Clusters

Before discussing the results, it is important to bear in mind the vehicle attribute scoring system, in which 1 represents "Extremely important" and 5 represents "Not at all important". Therefore, in the standardised format (in which data are scaled to have a mean of 0 and a standard deviation of 1), the more negative the value, the more important it is. In Table 6.12, the most important rating in each latent factor and two most important ratings in each cluster is highlighted in red.

***Cluster 1*:** Customers in *Cluster 1* are the ones that are conscious about their personal experience and perception when they buy a vehicle. They also look for a vehicle with good performance and driving comfort/safety, but do not place too much emphasis on the long-term value of the vehicle. Customers in this cluster are more loyal to their brand.

[1]The changes are from the previous number of clusters in the table.

[2]The ratios of changes are relative to the change for the two cluster solution.

[3]The ratios of distance measures are based on the current number of clusters against the previous number of clusters.

Table 6.12: Attributes centroid for the 5 clusters

		Clusters					
		1	**2**	**3**	**4**	**5**	**Combined**
Vehicle driving comfort/safety	**Mean**	-0.07	-0.07	-0.12	0.08	0.24	0.02
Vehicle toughness	**Mean**	0.03	0.22	-0.02	-0.17	-0.01	0.00
Vehicle appearance	**Mean**	0.02	-0.09	-0.07	0.19	-0.07	0.00
Vehicle performance	**Mean**	-0.08	0.05	0.16	-0.11	0.01	0.01
Vehicle interior comfort	**Mean**	-0.02	0.14	-0.17	0.05	0.05	0.01
Vehicle long-term value	**Mean**	0.15	-0.20	0.04	0.21	-0.26	-0.01
Vehicle customisation	**Mean**	0.03	-0.26	-0.07	0.29	-0.04	0.00
Customer experience	**Mean**	-0.18	-0.03	0.18	0.02	0.05	0.01
Intended positioning	**Mean**	-0.19	-0.11	0.03	0.25	0.06	0.01
Vehicle reliability	**Mean**	0.06	-0.03	-0.07	-0.04	0.09	0.00

***Cluster 2*:** From Table 6.12 we can see that *Cluster 2* has the highest number of negative centroids, followed by *Clusters 3* and *1*. This suggests that customers in this cluster are more conscious of their purchase decision and tend to consider most aspects of the vehicle. In particular, *Cluster 2* customers tend to base their purchase decision strongly on the vehicle's flexibility to modify/personalise and its long-term value. Compared to the other four clusters, *Cluster 2* also scores a higher importance rating on "Vehicle appearance". While customers in this cluster seem to be more cautious with their choice, they do not seem to pay much attention to the "Vehicle interior comfort" or "Vehicle toughness".

***Cluster 3*:** Unlike customers in *Cluster 1*, *Cluster 3* customers do not base their vehicle choice on their experience and vehicle performance. Instead, they value more the vehicle's comfort and reliability. Table 6.12 shows relatively high importance ratings for "Vehicle driving comfort/safety", "Vehicle interior comfort" and "Vehicle reliability". Customers in *Cluster 3* are those who look for an enjoyable day-to-day driving experience with a worry-free vehicle.

***Cluster 4*:** In contract to *Cluster 2*, *Cluster 4* has most centroids opposite to those in *Cluster 2*. Customers in *Cluster 4* are more concerned about the "Vehicle toughness" and "Vehicle performance". They pay only little attention to vehicle appearance, long-term value, flexibility to customise, and their own attitude to a vehicle. Customers in this cluster base their purchase decision primarily on the vehicle's specification and its ability to travel on different terrains. They also look for vehicles that are 'ready-to-go' and do not place too much emphasis on future customisation/modification.

***Cluster 5*:** The last cluster, *Cluster 5*, has customers who are quite neutral in their purchase decision making (i.e. centroids near to zero). They are more concerned about the long-term value of the vehicle, and also tend to choose a vehicle with good appearance internally as well as externally. Customers in this cluster, however, do not take too much notice of the "Vehicle driving comfort/safety", this maybe due to one or both of the following reasons: 1) customers might take vehicle technologies for granted and fail to see the importance of safety features in vehicle, and/or 2) customers might consider themselves to be more careful drivers and oversee the importance of safety features in a vehicle. Customers in this cluster seem to be more fashionable and have greater self-confidence.

The TwoStep Clustering method used here also produces five t-statistic charts, Figures F.1 to F.5. Comparing these figures and Table 6.12, it can be observed that the latent factors are accepted as significant for a cluster when its value of the t-statistic is above a magnitude of 0.03. It is of further note that customers in *Cluster 4* are more critical in their purchase decision, i.e. they either give a score of important or not important and seldom neutral, see also Figure 6.6.

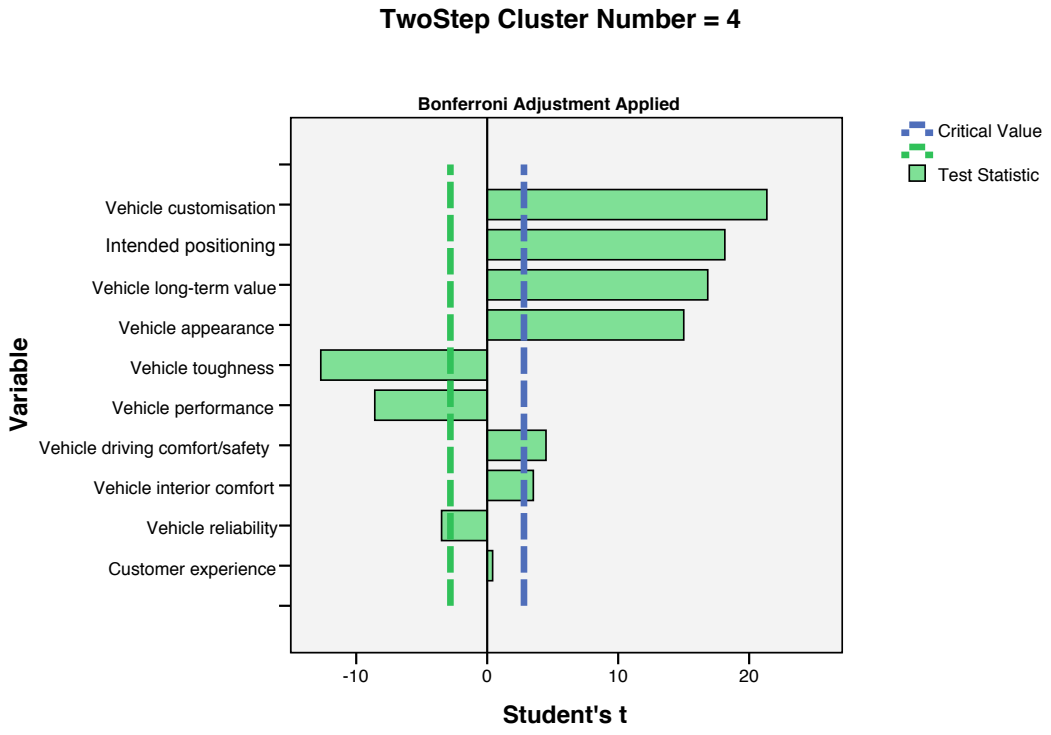

Figure 6.6: T-statistic for the latent factor in Cluster 4 for NVES_US

Age in the Five Clusters

Table 6.13 shows the age group for the respondents in the NVES_US. It indicates that most respondents come from the age group of "45-54" and "55-64". Together, these two age groups contain more than 12,000 respondents, which is almost half of the total valid cases studied for this analysis. The next largest age group is the "35-44" and then the "65 or over". The youngest age group of "18-24" has a very limited number, which is 6 times less than the most populated age group "45-54".

Table 6.13: Age of customers in the five segments

		Cluster					
Age		**1**	**2**	**3**	**4**	**5**	**Combined**
18-24	**N**	0	0	14	1075	1	1090
	%	0.00	0.00	1.28	98.62	0.09	100.00
25-34	**N**	0	0	1192	2072	743	4007
	%	0.00	0.00	29.75	51.71	18.54	100.00
35-44	**N**	4	2	1962	1067	2069	5104
	%	0.08	0.04	38.44	20.91	40.54	100.00
45-54	**N**	287	58	2263	1291	2726	6625
	%	4.33	0.88	34.16	19.49	41.15	100.00
55-64	**N**	2898	2958	205	158	211	6430
	%	45.07	46.00	3.19	2.46	3.28	100.00
65 or over	**N**	2329	2009	6	1	6	4351
	%	53.53	46.17	0.14	0.02	0.14	100.00

***Cluster 1* and *Cluster 2*:** From previous discussion, customers in these two clusters are more conscious of their purchase. As shown in Table 6.13, customers in these two clusters are primarily aged 55 or above (94% of the population in each cluster). This implies that customers in these two clusters have more experience in life, so they may be more reluctant to change, and be more loyal towards a particular brand;

***Cluster 3* and *Cluster 5*:** Nearly 80% of customers in these two clusters are aged between 25 to 54. In this age bracket, customers are in the middle of their career and driving to work has typically become a daily task. Customers in these two clusters are likely to seek a vehicle which reflects their status, as well as one that is comfortable and reliable to ride in;

***Cluster 4*:** Customers in this cluster are highly concentrated within the youth group of "18-24" and young adults of "25-34". Their experience of life is limited and many of them may not even have working experience. They are

likely to have tight budgets and therefore less likely to be a customer of the expensive brands; instead, they look for cheap and powerful alternatives in order to stand out in their group.

Gender in the Five Clusters

Table 6.14: Customers' gender in the five segments

		Cluster					
Gender		**1**	**2**	**3**	**4**	**5**	**Combined**
Male	**N**	3646	3901	5	2760	5705	16017
	%	22.76	24.36	0.03	17.23	35.62	100.00
Female	**N**	1872	1126	5637	2904	51	11590
	%	16.15	9.72	48.64	25.06	0.44	100.00

In terms of male/female frequency among the five clusters, the TwoStep clustering method shows that the overall male to female ratio is approximately 14 to 10, which implies that there are more male buyers.

With the age of customers as shown in Table 6.13, the male-to-female ratio in Table 6.14 shows that customers with more life experience (55 or above in *Clusters 1* and *2*) are predominantly male while the younger generation (18 to 34 in *Cluster 4*) are well-balanced between the two genders. The working class (aged 25 to 54 in *Clusters 3* and *5*) are split into two clusters, each dominated by a type of gender. Referring to the age and gender, we can see that the number of female buyers greatly decreases once they reach the age of 54. With this knowledge, more suitable marketing strategies can be employed more effectively to target different audiences.

Marital Status in the Five Clusters

Regarding the marital status of the customers in Table 6.15 reveals that about 71% of respondents are "Married", 24% are "Single" and 5% are "Other". The table shows that *Clusters 1* and *3* are occupied mostly by "Married" and "Other" while *Clusters 2* and *5* contain customers who are mostly "Married". *Cluster 4* discriminates itself from the rest with a high percentage of "Single" respondents.

The high proportion of married buyers amongst the five clusters indicates that customers at the age of 34 or above are very likely to have been married. Married female customers such as those in *Cluster 3*, are more family orientated seeking comfort and reliability. On the other hand single young adults in *Cluster 4* do not have much responsibility in the family and tend to buy vehicles that attract their peers in terms of performance and toughness.

Table 6.15: Marital status of customers in the five segments

		Cluster					
Marital status		**1**	**2**	**3**	**4**	**5**	**Combined**
Married	**N**	4251	4163	4778	948	5514	19654
	%	21.63	21.18	24.31	4.82	28.06	100
Single	**N**	820	667	598	4454	91	6630
	%	12.37	10.06	9.02	67.18	1.37	100
Other	**N**	447	197	266	262	151	1323
	%	33.79	14.89	20.11	19.80	11.41	100

Number of Children in the Household in the Five Clusters

Table 6.16 shows that 69% of respondents have no children and that they are distributed evenly among *Clusters 1*, *2* and *4*. Although it was shown previously that approximately 71% of respondents are married, only 31% of respondents have more than one child. This finding is mainly due to the age of the respondents. As described earlier, the majority of population in *Clusters 1* and *2* are aged 55 or above. Married couples in this age bracket are most likely to have grown up children who live away from home for work or study. On the other hand, the young adults (mostly under 34) in *Cluster 4* are mainly respondents who are single or with a young family without children.

Families who have more than one child are mainly segmented in *Clusters 3* and

Table 6.16: Number of children in the customer's household in the five segments

		Cluster					
Number of children		**1**	**2**	**3**	**4**	**5**	**Combined**
0-None	**N**	5306	4838	2511	4412	2072	19139
	%	27.72	25.28	13.12	23.05	10.83	100
1	**N**	123	155	1318	776	1308	3680
	%	3.34	4.21	35.82	21.09	35.54	100
2	**N**	59	20	1266	297	1607	3249
	%	1.82	0.62	38.97	9.14	49.46	100
3	**N**	12	8	418	119	579	1136
	%	1.06	0.70	36.80	10.48	50.97	100
4	**N**	9	2	87	47	137	282
	%	3.19	0.71	30.85	16.67	48.58	100
5	**N**	5	0	24	6	30	65
	%	7.69	0.00	36.92	9.23	46.15	100
6 Or More	**N**	4	4	18	7	23	56
	%	7.14	7.14	32.14	12.50	41.07	100

5, of which *Cluster 3* is mostly female customers and *Cluster 5* is dominated by male customers. While female customers in *Cluster 3* show more motherly care by giving higher importance ratings for comfort/safety and reliability, male customers in *Cluster 5* show a higher technical knowledge by rating long-term value higher.

Education in the Five Clusters

Table 6.17 shows the cluster profile for the educational background of the respondents. The table uncovers the high proportion of customers with experience in college (aka university) and post-grad. *Clusters 1* and *2* distinguish themselves from the other three clusters by having the most non-college graduates and the most post-grad education, respectively. The remaining respondents are spread among *Clusters 3*, *4* and *5* without obvious distinction between them with respect to the educational level. But in general, "College Graduate" and "Some Post-Grad" are distributed evenly between the three clusters. While *Clusters 4* and *5* have a mixture of educational backgrounds, *Cluster 3* consists of respondents who have a higher educational background.

The fact that customers are highly educated suggests that they may not be gullible beings. Information about a vehicle given by a car manufacturer to an individual is analysed before a conclusion is drawn. Information therefore needs to

Table 6.17: Education of customers in the five segments

		Cluster					
Education		**1**	**2**	**3**	**4**	**5**	**Combined**
Grade School Grad only	**N**	36	0	0	19	23	78
	%	46.15	0.00	0.00	24.36	29.49	100.00
Some High School	**N**	178	1	14	116	31	340
	%	52.35	0.29	4.12	34.12	9.12	100.00
High School Graduate	**N**	1639	0	517	814	510	3480
	%	47.10	0.00	14.86	23.39	14.66	100.00
Some College	**N**	2659	19	1180	1525	1240	6623
	%	40.15	0.29	17.82	23.03	18.72	100.00
College Graduate	**N**	571	1671	2068	2041	1956	8307
	%	6.87	20.12	24.89	24.57	23.55	100.00
Some Post-Grad	**N**	71	861	377	361	394	2064
	%	3.44	41.72	18.27	17.49	19.09	100.00
Post-Graduate Degree	**N**	6	2475	1346	562	1423	5812
	%	0.10	42.58	23.16	9.67	24.48	100.00
Other (Trade School)	**N**	358	0	140	226	179	903
	%	39.65	0.00	15.50	25.03	19.82	100.00

be true and accurate. Moreover, based on the age and education of each cluster, new ideas and terminologies can also be introduced to enhance understanding of customers with a new technology.

Occupation in the Five Clusters

The Occupation of respondents are divided into two tables, Tables 6.18 and F.4. Table 6.18 refers to the current occupation of respondents and Table F.4 corresponds to the last occupation of retired respondents. In this study, about 82% of respondents are working (18% retired). Table 6.18 shows that most respondents have a job in either the "Executive/Managerial" or the "Professional Specialty" sectors. Respondents in these two sectors are mostly located in *Clusters 2*, *3* and *5*. Four occupations are loaded quite heavily with more than 50% in one of the clusters, they are "Farmer", "Homemaker", "Service Worker" and "Student": over 50% of "Farmer" in *Cluster 1*, over 70% of "Homemaker" in *Cluster 3*, and over 50% of "Service Worker" and 90% of "Student" in *Cluster 4*. "Armed Services" is mainly concentrated in *Clusters 4* and *5* with more than 40% in each. Table F.4 shows the occupation of respondents before they retired. It clearly indicates that most respondents fall into *Clusters 1* and *2*, with *Cluster 1* having a higher proportion of respondents. *Cluster 2* can be further described to contain retired respondents who are highly skilled and knowledgeable in their field of expertise.

In general, the characteristics for occupation in the five clusters are summarised as follows:

Cluster 1 includes occupations which require repetitive work and patience, e.g. "Factory Worker" and "Farmer". Customers in this cluster are less willing to change, they are more practical and loyal to brands. The high proportion of retired customers also means they are more cautious with what and how they spend their pension on;

Cluster 2 includes occupations that require fewer skills but more knowledge, e.g. "Executive/Managerial" and "Professional Specialty". Customers in this cluster are aged 55 or above on average. In terms of career, customers are most likely to be in the senior/executive level and look for vehicles that are commensurate with their status;

Cluster 3 includes respondents who work in a social-orientated background, e.g. "Administrative Clerical", "Health Care", "Homemaker" and "Teacher, Educator". There is a high proportion of married female customers who are aged between 25 and 54 with children. Customers in this cluster generally put their

Table 6.18: Occupation of respondents in the five segments

		Cluster					
Occupation		**1**	**2**	**3**	**4**	**5**	**Combined**
Administrative Clerical	**N**	407	29	679	599	37	1751
	%	23.24	1.66	38.78	34.21	2.11	100
Armed Services	**N**	24	15	19	145	152	355
	%	6.76	4.23	5.35	40.85	42.82	100
Executive/Managerial	**N**	332	831	760	438	1368	3729
	%	8.90	22.28	20.38	11.75	36.69	100
Factory Worker	**N**	151	0	35	211	93	490
	%	30.82	0.00	7.14	43.06	18.98	100
Farmer	**N**	92	9	0	32	38	171
	%	53.80	5.26	0.00	18.71	22.22	100
Health Care	**N**	90	178	871	480	228	1847
	%	4.87	9.64	47.16	25.99	12.34	100
Homemaker	**N**	232	1	710	26	3	972
	%	23.87	0.10	73.05	2.67	0.31	100
Owner/Proprietor	**N**	287	228	226	139	474	1354
	%	21.20	16.84	16.69	10.27	35.01	100
Police, Postal, Fire	**N**	95	10	54	182	337	678
	%	14.01	1.47	7.96	26.84	49.71	100
Professional Specialty	**N**	218	858	926	736	1075	3813
	%	5.72	22.50	24.29	19.30	28.19	100
Sales Work	**N**	204	146	220	446	420	1436
	%	14.21	10.17	15.32	31.06	29.25	100
Service Worker	**N**	76	0	42	216	50	384
	%	19.79	0.00	10.94	56.25	13.02	100
Skilled Trade	**N**	358	0	13	341	448	1160
	%	30.86	0.00	1.12	29.40	38.62	100
Student	**N**	1	0	15	297	0	313
	%	0.32	0.00	4.79	94.89	0.00	100
Teacher, Educator	**N**	12	420	706	325	217	1680
	%	0.71	25.00	42.02	19.35	12.92	100
Technical Specialty	**N**	156	133	106	404	506	1305
	%	11.95	10.19	8.12	30.96	38.77	100
Other	**N**	113	55	225	611	223	1227
	%	9.21	4.48	18.34	49.80	18.17	100
				total number of respondents			22665

family needs as the highest priority and look for vehicles that are bigger, safer, more comfortable and more reliable;

Cluster 4 includes respondents who require fewer skills in their work, e.g. "Armed

Services", "Factory Worker", "Service Worker" and "Student". Customers in this cluster are the youngest amongst all the clusters. They have less or no experience in work and are typically unmarried. The nature of their occupations also suggests that they are the 'tough' ones, who looks for power and performance at a low price with the option of upgrades;

Cluster 5 includes occupations that require more technical knowledge and skills, e.g. "Executive/Managerial", "Police, Postal, Fire", "Professional Specialty", "Skilled Trade" and "Technical Specialty". Customers in this cluster are mainly married men aged 25 to 54 with children. Considering their age and occupations, they are mostly in the 'golden' period of their career. They are eager for success and tend to have self-confidence. They focus their life on the career and family and place little or no effort at all on researching and learning different vehicle models. They take technology for granted and accept most information from manufacturers/dealers. They judge vehicles visually.

Household Income in the Five Clusters

For the total household income before tax in the five clusters, Table 6.19 reveals a clear difference between the clusters. But in order to make it easier to interpret and understand, the income categories are grouped into five bands:

Band 1: US$30,000 Or Less,

Band 2: US$30,001 To US$55,000,

Band 3: US$55,001 To US$80,000,

Band 4: US$80,001 To US$175,000,

Band 5: US$175,001 Or Over.

Overall, most respondents are earning an income in the Band 3 and Band 4, and least in the Band 1. For each cluster, the income band is described as follows:

Cluster 1 has a high percentage of respondents in the Band 1, Band 2, and Band 3 incomes. Customers in this cluster are mostly retired and live on pensions. This implies that they are more careful with their spending and most likely to consider cheaper cars which suit their purpose of living;

Cluster 2 contains respondents who are mainly in the Band 4 and Band 5 incomes. They are rich but near or already at their retirement stage. Unlike customers

in *Cluster 1*, they have a much higher income/pension. They tend to consider vehicles are a luxury with a good exterior/interior design to reflect their status in life;

Cluster 3 has a high proportion of respondents in the Band 3 and Band 4 incomes. This cluster contains a high proportion of female working class with children. Although customers in this cluster are not in the top income band, they have the potential power to spend as they consider their family first when making decisions. They are willing to spend more on the safety, comfort and reliability aspects of a vehicle;

Cluster 4 contains respondents mainly in the Band 1 and Band 2 income. This is expected as customers in this cluster are mainly younger students and factory workers. They are more adventurous and tend to buy cheap vehicles which are upgradable;

Cluster 5 has the highest percentage of respondents who are earning either the Band 4 or the Band 5 income. As discussed, customers in this cluster are in the 'golden' period of their career. They are career-focused and make their decisions according to the styling of the vehicle.

Table 6.19: Total household income before tax of customers in the five segments

			Cluster					
			1	**2**	**3**	**4**	**5**	**Combined**
Band 1	**$10,000 Or Less**	**N**	29	7	5	86	4	131
		%	22.14	5.34	3.82	65.65	3.05	100
	$10,001 To $15,000	**N**	65	4	9	97	1	176
		%	36.93	2.27	5.11	55.11	0.57	100
	$15,001 To $20,000	**N**	115	7	10	148	4	284
		%	40.49	2.46	3.52	52.11	1.41	100
	$20,001 To $25,000	**N**	182	22	26	218	2	450
		%	40.44	4.89	5.78	48.44	0.44	100
	$25,001 To $30,000	**N**	276	23	33	358	7	697
		%	39.60	3.30	4.73	51.36	1.00	100

continue...

Continue from Table 6.19

			Cluster					
			1	2	3	4	5	Combined
Band 2	$30,001 To $35,000	N	370	49	70	483	21	993
		%	37.26	4.93	7.05	48.64	2.11	100
	$35,001 To $40,000	N	387	81	80	494	66	1108
		%	34.93	7.31	7.22	44.58	5.96	100
	$40,001 To $45,000	N	300	72	72	435	55	934
		%	32.12	7.71	7.71	46.57	5.89	100
	$45,001 To $50,000	N	408	114	149	409	90	1170
		%	34.87	9.74	12.74	34.96	7.69	100
	$50,001 To $55,000	N	385	116	145	397	119	1162
		%	33.13	9.98	12.48	34.17	10.24	100
Band 3	$55,001 To $60,000	N	371	190	262	342	178	1343
		%	27.62	14.15	19.51	25.47	13.25	100
	$60,001 To $65,000	N	260	190	245	251	169	1115
		%	23.32	17.04	21.97	22.51	15.16	100
	$65,001 To $70,000	N	290	191	305	245	213	1244
		%	23.31	15.35	24.52	19.69	17.12	100
	$70,001 To $75,000	N	267	223	255	236	211	1192
		%	22.40	18.71	21.39	19.80	17.70	100
	$75,001 To $80,000	N	255	256	391	245	298	1445
		%	17.65	17.72	27.06	16.96	20.62	100
Band 4	$80,001 To $90,000	N	279	309	473	252	436	1749
		%	15.95	17.67	27.04	14.41	24.93	100
	$90,001 To $100,000	N	296	409	515	222	501	1943
		%	15.23	21.05	26.51	11.43	25.78	100
	$100,001 To $125,000	N	368	712	904	300	1001	3285
		%	11.20	21.67	27.52	9.13	30.47	100
	$125,001 To $150,000	N	176	532	544	164	602	2018
		%	8.72	26.36	26.96	8.13	29.83	100
	$150,001 To $175,000	N	117	328	357	96	455	1353
		%	8.65	24.24	26.39	7.10	33.63	100
Band 5	$175,001 To $200,000	N	86	287	186	83	321	963
		%	8.93	29.80	19.31	8.62	33.33	100
	$200,001 To $300,000	N	98	442	306	54	512	1412
		%	6.94	31.30	21.67	3.82	36.26	100
	$300,001 To $400,000	N	44	156	114	13	162	489
		%	9.00	31.90	23.31	2.66	33.13	100
	$400,001 to $500,000	N	21	75	52	12	90	250
		%	8.40	30.00	20.80	4.80	36.00	100
	Over $500,000	N	73	232	134	24	238	701
		%	10.41	33.10	19.12	3.42	33.95	100

Summary: the Five Segments

With the use of SPSS TwoStep Clustering method, five clusters are generated and their summaries are provided in Table 6.20 to 6.24. Each table shows the top two most important and the least important purchase decisions. It also shows the dominant group for each customer detail considered in this study. Note that the gender is presented in terms of percentage ratio of male to female.

***Cluster 1*, Table 6.20:** customers in this cluster make their decision based on their experience and feeling. Customers in this cluster are in the Band 1 income and are near to or have already retired. They have little education and most of them do not have college education. Their job requires low skill and most of them are married men without children in the household. Their background may mean they are financially insecure and they try to avoid risk when purchasing a new vehicle. In order to reduce the risk, they choose a vehicle which they know well through past experience, their own interpretation and word of mouth.

Squares: insecure, conservative, stubborn. Self opinion and interpretation matter.

Table 6.20: Description for *Cluster 1 - Squares*

Cluster 1 - Squares	
Attributes and customer profile	
Most important	Intended positioning
2nd most important	Customer experience
Least important	Vehicle long-term value
Age	55 or above
Gender in survey (%Male : %Female)	23:16
Marital status	Other/Married
Number of children in household	0 or None
Education	non-college grad
Occupation	Repetitive work and patience OR retired e.g. Factory worker, Farmer
Total household income before tax	Band 1 (US$30,000 Or Less)
UK classification of social class	D, E

***Cluster 2*, Table 6.21:** customers in this cluster make their decision based on the vehicle flexibility in customising and its long-term value. Similar to customers in *Cluster 1*, they are mostly married men without children in the household who are aged 55 or above. But different to *Cluster 1*, customers in this cluster earns the highest band of income, Band 5. Apart from this, they are also highly educated with technical knowledge. As a result, they tend to consider different vehicle attributes and will be more careful with what they buy. Due to their background, they tend to be more forward-thinking and consider on vehicle value and customisation. In addition, customers in this cluster are or once were employees with a high position, so their choice of vehicle also tend to be dependent on its appearance.

Yodas: young-at-heart, wise. Cars must last long with future upgrades possible.

Table 6.21: Description for *Cluster 2 - Yodas*

Cluster 2 - Yodas	
Attributes and customer profile	
Most important	Vehicle customisation
2nd most important	Vehicle long-term value
Least important	Vehicle toughness
Age	55 or above
Gender in survey (%Male : %Female)	12:5
Marital status	Married
Number of children in household	0 or None
Education	post-grad
Occupation	Technical knowledge but less skilled OR retired e.g. Professional specialty, Executive/Managerial
Total household income before tax	Band 5 (US$175,001 Or Over)
UK classification of social class	B

***Cluster 3*, Table 6.22:** customers in *Cluster 3* make their decision based on the vehicle interior and driving comfort. Customer experience is not important to them. In this cluster, most customers are married women who have one or more children. They are aged between 25 to 54, and have high school education or above. Their work is primarily social-orientated with pay in the Band 3/4. When customers, who are more caring with motherly love, choose a vehicle they tend to make their decision with more considerations towards the family. As a result, they rate vehicle comfort, safety and reliability highly.

Comfort-goers: careful, conscious, family focus. Cars for comfort, safety and harmony.

Table 6.22: Description for *Cluster 3 - Comfort-goers*

Cluster 3 - Comfort-goers	
Attributes and customer profile	
Most important	Vehicle interior comfort
2nd most important	Vehicle driving comfort/safety
Least important	Customer experience
Age	25-54
Gender in survey (%Male : %Female)	Female dominate
Marital status	Married/Other
Number of children in household	1 or more
Education	high school or above
Occupation	Social-orientated e.g. Health care, Homemaker, Teacher
Total household income before tax	Band 3 (US$55,001 To US$80,000) or Band 4 (US$80,001 To US$175,000)
UK classification of social class	C1, C2

***Cluster 4*, Table 6.23:** customers in this cluster make their decision based on the vehicle toughness and performance. They are not concerned about vehicle flexibility to customise and only want an 'instant', 'ready-to-go' vehicle. The fact that they are in the Band 1/2/3 income means that they may be restricted by the price of future vehicle customisation. *Cluster 4* has the youngest age groups of all five clusters and its population includes students. This cluster is also the one that contains a high percentage of singles with more female than male drivers. The fact that they are single and young may explains the reason for their low income and spending power. They prefer vehicles that are powerful in performance rather than good appearance or comfort. Customers in this cluster tend to be interested in the specification (e.g. engine) of the vehicle; safety and long-term value do not appeal to them.

Die Hards: adventurous. All about power, excitement and performance.

Table 6.23: Description for *Cluster 4 - Die Hards*

Cluster 4 - Die Hards	
Attributes and customer profile	
Most important	Vehicle toughness
2nd most important	Vehicle performance
Least important	Vehicle customisation
Age	18-34
Gender in survey (%Male : %Female)	17:25
Marital status	Single
Number of children in household	mix
Education	mix
Occupation	Little-skilled e.g. Armed Services, Factory Worker, Student
Total household income before tax	Band 1 (US$30,000 Or Less) or Band 2 (US$30,001 To US$55,000) or Band 3 (US$55,001 To US$80,000)
UK classification of social class	C2, D

***Cluster 5*, Table 6.24:** customers in *Cluster 5* belong to the middle aged group between 35 and 54. They are mostly male with at least one child in the family. These customers vary with their educational background but the majority of them are secure with a job in a professional specialty or executive/managerial sector. They earn a high income in Band 4/5. Based on their background, it is not hard to see that their top two purchase decisions are vehicle appearance and long-term value. Similar to *Cluster 2*, customers in this cluster have the same forward-thinking mind. Since they are middle aged, their personal image is still important to them and this has a direct bearing on their choice of vehicle. To these customers, a vehicle may only be an instrument that reflects their status and image, whether it is safe and comfortable during driving may not be the reason for their particular choice.

Ego show-offs: ambitious, driven. Seeking personal image and self-esteem.

Table 6.24: Description for *Cluster 5 - Ego show-offs*

Cluster 5 - Ego show-offs	
Attributes and customer profile	
Most important	Vehicle long-term value
2nd most important	Vehicle appearance
Least important	Vehicle driving comfort/safety
Age	35-54
Gender in survey (%Male : %Female)	Male dominate
Marital status	Married
Number of children in household	1 or more
Education	mix
Occupation	Technical knowledge and skills e.g. Professional specialty, Executive/Managerial
Income before tax	Band 4 (US$80,001 To US$175,000) or Band 5 (US$175,001 Or Over)
UK classification of social class	A

Importance of Vehicle Handling: the Discriminant Analysis Approach

Using the SPSS TwoStep Clustering method, five customer groups are identified. In general, vehicle handling (in terms of "Vehicle driving comfort/safety" and "Vehicle toughness") is important for the *Squares*, the *Yodas*, the *Comfort-goers* and the *Die Hards*. This is especially true for the *Comfort-goers*, who look for safe trouble-free vehicle for their family; and the *Die Hards*, who look for high performance vehicles to travel on various terrains. From the analysis, *Ego show-offs* have rated vehicle handling the lowest. They are not aware of the importance of handling, because customers have taken safety and comfort features for granted (or simply expect them to be well designed) when they buy expensive stylish vehicles. From the perspective of *Ego show-offs*, the underrated importance of handling no longer adds value to the vehicle, but it becomes an entry requirement for the types of vehicle the *Ego show-offs* buy.

Although the TwoStep Clustering method is able to conclude the types of customer who consider handling an important feature, only 59% of the respondents' data are utilised, see Table 6.9. An alternative method is the use of discriminant analysis, which predicts a model for the dependent variable using various specified independent variables. In this analysis, the dependent variable is the importance ratings of "Ease of handling"; and the independent variables are the seven factors that describe the customers' background throughout this section (i.e. age group, gender, number of children in household, education, total household income before tax, occupation and marital status).

A first look at the data sample reveals that almost 80% of cases are valid for discriminant analysis, Table 6.25. Initial results from discriminant analysis also show that the seven factors have a significant level of 0.00 (<0.1), indicating that they are all significant for the modelling, see Table 6.26.

With the seven independent variables, the discriminant analysis has produced four discriminant functions for the model, see Table 6.27. The first and second functions include over 88% and 10% of the total variance respectively. Their high percentage of variance implies that the model can be explained using only the first two functions. Furthermore, by inspection, Table 6.28 reveals that functions 3 and

Table 6.25: Summary for cases used in discriminant analysis

Unweighted Cases	**N**	**Percent**
Valid	37369	79.99
Excluded	9349	20.01
Total	46718	100.00

Table 6.26: Tests of Equality of Group Means of the six independent variables

	Wilks' Lambda	F	df1	df2	Sig.
Age	1.00	14.55	4	37364	0.00
Gender	0.99	117.41	4	37364	0.00
Number of children in household	1.00	8.25	4	37364	0.00
Education	1.00	10.64	4	37364	0.00
Total household income before tax	1.00	3.55	4	37364	0.01
Occupation	1.00	5.00	4	37364	0.00
Marital status	1.00	5.88	4	37364	0.00

Table 6.27: Eigenvalues for discriminant functions of the "Ease of handling" model

Function	Eigenvalue	% of Variance	Cumulative %	Canonical Correlation
1	0.02	88.48	88.48	0.13
2	0.00	10.16	98.63	0.04
3	0.00	1.12	99.75	0.01
4	0.00	0.25	100.00	0.01

Table 6.28: Wilks' Lamda test for discriminant functions of the "Ease of handling" model

Test of Function(s)	Wilks' Lambda	Chi-square	df	Sig.
1 through 4	0.98	695.57	28	0.00
2 through 4	1.00	80.67	18	0.00
3 through 4	1.00	9.56	10	0.48
4	1.00	1.73	4	0.79

Table 6.29: Rotated structure matrix for the "Ease of handling" model

	Function			
	1	**2**	**3**	**4**
Gender	0.92	-0.16	-0.05	0.00
Age	0.02	0.79	0.11	0.15
Marital status	0.24	-0.67	0.12	-0.01
Education	-0.05	-0.01	0.96	0.12
Total household income before tax	-0.06	0.23	0.07	0.55
Number of children in household	0.23	0.34	0.22	-0.55
Occupation	0.15	0.05	0.15	0.38

4 are insignificant to the modelling (significant level, Sig.$>$ 0.1). This indicates that functions 1 and 2 are the two key modelling functions.

With the discriminant analysis, the correlation between the four discriminant functions and the seven independent variables are determined and presented in the form of a structure matrix. To simplify the structure matrix, it is rotated using the varimax rotation. The rotated solution is shown in Table 6.29 and it reveals the discriminant loadings for each variable on the four functions. For the first function,

Table 6.30: Classification results for the "Ease of handling" model"

			Predicted Group Membership					
			Extremely Important	**Very Important**	**Somewhat Important**	**Not Very Important**	**Not At All Important**	**Total**
Original	**Count**	**Extremely Important**	6698	2621	3714	1845	3209	18087
		Very Important	4423	2413	3739	1560	2698	14833
		Somewhat Important	962	571	1162	504	768	3967
		Not Very Important	71	33	86	54	67	311
		Not At All Important	35	18	32	33	53	171
		Ungrouped cases	274	183	178	61	127	823
	%	**Extremely Important**	37.03	14.49	20.53	10.20	17.74	100
		Very Important	29.82	16.27	25.21	10.52	18.19	100
		Somewhat Important	24.25	14.39	29.29	12.70	19.36	100
		Not Very Important	22.83	10.61	27.65	17.36	21.54	100
		Not At All Important	20.47	10.53	18.71	19.30	30.99	100
		Ungrouped cases	33.29	22.24	21.63	7.41	15.43	100

27.8% of original grouped cases correctly classified.

"Gender" is the only one that is heavily loaded and therefore this function is labelled "Gender". For the second function, the absolute loadings for "Age" and "Marital status" are both large, so it is named the "Stage of life".

Having plotted and interpreted the map, it is important to see how well the model predicts. Table 6.30 shows the classification results for the comparison between the original and the predicted data. It shows that 27% of original cases are correctly predicted using the model. This percentage accuracy, however, does not satisfy the maximum chance criterion, 60% (i.e. multiply the maximum importance rating likelihood, "Extremely important" 47%, by 1.25 tolerance, $60\% = 47\% \times 1.25$). Although the proposed model does not pass the statistical criterion, the results are consistent with those obtained from the SPSS TwoStep Clustering method. Examining the components of the classification results, "Extremely Important" is the most accurately predicted (37% correctly predicted) while "Very Important" is the least (16% correctly predicted). This inaccuracy of the model means that the importance of handling is not a discriminating variable based on the independent variables used here, and more discriminating independent variables may exist probably based around factors other than demographics. Improvements can be made by including these better variables and also being more specific with the segments in the study.

To conclude, vehicle handling is rated more important if a customer satisfies one or more of the following criteria: 1) is female, 2) is in a latter stage of life (i.e. older), 3) is married, 4) is a Comfort-goer, or 5) is a Die Hard. If a customer does not have any of these criteria, marketing with emphasis on the handling technology and its benefit may not be effective to sales.

6.4.3 Customer Perceptions of Brands

In the last section, five segments based on the customers' demographic details and psychographic characteristics were identified. Their importance on the customers' purchase reasons, especially vehicle handling, were discussed. This section explores the relative importance of the purchase decisions from the perspective of customers, and associates their decisions with their vehicle choice. This study assumes a straight-forward relationship between the purchase decision ratings and the purchased vehicle. In other words, importance ratings given by customers reflect their attitude towards the vehicle of their choice.

Using discriminant analysis on different brands of vehicle a model for customers' choice is predicted. Customer profiling for a particular brand is a complex procedure. It involves judgement and weighing of different vehicle attributes and features. Moreover, decision making is also influenced by an individual's background and stage of life. In this study the model is based upon two sets of independent variables, customers' background and customers' purchase decision. The former set is similar to the one used in the previous TwoStep analysis, see Table 6.31, and the latter set is taken from the latent factor identified previously in Section 6.4.1. Note that the sign has reversed for this study so results are more easily interpreted. Hence, the more positive the value is the more important the purchase decision is.

With the dependent variable in brands and independent variables based on customers' background and latent factors, discriminant analysis shows that 60% of data are valid in this study, Table 6.32.

With the independent variables, the equality group mean tests, Table 6.33, have

Table 6.31: Definition for independent variables in NVES_US

Independent variable	Definition	
Age	0 - 100	
Total household income before tax	1 - 10,000 or less	30 - over 500,000
Family size	1 - 0 or none	7 - 6 or more
Education	1- no education	9 - post grad
Gender	1- Male	2 - Female

Table 6.32: Summary for the cases involve in the study of brand discriminant analysis

Unweighted Cases	N	Percent
Valid	27814	59.54
Excluded	18904	40.46
Total	46718	100.00

Table 6.33: Tests of Equality of Group Means of the six independent variables

	Wilks' Lambda	F	df1	df2	Sig.
Vehicle driving comfort/safety	0.94	46.50	36	27777	0.00
Vehicle toughness	0.90	81.63	36	27777	0.00
Vehicle appearance	0.92	71.21	36	27777	0.00
Vehicle performance	0.98	18.04	36	27777	0.00
Vehicle interior comfort	0.91	74.13	36	27777	0.00
Vehicle long-term value	0.92	64.18	36	27777	0.00
Vehicle customisation	0.96	35.35	36	27777	0.00
Customer experience	0.91	76.67	36	27777	0.00
Intended positioning	0.95	37.71	36	27777	0.00
Vehicle reliability	0.95	37.41	36	27777	0.00
Age	0.93	59.60	36	27777	0.00
Gender	0.98	18.71	36	27777	0.00
Family size	0.99	9.43	36	27777	0.00
Education	0.93	60.35	36	27777	0.00
Total household income before tax	0.82	166.40	36	27777	0.00

shown that all variables are significant in discriminating the brands. The F-value in the Table shows the discriminating power of individual variables. "Total household income before tax (IBT)" has the highest discriminating power of 166.4, followed by "Vehicle toughness" (81.63) and "Vehicle interior comfort" (74.13); "Vehicle driving comfort/safety", however, only has a F-value of 46.50, position at tenth with the most discriminating power. In other words, the total family income separates the brands more readily than the other variables. Moreover, the table shows that "Vehicle performance", "Gender (SEX)" and "Family size (FAM)" do not offer much influence in discriminating the brands.

To predict the 'best' model for the brand choice, 15 discriminant functions are identified, see Table 6.34. It reveals that Functions 1 to 7 explain just over 95% of the variance, and the remaining 10% is contributed by the rest of the ten functions. In Table 6.35, it shows that all the functions apart from Function 15 have a significance level below 0.1. This suggests that these 14 functions play an important role in the brand discrimination.

From previous eigenvalue and wilks' lambda tests, see Tables 6.33 to 6.35, 15 functions are identified and their correlation are presented in Table F.5. As discussed

Table 6.34: Eigenvalues for the discriminant functions on brand choice

Function	Eigenvalue	% of Variance	Cumulative %	Canonical Correlation
1	0.45	39.79	39.79	0.56
2	0.22	19.87	59.66	0.43
3	0.12	10.95	70.61	0.33
4	0.12	10.50	81.11	0.33
5	0.10	9.04	90.15	0.30
6	0.04	3.93	94.07	0.21
7	0.02	1.79	95.86	0.14
8	0.01	1.21	97.08	0.12
9	0.01	1.00	98.08	0.11
10	0.01	0.74	98.82	0.09
11	0.01	0.47	99.29	0.07
12	0.00	0.30	99.59	0.06
13	0.00	0.21	99.80	0.05
14	0.00	0.11	99.91	0.03
15	0.00	0.09	100.00	0.03

Table 6.35: Wilks' Lamda test for the discriminant functions of brand choice

Test of Function(s)	Wilks' Lambda	Chi-square	df	Sig.
1 through 15	0.36	28041.86	540	0.00
2 through 15	0.53	17730.14	490	0.00
3 through 15	0.65	12105.62	442	0.00
4 through 15	0.73	8867.32	396	0.00
5 through 15	0.81	5754.70	352	0.00
6 through 15	0.90	3053.29	310	0.00
7 through 15	0.94	1848.21	270	0.00
8 through 15	0.95	1291.73	232	0.00
9 through 15	0.97	913.73	196	0.00
10 through 15	0.98	600.61	162	0.00
11 through 15	0.99	368.26	130	0.00
12 through 15	0.99	222.17	100	0.00
13 through 15	1.00	127.67	72	0.00
14 through 15	1.00	62.46	46	0.05
15	1.00	28.89	22	0.15

previously, the first 7 functions explain 95% of the total variance. By identifying the large loadings in each function, the representative variable/s for the particular function can be determined. To make the interpretation easier, the structure matrix in Table F.5 is rotated using the varimax rotation. Table 6.36 shows the first 7 rotated discriminant functions taken from the full rotated structure matrix in Table F.6. The seven functions in Table F.6 are represented by the variable with the highest loading, which is shaded in red. Function 1 is heavily loaded with "Total household income before tax (IBT)" and therefore is labelled "Family income". Function 2 has a strong loading in "Vehicle interior comfort" and so it is labelled "Importance of vehicle comfort".

Table 6.36: Unrotated structure matrix for the discriminant analysis of brand choice, part of Table F.6

	Function						
	1	**2**	**3**	**4**	**5**	**6**	**7**
Total household income before tax	0.97	0.01	-0.01	-0.02	0.00	0.09	0.02
Vehicle interior comfort	0.01	0.96	0.09	0.06	-0.07	-0.10	-0.02
Vehicle toughness	-0.01	0.09	0.97	0.09	-0.05	-0.08	-0.05
Customer experience	-0.02	0.06	0.10	0.96	-0.10	-0.10	0.04
Vehicle appearance	0.00	-0.07	-0.05	-0.10	0.95	0.05	0.04
Vehicle long-term value	0.10	-0.10	-0.08	-0.10	0.05	0.96	0.00
Age	0.02	-0.02	-0.05	0.04	0.04	0.00	0.98
Vehicle driving comfort/safety	0.01	0.14	0.04	0.06	-0.15	-0.09	0.04
Intended positioning	0.01	-0.04	-0.05	-0.09	0.09	0.07	0.07
Vehicle reliability	0.00	0.11	-0.02	0.06	-0.08	-0.10	-0.02
Education	0.15	0.00	-0.04	-0.04	0.05	0.03	-0.01
Vehicle customisation	0.04	-0.09	-0.16	-0.09	0.11	0.07	0.04
Vehicle performance	0.00	0.10	0.07	0.13	-0.15	-0.09	0.01
Gender	-0.05	0.03	0.02	-0.02	-0.01	-0.06	-0.11
Family size	0.12	0.06	0.03	0.00	0.01	0.01	-0.13

Using Functions 1 and 2 from the rotated structure matrix, Table 6.36, a customer perceptual map can be constructed, see Figure 6.7. The position for each brand in the map is a measure of its own centroid per average dollar. This is done because price of vehicle varies from brand to brand. Apart from the two main axes, "Family income" and "Importance of vehicle comfort", other independent variables are also added into the map as a vector to show their relative importance to each brand. In the map, the blue terms represent the latent factors and the red terms indicate the customer background. By comparing the direction of the vectors, the relative importance of the attributes can be determined. The map shows that "Vehicle appearance", "Vehicle long-term value", "Vehicle customisation" and "Intended positioning" are in the opposite direction to the rest. This suggests that customers who weigh high for these purchase decisions are likely to score low for the others.

As assumed previously, the perception of a customer towards a particular purchase decision (i.e. their judgement on the importance of different vehicle attributes) leads to his/her final choice of brand. Therefore, it must be noted that a high or low importance rating does not necessarily mean a brand fails or excels in delivering a particular attribute to customers; rather, it shows the awareness and importance placed by customers on a particular brand purchase decision. For example, in Figure 6.7, when comparing the vehicle comfort importance scoring for Jaguar and Land Rover, the more negative value of Jaguar does not mean that Jaguar is less comfortable than Land Rover. It only means the awareness and needs of Jaguar customers for vehicle comfort are lower than that of Land Rover. One reason for this is due

to the off-road and multi-terrain drivability of Land Rover. Moreover, the map is also used for brand comparison in terms of different vehicle attributes. Take Kia and Jaguar for example, Kia has a higher rating in "Gender (SEX)" than Jaguar, implying Kia has more female customers.

In order to determine the relation of a brand to an independent variable, a line perpendicular to the vector of the variable is drawn from the brand centroid. As shown in Figure 6.7, a perpendicular line to the "vehicle customisation" is drawn from both Jaguar and Mercedes. Inspecting the interception of the lines, Jaguar has a higher importance score than Mercedes. This suggests that Jaguar customers are more aware of the ability to customise than Mercedes customers.

By Inspecting the perceptual map, Figure 6.7, one can see an obvious discrimination of brands to the right. This group of brands belongs to the luxury car segment, which includes Mercedes, BMW, Jaguar, Audi and Lexus. This luxury segment is positioned in the upper spectrum of the family income when compared with other brands such as Ford, Honda and Suzuki. Buyers from this luxury car segment are older and also more highly educated. In addition, they are more aware of the vehicle's long-term value and their own personal feeling (i.e. prestigiousness of vehicle). On the other hand, they do not put too much emphasis on vehicle comfort, toughness and previous experience.

While the right hand side of the perceptual map is occupied by the luxury brands, the far left of the map is mainly populated with the Asian brands, such as Suzuki, Kia and Isuzu. Customers of these brands are generally younger and less wealthy in their household. They are most likely to be single with a high demand for vehicle performance and toughness.

Apart from these two segments, another interesting observation is the country of origin of the brands. In general, the European makes are located in the south-east of the map while the American and Asian (A&A) makes are positioned in the north-west of the map. Their locations suggest that the A&A makes have younger audiences, who emphasise the importance of vehicle performance, toughness and interior comfort; and the European makes have older but more successful customers, who rate technical aspects less important and place a greater emphasis on appearance, their intended positioning and value of the vehicle.

To summarise, this Section has predicted a model for the customer brand choice according to the latent factors and customers' background. A customer importance perceptual map for the American auto-market is presented

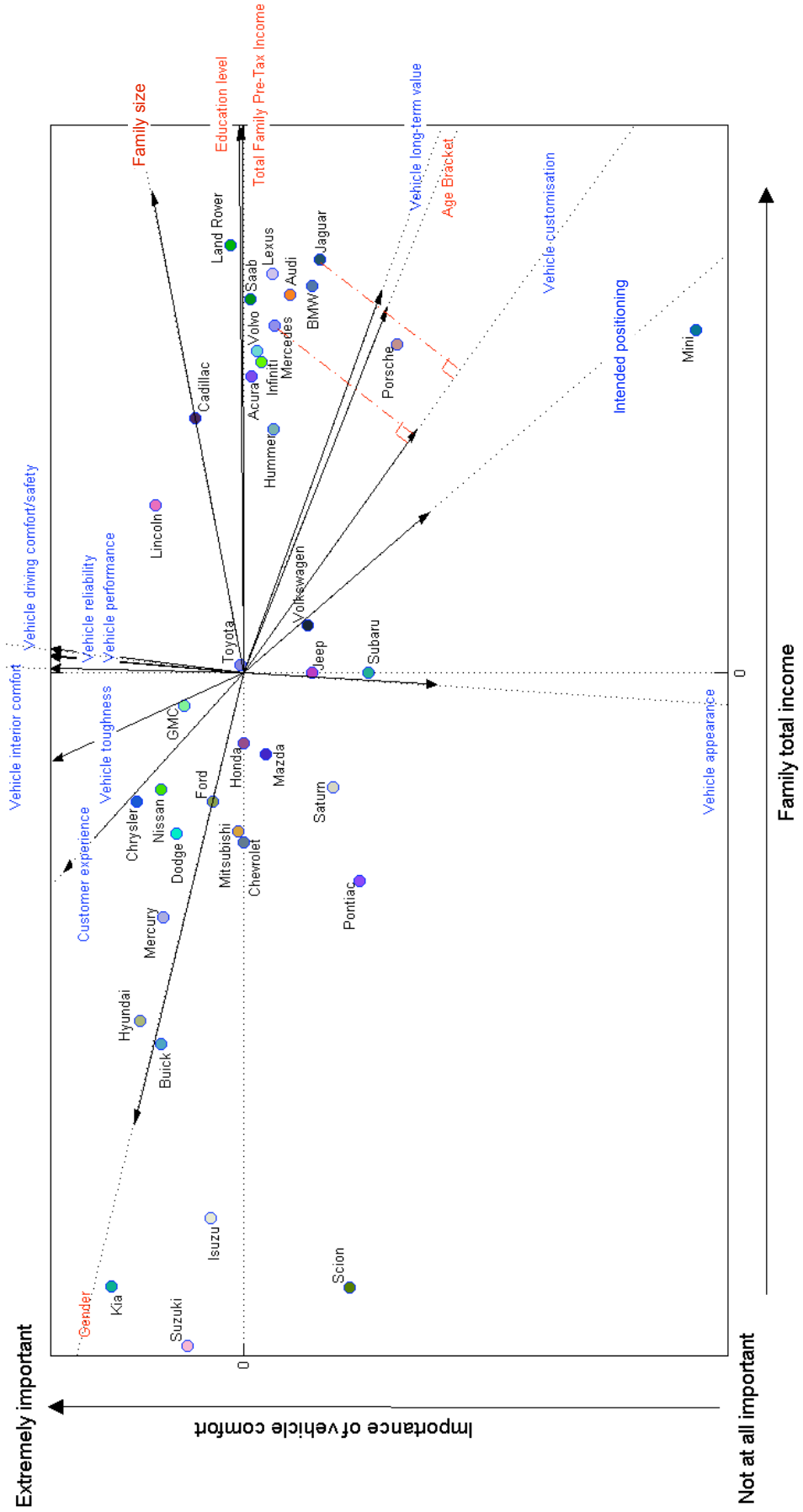

Figure 6.7: Perceptual map of customer perceptions on brand in a per US$ scale

and Table F.7 shows the classification of the accuracy for this model with the original data. The hit ratio for the original cases was 13.2%. Although small, this value is above the maximum chance criterion, 10.1% (calculated from maximum brand choice likelihood from the NVES_US, Nissan 8.1%, multiplied by 25% tolerance = 8.1% × 1.25). This suggests that the independent variables are sufficient to discriminate the brand choice of respondents in the NVES_US. This is especially true for respondents who have purchased Jaguar and Land Rover, which has a hit ratio of over 60% and 56% respectively. However, other independent variables may be needed to properly discriminate brands such as Chervolet and Ford (hit ratio of 1.7% and 3.4% respectively).

The UK Automotive Market

Using the NCBS_UK conducted in year 2007, the relative importance of customers' reasons of purchase are studied.

6.4.4 The British Perspective on Purchase Criteria

In the survey, the part that is relevant to this study is a qualitative open ended question,

> "D3: For what reasons did you buy this particular new car rather than some other one?"

Respondents are required to give one or more reasons for their choice of vehicle. It is assumed that the first reason mentioned by any customer in this question is the most representative and/or most important reason for their vehicle choice. Figure 6.8 shows a summary for the purchase reasons first mentioned; the second and third reason mentioned are included in the appendix, Figures F.6 and F.7.

In the survey, 33,818 respondents give at least one reason of purchase, 23,277 respondents give at least two and 15,530 respondents give three or more. In addition, it is recorded that only 88 respondents give 10 reasons. This indicates that customers may tend to view vehicle purchase holistically rather than analytically; they may not necessarily have a list of vehicle attributes to 'tick-off' when they choose a vehicle.

From Figure 6.8, we can see a high proportion of customers (28.6%) giving "Always Buy the Same" as their first reason of purchase. This reason has a percentage that is more than twice that of the second reason, "Exterior Styling/Appearance" (12%). The third and forth reasons, 'Reputation' and 'Price', have similar proportions of 5.3% and 5.2% respectively.

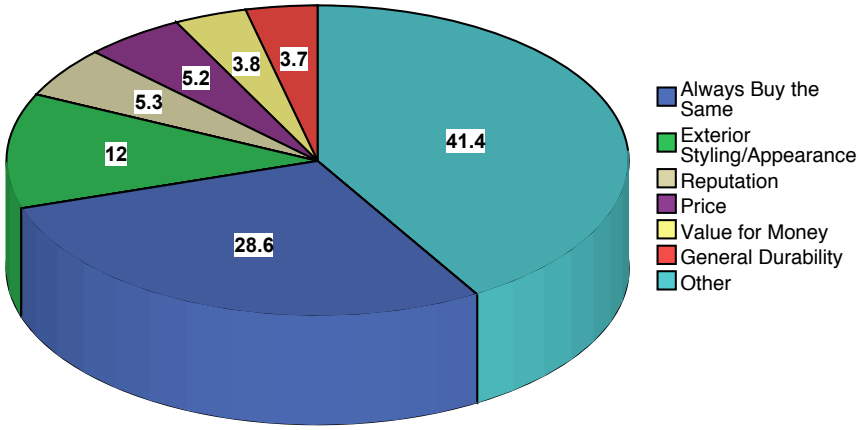

Figure 6.8: Reason of purchase (1st mention) for NCBS_UK

On the pie chart on the second mentioned reason of purchase, Figure F.6, "Exterior Styling/Appearance" has gained first place with 10.4% while "Always Buy the Same" drops to 4th place with 4.3% of respondents. The second and third places are occupied by "General Durability" and "Price", with 5.2% and 5% of the respondents respectively. In Figure F.7, the third mentioned reason of purchase, "Exterior Styling/Appearance" remains the top reason with 8.8% respondents and is followed by "Equipment/Equipment level" (5.2%). "Price" and "General Durability" remain in the same order with similar proportions of 5% and 4.8% respectively. "Always Buy the Same", however, only has 3.1% of respondents. For the first 3 reasons mentioned, see Table 6.37, the most mentioned reason is "Always Buy the Same", which has 11,154 respondents, nearly one third of all the respondents in the survey. From Table 6.37, the second most mentioned reason is "Exterior Styling/Appearance" and then "Price" and "General Durability", with "Equipment/Equipment level" only in sixth position.

Apart from the top reasons identified from each pie chart, a proportion of 40% or more also exists in each case representing "Other", with 70 plus purchase reasons. These reasons can be found in Tables F.8 and F.9. As it is difficult and inefficient to analyse such a large set of purchase reasons, they are categorised in terms of the latent factors as defined previously for the NVES_US, see Table 6.8. Table F.8 and F.9 show the results for this categorisation. Notice that two new categories are created: "Purchase convenience" and "Vehicle short-term value". "Purchase convenience" refers to the dealers, delivery time and types of payment; and "Vehicle short-term value" refers to the cost in tax and insurance, and the current economic climate.

Table 6.37: Total number of respondents mentioned for the first 3 reasons

		1st mention	2nd mention	3rd mention	Total mention
Total number of respondents		33818	23277	15530	
Always Buy the Same	%	28.6	4.3	3.1	
	N	9672	1001	481	11154
Exterior Styling/Appearance	%	12	10.4	8.8	
	N	4058	2421	1367	7846
Price	%	5.2	5	5	
	N	1759	1164	777	3699
General Durability	%	3.7	5.2	4.8	
	N	1251	1210	745	3207
Reputation	%	5.3	3.6	3.3	
	N	1792	838	512	3143
Equipment/Equipment level	%	1.3	4.1	5.2	
	N	440	954	808	2202

6.4.5 Customer Segmentation

In order to understand the vehicle attributes that affect a customer purchase choice, customers who have similar reasons for purchase are segmented in terms of the latent factors as defined in Tables F.8 and F.9. To perform the segmentation, a discriminant analysis is carried out, with the dependent variable as "The reason of purchase (1st mentioned)" and the independent variables as the age, gender, education, total family income before tax, family size and the total number of children in household of the respondents. The definition for these variables are given in Table 6.38.

Apart from the influence of customers' background, purchase decision is also affected by their daily driving behaviour, and expected distance of travel. As a result, another 18 factors are added to the original list of independent variables. These additional factors are given in Table 6.39, in which the expected distance of travel is a numerical metric value while the others are rated from 1 ("Almost everyday") to 5 ("Never/Not applicable").

The methodology for this section is the same as that for the previous study of

Table 6.38: Definition for independent variables in NCBS_UK

Age	0 - 100
Family size	0 – 9
Number of children in household	0 – 9
Gender	1:Male – 2:Female
Education	1:Secondary school without qualification – 5:University (higher degree)
Total household income before tax	1:Under 10,000 – 15:150,000 or more

Table 6.39: Additional independent variables for the discriminant analysis of the purchase decision in NCBS_UK

Distance expected to travel
Motorway driving
Out of town driving
Driving in town/city
Commuting to and from work
Business purposes
Shopping
Taking children to school
Towing a trailer/caravan
Carrying a passenger in the front of the car
Carrying adults in the back
Carrying children in the back
Carrying at least 3 people in the back
Carrying large items, luggage, sports equipment, etc. inside the car/boot
Carrying items on a roof rack
With the rear seat(s) folded down
Weekend trips
Holidays

Table 6.40: Summary for the cases involved in the study of brand discriminant analysis

Unweighted Cases	**N**	**Percent**
Valid	14574	40.21
Excluded	21670	59.79
Total	36244	100.00

the NVES_US. By utilising the 24 independent variables (customers' background information plus their driving behaviour, Tables 6.38 and 6.39), Table 6.41 shows that all variables are significant for describing a model for purchase reasons. From Table 6.41, "Age (AGE)" has the highest discriminating power (37.09), followed by "Commuting to and from Work" (19.23) and "Total household income before tax (IBT)" (12.61). This suggests that age, driving distance and income have a great effect on the purchase reason model, while holidays and transportation of goods/people do not have much influence on the model. In other words, the purchase reasons given by respondents are more influential by variables with a high discriminating power.

Using a step-wise method, eight functions entered the model. Table 6.42 reveals that the first and second functions contribute 47.22% and 24.67% of variance to the overall model respectively. But only 3.24% ($0.18^2 \times 100$) of variance in the dependent variable (purchase reason first mentioned) are accounted for by the first function of this model. Further investigation with the Wilks' Lambda test, Table 6.43, shows that only the first 6 discriminant functions have a significant level (Sig.) below 0.1,

Table 6.41: Tests of Equality of Group Means of the independent variables for purchase reason modelling

	Wilks' Lambda	F	df1	df2	Sig.
Total household income before tax	0.99	12.61	11	14,566	0.00
Number of children in household	0.99	10.83	11	14,566	0.00
Age	0.97	37.09	11	14,566	0.00
Family size	0.99	11.18	11	14,566	0.00
Gender	0.99	11.20	11	14,566	0.00
Education	0.99	9.25	11	14,566	0.00
Expected Miles, Next 12 Months	0.99	8.88	11	14,566	0.00
Motorway Driving	0.99	8.18	11	14,566	0.00
Out of Town Driving	1.00	2.80	11	14,566	0.00
Driving in Town/City	1.00	3.12	11	14,566	0.00
Commuting to and from Work	0.99	19.23	11	14,566	0.00
For Business Purposes	1.00	5.33	11	14,566	0.00
For Shopping	1.00	6.18	11	14,566	0.00
Taking Children to School	1.00	4.38	11	14,566	0.00
Towing A Trailer/Caravan	1.00	4.05	11	14,566	0.00
Carrying a Passenger in the Front	1.00	2.19	11	14,566	0.01
Carrying Adults in the Back	1.00	2.05	11	14,566	0.02
Carrying Children in the Back	1.00	5.44	11	14,566	0.00
Carrying 3+ People in the Back	1.00	3.40	11	14,566	0.00
Carrying Large Items in Car/Boot	1.00	5.95	11	14,566	0.00
Carrying Items on a Roof Rack	1.00	1.96	11	14,566	0.03
With the Rear Seat(s) Folded Down	0.99	6.88	11	14,566	0.00
Week-End Trips	1.00	1.94	11	14,566	0.03
Holidays	1.00	4.02	11	14,566	0.00

Table 6.42: Eigenvalues for the discriminant functions of the NCBS_UK purchase reason

Function	Eigenvalue	%Var	%Cum	Canonical Correlation
1	0.03	47.22	47.22	0.18
2	0.02	24.67	71.89	0.13
3	0.01	13.82	85.71	0.10
4	0.00	6.73	92.44	0.07
5	0.00	4.19	96.63	0.05
6	0.00	1.92	98.55	0.04
7	0.00	1.15	99.70	0.03
8	0.00	0.30	100.00	0.01

implying that Functions 7 and 8 are insignificant in the modelling.

Examining the unrotated structure matrix, Table F.10, Function 1 is loaded strongly by "Age (AGE)" and "Commuting to and from work" while Function 2 is heavily loaded by "Total household income before tax (IBT)" and "Gender (SEX)". Using the varimax rotation method, the rotated structure matrix, Table F.11 shows eight functions with loadings. An abstract of this rotated structure matrix is given in Table 6.44. The rotated Function 1 has a large discriminant loading on "Age

Table 6.43: Wilks' Lamda test for the discriminant functions of the NCBS_UK purchase reason

Test of Function(s)	Wilks' Lambda	Chi-square	df	Sig.
1 through 8	0.93	1004.77	88	0.00
2 through 8	0.96	532.95	70	0.00
3 through 8	0.98	284.52	54	0.00
4 through 8	0.99	144.88	40	0.00
5 through 8	0.99	76.71	28	0.00
6 through 8	1.00	34.24	18	0.01
7 through 8	1.00	14.74	10	0.14
8	1.00	3.05	4	0.55

Table 6.44: Rotated Structure Matrix for the discriminant analysis of purchase reason in NCBS_UK, detail table please refer to Table F.11

	Function					
	1	**2**	**3**	**4**	**5**	**6**
Total household income before tax	0.93	0.00	-0.01	-0.15	-0.10	-0.10
Gender	0.03	0.98	0.04	0.09	-0.11	-0.01
With the Rear Seat(s) Folded Down	0.00	-0.01	0.97	0.13	-0.04	0.00
Expected Miles, Next 12 Months	0.02	-0.01	0.02	-0.99	-0.05	-0.07
Age	-0.11	-0.10	-0.04	0.10	0.88	0.04
For Business Purposes	-0.09	0.00	0.00	0.29	0.03	0.92
Commuting to and from Work	-0.11	-0.05	-0.03	0.22	0.18	0.11
Carrying Adults in the Back	-0.02	-0.02	0.01	0.08	0.05	0.04
Carrying 3+ People in the Back	0.01	-0.01	0.03	0.08	0.02	0.02
Carrying Large Items in Car/Boot	-0.01	-0.01	0.13	0.19	0.00	0.03
Education	0.14	0.03	-0.04	-0.11	-0.07	-0.06
Carrying Items on a Roof Rack	-0.05	-0.01	0.04	0.03	0.04	0.00
Family size	0.15	-0.08	0.00	-0.02	-0.02	-0.01

(AGE)" and is therefore labelled "Life stage". The rotated Function 2 has a strong loading on "Gender (SEX)", so it is labelled "Gender mix". Notice that some of the variables in the structure matrix (both unrotated and rotated) are marked 'not used in the analysis'. This is due to their high correlation with other variables.

For the customer perceptual map, each purchase reason is averaged to produce a centroid, see Figure 6.9. The two main axes are described by "Life stage" on the horizontal and "Gender mix" on the vertical. The centroids of the 12 purchase reasons and the vectors of independent variables are plotted on the map according to the data found in Table 6.44. The red labels represent the customer background variables and the blue labels represent the driving behaviour variables. The length of the vectors are scaled with the F-values in Table 6.41, which indicate their discrimination power. It must be pointed out that the vectors of the driving behaviour variables are reversed in direction so they are now pointing towards an increasing

frequency. Four circles are also drawn on the map, they represent the four clusters of people who share similar reasons, and their sizes are proportional to the total number of respondents with the purchase reasons.

Cluster 1 (Conservatives) from the map is the most populated (17,467 respondents in total, i.s. 48%). It is composed of mature respondents with a moderate number of female customers. Respondents in this group also commute less and drive less. They tend to have fewer children in their house with a lower family income. Customers in *Cluster 1* seem to be more loyal to a brand and they are more reluctant to change to a different vehicle make. They tend to buy vehicles according to their previous experience and consider their purchase in terms of interior comfort. In short, *Cluster 1* is highly sensitive to what they buy and also more economically minded than others.

Cluster 2 (Investors) is made up of younger respondents, who commute frequently to work with a moderate income. The ratio of male to female is quite balanced with children in the family. This cluster has a total of 12,078 respondents (34%), they tend to be concerned with the value of the vehicle as well as its styling. Respondents in this cluster are forward looking with a future vision. They are also more aware of the vehicle's resale value, security, trade-in price, etc.

Cluster 3 (Perfectionists) contains a total of 4,452 respondents (12%), who have a high income but do less travelling to and from work. Despite their low mileage in getting to work, their expected mileage for the next 12 months remains high. This cluster has a high proportion of males who are average aged in the survey (50-55) with family members and children above average. During a purchase, respondents' decisions are made based on the vehicle specifications as well as reliability. Moreover, they also seem to have more affection towards vehicles, as they see them as something that can reflect themselves and their life. Customers in this cluster are complicated thinkers. They are conscious about their own feelings and self-image, and at the same time, also concerned with the details of the vehicle that they are going to buy. They tend to look for the perfect vehicle for themselves.

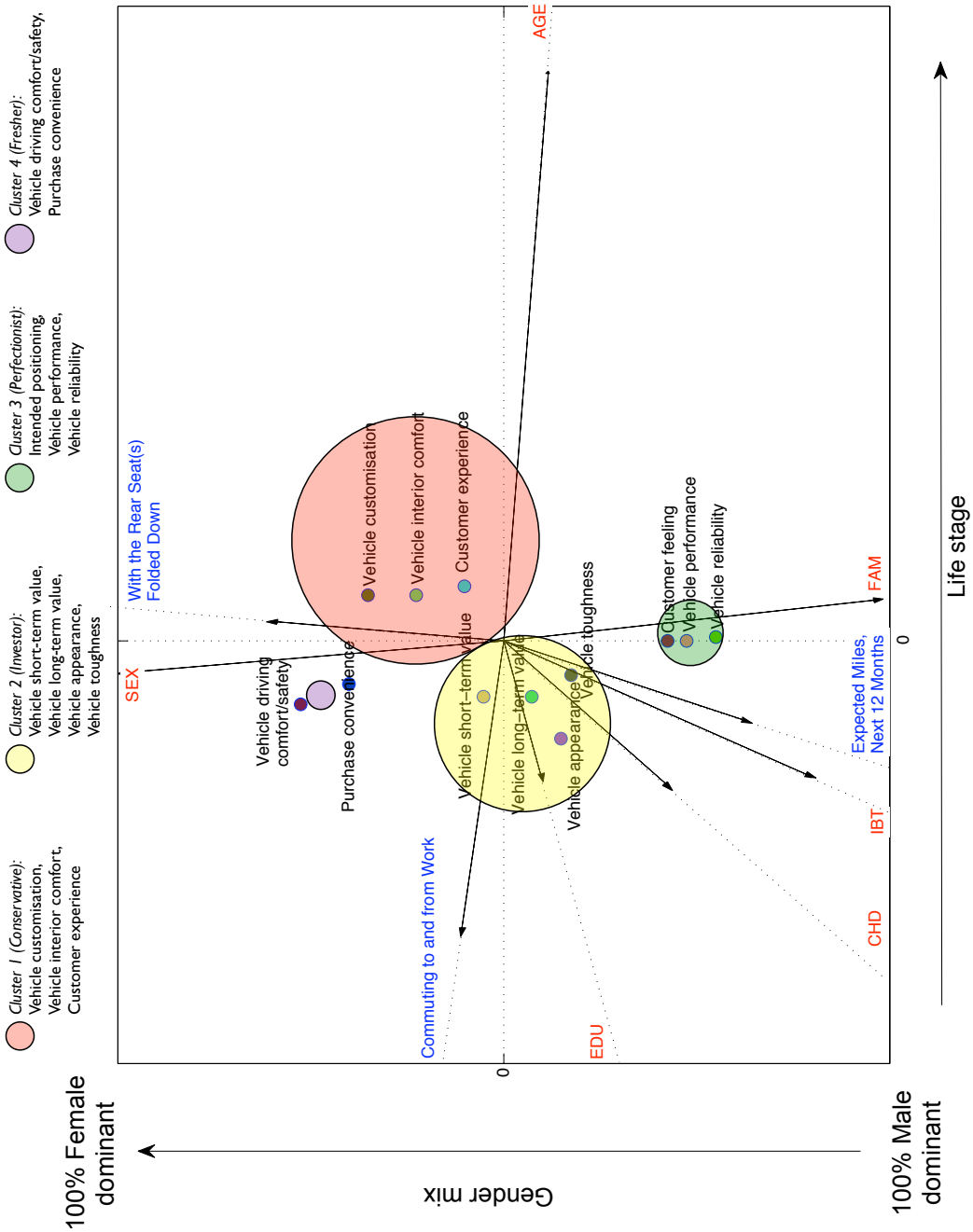

Figure 6.9: Perceptual map of respondents in NCBS_UK on reasons of purchase

Cluster 4 (Freshers) has the smallest number of respondents, about 2,011 respondents (6%). This segment has a high female-to-male ratio. Respondents in this cluster have a lower income and fewer members in the family. They are also young with an average level education. Customers in this segment therefore are likely to be single fresh graduates from schools/universities. Their purchase reasons for driving comfort and safety may also imply that they are new drivers who lack experience in driving. In addition, the map shows that *Cluster 4* respondents tend to look for convenience and simplicity of purchase. They, generally, want things to happen in a fast and simple manner, without delay and extra tasks.

Purchase reasons that are related to vehicle handling are categorised under "Vehicle driving comfort/safety" and "Vehicle toughness". These two categories can be found in the cluster of *Investors* or *Freshers*, in which respondents of these two segments are younger with a longer distance to commute to work. The respondents of *Investors* and *Freshers*, however, differ in their family size, income and gender ratio. Together, the total number of respondents in *Investors* and *Freshers* is 14089. This value, however, is still smaller than that of the *Conservatives*, which indicates that customers in the UK are more reluctant to experience technological change and tend to purchase a vehicle according to their past experience. But in a positive perspective, customers in the *Conservatives* are more loyal to their brand and less likely to switch to another make.

The fitness of the model is examined through the classification matrix, Table F.12. As shown, the hit ratio for this analysis sample is 10.1%, which is lower than the maximum chance criterion (33.9% of "Customer experience"). The low hit ratio of the model suggests that the independent variables are not sufficient and other variables may be required to more accurately discriminate purchase reasons.

6.4.6 Customer Perceptions of Brands

This section provides a model for the respondents' brand choice according to their purchase reasons, background and driving behaviour. Since the purchase reasons given in the NCBS_UK are non-metric qualitative data, they cannot be used as one of the independent variable in discriminant analysis. Therefore, a perceptual map of brand choice with customers' background and driving behaviour (same independent variables as previous study) is first constructed with discriminant analysis. Then the four customers' segments, namely the *Conservatives*, *Investors*, *Perfectionist* and *Freshers*, are superimposed onto the map with brand choice to interpret the

relationship between the purchase reasons and the brand choice. As the independent variables are the same as those in the last section, the number of valid cases for this study is the same previous, see Table 6.40.

In the equality tests for the independent variables, Table 6.45, results show that most variables are significant, especially the "Total household income before tax (IBT)" and "Gender (SEX)" which are the two with the largest F-values at 95.71 and 38.94 respectively. For the driving behaviour, the "Expected Miles, Next 12 Months", "For Business Purposes" and "With the Rear Seat(s) Folded Down" also have large F-values.

A step-wise approach has confirmed the use of 13 functions, in which the first function explains 26.01% ($0.51^2 \times 100\%$) of the variance of the dependent variable and accounts for 61.26% of the variance of the model, see Table 6.46. For the first five functions alone, they have already explained over 90% of the variance of the model. The insignificance of Functions 11, 12 and 13 which have a significant level (Sig.) over 0.1 is further shown in Table 6.47.

Inspecting the discriminant loadings in the unrotated structure matrix, Table

Table 6.45: Tests of Equality of Group Means of the independent variables for brand choice modeling

	Wilks' Lambda	F	df1	df2	Sig.
Total household income before tax	0.84	95.71	30	14642	0.00
Total number of children in household	0.99	5.11	30	14642	0.00
Age	0.95	25.41	30	14642	0.00
Family size	0.99	4.69	30	14642	0.00
Gender	0.93	38.94	30	14642	0.00
Education	0.97	16.56	30	14642	0.00
Expected Miles, Next 12 Months	0.95	25.79	30	14642	0.00
Motorway Driving	0.96	18.48	30	14642	0.00
Out of Town Driving	0.98	7.74	30	14642	0.00
Driving in Town/City	1.00	1.85	30	14642	0.00
Commuting to and from Work	0.98	11.43	30	14642	0.00
For Business Purposes	0.95	24.14	30	14642	0.00
For Shopping	0.98	8.25	30	14642	0.00
Taking Children to School	0.99	2.50	30	14642	0.00
Towing A Trailer/Caravan	0.99	5.83	30	14642	0.00
Carrying a Passenger in the Front	0.99	3.36	30	14642	0.00
Carrying Adults in the Back	0.98	12.43	30	14642	0.00
Carrying Children in the Back	0.99	3.44	30	14642	0.00
Carrying 3+ People in the Back	0.97	14.24	30	14642	0.00
Carrying Large Items in Car/Boot	0.97	14.73	30	14642	0.00
Carrying Items on a Roof Rack	0.98	9.13	30	14642	0.00
With the Rear Seat(s) Folded Down	0.95	23.19	30	14642	0.00
Week-End Trips	0.98	8.23	30	14642	0.00
Holidays	0.98	11.84	30	14642	0.00

Table 6.46: Eigenvalues for the discriminant functions of brand choice in UK

Function	Eigenvalue	%Var	%Cum	Canonical Correlation
1	0.35	61.25	61.25	0.51
2	0.08	13.42	74.67	0.27
3	0.04	7.64	82.31	0.21
4	0.04	6.80	89.11	0.19
5	0.02	3.24	92.35	0.14
6	0.01	2.55	94.90	0.12
7	0.01	1.71	96.61	0.10
8	0.01	1.27	97.88	0.09
9	0.00	0.74	98.62	0.07
10	0.00	0.51	99.13	0.05
11	0.00	0.42	99.55	0.05
12	0.00	0.28	99.83	0.04
13	0.00	0.17	100.00	0.03

Table 6.47: Wilks' Lamda test for the discriminant functions of brand choice in UK

Test of Function(s)	Wilks' Lambda	Chi-square	df	Sig.
1 through 13	0.59	7609.92	390	0.00
2 through 13	0.80	3191.34	348	0.00
3 through 13	0.87	2102.65	308	0.00
4 through 13	0.90	1473.36	270	0.00
5 through 13	0.94	911.38	234	0.00
6 through 13	0.96	640.95	200	0.00
7 through 13	0.97	428.19	168	0.00
8 through 13	0.98	285.10	138	0.00
9 through 13	0.99	178.44	110	0.00
10 through 13	0.99	116.01	84	0.01
11 through 13	1.00	73.22	60	0.12
12 through 13	1.00	37.90	38	0.47
13	1.00	13.96	18	0.73

F.13, Function 1 is loaded strongly in "Total household income before tax (IBT)" and "Gender (SEX)", and Function 2 in "Age (AGE)" and "Total household income before tax (IBT)". Similar to previous analysis, a few independent variables are ignored as they are similar to other variables and may results in multicollinearity issues. Again, as in previous studies, the unrotated matrix is rotated with the varimax rotation approach, see Table 6.48.

As shown in the rotated structure matrix, Table 6.48, the discriminant loading of "Total household income before tax (IBT)" is the largest in Function 1, so it is labelled "Total family income". In Function 2, the discriminant loading in "Gender (SEX)" is the strongest therefore it is labelled "Gender mix".

As price of vehicle varies a lot between brands, the perceptual map is constructed using the per sterling approach to reduce the effect of vehicle price on the brand choice model. This approach is carried out by dividing each brand's centroid by its

Table 6.48: Rotated Structure Matrix for the discriminant analysis of brand choice in UK, detail matrix please refer to Table F.14

	Function					
	1	**2**	**3**	**4**	**5**	**6**
Total household income before tax	0.93	0.00	-0.01	-0.15	-0.10	-0.10
Gender	0.03	0.98	0.04	0.09	-0.11	-0.01
With the Rear Seat(s) Folded Down	0.00	-0.01	0.97	0.13	-0.04	0.00
Expected Miles, Next 12 Months	0.02	-0.01	0.02	-0.99	-0.05	-0.07
Age	-0.11	-0.10	-0.04	0.10	0.88	0.04
For Business Purposes	-0.09	0.00	0.00	0.29	0.03	0.92
Commuting to and from Work	-0.11	-0.05	-0.03	0.22	0.18	0.11
Carrying Adults in the Back	-0.02	-0.02	0.01	0.08	0.05	0.04
Carrying 3+ People in the Back	0.01	-0.01	0.03	0.08	0.02	0.02
Carrying Large Items in Car/Boot	-0.01	-0.01	0.13	0.19	0.00	0.03
Education	0.14	0.03	-0.04	-0.11	-0.07	-0.06
Carrying Items on a Roof Rack	-0.05	-0.01	0.04	0.03	0.04	0.00
Family size	0.15	-0.08	0.00	-0.02	-0.02	-0.01

average price in the NCBS_UK. On the perceptual map, Figure 6.10, the red labels correspond to the customers' background variables and the blue labels represent the variables of driving behaviour. Apart from the variable "Expected Miles, Next 12 Months", all other driving behaviour variables are reversed (multiply by negative one) so their vectors are also pointing towards an increasing amount of likelihood. The vector length, which is a function of the F-value in Table 6.45, corresponds to the relative importance of the variable to the model.

On the perceptual map the luxury brands (e.g. Mercedes, BMW, Lexus and Jaguar) have been separated away from the rest, occupying the south-east region of the map. This region is defined as above average "Total household income before tax (IBT)" with a greater proportion of male respondents. Amongst all the brands in this region, Lexus is the furthest away from the origin and Volvo is the nearest. As the effect of vehicle price is minimised, the position of Lexus suggests that Lexus buyers have a higher average family income than buyers of other luxury brands.

Another interesting observation are the locations of BMW and Audi, which are both very close to the location of Volvo. This means that the average family income of the BMW and Audi customers are relatively low within the luxury segment. In the same segment, one unexpected candidate is the Subaru brand. Although Subaru does not belong to the luxury car segment, its brand image allows it to attract customers who have an average family income as high as those who buy a luxury vehicle such as Mercedes and Jaguar. However, when comparing this position of Subaru in the UK with that in the US, one can see the difference in customers' buying behaviour and perception in another market (refer to Figure 6.7; Subaru

in the US is merely a vehicle with customers who have an average family income, similar to that of the Toyota in the US). In addition, the luxury brands also tend to attract customers who are more mature with business purposes. On the other side of the luxury brands are the more affordable brands such as Kia, Vauxhall and Ford. These brands are more clustered closer together than the luxury brands along the "Total household income before tax (IBT)" axis, which indicates a smaller variation in customers' average family income among the affordable brands.

In the south-west region on the perceptual map, there are brands such as Mazda, Honda, Skoda and Dodge; and in the north-east region, there are brands such as VW and Mini (From 2002 MY). The SW region is in between the luxury and affordable brands, which has an almost balanced proportion of male to female customers with moderate family income. The NE region, especially the Mini, has a very higher proportion of young female customers with an income comparable to those who buy a BMW or Audi.

As discussed, the four derived clusters from the purchase reasons model are superimposed onto the perceptual map in Figure 6.10 as four circles. The centre of these four circles (clusters) are estimated according to the customers' background, namely "Gender (SEX)", "Total household income before tax (IBT)", "Age (AGE)" and "Family size (FAM)", and their size are scaled in proportion to the total number of respondents in each cluster. As shown on the map, *Conservatives* is located in the north-west with the affordable makes while *Perfectionists* is situated in the south-east covering the luxury segment. In between the two clusters are *Investors* and in the far north-west corner *Freshers*. As a reminder, each cluster contains purchase reasons that are given by a similar group of respondents. By knowing the position of a brand on the map, the nearest cluster provides a potential marketing opportunity to attract new customers who have similar backgrounds. For example on the perceptual map, Jaguar is in a position where customers are mainly mature males with high family income. This location is close to the *Perfectionist* segment, implying Jaguar's potential customers are those who purchase vehicles based on performance, reliability and the customers' own intended positioning of the brand. Marketers and designers of Jaguar, therefore, should see this as an opportunity and focus on these three reasons.

Finally, the perceptual map presented here is based on the brand choice model with the pre-specified independent variables. The classification for this model is given in Table F.15, which has a hit ratio of 5.6%. When this percentage is compared with the maximum chance criterion, 12.17% (from Honda, $9.7\% \times 1.25 = 12.17\%$), it suggests that other independent variables may exist which can discriminate

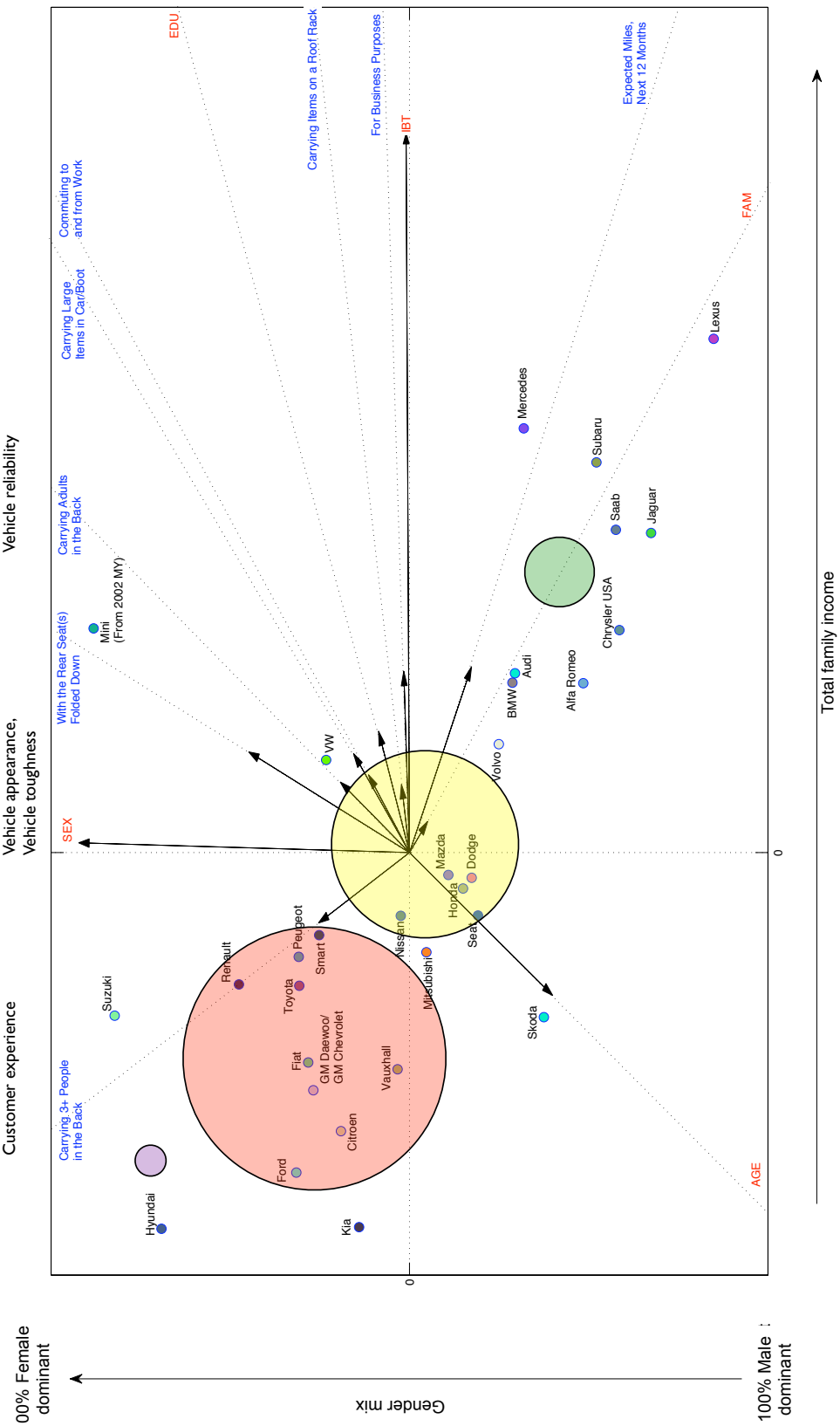

Figure 6.10: Perceptual map of respondents in NCBS_UK on their choice of brand per sterling

the brands more effectively with higher precision. This study, therefore, gives an exploratory background to the brand choice, with consideration of the customers' background and purchase reasons.

6.5 Managerial Implications and Recommendations

In this section, the focus will be on the marketing aspect for Jaguar Cars in the US and UK market.

6.5.1 The US Market

From the analysis of the NVES_US in the last section, it is found that the top five most important vehicle attributes for American customers are, (Table 6.3): 1) reliability, 2) a well made vehicle, 3) durability, 4) good running engine, and 5) ease of handling. The top five least important attributes are, (Table 6.3): 1) leasing terms, 2) off-road capability, 3) towing capability, 4) advice of friends, and 5) ease of customisation. Using the SPSS TwoStep Clustering method, five American customers segments are identified (Table 6.20 to 6.24): 1) *Squares*, 2) *Yodas*, 3) *Comfort-goers*, 4) *Die Hards*, and 5) *Ego show-offs*.

Jaguar Cars in the US Market

To market the Jaguar brand successfully, it is important to know both new and existing customers in Jaguar and in the market. As shown in the perceptual map, Figure 6.7, the Jaguar brand belongs to the luxury car segment. Its customers are primarily male, who are more mature in age with a higher education and family income.

Amongst these, Jaguar buyers can be categorised into two segments: the *Yodas* or the *Ego show-offs*. These two segments differ mainly by age group, in which *Yodas* are customers who are near or already at retirement and *Ego show-offs* are customers who are in their golden period for success. This age difference is the main driver for their difference in awareness. As explained in Tables 6.21 and 6.24, *Yodas* are more aware of the customisation of the vehicle while *Ego show-offs* are more aware of the styling of the vehicle.

Although there is an age difference, *Yodas* and *Ego show-offs* share common customer characteristics such as their occupation and high income. Moreover, the two segments also have a common awareness of long-term value.

From the perceptual map, relationships between latent factors can be determined from the direction of the purchase reason vectors. When two vectors are pointing away from one another, this implies the two vectors oppose one another. It shows from the map that Jaguar customers perceive highly on vehicle long-term value, appearance and customisation. These latent factors are pointing towards the south, opposing those directing towards the north. This means that Jaguar buyers are less

aware of the importance of their experience, the vehicle performance, toughness and driving comfort/safety. Although all of these features are important for a vehicle, Jaguar customers, generally, have underestimated their value and simply expect them to be well-made.

Recommendation for Jaguar Cars in US Market

Table 6.49 summarises the top five most important rated attributes in the US automotive market and the four most important areas to Jaguar customers. The table reveals that there is no agreement between US customers generally and US Jaguar customers in terms of those attributes that they perceive to be important. The absence of these US latent factors in Jaguar Cars does not mean they can be ignored in the company, it only means that the US latent factors are not the most critical and important ones in the mindset of Jaguar customers during their purchase. From another perspective, as buyers of a luxury brand, Jaguar customers may already have a high expectation in terms of reliability, performance and comfort/safety (which defines the luxury of a brand). Their purchase decisions are then based more importantly on their own perceptions, the vehicle appearance and value.

In the US, Jaguar Cars should concentrate on the luxury segment, emphasising in its marketing communications factors such as the vehicle's long term value, the customisability of the vehicle, the vehicle's appearance and the intended (luxury) positioning of the marque. In the long run, Jaguar Cars should also focus and continue to improve on the US latent factors (see Table 6.49) as they define the future standard and customer requirements.

The US vehicle attributes (and corresponding latent factors) should form the basis for the development of message content in advertisements and other promotional materials. By marketing those latent factors highly desired by customers of Jaguar Cars in the US, perceived customer value can be generated. For instance, engine performance can be marketed as a fuel efficient and environmental friendly feature. As a result, it is important for marketers to understand thoroughly how technolog-

Table 6.49: Areas of importance rated by customers in US and Jaguar

US automotive market		**Jaguar Cars**
Vehicle attributes	Corresponding latent factors	Latent factors
Reliability	Vehicle reliability	Vehicle long-term value
A well made vehicle	Vehicle reliability	Vehicle customisation
Durability	Vehicle reliability	Intended positioning
Good running engine	Vehicle performance	Vehicle appearance
Ease of handling	Vehicle driving comfort/safety	

ical features are comprehended by customers in order to identify those attributes whcih should be taken forward in marketing communications. Good management of this process in the US will give Jaguar Cars a competitive advantage in the luxury segment.

Handling Technology as a Purchase Criterion

In the US market, attributes that are related to the vehicle handling are ease of handling (positioned 5th), riding comfort (positioned 7th) and handling in inclement weather (positioned 19th). As shown previously in Table 6.8, these attributes fall into the latent factor of vehicle driving comfort/safety and vehicle toughness. Although the ranking of vehicle handling has proven to be important in the US market, Jaguar customers do not see it as the most important, see Table 6.49. If Jaguar believe they can generate a competitive advantage in the luxury car segment from promoting the car's handling features, they should develop a marketing communication strategy to emphasise Jaguar's superior handling technology.

For this project, a GPS/INS integrated system is proposed. It utilises the measurement from a GPS and other in-car sensors for vehicle dynamics estimations, thereby, improving vehicle handling and providing a better/safer driving experience under different inclement conditions and terrain changes. Without doubt, the GPS/INS system adds great value to the such perceived attributes as vehicle toughness and driving comfort/safety, but would not directly add to the most important perceived attributes (i.e. latent factors) identifed by Jaguar customers (though might contribute indirectly to vehicle customisation, particularly for 'worried' drivers). In order to make the GPS/INS system value adding, the system has to be marketed in terms of one or more of the Jaguar latent factors, in particular the vehicle long-term value. With the system's ability to predict vehicle dynamics, it can provide a better vehicle ride and handling, thereby, saving fuel and reducing wear on tyres.

6.5.2 The UK Market

In the UK market, the most frequently given purchase reason is "Always Buy the Same". This is then followed by "Exterior Styling/Appearance" and "Price", see Table 6.37. These statistics show that UK customers are more conservative and reluctant to change to another make. In general, the customers are segmented into four groups: 1) Conservatives, 2) Investors, 3) Perfectionists, and 4) Freshers, with Conservatives having more respondents than the other three segments combined.

Table 6.50: Purchase reasons of customers in terms of latent factors for the UK market, Jaguar Cars and the *Perfectionists* segment

The UK market (top five)	**Jaguar Cars (top four)**	***Perfectionists***
Customer experience	Customer experience	Intended positioning
Vehicle appearance	Vehicle appearance	Vehicle performance
Vehicle short-term value	Vehicle toughness	Vehicle reliability
Vehicle interior comfort	Intended positioning	
Vehicle toughness		

Jaguar Cars in the UK Market

As shown in the perceptual map, Figure 6.10, customers of Jaguar are mainly male with a large family and high household income. Moreover, the average age of Jaguar customers is not the most mature, in fact, it is even younger than that of Smart or Vauxhall.

Using the same latent factors derived previously in NVES_US (i.e. 10 factors in total), 2 additional factors, namely "Purchase convenience" and "Vehicle short-term value",are added to categorise the purchase reasons of respondents in the NCBS_UK, see Tables F.8 and F.9. For Jaguar Cars, the NCBS_UK reveals that its customers' purchase reasons are mainly "Customer Experience" (42.7%), "Vehicle Appearance" (13.6%), "Vehicle Toughness" (9.1%) and "Intended Positioning" (8.7%), see Tables F.16 to F.18. From the UK customers perceptual map, Figure 6.10, we can see that the nearest customer segment is *Perfectionists*, in which customers give purchase reasons based on their intended positioning, and vehicle performance and reliability. Table 6.50 summarises the above purchase reasons of customers in terms of the latent factors for the UK, Jaguar Cars and *Perfectionists*.

An examination of Table 6.50 reveals that customers of Jaguar Cars have very similar reasons to the UK customers in general apart from "Vehicle short-term value", "Vehicle interior comfort" and "Intended positioning". This similarity implies that customers of Jaguar Cars have a similar mindset to the majority of the UK customers in the automotive market. What differentiates Jaguar Cars from other makes is highlighted by the different reasons given by the Jaguar customers, namely the "Intended positioning". In other words, Jaguar successfully persuades its customers with its promotional appeals, emphasising such attributes as pride and class, elements which are critical to the brand as this defnes its place in the luxury segment. Comparing the purchase reason of Jaguar customers with those in the *Perfectionists* segment, Table 6.50 shows that Jaguar Cars only fulfils one reason, "Intended positioning". The unfulfilled reasons, especially the vehicle reliability, cause Jaguar Cars to lose *Perfectionists* customers to other luxury brands such as

BMW and Mercedes. This is because Jaguar Cars only has 2.9% of its respondents with reason "Vehicle reliability" when compared to 4.5% of BMW respondents and 6.0% of Mercedes respondents, see Tables F.16 to F.18.

Recommendation for Jaguar Cars in UK Market

From Table 6.50, it is clear that Jaguar Cars has to improve its image on vehicle reliability and performance in order to attract customers from the *Perfectionists* segment (12% of respondents in the NCBS_UK). To achieve this, Jaguar Cars must combine technical developments with marketing strategies.

While Jaguar Cars continues to upgrade and develop new technologies for vehicle performance and reliability, it is also important to re-examine the technologies behind each model. By doing so, a list of benefits for each technology can be determined and marketed in terms of the latent factors of the *Perfectionists* segment. For example, Rear Wheel Drive (RWD) as a quality for "Vehicle toughness" can be marketed as a benefit for acceleration, i.e. "Vehicle performance".

Nevertheless, Jaguar should not lose focus on the purchase reasons given by its current customers. As customers in the UK are more reluctant to change, it is extremely important for Jaguar to sustain what it is good at and known for – e.g. building prestigious cars of the highest quality in their class.

Handling Technology as a Purchase Criterion

In terms of the NCBS_UK latent factors, vehicle handling technology contributes to purchase reasons in "Vehicle driving comfort/safety" and "Vehicle toughness". Respondents mentioning these two reasons, however, constitute only 10% of valid cases (i.e. total respondents are 22,333) in the survey, see Table F.12. This shows that less than one in ten respondents has the potential of being attracted by technology related to handling as a first choice criterion.

As discussed previously the GPS/INS integrated system is beneficial to the handling characteristics of a vehicle, especially to "Vehicle driving comfort/safety". This, however, is the least mentioned in the NCBS_UK (i.e. 574 in 22,333 respondents), which implies that customers do not consider "Vehicle driving comfort/safety" as their main reason for purchase when they choose a vehicle. This small proportion does not mean that "Vehicle driving comfort/safety" is insignificant in the automobile industry, but rather, that it has become an entry requirement to the market and no longer provides a competitive advantage. With technological advancement, customers no longer choose a vehicle because of its good handling ability, they simply assume handling to be reasonable and begin to focus more heav-

ily on the vehicle's performance and its long-term value. To market the GPS/INS system, therefore, Jaguar Cars should focus on the benefits of the system in terms of "Vehicle toughness","Vehicle performance" and "Vehicle reliability" - attributes which customers perceive as highly important. For instance, the GPS/INS system can be marketed as a "Vehicle toughness" feature, providing road holding ability in adverse weather conditions.

6.6 Conclusion and Future Study

This chapter has studied the purchase reasons and their effects on customers' brand choice in the US and UK automotive markets. For each market the population is segmented according to the customers' demographic details and their purchase reasons. Using customer information as independent variables, a brand choice model is constructed for each market to simulate actual customers' choices.

In both markets, analysis has shown that Jaguar is positioned in the luxury segment together with BMW, Audi and Mercedes. Its customers are predominantly male with large family size and income in the family. Comparing the two markets, Jaguar customers are more mature in the US than in the UK. While Jaguar buyers in the US have the oldest average age amongst the luxury brands, UK Jaguar customers have one of the younger profiles amongst the luxury brands.

In the two markets, results show that customer purchase decisions are very different. US customers tend to be more practical. They are more aware of the technology in operation and how the vehicle can actually perform. UK buyers, on the other hand, are more sentimental, and are more aware of their past experience, the vehicle appearance and how the vehicle represents them. Although the attitudes towards buying a vehicle in the two markets are different, Jaguar customers, in general, have similar purchase reasons: 1) "Intended positioning" and 2) "Vehicle appearance".

The US Market

From NVES_US, the top five most important vehicle attributes are: 1) "Reliability", 2) "A well made vehicle", 3) "Durability", 4) "Good running engine", and 5) "Ease of handling". In terms of the latent factors, these are reduced to three groups: 1) "Vehicle reliability", 2) "Vehicle performance", and 3) "Vehicle driving comfort/safety". Among the US automotive buyers, five segments are identified with unique characteristics, see Section 6.4.2: 1) *Squares*, 2) *Yodas*, 3) *Comfort-goers*, 4) *Die Hards*, and 5) *Ego show-offs*.

The brand choice model from the discriminant analysis shows that the independent variables are able to distinguish the brands and provides a good model to estimate (and predict) customers' choice behaviours. Using this model demonstrates that the majority of Jaguar Cars customers come from "Yodas" or "Ego show-offs". Although the US automotive market is in favour of vehicle handling technology, it does not appeal much to the US customers of Jaguar Cars. It is recommended that new technologies which are associated with vehicle handling, such as the GPS/INS integrated system in this project, are to be marketed in terms of "Vehicle long-term value".

The UK Market

According to the NCBS_UK, automotive buyers are very conservative, with almost 30% of respondents giving "Always Buy the Same" as a purchase reason; and over 33% of respondents buy a vehicle because of "Customer Experience". The next most important purchase reasons are "Vehicle Appearance" (12.5%), "Vehicle short-term value" (7.4%), "Vehicle interior comfort" (7.1%), and "Vehicle Toughness" (7.0%). Latent factors which are related to vehicle handling (i.e. "Vehicle Toughness" and "Vehicle driving comfort/safety") constitute less than 10% of the valid population. Using customers' demographic details and the latent factors, four customer segments are identified: 1) *Conservatives*, 2) *Investors*, 3) *Perfectionists*, and 4) *Freshers*.

In the NCBS_UK, a discriminant analysis is carried out to model customers' brand choice in the automotive market. The independent variables are the latent factors and customers' demographic details from the survey. Results show that the model is not accurate (i.e. a low hit ratio for the estimations) and other independent variables may exist within the survey, which can discriminate the customers' brand choice more sufficiently. Nevertheless, the customer perceptual map provides some insights into the relative positioning for Jaguar in the luxury car segment. It has been identified that Jaguar Cars must focus on its "Vehicle reliability" in order to attract more customers from the *Perfectionists* segment. Similarly, for new handling technology, Jaguar Cars should market in terms of the latent factors of the *Perfectionists* segment, "Vehicle performance" and "Vehicle reliability". This is because customers in the *Perfectionists* segment underrate the importance of handling in a vehicle and simply take it for granted.

.

Future Studies

For future studies, there are several areas where the analysis could be further built upon as follows:

1. a specifically-designed survey (incorporating questions relevant to the nature of handling), or a new buyers survey which incorporated more questions on handling; this is important as statistical methods are closely related to the nature of the data collected,

2. a more up-to-date analysis; this is necessary as customers' attitudes towards vehicle purchase may be different after the credit crunch,

3. a specialised analysis, to include luxury brands buyers only so they can be segmented more distinctively,

4. a study focusing on whether vehicle system handling could improve customer satisfaction, and if so, amongst which segment will the improvement be most prominent.

Chapter 7

Conclusion and Future Work

7.1 Conclusion

7.1.1 Engineering research

In order to improve the performance of current automotive electronic control systems, such as the Anti-lock Braking System (ABS) and Electronic Stability Program (ESP), accurate dynamic measurements are essential. In the existing literature, there are four ways in general to achieve this requirement: 1) direct, 2) indirect, 3) vehicle-model, and 4) integrated approach. While the first two approaches are related to measuring techniques, the last two are associated with estimation. In Chapter 2, the advantages and disadvantages for the first three approaches were discussed in detail, and it was concluded that the most valid and appropriate method is to combine the three – an integrated approach. Amongst the many integrated methods, the Kalman Filter (KF) is the most widely used and preferred estimator in the automotive sector. In addition, motivated by the increase in their popularity, accuracy, as well as the cost reduction of Global Positioning System (GPS) receivers, this project focuses on the KF estimator design using GPS and in-car sensors, such as the Inertial Navigation System (INS), Wheel Speed Sensor (WSS) and steering wheel sensor), to estimate vehicle dynamic states. This project is based on simulation, while the vehicle plant models are based on IPG CarMaker, the sensor noise model and KF designs built in MATLAB/Simulink.

Using the KF estimator as a basis, three approaches can be devised: 1) Kinematic Kalman Filter (KKF), 2) Model-based Kalman Filter (MKF), and 3) Integrated Kalman Filter (IKF), see Figure 7.1. Chapter 4 dealt with the KKF approach, and an overview of the dual KF was discussed. It showed that the dual KKF design suffers from errors due to the approximation of the discrete time model,

the inaccuracy of the sensor model, and loss of information in the Controller Area Network (CAN-bus). These errors lead to the inaccuracy of state estimations, in particular the sideslip angle, which is a function of either the tracking and heading angle, or the longitudinal and lateral velocities.

Using the dual KKF, simulation results show that as long as there are straight roads with GPS tracking measurements, the yaw rate bias in the gyroscope is corrected; but additional sources of heading reference measurement are only able to improve the sideslip estimation by 3 to 4%. With the use of the WSS, it is found that the proposed design of the triple KF ($wssEKF$ + $yawKKF$ + $velKKF$) does not provide a significant improvement to the heading estimation in the dual KKF, but that there is benefit in the estimation of tyre radius bias, and subsequently in the longitudinal velocity. Moreover, it is found that consumer-grade GPS receivers of 1Hz cause discontinuity on the estimated states whenever GPS measurements are available (i.e. every one second excluding outages). It is proposed in this thesis to use first and second order interpolation to extend the latest available estimations during the outages. Results show that the first order interpolation is better than the second as less overshoot occurs during the change in dynamics. Moreover, when the GPS receiver rate is less than 5Hz, the dual KKF must be set to depend on the GPS measurement at all times apart from cornering during GPS absence.

Utilising the benefit of the triple KF (i.e. good estimation in longitudinal velocity and heading angle), Chapter 5 proposed to combine it with MKF to form an IKF. The selection of the vehicle model in the MKF was discussed in Chapter 3. Amongst the bicycle and twin-track models with different Degrees of Freedom (DoF), the 2DoF bicycle model is the best that can be used in the Model-based Extended Kalman Filter (MEKF) because of its simplicity and small number of parameters. Using the linear tyre model in the MEKF, it is combined with the triple KF design to form the new IKF design. The IKF uses the longitudinal estimation and the corrected yaw rate from the triple KF as inputs to the MEKF. Simulation results are favourable to the IKF, but only when linear tyre model is applicable in the driving manoeuvres.

Apart from analysing the numerous KF designs, this thesis also provides guidelines for engineers to design a GPS/INS KF estimator. The guidelines also highlight some of the pitfalls that engineers should be aware of. In Chapter 4, three working frameworks on the vehicle were identified: the East, North, Up framework (e-frame) for the GPS, the Vehicle-frame (v-frame) for the vehicle motion and the Body-frame (b-frame) for the in-car sensors. It is important to understand the transformation between the three frameworks (via the Direct Cosine Matrix (DCM)) as sensor mea-

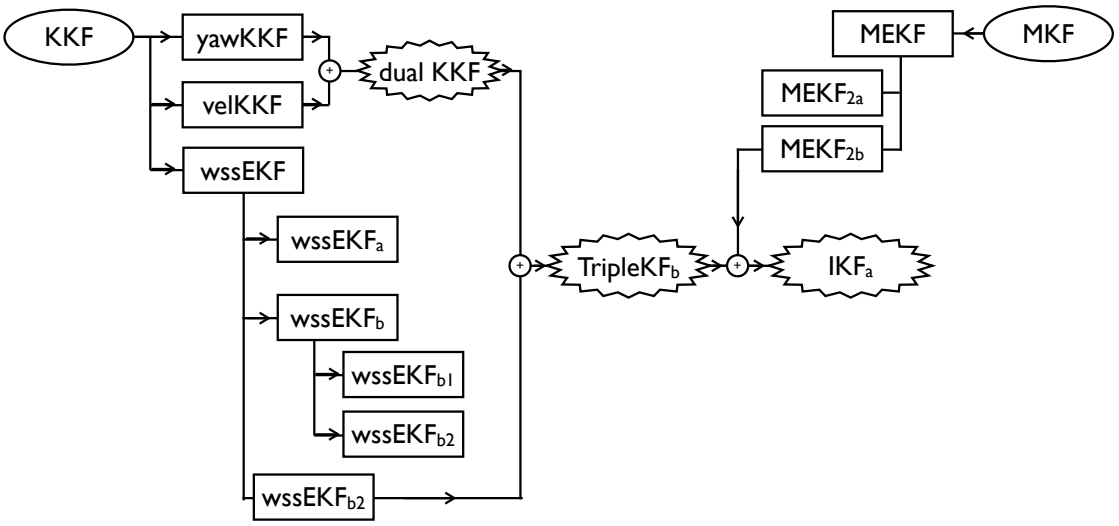

Figure 7.1: Summary for the KF designs in this thesis

surements are only comparable when they are derived in the same frame of reference. However, due to the lack of measurements, the three frameworks are reduced to two by assuming zero tilt angles between the vehicle body and the surface of the road (i.e. the b-frame lies on the v-frame). In some practice, the two frameworks often reduce to one by assuming the vehicle is travelling on a flat surface. But in reality, a vehicle climbs and descends with non-zero tilt angles, so by incorporating additional sensors, new measurements can be made available for the construction of a more accurate sensor model.

As the GPS is one of the most important sources for information in the KF design, in this thesis, a study of the GPS receiver sampling rate and precision was carried out based on the dual KKF design. Results show that state estimations are accurate when the GPS receiver is at 5Hz or above, and when the GPS receiver's velocity variance is under $0.001m^2/s^2$. Interestingly, in the year 2005, this velocity variance is within the survey grade GPS receiver; today, this precision is achieved by some high-street GPS receiver with antenna (e.g. GlobalSat DG-100). In the future, it is anticipated that GPS receivers will become even cheaper and more accurate, the only concern is the update rate of the GPS receiver. Currently in the consumer market most GPS receivers are running at a low frequency of 1Hz. With this low GPS sampling rate and 100Hz in-car sensors, the sideslip estimation and accuracy of the GPS and INS is investigated and presented in graphical form. A recommended design procedure is also given to help engineers in choosing an appropriate sensor to match their design specification. In addition, for the 2DoF linear vehicle model, a graphical and theoretical analysis on the parametric sensitivity was provided in

Chapter 5. It is found that the cornering stiffness is the most critical parameter in the vehicle model. When the tyre behaves linearly on the road, it is better to overestimate the cornering stiffness than underestimate it.

To conclude, the following suggestions are recommended during the implementation of GPS/INS state estimators:

1. Use a second order or higher for the approximation of the discrete time model. This can ensure that the errors from the discretisation is reduced. However, during implementation, designers must also be aware that this comes with an increase in computational cost.

2. Use of additional sensors, such as gyroscopes and a magnetometer means that roll and pitch rates can be measured and incorporated into the KF design. Magnetometers also provide an extra source of heading information for the KF to update and correct. Designers must prepare to weigh the cost against the estimation accuracy.

3. Direct measurement from the sensors, by-passing the CAN-bus, provides more accurate sensor measurements without error from scaling.

4. Use of the *wssEKF* in the triple KF design allows the correction of tyre radius and aids the determination of longitudinal velocity.

5. The GPS receiver is recommended to have a sampling rate of 5Hz or above for precise measurements. For such GPS/INS KF designs, correction is only made when GPS is present (i.e. every one-fifth of a second). Where the sampling rate is lower than 5Hz, significant discontinuities occur when the GPS returns. These errors can be reduced by applying the first order line interpolation technique to the states to extend the last available estimations.

6. If accuracy is the most important factor, it is recommended to use a dual antennae setup, which allows the KF to measure the heading angle accurately.

7. When the parameters are roughly known, it is better to use the IKF, in which the longitudinal velocity and heading angles are estimated by the triple KF while the lateral velocity is estimated by the MEKF.

7.1.2 Marketing research

In their review paper, of Manning and Crolla [2007] have commented that a significant research effort is needed to address the subjective performance of vehicle

handling systems. Such systems can be categorised into 3 main control approaches: 1) yaw rate control, 2) sideslip control, and 3) combined yaw and sideslip control. It is clear from the discussion and conclusion of Manning and Crolla [2007] that these control strategies require an accurate estimation of vehicle dynamic states, namely the sideslip angle. With the proposed GPS/INS state estimator in this project, the longitudinal, lateral, yaw, and sideslip estimation is enhanced. This system, when integrated with current/future controllers, will add value to vehicle handling. Although vehicle handling is crucial to a manufactured vehicle, from the market research based on two surveys (the New Vehicle Experience Survey (NVES) in US and the New Car Buyer Survey (NCBS) in UK) in year 2007, it shows that customers under-rate vehicle handling as their purchase criteria.

In the US market, customers are clustered into 5 segments, namely the "Squares", the "Yodas", the "Comfort-goers", the "Die Hards", and the "Ego show-offs". Each of these segments is different in terms of its purchase reasons and demographic details. For Jaguar Land Rover (JLR), as shown in the perceptual map, Figure 6.7, it belongs to the luxury brand with customers mainly from the "Yodas" or the "Ego show-offs" (i.e. high income, mature and male dominate customers with a latent factors of vehicle long-term value, appearance and customisation). In order to market the GPS/INS integrated technology to these 2 segments, the benefits of having this technology must be marketed in terms of the latent factors of the "Yodas" and the "Ego show-offs". For example, the improvement of vehicle handling using the GPS/INS system can be marketed as a fuel saving and/or cost reduction feature (i.e. vehicle long-term value). Furthermore, it is recommended that JLR should continue to research in the technologies related to the vehicle reliability, performance and driving comfort/safety, as these latent factors define the customers' expected needs in the future of the US automotive market.

In the UK market, customers are generally more conservative with their purchase reasons than those in the US. From Figure 6.9, the UK customers are clustered into 4 segments: the "Conservative", the "Investor", the "Perfectionist", and the "Fresher". For JLR, as can be observed from Figure 6.10 that it belongs to the luxury brands with customers who are mainly mature male with a relatively big family size and high income. These customers' details are similar to that from the US but when considering the latent factors, the 2 countries are very different. From Figure 6.10, the nearest segment to JLR is the "Perfectionist", who has a high importance rating on intended positioning, vehicle performance and reliability. When analysing the reason of purchase of JLR customers' alone, results show that JLR have only fulfilled 1 of the latent factor (Intended positioning) of the "Perfectionist", but

3 of the latent factors of the UK (customer experience, vehicle appearance and toughness). This indicates that JLR is fulfilling the customers' needs in the UK automotive market but not those in the "Perfectionist". JLR, therefore, would require a better strategy to market its quality in terms of vehicle performance and reliability as the "Perfectionist" is the main segment in the luxury brand in UK. The GPS/INS state estimator should, hence, be marketed as a technology that will improve, for example, the speed going through a corner.

7.2 Recommendation for future opportunities

This section discusses the recommendations and future opportunities for the engineering aspects of the project. For the management aspect, refer to Section 6.5 and Section 6.6. In terms of the engineering aspect, expanding from the ideas and discussion in Deng and Zhang [2006], there are in total seven ways to obtain vehicle dynamic states (see also Figure 7.2):

1. numerical integration of INS/sensors measurements;
2. direct measurement from the Global Navigation Satellite System (GNSS) device;
3. direct determination from a Vehicle Model (VM);
4. estimation via a GNSS/INS Kinematic Estimator (KE);
5. estimation via a GNSS/VM Model-based Estimator (ME);
6. estimation via a INS/VM ME; and
7. estimation via a GNSS/INS/VM Integrated Estimator (IE).

Region 1 - INS only

Numerical integration relies heavily on the INS quality, i.e. sampling rate and precision. In most cases, INS suffers from bias and disturbances. Integrating these noisy signals may cause severe drifting. Furthermore, most INS operate at 100Hz on a manufactured vehicle and measured data are transmitted via a CAN-bus. As discussed in Section 7.1, future improvements can be made by having additional sensors as well as direct measurements by-passing the CAN-bus.

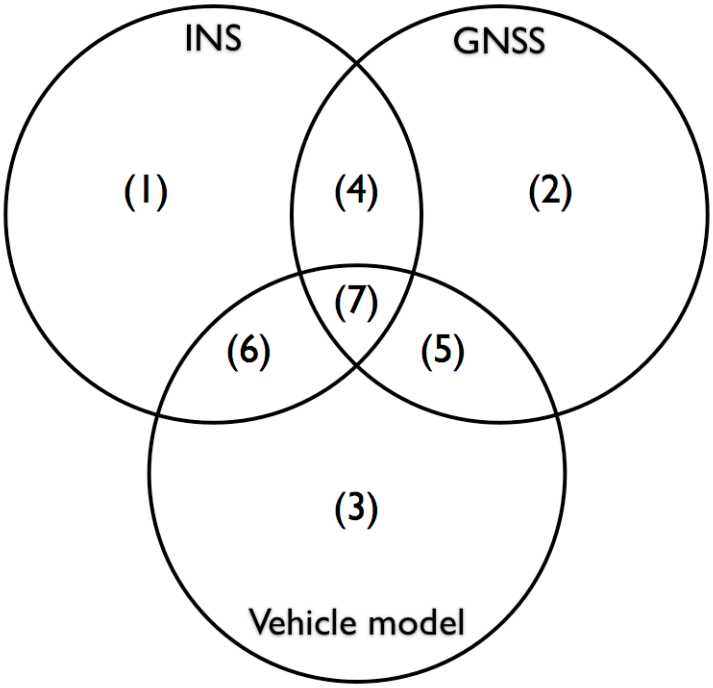

Figure 7.2: Seven ways of obtaining vehicle state estimations

Region 2 - GNSS only

Other than vehicle on-board sensors, the GNSS technology is also becoming more popular in standalone modern production vehicles. GNSS is capable of measuring not only the positions of the user, but also the velocities of the user via Doppler measurements. With multiple GNSS receivers, the heading angle, the pitching angle, the rolling angle as well as the road grade can also be determined. Due to increased competition from Chinese, European and Russian GNSS, GPS has become more widely available and accurate, which has led to cheaper GPS receivers with increased accuracy. However, drawbacks of the GPS still exist. These are the low sampling rate of the receiver, typically 1Hz, and the outages due to heavy foliage or urban canyons. In future studies, it will be interesting to compare the effectiveness of state estimations using individual and/or a combination of GNSS.

Region 3 - VM only

Typically, vehicle models based on a reduced four wheeled model are used – in particular the 2DoF bicycle model, which assumes identical motion on the left and right wheels [Liu et al. 2005, Cherouat et al. 2005, Rock et al. 2005, Chen and Hsieh 2008]. The motions that are of interest are the lateral motion and the rotational

motion about the z-axis of the vehicle. Assumptions made for this model include constant longitudinal velocity, small steer angles and slip angles on tyres, and linear tyre characteristics. The 2DoF model is favoured by researchers and in industrial applications due to its simple equations and freedom from sensor errors. However, it tends to suffer from inaccuracy when the tyres behave non-linearly and/or when the load on the left and right tyres differ significantly. This is because cornering stiffness is not only a function of slip angle, α, but also a function of the load applied on the tyre. To resolve these issues, a 5DoF twin track model [Wenzel et al. 2007] can be applied to determine the load on each wheel. Although the 5DoF model is able to give more precise solutions, more parameters are required. Without accurate parameters, especially the cornering coefficients (C_f and C_r), state estimations will be inaccurate. For this reason, the future for VM based dynamic estimation relies on research in realtime parameter estimation.

Region 4 - GNSS/INS Kinematic Estimator

It is clear from the above discussion that vehicle states can not be estimated cheaply (economically or computationally) and accurately with only one system; integrated systems are therefore required. From the existing literature it is found that the majority of the IEs are designed using the kinematic approach. This is because the KE is easy to implement and does not require any parameters such as mass, inertia and tyre cornering coefficients. KE is particularly attractive to car manufacturers as it can be applied to a number of different vehicle models with ease, thereby reducing the cost per vehicle by reducing complicated and expensive calibration. As described previously, GNSS/INS KE operates at the INS frequency, typically 100Hz. During KE operation, the bias of the INS is partially eliminated and in between GNSS sampling times, the corrected INS is numerically integrated. Although this approach is able to provide continuous estimations, INS bias can never be completely removed. As a result, measurements from the low update rate GNSS receiver may cause discontinuity at each GNSS sample [Leung et al. 2009*a*]. It is, therefore, important to sustain the INS estimation accuracy in between GNSS outages. As described in earlier sections, this can be done in two ways: improving the sensor/disturbance kinematic model and/or applying a numerical interpolation technique to extend estimations. In addition, another approach that may be worth exploring is the modelling of sensor errors in real-time using numerical approximation.

Region 5 & 6 - GNSS/VM & INS/VM Model-based Estimator

Most ME are constructed using the architecture of GNSS/VM [Bayliss et al. 2006] or INS/VM [Best et al. 2000, Cherouat et al. 2005]. As INS/VM is not within the scope of this work, only GNSS/VM is discussed. From the previous discussion, the most popular vehicle model is the 2DoF bicycle model. In standalone VM estimations, the inputs to the system are limited to steer angle and speed measurement from WSS. With GNSS installed, an extra source of information is available (velocity and yaw rate), which will allow states to be estimated more precisely. Assuming accurate parameters are available, the GNSS/VM ME will be able to produce the best estimations with errors bounded even during the absence of GPS. The role for the GPS is solely to correct the errors generated from unmodelled dynamics (such as dynamics of vehicle compliance). As shown in the literature, this is achievable but requires a dual or triple antenna GPS receiver unit, which is unfavourable to automobile manufacturers because of the extra cost. As pointed out in Anderson and Bevly [2005], ME can generate inaccurate states estimation when the parameters are wrong. Although most parameters, such as the mass and inertia, stay relatively constant and only undergo minor changes during the drive, forces on the tyres are greatly dependent on the slip angle and the vertical load applied. It is, therefore, essential to update the cornering stiffness continuously during the drive. Future research on GNSS/VM ME may extend from simplified bicycle models to using more sophisticated twin track models to incorporate the changes in the cornering stiffness coefficients on each tyre.

Region 7 - GNSS/INS/VM Model-based Estimator

Judging from the advantages and disadvantages of KE and ME, state estimations can be further improved when the two approaches are integrated into a combined GNSS/INS/VM IE, so providing estimations for both dynamic states and parameters. Anderson and Bevly [2005], Rock et al. [2005], Best et al. [2007], have used multiple GPS antennae or expensive GPS/INS units to predict the vehicle sideslip, velocities and heading angle, thereby, estimating the mass, inertia and cornering stiffness for the VM. Although these IE show good agreement with actual measurements, the devices that are used in the studies are expensive. From an automobile manufacturer's perspective these are not feasible solutions as one of the main priorities for an automotive company is to reduce cost of production by using existing vehicle-mounted sensors. Moreover, the GNSS/INS/VM IE are based upon an ME, which means estimations are dependent heavily on the accuracy of the model. GNSS and INS information only plays a part in identifying parameters for the VM and

moreover, GNSS is not used as a corrective agent for the INS error. Future IE should have the capability to estimate states and parameters with KE running alongside of another ME, compensating one another.

When GNSS signals are available, both INS and VM are updated to reduce errors in each system while providing estimations for parameters and dynamic states. During GNSS outages, the corrected INS and VM should compensate one another to produce better estimations. A similar concept for the INS/VM collaborative idea can be found in a recent paper, [Piyabongkarn et al. 2009], in which a combined low and high pass filter is used. The sideslip, $\hat{\beta}$, is estimated by passing the VM estimations, $\hat{\beta}_{vm}$, through a low pass filter and INS estimations, $\hat{\beta}_{ins}$, through a high pass filter:

$$\hat{\beta} = \frac{1}{\tau s + 1}\hat{\beta}_{vm} + \frac{\tau s}{\tau s + 1}\hat{\beta}_{ins} \tag{7.1}$$

The VM sideslip predicted in (7.1) uses GPS and WSS tyre measurements for longitudinal and wheel rotational velocity to determine the cornering stiffness, while the INS prediction utilises measurements from a lateral and a vertical accelerometer as well as a yaw rate gyroscope. As commented in Piyabongkarn et al. [2009], although the observer produces some good estimations, it has a limitation for large slip angles for a long duration of time (i.e. when the vehicle goes out of control). This finding is due to the non-linearity of the tyre model, but estimations can be improved if INS error (i.e. bias) are corrected with the GNSS initially.

Other state estimator designs

Apart from the design architecture of estimators, further studies are also required in the use of other types of estimators, such as the unscented Kalman filter and the particle filter. Since the estimator depends highly on the types of sensors, designers need to be aware of the latest sensor technology available.

Appendix A

Vehicle Parameters

In this project, the simulation is based on a rear wheel drive Jaguar Saloon, which has the parameters as shown in Table A.1.

Table A.1: Vehicle parameters used for this project

	Value	**Unit**
Dimension		
distance from front axle to cg (a)	1.360	m
distance from rear axle to cg (b)	1.546	m
cg height	0.554	m
front track (T_F)	0.768	m
rear track (T_R)	0.768	m
Masses and inertia		
sprung mass (M_s)	1665.900	kg
unsprung mass per wheel (M_u)	48.080	kg
total mass of vehicle (M)	1858.000	kg
roll inertia about cg (J_{xx})	655.200	kgm^2
pitch inertia about cg (J_{yy})	3319.000	kgm^2
yaw inertia about cg (J_{zz})	3515.000	kgm^2
wheel inertia (J_w)	1.000	kgm^2
Steering		
On centre rack ratio	17.58	
Aerodynamics		
aerodynamic coefficient (C_{dx})	0.305	
frontal cross-sectional area (A_x)	2.200	m^2
air density (ρ)	1.205	kgm^{-3}

This page intentionally left blank.

Appendix B

Sensor Parameters and Validation

This section shows the parameters of the vehicle and the noise of the sensors that are used in this thesis. Unless specify, the following data is applied onto all the simulations.

B.1 Inertial Navigation System

Below shows the standard deviation and biases of the Inertial Navigation Sensors (INS) that are used in most of the simulations in this thesis. The noise are assumed to be white and the bias to be a constant. The errors are added into the corresponding sensors and then passed through a CAN bus simulator, before using as measurements for the GPS/INS estimators.

Table B.1: Simulated INS errors

		Standard deviation, σ		**Bias**	
Sensor ($100Hz$)		Value	Unit	Value	Unit
Roll rate gyroscope	p_m	1.0×10^{-1}	$deg/s.$	1.0	deg/s
Pitch rate gyroscope	q_m	1.0×10^{-1}	$deg/s.$	1.0	deg/s
Yaw rate gyroscope	r_m	1.0×10^{-1}	$deg/s.$	1.0	deg/s
Longitudinal accelerometer	$\ddot{x}_b$	5.0×10^{-1}	m/s^2	1.0	m/s^2
Lateral accelerometer	$\ddot{y}_b$	5.0×10^{-1}	m/s^2	1.0	m/s^2
Vertical accelerometer	$\ddot{z}_b$	5.0×10^{-1}	m/s^2	1.0	m/s^2
Steering wheel sensor	δ_w	1.0	deg	5.0	deg

B.2 Global Positioning System

Figure B.1 shows the GPS static measurements collected during a 9-hours period using the GlobalSat® DG-100 DataLogger unit. The yellow star shows the actual position of the DataLogger on earth; the red patch shows the positions recorded by the DataLogger without an antenna; and the purple blue patch shows the positions recorded by the DataLogger with an antenna.

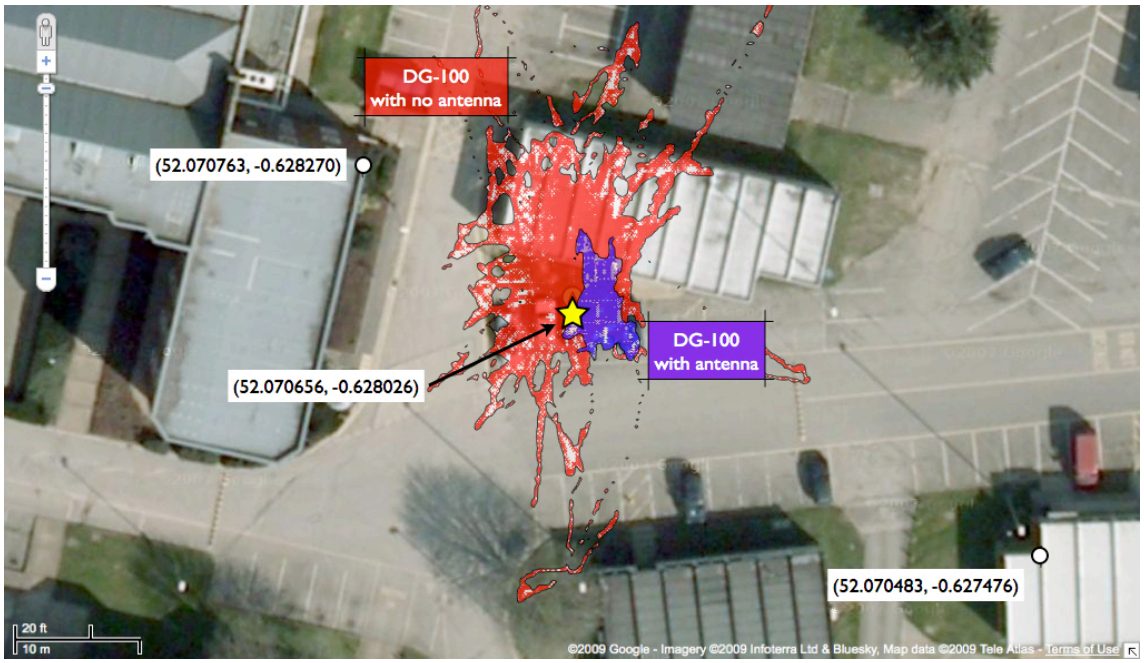

Figure B.1: The GlobalSat® DG-100 recorded positions on the Google [2009]

Table B.2: GPS errors based on DG-100 without an antenna

		Standard deviation, σ
GPS $(1Hz)$		Value
Eastings position	σ_{x_e}	3.0
Northings position	σ_{y_e}	3.0
Longitudinal velocity	$\sigma_{\dot{x}_e}$	2.5×10^{-2}
Lateral velocity	$\sigma_{\dot{y}_e}$	2.5×10^{-2}
Resultant velocity	σ_V	$\sqrt{\left(\frac{\dot{x}_e}{V}\sigma_{\dot{x}_e}\right)^2 + \left(\frac{\dot{y}_e}{V}\sigma_{\dot{y}_e}\right)^2}$
Tracking angle[1]	σ_ν	$\sqrt{\left(\frac{\dot{y}_e}{\dot{x}_e^2}\sigma_{\dot{x}_e}\right)^2 + \left(\frac{1}{\dot{x}_e}\sigma_{\dot{y}_e}\right)^2}$
	$\sigma_{\cos\nu}$	$\sqrt{\left(\sin\left(\frac{\dot{y}_e}{\dot{x}_e}\right)\left(\frac{\dot{y}_e}{\dot{x}_e^2}\right)\sigma_{\dot{x}_e}\right)^2 + \left(\sin\left(\frac{\dot{y}_e}{\dot{x}_e}\right)\left(\frac{1}{\dot{x}_e}\right)\sigma_{\dot{y}_e}\right)^2}$
	$\sigma_{\sin\nu}$	$\sqrt{\left(\cos\left(\frac{\dot{y}_e}{\dot{x}_e}\right)\left(\frac{\dot{y}_e}{\dot{x}_e^2}\right)\sigma_{\dot{x}_e}\right)^2 + \left(\cos\left(\frac{\dot{y}_e}{\dot{x}_e}\right)\left(\frac{1}{\dot{x}_e}\right)\sigma_{\dot{y}_e}\right)^2}$

[1] $\nu = \tan^{-1}\left(\frac{\dot{y}_e}{\dot{x}_e}\right) \approx \frac{\dot{y}_e}{\dot{x}_e}$

Appendix C

IPG CarMaker Simulation

In this project, various tracks are used in simulations for the comparison of the performance of KF designs. These tracks includes:

1. *DoubleOval* track
2. *LaneChangeISO* track
3. *Right Turn* (*RT*) track
4. *Figure Eight* (*8C*) track
5. *Self-Defined* (*SD*) track

In CarMaker, these tracks are defined using straight roads and corners. Their road definition are given in this section with ST representing the length of the straight road; LT representing the angle in degrees for the left turn; RT representing the angle in degrees for the right turn; and R representing the radius of turn.

C.1 *DoubleOval* track

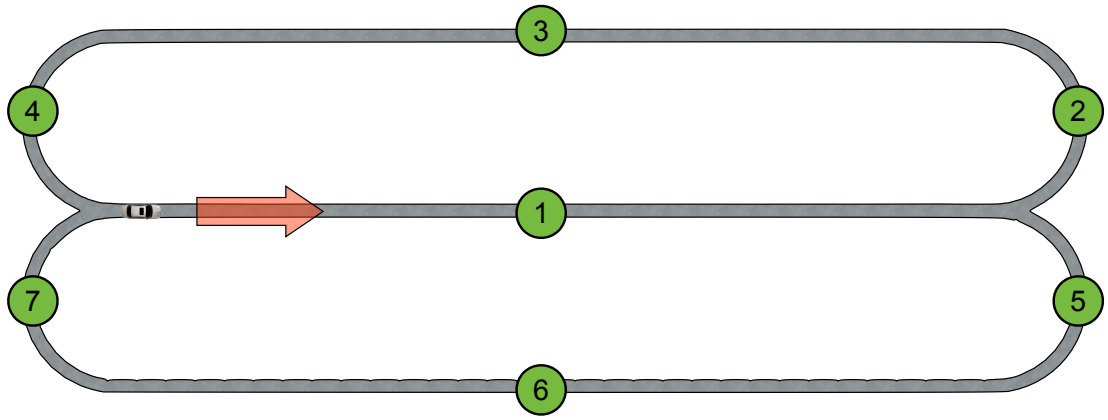

Figure C.1: Schematic diagram for *DoubleOval* track in CarMaker

Table C.1: Section definition for the *DoubleOval* track

Section	**Definition**
1	ST300
2	R30 LT180°
3	ST300
4	R30 LT180°
5	R30 RT180°
6	ST300
7	R30 RT180°

C.2 *LaneChangeISO* track

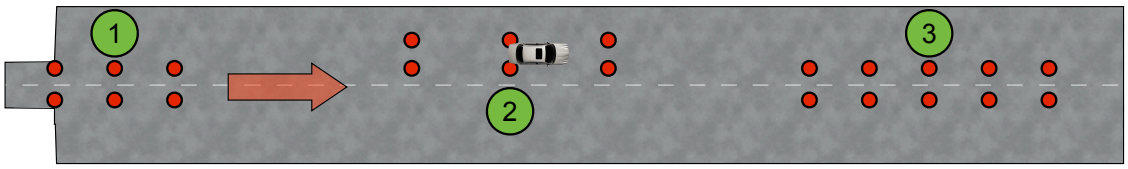

Figure C.2: Schematic diagram for *LaneChangeISO* track in CarMaker

The *LaneChangeISO* manoeuvre in CarMaker is modelled by driving the virtual vehicle in between pylons. The pylons positions are defined in pairs with x_e, y_e and their distance apart. For the ISO standard lane change, these pylons are defined as,

Table C.2: Section definition for the *LaneChangeISO* track

	Pylons definition		
Section	x_e	y_e	Distance apart
1	400.0	0.0	2.142
	407.5	0.0	2.142
	415.0	0.0	2.142
2	445.0	3.586	2.314
	457.5	3.586	2.314
	470.0	3.586	2.314
3	495.0	0.172	2.486
	502.5	0.172	2.486
	510.0	0.172	2.486
	517.5	0.172	2.486
	625.0	0.172	2.486

C.3 *Right Turn* (*RT*) track

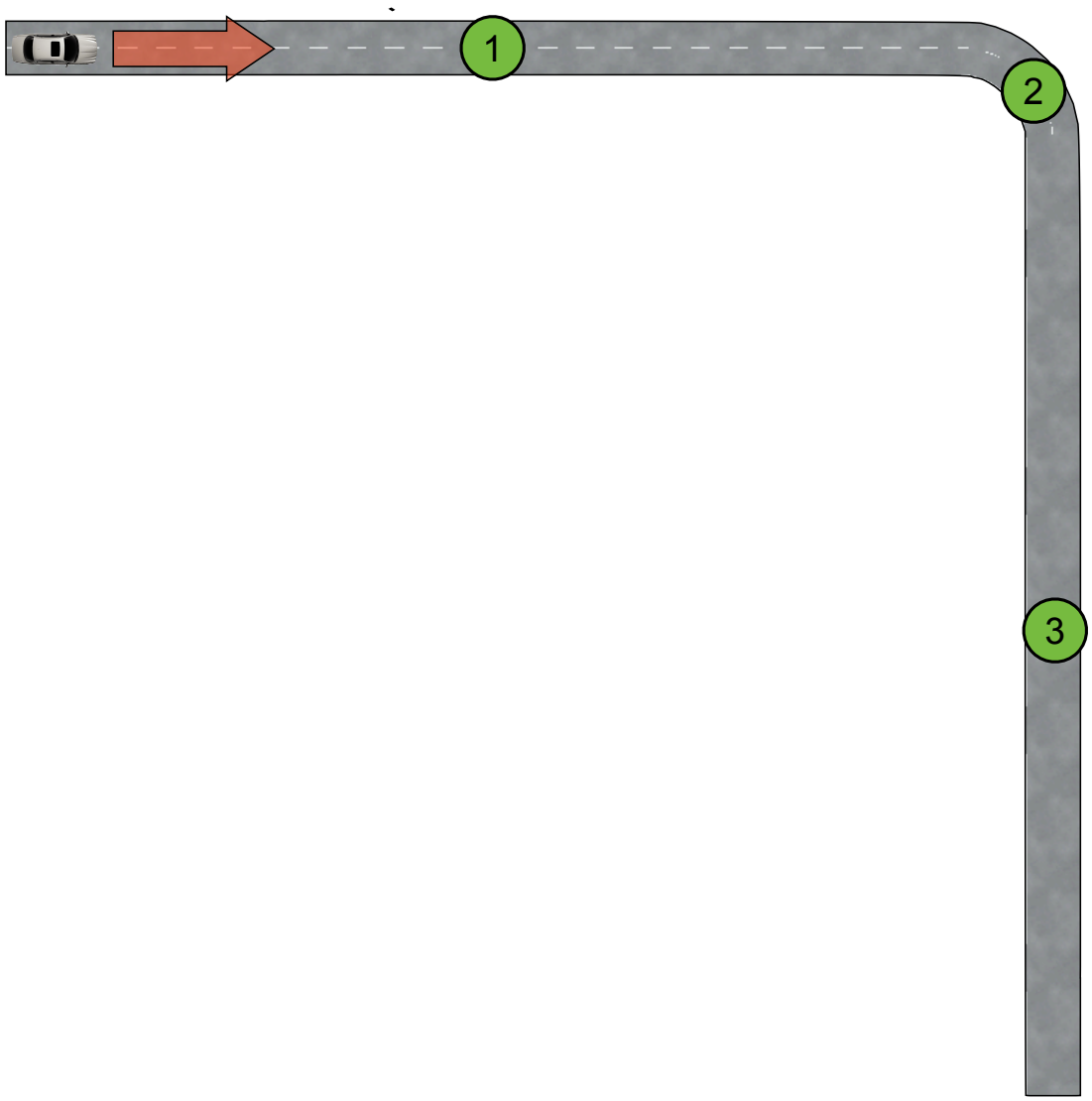

Figure C.3: Schematic diagram for *Right Turn* track in CarMaker

Table C.3: Section definition for the *Right Turn* track

Section	**Definition**
1	ST100
2	R5 RT90°
3	ST100

C.4 *Figure Eight* (*8C*) track

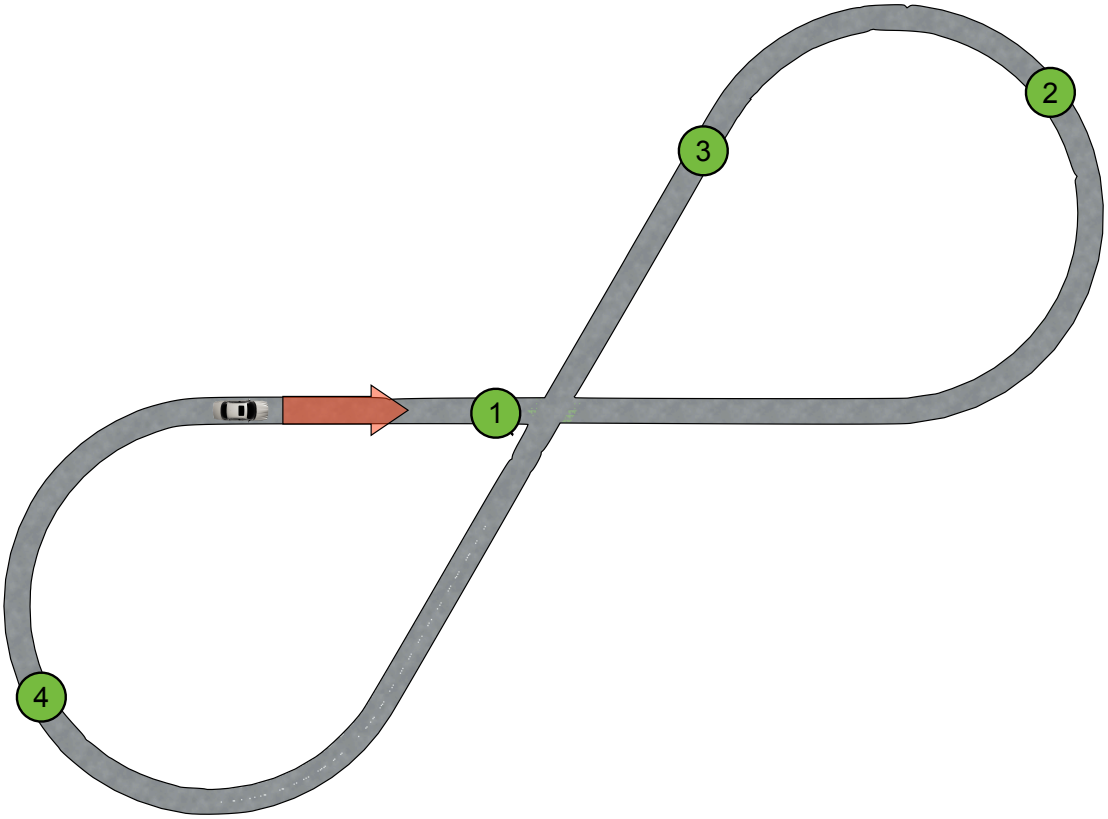

Figure C.4: Schematic diagram for *Figure Eight* track in CarMaker

Table C.4: Section definition for the *Figure Eight* track

Section	Definition
1	ST145
2	R42 LT240°
3	ST145
4	R43 RT240°

C.5 *Self-Defined* (*SD*) track

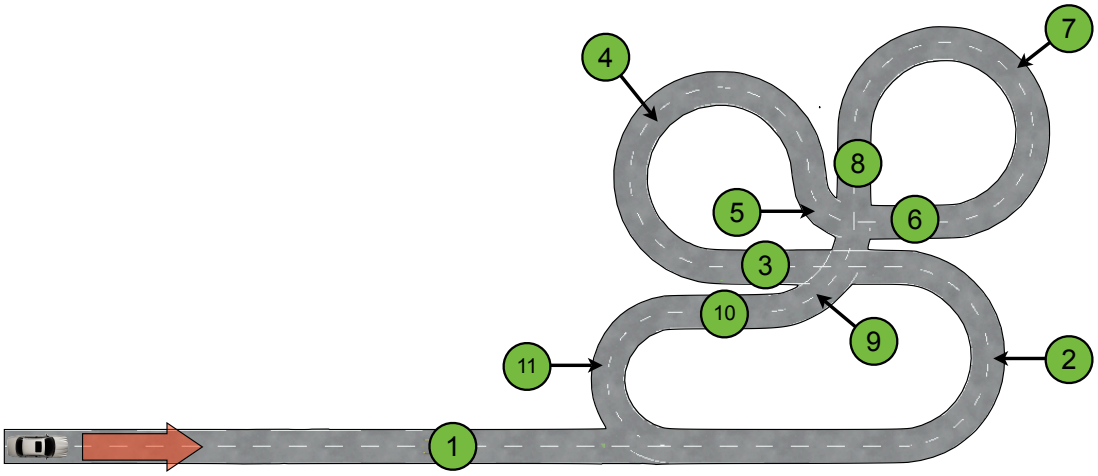

Figure C.5: Schematic diagram for *Self-Defined* track in CarMaker

Table C.5: Section definition for the *Self-Defined* track

Section	Definition
1	ST100
2	R10 LT180°
3	ST20
4	R10 RT270°
5	R5 LT90°
6	ST10
7	R10 LT270°
8	ST10
9	R10 RT90°
10	ST10
11	R7.5 LT180°

Appendix D

Vehicle Frequency Response

Here, the complete results for the vehicle frequency response are given. Frequency responses are performed on five different vehicle models: 2DoF bicycle, 3DoF bicycle, 3DoF twin-track, 5DoF bicycle, and 7DoF twin-track. Each model is run at a constant speed of 10kph, 20kph, 30kph, 40kph, 50kph, 60kph, 70kph, 80kph, 90kph, and 100kph.

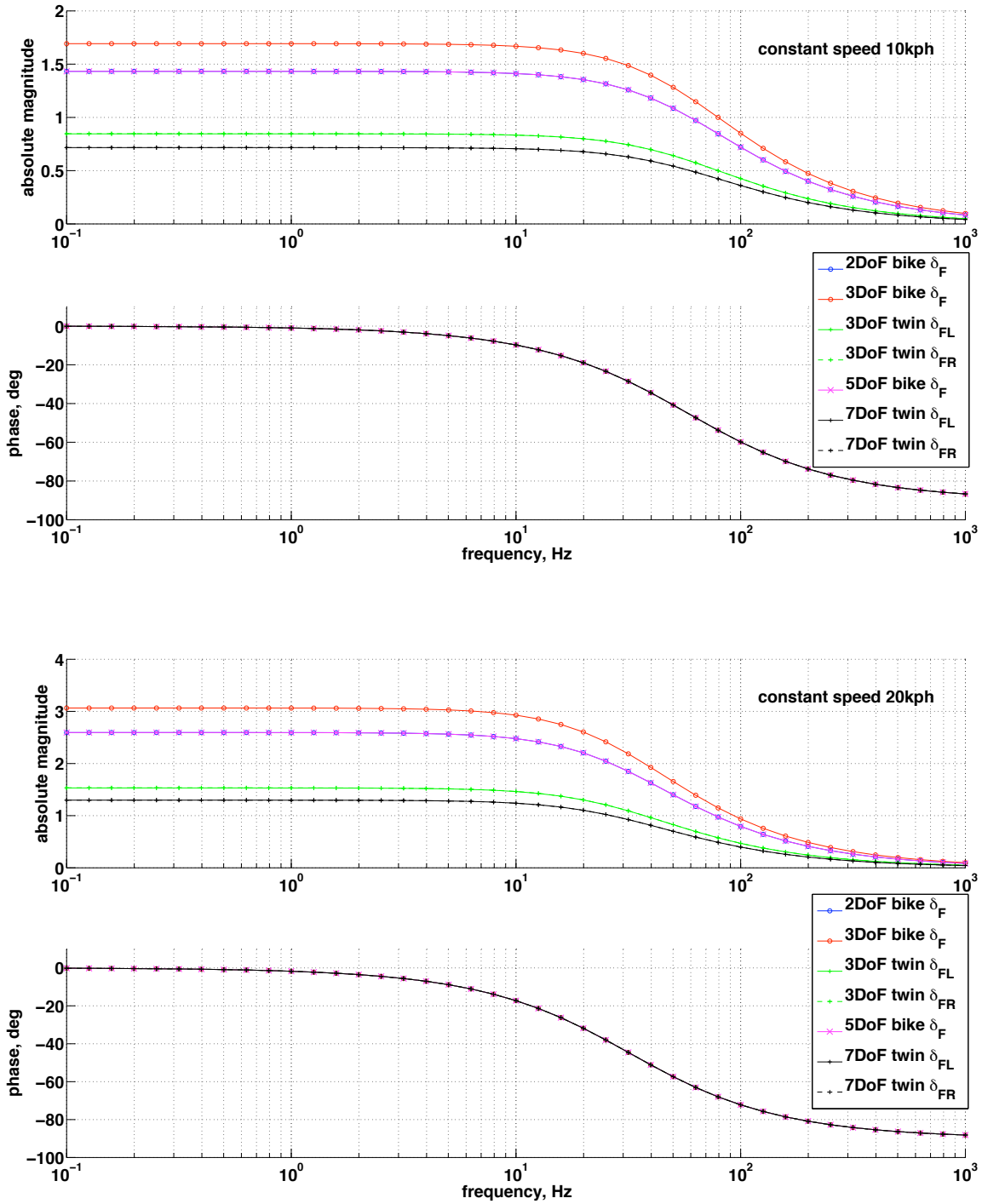

Figure D.1: Frequency response of lateral velocity with steering inputs for different models, 10 and 20kph

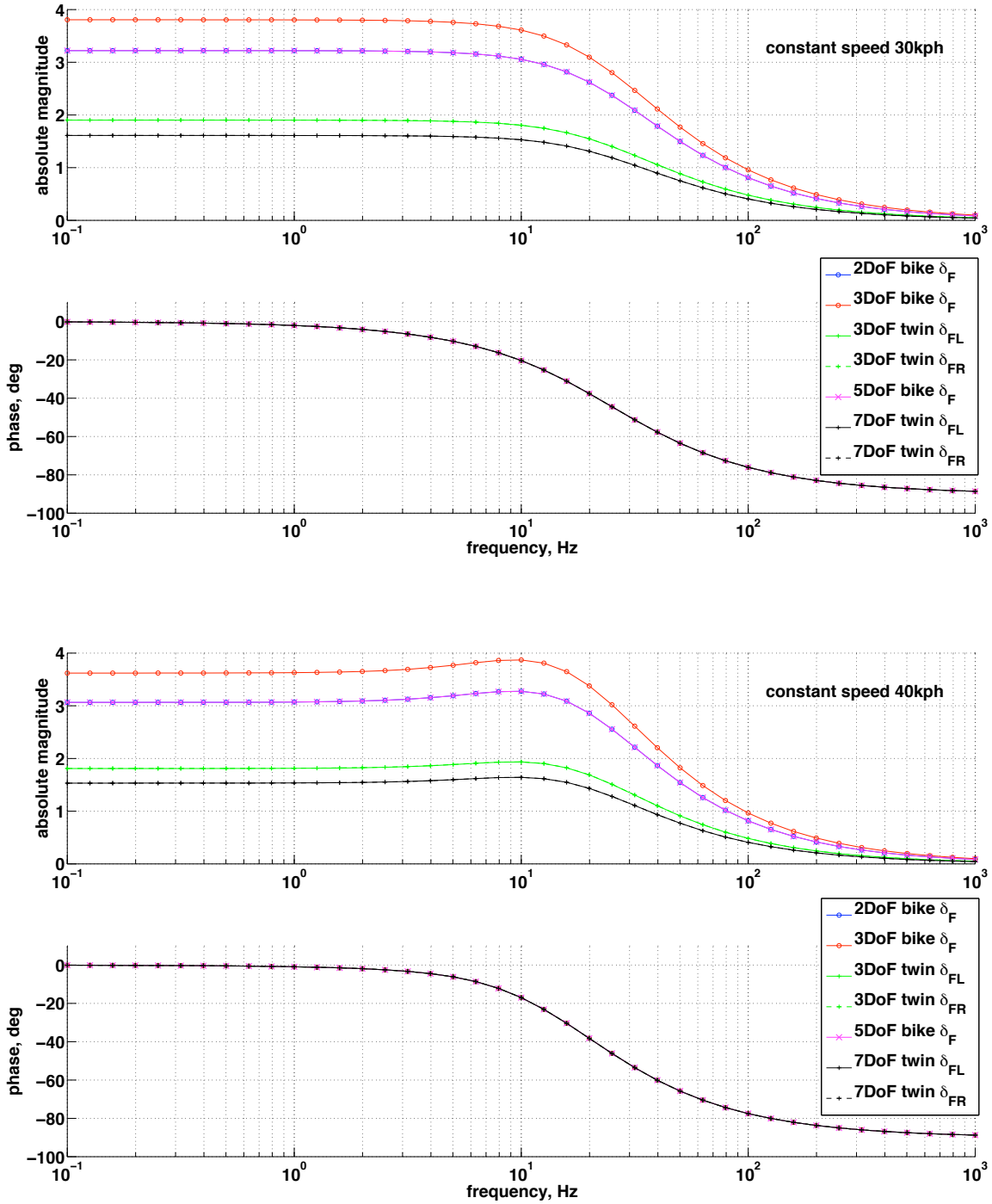

Figure D.2: Frequency response of lateral velocity with steering inputs for different models, 30 and 40kph

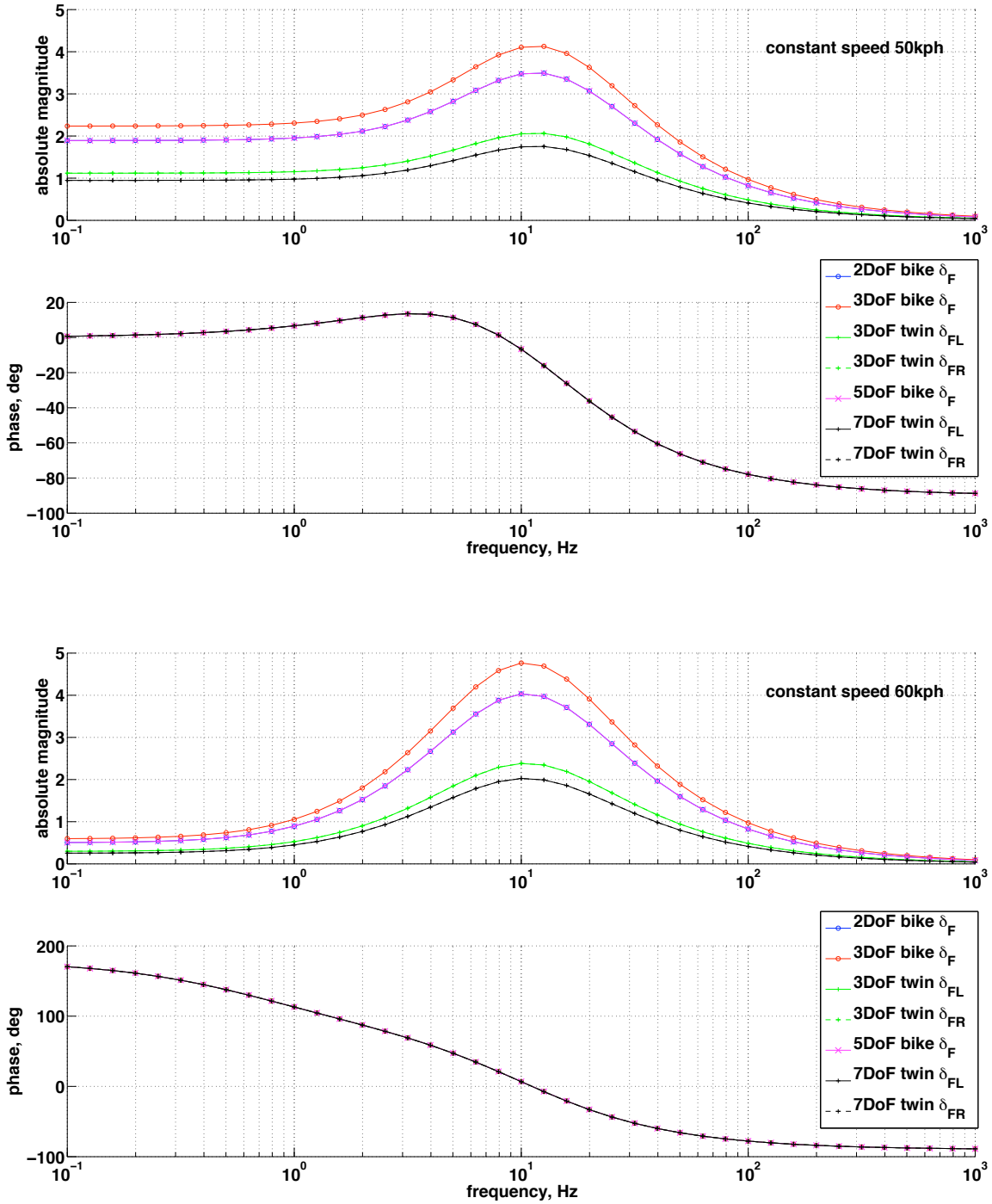

Figure D.3: Frequency response of lateral velocity with steering inputs for different models, 50 and 60kph

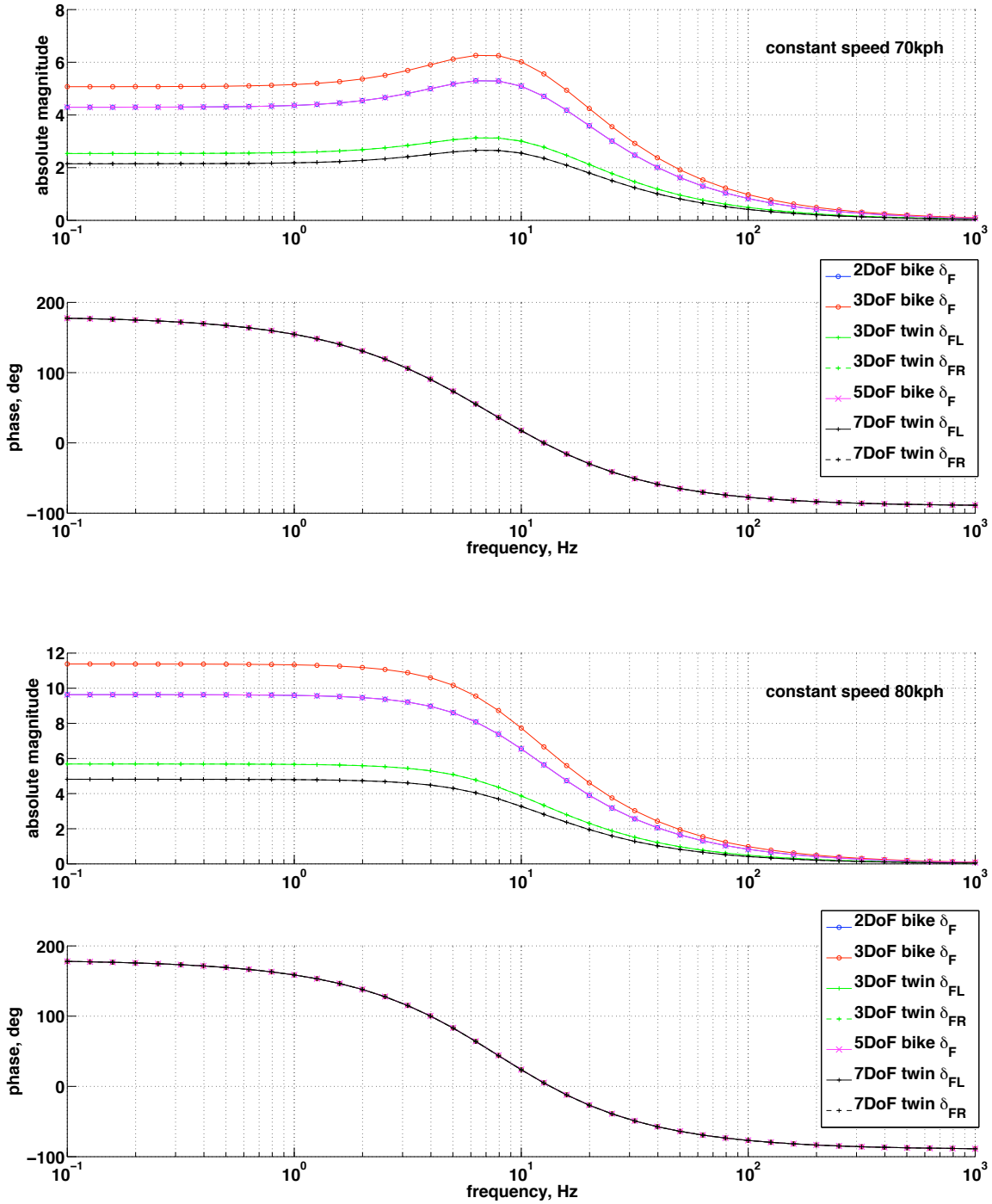

Figure D.4: Frequency response of lateral velocity with steering inputs for different models, 70 and 80kph

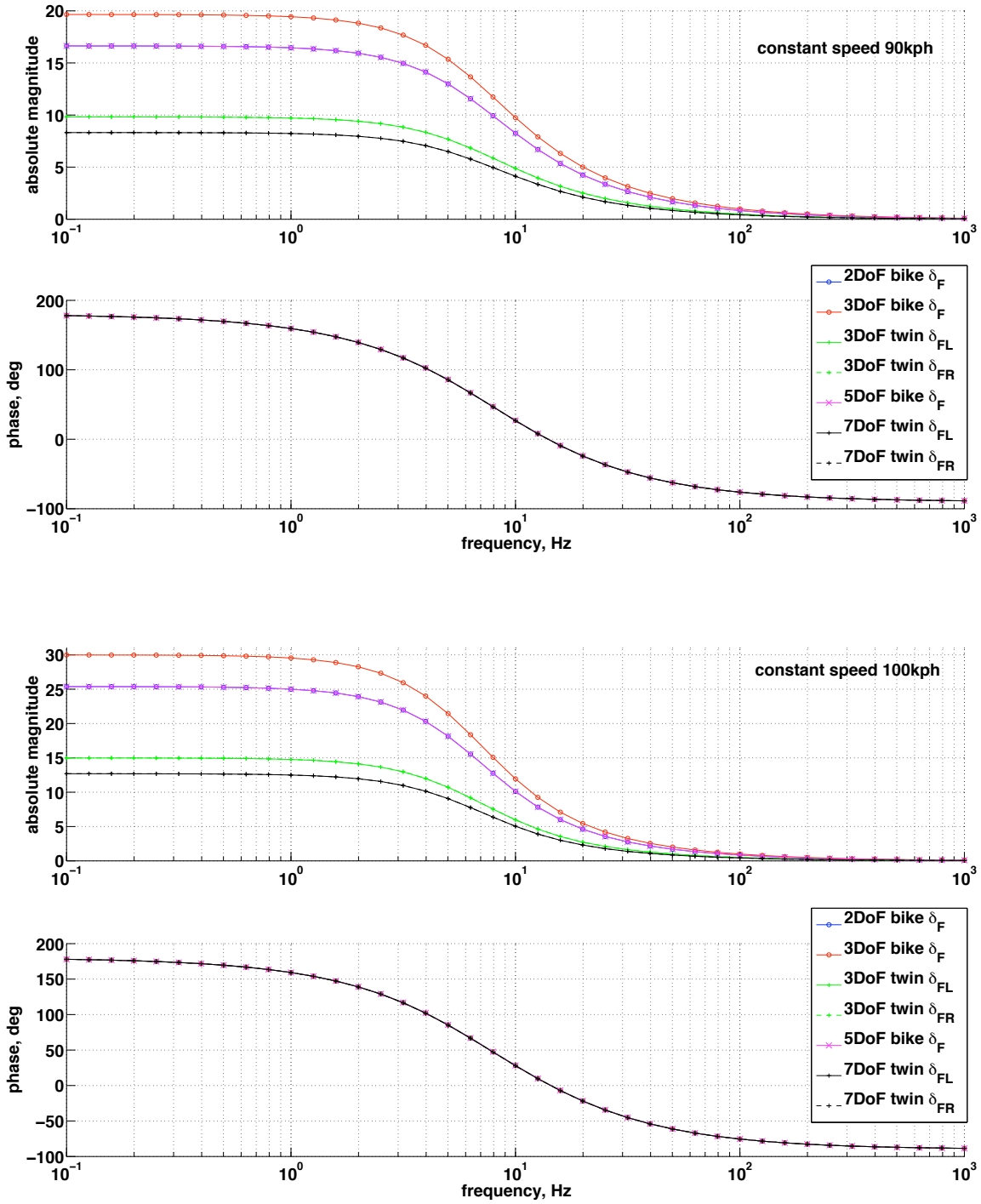

Figure D.5: Frequency response of lateral velocity with steering inputs for different models, 90 and 100kph

Appendix E

Vehicle Model Parametric Sensitivity

E.1 IKF_a state estimations comparison

In this section, additional results are shown for the comparison of four KF designs, namely, the IKF_a, the $MEKF_{2c}$, the $TripleKF_b$, and the 2DoF. The comparison for the state estimations and their erros for the *DoubleOval* and *LaneChangeISO* are shown in:

- Figures E.1 to E.2 – *DoubleOval_15kph*;
- Figures E.3 to E.4 – *DoubleOval_15kph*;
- Figures E.5 to E.6 – *DoubleOval_15kph*;
- Figures E.7 to E.8 – *DoubleOval_15kph*;
- Figures E.9 to E.10 – *DoubleOval_15kph*;
- Figures E.11 to E.12 – *LaneChangeISO_15kph*;
- Figures E.13 to E.14 – *LaneChangeISO_15kph*;
- Figures E.15 to E.16 – *LaneChangeISO_15kph*;
- Figures E.17 to E.18 – *LaneChangeISO_15kph*;
- Figures E.19 to E.20 – *LaneChangeISO_15kph*.

E.1.1 Analysis on the *DoubleOval* track

DoubleOval_15kph

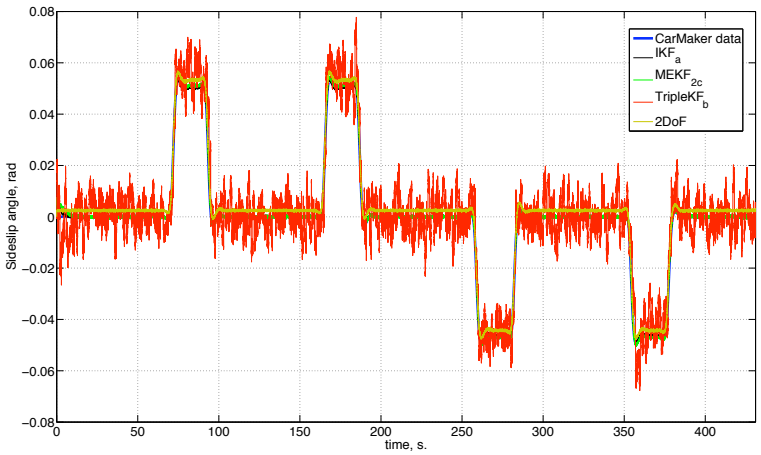

(a) Sideslip estimations

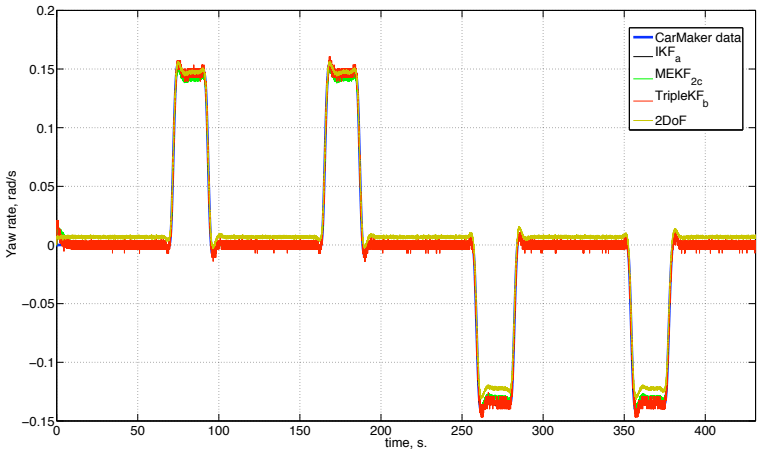

(b) Yaw rate estimations

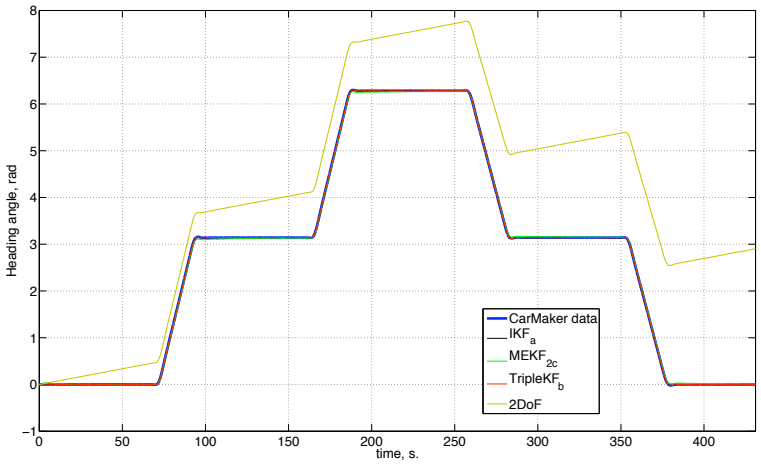

(c) Heading estimations

Figure E.1: State estimation on *DoubleOval_15kph* manoeuvre

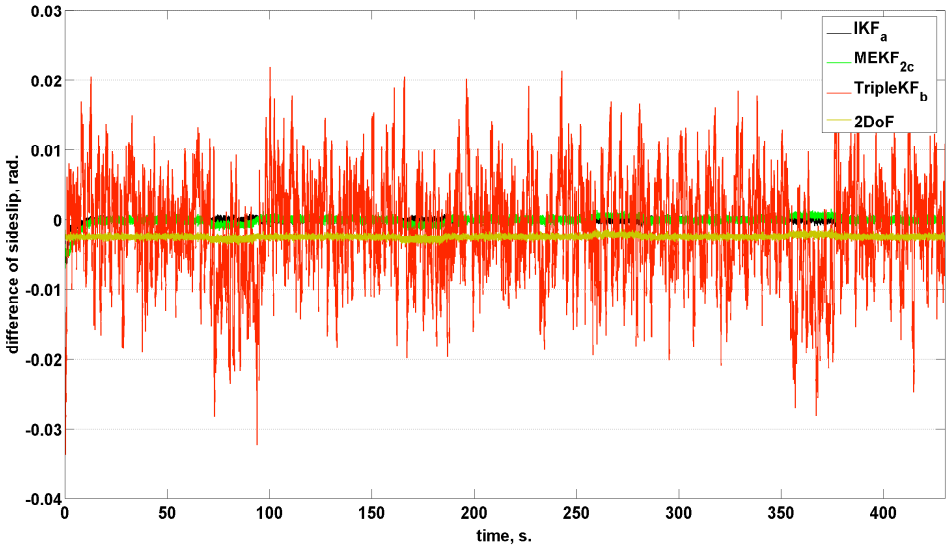

(a) Error in sideslip angle estimations

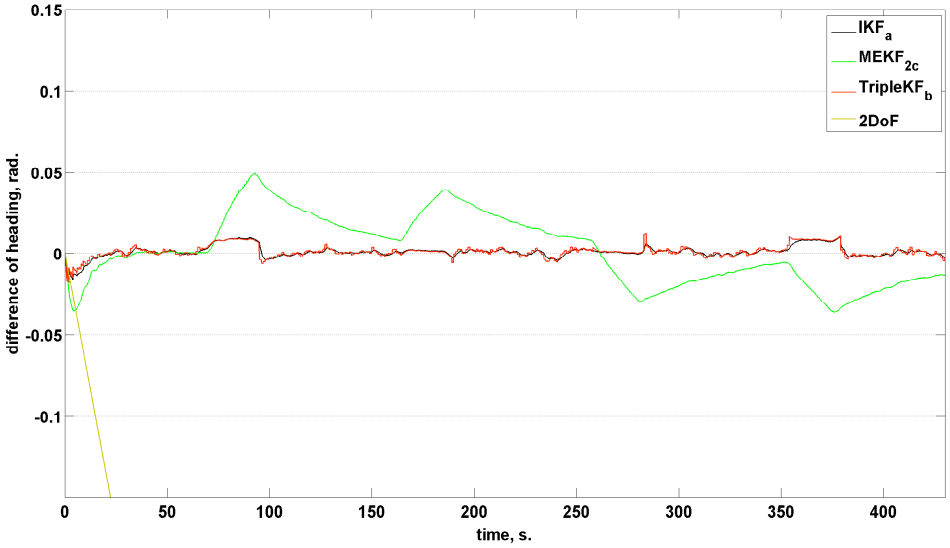

(b) Error in heading angle estimations

Figure E.2: State estimation error on *DoubleOval_15kph* manoeuvre with different KFs

DoubleOval_25kph

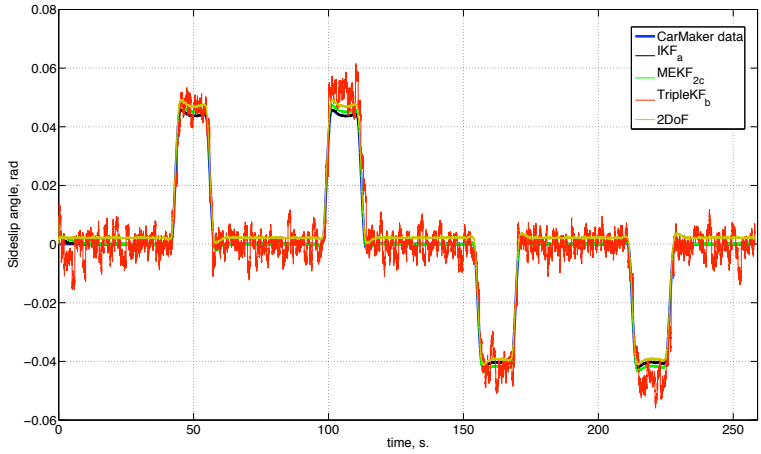

(a) Sideslip estimations

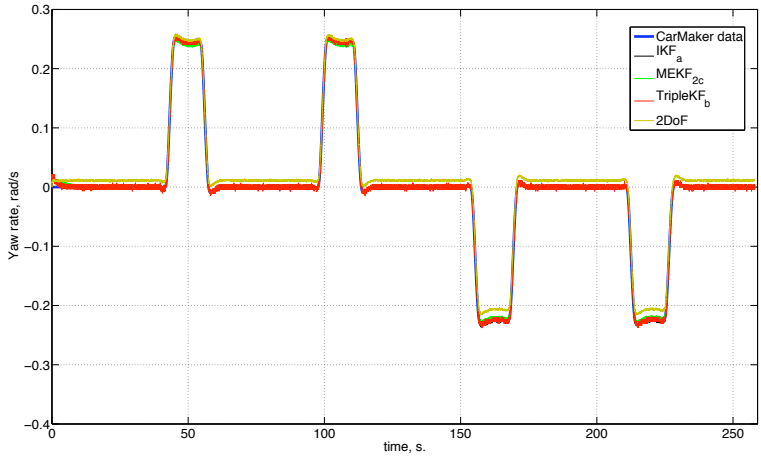

(b) Yaw rate estimations

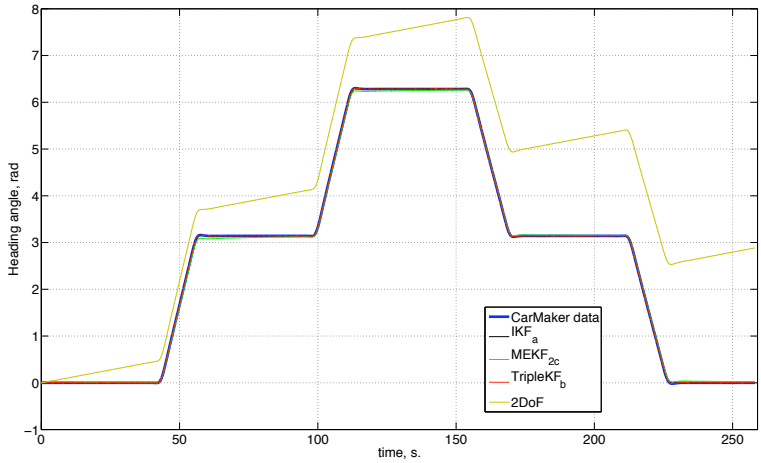

(c) Heading estimations

Figure E.3: State estimation on *DoubleOval_25kph* manoeuvre

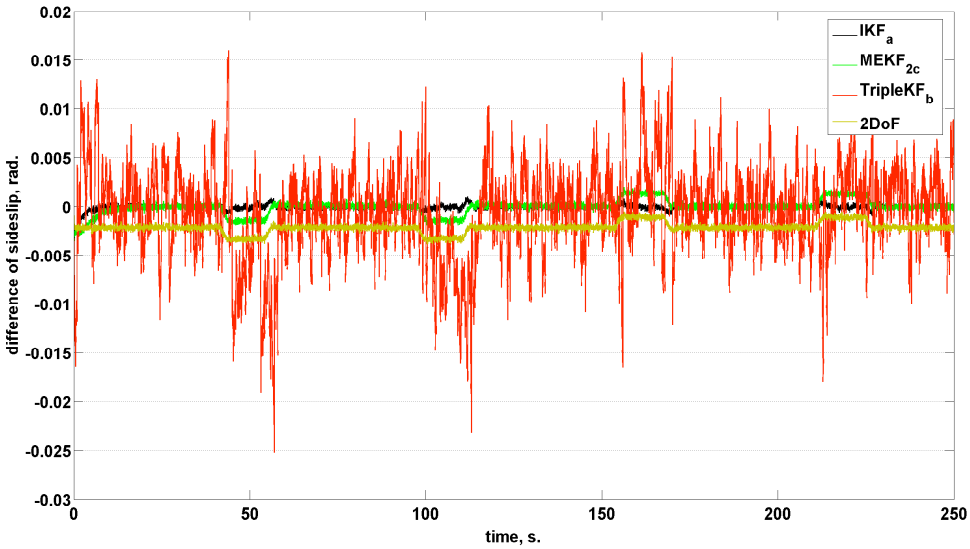

(a) Error in sideslip angle estimations

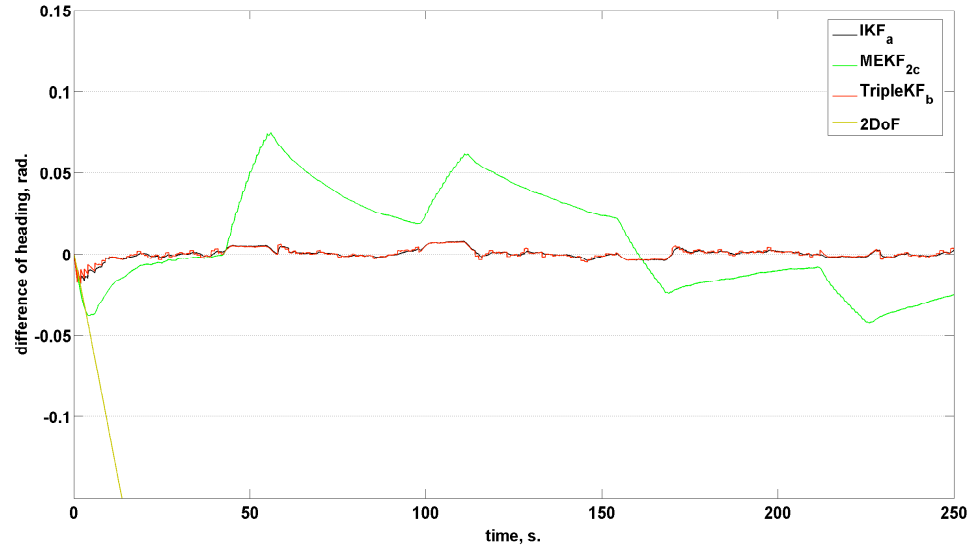

(b) Error in heading angle estimations

Figure E.4: State estimations error on *DoubleOval_25kph* manoeuvre with different KFs

DoubleOval_35kph

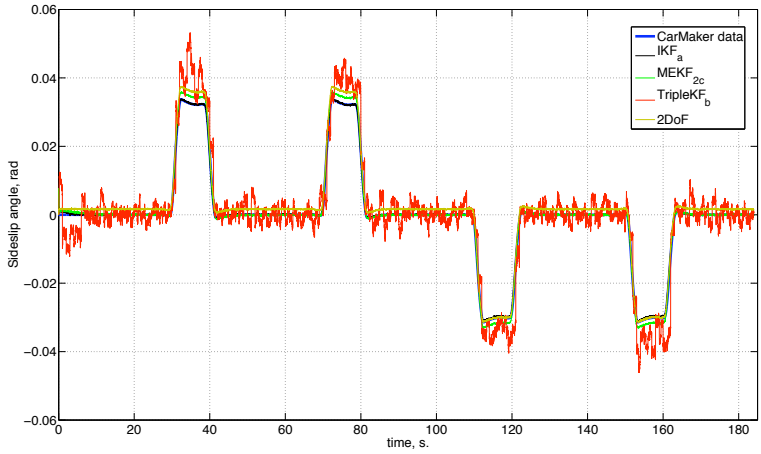

(a) Sideslip estimations

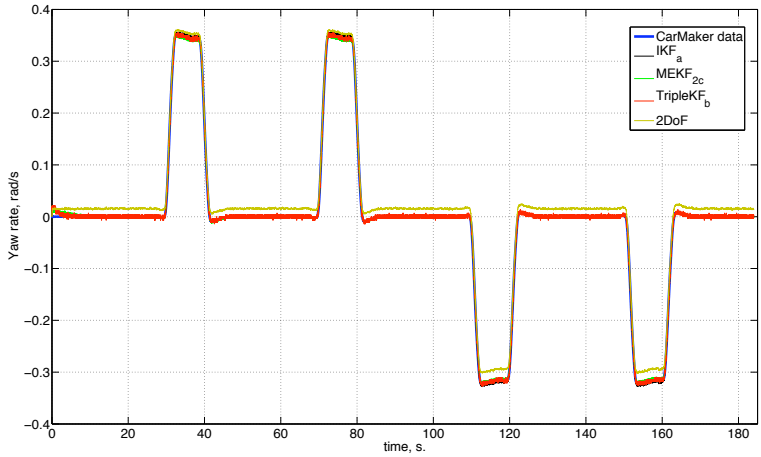

(b) Yaw rate estimations

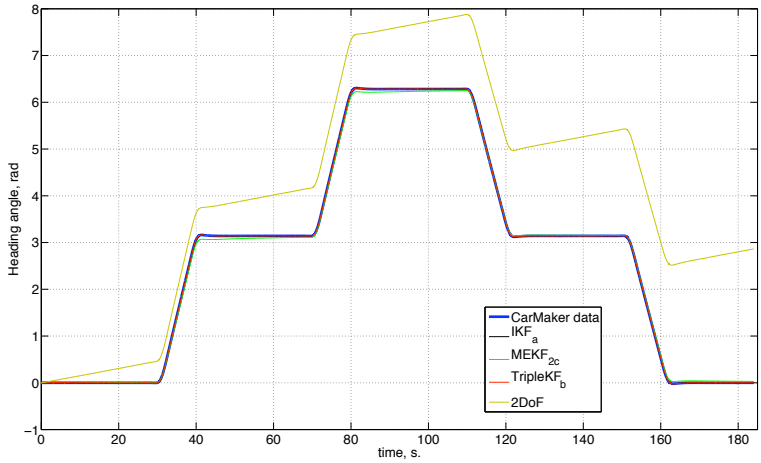

(c) Heading estimations

Figure E.5: State estimation on *DoubleOval_35kph* manoeuvre

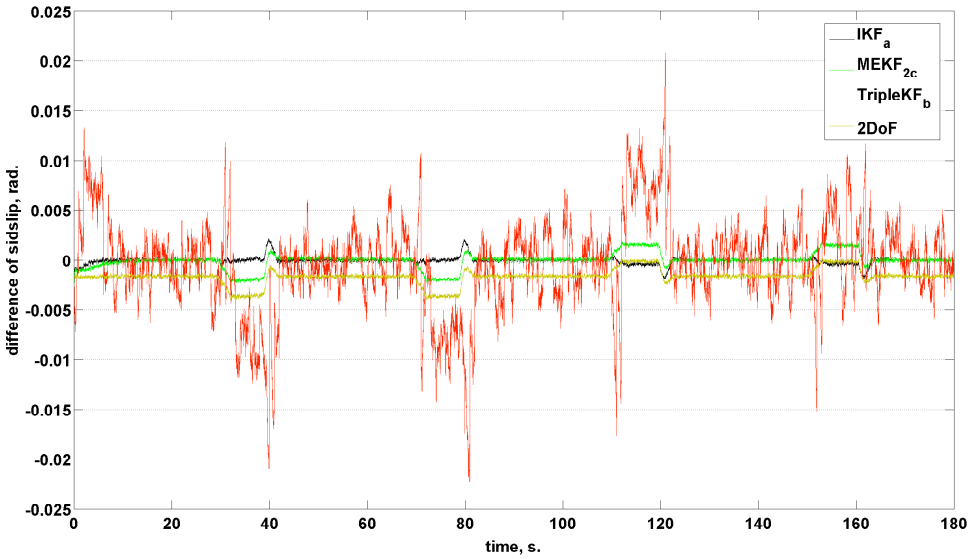

(a) Error in sideslip angle estimations

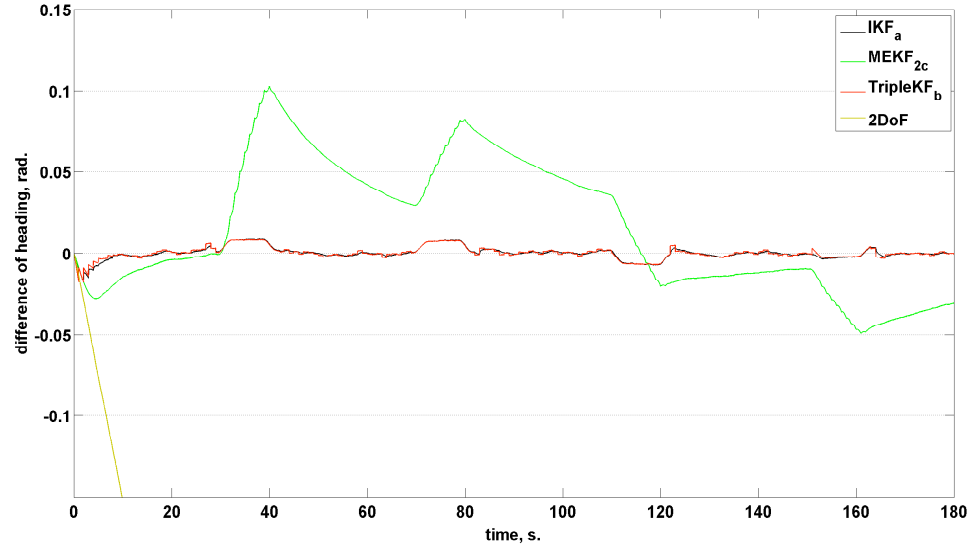

(b) Error in heading angle estimations

Figure E.6: State estimations error on *DoubleOval_35kph* manoeuvre with different KFs

DoubleOval_45kph

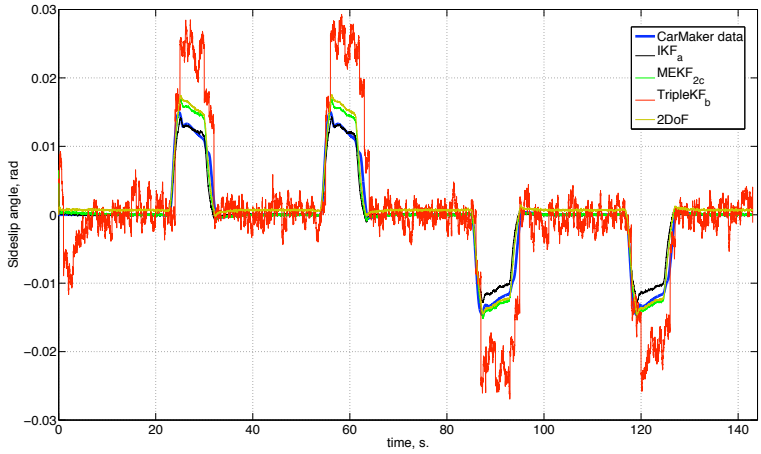

(a) Sideslip estimations

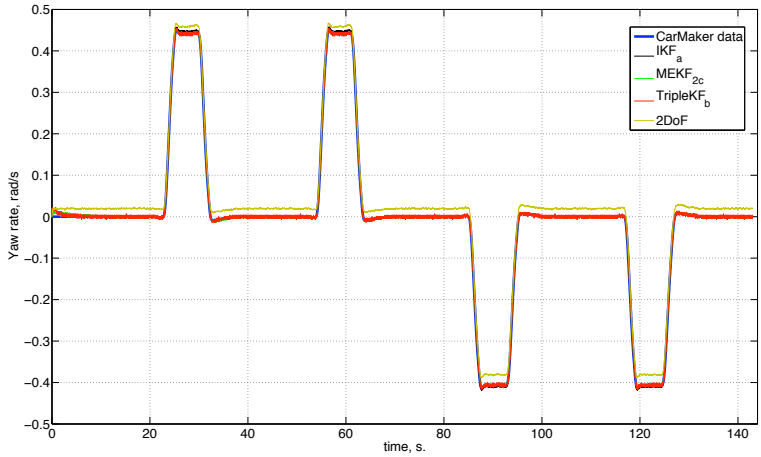

(b) Yaw rate estimations

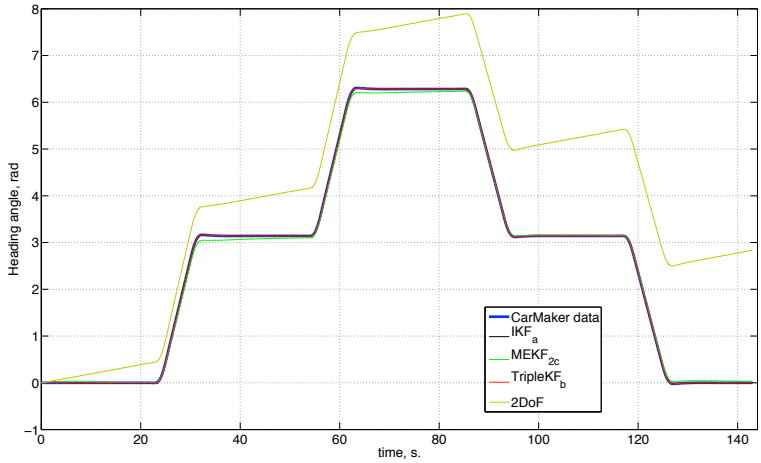

(c) Heading estimations

Figure E.7: State estimation on *DoubleOval_45kph* manoeuvre

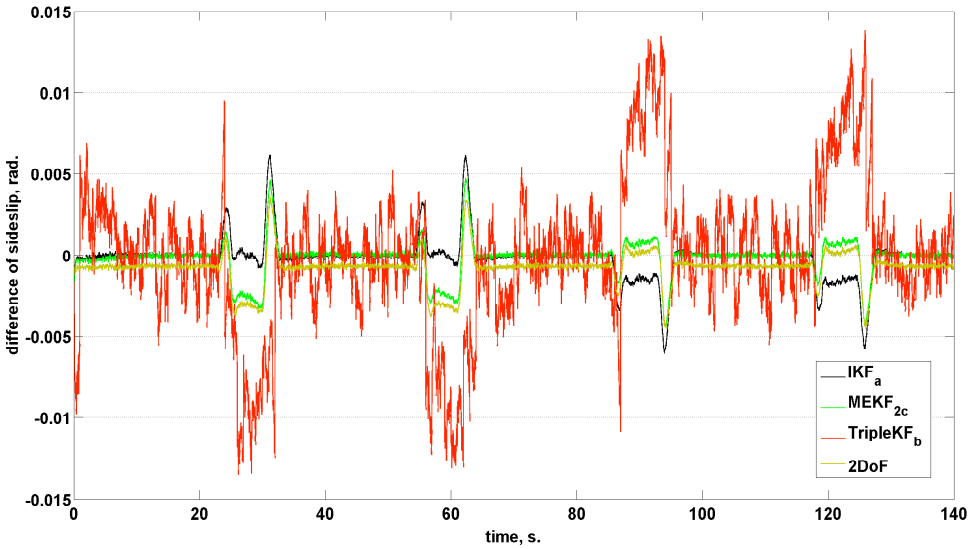

(a) Error in sideslip angle estimations

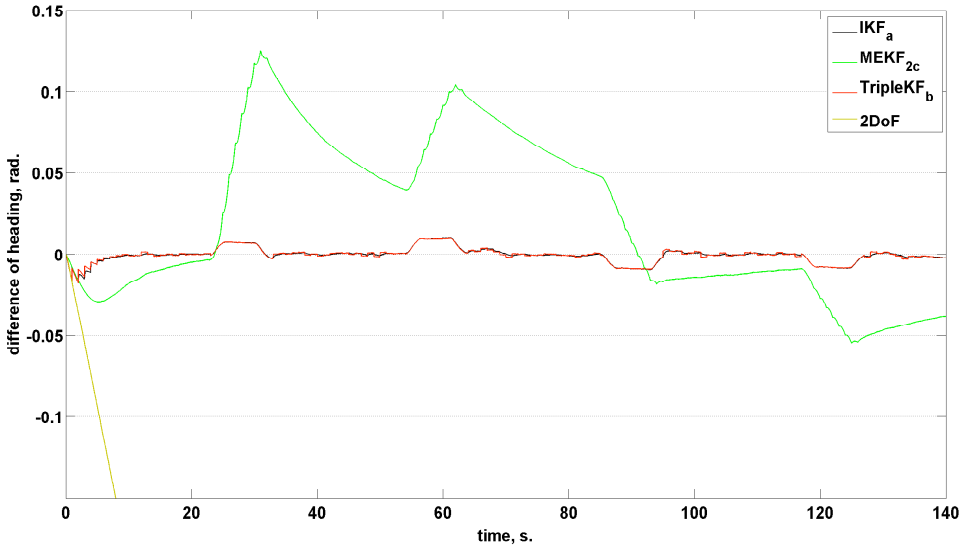

(b) Error in heading angle estimations

Figure E.8: State estimations error on *DoubleOval_45kph* manoeuvre with different KFs

DoubleOval_55kph

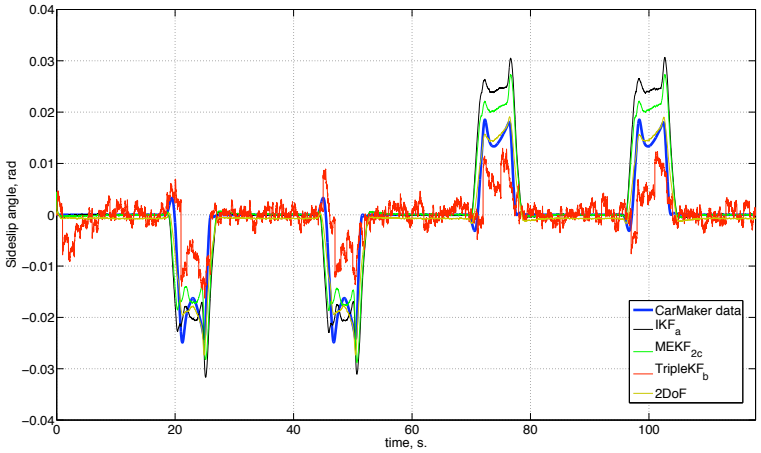

(a) Sideslip estimations

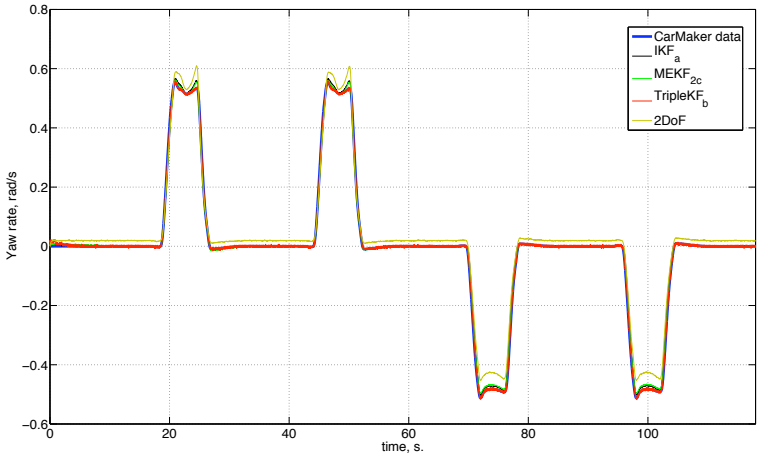

(b) Yaw rate estimations

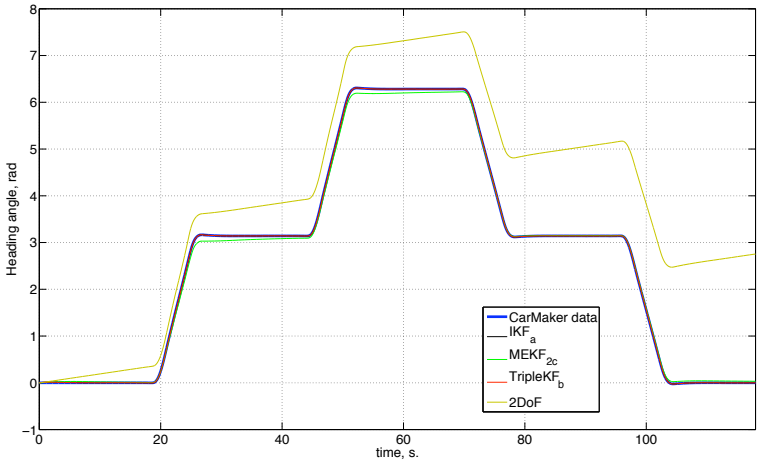

(c) Heading estimations

Figure E.9: State estimation on *DoubleOval_55kph* manoeuvre

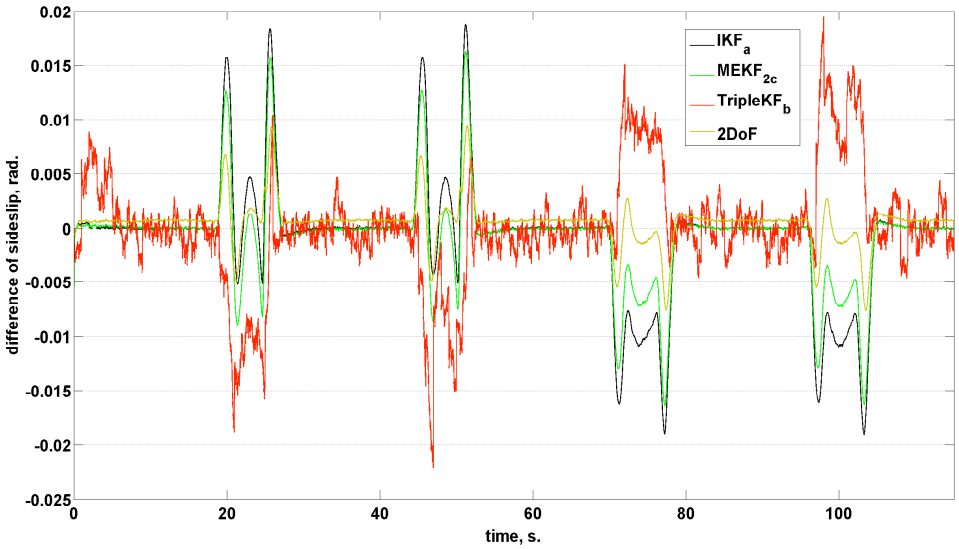

(a) Error in sideslip angle estimations

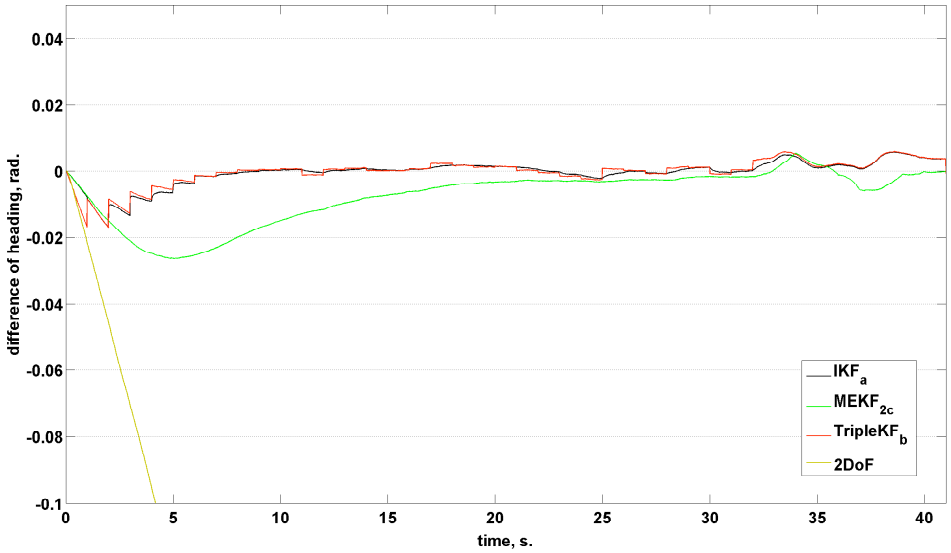

(b) Error in heading angle estimations

Figure E.10: State estimations error on *DoubleOval_55kph* manoeuvre with different KFs

E.1.2 Analysis on the *LaneChangeISO* track

LaneChangeISO_15kph

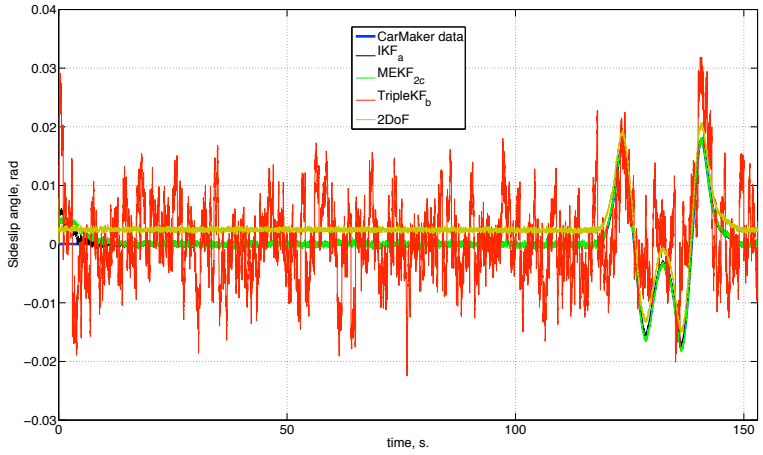

(a) Sideslip estimations

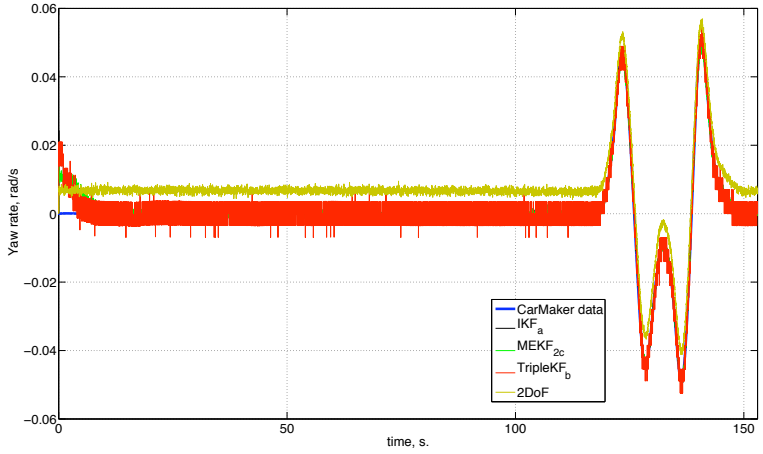

(b) Yaw rate estimations

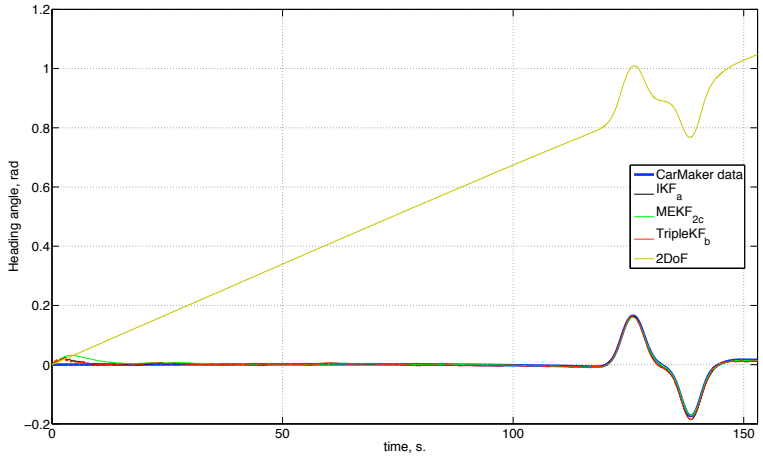

(c) Heading estimations

Figure E.11: State estimation on *LaneChangeISO_15kph* manoeuvre

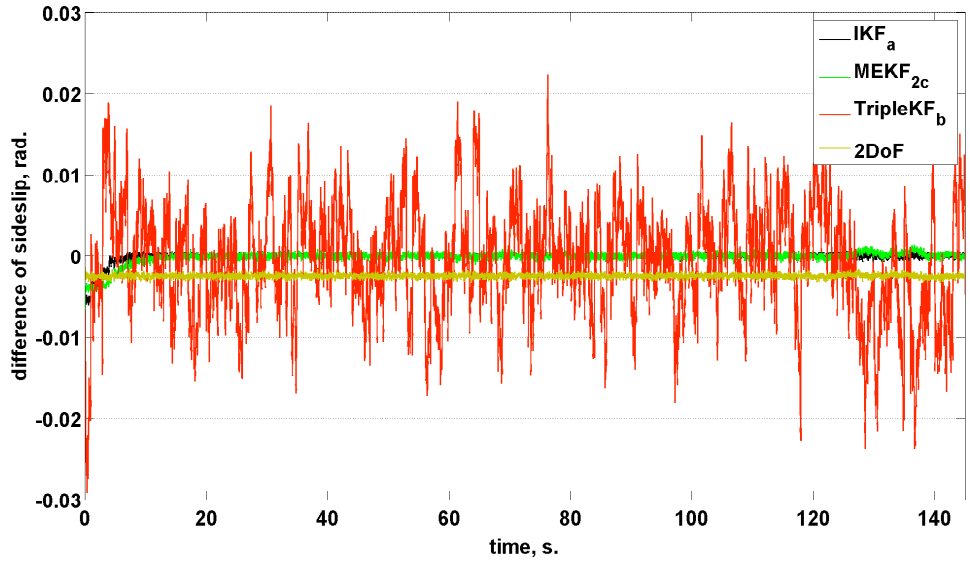

(a) Error in sideslip angle estimations

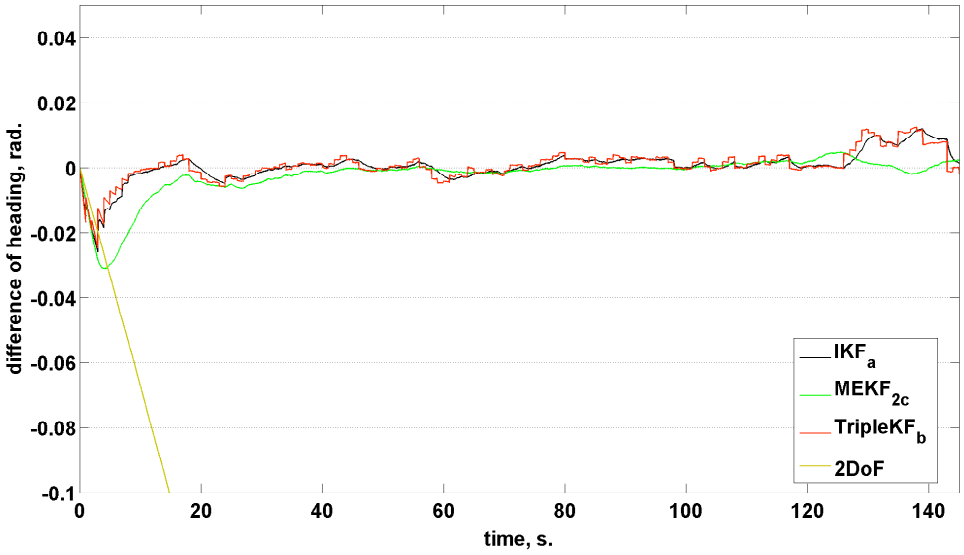

(b) Error in heading angle estimations

Figure E.12: State estimation error on *LaneChangeISO_15kph* manoeuvre with different KFs

LaneChangeISO_25kph

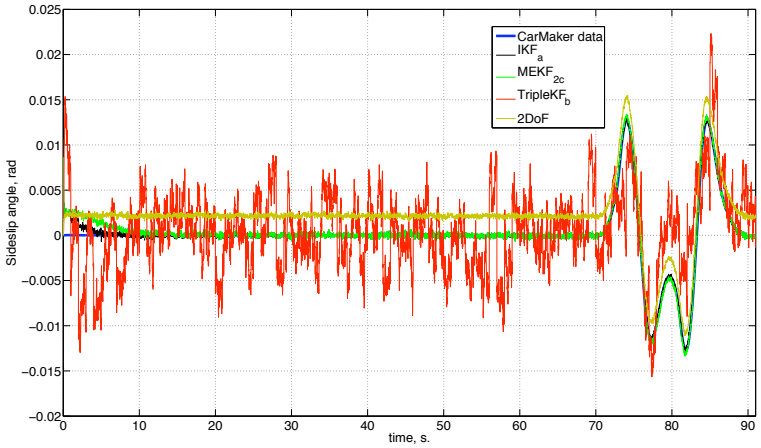

(a) Sideslip estimations

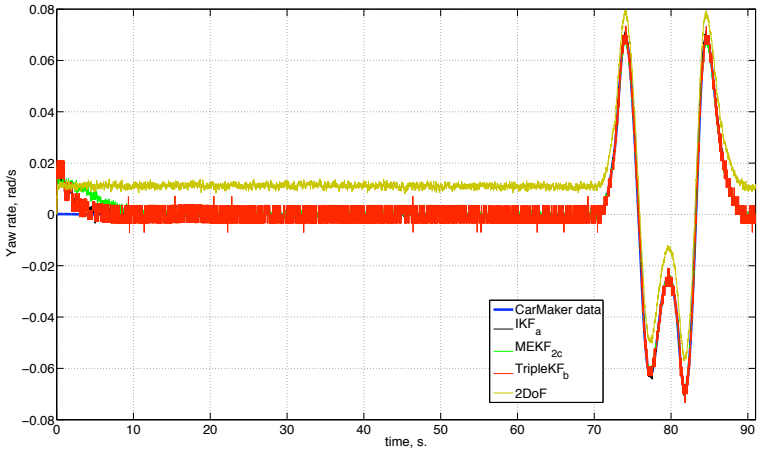

(b) Yaw rate estimations

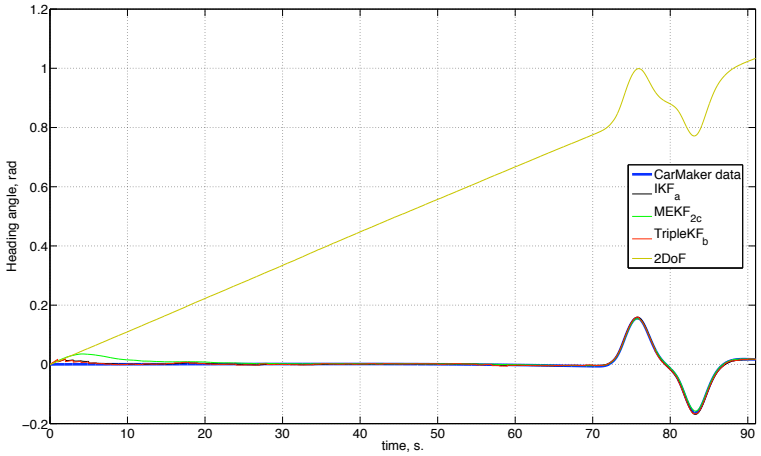

(c) Heading estimations

Figure E.13: State estimation on *LaneChangeISO_25kph* manoeuvre

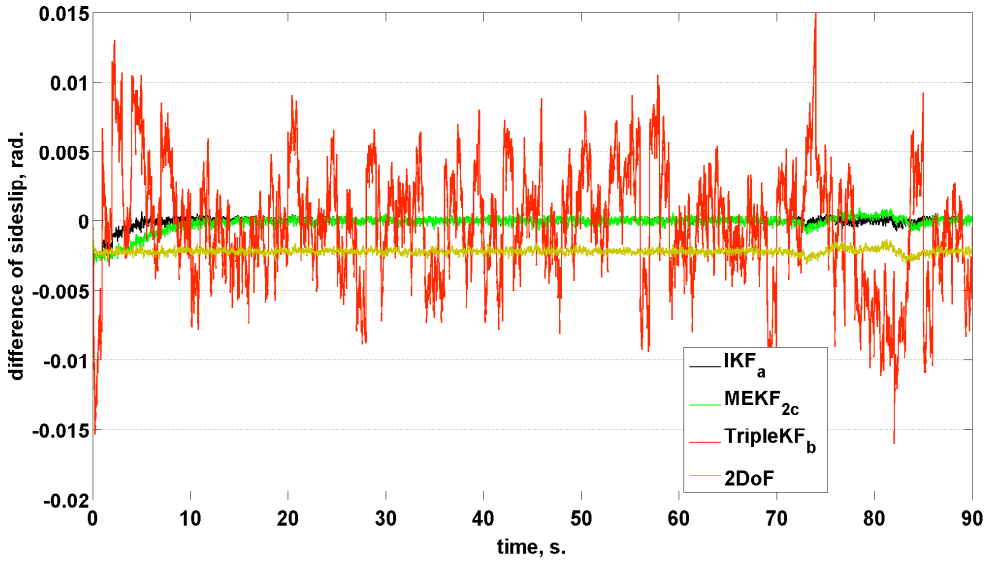

(a) Error in sideslip angle estimations

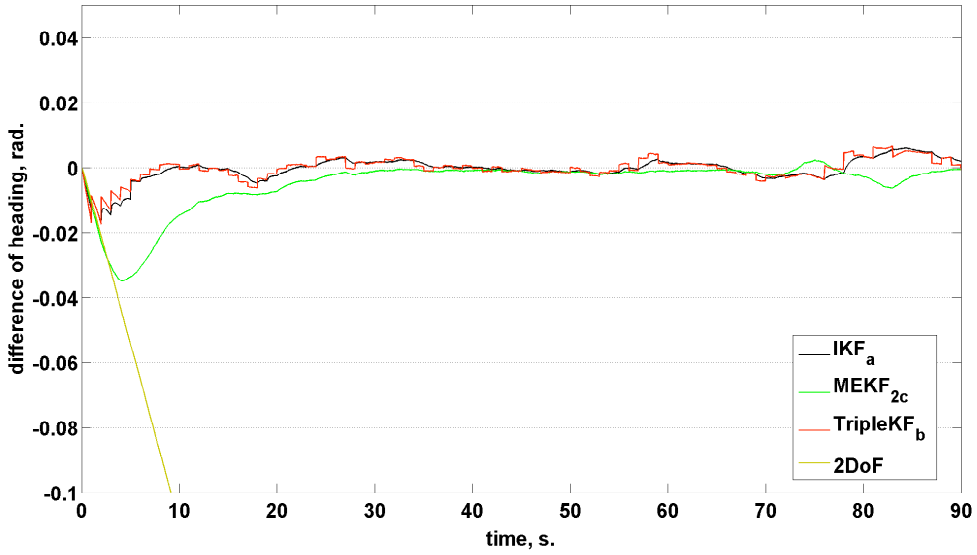

(b) Error in heading angle estimations

Figure E.14: State estimation error on *LaneChangeISO_25kph* manoeuvre with different KFs

LaneChangeISO_35kph

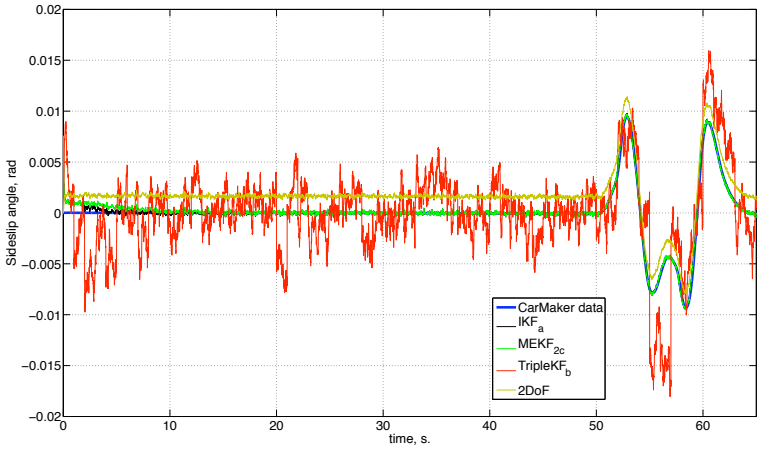

(a) Sideslip estimations

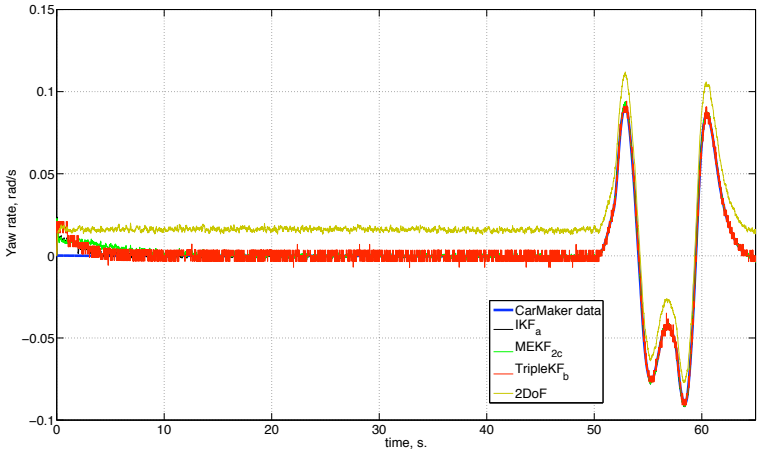

(b) Yaw rate estimations

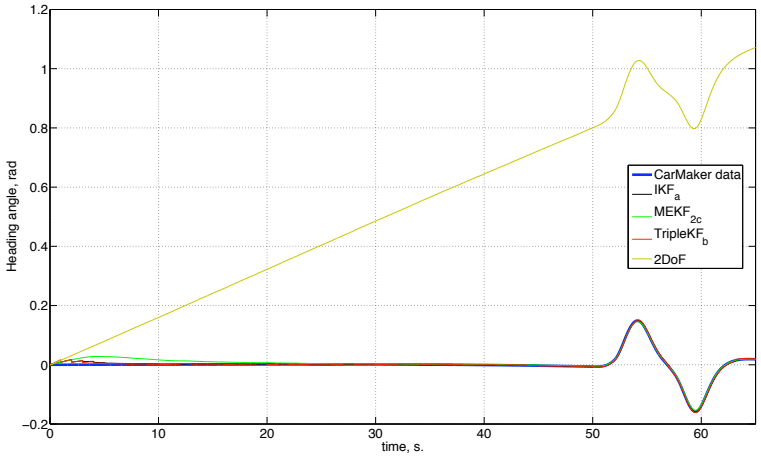

(c) Heading estimations

Figure E.15: State estimation on *LaneChangeISO_35kph* manoeuvre

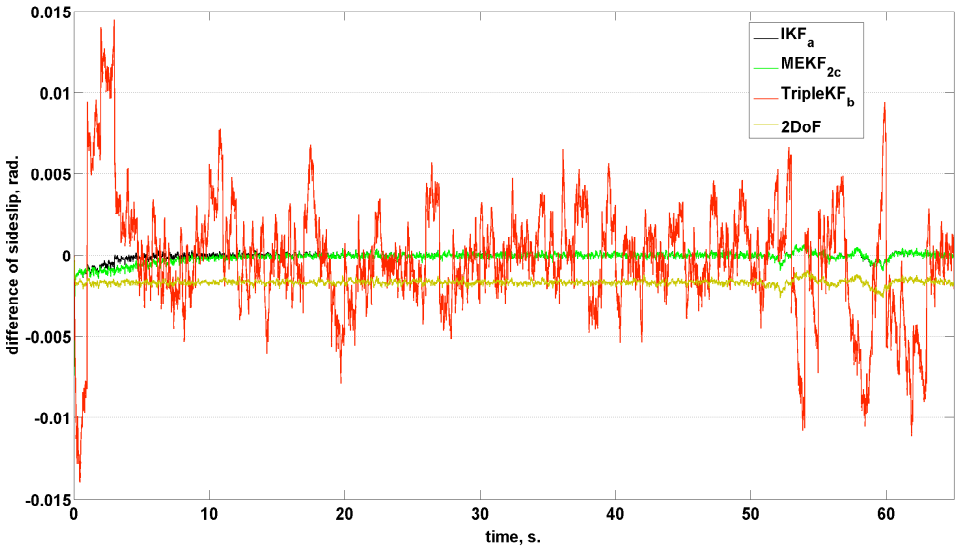

(a) Error in sideslip angle estimations

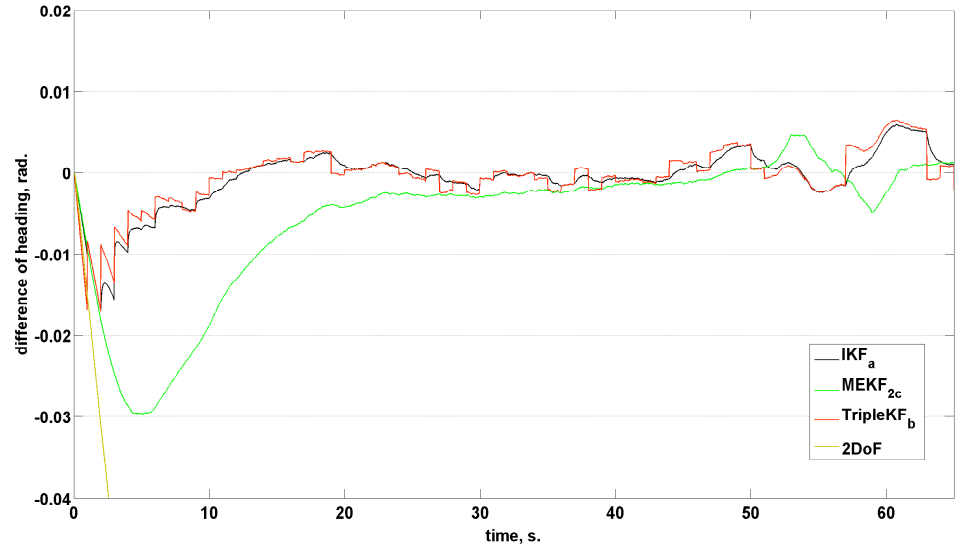

(b) Error in heading angle estimations

Figure E.16: State estimation error on *LaneChangeISO_35kph* manoeuvre with different KFs

LaneChangeISO_45kph

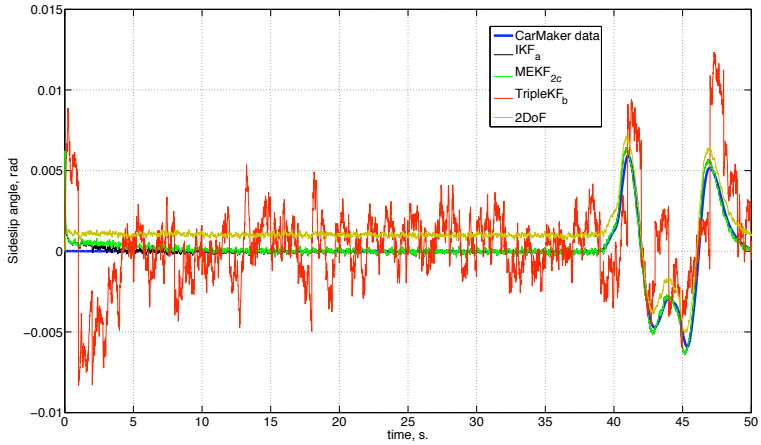

(a) Sideslip estimations

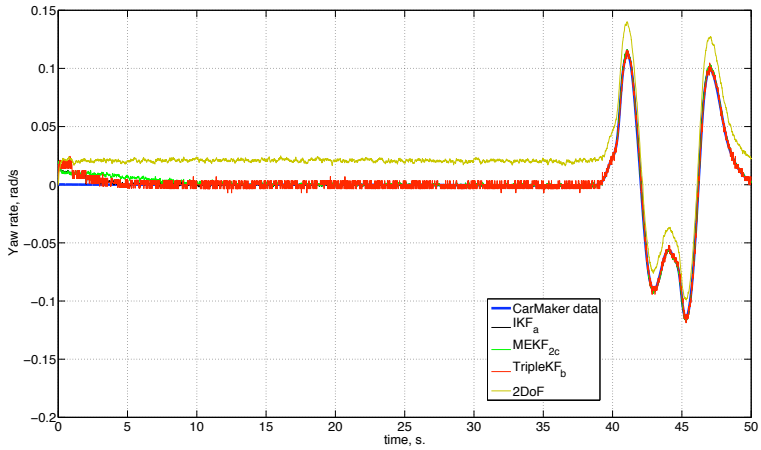

(b) Yaw rate estimations

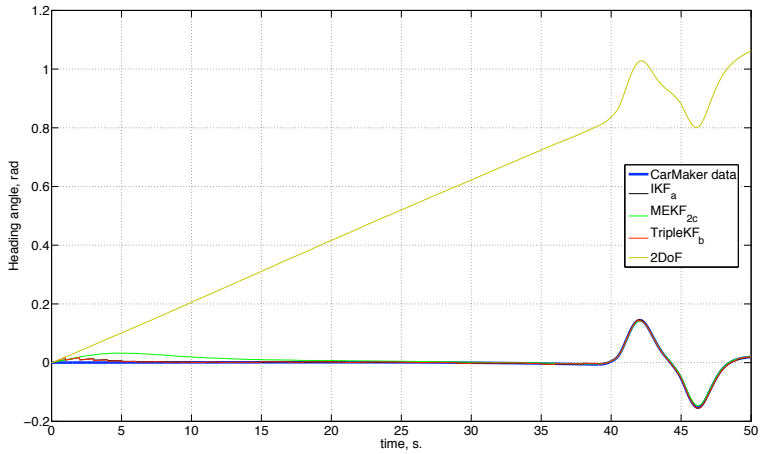

(c) Heading estimations

Figure E.17: State estimation on *LaneChangeISO_45kph* manoeuvre

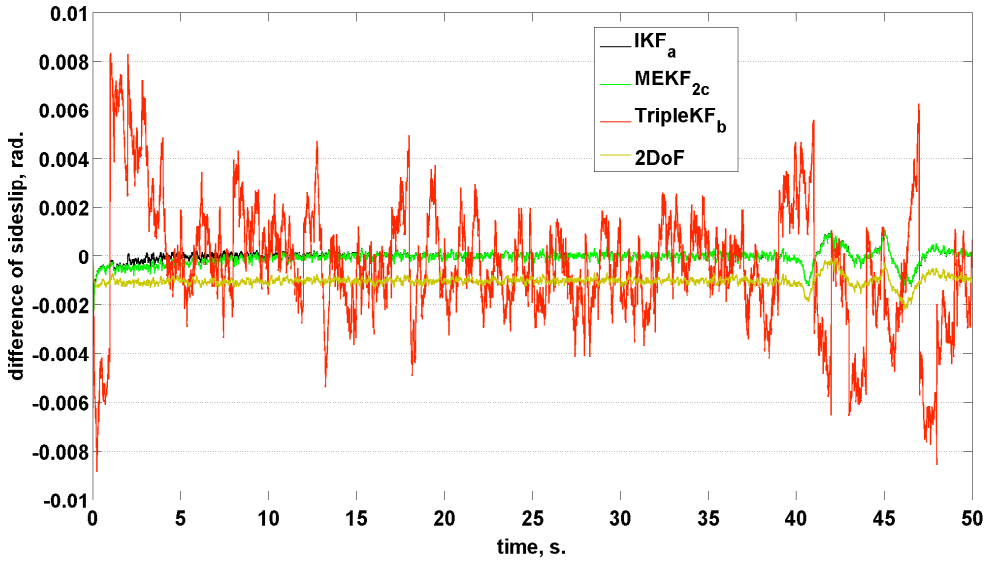

(a) Error in sideslip angle estimations

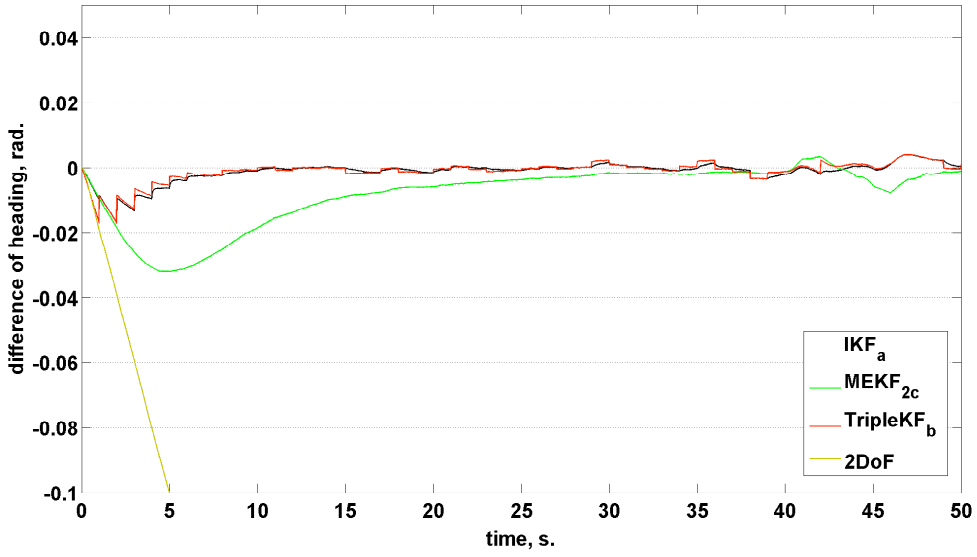

(b) Error in heading angle estimations

Figure E.18: State estimation error on *LaneChangeISO_45kph* manoeuvre with different KFs

LaneChangeISO_55kph

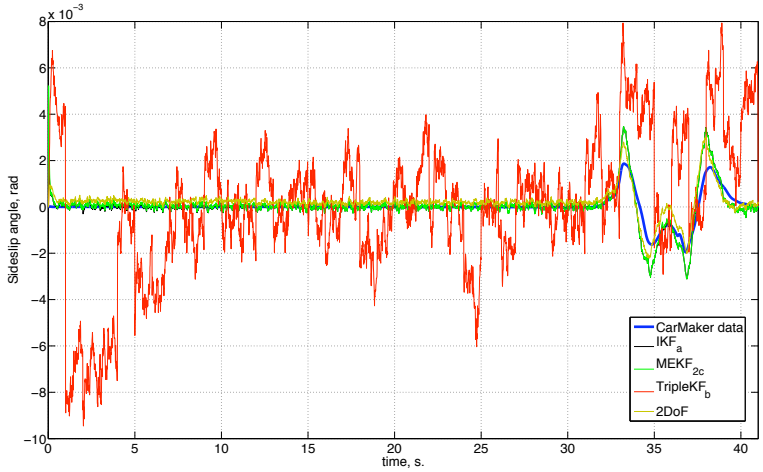

(a) Sideslip estimations

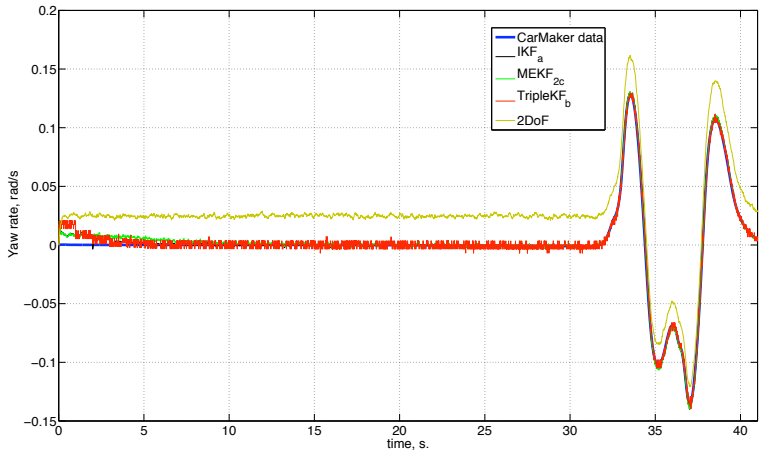

(b) Yaw rate estimations

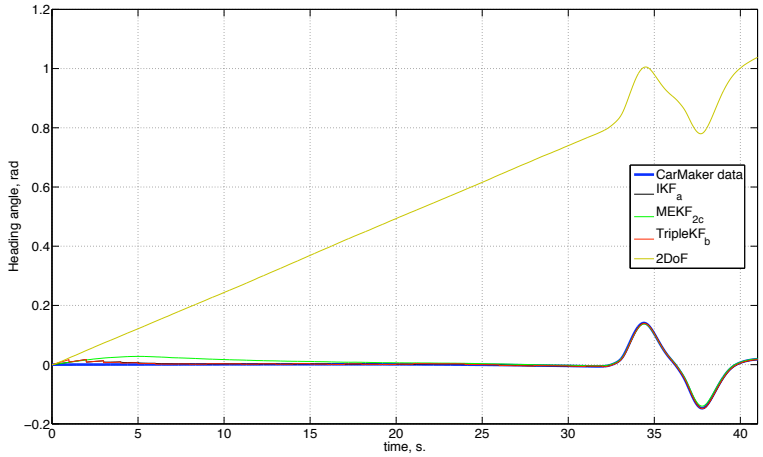

(c) Heading estimations

Figure E.19: State estimation on *LaneChangeISO_55kph* manoeuvre

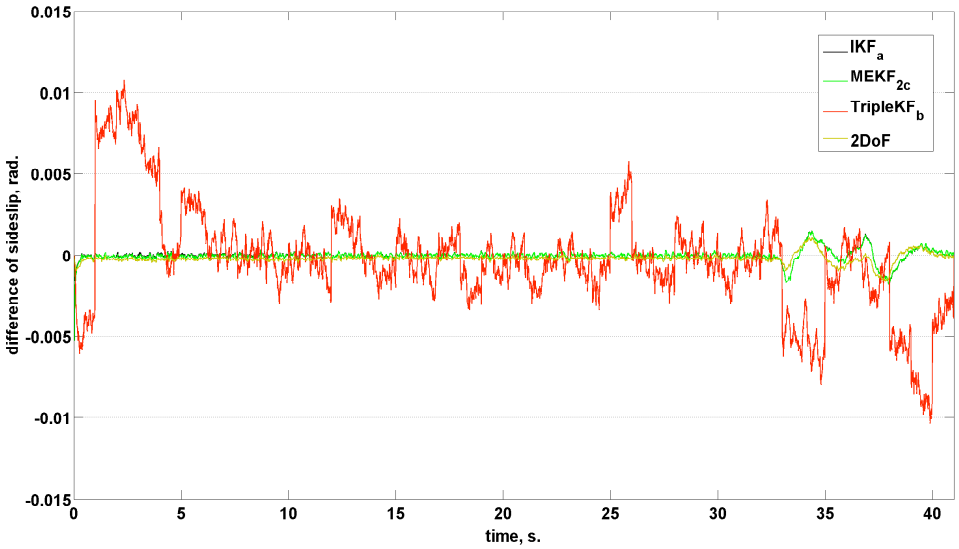

(a) Error in sideslip angle estimations

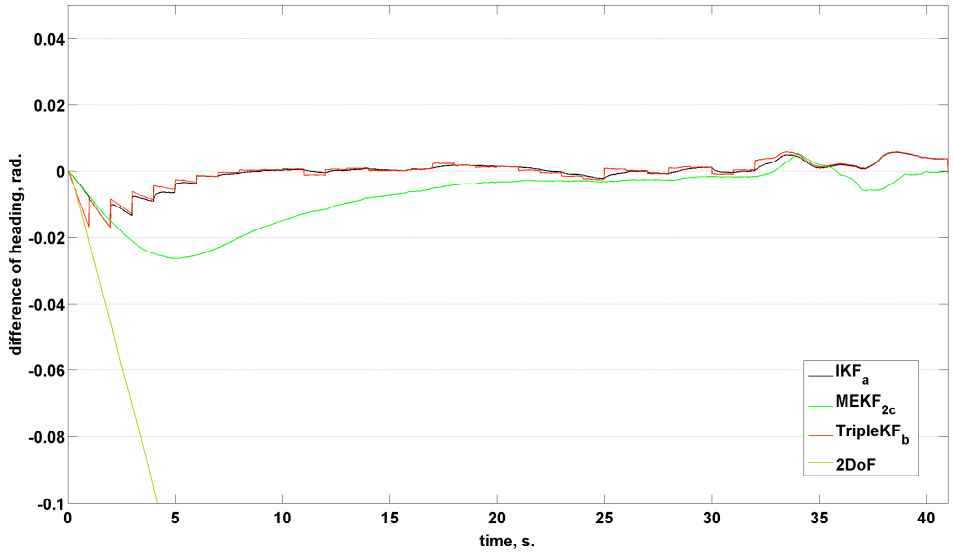

(b) Error in heading angle estimations

Figure E.20: State estimation error on *LaneChangeISO_55kph* manoeuvre with different KFs

This page intentionally left blank.

Appendix F

Business Research

%Var	percentage of variance
%Cum	cumulative percentage

F.1 Car segmentation

Table F.1: Car segmentation in the UK suggested by Truscott [1967]

Basic segments (Car sizes/performance)	**Price**	**Car type**	**Example**
small	lower	basic	N/A
		luxury & speciality	N/A
		estate	N/A
	upper	basic	Mini
		luxury & speciality	Mini Cooper
		estate	Mini
light	lower	basic	Cortina 1200
		luxury & speciality	MG 1100
		estate	Cortina 1200
	upper	basic	Cortina 1300
		luxury & speciality	Cortina GT
		estate	Cortina Super
medium	lower	basic	Austin A60
		luxury & speciality	Riley 4/72
		estate	Victor
	upper	basic	Rover 2000
		luxury & speciality	Jaguar 240
		estate	Triumph 2000
large	lower	basic	Zodiac V6
		luxury & speciality	Viscount
		estate	N/A
	upper	basic	Rover 3 Litre
		luxury & speciality	Jaguar Mk X
		estate	N/A
sports	lower	basic	Sprite
		luxury & speciality	Mini Cooper 1275 ‘s’
		estate	N/A
	upper	basic	MG C
		luxury & speciality	Jaguar ‘E’ Open
		estate	N/A
grand touring	lower	basic	MG B GT
		luxury & speciality	N/A
		estate	N/A
	upper	basic	Jaguar ’E’ FH
		luxury & speciality	Aston Martin
		estate	N/A

F.2 NVES_US

This section shows additional tables and figures for the statistical analysis of the US automotive market presented in section 6.4. All analyses are carried out in SPSS.

The 38 attributes are reduced to 10 latent factors by using the factor analysis:

- Table F.2 – Total variance explained with Principle Component Analysis (PCA)
- Table F.3 – Rotated total variance explained with Principle Component Analysis (PCA)

Using the SPSS TwoStep clustering, the 10 latent factors are segmented into 5 clusters with regards to customers' details:

- Table F.4 – Pre-retirement of customers in the five segments
- Figure F.1 – T-statistic for the latent factors in Cluster 1
- Figure F.2 – T-statistic for the latent factors in Cluster 2
- Figure F.3 – T-statistic for the latent factors in Cluster 3
- Figure F.4 – T-statistic for the latent factors in Cluster 4
- Figure F.5 – T-statistic for the latent factors in Cluster 5

The customers' choice of brands in terms of their demographic details and ratings on the 10 latent factors are modelled using the discriminant analysis:

- Table F.5 – Unrotated Structure Matrix for the discriminant analysis of brand choice
- Table F.6 – Rotated Structure Matrix for the discriminant analysis of brand choice
- Table F.7 – Classification of brand choice model

Table F.2: Total variance explained with Principle Component Analysis (PCA)

	Initial Eigenvalues		
Component	**Total**	**%Var**	**%Cum**
1	12.70	31.74	31.74
2	3.59	8.98	40.72
3	2.33	5.82	46.54
4	1.59	3.98	50.51
5	1.41	3.51	54.03
6	1.12	2.81	56.84
7	1.02	2.55	59.38
8	0.98	2.46	61.85
9	0.86	2.14	63.99
10	0.85	2.12	66.10
11	0.77	1.92	68.02
12	0.76	1.90	69.92
13	0.66	1.66	71.58
14	0.64	1.61	73.19
15	0.63	1.57	74.77
16	0.60	1.51	76.28
17	0.58	1.46	77.73
18	0.57	1.42	79.15
19	0.56	1.41	80.56
20	0.55	1.37	81.93
21	0.54	1.34	83.26
22	0.50	1.24	84.50
23	0.48	1.21	85.71
24	0.47	1.17	86.88
25	0.44	1.11	87.99
26	0.43	1.07	89.06
27	0.41	1.02	90.08
28	0.40	1.00	91.08
29	0.39	0.97	92.05
30	0.37	0.94	92.99
31	0.36	0.91	93.90
32	0.33	0.82	94.72
33	0.31	0.78	95.50
34	0.31	0.77	96.28
35	0.30	0.75	97.03
36	0.28	0.71	97.74
37	0.26	0.66	98.40
38	0.25	0.61	99.01
39	0.22	0.54	99.55
40	0.18	0.45	100.00

Table F.3: Rotated total variance explained with Principle Component Analysis (PCA)

	Initial Eigenvalues			**Extraction Sums of Squared Loadings**		
Component	**Total**	**%Var**	**%Cum**	**Total**	**%Var**	**%Cum**
1	12.33	32.45	32.45	12.33	32.45	32.45
2	3.44	9.04	41.49	3.44	9.04	41.49
3	2.32	6.11	47.60	2.32	6.11	47.60
4	1.53	4.02	51.62	1.53	4.02	51.62
5	1.36	3.59	55.20	1.36	3.59	55.20
6	1.08	2.85	58.05	1.08	2.85	58.05
7	0.99	2.61	60.65	0.99	2.61	60.65
8	0.94	2.47	63.13	0.94	2.47	63.13
9	0.85	2.25	65.38	0.85	2.25	65.38
10	0.81	2.14	67.52	0.81	2.14	67.52
11	0.76	1.99	69.51			
12	0.71	1.87	71.38			
13	0.63	1.66	73.04			
14	0.63	1.66	74.69			
15	0.62	1.62	76.31			
16	0.58	1.54	77.85			
17	0.57	1.50	79.35			
18	0.56	1.46	80.81			
19	0.54	1.41	82.22			
20	0.50	1.32	83.54			
21	0.49	1.30	84.84			
22	0.48	1.27	86.11			
23	0.45	1.18	87.29			
24	0.44	1.15	88.44			
25	0.41	1.08	89.51			
26	0.40	1.06	90.58			
27	0.39	1.03	91.61			
28	0.38	0.99	92.60			
29	0.36	0.96	93.56			
30	0.33	0.87	94.43			
31	0.31	0.82	95.26			
32	0.31	0.82	96.07			
33	0.30	0.80	96.87			
34	0.28	0.75	97.62			
35	0.26	0.69	98.31			
36	0.25	0.65	98.96			
37	0.22	0.57	99.53			
38	0.18	0.47	100.00			

Table F.4: Pre-retirement of customers in the five segments

		Cluster					
Pre-retirement		**1**	**2**	**3**	**4**	**5**	**Combined**
Administrative Clerical	**N**	287	14	3	0	0	304
	%	94.41	4.61	0.99	0.00	0.00	100
Armed Services	**N**	134	82	0	9	43	268
	%	50.00	30.60	0.00	3.36	16.04	100
Executive/Managerial	**N**	400	706	4	0	14	1124
	%	35.59	62.81	0.36	0.00	1.25	100
Factory Worker	**N**	158	3	0	2	0	163
	%	96.93	1.84	0.00	1.23	0.00	100
Farmer	**N**	36	4	0	0	0	40
	%	90.00	10.00	0.00	0.00	0.00	100
Health Care	**N**	67	88	8	3	0	166
	%	40.36	53.01	4.82	1.81	0.00	100
Homemaker	**N**	46	2	0	1	0	49
	%	93.88	4.08	0.00	2.04	0.00	100
Owner/Proprietor	**N**	157	69	2	0	1	229
	%	68.56	30.13	0.87	0.00	0.44	100
Police, Postal, Fire	**N**	220	35	3	1	16	275
	%	80.00	12.73	1.09	0.36	5.82	100
Professional Specialty	**N**	196	418	6	2	5	627
	%	31.26	66.67	0.96	0.32	0.80	100
Sales Work	**N**	153	55	6	1	1	216
	%	70.83	25.46	2.78	0.46	0.46	100
Service Worker	**N**	69	3	1	1	0	74
	%	93.24	4.05	1.35	1.35	0.00	100
Skilled Trade	**N**	354	0	2	1	3	360
	%	98.33	0.00	0.56	0.28	0.83	100
Student	**N**	1	0	0	1	0	2
	%	50.00	0.00	0.00	50.00	0.00	100
Teacher, Educator	**N**	4	484	0	1	2	491
	%	0.81	98.57	0.00	0.20	0.41	100
Technical Specialty	**N**	220	79	0	4	0	303
	%	72.61	26.07	0.00	1.32	0.00	100
Other	**N**	77	38	0	9	2	126
	%	61.11	30.16	0.00	7.14	1.59	100
No Answer	**N**	91	34	0	0	0	125
	%	72.80	27.20	0.00	0.00	0.00	100
				total number of respondents			4942

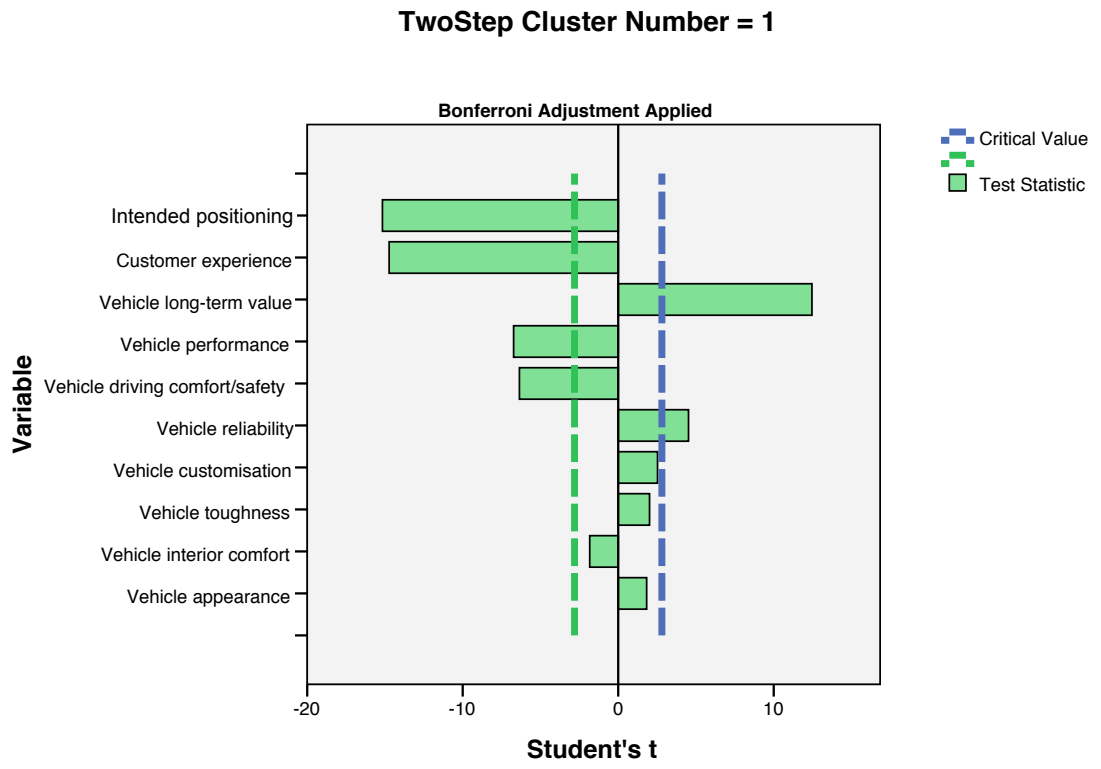

Figure F.1: T-statistic for the latent factors in Cluster 1

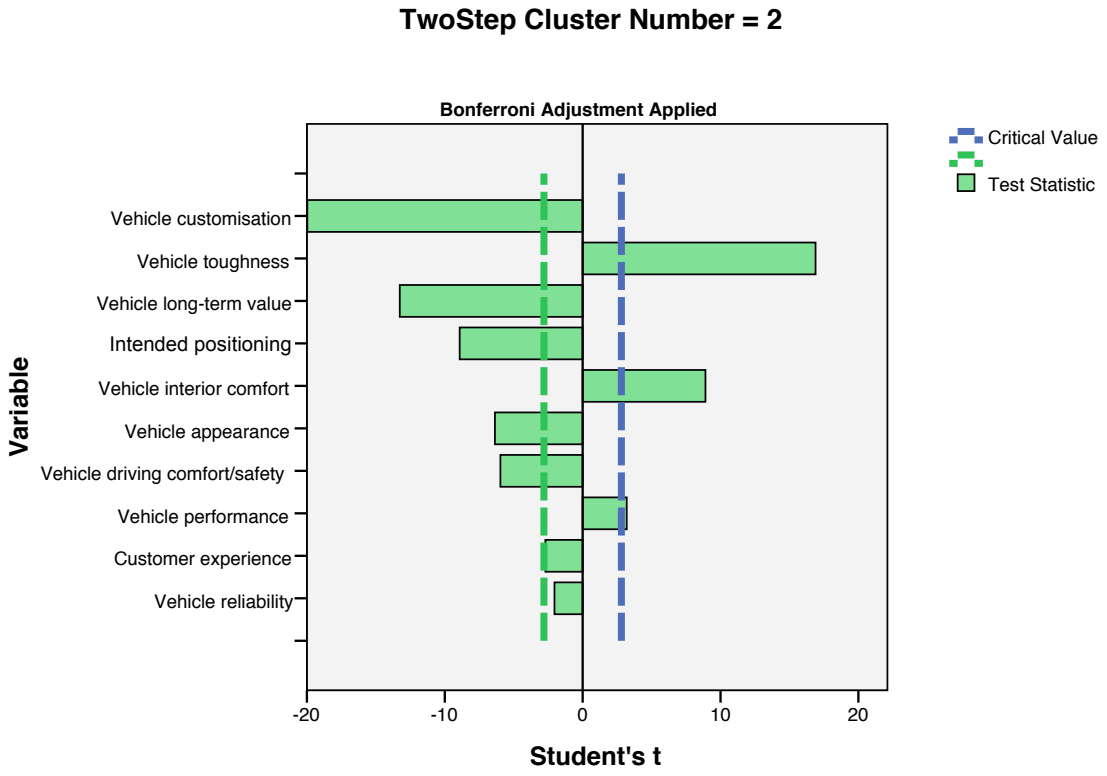

Figure F.2: T-statistic for the latent factors in Cluster 2

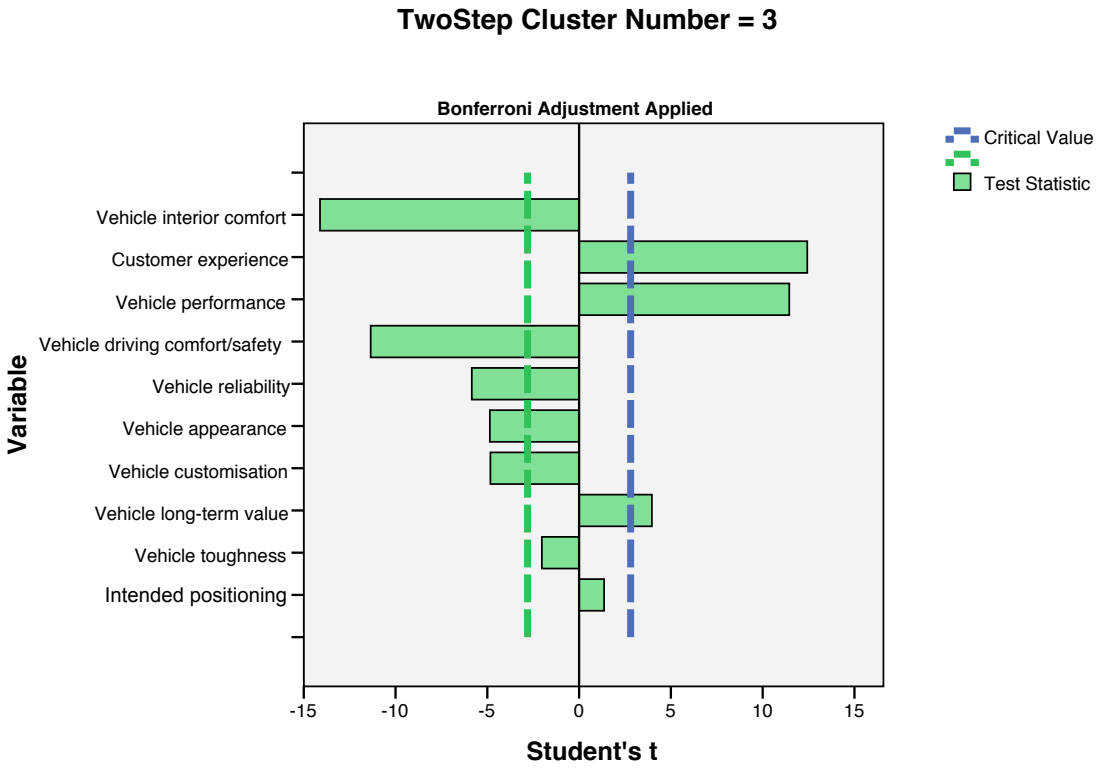

Figure F.3: T-statistic for the latent factors in Cluster 3

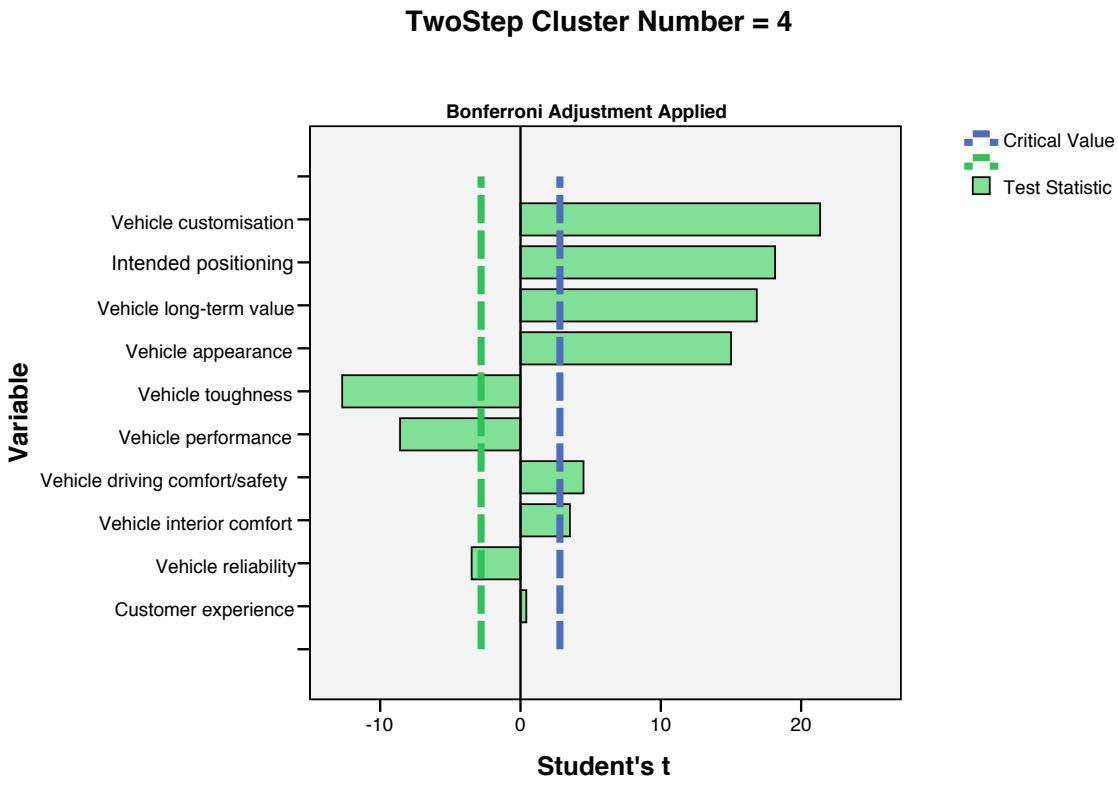

Figure F.4: T-statistic for the latent factors in Cluster 4

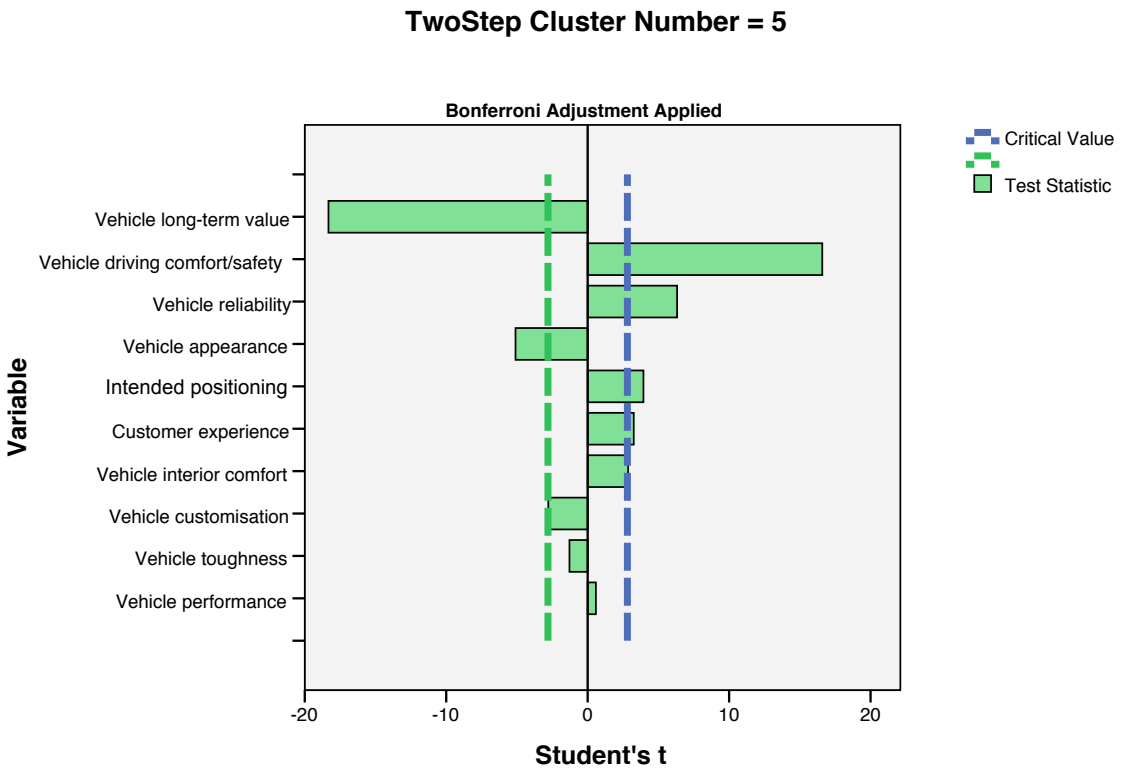

Figure F.5: T-statistic for the latent factors in Cluster 5

Table F.5: Unrotated Structure Matrix for the discriminant analysis of brand choice

	Function														
	1	**2**	**3**	**4**	**5**	**6**	**7**	**8**	**9**	**10**	**11**	**12**	**13**	**14**	**15**
Total Family Pre-Tax Income	0.67	0.16	0.06	0.04	0.04	0.22	-0.20	0.29	0.29	0.31	0.25	0.06	-0.30	-0.05	-0.06
Vehicle toughness	-0.03	0.46	0.59	-0.11	-0.31	-0.20	-0.11	0.26	-0.25	-0.12	-0.03	0.03	0.18	-0.21	0.25
Vehicle appearance	-0.33	-0.21	0.47	0.02	0.14	0.01	0.36	-0.19	0.15	0.30	0.35	0.05	-0.42	0.05	-0.17
Age Bracket	0.08	0.22	-0.15	0.57	0.20	-0.56	0.37	0.04	0.29	-0.05	0.01	0.11	-0.08	-0.01	0.00
Vehicle interior comfort	-0.28	0.19	0.15	0.54	-0.11	0.47	-0.39	0.11	0.18	-0.07	-0.19	0.11	0.22	-0.19	0.11
Vehicle driving comfort/safety	0.23	-0.19	0.03	0.45	-0.08	0.04	0.00	0.16	-0.32	0.41	-0.43	0.02	0.41	-0.13	0.17
Customer experience	0.05	0.51	0.00	0.00	0.60	0.21	0.16	0.01	-0.26	-0.04	-0.09	-0.10	0.32	-0.29	0.20
Vehicle long-term value	0.32	0.26	-0.01	-0.10	-0.35	0.09	0.19	-0.62	0.25	0.18	0.10	-0.04	-0.02	0.28	-0.27
Vehicle performance	0.06	0.10	-0.17	-0.07	-0.15	0.35	0.43	0.47	0.07	-0.16	-0.19	0.32	0.39	-0.26	0.13
Total in the family	-0.07	0.03	0.02	-0.06	-0.14	0.25	-0.13	0.25	0.23	0.28	0.43	-0.53	0.25	0.23	0.34
Vehicle reliability	0.16	-0.23	0.29	0.08	0.32	0.11	-0.06	0.31	0.20	-0.09	-0.37	0.09	0.59	0.19	-0.21
Gender	-0.08	-0.26	0.00	0.01	-0.04	-0.09	-0.34	-0.11	-0.25	0.10	0.49	0.26	0.50	-0.32	-0.22
Intended positioning	-0.25	0.25	-0.14	0.03	0.02	-0.15	-0.03	0.10	-0.10	0.39	0.10	0.43	-0.13	0.62	-0.24
Vehicle customisation	0.20	-0.20	-0.02	0.34	0.02	0.18	0.25	-0.01	-0.29	-0.26	0.40	-0.07	-0.24	0.47	-0.33
Education level	0.36	-0.22	0.18	0.03	0.16	0.13	-0.10	-0.25	0.14	-0.04	0.18	0.46	-0.13	0.24	0.57

Table F.6: Rotated Structure Matrix for the discriminant analysis of brand choice

	Functions														
	1	**2**	**3**	**4**	**5**	**6**	**7**	**8**	**9**	**10**	**11**	**12**	**13**	**14**	**15**
Total household income before tax	0.97	0.01	-0.01	-0.02	0.00	0.09	0.02	0.01	0.01	0.00	0.15	0.04	0.00	-0.05	0.12
Vehicle interior comfort	0.01	0.96	0.09	0.06	-0.07	-0.10	-0.02	0.14	-0.04	0.11	0.00	-0.09	0.09	0.04	0.07
Vehicle toughness	-0.01	0.09	0.97	0.09	-0.05	-0.08	-0.05	0.04	-0.05	-0.02	-0.04	-0.16	0.06	0.03	0.03
Customer experience	-0.02	0.06	0.10	0.96	-0.10	-0.10	0.04	0.06	-0.10	0.06	-0.04	-0.09	0.12	-0.02	0.00
Vehicle appearance	0.00	-0.07	-0.05	-0.10	0.95	0.05	0.04	-0.14	0.10	-0.08	0.05	0.11	-0.15	-0.01	0.01
Vehicle long-term value	0.10	-0.10	-0.08	-0.10	0.05	0.96	0.00	-0.09	0.07	-0.09	0.04	0.07	-0.08	-0.06	0.01
Age	0.02	-0.02	-0.05	0.04	0.04	0.00	0.98	0.03	0.07	-0.02	-0.01	0.04	0.01	-0.11	-0.14
Vehicle driving comfort/safety	0.01	0.14	0.04	0.06	-0.15	-0.09	0.04	0.94	-0.03	0.18	0.00	-0.06	0.10	0.08	0.00
Intended positioning	0.01	-0.04	-0.05	-0.09	0.09	0.07	0.07	-0.03	0.98	-0.02	-0.01	0.09	-0.06	0.00	-0.03
Vehicle reliability	0.00	0.11	-0.02	0.06	-0.08	-0.10	-0.02	0.17	-0.02	0.96	0.01	-0.01	0.14	0.03	-0.01
Education	0.15	0.00	-0.04	-0.04	0.05	0.03	-0.01	0.00	-0.01	0.01	0.98	0.03	-0.03	-0.01	-0.01
Vehicle customisation	0.04	-0.09	-0.16	-0.09	0.11	0.07	0.04	-0.06	0.09	-0.01	0.04	0.96	-0.07	-0.01	-0.01
Vehicle performance	0.00	0.10	0.07	0.13	-0.15	-0.09	0.01	0.10	-0.07	0.14	-0.04	-0.07	0.95	-0.04	-0.02
Gender	-0.05	0.03	0.02	-0.02	-0.01	-0.06	-0.11	0.07	0.00	0.03	-0.01	-0.01	-0.03	0.99	0.00
Family size	0.12	0.06	0.03	0.00	0.01	0.01	-0.13	0.00	-0.03	-0.01	-0.01	-0.01	-0.02	0.00	0.98

Table F.7: Classification of brand choice model

Classification Results[a]

		New Model Purchased - Brand	Predicted Group Membership																																							
			Acura	Audi	BMW	Buick	Cadillac	Chevrolet	Chrysler	Dodge	Ford	GMC	Honda	Hyundai	Infiniti	Isuzu	Jaguar	Jeep	Kia	Lexus	Lincoln	Mazda	Mercedes	Mercury	Mitsubishi	Nissan	Pontiac	Porsche	Land Rover	Saab	Saturn	Subaru	Suzuki	Toyota	Volkswagen	Volvo	Mini	Hummer	Scion	Total
Original	Count	Acura	79	22	14	22	6	2	2	1	0	5	9	3	29	7	12	2	6	28	30	1	5	3	2	3	3	4	27	57	1	23	13	4	11	17	11	16	13	493
		Audi	20	81	10	4	6	0	1	1	1	2	2	2	19	0	26	2	0	16	15	4	11	4	5	0	0	23	22	18	0	19	6	3	7	16	17	14	3	380
		BMW	50	47	72	10	16	1	1	1	2	8	3	1	39	1	49	3	1	50	24	3	29	5	1	1	8	66	33	49	3	14	7	2	8	19	22	29	4	682
		Buick	2	1	2	148	5	0	3	2	3	3	1	3	4	6	1	2	5	7	21	0	0	5	0	0	3	0	0	18	4	1	2	1	0	2	0	1	3	259
		Cadillac	8	3	1	23	45	1	2	1	0	6	1	1	3	8	12	1	1	5	39	0	7	2	0	0	0	1	18	8	1	2	4	0	2	0	0	19	0	225
		Chevrolet	22	4	11	188	37	33	42	33	27	241	34	19	15	146	42	47	62	9	108	8	20	43	14	38	42	53	37	50	28	24	114	35	20	11	19	141	110	1927
		Chrysler	23	5	1	148	32	2	59	16	8	27	10	22	9	41	19	5	36	12	75	7	6	21	8	8	27	3	23	40	12	6	23	4	6	22	11	32	21	830
		Dodge	23	6	7	97	31	11	35	88	23	130	23	9	43	118	18	47	52	10	61	17	8	31	24	30	26	18	33	30	16	18	85	16	14	9	8	92	42	1349
		Ford	42	5	16	205	56	12	52	35	68	211	63	20	17	121	24	47	57	9	132	13	12	65	22	29	53	36	53	51	24	56	96	50	14	27	21	115	71	2000
		GMC	10	1	3	44	33	6	12	14	16	150	3	2	7	55	2	16	12	5	48	3	5	10	5	14	2	0	33	9	3	7	20	13	5	7	1	61	14	651
		Honda	42	7	11	84	7	5	9	10	7	40	205	32	9	44	9	17	48	21	26	11	5	23	14	10	10	15	24	38	16	65	36	49	27	21	41	37	133	1208
		Hyundai	50	18	8	180	8	4	43	11	9	29	61	171	21	92	13	18	193	13	85	29	4	41	17	14	24	5	15	111	20	75	154	26	30	32	34	51	115	1824
		Infiniti	13	12	15	10	12	1	3	2	0	4	0	1	62	3	12	3	3	14	23	2	6	2	1	2	6	15	16	25	3	8	3	1	2	4	8	14	1	312
		Isuzu	0	0	0	3	0	3	0	0	0	2	0	0	0	31	1	0	3	0	0	0	0	0	0	1	0	0	0	0	0	2	1	0	0	0	0	2	0	49
		Jaguar	2	3	1	2	4	0	2	1	0	0	0	0	0	0	53	0	2	4	3	0	1	0	0	0	1	4	0	0	0	1	0	0	0	2	2	0	0	88
		Jeep	20	16	6	36	12	6	11	18	8	43	14	7	14	36	16	160	31	8	37	6	9	19	8	15	10	17	41	18	3	58	61	14	5	12	12	112	26	945
		Kia	17	5	0	98	5	1	23	9	3	22	28	69	2	92	7	14	253	7	34	28	2	29	15	7	10	2	4	36	16	23	139	12	14	10	10	30	58	1134
		Lexus	40	25	15	40	20	2	4	1	0	5	4	0	28	3	32	5	2	121	64	2	21	6	2	0	7	15	31	36	3	8	3	7	4	27	21	22	7	633
		Lincoln	3	4	1	42	18	0	7	2	0	5	3	3	7	3	6	2	4	10	92	0	6	4	0	0	1	1	10	11	1	3	5	0	0	5	1	17	0	277
		Mazda	24	8	6	33	7	2	8	8	2	13	23	26	19	45	11	9	33	7	14	38	1	12	6	9	17	19	8	59	12	11	52	7	32	17	50	20	47	715
		Mercedes	35	42	33	32	49	1	4	1	3	17	9	3	38	6	84	9	5	73	77	0	88	6	4	0	6	52	73	48	6	19	4	4	5	28	29	53	12	958
		Mercury	15	2	0	105	7	0	9	4	0	11	2	10	3	14	2	6	14	6	36	7	0	26	5	2	6	0	7	20	2	19	20	2	8	12	3	11	9	405
		Mitsubishi	15	2	2	16	2	3	10	7	3	17	7	7	5	24	3	11	25	3	20	5	1	11	20	7	16	8	11	29	9	19	30	9	13	11	23	14	22	440
		Nissan	81	6	13	129	49	15	36	76	14	185	61	54	27	161	15	84	90	17	93	28	9	42	39	98	33	20	52	96	19	62	153	42	52	39	19	182	121	2312
		Pontiac	25	4	6	70	11	7	9	9	7	8	20	7	13	30	16	10	33	9	33	11	3	17	6	4	67	27	6	49	25	3	31	7	27	9	52	14	69	754
		Porsche	3	6	5	2	1	0	0	0	1	2	1	0	3	0	13	2	1	6	2	0	2	0	0	0	3	105	11	4	3	1	1	0	0	2	10	6	0	196
		Land Rover	1	7	3	0	3	0	2	0	0	2	0	0	2	0	0	1	0	0	8	1	1	0	0	0	0	2	65	1	0	3	0	0	0	3	0	10	0	115
		Saab	1	2	0	3	2	0	0	0	0	0	1	0	0	0	1	0	2	0	2	0	0	1	0	1	0	0	3	31	0	1	0	0	1	0	2	0	1	55
		Saturn	24	0	8	97	10	1	9	6	1	11	33	18	4	28	14	13	36	12	26	3	5	22	13	13	39	32	4	46	55	10	26	14	13	10	68	19	49	792
		Subaru	35	22	3	14	4	0	3	4	1	11	12	10	8	22	6	23	14	7	20	4	6	23	9	5	1	9	22	19	0	248	44	15	9	27	4	26	6	696
		Suzuki	6	4	1	29	7	0	6	4	3	20	6	16	4	58	3	16	56	2	20	10	2	12	9	9	6	0	6	10	3	28	184	4	5	4	6	35	26	620
		Toyota	66	12	11	190	27	12	17	25	22	160	165	38	18	115	19	80	81	40	118	11	9	43	21	30	18	6	49	112	32	122	65	149	24	61	58	110	158	2294
		Volkswagen	51	19	16	43	5	1	16	8	6	7	34	24	28	23	16	15	32	32	23	31	15	14	14	4	27	8	20	160	22	42	42	18	127	46	91	21	85	1186
		Volvo	15	19	8	27	8	0	5	1	0	1	13	5	11	7	10	5	4	10	23	1	8	8	3	1	1	3	14	46	2	17	5	2	6	58	13	13	11	384
		Mini	10	1	2	1	0	0	0	0	1	1	5	1	6	2	6	4	2	8	1	1	1	1	1	1	13	23	5	14	4	1	1	1	6	5	214	4	16	363
		Hummer	1	0	0	0	0	0	2	1	0	1	0	0	0	0	1	3	0	0	1	0	0	0	0	1	0	1	2	0	0	0	1	0	0	2	0	45	0	62
		Scion	3	0	0	7	0	2	2	2	0	4	13	2	1	5	1	6	7	0	1	3	3	3	1	0	5	0	0	11	1	4	11	4	9	1	15	2	72	201
	%	Acura	16.0	4.5	2.8	4.5	1.2	.4	.4	.2	.0	1.0	1.8	.6	5.9	1.4	2.4	.4	1.2	5.7	6.1	.2	1.0	.6	.4	.6	.6	.8	5.5	11.6	.2	4.7	2.6	.8	2.2	3.4	2.2	3.2	2.6	100.0
		Audi	5.3	21.3	2.6	1.1	1.6	.0	.3	.3	.3	.5	.5	.5	5.0	.0	6.8	.5	.0	4.2	3.9	1.1	2.9	1.1	1.3	.0	.0	6.1	5.8	4.7	.0	5.0	1.6	.8	1.8	4.2	4.5	3.7	.8	100.0
		BMW	7.3	6.9	10.6	1.5	2.3	.1	.1	.1	.3	1.2	.4	.1	5.7	.1	7.2	.4	.1	7.3	3.5	.4	4.3	.7	.1	.1	1.2	9.7	4.8	7.2	.4	2.1	1.0	.3	1.2	2.8	3.2	4.3	.6	100.0
		Buick	.8	.4	.8	57.1	1.9	.0	1.2	.8	1.2	1.2	.4	1.2	1.5	2.3	.4	.8	1.9	2.7	8.1	.0	.0	1.9	.0	.0	1.2	.0	.0	6.9	1.5	.4	.8	.4	.0	.8	.0	.0	.4	1.2	100.0
		Cadillac	3.6	1.3	.4	10.2	20.0	.4	.9	.4	.0	2.7	.4	.4	1.3	3.6	5.3	.4	.4	2.2	17.3	.0	3.1	.9	.0	.0	.0	.4	8.0	3.6	.4	.9	1.8	.0	.9	.0	.0	8.4	.0	100.0
		Chevrolet	1.1	.2	.6	9.8	1.9	1.7	2.2	1.7	1.4	12.5	1.8	1.0	.8	7.6	2.2	2.4	3.2	.5	5.6	.4	1.0	2.2	.7	2.0	2.2	2.8	1.9	2.6	1.5	1.2	5.9	1.8	1.0	.6	1.0	7.3	5.7	100.0
		Chrysler	2.8	.6	.1	17.8	3.9	.2	7.1	1.9	1.0	3.3	1.2	2.7	1.1	4.9	2.3	.6	4.3	1.4	9.0	.8	.7	2.5	1.0	1.0	3.3	.4	2.8	4.8	1.4	.7	2.8	.5	.7	2.7	1.3	3.9	2.5	100.0
		Dodge	1.7	.4	.5	7.2	2.3	.8	2.6	6.5	1.7	9.6	1.7	.7	3.2	8.7	1.3	3.5	3.9	.7	4.5	1.3	.6	2.3	1.8	2.2	1.9	1.3	2.4	2.2	1.2	1.3	6.3	1.2	1.0	.7	.6	6.8	3.1	100.0
		Ford	2.1	.2	.8	10.2	2.8	.6	2.6	1.8	3.4	10.6	3.2	1.0	.8	6.0	1.2	2.4	2.8	.4	6.6	.6	.6	3.2	1.1	1.4	2.6	1.8	2.6	2.6	1.2	2.8	4.8	2.5	.7	1.4	1.0	5.8	3.6	100.0
		GMC	1.5	.2	.5	6.8	5.1	.9	1.8	2.2	2.5	23.0	.5	.3	1.1	8.4	.3	2.5	1.8	.8	7.4	.5	.8	1.5	.8	2.2	.3	.0	5.1	1.4	.5	1.1	3.1	2.0	.8	1.1	.2	9.4	2.2	100.0
		Honda	3.5	.6	.9	7.0	.6	.4	.7	.8	.6	3.3	17.0	2.6	.7	3.6	.7	1.4	4.0	1.7	2.2	.9	.4	1.9	1.2	.8	.8	1.2	2.0	3.1	1.3	5.4	3.0	4.1	2.2	1.7	3.4	3.1	11.0	100.0
		Hyundai	2.7	1.0	.4	9.9	.4	.2	2.4	.6	.5	1.6	3.3	9.4	1.2	5.0	.7	1.0	10.6	.7	4.7	1.6	.2	2.2	.9	.8	1.3	.3	.8	6.1	1.1	4.1	8.4	1.4	1.6	1.8	1.9	2.8	6.3	100.0
		Infiniti	4.2	3.8	4.8	3.2	3.8	.3	1.0	.6	.0	1.3	.0	.3	19.9	1.0	3.8	1.0	1.0	4.5	7.4	.6	1.9	.6	.3	.6	1.9	4.8	5.1	8.0	1.0	2.6	1.0	.3	.6	1.3	2.6	4.5	.3	100.0
		Isuzu	.0	.0	.0	6.1	.0	6.1	.0	.0	.0	4.1	.0	.0	.0	63.3	2.0	.0	6.1	.0	.0	.0	.0	.0	.0	2.0	.0	.0	.0	.0	.0	4.1	2.0	.0	.0	.0	.0	4.1	.0	100.0
		Jaguar	2.3	3.4	1.1	2.3	4.5	.0	2.3	1.1	.0	.0	.0	.0	.0	.0	60.2	.0	2.3	4.5	3.4	.0	1.1	.0	.0	.0	.0	1.1	4.5	.0	.0	1.1	.0	.0	.0	2.3	2.3	.0	.0	100.0
		Jeep	2.1	1.7	.6	3.8	1.3	.6	1.2	1.9	.8	4.6	1.5	.7	1.5	3.8	1.7	16.9	3.3	.8	3.9	.6	1.0	2.0	.8	1.6	1.1	1.8	4.3	1.9	.3	6.1	6.5	1.5	.5	1.3	1.3	11.9	2.8	100.0
		Kia	1.5	.4	.0	8.6	.4	.1	2.0	.8	.3	1.9	2.5	6.1	.2	8.1	.6	1.2	22.3	.6	3.0	2.5	.2	2.6	1.3	.6	.9	.2	.4	3.2	1.4	2.0	12.3	1.1	1.2	.9	.9	2.6	5.1	100.0
		Lexus	6.3	3.9	2.4	6.3	3.2	.3	.6	.2	.0	.8	.6	.0	4.4	.5	5.1	.8	.3	19.1	10.1	.3	3.3	.9	.3	.0	1.1	2.4	4.9	5.7	.5	1.3	.5	1.1	.6	4.3	3.3	3.5	1.1	100.0
		Lincoln	1.1	1.4	.4	15.2	6.5	.0	2.5	.7	.0	1.8	1.1	1.1	2.5	1.1	2.2	.7	1.4	3.6	33.2	.0	2.2	1.4	.0	.0	.4	.4	3.6	4.0	.4	1.1	1.8	.0	.0	1.8	.4	6.1	.0	100.0
		Mazda	3.4	1.1	.8	4.6	1.0	.3	1.1	1.1	.3	1.8	3.2	3.6	2.7	6.3	1.5	1.3	4.6	1.0	2.0	5.3	.1	1.7	.8	1.3	2.4	2.7	1.1	8.3	1.7	1.5	7.3	1.0	4.5	2.4	7.0	2.8	6.6	100.0
		Mercedes	3.7	4.4	3.4	3.3	5.1	.1	.4	.1	.3	1.8	.9	.3	4.0	.6	8.8	.9	.5	7.6	8.0	.0	9.2	.6	.4	.0	.6	5.4	7.6	5.0	.6	2.0	.4	.4	.5	2.9	3.0	5.5	1.3	100.0
		Mercury	3.7	.5	.0	25.9	1.7	.0	2.2	1.0	.0	2.7	.5	2.5	.7	3.5	.5	1.5	3.5	1.5	8.9	1.7	.0	6.4	1.2	.5	1.5	.0	1.7	4.9	.5	4.7	4.9	.5	2.0	3.0	.7	2.7	2.2	100.0
		Mitsubishi	3.4	.5	.5	3.6	.5	.7	2.3	1.6	.7	3.9	1.6	1.6	1.1	5.5	.7	2.5	5.7	.7	4.5	1.1	.2	2.5	4.5	1.6	3.6	1.8	2.5	6.6	2.0	4.3	6.8	2.0	3.0	2.5	5.2	3.2	5.0	100.0
		Nissan	3.5	.3	.6	5.6	2.1	.6	1.6	3.3	.6	8.0	2.6	2.3	1.2	7.0	.6	3.6	3.9	.7	4.0	1.2	.4	1.8	1.7	4.2	1.4	.9	2.2	4.2	.8	2.7	6.6	1.8	2.2	1.7	.8	7.9	5.2	100.0
		Pontiac	3.3	.5	.8	9.3	1.5	.9	1.2	1.2	.9	1.1	2.7	.9	1.7	4.0	2.1	1.3	4.4	1.2	4.4	1.5	.4	2.3	.8	.5	8.9	3.6	.8	6.5	3.3	.4	4.1	.9	3.6	1.2	6.9	1.9	9.2	100.0
		Porsche	1.5	3.1	2.6	1.0	.5	.0	.0	.0	.5	1.0	.5	.0	1.5	.0	6.6	1.0	.5	3.1	1.0	.0	1.0	.0	.0	.0	1.5	53.6	5.6	2.0	1.5	.5	.5	.0	.0	1.0	5.1	3.1	.0	100.0
		Land Rover	.9	6.1	2.6	.0	2.6	.0	1.7	.0	.0	1.7	.0	.0	1.7	.0	.0	.9	.0	.0	7.0	.9	.9	.0	.0	.0	.0	1.7	56.5	.9	.0	2.6	.0	.0	.0	2.6	.0	8.7	.0	100.0
		Saab	1.8	3.6	.0	5.5	3.6	.0	.0	.0	.0	.0	1.8	.0	.0	.0	1.8	.0	3.6	.0	3.6	.0	.0	1.8	.0	1.8	.0	.0	5.5	56.4	.0	1.8	.0	.0	1.8	.0	3.6	.0	1.8	100.0
		Saturn	3.0	.0	1.0	12.2	1.3	.1	1.1	.8	.1	1.4	4.2	2.3	.5	3.5	1.8	1.6	4.5	1.5	3.3	.4	.6	2.8	1.6	1.6	4.9	4.0	.5	5.8	6.9	1.3	3.3	1.8	1.6	1.3	8.6	2.4	6.2	100.0
		Subaru	5.0	3.2	.4	2.0	.6	.0	.4	.6	.1	1.6	1.7	1.4	1.1	3.2	.9	3.3	2.0	1.0	2.9	.6	.9	3.3	1.3	.7	.1	1.3	3.2	2.7	.0	35.6	6.3	2.2	1.3	3.9	.6	3.7	.9	100.0
		Suzuki	1.0	.6	.2	4.7	1.1	.0	1.0	.6	.5	3.2	1.0	2.6	.6	9.4	.5	2.6	9.0	.3	3.2	1.6	.3	1.9	1.5	1.5	1.0	.0	1.0	1.6	.5	4.5	29.7	.6	.8	.6	1.0	5.6	4.2	100.0
		Toyota	2.9	.5	.5	8.3	1.2	.5	.7	1.1	1.0	7.0	7.2	1.7	.8	5.0	.8	3.5	3.5	1.7	5.1	.5	.4	1.9	.9	1.3	.8	.3	2.1	4.9	1.4	5.3	2.8	6.5	1.0	2.7	2.5	4.8	6.9	100.0
		Volkswagen	4.3	1.6	1.3	3.6	.4	.1	1.3	.7	.5	.6	2.9	2.0	2.4	1.9	1.3	1.3	2.7	2.7	1.9	2.6	1.3	1.2	1.2	.3	2.3	.7	1.7	13.5	1.9	3.5	3.5	1.5	10.7	3.9	7.7	1.8	7.2	100.0
		Volvo	3.9	4.9	2.1	7.0	2.1	.0	1.3	.3	.0	.3	3.4	1.3	2.9	1.8	2.6	1.3	1.0	2.6	6.0	.3	2.1	2.1	.8	.3	.3	.8	3.6	12.0	.5	4.4	1.3	.5	1.6	15.1	3.4	3.4	2.9	100.0
		Mini	2.8	.3	.6	.3	.0	.0	.0	.0	.3	.3	1.4	.3	1.7	.6	1.7	1.1	.6	2.2	.3	.3	.3	.3	.3	.3	3.6	6.3	1.4	3.9	1.1	.3	.3	.3	1.7	1.4	59.0	1.1	4.4	100.0
		Hummer	1.6	.0	.0	.0	.0	.0	3.2	1.6	.0	1.6	.0	.0	.0	.0	1.6	4.8	.0	.0	1.6	.0	.0	.0	.0	1.6	.0	1.6	3.2	.0	.0	.0	1.6	.0	.0	3.2	.0	72.6	.0	100.0
		Scion	1.5	.0	.0	3.5	.0	1.0	1.0	1.0	.0	2.0	6.5	1.0	.5	2.5	.5	3.0	3.5	.0	.5	1.5	1.5	1.5	.5	.0	2.5	.0	.0	5.5	.5	2.0	5.5	2.0	4.5	.5	7.5	1.0	35.8	100.0

a. 13.2% of original grouped cases correctly classified.

F.3 NCBS_UK

This section shows additional tables and figures for the statistical analysis of the UK automotive market presented in section 6.4. All analyses are carried out in SPSS.

Two pie charts are shown here for the 2nd and 3rd mentioned reason of purchase:

- Figure F.6 – Reason of purchase (2nd mentioned) for NCBS_UK survey
- Figure F.7 – Reason of purchase (3rd mentioned) for NCBS_UK survey

Using the 12 latent factors (in which 10 are identified in NVES_US), the reason of purchase from the NCBS_UK is categorised:

- Table F.8 – Summary for latent factors, table 1 of 2
- Table F.9 – Summary for latent factors, table 2 of 2

The purchase reasons are modelled using the discriminant analysis with respect to the customers' demographic details and behaviour:

- Table F.10 – Unrotated Structure Matrix for the discriminant analysis of purchase reason in NCBS_UK
- Table F.11 – Rotated Structure Matrix for the discriminant analysis of purchase reason in NCBS_UK
- Table F.12 – Classification of reduced purchase reason model in UK

The customers' choice of brands in terms of their demographic details and ratings on the 12 latent factors are modelled using the discriminant analysis

- Table F.13 – Unrotated Structure Matrix for the discriminant analysis of brand choice in UK
- Table F.14 – Rotated Structure Matrix for the discriminant analysis of brand choice in UK
- Table F.15 – Classification of brand choice model in UK
- Table F.16 – Latent factors (1st mention) of brand of cars, table 1 of 3
- Table F.17 – Latent factors (1st mention) of brand of cars, table 2 of 3
- Table F.18 – Latent factors (1st mention) of brand of cars, table 3 of 3

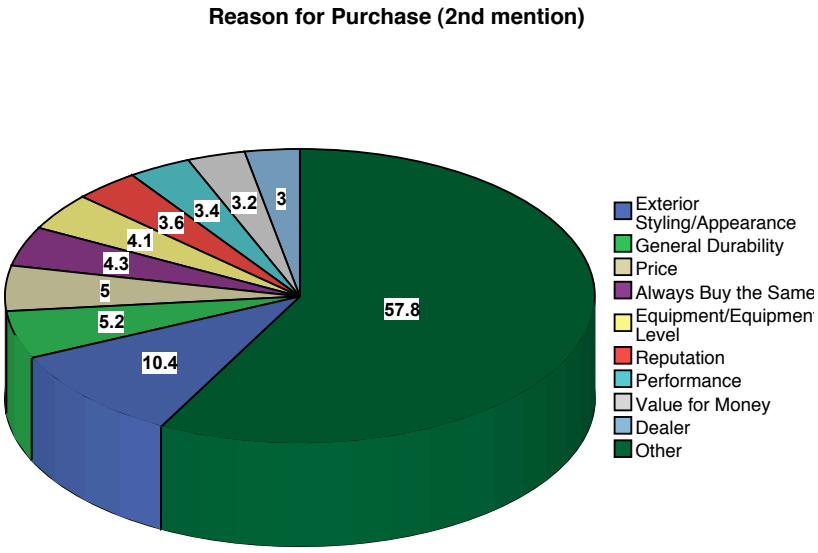

Figure F.6: Reason of purchase (2nd mention) for NCBS_UK survey

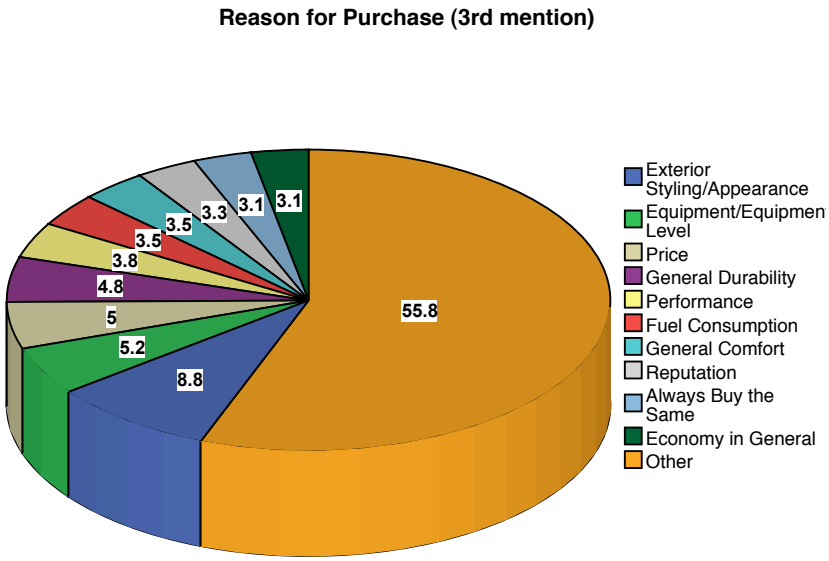

Figure F.7: Reason of purchase (3rd mention) for NCBS_UK survey

Table F.8: Summary for latent factors, table 1 of 2

Latent factors	NCBS_UK customers' purchase reason
Vehicle driving comfort/safety	Manoeuvrability
	Road holding/handling
	Ease of driving
	Driving position
	Quiet when driving
	GPS/Navigation system
	Brakes (ABS)
	Position/Operation of features
	Visibility
	General safety features
	Suits local roads
Vehicle toughness	FWD/RWD/4WD
	Body type
Vehicle appearance	Exterior finish
	Interior design/appearance
	Quality of interior/equipment
	Exterior styling/appearance
	Colour of car
Vehicle performance	Acceleration
	Ease of starting
	New technology
	Manual gearbox
	Automatic gearbox
	Fuel tank capacity
	Engine size
	Engine design
	Diesel
	Power
	Performance
Vehicle interior comfort	Comfortable ride
	Interior roominess
	Size of boot
	Number/Verssatility of seats
	Seat comfort
	General comfort
	Vent/Heating/Aircond
	Door system
	Equipement/Equipment level
	Interior storage space

Table F.9: Summary for latent factors, table 2 of 2

Reduced factors	**NCBS_UK customers' purchase reason**
Vehicle long-term value	Resale value
	Fuel consumption
	Security
	Spares availability
	Low pollution
	Trade-in price
	Car receyclable
	Mainteanance cost
	Value of money
Vehicle customisation	Compact size
	Engine access
	Large size
	Size
	Access to interior
	Rear load space versatility
	Access to boot
	Practicle/Versatile
Customer experience	New model
	Test drive
	Car characteristic
	Nationality
	Reputation
	Always buy the same
Intended positioning	Car overall
	Prestige/Class
	Reflects lifestyle
	Good publicity
	Limited/Special edition
	Wanted a change
Vehicle reliability	Bodywork durability
	Engine durability
	General durability
Purchase convenience	Salesman
	Dealer
	Dealer Network
	Delivery Period
	Terms of payment
	Simple specification
Vehicle short-term value	Economy in general
	Discount of new car
	Price of options/Extras
	Price
	Tax cost
	Insurance cost
	Value of money

Table F.10: Unrotated Structure Matrix for the discriminant analysis of purchase reason in NCBS_UK

	Function							
	1	**2**	**3**	**4**	**5**	**6**	**7**	**8**
Age	0.91	0.01	-0.17	-0.24	0.15	0.15	-0.06	0.18
Commuting to and from Work	0.62	0.03	0.12	-0.48	-0.44	-0.06	0.38	-0.17
Carrying Children in the Back *	0.27	0.09	-0.11	0.03	0.01	-0.14	-0.21	-0.22
Carrying 3+ People in the Back*	0.20	0.05	-0.12	0.05	-0.06	-0.15	-0.09	-0.10
Driving in Town/City*	0.18	0.01	-0.06	-0.12	-0.12	-0.03	0.08	-0.04
Total household income before tax	-0.18	0.59	0.30	0.53	-0.30	0.11	-0.13	0.36
Motorway Driving*	0.18	-0.26	-0.20	-0.14	-0.18	-0.16	0.02	0.12
For Shopping*	-0.10	0.17	0.03	-0.02	0.02	-0.07	-0.01	0.06
Education	0.05	0.09	0.78	0.34	0.20	-0.48	-0.01	0.05
Carrying Large Items in Car/Boot*	0.02	-0.05	-0.25	0.04	-0.02	-0.17	0.14	0.07
Week-End Trips*	0.04	-0.11	-0.18	0.03	-0.05	-0.11	0.10	0.07
Carrying Items on a Roof Rack*	0.03	-0.05	-0.14	0.04	0.00	-0.10	0.07	-0.01
Holidays*	-0.08	-0.11	-0.13	0.11	-0.10	-0.08	0.10	0.07
Gender	-0.01	-0.58	-0.05	0.71	-0.22	0.05	0.27	-0.18
For Business Purposes*	0.19	-0.24	-0.14	-0.28	-0.24	-0.14	0.10	-0.03
Towing A Trailer/Caravan*	-0.03	-0.03	-0.04	0.09	-0.04	-0.07	0.02	0.01
Expected Miles, Next 12 Months	-0.18	0.44	0.31	0.18	0.50	0.52	0.16	-0.32
Out of Town Driving*	0.03	-0.14	-0.13	-0.04	-0.19	-0.22	0.05	0.08
Carrying a Passenger in the Front*	0.06	0.07	-0.04	0.16	-0.03	-0.17	-0.08	-0.11
Carrying Adults in the Back*	0.11	0.06	-0.07	0.06	-0.07	-0.14	-0.03	-0.05
With the Rear Seat(s) Folded Down	-0.07	0.31	-0.52	0.17	0.16	-0.45	0.59	0.15
Family size	-0.47	-0.09	0.25	-0.05	-0.02	0.29	0.37	0.69
Number of children in household	-0.40	-0.09	0.21	-0.02	0.00	0.19	0.31	0.46
Taking Children to School*	0.24	0.09	-0.11	-0.02	0.02	-0.13	-0.20	-0.25

*This variable not used in the analysis

Table F.11: Rotated Structure Matrix for the discriminant analysis of purchase reason in NCBS_UK

	Function							
	1	**2**	**3**	**4**	**5**	**6**	**7**	**8**
Age	0.87	-0.03	0.35	0.29	-0.10	-0.09	0.08	-0.05
Gender	-0.18	0.94	-0.10	-0.04	0.07	0.09	0.08	0.25
For Shopping*	-0.06	-0.18	-0.04	-0.03	0.09	0.04	-0.04	0.03
Commuting to and from Work	0.16	-0.01	0.95	0.13	-0.08	0.02	0.19	-0.06
Driving in Town/City*	0.06	-0.01	0.23	0.08	-0.02	-0.05	0.08	0.03
Family size	0.02	-0.08	-0.10	-0.97	0.21	0.05	0.04	0.03
Number of children in household	-0.06	-0.03	-0.08	-0.73	0.11	0.07	0.00	0.04
Carrying Children in the Back*	0.08	-0.02	0.03	0.44	-0.02	0.00	0.01	-0.02
Taking Children to School*	0.05	-0.05	0.05	0.43	-0.06	-0.02	0.00	-0.03
Carrying 3+ People in the Back*	0.05	0.01	0.05	0.30	0.03	0.00	0.08	0.07
Carrying a Passenger in the Front*	-0.06	0.03	-0.04	0.23	0.08	0.08	0.01	0.07
Carrying Adults in the Back*	0.00	0.00	0.05	0.18	0.06	0.04	0.06	0.08
Total household income before tax	-0.09	-0.09	-0.17	-0.12	0.93	0.17	-0.20	-0.09
Education	-0.08	-0.01	-0.10	0.04	0.16	0.96	-0.12	-0.14
Expected Miles, Next 12 Months	-0.03	-0.04	-0.10	-0.12	0.01	0.02	-0.97	-0.17
Motorway Driving*	0.11	0.07	0.13	0.04	-0.10	-0.06	0.41	0.12
For Business Purposes*	0.01	0.04	0.31	0.05	-0.19	-0.09	0.36	0.06
Out of Town Driving*	-0.06	0.03	0.08	0.02	0.00	0.01	0.32	0.15
With the Rear Seat(s) Folded Down	-0.04	-0.21	0.07	0.00	0.07	0.04	-0.08	0.97
Carrying Large Items in Car/Boot*	0.01	0.02	0.01	0.03	-0.03	-0.04	0.14	0.32
Week-End Trips*	0.02	0.07	0.02	0.00	-0.02	-0.04	0.15	0.20
Holidays*	-0.08	0.11	-0.04	-0.06	0.05	-0.03	0.13	0.18
Carrying Items on a Roof Rack*	0.00	0.04	0.00	0.05	-0.04	-0.02	0.07	0.17
Towing A Trailer/Caravan*	-0.05	0.05	-0.04	0.02	0.04	0.02	0.05	0.08

This page intentionally left blank.

Table F.12: Classification of reduced purchase reason model in UK

		Predicted Group Membership												
		Vehicle driving comfort/safety	Vehicle toughness	Vehicle appearance	Vehicle performance	Vehicle interior comfort	Vehicle long-term value	Vehicle customisation	Customer experience	Intended positioning	Vehicle reliability	Purchase convenience	Vehicle short-term value	Total
Original	Count Vehicle driving comfort/safety	105	5	55	71	28	20	101	12	28	62	54	33	574
	Vehicle toughness	190	41	202	169	63	48	241	43	179	180	135	79	1570
	Vehicle appearance	301	47	467	270	89	105	403	76	285	285	276	203	2807
	Vehicle performance	62	20	74	152	45	27	138	12	76	103	43	36	788
	Vehicle interior comfort	211	28	122	155	102	48	350	31	78	180	157	133	1595
	Vehicle long-term value	143	23	183	181	63	73	208	26	123	171	154	95	1443
	Vehicle customisation	161	16	151	142	86	39	469	39	92	130	145	95	1565
	Customer experience	740	94	833	919	332	224	1612	257	694	729	718	375	7527
	Intended positioning	98	14	119	142	44	31	194	31	142	121	84	55	1075
	Vehicle reliability	71	10	88	132	33	40	113	16	96	149	67	43	858
	Purchase convenience	94	4	81	62	20	19	119	11	66	74	119	48	717
	Vehicle short-term value	155	21	240	138	66	54	315	41	121	156	192	170	1669
	Ungrouped cases	14	1	13	18	3	5	26	6	17	24	12	6	145
	% Vehicle driving comfort/safety	18.29	0.87	9.58	12.37	4.88	3.48	17.60	2.09	4.88	10.80	9.41	5.75	100
	Vehicle toughness	12.10	2.61	12.87	10.76	4.01	3.06	15.35	2.74	11.40	11.46	8.60	5.03	100
	Vehicle appearance	10.72	1.67	16.64	9.62	3.17	3.74	14.36	2.71	10.15	10.15	9.83	7.23	100
	Vehicle performance	7.87	2.54	9.39	19.29	5.71	3.43	17.51	1.52	9.64	13.07	5.46	4.57	100
	Vehicle interior comfort	13.23	1.76	7.65	9.72	6.39	3.01	21.94	1.94	4.89	11.29	9.84	8.34	100
	Vehicle long-term value	9.91	1.59	12.68	12.54	4.37	5.06	14.41	1.80	8.52	11.85	10.67	6.58	100
	Vehicle customisation	10.29	1.02	9.65	9.07	5.50	2.49	29.97	2.49	5.88	8.31	9.27	6.07	100
	Customer experience	9.83	1.25	11.07	12.21	4.41	2.98	21.42	3.41	9.22	9.69	9.54	4.98	100
	Intended positioning	9.12	1.30	11.07	13.21	4.09	2.88	18.05	2.88	13.21	11.26	7.81	5.12	100
	Vehicle reliability	8.28	1.17	10.26	15.38	3.85	4.66	13.17	1.86	11.19	17.37	7.81	5.01	100
	Purchase convenience	13.11	0.56	11.30	8.65	2.79	2.65	16.60	1.53	9.21	10.32	16.60	6.69	100
	Vehicle short-term value	9.29	1.26	14.38	8.27	3.95	3.24	18.87	2.46	7.25	9.35	11.50	10.19	100
	Ungrouped cases	9.66	0.69	8.97	12.41	2.07	3.45	17.93	4.14	11.72	16.55	8.28	4.14	100

10.1% of original grouped cases correctly classified.

Table F.13: Unrotated Structure Matrix for the discriminant analysis of brand choice in UK

	Function												
	1	**2**	**3**	**4**	**5**	**6**	**7**	**8**	**9**	**10**	**11**	**12**	**13**
Total household income before tax	0.70	0.52	0.03	-0.16	-0.25	0.19	0.05	-0.07	-0.19	0.20	-0.06	0.16	0.00
Carrying 3+ People in the Back	-0.01	0.47	0.05	0.44	0.18	-0.36	-0.26	0.27	0.16	-0.18	-0.33	-0.23	0.23
Towing A Trailer/Caravan*	-0.03	0.09	-0.08	0.03	-0.05	0.02	0.05	0.06	0.00	0.01	0.00	0.01	-0.01
With the Rear Seat(s) Folded Down	0.16	-0.09	-0.88	0.29	0.10	0.12	-0.17	0.14	-0.04	-0.08	0.03	0.17	0.01
Holidays*	-0.09	0.17	-0.18	0.10	-0.03	-0.02	0.00	-0.03	-0.06	0.02	0.01	0.05	0.01
Age	0.11	-0.55	0.33	0.69	0.01	-0.25	0.12	-0.01	0.02	0.04	-0.16	0.04	0.05
Motorway Driving*	-0.20	-0.04	-0.03	0.30	0.00	-0.13	-0.03	0.01	-0.24	0.04	0.03	-0.05	-0.10
Carrying Children in the Back*	0.04	0.09	0.10	0.24	0.12	-0.13	0.08	0.21	0.08	-0.22	-0.23	-0.10	-0.06
Driving in Town/City*	-0.02	-0.02	0.04	0.20	0.10	-0.10	0.01	0.01	-0.10	-0.11	0.10	-0.01	0.01
Week-End Trips*	-0.10	0.09	-0.16	0.20	0.02	-0.06	0.00	-0.03	-0.06	0.00	0.00	0.06	-0.03
Carrying Adults in the Back	0.01	0.37	-0.10	0.31	0.66	-0.13	0.41	-0.19	-0.19	-0.04	-0.07	-0.16	0.19
Carrying a Passenger in the Front*	0.03	0.23	-0.07	0.15	0.23	0.02	0.18	0.00	-0.01	-0.09	-0.11	-0.08	-0.05
For Shopping*	0.10	0.12	-0.08	-0.05	0.16	-0.08	-0.01	0.01	-0.02	0.05	0.00	0.02	0.00
Gender	-0.40	0.38	-0.09	0.27	-0.38	0.62	0.10	-0.21	0.00	-0.15	-0.01	-0.01	0.13
Education	0.22	0.29	0.22	0.02	0.28	0.58	-0.03	0.34	0.25	0.40	0.12	-0.05	-0.20
Carrying Items on a Roof Rack	-0.12	0.11	-0.29	0.13	-0.34	-0.27	0.55	0.45	0.27	0.17	0.24	0.00	0.15
Taking Children to School*	0.03	0.00	0.10	0.16	0.08	-0.11	0.08	0.24	0.06	-0.23	-0.18	-0.09	-0.08
For Business Purposes	-0.35	-0.11	0.17	0.21	0.10	-0.09	-0.08	0.45	-0.59	-0.17	0.21	0.33	0.21
.Expected Miles, Next 12 Months	0.35	-0.04	0.11	-0.40	0.13	0.20	0.06	-0.13	0.58	-0.20	-0.03	0.28	0.42
Out of Town Driving*	-0.13	0.06	-0.11	0.15	-0.02	-0.05	-0.04	0.03	-0.19	0.02	0.08	-0.03	-0.17
Family size	0.04	0.15	-0.15	-0.24	-0.15	-0.04	-0.32	-0.37	-0.09	0.62	0.32	0.22	0.30
Number of children in household*	-0.01	0.09	-0.15	-0.23	-0.02	0.06	-0.18	-0.34	-0.08	0.45	0.29	0.14	0.19
Commuting to and from Work	0.07	-0.26	0.27	0.54	0.06	-0.19	-0.10	0.06	-0.13	-0.29	0.61	-0.19	-0.05
Carrying Large Items in Car/Boot	-0.20	0.30	-0.21	0.35	0.13	-0.27	-0.04	-0.10	0.14	-0.10	0.03	0.63	-0.42

*This variable not used in the analysis

Table F.14: Rotated Structure Matrix for the discriminant analysis of brand choice in UK

	Function												
	1	**2**	**3**	**4**	**5**	**6**	**7**	**8**	**9**	**10**	**11**	**12**	**13**
Total household income before tax	0.93	0.00	-0.01	-0.15	-0.10	-0.10	-0.15	0.08	0.01	-0.02	0.16	0.02	-0.20
Gender	0.03	0.98	0.04	0.09	-0.11	-0.01	-0.08	0.04	0.01	0.05	0.06	0.08	-0.07
With the Rear Seat(s) Folded Down	0.00	-0.01	0.97	0.13	-0.04	0.00	0.00	0.07	0.01	0.15	-0.03	0.11	-0.04
Expected Miles, Next 12 Months	0.02	-0.01	0.02	-0.99	-0.05	-0.07	-0.06	0.00	-0.02	0.02	0.02	-0.05	-0.07
Motorway Driving*	-0.09	0.03	0.02	0.40	0.12	0.10	0.11	0.04	0.05	0.06	-0.07	0.00	0.03
Out of Town Driving*	-0.01	0.03	0.07	0.33	-0.05	0.04	0.07	0.02	-0.01	0.08	0.00	0.02	0.00
Week-End Trips*	-0.02	0.07	0.12	0.17	0.03	0.02	0.02	0.10	0.07	0.16	-0.05	0.05	-0.01
Holidays*	0.04	0.11	0.10	0.13	-0.06	0.01	-0.03	0.10	0.08	0.12	-0.05	0.08	-0.07
Age	-0.11	-0.10	-0.04	0.10	0.88	0.04	0.31	-0.05	0.03	0.01	-0.09	-0.04	0.29
For Business Purposes	-0.09	0.00	0.00	0.29	0.03	0.92	0.22	-0.05	0.02	0.04	-0.06	0.03	0.07
Commuting to and from Work	-0.11	-0.05	-0.03	0.22	0.18	0.11	0.93	-0.07	0.00	-0.04	0.00	-0.03	0.13
Driving in Town/City*	-0.04	-0.01	0.02	0.10	0.06	0.09	0.22	0.10	0.03	0.05	-0.05	-0.02	0.08
Carrying Adults in the Back	-0.02	-0.02	0.01	0.08	0.05	0.04	0.10	0.98	0.10	0.03	-0.02	0.01	0.08
Carrying a Passenger in the Front*	0.05	0.05	0.04	0.04	-0.04	-0.05	-0.02	0.37	0.05	0.06	0.06	0.01	0.19
For Shopping*	0.06	-0.15	0.05	-0.02	-0.08	-0.01	-0.03	0.16	0.06	0.04	0.03	0.00	-0.04
Carrying 3+ People in the Back	0.01	-0.01	0.03	0.08	0.02	0.02	0.06	0.26	0.87	0.08	-0.01	0.05	0.39
Carrying Large Items in Car/Boot	-0.01	-0.01	0.13	0.19	0.00	0.03	0.03	0.09	0.04	0.96	-0.03	0.05	0.05
Education	0.14	0.03	-0.04	-0.11	-0.07	-0.06	-0.06	0.07	-0.01	-0.05	0.97	0.00	-0.01
Carrying Items on a Roof Rack	-0.05	-0.01	0.04	0.03	0.04	0.00	0.02	-0.01	0.00	0.02	-0.03	0.99	0.07
Towing A Trailer/Caravan*	0.04	0.06	0.04	0.05	-0.04	0.01	-0.04	0.02	0.02	0.03	0.02	0.11	0.01
Family size	0.15	-0.08	0.00	-0.02	-0.02	-0.01	-0.09	-0.09	0.13	0.03	0.01	0.02	-0.97
Number of children in household*	0.05	-0.02	0.02	-0.02	-0.07	-0.03	-0.06	0.02	-0.03	0.01	0.03	-0.02	-0.76
Carrying Children in the Back*	0.00	-0.04	-0.02	0.02	0.08	0.00	0.03	0.13	0.20	0.05	0.02	0.03	0.46
Taking Children to School*	-0.02	-0.06	-0.01	0.01	0.05	0.03	0.04	0.04	0.10	0.01	0.00	0.03	0.45

*This variable not used in the analysis

This page intentionally left blank.

Table F.15: Classification of brand choice model in UK

		Predicted Group Membership																															
		Alfa Romeo	Audi	BMW	Chrysler USA	Citroen	Fiat	Ford	Honda	Hyundai	Jaguar	Kia	Mazda	Mercedes	Mitsubishi	Nissan	Peugeot	Renault	Saab	Seat	Skoda	Subaru	Suzuki	Toyota	Vauxhall	VW	Volvo	Smart	Lexus	Mini (From 2002 MY)	GM Daewoo/GM Chevrolet	Dodge	Total
Original Count																															1	131
	Audi	72	22	14	107	1	4	1	4	1	25	0	4	6	24	23	8	1	44	23	11	28	149	6	0	1	31	42	130	92	18	13	905
	BMW	51	10	9	84	1	1	0	1	3	27	0	0	6	29	21	4	0	27	16	4	31	108	5	0	1	17	44	189	72	17	6	784
	Chrysler USA	4	2	0	36	0	0	0	0	1	2	0	0	0	5	1	0	0	3	0	0	1	8	0	0	0	3	1	27	2	4	4	104
	Citroen	16	1	1	14	4	5	0	0	9	7	2	5	2	32	7	6	0	4	14	8	7	155	3	1	1	8	23	17	63	57	9	481
	Fiat	10	2	1	5	0	9	0	2	3	2	1	1	0	32	4	4	1	4	14	3	5	156	1	1	1	7	23	12	53	32	11	400
	Ford	49	6	4	38	3	14	1	3	12	13	8	10	4	136	22	29	1	9	40	11	15	558	16	1	0	25	76	64	169	144	28	1509
	Honda	50	6	0	55	4	8	0	6	8	24	5	8	8	106	17	7	1	14	42	9	22	323	14	0	3	15	34	62	90	77	39	1057
	Hyundai	5	2	0	1	0	0	0	0	6	0	1	0	0	10	4	1	0	1	2	0	3	49	0	0	0	1	7	4	22	19	2	140
	Jaguar	8	1	1	44	0	0	1	2	1	31	1	1	6	11	6	0	0	15	2	2	8	36	3	0	0	14	9	125	5	9	1	343
	Kia	2	1	0	4	0	1	0	0	1	1	2	0	0	19	3	2	0	1	6	0	0	88	5	0	0	2	8	7	10	13	2	178
	Mazda	16	1	2	22	0	6	0	0	4	12	2	5	2	35	9	8	0	7	8	5	13	120	9	1	1	7	21	25	35	30	16	422
	Mercedes	35	10	11	77	0	1	0	2	5	21	2	1	26	51	15	2	0	27	7	0	24	133	10	0	1	18	16	246	76	24	12	853
	Mitsubishi	2	0	0	1	0	0	0	0	0	1	1	1	1	22	0	1	0	1	4	4	2	47	1	0	0	0	5	12	14	9	2	131
	Nissan	7	1	1	7	1	2	0	0	1	3	1	1	1	18	35	1	1	2	2	1	5	87	4	0	0	2	30	9	22	16	3	264
	Peugeot	10	1	0	19	2	4	0	1	8	4	4	3	2	48	10	28	1	4	16	7	8	261	10	0	0	11	39	27	87	61	13	689
	Renault	40	6	0	39	5	13	0	6	6	32	4	9	9	98	24	30	2	9	43	10	18	550	13	2	1	27	57	47	157	127	24	1408
	Saab	13	3	0	30	0	0	0	0	0	17	1	2	1	7	7	2	0	34	2	0	8	27	2	0	1	12	6	21	16	4	3	219
	Seat	21	2	3	16	1	4	0	0	1	4	4	2	3	27	5	8	0	4	36	7	6	140	2	0	0	4	12	13	54	20	13	412
	Skoda	16	5	1	20	2	5	0	0	3	10	3	6	0	37	10	3	0	12	14	10	12	95	10	0	0	19	13	23	16	35	9	389
	Subaru	0	1	0	6	0	0	0	0	1	3	0	0	1	2	2	0	0	2	1	0	13	12	2	0	0	1	2	9	8	2	0	68
	Suzuki	0	0	0	0	0	0	0	0	0	0	1	0	0	0	0	0	0	0	0	0	0	38	0	0	0	0	2	0	2	1	2	46
	Toyota	27	1	2	33	1	3	0	4	3	19	7	4	1	67	9	12	0	10	12	8	18	242	25	0	2	13	30	36	82	65	10	746
	Vauxhall	36	6	0	30	4	9	0	2	4	12	11	7	2	81	10	11	2	14	29	9	21	389	14	2	4	22	50	56	84	106	33	1060
	VW	58	10	3	78	4	7	0	2	10	39	10	6	12	95	21	12	0	37	39	13	44	400	21	1	1	48	55	76	173	66	33	1374
	Volvo	12	6	4	39	1	1	0	1	2	15	1	2	6	33	4	2	0	31	3	5	15	81	15	0	0	41	15	53	33	23	5	449
	Smart	0	0	0	0	0	0	0	0	0	0	0	0	0	1	2	0	0	0	0	0	0	1	0	0	0	0	40	1	1	0	0	46
	Lexus	1	0	4	6	0	0	0	0	1	1	0	1	1	1	2	0	0	2	0	0	0	11	0	0	0	0	4	74	1	0	0	110
	Mini (From 2002 MY)	10	2	0	2	0	1	0	0	1	3	2	0	0	7	1	0	1	0	7	1	1	126	0	0	0	1	28	3	208	2	4	411
	GM Daewoo/GM Chevrolet	2	1	0	4	1	0	0	0	0	0	2	0	0	17	0	2	0	1	3	3	2	75	1	1	0	0	12	4	10	47	2	190
	Dodge	6	1	1	13	0	0	0	0	2	5	1	1	2	14	0	2	1	1	8	2	4	58	1	0	0	2	4	9	7	13	25	183
%	Alfa Romeo	20.61	0.76	0.00	9.16	0.00	0.00	0.00	0.00	0.00	2.29	0.00	0.00	0.76	2.29	3.82	0.00	0.76	1.53	2.29	0.00	0.76	15.27	0.76	0.00	0.00	0.76	6.11	12.98	14.50	3.82	0.76	100
	Audi	7.96	2.43	1.55	11.82	0.11	0.44	0.11	0.44	0.11	2.76	0.00	0.44	0.66	2.65	2.54	0.88	0.11	4.86	2.54	1.22	3.09	16.46	0.66	0.00	0.11	3.43	4.64	14.36	10.17	1.99	1.44	100
	BMW	6.51	1.28	1.15	10.71	0.13	0.13	0.00	0.13	0.38	3.44	0.00	0.00	0.77	3.70	2.68	0.51	0.00	3.44	2.04	0.51	3.95	13.78	0.64	0.00	0.13	2.17	5.61	24.11	9.18	2.17	0.77	100
	Chrysler USA	3.85	1.92	0.00	34.62	0.00	0.00	0.00	0.00	0.96	1.92	0.00	0.00	0.00	4.81	0.96	0.00	0.00	2.88	0.00	0.00	0.96	7.69	0.00	0.00	0.00	2.88	0.96	25.96	1.92	3.85	3.85	100
	Citroen	3.33	0.21	0.21	2.91	0.83	1.04	0.00	0.00	1.87	1.46	0.42	1.04	0.42	6.65	1.46	1.25	0.00	0.83	2.91	1.66	1.46	32.22	0.62	0.21	0.21	1.66	4.78	3.53	13.10	11.85	1.87	100
	Fiat	2.50	0.50	0.25	1.25	0.00	2.25	0.00	0.50	0.75	0.50	0.25	0.25	0.00	8.00	1.00	1.00	0.25	1.00	3.50	0.75	1.25	39.00	0.25	0.25	0.25	1.75	5.75	3.00	13.25	8.00	2.75	100
	Ford	3.25	0.40	0.27	2.52	0.20	0.93	0.07	0.20	0.80	0.86	0.53	0.66	0.27	9.01	1.46	1.92	0.07	0.60	2.65	0.73	0.99	36.98	1.06	0.07	0.00	1.66	5.04	4.24	11.20	9.54	1.86	100
	Honda	4.73	0.57	0.00	5.20	0.38	0.76	0.00	0.57	0.76	2.27	0.47	0.76	0.76	10.03	1.61	0.66	0.09	1.32	3.97	0.85	2.08	30.56	1.32	0.00	0.28	1.42	3.22	5.87	8.51	7.28	3.69	100
	Hyundai	3.57	1.43	0.00	0.71	0.00	0.00	0.00	0.00	4.29	0.00	0.71	0.00	0.00	7.14	2.86	0.71	0.00	0.71	1.43	0.00	2.14	35.00	0.00	0.00	0.00	0.71	5.00	2.86	15.71	13.57	1.43	100
	Jaguar	2.33	0.29	0.29	12.83	0.00	0.00	0.29	0.58	0.29	9.04	0.29	0.29	1.75	3.21	1.75	0.00	0.00	4.37	0.58	0.58	2.33	10.50	0.87	0.00	0.00	4.08	2.62	36.44	1.46	2.62	0.29	100
	Kia	1.12	0.56	0.00	2.25	0.00	0.56	0.00	0.00	0.56	0.56	1.12	0.00	0.00	10.67	1.69	1.12	0.00	0.56	3.37	0.00	0.00	49.44	2.81	0.00	0.00	1.12	4.49	3.93	5.62	7.30	1.12	100
	Mazda	3.79	0.24	0.47	5.21	0.00	1.42	0.00	0.00	0.95	2.84	0.47	1.18	0.47	8.29	2.13	1.90	0.00	1.66	1.90	1.18	3.08	28.44	2.13	0.24	0.24	1.66	4.98	5.92	8.29	7.11	3.79	100
	Mercedes	4.10	1.17	1.29	9.03	0.00	0.12	0.00	0.23	0.59	2.46	0.23	0.12	3.05	5.98	1.76	0.23	0.00	3.17	0.82	0.00	2.81	15.59	1.17	0.00	0.12	2.11	1.88	28.84	8.91	2.81	1.41	100
	Mitsubishi	1.53	0.00	0.00	0.76	0.00	0.00	0.00	0.00	0.00	0.76	0.76	0.76	0.76	16.79	0.00	0.76	0.00	0.76	3.05	3.05	1.53	35.88	0.76	0.00	0.00	0.00	3.82	9.16	10.69	6.87	1.53	100
	Nissan	2.65	0.38	0.38	2.65	0.38	0.76	0.00	0.00	0.38	1.14	0.38	0.38	0.38	6.82	13.26	0.38	0.38	0.76	0.76	0.38	1.89	32.95	1.52	0.00	0.00	0.76	11.36	3.41	8.33	6.06	1.14	100
	Peugeot	1.45	0.15	0.00	2.76	0.29	0.58	0.00	0.15	1.16	0.58	0.58	0.44	0.29	6.97	1.45	4.06	0.15	0.58	2.32	1.02	1.16	37.88	1.45	0.00	0.00	1.60	5.66	3.92	12.63	8.85	1.89	100
	Renault	2.84	0.43	0.00	2.77	0.36	0.92	0.00	0.43	0.43	2.27	0.28	0.64	0.64	6.96	1.70	2.13	0.14	0.64	3.05	0.71	1.28	39.06	0.92	0.14	0.07	1.92	4.05	3.34	11.15	9.02	1.70	100
	Saab	5.94	1.37	0.00	13.70	0.00	0.00	0.00	0.00	0.00	7.76	0.46	0.91	0.46	3.20	3.20	0.91	0.00	15.53	0.91	0.00	3.65	12.33	0.91	0.00	0.46	5.48	2.74	9.59	7.31	1.83	1.37	100
	Seat	5.10	0.49	0.73	3.88	0.24	0.97	0.00	0.00	0.24	0.97	0.97	0.49	0.73	6.55	1.21	1.94	0.00	0.97	8.74	1.70	1.46	33.98	0.49	0.00	0.00	0.97	2.91	3.16	13.11	4.85	3.16	100
	Skoda	4.11	1.29	0.26	5.14	0.51	1.29	0.00	0.00	0.77	2.57	0.77	1.54	0.00	9.51	2.57	0.77	0.00	3.08	3.60	2.57	3.08	24.42	2.57	0.00	0.00	4.88	3.34	5.91	4.11	9.00	2.31	100
	Subaru	0.00	1.47	0.00	8.82	0.00	0.00	0.00	0.00	1.47	4.41	0.00	0.00	1.47	2.94	2.94	0.00	0.00	2.94	1.47	0.00	19.12	17.65	2.94	0.00	0.00	1.47	2.94	13.24	11.76	2.94	0.00	100
	Suzuki	0.00	0.00	0.00	0.00	0.00	0.00	0.00	0.00	0.00	0.00	2.17	0.00	0.00	0.00	0.00	0.00	0.00	0.00	0.00	0.00	0.00	82.61	0.00	0.00	0.00	0.00	4.35	0.00	4.35	2.17	4.35	100
	Toyota	3.62	0.13	0.27	4.42	0.13	0.40	0.00	0.54	0.40	2.55	0.94	0.54	0.13	8.98	1.21	1.61	0.00	1.34	1.61	1.07	2.41	32.44	3.35	0.00	0.27	1.74	4.02	4.83	10.99	8.71	1.34	100
	Vauxhall	3.40	0.57	0.00	2.83	0.38	0.85	0.00	0.19	0.38	1.13	1.04	0.66	0.19	7.64	0.94	1.04	0.19	1.32	2.74	0.85	1.98	36.70	1.32	0.19	0.38	2.08	4.72	5.28	7.92	10.00	3.11	100
	VW	4.22	0.73	0.22	5.68	0.29	0.51	0.00	0.15	0.73	2.84	0.73	0.44	0.87	6.91	1.53	0.87	0.00	2.69	2.84	0.95	3.20	29.11	1.53	0.07	0.07	3.49	4.00	5.53	12.59	4.80	2.40	100
	Volvo	2.67	1.34	0.89	8.69	0.22	0.22	0.00	0.22	0.45	3.34	0.22	0.45	1.34	7.35	0.89	0.45	0.00	6.90	0.67	1.11	3.34	18.04	3.34	0.00	0.00	9.13	3.34	11.80	7.35	5.12	1.11	100
	Smart	0.00	0.00	0.00	0.00	0.00	0.00	0.00	0.00	0.00	0.00	0.00	0.00	0.00	2.17	4.35	0.00	0.00	0.00	0.00	0.00	0.00	2.17	0.00	0.00	0.00	0.00	86.96	2.17	2.17	0.00	0.00	100
	Lexus	0.91	0.00	3.64	5.45	0.00	0.00	0.00	0.00	0.91	0.91	0.00	0.91	0.91	0.91	1.82	0.00	0.00	1.82	0.00	0.00	0.00	10.00	0.00	0.00	0.00	0.00	3.64	67.27	0.91	0.00	0.00	100
	Mini (From 2002 MY)	2.43	0.49	0.00	0.49	0.00	0.24	0.00	0.00	0.24	0.73	0.49	0.00	0.00	1.70	0.24	0.00	0.24	0.00	1.70	0.24	0.24	30.66	0.00	0.00	0.00	0.24	6.81	0.73	50.61	0.49	0.97	100
	GM Daewoo/GM Chevrolet	1.05	0.53	0.00	2.11	0.53	0.00	0.00	0.00	0.00	0.00	1.05	0.00	0.00	8.95	0.00	1.05	0.00	0.53	1.58	1.58	1.05	39.47	0.53	0.53	0.00	0.00	6.32	2.11	5.26	24.74	1.05	100
	Dodge	3.28	0.55	0.55	7.10	0.00	0.00	0.00	0.00	1.09	2.73	0.55	0.55	1.09	7.65	0.00	1.09	0.55	0.55	4.37	1.09	2.19	31.69	0.55	0.00	0.00	1.09	2.19	4.92	3.83	7.10	13.66	100

a. 5.6% of original grouped cases correctly classified.

This page intentionally left blank.

Table F.16: Latent factors (1st mention) of brand of cars, table 1 of 3

		Reduced Purchase Decision 1st															
		Vehicle driving comfort/safety		Vehicle toughness		Vehicle appearance		Vehicle performance		Vehicle interior comfort		Vehicle long-term value		Vehicle customisation		Customer experience	
		Count	Row N %	Count	Row N %	Count	Row N %	Count	Row N %	Count	Row N %	Count	Row N %	Count	Row N %	Count	Row N %
A2.Make of New Car	Alfa Romeo	4	2.2%	9	4.9%	69	37.7%	4	2.2%	5	2.7%	1	.5%	6	3.3%	64	35.0%
	ARO	0	.0%	0	.0%	0	.0%	0	.0%	0	.0%	0	.0%	0	.0%	0	.0%
	Audi	28	1.8%	166	10.4%	234	14.7%	59	3.7%	72	4.5%	57	3.6%	64	4.0%	562	35.2%
	Autobianchi	0	.0%	0	.0%	0	.0%	0	.0%	0	.0%	0	.0%	0	.0%	0	.0%
	BMW	49	3.2%	177	11.6%	166	10.9%	68	4.5%	59	3.9%	59	3.9%	54	3.5%	599	39.4%
	Chrysler USA	0	.0%	18	5.8%	98	31.4%	4	1.3%	36	11.5%	21	6.7%	31	9.9%	62	19.9%
	Citroen	30	2.1%	93	6.4%	161	11.0%	44	3.0%	181	12.4%	114	7.8%	154	10.5%	371	25.4%
	Daewoo	0	.0%	0	.0%	0	.0%	0	.0%	0	.0%	0	.0%	0	.0%	0	.0%
	Daihatsu	0	.0%	0	.0%	0	.0%	0	.0%	0	.0%	0	.0%	0	.0%	0	.0%
	Fiat	22	2.9%	67	8.9%	86	11.5%	20	2.7%	37	4.9%	47	6.3%	62	8.3%	218	29.0%
	Ford	49	1.6%	296	9.6%	229	7.4%	81	2.6%	205	6.7%	190	6.2%	266	8.7%	1157	37.6%
	Ford USA	0	.0%	0	.0%	0	.0%	0	.0%	0	.0%	0	.0%	0	.0%	0	.0%
	FSO	0	.0%	0	.0%	0	.0%	0	.0%	0	.0%	0	.0%	0	.0%	0	.0%
	GM USA	0	.0%	0	.0%	0	.0%	0	.0%	0	.0%	0	.0%	0	.0%	0	.0%
	Honda	67	2.7%	180	7.3%	412	16.7%	117	4.7%	209	8.5%	122	4.9%	148	6.0%	773	31.3%
	Hyundai	23	3.6%	54	8.4%	73	11.3%	17	2.6%	40	6.2%	97	15.1%	61	9.5%	154	23.9%
	Innocenti	0	.0%	0	.0%	0	.0%	0	.0%	0	.0%	0	.0%	0	.0%	0	.0%
	Isuzu	0	.0%	0	.0%	0	.0%	0	.0%	0	.0%	0	.0%	0	.0%	0	.0%
	Jaguar	3	.5%	54	9.1%	81	13.6%	27	4.5%	23	3.9%	36	6.1%	10	1.7%	254	42.7%
	Kia	13	1.9%	49	7.2%	76	11.2%	43	6.3%	58	8.6%	110	16.2%	55	8.1%	103	15.2%
	Lada	0	.0%	0	.0%	0	.0%	0	.0%	0	.0%	0	.0%	0	.0%	0	.0%
	Lancia	0	.0%	0	.0%	0	.0%	0	.0%	0	.0%	0	.0%	0	.0%	0	.0%
	Lotus	0	.0%	0	.0%	0	.0%	0	.0%	0	.0%	0	.0%	0	.0%	0	.0%
	Mazda	21	2.3%	68	7.6%	107	11.9%	38	4.2%	70	7.8%	59	6.6%	40	4.5%	280	31.2%
	Mercedes	65	2.8%	215	9.4%	313	13.6%	67	2.9%	200	8.7%	75	3.3%	172	7.5%	716	31.2%
	Mitsubishi	12	2.5%	45	9.2%	65	13.3%	29	5.9%	37	7.6%	40	8.2%	36	7.4%	120	24.5%
	Nissan	28	2.7%	98	9.5%	150	14.5%	41	4.0%	87	8.4%	48	4.7%	108	10.5%	301	29.2%
	Opel	0	.0%	0	.0%	0	.0%	0	.0%	0	.0%	0	.0%	0	.0%	0	.0%
	Peugeot	32	2.0%	164	10.5%	235	15.0%	33	2.1%	91	5.8%	94	6.0%	122	7.8%	544	34.7%
	Porsche	0	.0%	0	.0%	0	.0%	0	.0%	0	.0%	0	.0%	0	.0%	0	.0%
	Proton	0	.0%	0	.0%	0	.0%	0	.0%	0	.0%	0	.0%	0	.0%	0	.0%
	Renault	98	3.1%	251	8.0%	271	8.7%	58	1.9%	205	6.6%	145	4.6%	246	7.9%	1282	41.0%
	MG Rover	0	.0%	0	.0%	0	.0%	0	.0%	0	.0%	0	.0%	0	.0%	0	.0%
	Saab	18	4.5%	43	10.8%	31	7.8%	13	3.2%	23	5.8%	27	6.8%	10	2.5%	173	43.2%
	Santana	0	.0%	0	.0%	0	.0%	0	.0%	0	.0%	0	.0%	0	.0%	0	.0%
	Seat	13	1.9%	37	5.4%	116	16.8%	27	3.9%	51	7.4%	79	11.4%	30	4.3%	204	29.6%
	Skoda	9	1.1%	68	8.6%	34	4.3%	38	4.8%	77	9.7%	88	11.1%	50	6.3%	229	28.9%
	Ssang Yong	0	.0%	0	.0%	0	.0%	0	.0%	0	.0%	0	.0%	0	.0%	0	.0%
	Subaru	8	4.4%	26	14.2%	3	1.6%	14	7.7%	10	5.5%	7	3.8%	8	4.4%	71	38.8%
	Suzuki	14	7.8%	4	2.2%	30	16.8%	3	1.7%	8	4.5%	9	5.0%	26	14.5%	49	27.4%
	Talbot	0	.0%	0	.0%	0	.0%	0	.0%	0	.0%	0	.0%	0	.0%	0	.0%

This page intentionally left blank.

Table F.17: Latent factors (1st mention) of brand of cars, table 2 of 3

		Reduced Purchase Decision 1st									
		Intended positioning		Vehicle reliability		Purchase convenience		Vehicle short-term value		Other	
		Count	Row N %	Count	Row N %	Count	Row N %	Count	Row N %	Count	Row N %
A2.Make of New Car	Alfa Romeo	14	7.7%	1	.5%	0	.0%	6	3.3%	0	.0%
	ARO	0	.0%	0	.0%	0	.0%	0	.0%	0	.0%
	Audi	116	7.3%	158	9.9%	32	2.0%	30	1.9%	19	1.2%
	Autobianchi	0	.0%	0	.0%	0	.0%	0	.0%	0	.0%
	BMW	123	8.1%	69	4.5%	40	2.6%	46	3.0%	13	.9%
	Chrysler USA	19	6.1%	3	1.0%	3	1.0%	14	4.5%	3	1.0%
	Citroen	50	3.4%	10	.7%	49	3.3%	195	13.3%	11	.8%
	Daewoo	0	.0%	0	.0%	0	.0%	0	.0%	0	.0%
	Daihatsu	0	.0%	0	.0%	0	.0%	0	.0%	0	.0%
	Fiat	27	3.6%	9	1.2%	44	5.9%	107	14.2%	5	.7%
	Ford	131	4.3%	44	1.4%	100	3.3%	308	10.0%	18	.6%
	Ford USA	0	.0%	0	.0%	0	.0%	0	.0%	0	.0%
	FSO	0	.0%	0	.0%	0	.0%	0	.0%	0	.0%
	GM USA	0	.0%	0	.0%	0	.0%	0	.0%	0	.0%
	Honda	126	5.1%	156	6.3%	52	2.1%	96	3.9%	11	.4%
	Hyundai	25	3.9%	12	1.9%	12	1.9%	72	11.2%	4	.6%
	Innocenti	0	.0%	0	.0%	0	.0%	0	.0%	0	.0%
	Isuzu	0	.0%	0	.0%	0	.0%	0	.0%	0	.0%
	Jaguar	52	8.7%	17	2.9%	19	3.2%	15	2.5%	4	.7%
	Kia	35	5.2%	10	1.5%	21	3.1%	103	15.2%	2	.3%
	Lada	0	.0%	0	.0%	0	.0%	0	.0%	0	.0%
	Lancia	0	.0%	0	.0%	0	.0%	0	.0%	0	.0%
	Lotus	0	.0%	0	.0%	0	.0%	0	.0%	0	.0%
	Mazda	58	6.5%	43	4.8%	40	4.5%	70	7.8%	4	.4%
	Mercedes	193	8.4%	137	6.0%	61	2.7%	65	2.8%	19	.8%
	Mitsubishi	19	3.9%	17	3.5%	17	3.5%	46	9.4%	6	1.2%
	Nissan	61	5.9%	24	2.3%	26	2.5%	52	5.0%	7	.7%
	Opel	0	.0%	0	.0%	0	.0%	0	.0%	0	.0%
	Peugeot	58	3.7%	14	.9%	58	3.7%	115	7.3%	6	.4%
	Porsche	0	.0%	0	.0%	0	.0%	0	.0%	0	.0%
	Proton	0	.0%	0	.0%	0	.0%	0	.0%	0	.0%
	Renault	95	3.0%	33	1.1%	174	5.6%	250	8.0%	20	.6%
	MG Rover	0	.0%	0	.0%	0	.0%	0	.0%	0	.0%
	Saab	17	4.2%	12	3.0%	10	2.5%	21	5.2%	2	.5%
	Santana	0	.0%	0	.0%	0	.0%	0	.0%	0	.0%
	Seat	33	4.8%	10	1.4%	24	3.5%	60	8.7%	6	.9%
	Skoda	64	8.1%	47	5.9%	20	2.5%	65	8.2%	3	.4%
	Ssang Yong	0	.0%	0	.0%	0	.0%	0	.0%	0	.0%
	Subaru	10	5.5%	12	6.6%	4	2.2%	8	4.4%	2	1.1%
	Suzuki	11	6.1%	3	1.7%	6	3.4%	13	7.3%	3	1.7%
	Talbot	0	.0%	0	.0%	0	.0%	0	.0%	0	.0%

This page intentionally left blank.

Table F.18: Latent factors (1st mention) of brand of cars, table 3 of 3

		Reduced Purchase Decision 1st															
		Vehicle driving comfort/safety		Vehicle toughness		Vehicle appearance		Vehicle performance		Vehicle interior comfort		Vehicle long-term value		Vehicle customisation		Customer experience	
		Count	Row N %	Count	Row N %	Count	Row N %	Count	Row N %	Count	Row N %	Count	Row N %	Count	Row N %	Count	Row N %
A2.Make of New Car	Toyota	47	2.5%	126	6.7%	124	6.6%	65	3.5%	107	5.7%	153	8.2%	136	7.3%	760	40.6%
	Vauxhall	60	2.2%	274	9.9%	439	15.8%	78	2.8%	222	8.0%	116	4.2%	276	9.9%	812	29.3%
	VW	67	2.2%	234	7.8%	236	7.9%	127	4.2%	205	6.9%	156	5.2%	217	7.3%	1161	38.8%
	Volvo	69	6.2%	126	11.3%	127	11.4%	27	2.4%	75	6.7%	37	3.3%	77	6.9%	437	39.1%
	Yue Loong	0	.0%	0	.0%	0	.0%	0	.0%	0	.0%	0	.0%	0	.0%	0	.0%
	Yugo	0	.0%	0	.0%	0	.0%	0	.0%	0	.0%	0	.0%	0	.0%	0	.0%
	Smart	0	.0%	6	6.8%	8	9.1%	3	3.4%	1	1.1%	9	10.2%	22	25.0%	14	15.9%
	Lexus	8	2.6%	21	6.8%	21	6.8%	30	9.7%	13	4.2%	28	9.1%	6	1.9%	102	33.1%
	Land Rover	55	10.5%	31	5.9%	54	10.3%	34	6.5%	44	8.4%	12	2.3%	36	6.9%	190	36.3%
	Mini (From 2002 MY)	21	2.7%	75	9.8%	108	14.1%	20	2.6%	17	2.2%	37	4.8%	58	7.6%	318	41.5%
	GM Daewoo/GM Chevrolet	5	1.2%	31	7.6%	27	6.6%	4	1.0%	15	3.7%	42	10.2%	50	12.2%	116	28.3%
	Dacia	0	.0%	0	.0%	0	.0%	0	.0%	0	.0%	0	.0%	0	.0%	0	.0%
	Jeep	9	6.0%	13	8.7%	24	16.1%	15	10.1%	15	10.1%	13	8.7%	5	3.4%	36	24.2%
	Dodge	4	1.3%	18	5.9%	90	29.3%	4	1.3%	14	4.6%	30	9.8%	14	4.6%	67	21.8%
	Others	0	.0%	0	.0%	0	.0%	0	.0%	0	.0%	0	.0%	0	.0%	0	.0%
	Not Identified	0	.0%	0	.0%	0	.0%	0	.0%	0	.0%	0	.0%	0	.0%	0	.0%

		Reduced Purchase Decision 1st									
		Intended positioning		Vehicle reliability		Purchase convenience		Vehicle short-term value		Other	
		Count	Row N %	Count	Row N %	Count	Row N %	Count	Row N %	Count	Row N %
A2.Make of New Car	Toyota	68	3.6%	106	5.7%	43	2.3%	129	6.9%	7	.4%
	Vauxhall	113	4.1%	30	1.1%	82	3.0%	261	9.4%	11	.4%
	VW	135	4.5%	219	7.3%	65	2.2%	140	4.7%	27	.9%
	Volvo	43	3.8%	40	3.6%	24	2.1%	28	2.5%	7	.6%
	Yue Loong	0	.0%	0	.0%	0	.0%	0	.0%	0	.0%
	Yugo	0	.0%	0	.0%	0	.0%	0	.0%	0	.0%
	Smart	2	2.3%	0	.0%	1	1.1%	19	21.6%	3	3.4%
	Lexus	27	8.8%	41	13.3%	5	1.6%	6	1.9%	0	.0%
	Land Rover	39	7.5%	10	1.9%	5	1.0%	10	1.9%	3	.6%
	Mini (From 2002 MY)	75	9.8%	13	1.7%	7	.9%	11	1.4%	6	.8%
	GM Daewoo/GM Chevrolet	18	4.4%	1	.2%	10	2.4%	89	21.7%	2	.5%
	Dacia	0	.0%	0	.0%	0	.0%	0	.0%	0	.0%
	Jeep	4	2.7%	3	2.0%	1	.7%	10	6.7%	1	.7%
	Dodge	30	9.8%	5	1.6%	5	1.6%	25	8.1%	1	.3%
	Others	0	.0%	0	.0%	0	.0%	0	.0%	0	.0%
	Not Identified	0	.0%	0	.0%	0	.0%	0	.0%	0	.0%

References

Anderson, R. and D. Bevly [2005], Estimation of tire cornering stiffness using GPS to improve model based estimation of vehicle states, *in* 'Proceedings of IEEE Intelligent Vehicles Symposium', pp. 801–806.

Aoki, Y., T. Inoue and Y. Hori [2004], Robust design of gain matrix of body slip angle observer for electric vehicles and its experimental demonstration, *in* 'Proceedings of 8th IEEE International Workshop on Advanced Motion Control', Kawasaki, Japan.

Aykan, R., C. Hajiyev and F. Caliskan [2005], 'Kalman filter and neural network-based icing identification applied to A340 aircraft dynamics', *Aircraft Engineering and Aerospace Technology* **77**(1), 23–33.

Bae, H., J. Ryu and J. Gerdes [2001], Road grade and vehicle parameter estimation for longitudinal control using GPS, *in* 'Proceedings of IEEE Conference on Intelligent Transport Systems', Oakland, CA, USA.

Baek, W., B. Song, Y. Kim and S. K. Hong [2007], 'Roll and pitch estimation via an accelerometer array and sensor networks', *International Journal of Automotive Technology* **8**(6), 753–760.

Baines, P. [2010], Email communication. 9th January, 2010.

Baines, P., C. Fill and K. Page [2008], *Marketing*, Oxford University Press.

Bakker, E., H.B. Pacejka and L. Lidner [1989], A new tyre model with application in vehicle dynamics studies., *in* 'Proceedings of the 4th Auto Technologies Conference', Monte Carlo, SAE paper 890087.

Bakker, E., L. Nyborg and H.B. Pacejka [1986], 'Tyre modelling for use in vehicle dynamics studies', *SAE International* .

Barlett, M.S. [1954], 'A note on the multiplying factors for various chi square approximations', *Journal of the Royal Statistical Society* **16 (Series B)**, 296–298.

Bayliss, M., K-T. Leung, J. Whidborne, D. Purdy and R. Williams [2006], Four wheel steer controller development utilising a GPS (global positioning satellite) system compensated inertial sensor suite, *in* 'Proceedings of FISITA World Automotive Congress', Yokohama, Japan.

Belch, M. A. and L. A. Willis [2001], 'Family decision at the turn of the century: Has the changing structure of households impacted the family decision-making process?', *Journal of Consumer Behaviour* **2**(2), 111–124.

Best, M., A. Newton and S. Tuplin [2007], The identifying extended Kalman filter: parametric system identification of a vehicle handling model, *in* 'Proceedings of the Institution of Mechanical Engineers, Part K (Journal of Multi-Body Dynamics)', Vol. 221, pp. 87–98.

Best, M., T. Gordon and P. Dixon [2000], 'An extended adaptive Kalman filter for real-time state estimation of vehicle handling dynamics', *Vehicle System Dynamics* **34**, 57–75.

Bevly, D. [2004], 'Global positioning system (GPS): a low-cost velocity sensor for correcting inertial sensor errors on ground vehicles', *Journal of Dynamic Systems, Measurement and Control* **126**(2), 255–64.

Bevly, D., J. Gerdes and C. Wilson [2002], 'The use of GPS based velocity measurements for measurement of sideslip and wheel slip', *Vehicle System Dynamics* **38**(2), 127–47.

Bevly, D., J. Gerdes, C. Wilson and G. Zhang [2000], The use of GPS based velocity measurements for improved vehicle state estimation, *in* 'Proceedings of American Control Conference', Vol. 4, Chicago, USA, pp. 2538–2542.

Bevly, D., J. Ryu and J. Gerdes [2006], 'Integrating INS sensors with GPS measurements for continuous estimation of vehicle sideslip, roll, and tire cornering stiffness', *IEEE Transactions on Intelligent Transportation Systems* **7**(4), 483–493.

Bevly, D., R. Sheridan and J. Gerdes [2001], 'Integrating INS sensors with GPS velocity measurements for continuous estimation of vehicle sideslip and tire cornering stiffness', *Proceedings of the American Control Conference* **1**, 25–30.

Birmingham Post [2009], 'Traditional media hardest hit as uk ad spend drops by 4.3pc; ADVERTISING', 30 June.

Blundell, M. and D. Harty [2004], *The Multibody Systems Approach to Vehicle Dynamics*, 1st edn, Butterworth-Heinemann.

Britannica [2009], 'Automotive industry'.
URL: *http://www.britannica.com/*

Brown, R. and P. Hwang [1997], *Introduction to random signals and applied Kalman filtering*, John Wiley & sons.

Chen, B-C. and F. Hsieh [2008], 'Sideslip angle estimation using extended Kalman filter', *Vehicle System Dynamics* **46**, 353–364.

Cherouat, H., M. Braci and S. Diop [2005], 'Vehicle velocity, side slip angles and yaw rate estimation', *IEEE International Symposium on Industrial Electronics* **1**, 349–354.

Clay, L. and A. James [2009], TV is the best medium to market most things, *in* 'Campaign', p. 15.
URL: *http://www.campaignlive.co.uk*

Creative Research Systems [2007], 'Sample size calculator'.
URL: *http://www.surveysystem.com/sscalc.htm*

Daily, R. and D. Bevly [2004], The use of GPS for vehicle stability comtrol systems for vehicle stability comtrol systems, *in* 'IEEE Transaction Industrial Electronics', Vol. 51 of *2*, pp. 270–277.

Davies, C. and A. Schreck [2008], Environmental leads sae survey results, Technical report, DuPont Automotive.

Davis, H. and B. Rigaux [1974], 'Perceptions of marital roles in decision processes', *Journal of consumer research* **1**(1).

Deng, W. and H. Zhang [2006], Rls-based online estimation on vehicle linear sideslip, *in* 'Proceedings of American Control Conference', Minneapolis, USA, pp. 3960–3965.

Dissanayake, G., S. Sukkarieh, E. Nebot and H. Durrant-Whyte [2001], 'The aiding of a low cost strapdown inertial measurement unit suing vehicle model constraints for land vehicle application', *IEEE Transactions on Robotics and Automation* **17**(5), 731–747.

Djuric, P., J. Kotecha, J. Zhang, Y. Huang, M. Bugallo and J. Miguez [2003], Particle filtering, *in* 'IEEE Signal Processing Magazine'.

Eckermann, E. [2001], *World history of automobile*, SAE press.

Ellis, J. [1994], *Vehicle Handling Dynamics*, Professional Engineering Publishing.

Evans, M., A. Jamal and G. Foxall [2006], *Consumer behaviour*, John Wiley & Sons, Ltd.

Farmer, C. [2001], 'New evidence concerning fatal crashes of passenger vehicles before and after adding antilock braking systems', *Accident Analysis and Prevention* **33**, 361–369.

Farmer, C., A. Lund, R. Trempel and E. Braver [1997], 'Fatal crashes of passenger vehicles before and after adding antilock braking', *Accident Analysis and Prevention* **29**(6), 745–757.

Farrelly, J. and P. Wellstead [1996], Estimation of vehicle lateral velocity, *in* 'Proceedings of IEEE International Conference on Control Applications', Dearborn, MI, pp. 552–557.

Fisher, W. and H. Rauch [1994], Augmentation of an extended Kalman filter with /neural network, *in* 'Proceedings of the IEEE International Conference on Neural Networks', Vol. 2, pp. 1191–1196.

Gao, J. [2006], GPS/INS/G sensors/yaw rate sensor/wheel speed sensors integrated vehicular positioning system, *in* 'Proceedings of the Institute of Navigation', Vol. 3, pp. 1427–1439.

Genta, G. [2003], *Motor Vehicle Dynamics, Modelling and Simulation*, World Scientific.

Google [2009], 'Google Map'.
URL: *http://maps.google.com/*

Grewal, M., L. Weill and A. Andrews [2007], *Global Positioning Systems, Inertial Navigation, and Integration*, Wilney.

Grip, H., L. Imsland, T. Johansen, T. Fossen, J. Kalkkuhl and A. Suissa [2006], Nonlinear vehicle velocity observer with road-tire friction adaptation, *in* 'Proceedings of the 45th IEEE Conference on Decision and Control', San Diego.

Grip, H., L. Imsland, T. Johansen, T. Fossen, J. Kalkkuhl and A. Suissa [2007], 'Nonlinear vehicle side-slip estimation with friction adaptation', *Automatica* **44**, 611–622.

Gustafsson, F., F. Gunnarsson, N. Bergman, U. Forssell, J. Jansson, R. Karlsson and P-J. Nordlund [2002], 'Particle filters for positioning, navigation and tracking', *IEEE Transactions on Signal Processing* **50**(2), 425–437.

He, B. [2006], 'Precise navigation for a 4ws mobile robot', *Journal of Zhejiang University: Science* **7**(2), 185–193.

He, B., D. Wang, M. Phain and T. Yu [2002], Position and orientation estimation with high accuracy for a car-like vehicle, *in* 'Proceedings of IEEE 5th International Conference on Intelligent Transportation Systems', pp. 528–33.

Hirschberg, W., G. Rill and H. Weinfurter [2003], 'User-appropriate tyre-modelling for vehicle dynamics in standard and limit situations', *Vehicle System Dynamics* **38**(2), 103–125.

Ho, Y-C. and R-C. Lee [1964], 'A bayesian approach to problems in stochastic estimation and control', *Automatic Control* **9**, 333–339.

IPG CarMaker [2009].
URL: *http://www.ipg.de*

Jamison, C. [1999], 'Do you know what your customers really want?', *The British Journal of Adminstrative Management* pp. 24–25.

Jean Philippe, Deschamps [1989], 'Creating the products the market wants', *Marketing and Research Today* **17**(1), 4–16.

Julier, S.E. and J.K. Uhlmann [1997], A new extension of the Kalman filter to nonlinear systems, *in* 'SPIE proceeding series', Vol. 3068, pp. 182–193.

Kaiser, H. [1970], 'A second generation little jiffy.', *Psychometrika* **35**, 401–415.

Kaiser, H. [1974], 'An index of factorial simplicity', *Psychometrika* **39**, 31–36.

Kenkel, W.F. [1961], 'Husband wife interaction in decision-making and decision choice', *Journal of Social Psychology* **54**.

KeyNote [2008], Motor industry, Technical report, Key Note Ltd.

KeyNote [2009], Marketing in the digital age, Technical report, Key Note Ltd.

Kickert, W. and E. Mamdani [1978], 'Analysis of a fuzzy logic controller', *Journal of Fuzzy Sets and Systems* **1**, 29–44.

Kiencke, U. and L. Nielsen [2005], *Automotive Control Systems: For Engine, Driveline, and Vehicle*, 2nd edn, Springer.

Klier, W., A. Reim and D. Stapel [2008], 'Robust estimation of vehicle sideslip angle - an approach w/o vehicle and tire models', *SAE International* .

KPMG [2009], Kpmg global auto executive survey 2009, Technical report, KPMG.

Lawrence, A. [1998], *Modern inertia technology, navigation guidance and control*, Springer-Verlag.

Lenain, R., B. Thuilot, C. Cariou and P. Martinet [2006], Sideslip angles observer for vehicle guidance in sliding conditions: Application to agricultural path tracking tasks, *in* 'Proceedings of IEEE International Conference on Robotics and Automation', Vol. 2006, pp. 3183–3188.

Leung, K-T., J. Whidborne, D. Purdy and A. Dunoyer [2009*a*], 'Ideal vehicle sideslip estimation using consumer grade GPS and ins', *SAE International* .

Leung, K-T., M. Bayliss, J. Whidborne and R. Williams [2006], Simulations for the use of GPS compensated sensors for vehicle dynamic systems control, *in* 'Proceedings of 18th International Conference on Systems Engineering', Coventry, UK.

Leung, K.T., J. Whidborne, D. Purdy and A. Dunoyer [2009*b*], 'A review of ground vehicle dynamic state estimations utilising GPS/INS', *Vehicle System Dynamics* .

Leung, K.T., J. Whidborne, D. Purdy, A. Dunoyer and R. Williams [2008], A study on the effect of GPS accuracy on a GPS/INS Kalman filter, *in* 'Proceedings of UKACC International Conference on Control', Manchester, UK.

Li, L., F. Wang and Q. Zhou [2005], A robust observer designed for vehicle lateral motion estimation, *in* 'Proceedings of IEEE Intelligent Vehicles Symposium', Vol. 2005, Las Vegas, USA, pp. 417–422.

Li, P., R. Goodall and V. Kadirkamanathan [2004], Estimation of parameters in a linear state space model using a rao-blackwellised particle filter, *in* 'IEEE Proceedings of Control Theory Application', Vol. 151, pp. 727–738.

Lingman, P. and B. Schmidtbauer [2002], 'Road slope and vehicle mass estimation using Kalman filtering', *Vehicle System Dynamics* **37**, 12–23.

Liu, B., M. Adams and J. Ibanez-Guzman [2005], Multi-aided inertial navigation for ground vehicles in outdoor uneven environments, *in* 'Proceedings of IEEE International Conference on Robotics and Automation', Barcelona, Spain, pp. 4703–4708.

Liu, H., H. Wang and X. Liu [2006], 'Attitude measurement using quaternion based on UKF', *Journal of Nanjing University of Aeronautics & Astronautics* **38**(1), 37–42.

Luckhurst, J. and E. Smith [2006], 'Now try it without ABS, EBD, ESP, EBA ...'. **URL:** *http://www.timesonline.co.uk/tol/driving/features/article785747.ece*

Makita, M. and S. Torii [1992], An analysis of tire cornering characteristics using a magic formula tire model, *in* 'Proceedings of the International Symposium on Advanced Vehicle Control 1992', Yokohama, Japan.

Manning, W. and D. Crolla [2007], 'A review of yaw rate and sideslip controllers for passenger vehicles', *Transactions of the Institute of Measurement and Control* **29**(2), 117–135.

Maskell, S. and N. Gordon [2001], 'A tutorial on particle filters for online nonlinear/non-gaussian bayesian tracking', *IEEE Transactions on Signal Processing* **50**, 174–188.

Maurer, R. [2007], 'This just in-listen to your customers', *The Journal for Quality and Participation* **30**(4), 41–42.

McIntyre, M., T. Ghotikar, A. Vahidi, X. Song and D. Dawson [2009], 'A two-stage lyapunov-based estimator for estimation of vehicle mass and road grade', *IEEE Transactions on Vehicular Technology* **58**(7), 3177–3185.

McMains, Andrew and Brian Morrissey [2009], 'Online brands turn to traditional ads', *Adweek* **50**(25), 7.

Mintel [2007], In car technology, Technical report, Mintel Int. Group.

Mintel [2008*a*], Car retailing - uk, Technical report, Mintel Int. Group.

Mintel [2008*b*], Cars, Technical report, Mintel Int. Group.

Mintel [2009*a*], The car market: 'into and out of recession', Technical report, Mintel Int. Group.

Mintel [2009*b*], Market re-forecasts: Cars, Technical report, Mintel Int. Group.

Mintel [2009*c*], The rise of the online shopper, Technical report, Mintel Int. Group.

Mitchell, V. [1994], 'How to identify psychographic segments: Part 1', *Marketing Intelligence & Planning* **12**(7), 4–10.

Myers, J. [1997], *Segmentation and positioning for strategic marketing decisions*, American Marketing Association.

Ng, B., A. Pfeffer and R. Dearden [2005], Continuous time particle filtering, *in* 'Proceedings of the 19th international joint conference on Artificial intelligence', Edinburgh, Scotland.

Oxlade, A. [2009], 'Recession watch: History & predictions'.
URL: *www.thisismoney.co.uk*

OXTS [2008], 'Oxford technical solution'.
URL: *http://www.oxts.co.uk/*

Pacejka, H. and E. Bakker [1993], The magic formula tyre model, tyre models for vehicle dynamic analysis, *in* 'Proceedings of the 1st International Colloquium on Tyre Models for Vehicle Dynamic Analysis', pp. 1–18.

Pacejka, H. and I. Besselink [1997], Magic formula tyre model with transient properties, *in* 'Proceedings of the Berlin Tyre Colloquium, Vehicle System Dynamics Suppliment', Vol. 27, pp. 145–155.

Parikh, N. [2006], Low-cost multi global positioning system for short baseline attitude determination, Master's thesis, Russ College of Engineering and Technology of Ohio University.

Paul, P., J. Olson and K. Grunert [1999], *Consumer behaviour and marketing strategy*, McGrawHill.

Pettit, R. [2008], 'Learning from winners: How research drove a new model for the automotive industry', *Journal of Advertising Research* **48**(4), 583–590.

Piyabongkarn, D., R. Rajamani, J. Grogg and J. Lew [2009], 'Development and experimental evaluation of a slip angle estimator for vehicle stability control', *IEEE Transactions on control systems technology* **17**(1), 78–88.

Polk, R. L. [2009], 'The leader in global automotive intelligence'.
URL: *http://www.polk.com/*

Prasad, R. and M. Ruggieri [2005], *Applied Satellite Navigation Using GPS, GALILEO, and Augmentation System*, Artect House.

Prasitphol, W. [2002], A cross-cultural investigation of consumer behavior in Japan, Thailand, and the United States, PhD thesis, Alliant Internation University.

Rock, K., S. Beiker, S. Laws and J. Gerdes [2005], Validating GPS based measurements for vehicle control, *in* '2005 ASME International Mechanical Engineering Congress and Exposition, IMECE 2005, Nov 5-11 2005', Vol. 74 DSC, pp. 583–592.

Ryu, J. [2004], State and parameter estimation for vehicle dynamics control using GPS, PhD thesis, Standford University.

Ryu, J. and J. Gerdes [2004*a*], Estimation of vehicle roll and road bank angle, *in* 'Proceedings of 2004 American Control Conference', Boston, USA.

Ryu, J. and J. Gerdes [2004*b*], 'Integrating inertial sensors with global positioning system (GPS) for vehicle dynamics control', *Journal of Dynamic Systems, Measurement and Control* **126**(2), 243–254.

Ryu, J., J. Rossetter and J. Gerdes [2002], Vehicle sideslip and roll parameter estimation using GPS, *in* 'AVEC 2002 6th International Symposium on Advanced Vehicle Control', Hiroshima, Japan.

Sahlholm, P., H. Jansson, E. Kozica and K.H. Johansson [2007], A sensor and data fusion algorithm for road grade estimation, *in* 'Proceedings of 5th IFAC Symposium on Advances in Automotive Control', Monterey Coast, CA.

Sahlholm, P., H. Jansson and K. Johansson [2007], Road grade estimation results using sensor and data fusion, *in* 'Proceedings of 14th World Congress on Intelligent Transport Systems', Beijing, China.

Sahlholm, P., K. Johansson and K. Henrik [2008], Road grade estimation for look-ahead vehicle, *in* 'Proceedings of 17th IFAC World Congress', Seoul, South Korea.

Sharp, B., V. Beal and M. Collins [2009], 'Television: Back to the future', *Journal of Advertising Research* pp. 211–219.

Shieh, L. [2005], 'Extended-Kalman-filter-based chaotic communication', *Journal of Mathematical Control and Information* **22**, 58–79.

Skillern, P. [1967], Market segmentation in the bristish car market, Master's thesis, Cranfield University.

Solomon, M., G. Bamossy and S. Askegaard [2002], *Consumer behaviour: A European Perspective*, Pearson Education.

Stephant, J., A. Charara and D. Meizel [2004], 'Virtual sensor: Application to vehicle sideslip angle and transversal forcesrtual sensor: Application to vehicle sideslip angle and transversal force', *IEEE Transactions on Industrial Electronics* **51**(2), 278–289.

Tan, Y. and M. Saif [2000], 'Neural-networks-based nonlinear dynamic modeling for automotive engines', *Neurocomputing* **30**, 129–142.

Tardy, S. [2007], Active steering for vehicle stability control, Master's thesis, School of Engineering, Cranfield University.

Taylor, A. [1995], 'Porsche slices up its buyers', *Fortune* **131**, 24.

Taylor-West, P., H. Fulford, G. Reed, V. Story and J. Saker [2008], 'Familiarity, expertise and involvement: key consumer segmentation factors', *Journal of Consumer Marketing* **25**(6), 361–368.

Towriss, J. [1981], The new car buyer: the determinants of choice, Technical report, Cranfield Institute of Technology.

Travis, W. and D. Bevly [2005], Navigation errors introduced by ground vehicle dynamics, *in* 'Proceedings of ION GNSS 18th International Technical Meeting of the Satellite Division', California, USA.

Travis, W. and D. Bevly [2008], 'Compensation of vehicle dynamic induced navigation errors with dual antenna GPS attitude measurements', *International Journal of Modelling, Identification and Control* **3**(3), 212–224.

Truscott, B.G. [1967], Market segmentation and characteristics, fundamental trends and forecasting in the UK car market, Master's thesis, Cranfield University.

Uhlmann, J. [1994], Simultaneous map building and localization for real time applications, Technical report, University of Oxford.

Vahidi, A., A. Stefanopoulou and H. Peng [2005], 'Recursive least squares with forgetting for online estimation of vehicle mass and road grade: theory and experiments', *Vehicle System Dynamics* **43**, 31 – 55.

Van Graas, F. and M. Braasch [1991], 'GPS interferometric attitude and heading determination: Initial flight test results', *Journal of The Institute of Navigation* **38**(4), 297–316.

Van Miert, K. [1999], 'Regulation (EEC) No 4064/89 merger procedure', *Commission of the European Communities* .
URL: *http://ec.europa.eu/*

Van Zanten, A. [2002], Evolution of electronic control systems for improving the vehicle dynamic behaviour, *in* 'Proceedings of International Symposium on Advanced Vehicle Control', Hiroshima, Japan.

Verespej, M. [2003], 'Do you know what your customers really want?', *Frontline Solutions* .

Wang, H. and C. Goh [1999], Fuzzy logic Kalman filter estimation for 2-wheel steerable vehicles, *in* 'Proceedings of IEEE/RSJ International Conference on Intelligent Robots and Systems', Kyongju, Korea, pp. 88–93.

Welch, G. and G. Bishop [2001], An introduction to the Kalman filter, Technical report, University of North Carolina at Chapel Hill.

Wenzel, T. [2005], State and parameter estimation for vehicle dynamic control, PhD thesis, Coventry University.

Wenzel, T., K. Burnham, M. Blundell and R. Williams [2006], 'Dual extended Kalman filter for vehicle state and parameter estimation', *Vehicle System Dynamics* **44**, 153–71.

Wenzel, T., K. Burnham, M. Blundell and R. Williams [2007], 'Kalman filter as a virtual sensor: applied to automotive stability systems', *Transactions of the Institute of Measurement and Control* **29**(2), 95–115.

Wing, M., A. Eklund and L. Kellogg [2005], 'Consumer-grade global positioning system (GPS) accuracy and reliability', *Journal of Forestry* **103**, 169–173.

Wolin, L. and P. Korgaonkar [2003], 'Web advertising: gender differences in beliefs, attitudes and behavior', *Internet Research* **13**(5), 375–385.

Yang, N., W-F. Tian, Z-H. Jin and C-B. Zhang [2005], 'Particle filter for sensor fusion in a land vehicle navigation system', *Measurement Science and Technology* **16**, 677–681.

Zhang, P., J. Gu, E. Millios and P. Huynh [2005], Navigation with IMU/GPS/digital compass with unscented Kalman filter, *in* 'Proceedings of IEEE International Conference on Mechatronics and Automation, ICMA 2005', Niagara Falls, Canada, pp. 1497–1502.

Zhou, Z-X., Y-N. Gao and J-B. Chen [2006], 'Application of unscented Kalman filter for large misalignment errors in INS alignment', *Journal of System Simulation* **18**(1), 173–180.

Zino, K. [2009], 'Global auto sales will continue decline in 2009'.
URL: *www.thedetroitbureau.com*

Zlotin, B., A. Zusman and L. Smith [2002], Futuring the next industrial revolution, *in* 'Annual Quality Congress Proceedings', Denver, USA.